Fakultät für Medizin

Institut für Virologie

Inflammation Induced Liver Damage Caused by Viral Infection or Aberrant Metabolism

Florian Reisinger

Vollständiger Abdruck der von der Fakultät für Medizin der Technischen Universität München zur Erlangung des akademischen Grades eines Doktors der Naturwissenschaften genehmigten Dissertation.

Vorsitzender: Univ.-Prof. Dr. Percy Knolle

Prüfer der Dissertation:

1. Univ.-Prof. Dr. Mathias Heikenwälder
2. Univ.-Prof. Dr. Iris Antes

Die Dissertation wurde am 07.10.2014 bei der Technischen Universität eingereicht und durch die Fakultät für Medizin am 11.03.2015 angenommen.

Summary

Hepatitis – inflammation of the liver – can manifest itself as an acute or chronic disease. It comprises of a diverse spectrum of diseases ranging from no or only minor clinical symptoms to jaundice and fulminant liver failure. Chronic hepatitis leads to liver damage, compensatory hepatocyte proliferation, fibrosis and eventually liver cirrhosis and hepatocellular carcinoma (HCC). Many different etiologies are mediating chronic hepatitis like for example infection with hepatotropic viruses, bacteria, autoimmune diseases as well as mal nutrition and toxins.

With 350 – 400 million chronic carriers, hepatitis B virus (HBV) infection is the most prevalent viral liver infection and the leading cause for chronic hepatitis worldwide. Despite the availability of a preventive vaccine, HBV remains a major health problem especially in eastern Asia and sub-Saharan Africa. Persistent HBV infection is accounting for approximately 1 million deaths per year.

While in developing countries HBV infection is the major cause for developing chronic hepatitis, in industrialized countries non-alcoholic fatty liver disease (NAFLD) has become a commonly diagnosed chronic liver disease. The incidence of NAFLD, which is induced by high fat, high sugar diet and a sendentary life-style, has strongly increased in the last two decades with approximately 90 million peoble suffering from this disease in the U.S. Therefore, obesity has evolved as a main etiology causing chronic liver inflammation and HCC in the Western world. Consequently, HCC has become the most rapidly increasing type of cancer in the U.S. Globally, HCC is the sixth most frequent type of cancer and the third most frequent cause of cancer related death. The 5-year survival rate in this highly chemo-resistant cancer is below 12%. Only recently, the first systemic chemotherapy for advanced stage HCC has become available - however, showing only limited survival benefit of 2 – 3 months.

Hence, a better understanding of the molecular underpinnings in the progression from chronic liver inflammation to HCC, as well as new treatment regimens for advanced HCC and its underlying liver diseases like chronic HBV infection and NAFLD are urgently needed.

Therefore my PhD thesis focused on new treatment options for chronic HBV infection and molecular signaling pathways in the progression from NAFLD to non-alcoholic steatohepatits (NASH) and HCC development.

In the first study, termed ‘Intrahepatic myeloid-cell aggregates enable local proliferation of CD8+ T cells and successful immunotherapy against chronic viral liver infection’ my colleagues and I were able to break immune-tolerance in a mouse model of chronic viral infection and induce a sufficient cytotoxic T-lymphocyte (CTL) population that was able to control viral infection. We found that by *in vitro* stimulation of the T cell receptor, CD28 and IL-12 together with Toll-like receptor 9 (TLR9) treatment, a 50-fold increased expansion CTLs in the liver was induced. By histological and

immunohistochemical analyises we identified a previously unrecognized cocoon-like structure, which we termed intrahepatic myeloid-cell aggregates of T-cell expansion (iMATEs), arising upon TLR9 stimulation or acute viral infection. These iMATEs consist of monocyte-derived $CD11b^+$ dendritic cells (DC) and mediate extremely efficient local CTL proliferation and antiviral immunity, leading to the clearance of chronic viral infection in mice.

In the second study 'Specific and Nonhepatotoxic Degradation of Nuclear Hepatitis B Virus cccDNA' we were able to identify a different mechanism for clearing chronic HBV infection from infected hepatocytes. The main hurdle in the treatment of chronic HBV infection is, that the virus establishes a stable episomal DNA, the so-called covalently-closed circular (ccc) DNA, which so far could not be cleared from infected hepatocyte nuclei. Here we can show for the first time that, either by treatment with high doses of interferon-alpha (IFNα) or by activation of the lymphotoxin-beta receptor pathway (LTβR) we can induce degradation of nuclear cccDNA. IFNα treatment as well as LTβR-activation upregulated APOBEC3A and APOBEC3B cytidine-deaminases, respectively, which subsequently deaminated cccDNA marking it for subsequent degradation without any cytotoxicity to the host cell. This indicates that induction of nuclear deaminases by cytokine signaling pathways might allow development of novel therapeutics for curing chronic HBV infection.

In the third study presented in this thesis 'A positive feedback loop between RIP3 and JNK controls non-alcoholic steatohepatitis' my colleagues and I investigating the role of receptor-interacting protein 3 (RIP3) mediated necroptosis in the development of NASH. Here we show that RIP3 is upregulated in a dietary mouse model of NASH as well as in human NASH patients. RIP3 mediated release of pro-inflammatory cytokines, inflammation induced liver damage, fibrosis and proliferation of biliary cells by activation of Jun-(N)-terminal kinase (JNK). This activation was counterbalanced by Caspase-8, the main mediator of apoptotic cell death, and thereby preventing RIP3-induced liver damage and fibrosis. Hence, blocking of RIP3 dependent necroptosis might represent a novel pathway for therapeutic intervention in the development of NASH.

The last study included in my thesis termed 'RIP3 inhibits inflammatory hepatocarcinogenesis but promotes cholestasis by controlling Caspase-8 and JNK-dependent compensatory proliferation' focuses on the role of RIP3-dependent necroptosis in development of HCC. Here my colleagues and I describe in a genetic HCC mouse model of chronic inflammation induced liver damage, that RIP3 prevents Caspase-8-mediated liver damage by suppressing immune responses and compensatory proliferation of liver parenchymal cells. Consequently, RIP3 prevented HCC formation but promoted cholestasis by inhibiting compensatory proliferation of biliary cells upon liver damage.

Zusammenfassung

Als Hepatitis wird eine akute oder chronische Entzündung der Leber bezeichnet. Diese beschreibt ein weites Spektrum von Erkrankungen, die von entweder keinen oder nur geringen klinischen Symptomen bis hin zur Gelbsucht und fulminantem Leberversagen reichen. Chronische Hepatitis führt zu Leberschaden, kompensatorischer Proliferation von Hepatozyten, Fibrose und in manchen Fällen zu Leberzirrhose und zur Entstehung eines Hepatozellulären Karzinoms (HCC). Es gibt vielfältige Ursachen für die Entstehung einer chronischen Leberentzündung, wie zum Beispiel virale und bakterielle Infektionen, Autoimmunerkrankungen sowie auch fehlerhafter Ernährung oder Toxine

Mit 350 – 400 Millionen infizierten Menschen weltweit, ist chronische Infektion mit dem Hepatitis B Virus (HBV) die häufigste virale Leberinfektion und der führende Auslöser für chronische Hepatitis. Obwohl ein präventiver Impfstoff erhältlich ist, stellt HBV vor allem in Ost-Asien und in Afrika südlich der Sahara noch immer ein enormes Gesundheitsproblem dar. Persistierende HBV-Infektion ist vermutlich für mehr als 1 Million Todesfälle pro Jahr verantwortlich.

Während in Entwicklungsländern HBV-Infektion die Hauptursache für chronische Hepatitis darstellt, ist in Industrienationen die nicht-alkohol-induzierte Fettlebererkrankung (NAFLD), eine der häufigsten diagnostizierten, chronischen Leberkrankung. Die Inzidenz von NAFLD ist in den letzten zwei Jahrzehnten stark gestiegen mit etwa 90 Millionen Erkrankten allein in den USA. Daher zählt Fettleibigkeit zu den Hauptursachen für chronische Leberentzündung und der Entstehung von Hepatozellulären Karzinomen (HCC) in der westlichen Welt. Infolgedessen ist das HCC, die am schnellsten zunehmende Krebserkrankung in den USA. Weltweit gesehen ist das HCC die sechst-häufigste Krebserkrankung und die dritt-häufigste durch Krebs verschuldete Todesursache. Das HCC ist resistent gegen die meisten Chemotherapeutika, und die 5-Jahres-Überlebensrate liegt daher unter 12%. Seit wenigen Jahren, gibt es nun die erste systemische Chemotherapie für die Behandlung von fortgeschrittenem HCC, jedoch führt auch diese nur zu einem geringfügig verlängertem Überleben von 2 – 3 Monaten.

Aus diesen Gründen ist es unerlässlich, die molekularen Mechanismen die für die Entstehung des HCC während einer chronischen Entzündung verantwortlich sind, noch genauer zu untersuchen und besser zu verstehen. Außerdem werden neue Behandlungsoptionen für fortgeschrittenes HCC und zugrundeliegende Lebererkrankungen, wie zum Beispiel chronische HBV-Infektion, dringend benötigt.

Daher fokussiert sich meine Doktorarbeit auf die Untersuchung neuer Behandlungsmethoden für chronische HBV-Infektion und die Analyse der molekularen Signalwege, welche der Entwicklung von

NAFLD zur nicht-alkohol-induzierten Fettleberenzündung (NASH) und der HCC-Entstehung zu Grunde liegen.

In der ersten Studie mit dem Titel 'Intrahepatic myeloid-cell aggregates enable local proliferation of $CD8^+$ T cells and successful immunotherapy against chronic viral liver infection' waren meine Kollegen und ich in der Lage in einem Mausmodel für für chronische virale Leberinfektion die Immuntoleranz zu brechen und somit eine ausreichend große Population an cytotoxischen T-Zellen (CTL) zu induzieren, welche die virale Infektion kontrollieren konnte. Wir konnten zeigen, dass Stimulation des T-Zell-Rezeptors, CD28 und IL-6, bei gleichzeitiger Toll-like Rezeptor 9 (TLR9)-Aktivierung, zu einer 50-fachen Expansion der CTL Population führt. Durch histologische und immunohistochemische Charakterisierung von Mäuselebern nach TLR9-Stimulation und während akuter viraler Infektion, konnten wir eine bis dahin unbekannte Kokon-artige Struktur identifizieren, welche wir als ‚intrahepatic myeloid-cell aggregates of T-cell expansion' (iMATEs) bezeichneten. Diese iMATEs bestehen aus $CD11b^+$ dendritischen Zellen und vermitteln eine effiziente, lolake Expansion von funktionellen CTLs und führen somit zur Bekämpfung von chronischen viralen Infektionen in Mäusen.

In der zweiten Studie 'Specific and Nonhepatotoxic Degradation of Nuclear Hepatitis B Virus cccDNA' konnten wir einen weiteren Mechanismus zur Bekämpfung einer chronischen HBV-Infektion identifizieren. Eines der Hauptpobleme in der Behandlung von chronischen HBV-Infektionen ist, dass das Virus im Kern von infizierten Hepatozyten ein stabile, episomale DNA, die sogenannte cccDNA, etabliert, welche mit bisherigen Behandlungsmethoden nicht beseitigt werden kann. Wir zeigen hier nun zum ersten Mal, dass Behandlung mit interferon-alpha (IFNα) oder Aktivierung des Lymphotoxin-beta Rezeptor-Pathways (LTβR) zur Degradierung der cccDNA führen. IFNα und LTβR-Aktivierung erzielten, ohne Schädigung der infizierten Zelle, eine Überexpression von APOBEC3A, beziehungsweise 3B Cytidine-Deaminasen, welche die cccDNA deaminierten, sodass diese daraufhin abgebaut wurde. Somit stellt die Induktion von nukleären Deaminasen durch Zytokine eine potentielle neue Behandlungsmethode für chronische HBV-Infektion dar.

In der dritten Studie 'A positive feedback loop between RIP3 and JNK controls non-alcoholic steatohepatitis' untersuchten meine Kollegen und ich die Rolle des, durch das receptor-interacting protein 3 (RIP3)-induzierten, necroptotoischen Zelltod-Signalweges in der Entstehung von NASH. Wir präsentieren, dass RIP3 sowohl in unserem Mausmodel für NASH als auch in humanen NASH-Patienten hochreguliert ist. RIP3-Überexpression führte zu einem Anstieg in pro-inflammatorischen Zytokinen, Leberschaden, Fibrose und kompensatorischer Proliferation von biliären Zellen durch Aktivierung der Jun-(N)-terminalen Kinase (JNK). Wohingegen Caspase-8, das zentrale Molekül im apoptotischen Zelltod-Signalweg, dieser Aktivierung gegensteuerte und somit RIP-3 induzierten Leberschaden dämpfte. Daher denken wir, dass RIP-3 abhängige Nekroptose einen möglichen Signalweg zur therapeutischen Intervention in NASH darstellt.

Die letzte Studie in meiner Doktorarbeit mit dem Titel ‚RIP3 inhibits inflammatory hepatocarcinogenesis but promotes cholestasis by controlling Caspase-8 and JNK-dependent compensatory proliferation', befasst sich mit der Rolle von RIP3-abhängiger Nekroptose in der Entstehung von HCC. In einem genetischen Mausmodel für chronische Entzündung, Leberschaden und HCC können wir zeigen, dass RIP3 Leberschaden, hervorgerufen durch Caspase-8, verhindert. RIP3 unterdrückte die Aktivierung von Immunzellen und verhinderte die kompensatorische Proliferation von Parenchymzellen und somit die Entstehung von HCC. Allerdings führte diese Unterdrückung der kompensatorischen Proliferation zu Cholestase, da sich auch biliäre Zellen nicht mehr regenerieren konnten.

1. Introduction

1.1. The liver

1.1.1. Physiology and function

With 1200 – 1500g the liver is the largest and metabolic most active human organ. Characteristic for the liver is a high regenerative capacity. Its main functions are the metabolism of carbohydrates, proteins and lipids. Furthermore, the liver serves as reservoir for glycogen, lipids in form of triglycerides and vitamins A, D, E and B_{12}. Hence, due to its metabolic and reservoir function the liver is the vital organ in regulating the nutrient demand of all somatic cells. Additionally, the liver is involved in the detoxification of foreign substances like alcohol or drugs releasing solutes into the bile and liposoluble substances into the gut. Besides its involvement in metabolism and detoxification, the liver has also immune-regulatory functions due to its high number of macrophages (Kupffer cells), production of complement factors and acute phase proteins.[1]

1.1.2. The liver – an immunogenic organ

To prevent local organ damage due to immune responses against antigens metabolized in the liver, these responses are strictly and uniquely regulated. Antigen uptake by tolerogenic non-parenchymal liver cells or direct antigen expression and presentation by hepatocytes induces immune tolerance by the liver microenvironment. Due to this combination of functions in metabolism, toxin and pathogen clearance and its unique immuno-tolerant features, the liver is strongly predisposed to infections with pathogens circulating in the blood. [2, 3] However, in most of the cases the immune system can clear acute liver infections and resolve liver damage.

Initiation of the innate immune response via pattern recognition receptors (PRRs) is the first line of defense against pathogens invading the liver. Interestingly, these PRRs, like for example Toll-like receptors (TLRs), RIG-I-like receptors (RLRs) and NOD-like receptors (NLRs) are not only expressed on bone-marrow derived cells, like Kupffer cells or dendritic cells but also by cells residing in the liver such as hepatocytes, hepatic stellate cells and liver sinusoidal endothelial cells (LSECs). [4-7] Activation of PRRs upon sensing of pathogens triggers the expression of pro-inflammatory cytokines like tumor necrosis factor-alpha (TNFα) and interleukin-6 (IL-6) or antiviral effector molecules like type I interferons (IFNs) leading to increased natural killer (NK) cell activation and improved antigen presentation. [2]

However, the liver is constantly exposed to lipopolysaccharide (LPS) from portal venous blood causing a hypo-responsiveness towards further pro-inflammatory immune stimuli.[8] Thus, this so-

called LPS-tolerance most likely leads to impairment in the induction of adaptive immune system components like cytotoxic T lymphocytes (CTLs).[9] Immunoreglatory mechansims that protect the liver from an overwhelming CTL activation and expansion are the expression of inhibitory molecules like arginase, PDL-1 and galectin-9.[2, 10] But these mechanisms used to inhibit liver damage are also affecting pathogen-specific CTLs and hence might also prevent a sufficient immune response against pathogens.

1.1.3. Viral liver infections

While bacterial liver infections are mainly cleared by the innate immune system, infections with hepatotropic viruses need a strong induction of adaptive immune responses following innate immune stimuli to eliminate infected hepatocytes.[2] When talking about viral liver infections, the most important ones are hepatitis B (HBV) and C (HCV) virus infections with 350 million chronically infected people worldwide for HBV and 170 million for HCV, respectively.[2] In approximately 10% of cases HBV leads to a chronic infection while HCV persists in 50%-80% of all infected patients.[2] Both viruses have established different strategies to evade the immune system. HBV as well as HCV are being recognized by TLR2 on macrophages and Kupffer cells[11, 12] leading to a release of immunoreguatlory cytokines like IL-6 and IL-10 but not of type I IFNs.[13-16]

Both viruses have also developed strategies to escape the humoral immune response with neutralizing antibodies. HBV for example releases large amounts of secreted surface antigen (HBsAg) which binds to and saturates circulating HBV antibodies. HCV on the other hand evades neutralizing antibodies due to the selection of escape variants.[2, 17]

The most important and most obvious immune system evading mechanism of HBV and HCV is the inactivation or depletion of virus-specific CTLs. It has been shown that large numbers of parasite-specific CTLs are necessary to find and clear infected hepatocytes.[18, 19] Due to the liver specific immune functions and a more tolerogenic priming of T-cells, CTLs in the liver are more susceptible to BCL-2-interacting mediator of cell death (BIM) induced apoptosis.[20-22] In the context of HBV and HCV infection, BIM has been shown to be a main player in the depletion of virus-specific CTLs.[21, 23, 24] Hence, overcoming these regulatory mechanisms of T-cell function and expansion would be crucial in efficient immunotherapy of acute and chronic viral liver infections.

1.2. Hepatitis B virus

1.2.1. Epidemiology

With 350 – 400 million chronic carriers worldwide, HBV infection is the most prevalent viral liver infection. Despite the availability of a preventive vaccine, HBV remains a major health problem especially in Asia and Africa accounting for approximately 1 million deaths per year by causing chronic hepatitis, cirrhosis, liver failure and hepatocellular carcinoma (HCC). [25] The main risk for developing chronic HBV infection is by perinatal transmission from chronically infected mothers, while in adults in more than 90% of cases infection is cleared spontaneously.[25, 26]

HBV is a small, enveloped, hepatotropic virus belonging to the family of *Hepadnaviridae*. [27, 28] The common feature of hepadnaviruses is a circular, partially double-stranded DNA genome and they replicate via an RNA intermediate.[29] The HBV genome is organized in a relaxed circular (rc) DNA structure with a lengths of around 3.2 kb and consists of 4 overlapping open reading frames. [28] HBV entry into hepatocytes is mediated by binding to the cell surface receptor NTCP.[30] Upon entering the host cell the rcDNA is being released from the nucleocapsid and transported to the nucleus were it is converted into covalently closed circular (ccc) DNA. cccDNA is a stable episomal DNA present in the nucleus of infected hepatocytes were it serves as template for transcription of all viral mRNAs.[27]

1.2.2. Treatment of chronic HBV infection

The stable expression of cccDNA is also the main obstacle in efficient therapy of chronically HBV-infected patients because current antiviral treatment with nucleo(t)side analogous inhibits viral replication occurring after establishment of the cccDNA. Hence, after treatment cessation cccDNA remains in the nucleus leading to viral rebound even after successful treatment.[28, 31, 32] Therefore, life-long treatment is necessary and also the risk of developing resistance against these drugs has been reported. [33] Another approved treatment option for chronic HBV infection are type I inferferons. For those, a clearance of chronic infection has been shown in a proportion of cases but in general antiviral effects are only moderate and usually accompanied with sometimes severe side effects like for example fatigue, fever, depression or even autoimmune disorders.[27] Hence, new therapeutic options for curing chronic HBV-infected patients without significant side-effects are urgently needed.

In several previous studies it could already be shown that cytokines like interferons and tumor necrosis factor-alpha (TNFα) can influence HBV RNA, capsid as well as cccDNA stability in a non-cytopathic fashion.[34-37] In addition to that, in recent years it has become evident that not only retroviruses like HIV but also DNA viruses and hepadnaviruses are exposed to genetic editing of their

genome by host cell defense mechanisms like APOBEC3 deaminases.[38-40] APOBEC3 genes have been shown to be upregulated in HBV-related inflammation[40] suggesting a role of pro-inflammatory cytokines in regulation of these enzymes. Therefore, modulating pro-inflammtory signaling cascades and downstream APOBEC3 expression might be a promising approach for new anti-viral therapies in chronic HBV infection.

1.3. Hepatitis – inflammation of the liver

That the above mentioned immune-regulatory mechanisms present in the liver are of utmost importance to maintain liver integrity and function becomes obvious when looking at inflammatory reactions in the liver.

Hepatitis – inflammation of the liver – comprises of a diverse spectrum of diseases ranging from no or only minor clinical symptoms to jaundice and fulminant liver failure.[41] Depending on disease duration and whether the inflammatory response is self-limited or persistent one distinguishes between acute and chronic hepatitis, respectively. There exist many different etiologies known today that can lead to hepatitis like for example infection with hepatotropic viruses like HBV and HCV[25, 42], bacteria, protozoa, or autoimmune hepatitis, and primary biliary cirrhosis.[43, 44] Furthermore, liver inflammation can also be caused by life-style and nutritive habits including alcohol consumption, various drugs, and high-fat diet causing non-alcoholic fatty liver disease (NAFLD) and non-alcoholic steatohepatitis (NASH).[45-47]

Acute hepatitis is histologically characterized by inflammatory cells in portal tracts and the parenchyma. Livers show necrotic foci and hepatocyte death, causing architectural liver damage and cholestasis. In later stages of the disease signs of resolving inflammation like pigment-laden macrophages and regenerating hepatocytes become visible. But the extent and timing in which these histological features can be observed is different in the various etiologies and clinical settings. In contrast to acute hepatitis, the characteristic features of chronic hepatitis are persistence of inflammatory cells and continuous destruction of liver cells. Also here, certain histological features can be distinguished between the different etiologies causing chronic hepatitis, like for example so called ground glass hepatocytes are a characteristic for HBV-induced chronic inflammation. [41]

Compared to most other organs, where chronic inflammation would lead to massive tissue destruction, the liver can withstand a significant loss of liver cells due to its regenerative capacity. Upon tissue damage neighboring, resting hepatocytes start to proliferate again to compensate for lost liver mass.[48] However, constant hepatocyte death and compensatory proliferation still leads to

liver damage and usually liver fibrosis. In a proportion of cases fibrosis may become progressive resulting in abnormal liver nodules due to hyperplasia. This late stage and irreversible form of fibrosis is termed cirrhosis which is linked with life-threatening complications and therefore a reduced life expectancy. One reason for this is that in most etiologies of chronic inflammation the sequel of fibrosis and cirrhosis can lead to hepatocellular carcinoma (HCC).[49, 50] Only in the case of HBV-related chronic inflammation direct hepatocarcinogenesis without preceding fibrosis and cirrhosis has been reported.[51]

1.4. Non-alcoholic fatty liver disease and non-alcoholic steatohepatitis

Non-alcoholic liver disease (NAFLD) characterizes a spectrum of disorders of the liver were 5% - 10% of its total weight are accounted for by accumulated fat not caused by alcohol consumption. Pathological features are ranging from simple steatosis (fatty liver) with no or only minor inflammation to non-alcoholic steatohepatitis (NASH) showing strong inflammation, fibrosis, cirrhosis, and hepatocyte apoptosis and necroptosis.[52-54]

1.4.1. Epidemiology

NAFLD has become the most commonly diagnosed chronic liver disease in the Western world. The reasons for this are on the one hand the greater awareness of the disease and on the other hand the increase in metabolic risk factors.[55, 56] Between 1998 and 2008 the US National Health and Nutrition Examination Survey reported an increase of NAFLD among chronic liver diseases from 47% to 75% along with an increase in obesity, type 2 diabetes, insulin resistance and arterial hypertension.[56] The estimated prevalence of NAFLD in Europe is 20% to 30% and worldwide between 6% and 33%. The prevalence estimated for NASH is significantly lower but still 3% to 5%.[55, 57]

The best known risk factor for NAFLD is obesity. A high BMI and increased amounts of visceral fat have been shown to increase the risk of developing NAFLD. But also patients with type 2 diabetes show a markedly higher correlation with NAFLD compared to the general population.[58, 59] Furthermore, male sex, older age and Hispanic origin could be associated with an increased danger for developing NAFLD.[57, 60]

1.4.2. Characterization and clinical course of NAFLD

In general NAFLD can be divided into two groups. Patients simply suffering from a fatty liver, namely steatosis, with no or only very mild symptoms of a hepatic disease like for example fatigue and a slight pressure in the right upper abdomen. They show no or only a very slow progression of disease

and the histologic phenotype can be reverted by weight reduction and physical activity. But in 5% to 20% of cases fatty liver disease develops into NASH.[53] For the progression from steatosis to NASH a 'two-hit hypothesis' has been proposed. [61] Accumulation of lipids in the cytoplasm of hepatocytes is only the first step in the development of NASH. A second hit causing inflammation, hepatocyte cell death, fibrosis, and in advanced stages also cirrhosis and HCC is needed. Yet, the exact molecular underpinnings leading to this progression remain still elusive (**Fig 1**).[61, 62]

atients suffering from NASH have a poor long-term survival and especially of those with cirrhosis 2% develop HCC every year.[62, 63] Treatment options for NASH are limited and so far no drug-based approach has managed to improve all the pathologic features ranging from steatosis, inflammation and fibrosis. [53] Hence, further studies investigating the molecular mechanisms in the progression from steatosis to NASH are urgently needed, especially due to the fast increasing prevalence of NAFLD.

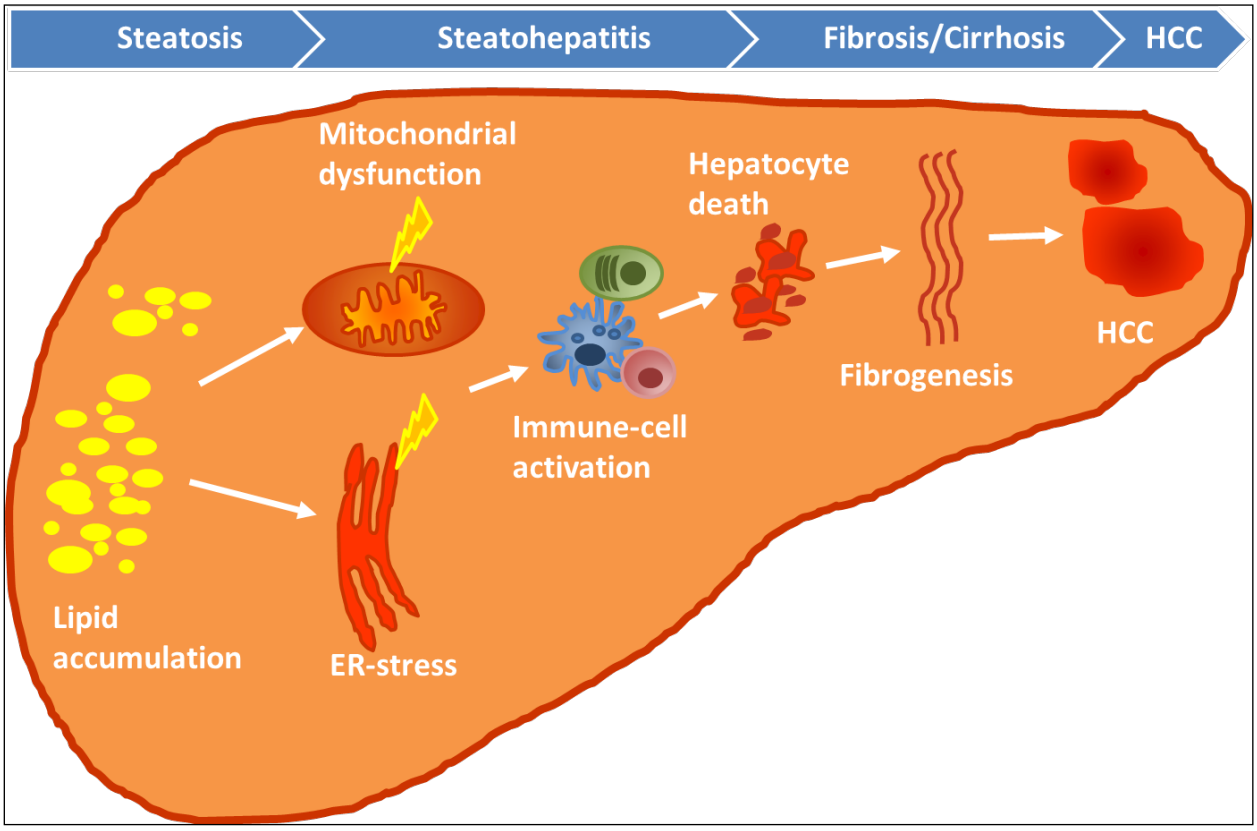

Figure 1: Clinical course of NAFLD and NASH. Accumulation of lipid droplets is the initial step in development of NAFLD. For progression to NASH a second hit causing ER-stress and mitochondrial dysfunction is needed. These triggers are then causing immune cell activation and chronic liver inflammation driving immune cell mediated hepatocyte death, compensatory proliferation, fibrosis and cirrhosis. Approximately 2% of cirrhotic patients will develop HCC.[52, 54]

1.5. Chronic inflammation and cancer

It was already in the late 19th century that Rudolph Virchow, a German physician, proposed a link between wound healing, scar formation, inflammation and tumor development.[64] Remarkably, he even speculated on the existence of a cancer-causing bacillus, which turned out to be right. [65] In the last decades several studies have demonstrated that chronic inflammation is a risk factor and promoter for cancer development.[66] Therefore, inflammation was included in the hallmarks of cancer which in addition comprise of sustained proliferative signaling, evading growth suppressors, resistance to cell death, enabling replicative immortality, inducing angiogenesis, activation of invasion and metastasis, reprogramming energy metabolism and evading immune destruction.[67-69]

Chronic inflammation can be induced by viruses, like for example HBV and HCV, driving hepatocarcinogenesis,[51] or by pathogenic bacteria like *Helicobacter pylori* in gastritis promoting gastric cancer or mucosa-associated lymphoid tissue (MALT) lymphoma.[70] Also parasitic infections with Schistosoma have been reported to cause chronic inflammation that potentially can trigger liver, colorectal or bladder cancer.[71] Yet, not only infection with pathogens but also autoimmune diseases can cause cancer-promoting inflammation. For example, patients suffering from autoimmune hepatitis or inflammatory bowel diseases (e.g. Crohn's disease) show an increased risk for development of HCC or colon cancer, respectively. [72, 73] Additionally to pathogens and autoimmunity, also chronic and acute intoxication with certain drugs or alcohol are related with inflammation-induced carcinogenesis.[41] Furthermore, recent studies propose an additional role of genetic and dietary obesity in driving hepatitis and HCC development.[47, 74]

However, acute and chronic inflammation has also been reported to be anti-tumorigenic as tumor cells can be targeted and destroyed by innate and adaptive immune cells. [75, 76] Despite the enormous progress that has been made in understanding the exact molecular mechanisms and signaling pathways of chronic inflammation and its influence on cell death, proliferation, tissue integrity and its pro- and anti-carcinogenic effects remain still elusive. The complicated network of immune cells, their interaction with organ-specific epithelial cells, tumor stroma and the expression of a plethora of cytokines and chemokines by these cells are probably decisive for the outcome of a chronic inflammatory disease. Furthermore, it still needs to be investigated whether the transition from chronic inflammation to cancer is mediated by specific pathways or is occurring unspecifically by just increasing the probability of the development of aberrant cells due to tissue destruction and compensatory proliferation.[41]

1.6. Hepatocellular carcinoma

Hepatocellular carcinoma (HCC) is a clinically heterogeneous primary liver cancer consisting of a range of tumors arising from different etiologies. [77] HCC is mainly caused by prolonged liver damage and in most cases preceded by liver cirrhosis. With more than 800 000 new cases per year, HCC is the sixth most common type of cancer and the third most frequent cause of cancer related death. [78] The 5-year survival rate of patients suffering from HCC is below 12%. [79]

1.6.1. Risk factors for HCC

In 70% – 90% of patients HCC develops on the background of chronic liver disease. Around 80% of cases arise in eastern Asia and sub-Saharan Africa where the most prevailing risk factor is chronic HBV-infection in combination with aflatoxin B1 exposure. In contrast, in industrialized countries, for a long time most HCC cases were accounted for by persistent infection with HCV and chronic alcohol intake.[80] But in recent years obesity has evolved as the most common etiology causing liver cancer. Consequently, HCC has become the most rapidly increasing type of cancer in the U.S.[47] Still, more than 50% of all HCC cases worldwide arise on the background of a chronic HBV infection.

HBV *per se* is a non-cytopathic virus and during chronic HBV infection liver damage is mainly mediated by $CD8^+$ T-cells trying to clear the virus from infected hepatocytes.[81, 82] In persistent viral infections, insufficient T-cell responses lead to continuous inflammatory liver damage and repeated cycles of hepatocyte death (so-called necro-inflammation) and compensatory proliferation. Necro-inflammation may subsequently lead to fibrosis, cirrhosis and cancer.[81, 83, 84] The link between pro-inflammatory signaling pathways, like for example NF-κB, in driving chronic inflammation-induced liver damage, compensatory proliferation and finally HCC development could already be corroborated in several mouse models.[41, 85]

Additionally to causing necro-inflammation, HBV can also directly contribute to HCC development in the absence of inflammation, fibrosis and cirrhosis.[51] For example, in 86.4% of HCC cases HBV-DNA integration into the host genome can be found,[86] which might lead to expression of fusion proteins or a general genomic instability.[87, 88] However, it is still debated whether HBV integration is rather a consequence or an initiator of malignant hepatocyte transformation.[89] Furthermore, the non-structural viral HBx protein has been shown in several studies to have direct oncogenic effects.[90-92] Most likely, HBx mediates its pro-carcinogenic functions by influencing diverse signaling pathways involved in cell death, proliferation, differentiation, DNA repair and oxidative stress.[51]

While in Asia and Africa about 90% of HCC cases are related to HCV and HBV virus infection[93] in Western countries 30% to 40% of HCC patients were shown not to be infected with neither of these

viruses suggesting other reasons for hepatocarcinogenesis.[80] For example, sustained and heavy consumption of alcohol is a well-established risk factor for HCC development increasing the probability for liver cancer by a factor of 1.5 to 2.0.[94] Furthermore, as already mentioned above, several studies performed in the United States, Scandinavia, Taiwan and Japan could show that people suffering from fatty liver disease or the metabolic syndrome (e.g. type 2 diabetes) had a 1.5 to 2.0 fold increased risk for developing HCC compared to non-obese people.[95-97]

1.6.2. Treatment of HCC

HCC is a highly chemoresistant cancer which is most often diagnosed at a rather late stage. Potentially curative treatment options like surgical resection and liver transplantation are limited to early stage of disease.[98] Surgical intervention is the best treatment option for patients without cirrhosis and only small tumor nodules. Due to the underlying liver disease that caused the initial tumor, patients are still at risk of developing new HCC and hence the 5-year reoccurrence rate is around 70%.[80]

For patients suffering from HCC including cirrhosis, orthotopic liver transplantation is the treatment of choice with the lowest risk of tumor reoccurrence as also the underlying cirrhosis is being cured. Patients with only one tumor smaller than 5 cm or a maximum of 3 tumors smaller than 3 cm in diameter and no vascular invasion, the 4-year overall survival rate was shown to be 85% with a 92% probability of reoccurrence-free survival after liver transplantation.[99] Due to shortage of organs available for transplantation, patients have to meet strict criteria and hence only a limited number of patients who are likely to have the best outcome is eligible for liver transplantation.[80] Further treatment options for early stage HCC are radiofrequency ablation or **T**rans**a**rterial **C**hemoembolization and Radio**e**mbolization (TACE) but they are not efficacious in larger tumor nodules and patients show a high reoccurrence rate due to the non-curative nature of these treatments.[93]

Only recently, the first systemic chemotherapy that showed to be efficacious in treatment of advanced stage HCC – Sorafenib – became available. Sorafenib is an orally administered pan-kinase inhibitor with antiproliferative and antiangiogenic properties. However, also Sorafenib shows only a limited survival benefit of 2-3 months with partly severe side-effects.[100, 101]

This poor prognostic outcome most likely results from the fact, that HCC is not a single entity but in many patients rather comprises of several liver cancer-subtypes not only differing in genetics and morphology but also in their responsiveness to therapy. [98, 102] Consequently, further studies are urgently needed to identify common signaling pathways and biomarkers to provide more targeted and personalized treatment options for patients suffering from HCC.

1.7. NF-κB – linking inflammation, cell death, survival, and cancer

1.7.1. The NF-κB family

NF-kappa B proteins are a family of eukaryotic transcription factors that have been shown to be involved in diverse cellular processes, like for example cell proliferation and survival, cell death, developmental processes and inflammatory responses.[103-106] Members of the NF-κB family are characterized by a highly conserved DNA binding domain, the Rel homology (RH) domain. In humans the NF-κB family comprises of five different DNA-binding subunits: p65 (also called RelA), RelB, c-Rel, p52 (cleaved form of p100) and p50 (cleaved form of p105).[107] NF-kB activity can be induced by many different stimuli, such as pro-inflammatory cytokines like for example tumor necrosis factor alpha (TNFα), interleukin 1 beta (IL-1β) and lymphotoxin (LT), LPS, or reactive oxygen species (ROS).[108-110] In steady-state, NF-κB transcription factors are being kept in the cytoplasm either as inactive, uncleaved pro-forms, as in case of p100 and p105 or sequestered by inhibitor of kappa B (IκB) proteins as shown for RelA, RelB and c-Rel. Upon stimulation NF-κB transcription factors are either processed into their active form or released from IκB proteins enabling translocation into the nucleus were they initiate target gene transcription either as hetero- or homodimers.[111-113]

1.7.2. NF-κB signaling

NF-κB dependent target gene transcription is mediated via two different signaling pathways – the canonical pathway which is mainly downstream of tumor necrosis factor receptor (TNFR) I and II, and the non-canonical pathway which is initiated by another subset of TNFR superfamily members like for example LT-beta receptor (LTβR) or CD40 (**Fig. 2**).[113, 114]

The initial step in the non-canonical signaling cascade upon receptor engagement by their ligands (e.g. $LT\alpha_1\beta_2$ heterotrimers, CD40 ligand) is phosphorylation of the NF-κB-inducing kinase (NIK) and its downstream target IκB kinase-alpha ($IKK\alpha_2$). In the subsequent step $IKK\alpha_2$ mediates the proteasomal cleavage of p100 into p52 and hence enabling translocation of p52/RelB dimers into the nucleus. The physiological functions of the LTβR-pathway comprise development and organization of secondary lymphoid organs, the thymic stroma and recruitment of immune cells. Furthermore, non-canonical signaling via LTbR and CD40 is crucial for B-cell survival and maturation of follicular dendritic cells.[115, 116]

Notably, besides its physiological functions, LTs play a crucial role in the development and maintenance of tertiary lymphoid organs, thereby contributing to inflammatory and autoimmune diseases. In line, in a mouse model overexpressing LT specifically in hepatocytes, it could be shown

that constitutive activation of non-canonical NF-κB signaling leads to necro-inflammation, compensatory proliferation and subsequent development of hepatocellular carcinoma.[85]

While non-canonical signaling is initiated via NIK, the first step in the canonical signaling cascade downstream of TNFRI is recruitment of the so-called complex I, consisting of TNFRI associated death domain protein (TRADD), TNFRI associated factor (TRAF)2 and TRAF5, receptor-interacting protein (RIP)-1, and cellular inhibitor of apoptosis (cIAP).[117] Via transforming growth factor β activated kinase 1 (TAK1), Complex I then mediates activation of the IKK-complex comprising of a IKKα, β, γ heterotrimer which subsequently mediates nuclear translocation of the p50/RelA heterodimer (NF-κB1) by phosphorylation of IκBα (**Fig. 2**). The main tasks of canonical NF-κB are induction of pro-inflammatory cytokines and anti-apoptotic and pro-proliferative factors like for example inhibitor of apoptosis proteins (IAPs) or members of the cyclin family, respectively. [118, 119]

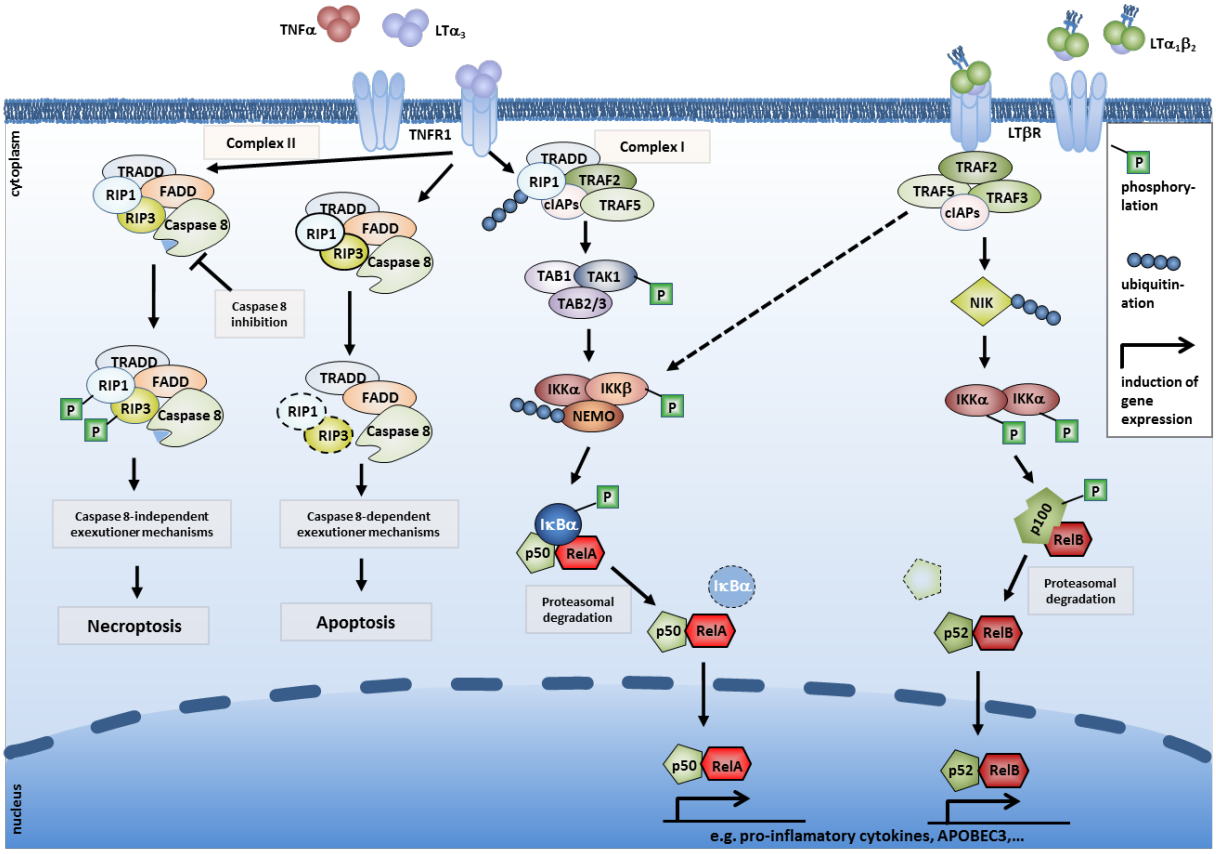

Figure 2: NF-κB and programmed cell death signaling. Activation of TNFRI can initiate canonical NF-κB signaling via complex I, TAK1 and the IKK-complex. Release of the p50/RelA dimer leads to the transcription of pro-inflammatory cytokines and anti-apoptotic and pro-proliferative target genes. In case canonical NF-κB is blocked or disturbed, complex II is being formed mediating TNF-induced cell death either via the apoptotic, or if caspase-8 is blocked, the necroptotic signaling cascade. The non-canonical NF-κB pathway is mediated by receptor trimerization of several TNFR superfamily members like for example LTβR. NIK-induced phosphorylation of IKKα_2 leads to processing of p100 to p52 and subsequent translocation of the p52/RelB dimer into the nucleus. (Adapted from [119])

However, in case canonical signaling is blocked or disturbed binding of TNFα to TNFRI can also activate programmed cell death pathways by recruiting complex II consisting of Fas-associated death domain (FADD), TRADD, Caspase-8, RIP1 and RIP3.[117] Until lately caspase-8 mediated apoptosis, via cleavage of RIP1 and RIP3 and activation of downstream effector caspases, was thought to be the only regulated cell death pathway. In contrast to that, necrosis was mainly viewed as an unregulated cellular burst due to stress. But recent studies could show that, in case apoptosis was blocked - for example by viruses expressing anti-apoptotic genes, complex II was still able to induce cell death via the RIP1/RIP3 complex. Consequently, this newly described form of programmed cell death was termed necroptosis (**Fig .2**). [117, 120 121]

1.7.3. NF-kB and liver cancer

NF-κB has a plethora of functions in different cellular compartments of the liver, for example influencing the survival of hepatocytes, activation of Kupffer cells, and induction of inflammatory responses. Hence, NF-κB is one of the main mediators in regulating anti-viral responses, inflammation induced liver damage, compensatory proliferation and wound healing. [122] Of note, NF-κB activation is frequently detected in chronic inflammation-induced human HCC and has been associated with hepatocyte transformation, independent of the underlying liver disease.[123] For example, in HBV-induced HCC it could be shown that the oncogenic HBx protein can trigger the NF-κB signaling pathway.[124] But also HCV-infection[125] and fatty acids causing NAFLD could be correlated with an increased NF-κB activity.[126]

The important role of NF-κB in the liver was also corroborated in several mouse models, were it could be shown that genetic deletion of canonical NF-κB regulators like IKKγ and TAK1, or constitutive activation of non-canonical NF-κB leads to inflammation, liver injury, fibrosis and HCC. [85, 127-129] Furthermore, in a recent study in mice fed with choline-deficient, high-fat diet, non-canonical NF-κB activation, via the TNF superfamily member LIGHT, links NASH to the development of HCC by activation of $CD8^+$ and NKT cells.[47]

2. Material and Methods

2.1. Material

2.1.1. Machines and Devices

Device	Source
Infinite F200 PRO microplate reader	Tecan, Männedorf, Switzerland
Molecular Imager® ChemiDoc™ XRS	Bio Rad, München, Germany
-80°C fridge Herafreeze	Heraeus, Hanau, Germany
-20°C fridge	Liebherr, Switzerland
4°C fridge	Bauknecht, Stuttgart, Germany
Biofuge Fresco Microcentrifuge	Heraeus, Hanau, Germany
Megafuge 1.0	Heraeus, Hanau, Germany
Micro centrifuge MiniStar Silverline	VWR, Darmstadt, Germany
Heracell CO_2 Incubator	Thermo Scientific, Ulm, Germany
Herasafe Cell Culture Bench	Thermo Scientific, Ulm, Germany
Vortexer Reax 200	Heidolpf, Kelheim, Germany
7900HT Fast Real Time PCR System	Applied Biosystems, Darmstadt, Germany
Nanodrop 2000 Spectrophotometer	Peqlab, Erlangen, Germany
Thermomixer comfort	Eppendorf, Hamburg, Germany
Microscope Axiovert 25	Zeiss, Jena, Germany
Microscope BX53	Olympus, Hamburg, Germany
SCN400 slide scanncer	Leica Microsystems, Wetzlar, Germany
Automatic Ice Machine AF10	Scotsman, USA
PCR-cycler	Biometra, Göttingen, Germany

Precision scale CP153	Sartorius, Göttingen, Germany
Water bath	Memmert, Schwabach, Germany
Power 300 Power Supply	Peqlab, Erlangen, Germany

2.1.2. Kits and Reagents

Kit	Source
Cell Proliferation Kit II (XTT)	Roche, Mannheim, Germany
RNeasy Mini Kit	Qiagen, Hilden, Germany
BCA Protein Assay kit	Thermo Scientific, Ulm, Germany
QuantiTect Reverse Transcription Kit	Qiagen, Hilden, Germany
Caspase-activity assay	Enzo Life Sciences, Lorrach, Germany

2.1.3. Cells

Cell line	Description
HepG2	human hepatocellular carcinoma cell line
Huh7	human hepatocellular carcinoma cell line
HepaRG	human hepatocellular carcinoma cell line
HepG2H1.3	human hepatocellular carcinoma cell line

2.1.4. Buffers/Medium

Buffer/Medium	Composition/Evidence	Source
Cell culture		
DMEM Medium with High	Supplemented with	Cat. No. E15-810. PAA

Glucose (4.5 g/l) and 2 mM L-glutamine	10% FCS 1% penicillin/streptomycin	Laboratories, Austria, Pasching
PBS		Cat. No. BE17-516F Lonza, Verviers, Belgium,
Trypsin/EDTA	10 x solution was diluted 1:10 in bidistilled water	Cat. No. L2153 BiochromeAG, Berlin, Germany
Cell lysis/ Determination of protein concentration		
RIPA buffer	50 mM TRIS-HCL (pH 7,4) 1% NP-40 (Igepal) 150 mM NaCl 0.25% DOC 1 mM EDTA	
RLT buffer		Cat. No. 74106 Qiagen, Germany, Hilden
Lysis buffer for protein extraction	RIPA buffer plus Roche complete protease inhibitor cocktail	
Lysis buffer for RNA extraction	RLT buffer plus 1% β-mercaptoethanol	
SDS-PAGE		
Running gel	8.1% acrylamide mix 0.375 M Tris (pH 8.8) 1% SDS	

	0.1% ammonium persulfate 0.04% TEMED in distilled water	
Stacking gel	5% acrylamide mix 0.125 M Tris (pH 8.8) 0.1% SDS 1% ammonium persulfate 0.1% TEMED in distilled water	
3x SDS Loading buffer	0.24 M TRIS-CL (pH 6.8) 6% SDS 30% glycerol 16% β-mercaptoethanol 0.6 mg/ml bromphenol blue	
10x Electrophoresis buffer	0.25 M TRIS 1.92 M glycine 1% SDS in distilled water	
Western blot		
PONCEAU-S	Diluted in 5% acetic acid	Cat. No. P-3504 Sigma, Steinheim, Germany
10 x TBST	0.1 M TRIS-HCl (pH 8.0)	

	1.5 M NaCl 0.5% TWEEN 20 in distilled water	
Ab-dilution / blocking buffer	1x TBST 5% BSA	
Blocking buffer	1 x TBST 5% Skim Milk	
Transfer buffer	0.3% TRIS base 1.4% glycin 20% methanol in ultra-filtered water	
HRP-Substrate	Super Signal West Dura	Cat. No. 34076 Thermo Scientific, Illinois, USA
Molecular-weight marker	Spectra Multicolor Broad Range Protein Ladder	Cat. No. 26634 Thermo Scientific, Illinois, USA
RT-PCR		
Master mix	ROCHE Fast SYBR Green Mix (2x) 100 µM forward Primer 100 µM reverse Primer in distilled water	Roche, Penzberg, Germany

2.1.5. Antibodies

Western Blot

Target	Species	Dilution	Clone	Company
Anti-phospho RelA	rabbit	1:1,000	93H1	Cell Signaling, Danvers, MA, USA
Anti-p100/p52	rabbit	1:1,000	polyclonal	Cell Signaling, Danvers, MA, USA
Anti-GAPDH	rabbit	1:5,000	D16H11	Cell Signaling, Danvers, MA, USA
Anti-phospho JNK	rabbit	1:1000	56G8	Cell Signaling, Danvers, MA, USA
Anti-Apobec3a	rabbit	1:1000	polyclonal	Acris, San Diego, CA, USA
Anti-Apobec3b	rabbit	1:1000	polyclonal	Santa Cruz Biotechnology, Dallas, TX, USA
Anti-TNFRI	rabbit	1:1000	C25C1	Cell Signaling, Danvers, MA, USA
Anti-LTbR	goat	1:1000	polyclonal	Santa Cruz Biotechnology, Dallas, TX, USA
HRP-anti-rabbit Ig	goat	1:10,000	polyclonal	Cell Signaling, Danvers, MA, USA
HRP-anti-goat Ig	donkey	1:4000	polyclonal	Dako, Hamburg, Gemany

Immunohistochemistry

Target	Source	Dilution	Clone	Company
Anti-Ki67	rabbit	1:500	SP6	Lab Vision / NeoMarkers, Fremont, CA, USA
Anti-cleaved	rabbit	1:300	polyclonal	Cell Signaling, Danvers, MA,

Caspase-3				USA
Anti-RelA	rabbit	1:500	polyclonal	Lab Vision / NeoMarkers, Fremont, CA, USA
Anti-RelB	rabbit	1:200	polyclonal	Santa Cruz Biotechnology, Dallas, TX, USA
Anti-phospho-JNK	mouse	1:250	56G8	Cell Signaling, Danvers, MA, USA
Anti-cJun	rabbit	1:400	polyclonal	Abcam, Cambridge, UK
Anti-B220	mouse	1:3000	RA36B2	BD Biosciences, San Jose, CA, USA
Anti-F4/80	mouse	1:120	BM8	BMA Biomedicals AG, Augst, Switzerland
Anti-CK19	rat	1:500	n/a	Hybridoma bank
Anti-CD3	rabbit	1:300	SP7	Lab Vision / NeoMarkers, Fremont, CA, USA
Anti-CD11b	rabbit	1:800	polyclonal	Novus Biologicals, Littleton, CO, USA
Anti-MHC class II	mouse	1:500	OX-6	Novus Biologicals, Littleton, CO, USA
Anti-OX40L	rat	1:100	OX89	MyBioSource, San Diego, CA, USA
Anti-TNF-alpha	rabbit	1:300	polyclonal	Abcam, Cambridge, UK
Anti-GP73	goat	1:100	polyclonal	Santa Cruz Biotechnology, Dallas, TX, USA
Anit- Collagen type IV	rabbit	1:50	polyclonal	Cedarlane, Burlington, ON, Canada

2.2. Methods

2.2.1. Quantitative Real-Time PCR

Total RNA was purified from liver tissue using Trizol reagent (Invitrogen, Darmstadt, Germany) or from cultured cells using the RNeasy Mini Kit (QIAGEN, Hildesheim, Germany) The quantity and quality of the RNA was determined with a Nanodrop2000 (Thermo Scientific). 1µg total RNA was used for reverse transcription using the Quantitect Reverse Transcription kit (QIAGEN) according to manufacturer's protocol. In the end reversely transcribed cDNA was diluted 1:20 in aqua bidest to a total volume of 400µl for further use in Real-Time PCR reaction.

For Real-Time PCR reaction, 3µl of 1:20 diluted cDNA were mixed with 2x Fast SYBR Green Mix (Roche, Penzberg, Germany) and specific forward and reverse primers and pipetted onto a 384-well qPCR plate (Biozol, Eching, Germany). All qPCR reactions were performed in triplicates on a 7900HT Sequence Detection System (Applied Biosystems, Foster City, CA, USA). Data analysis was performed using SDS 2.4 software (Applied Biosystems). All values shown are relative values normalized to values of RHOT2 and HPRT serving as house-keeping genes.

2.2.2. Western Blot

The SDS-gel as well as 8 pieces of 3 mm Whatman filter paper (Whatman, Dassel, Germany) and a nitrocellulose membrane were soaked in transfer buffer. The blot was assembled as following: anode, 4 pieces of Whatman paper, membrane, gel, 4 pieces of Whatman paper, cathode. The transfer was carried out for 30 min at 300 mA per gel and confirmed with PONCEAU-S solution, which was afterwards removed with distilled water. After 3-5 times washing for 5 min in TBST, free spots on the membrane were blocked for 1h in blocking buffer. Then the membrane was incubated with the primary antibody appropriately diluted in Ab-dilution buffer for 2h at room temperature or overnight at 4°C followed by 5 times washing with TBST for 5 min and incubation with of the secondary antibody appropriately diluted in Ab-dilution buffer for 1h. While the membrane was washed again 3-5 times for 5 minutes in TBST, a 1:1 mixture of stable peroxide solution and luminol/enhancer solution (Biorad) was prepared. The membrane was covered with this mixture, incubated for 5 minutes and developed in the Molecular Imager® ChemiDoc™ XRS (Biorad).

2.2.3. Immunohistochemical stainings

2µm paraffin sections were stained with H/E or various primary and secondary antibodies. Paraformaldehyde (4%) fixed and paraffin embedded liver tissue was incubated in Bond Primary antibody diluent (Leica Biosystems, Wetzlar, Germany) and staining was performed on a BondMax immunohistochemistry robot (Leica Biosystems) usind BOND polymer refine detection solution for

DAB or BOND polymer refine red detection for AP, respectively. Image acquisition was either performed on an Olympus BX53 microscope equipped with an Olympus DP72 digital camera or with a Leica SCN400 slide scanner.

2.2.4. Analysis and Quantification of Immunohistochemical Stainings

The number of cells positively stained for the different nuclear markers (e.g. Ki67, p-JNK) in various cell types (e.g. hepatocytes or non-parenchymal cells) was determined using SlidePath TissueIA image analysis software and normalized to tissue area or total cell number respectively. Alternatively, 4 different and independent areas ware randomly selected and analyzed in a blinded fashion and normalized to tissue area or total cell number on an Olympus BC53 microscope using CellSense software (Olympus, Hamburg, Germany).

Numbers of bile ducts or bile duct cells, positively stained for cytokeratin or A6 were counted manually or automatically using SlidePath TissueIA image analysis software on whole liver sections and normalized to tissue area. Hepatocytes positively stained for cleaved Caspase-3 as well as macrophages positive for F4/80 were quantified numerically (positive cells per total cells) or densitometrically (area stained per total area) using SlidePath TissueIA software on whole tissue sections and normalized to the total number of hepatocytes or total tissue area, respectively. For double stainings the number of bile duct cells, positively double stained for pan-cytokeratin and Ki67 or cleaved Caspase-3, respectively, were counted manually on whole liver sections and normalized to total number of cytokeratin-positive cells.

Images for representation were either taken with an Olympus BX53 Microscope equipped with a DP72 camera using CellSense Dimensions 1.7 software (Olympus) or by scanning of whole tissue sections using a Leica SCN400 slide scanner and SlidePath imaging software (Leica).

2.2.5. aCGH Analysis

In order to characterize copy number alterations, oligo array CGH using the Agilent (Boeblingen, Germany) platform was performed. Genomic DNA was extracted from formalin-fixed paraffin-embedded (FFPE) tissue sections, after enrichment for tumor cells by micro-dissection using the DNEeasy FFPE kit (QIAGEN). DNA extracted from four C57Bl/6 WT livers was pooled and used as reference DNA. 250ng of test and reference DNA was differentially labeled with Cy3-dUTP (test) and Cy5-dUTP (reference) by random primed labelling using CGH labelling kit for oligo arrays (Enzo, Loerrach, Germany). Hybridization, washing and scanning was performed acoording to manufacturer's protocol and data were extracted from the Feature Extraction Software (Agilent, Boeblingen, Germany) as tab-delimited text files. The arrays used were custom-designed 8x60k

arrays (AMADID 41078) with approximately 60000 probes covering the whole mouse genome. The probe set include the Agilent 44k (AMADID 15028) in order to enable merging of the 60k data with 44k data. The raw data were imported into the R statistical platform (R Development Core Team; R: A language and environment for statistical computing. R Foundation for Statistical Computing, Vienna, Austria, ISBN 3-900051-07-0, URL: http://www.R-project.org) and the background substracted median intensity signals were used to build log2 ratios. After median normalization values were quality filtered using flags as defined by AgilentFeature extraction software. The log2 ratios were subsequently segmented, called, and copy number regions were defined using functions from the CGHcall[130] and CGHregeions[131] packages. For the CGH call function 75% of tumor cells based on microscopic assessment of H/E stained FFPE sections, was used. In order to include profiles of liver tumors that developed in TAK1^{LPC-KO} mice from a former study[127] raw data from two samples (GSM473549 and GSM473553) were downloaded from GeneExpression Omnibus (GEO, http://www.ncbi.nlm.nih.gov/geo/), analyzed as described above and the resulting data were merged with the 60k array data. The copy number profiles were karyogram-style plotted using an in-house written R-function.

2.2.6. HBV inocula, cell cultures, HBV infection and treatments

HBV inocula were prepared as described previously.[132] Shortly, HBV was concentrated from the supernatant of HepG2.2.15 cells using centrifugal filter devices (Centricon Plus-70, Biomax 100.000m Millipore Corp., Bedford, MA) and tittered by HBV-DNA dot blot analysis after sedimentation into a CsCl density-gradient to determine enveloped DNA-containing viral particles (vp). Only inocula reaching a titer between $3x10^9$ and $3x10^{10}$ vp/ml were used. Immediately after collection, the virus stock was aliquoted and stored at -80°C until being used for infection. Primary Human Hepatocytes (PHH) were isolated from surgical liver resections, cultured and infected with HBV as described.[133, 134] Tissue samples and annotated data were obtained and experimental procedures were performed within the framework of the nonprofit foundation Human Tissue Cell Research (HTCR), including the informed patient's consent.[135] HepG2H1.3, HepaRG and HepaRG-tA cell culture, differentiation and HBV infection (at a multiplicity of infection of 600 vp / cell) were also performed as described.[136, 137] HepaRG-tAVifAU1 cell line was obtained after transduction of HepaRG-tA cells with a lentivirus expressing the HIV-Vif gene under a tetracyclin regulated promoter (Plvx-Tight-Puro lentiviral vector, Clontech, Saint-Germain-en-Laye, France) and selection using 0.25 µg/ml puromycin.

A3A or A3B overexpression in HepG2H1.3 cells was obtained by transfection of pLenti6.3, pLenti6.3-A3A, pTR600 orpTR600-A3B, respectively, using 'Lipofectamine 2000 Reagent' (Invitrogen). The HepG2H1.3-A3A cell line was obtained after lentiviral transduction of A3A into HepG2H1.3 cells[138] and selection using 5µg/ml blasticidin. HepaRG cells were transfected with episomal replicon

construct pEpi-H1.3 using 'Lipofectiamine 2000 Reagent' (Invitrogen, Darmstadt, Germany). pEpi-H1.3 was derived by cloning a 1.3-fold overlength HBV genome into extrachromosomal mammalian replicon pEpi-eGFP (kindly provided by H.J. Lipps, Witten-Herdecke, Germany). Two days after transfection, selection with 600 µg / ml geneticin was started and kept until cells expressed GFP and reached confluency and expressed GFP. HepaRG + pEpi-H1.3 cells were differentiated for 6 weeks to allow replication of HBV and establishment of HBV cccDNA by nuclear reimport of HBV rcDNA containing capsids. Lamivudin and Entecavir were used at 0.5 µM (5-fold and 1000-fold IC50, respectively), IFN-a (Roferon-A, Roche) at 1000 U/ml and BS1, CBE11 and hu-IgG at 0.5 µg/ml unless otherwise indicated.

2.2.7. Deep sequencing

Target genes were amplified from total DNA by PCR using primers designed to span around 2000bp of genomic sequence containing at least one exon and one intron. PCR reaction was performed with the Advantage®-HF2 PCR-kit (Clontech). Subsequently, amplicons were separated by a 0.8% agarose gel and purified using the S.N.A.P.TM UV-free gel purification kit (Life Technologies). Purified amplicons were submitted for deep sequencing to a commercial provider (GATC Biotech, Konstanz, Germany) and analyzed using Hiseq2000 sequencing system (Illumina, San Diego, CA, USA). Sequencing data were analyzed with CLC Genomics Workbench 6.01 (CLC bio, Aarhus, Denmark).

2.2.8. Immunofluorescence microscopy

Cells grown on 4-well-glass slide (Lab-Tek II, Fisher Scientific - Germany, Schwerte, Germany) were fixed with 4% paraformaldehyde (PFA) in PBS pH 7.4 for 10 min at room temperature and permeabilized with 0.5% saponin. Slides were blocked in PBS containing 0.5% saponin and 10% serum from the species that the secondary antibody was raised in at room temperature for two hours. After blocking, primary antibodies diluted in PBS with 0.1% saponin and 10% blocking serum were added overnight at 4°C. After extensive washing, slides were incubated with the secondary antibody in PBS with 0.1% saponin and 2% blocking serum for 2 hours at room temperature in the dark. Slides were mounted with Dapi Fluoromount-G (SouthernBiotech, Birmingham, Alabama, USA) and images were captured with a Olympus FV10i confocal Microscope (Olympus, Germany).

2.2.9. Expression profile analyses

Total RNA was amplified and labeled using WT Expression Kit (Ambion, Life Technologies) and Terminal labeling Kit (Affymetrix, Santa Clara, CA, USA) according to the manufacturer's recommendations. The amplified and fragmented, biotinylated complementary RNA was hybridized to Affymetrix Human Gene 1.0 ST Arrays (33297 probe sets) using standard procedures. The

experimental setup contained a total of 8 arrays, made up of 2 groups, with each group consisting of 4 biological replicates. Arrays were assessed for quality and robust multiarray average (RMA)-normalized. Quality assessment consisted of RNA degradation plots, Affymetrix quality control metrics, sample cross-correlation, and probe-level visualizations.

Normalization included (separately for each RNA-type data set) background correction, quantile normalization, and probe-level summation by RMA. Data were analyzed for differential gene expression using an empirical Bayes moderated t-test (52), implemented in the Bioconductor package Linear Models for Microarray Data LIMMA. Results were sorted by the adjusted pvalue and exported in tab-delimited format. Samples with an up- or downregulation ≥ 2 were reanalyzed by qRT-PCR. Microarray data have been submitted to the GEO database (http://www.ncbi.nlm.nih.gov/geo/) and have the accession number GSE46667.

2.2.10. HBV-transgenic mice and tissue analysis

6 months old, male hepatitis B virus transgenic mice (C57BL/6, strain HBV1.3.32) (59) received murine lymphotoxin-receptor agonizing (ACH6) or isotype control antibodies intra-peritoneally (2 mg/kg, body weight) three times a week. Animals were maintained under specified pathogenfree conditions. Experiments were performed in accordance to the German legislation governing animal studies and the Principles of Laboratory Animal Care guidelines, NIH (55.1-1-54-2531.3- 27-08). Mice were sacrificed at indicated time points and serum as well as liver tissues were obtained. Murine livers were fixed in phosphate buffered saline containing 4% PFA for 24 hours. Fixed liver specimens were embedded in paraffin and 2 µm sections were mounted on glass slides.

Fresh murine liver tissue was homogenized mechanically and lysed in buffer (Tris-HCL [10mM], NaCl [100mM], EDTA [5mM], Triton-X100 [5%]) containing protease inhibitor (Roche Diagnostics). Lysates (30 µg/ lane) were subjected to 15% SDS-PAGE (Bio-Rad, München, Germany) and blotted on nitrocellulose membranes (Bio-Rad) for Western blot analyses. Northern blot analyses were performed with total RNA isolated from cryopreserved liver tissue using TIRZOL® (Invitrogen).

2.2.11. Human chimeric uPA/SCID mice

Human liver-chimeric UPA/SCID mice were generated by transplanting one million thawed primary human hepatocytes and housed under specific pathogen-free conditions in accordance with protocols approved by the Ethical Committee of the city and state of Hamburg (permission number G12/015.[139] Levels of human chimerism were determined by measuring human serum albumin (HSA) in mouse serum (Human Albumin ELISA kit, Immunology Consultants Lab, Portland, USA) (61). HBV-infected mice received human lymphotoxin-receptor agonizing (CBE11) or isotype control antibodies

intra-peritoneally (2mg/kg, body weight) once per week after macrophage depletion using clodronate liposomes (http://clodronateliposomes.org). Liver specimens collected at sacrifice were snap-frozen in 2-methylbutane for molecular analyses.

2.2.12. Flow Cytometry

Six-color staining was conducted using combinations of the following mAbs: F4/80 (Serotec), CD11b (eBioscience), CD45, Ly6G, CD19, CD8, CD4 (all BD). Flow cytometric analysis was performed on a FACS-Canto II (BD). Absolute cell numbers were determined by adding 2x104 Calibrite APC beads (BD) to each sample before measurement as internal reference standard. Data were analyzed using FlowJo (Tree Star, Ashland, OR, USA).

2.2.13. Measurement of serum ALT (GPT) levels

Fresh serum of HBV-tg1.3 mice was diluted 1:15 in PBS and 32µl were loaded onto a Reflotron® GPT-measurement stripe (Roche). Measurements were performed on a Reflotron® Plus blood analysis unit (Roche) according to manufacturer's instructions.

3. Results

3.1. Intrahepatic myeloid-cell aggregates enable local proliferation of CD8+ T cells and successful immunotherapy against chronic viral liver infection

'Introduction', 'Material and Methods', 'Results' and 'Discussion' have been described in the following publication: Huang et al. *Nature Immunology,* **14**, 574–583 (2013)

3.1.1. Authors

Li-Rung Huang, Dirk Wohlleber, **Florian Reisinger**, Craig N Jenne, Ru-Lin Cheng, Zeinab Abdullah, Frank A Schildberg, Margarete Odenthal, Hans-Peter Dienes, Nico van Rooijen, Edgar Schmitt, Natalio Garbi, Michael Croft, Christian Kurts, Paul Kubes, Ulrike Protzer, Mathias Heikenwalder & Percy A Knolle

3.1.2. Summary

Chronic infection is difficult to overcome because of exhaustion or depletion of cytotoxic effector CD8+ T cells (cytotoxic T lymphoytes (CTLs)). Here we report that signaling via Toll-like receptors (TLRs) induced intrahepatic aggregates of myeloid cells that enabled the population expansion of CTLs (iMATEs: 'intrahepatic myeloid-cell aggregates for T cell population expansion') without causing immunopathology. In the liver, CTL proliferation was restricted to iMATEs that were composed of inflammatory monocyte–derived $CD11b^+$ cells. Signaling via tumor-necrosis factor (TNF) caused iMATE formation that facilitated costimulation dependent on the receptor OX40 for expansion of the CTL population. The iMATEs arose during acute viral infection but were absent during chronic viral infection, yet they were still induced by TLR signaling. Such hepatic expansion of the CTL population controlled chronic viral infection of the liver after vaccination with DNA. Thus, iMATEs are dynamic structures that overcome regulatory cues that limit the population expansion of CTLs during chronic infection and can be used in new therapeutic vaccination strategies.

3.1.3. Introduction

The liver has unique immunological functions that are determined by its particular microenvironment and its organ-resident antigen-presenting cells[1,2]. Because of this distinct regulation of T cell responses, the liver is considered a lymphoid organ[3]. Although the immune system can clear liver

infections, hepatotropic pathogens such as hepatitis B virus (HBV), hepatitis C virus or malaria parasites can persist and establish chronic infections, which affect hundreds of millions of people worldwide[4]. Mechanisms that limit the function and population expansion of cytotoxic $CD8^+$ T cells (cytotoxic T lymphocytes (CTLs)) in the liver include expression of the inhibitory molecules PD-L1 and galectin-9 or of arginase, which metabolizes amino acids required for the proliferation of CTLs, or the release of immunoregulatory cytokines such as interleukin 10 (IL-10) and transforming growth factor-β[4]. Such regulatory cues limit CTL function, which may protect the infected liver from overwhelming immunopathology by inducing oscillatory CTL effector function[5] but may also functionally compromise pathogen-specific CTLs[6,7]. However, large numbers of parasite-specific CTLs can eradicate infected hepatocytes[8,9], which indicates that large numbers of CTLs are needed to find and eliminate infected hepatocytes in the extensive maze of liver sinusoids. At present, no convincing immunotherapy exists for the treatment of chronic viral infection of the liver.

The generation of sufficient numbers of CTLs for defense against pathogens is regulated by the extent of antigen presentation in secondary lymphatic tissue by appropriately matured dendritic cells (DCs)[9,10]. CTLs may also proliferate in infected tissues after major histocompatibility complex (MHC) class I–restricted activation through the T cell antigen receptor[11], but local regulatory cues in the liver limit or even prevent such local proliferation. Tertiary lymphatic tissue generated during chronic inflammation is reported to increase CTL numbers in chronically inflamed tissue and augment immunity during infection of the lungs with influenza virus[12–14]. The relevance of tertiary lymphatic tissue for chronic infection of the liver is unclear. However, in hepatic granulomas formed after infection with mycobacteria, macrophage–T cell interactions, which lead to local antigen presentation in granulomas, trigger CTL effector function[15,16].

Here we report that induction of intrahepatic myeloid cell aggregates after signaling via Toll-like receptor 9 (TLR9) enabled massive expansion of the CTL population locally in the liver. Those myeloid-cell aggregates rapidly formed within 2 d after TLR9 signaling and provided a nonperfused cocoon-like anatomic structure for local proliferation of CTLs dependent on the T cell–costimulatory receptor OX40. Such population expansion of CTLs in the liver controlled acute and chronic viral infection of the liver and eradicated chronic viral infection.

3.1.4. Results

3.1.4.1. TLR9 signaling leads to population expansion of CTLs in the liver

In the liver, many layers of inhibitory mechanisms prevent the local population expansion and execution of effector functions of CTLs[4]. By adoptive transfer of CTLs, we studied which beneficial factors influence the CTLs or the microenvironment to achieve hepatic proliferation of CTLs. Through the use of antibody-coated microbeads as artificial antigen-presenting particles, we discovered that activation of CTLs by combined stimulation *in vitro* with antibody to the invariant signaling protein of the T cell receptor CD3 (anti-CD3) and antibody to the coreceptor CD28 (anti-CD28) together with IL-12 resulted in better *in vivo* survival of CTLs in the spleen and liver than did stimulation with antibody alone (data not shown). Costimulation with IL-12 improves CTL survival and promotes the differentiation of CTLs into effector and memory T cells[17–19]. Other stimulatory signals such as type I interferon (IFN-α/β), IFN-γ or retinoic acid together with transforming growth factor-β did not augment CTL numbers in the liver (data not shown).

We next investigated whether hepatic inflammation resulted in more proliferation of CTLs. We activated CD90.1$^+$ CTLs *in vitro* with anti-CD3, anti-CD28 and IL-12 and transferred the cells into CD90.2$^+$ host mice, then challenged the recipient mice by intravenous injection of TLR ligands. We found no greater abundance of CTLs in the liver or lungs but found fewer CTLs in the spleen at 4 h after injection of TLR9 ligand (**Fig. 1a**). At day 4 after challenge with TLR9 ligand, we found no greater abundance of splenic CTLs but over 20-fold more hepatic CTLs in mice treated with TLR9 ligand than in mice injected with a non–TLR9-binding control oligonucleotide (**Fig. 1b**). Challenge with a TLR4 ligand also elicited hepatic proliferation of CTLs, but TLR3 ligand or TLR7 ligand had little or no effect (data not shown). Dose-titration studies showed that a single application of TLR9 ligand sufficed for hepatic population expansion of CTLs but did not cause substantial liver damage (data not shown). The TLR9 ligand acted on recipient cells but not on transferred CTLs, as shown by the lack of proliferation of CTLs in *Tlr9*$^{-/-}$ mice (**Fig. 1c**); this also demonstrated the specificity of the TLR9 ligand used. These results suggested that TLR9 signaling caused changes in the liver that supported the hepatic proliferation of CTLs.

TLR9-induced proliferation of CTLs, as determined by expression of the proliferation marker Ki67, was most prominent in the liver and lungs (**Fig. 1d**), a result we confirmed by dilution of the cytosolic dye CFSE in CTLs (data not shown). Also, endogenous CTLs underwent proliferation in the liver after injection of TLR9 ligand (data not shown), which raised the question of whether naive or memory CD8+ T cells had proliferated. We sorted splenic naive CD44^{lo}KLRG1$^-$CD8$^+$ T cells or memory CD44^{hi}KLRG1$^-$CD127$^+$CD8$^+$ T cells by flow cytometry from CD45.1$^+$ mice and then adoptively

transferred those cells into CD45.2$^+$ recipient mice. Intrahepatic transferred naive CD8$^+$ T cells did not incorporate the thymidine analog BrdU, and we detected only low absolute numbers of T cells (data not shown). Transferred memory T cells present in the liver, however, incorporated BrdU after challenge with TLR9 ligand, which led to sevenfold more cells, but we detected lower absolute numbers of cells than after transfer of *in vitro*–activated CTLs (data not shown). The greater abundance of hepatic CTLs resulted from local proliferation but not from recirculation after activation in the spleen, as CTLs also proliferated in the liver after splenectomy (**Fig. 1e**).

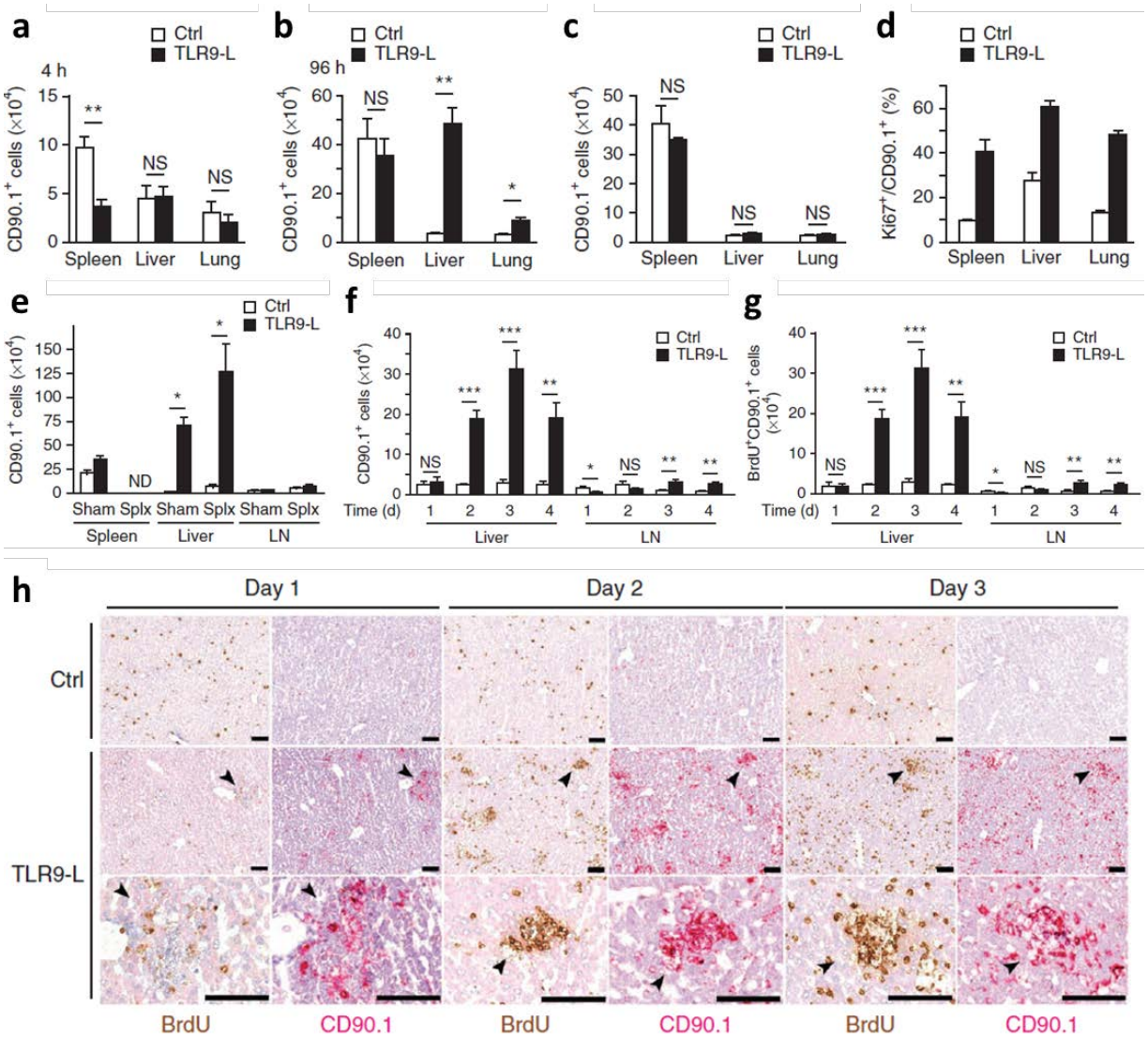

Figure 1: Injection of TLR9 ligand results in more IL-12-treated CTLs in the liver. (a,b) Quantification of CD90.1$^+$ CTLs 4 h (a) or 96 h (b) after transfer of CD90.1$^+$ CTLs (2 × 10^6), stimulated with anti-CD3, anti-CD28 and IL-12, into CD90.2$^+$ recipient mice (*n* = 3 per group) injected with non–TLR9-binding control oligonucleotide (Ctrl) or TLR9 ligand (TLR9-L). (c) Quantification of CD90.1$^+$ CTLs 96 h after transfer of CTLs into *Tlr9*$^{-/-}$ recipient mice (*n* = 3 per group) treated as in a,b. (d) Frequency of Ki67$^+$ cells among CD90.1$^+$ CTLs at day 3 after transfer and treatment as in a,b (*n* = 3 mice per group). (e) Quantification of CTLs in recipient mice (*n* = 3 per group) given sham surgery (Sham) or a splenectomy (Splx), assessed on day 3 after transfer and treatment as in a,b. ND, not detected; LN, lymph nodes. (f,g) Quantification of transferred CTLs (f) and BrdU incorporation by CTLs (g) in recipient mice (*n* = 3 per group) given splenectomy and treatment with FTY720, as well as BrdU in the drinking water, assessed on day 1, 2, 3 or 4 after adoptive transfer and treatment with the control oligonucleotide or TLR9 ligand. (h) Immunohistochemical analysis of BrdU or CD90.1 in consecutive liver sections from the mice in f,g. Arrowheads indicate the same position in consecutive sections. Scale bars, 100 μm. NS, not significant; **P* < 0.05, ***P* < 0.01 and ****P* < 0.001 (unpaired Student's *t*-test). Data are representative of two independent experiments (error bars (a–g), s.d.).

We obtained further evidence of hepatic expansion of the CTL population independently of lymphatic tissue by removing spleens from mice and treating the mice with the sphingosine 1-phosphate antagonist FTY720, which prevents egress of lymphocytes from the lymph nodes. As expected, treatment with FTY720 resulted in fewer endogenous CTLs in the liver and spleen (data not shown). We transferred CD90.1$^+$ CTLs into mice treated as described above (splenectomy plus FTY720) and found that the transferred cells increased in number in the livers and incorporated BrdU after challenge with TLR9 ligand (**Fig. 1f**,**g**), consistent with hepatic proliferation of CTLs rather than relocation from lymphatic tissue. Furthermore, BrdU$^+$CD90.1$^+$ CTLs accumulated in the liver in mice treated with TLR9 ligand (**Fig. 1h**). Notably, BrdU$^+$CD90.1$^+$ CTLs accumulated in certain areas in the liver, which raised the question of whether the proliferation of CTLs was related to their local clustering in the liver after challenge with TLR9 ligand.

3.1.4.2. Clustering of CD11b$^+$ cells promotes hepatic proliferation of CTLs

The lack of TLR9-induced hepatic proliferation of CTLs in *Tlr9*$^{-/-}$ mice indicated that recipient cells but not CTLs were the target of the TLR9 ligand. Depletion of phagocytic cells in mice completely abrogated the hepatic proliferation of CTLs but led to more CTLs in the lungs (**Fig. 2a**). This finding indicated that the CTL proliferation in the lung was independent of phagocytes and may have occurred in a compensatory way in the absence of phagocyte-dependent proliferation of CTLs in the liver.

Immunohistochemistry showed the presence of CD11b$^+$, MHC class II–positive (MHCII$^+$) and CCR2$^+$ cells after challenge with TLR9 ligand; these cells formed intrahepatic aggregates throughout the hepatic parenchyma (**Fig. 2b**). We observed aggregates formed by CD11b$^+$ cells only in mice treated with TLR9 ligand or TLR4 ligand, associated with hepatic proliferation of CTLs, but did not find such aggregates in mice treated with TLR3 ligand or TLR7 ligand (**Fig. S2a**). Those aggregates were not separated from the surrounding liver tissue by collagen IV or by cells that expressed platelet-derived growth-factor receptor-β or smooth muscle actin, but we did detect expression of gp38, a marker of stromal cells, on CD11b$^+$MHCII$^+$ cells in the aggregates (**Fig. 2c** and data not shown). These results demonstrated a fundamental difference between hepatic aggregates of CD11b$^+$MHCII$^+$ cells generated by TLR9 ligand and the tertiary lymphoid structures formed during chronic inflammation[20,21]. Pursuant to that, we found no role for signaling via the lymphotoxin-β receptor (LTβR) in the TLR9 ligand–mediated proliferation of CTLs (**Fig. S2b**).

We depleted CCR2-CFP-DTR mice (which have transgenic expression of a cyan fluorescent protein (CFP) reporter fused to the diphtheria toxin receptor (DTR) under the control of the promoter of the gene encoding the chemokine receptor CCR2) of CCR2$^+$ cells by injecting them with diphtheria toxin

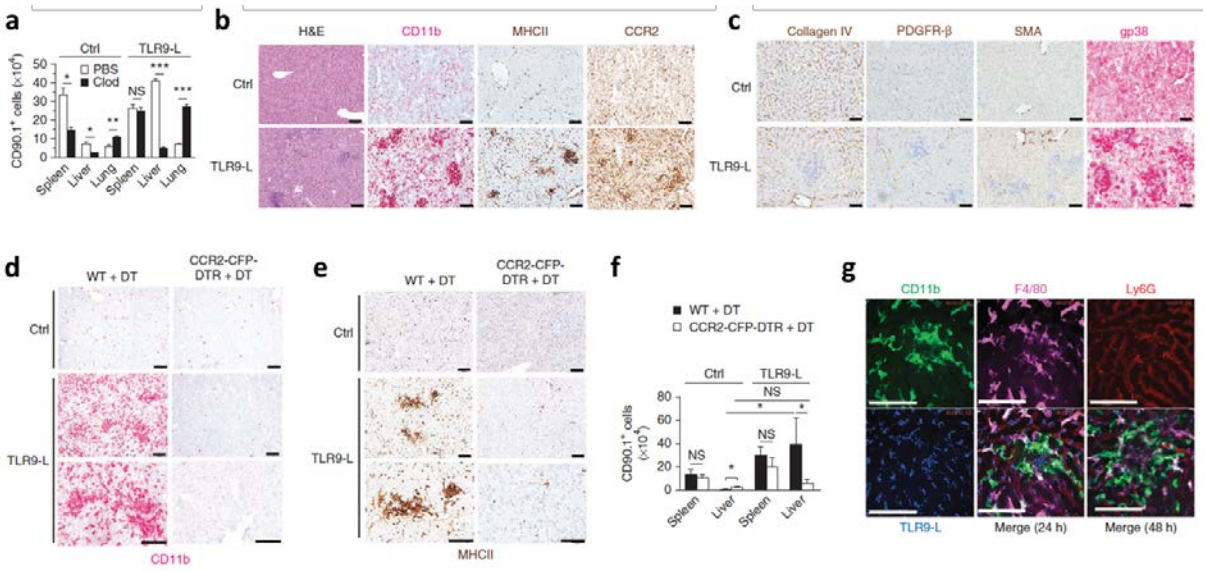

Figure 2: Characterization of iMATEs in the liver after injection of TLR9 ligand. (a) Quantification of CD90.1$^+$ CTLs after adoptive transfer into mice (*n* = 4 per group) treated with PBS or clodronate liposomes (Clod; for depletion of phagocytes), assessed at day 3 after challenge with TLR9 ligand or non–TLR9-binding control oligonucleotide. (b) Hematoxylin-and-eosin staining (far left) and immunohistochemical analysis of CD11b, MHC class II or CCR2 in liver tissue at day 3 after challenge with TLR9 ligand or the control oligonucleotide. (c) Immunohistochemical analysis of collagen IV, platelet-derived growth-factor receptor-β (PDGFR-β), smooth muscle actin (SMA) and gp38 in liver tissue at day 3 after challenge as in b. (d,e) Immunohistochemical analysis of CD11b (d) or MHC class II (e) in liver tissues from wild-type (WT) and CCR2-CFP-DTR mice treated with diphtheria toxin (+ DT), assessed at day 4 after challenge as in b. (f) Quantification of CD90.1$^+$ CTLs after transfer into wild-type or CCR2-CFP-DTR mice (*n* = 3 per group) treated with diphtheria toxin, assessed at day 4 after challenge as in b. (g) Images of intravital spinning-disc confocal microscopy of liver tissues obtained from mice 24 h or 48 h after injection of indodicarbocyanine-labeled TLR9 ligand and fluorochrome-labeled antibodies. Scale bars, 100 μm. **P* < 0.05, ***P* < 0.01 and ****P* < 0.001 (unpaired Student's *t*-test). Data are representative of two independent experiments (error bars (a,f), s.d.)

and found that aggregates of CD11b$^+$MHCII$^+$ cells did not form, which coincided with the loss of population expansion of CTLs (**Fig. 2d–f**). That observation led us to call this structure 'iMATE' ('intrahepatic myeloid-cell aggregate for T cell population expansion'). We found that iMATEs developed in a dynamic way after treatment with TLR9 ligand and gradually disappeared by day 8 (**Fig. S2c**,**d**). There was little liver damage associated with the formation of iMATEs, as evaluated by cleavage of caspase-3 (Supplementary Fig. 2e) and slightly higher serum concentrations of alanine aminotransferase (ALT). We found few infiltrating natural killer (NK) cells or B cells in iMATEs (**Fig. S2f**). Instead, cells in iMATEs stained with antibody to the marker Gr-1 (**Fig. S2f**), which identifies inflammatory monocytes (Ly6C) and neutrophils (Ly6G).

Anti-Ly6G-mediated depletion of neutrophils did not affect the hepatic proliferation of CTLs (**Fig. S2g**) which excluded the possibility of a prominent role for neutrophils in this. We depleted mice of CD11b$^+$ neutrophils and treated them with TLR9 ligand, then used intravital time-lapse spinning-disc microscopy to characterize the role of CD11b$^+$ monocytes in iMATE formation. Circulating CD11b$^+$F4/80$^-$ monocytes did not adhere to sinusoids immediately after treatment with TLR9 ligand, but 4 h later, some CD11b$^+$F4/80$^-$ monocytes adhered without affecting sinusoidal perfusion.

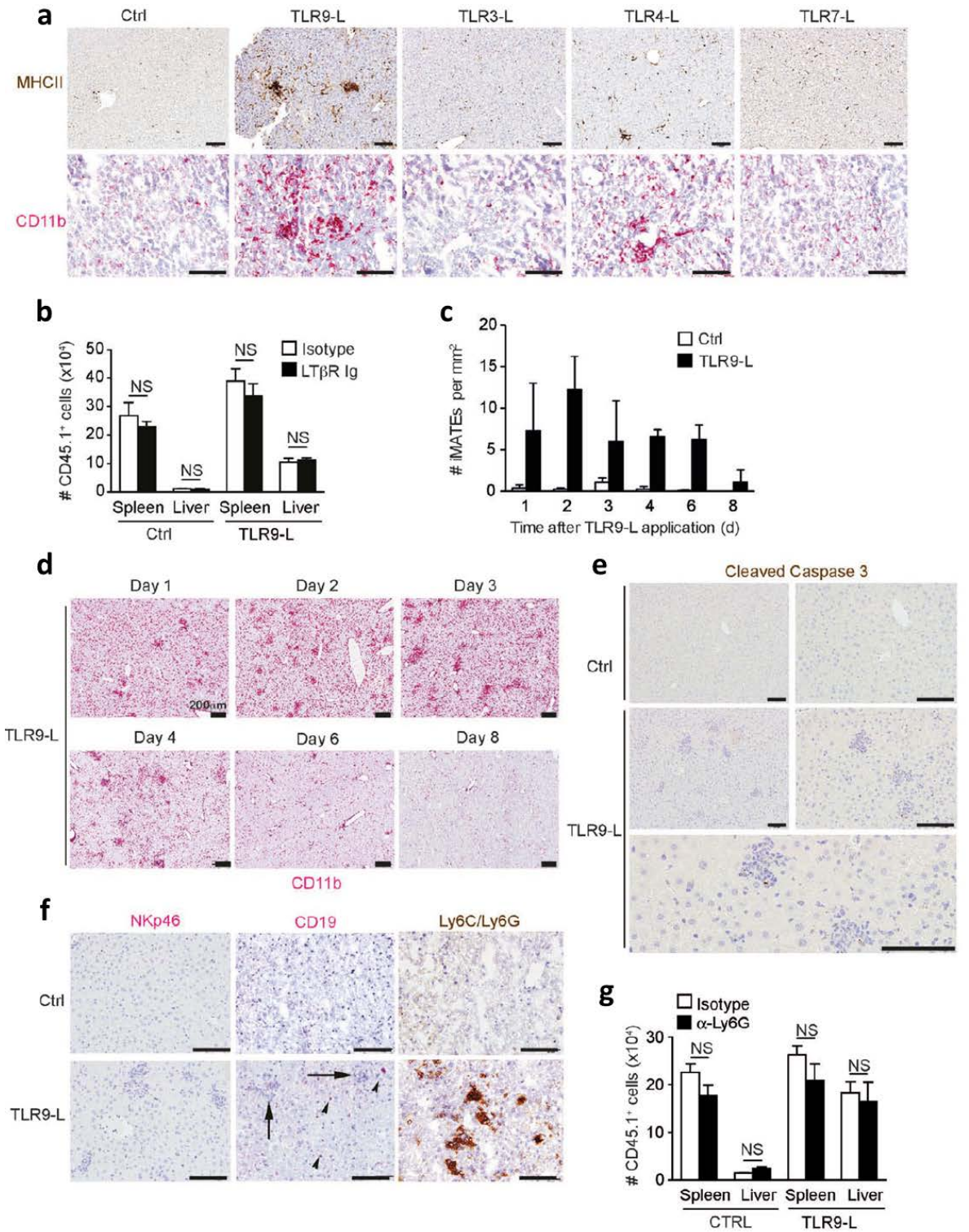

Figure S2: Characteristics of iMATEs. (a) Immunohistochemistry for MHCII and CD11b in the liver at d3 after application of TLR agonists. (b) Number of CD45.1$^+$ CTLs in different organs of TLR9-L-treated mice at d3 after daily application of LTbR-Ig (100µg per mouse i.p.) or control isotype Ig. (c) Quantification of the numbers of iMATEs at indicated time points after TLR9-L treatment (n=3 per group per time point). (d) Immunohistochemistry for CD11b in the liver at indicated time points after TLR9-L treatment. (e) Staining for cleaved caspase 3 in liver tissue of mice at d3 after TLR9-L challenge. (f) Immunohistochemistry for NKp46, CD19 or LY6C + Ly6G (Gr-1) in liver tissue at d3 after TLR9-L challenge. Arrows indicate iMATE and arrowhead point out CD19+ cells. (g) Number of CD45.1$^+$ CTLs in spleen or liver of TLR9-L-treated mice at d3 after daily application of anti-Ly6G Ig (1A8) or isotype Ig (2A3) (d-1-d2; 100µg per mouse i.v.) (n=3 per group). Scale bar, 100µm. NS, not significant. *P<0.05, **P<0.01, ***P<0.001 (unpaired Student's t-test). Data are representative of two independent experiments with 3 mice per group. (b,c,g; error bars, s.d.)

At 24 h and 48 h after treatment with TLR9 ligand, CD11b$^+$ monocytes with low to undetectable expression of F4/80 clustered in sinusoids (**Fig. 2g)**. These results suggested that iMATEs arose from inflammatory monocytes, but not Kupffer cells, that adhered to sinusoidal cells and thereby formed a non-perfused anatomical structure distinct from lymphatic tissue in which T cell proliferation occurred.

3.1.4.3. Hepatic CTL proliferation is restricted to iMATEs

After activation *in vitro* with anti-CD3, anti-CD28 and IL-12, CD45.1$^+$ CTLs or CTLs with transgenic expression of green fluorescent protein (GFP) localized together with CD11b$^+$MHCII$^+$ cells in iMATEs (**Fig. 3a**); this colocalization was constant (**Fig. 3b**) and independent of the proliferation of CTLs in the spleen or lymph nodes (**Fig. S3a**). BrdU incorporation was greater in CTLs isolated from the liver than in those isolated from lymph nodes, and it continuously increased from day 1 to day 3 (**Fig. S3b**). This suggested local proliferation of CTLs in iMATEs. Proliferating Ki67$^+$ CTLs were located in iMATEs but not elsewhere in parenchymal liver tissue, as shown by immunohistochemistry of serial liver sections (**Fig. 3c**). Quantification showed over 200-fold more Ki67$^+$ CTLs in iMATEs than in the remaining liver tissue (**Fig. 3d**).

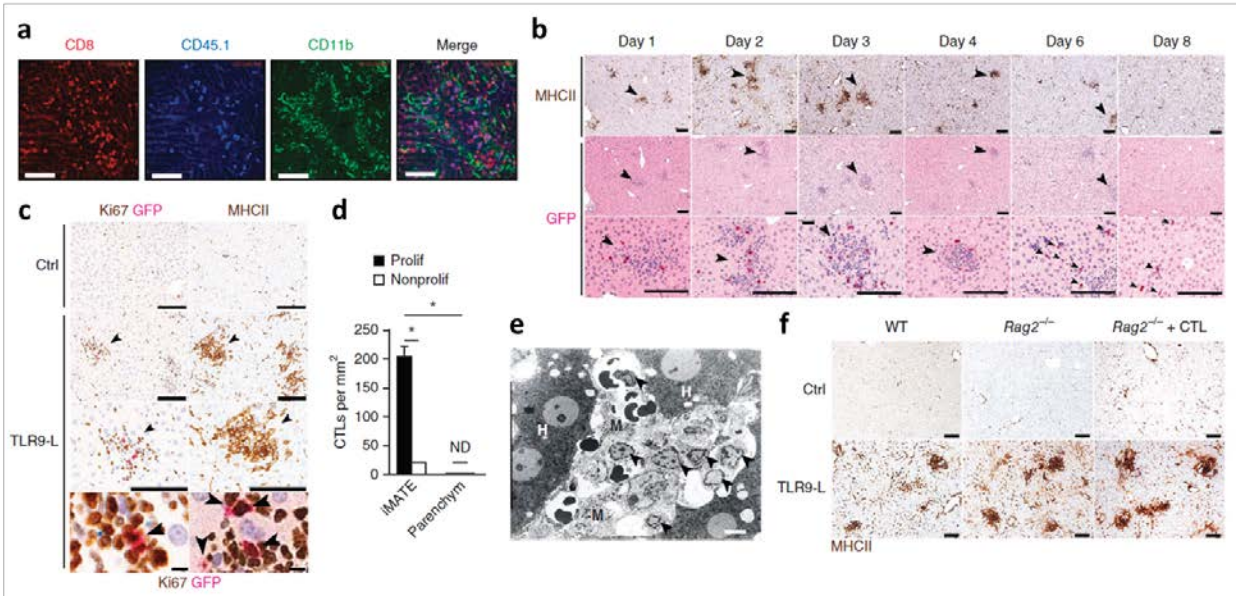

Figure 3: CTL proliferation in iMATEs. (a) Images of intravital spinning-disc confocal microscopy of an iMATE at day 3 after transfer of CD45.1$^+$ CTLs and treatment with TLR9 ligand; samples were costained for CD11b$^+$ cells (green), CD45.1$^+$ CTLs (blue) and total CD8$^+$ T cells (red). (b) Immunohistochemical analysis of MHC class II or GFP in consecutive liver sections obtained on days 1–8 (time, above images) after transfer of GFP+ CTLs (3×10^6) and treatment with TLR9 ligand. Large arrowheads indicate the same iMATE in consecutive sections; small arrowheads indicate single CTLs outside iMATEs. (c) Costaining for GFP, Ki67 and MHC class II in consecutive liver sections at day 3 after treatment with TLR9 ligand or non–TLR9-binding control oligonucleotide. Arrowheads indicate the same position in consecutive sections (middle two rows) or dividing GFP$^+$ CTLs (bottom row). (d) Quantification of proliferating (Prolif; Ki67$^+$) and nonproliferating (Nonprolif; Ki67−) transferred GFP$^+$ CTLs at day 3 after injection of TLR9 ligand, presented as cells per mm2 liver tissue. **P* < 0.01 (unpaired Student's *t*-test). (e) Ultrastructural analysis of iMATEs by electron microscopy at day 3 after treatment with TLR9 ligand, showing CTLs (arrowheads) interacting with myeloid cells (M) in the vicinity of hepatocytes (H). (f) Immunohistochemical analysis of MHC class II in liver tissue at day 3 after injection of TLR9 ligand or control oligonucleotide, with (right) or without (left and middle) CTLs, into wild-type mice and mice deficient in recombination-activating gene 2 (*Rag2*$^{-/-}$).

We observed three distinct iMATE structures: a condensed form with either few proliferating CTLs or many proliferating CTLs; a dispersed form with many proliferating CTLs; and a diffuse form with few Ki67$^+$ CTLs (data not shown). Three-dimensional reconstruction of serial sections recapitulated the distinct forms of iMATEs (data not shown), which allowed us to quantify the mean volume of iMATEs (73,851 µm3 ± 50,184 µm3) and number of CTLs per iMATE (94.4 ± 15). Ultrastructural analysis showed that monocyte-derived cells closely interacted with CTLs in iMATEs that were not demarcated from surrounding hepatocytes (**Fig. 3e**). The formation of iMATEs did not require cross-talk between myeloid cells and lymphocytes, as injection of TLR9 ligand into mice deficient in recombination-activating gene 2, which lack B cells and T cells, was sufficient to induce iMATEs, and this was not further improved by the transfer of additional CTLs (**Fig. 3f**). Thus, iMATE formation was triggered by inflammatory signals and did not require the presence of lymphocytes.

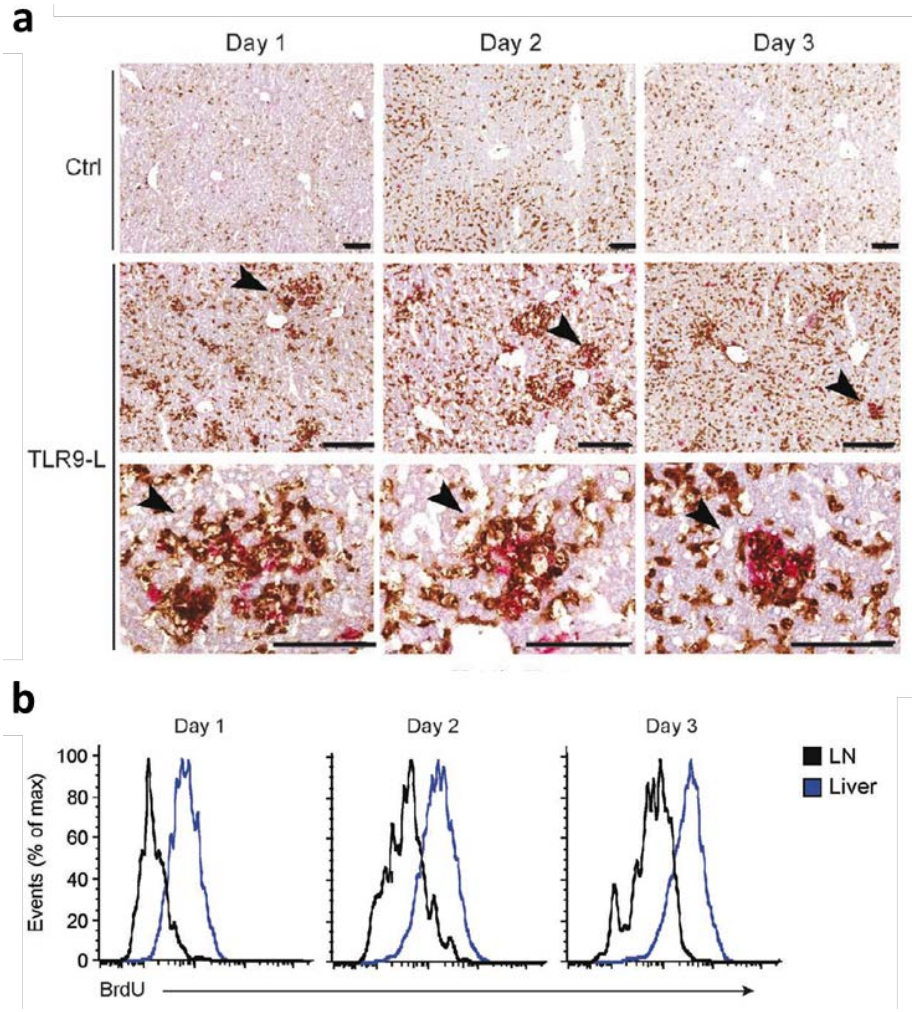

Figure S3: Preferential CTL expansion in iMATEs. (a) Immunohistochemistry for CD11b and CD90.1 in the liver of splenectomized FTY720-treated mice at indicated time points after transfer of CD90.1$^+$ CTLs and TLR9-L challenge. Mice received BrdU in drinking water (0.8 mg/ml) during the entire time of the experiment (n=3 per group per time point). Arrowheads indicate iMATEs. (b) BrdU-incorporation in transferred CD90.1$^+$ cells from liver or lymph node (LN) of TLR9-L-treated mice as described in (a). Data are representative of two independent experiments with 3 mice per group. Scale bar, 100µm.

3.1.4.4. Phenotype of myeloid cells in iMATEs

The results reported above raised the issue of how $CD11b^+$ cells (neutrophils, NK cells, Kupffer cells, monocytes and macrophages or DCs) facilitate the hepatic proliferation of CTLs. As neither neutrophils nor NK cells were present in iMATEs, we analyzed hepatic $NKp46^-Ly6G^-CD11b^+$ cells. Profiling by flow cytometry showed more $F4/80^{hi}$ Kupffer cells or $F4/80^-CD11b^+$ cells in mice treated with TLR9 ligand than in mice treated with the control (non-TLR9) ligand, whereas the number of $CD11b^+$ non-Kupffer cells that were $F4/80^+$ paralleled the hepatic proliferation of CTLs (**Fig. 1f**); this prompted us to investigate the role of inflammatory monocytes and DCs in the hepatic proliferation of CTLs[22]. Those $NKp46^-Ly6G^-CD11b^+F4/80^+$ cells were distinct from $F4/80^{hi}$ Kupffer cells, as assessed by Ly6C expression (data not shown). We categorized them into two main populations on the basis of their Ly6C expression in combination with expression of MHC class II or the common DC marker CD11c (data not shown); this defined $Ly6C^{hi}$ inflammatory monocytes that were $MHCII^-$ with low CD11c expression, and $MHCII^+$ cells with lower Ly6C expression and intermediate CD11c expression. After treatment with TLR9 ligand, there was a rapid increase in $Ly6C^{hi}MHCII^-$ inflammatory monocytes, a transient increase in $Ly6C^{hi}MHCII^+CD11b^+$ cells and a persistent increase in $Ly6C^{dim}MHCII^+CD11b^+$ cells in the liver (**Fig. 4a**). All those $CD11b^+$ cells expressed the macrophage-specific markers Mac-3 and CD64 (**Fig. 4b**), consistent with their monocytic origin. $Ly6C^{dim}MHCII^+$ cells also had CD11c expression, albeit less than that of conventional DCs (**Fig. 4b,c**). Notably, when we depleted CD11c.DOG mice (which have transgenic expression of DTR under control of the promoter of the gene encoding CD11c) of DCs by injection of diphtheria toxin, we found that this did not eliminate those $CD11b^+CD11c^{int}$ cells in the liver and did not affect the hepatic proliferation of CTLs or iMATE formation (data not shown). Thus, monocytes and monocyte-derived inflammatory DCs, but not conventional DCs, were responsible for the hepatic proliferation of CTLs.

After injection of TLR9 ligand into wild-type mice, there was substantial expression of tumor-necrosis factor (TNF) in the liver but not in the spleen (**Fig. 4d**). Analysis of gene expression showed that the $CD11b^+$ cells expressed TNF and inducible nitric oxide synthetase (iNOS; **Fig. 4e**,**f**). We found TNF- and iNOS-expressing cells in iMATEs (**Fig. 4g**, **h**), which indicated a critical role for signaling via the TNF receptor. Indeed, no iMATEs formed in mice doubly deficient in the TNF receptors TNFR1 and TNFR2 (TNFR1-TNFR2–deficient) after treatment with TLR9 ligand (**Fig. 4i**); similarly, the recruitment of inflammatory monocytes and proliferation of $CD11b^+MHCII^+$ cells were impaired in these mice (**Fig. 4j**,**k**). Predictably, there was less hepatic CTL proliferation in TNFR1-TNFR2–deficient mice than in wild-type mice after challenge with TLR9 (**Fig. 4l**). Signaling via the TNF receptor in T cells was not involved, as TNFR1-TNFR2–deficient CTLs proliferated in TNF receptor–sufficient mice after treatment with TLR9 ligand (data not shown). These data demonstrated a critical role for

inflammatory monocytes or inflammatory DCs in the formation of iMATEs and local hepatic proliferation of CTLs after challenge with TLR9 ligand.

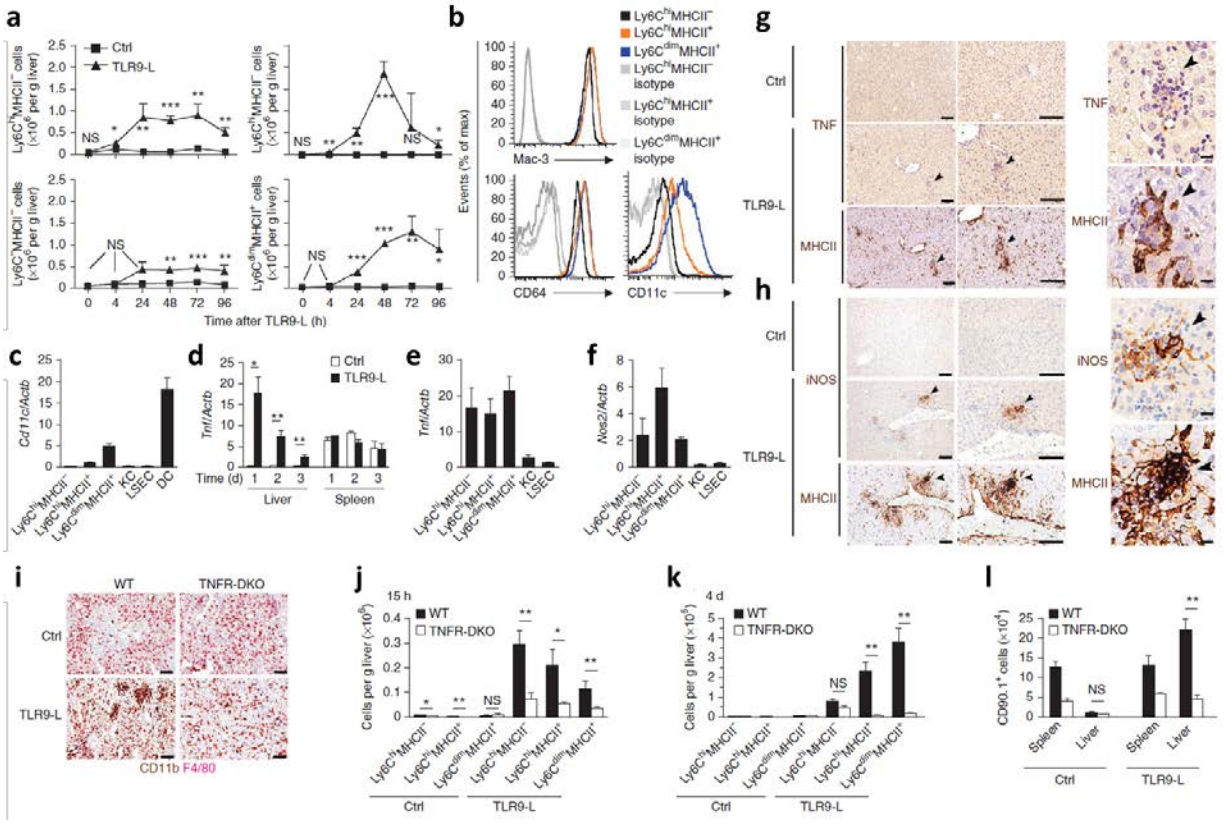

Figure 4: Phenotype of myeloid cells in iMATEs. (a) Kinetics of changes in the abundance of subpopulations of NKp46$^-$Ly6G$^-$F4/80$^+$CD11b$^+$ cells in livers from mice (*n* = 3 per group per time point) treated with TLR9 ligand or non–TLR9-binding control oligonucleotide. (b) Expression of CD64, CD11c and intracellular Mac-3 by subpopulations of NKp46$^-$Ly6G$^-$F4/80$^+$CD11b$^+$ cells, assessed by flow cytometry. Isotype, immunoglobulin isotype–matched control antibody. (c) Quantitative real-time PCR analysis of *Cd11c* in hepatic cell populations (left five bars) or splenic DCs (far right) obtained on day 3 after injection of TLR9 ligand and sorted by flow cytometry; results are presented relative to those of *Actb* (encoding β-actin). KC, Kupffer cell; LSEC, liver sinusoidal endothelial cell. (d) Time course of *Tnf* expression in livers and spleens from mice (*n* = 3 per group) treated with TLR9 ligand or control (as in a); presented as in c. (e,f) Quantitative real-time PCR analysis of *Tnf* (e) and *Nos2* (encoding iNOS; f) in cells as in c (presented as in c). (g,h) Immunohistochemical analysis of TNF and MHC class II (g) or iNOS and MHC class II (h) in consecutive liver sections on day 3 after treatment with TLR9 ligand or control (as in a). Arrowheads indicate the same position in consecutive sections. (i) Immunohistochemical analysis of CD11b and F4/80 in liver tissues from wild-type or TNFR1-TNFR2–deficient (TNFR-DKO) mice on day 3 after treatment with TLR9 ligand or control (as in a). (j,k) Total Ly6C^{hi}MHCII$^-$, Ly6C^{hi}MHCII$^+$ and Ly6C^{dim}MHCII$^+$ cells among NKp46$^-$Ly6G$^-$F4/80$^+$CD11b$^+$ cells in the liver at 15 h (j) or day 4 (k) after treatment of wild-type or TNFR1-TNFR2–deficient mice (*n* = 3 per group) with TLR9 ligand or control (as in a). (l) Quantification of CD90.1$^+$ CTLs from wild-type mice at day 3 after transfer into wild-type or TNFR1-TNFR2–deficient mice treated with TLR9 ligand or control (as in a). Scale bars, 100 μm (g,h, left two columns, and i) or 10 μm (g,h, right column). **P* < 0.05, ***P* < 0.01 and ****P* < 0.001 (unpaired Student's *t*-test). Data are representative of two independent experiments (error bars (a,c–f,j–l), s.d.).

3.1.4.5. Functional characterization of myeloid cells in iMATEs

To investigate the relevance of CD11b^{+}MHCII^{+} cells to CTL proliferation, we analyzed Ly6C^{hi}MHCII^{-} inflammatory monocytes and MHCII^{+}CD11b^{+} cells sorted from the liver of wild-type mice after treatment with TLR9 ligand. Only MHCII^{+} inflammatory DCs induced CTL proliferation independently of antigen presentation; inflammatory monocytes or liver sinusoidal endothelial cells did not (**Fig. 5a**). Costimulatory signals are important for the proliferation and survival of T cells[23,24]. Only CD11b^{+}MHCII^{+} cells had higher expression of mRNA encoding the costimulatory molecules CD80, CD86 and OX40L than did MHCII^{-} cells, Kupffer cells or liver sinusoidal endothelial cells (**Fig. 5b–d**). Individual blockade of CD86 or OX40L had some effect on but did not abrogate CTL proliferation (**Fig. 5e**), whereas simultaneous blockade of CD80, CD86 and OX40L led to almost complete inhibition of CTL proliferation (**Fig. 5f**).

CTLs activated i*n vitro* with anti-CD3, anti-CD28 and IL-12 expressed CD28, and approximately 50% of these CTLs expressed OX40 (data not shown), which suggested that costimulation might be relevant for the hepatic expansion of the CTL population *in vivo*. In the liver, OX40L expression was restricted to CD11b+ cells in iMATEs but not in parenchymal liver tissue (**Fig. 5g**).

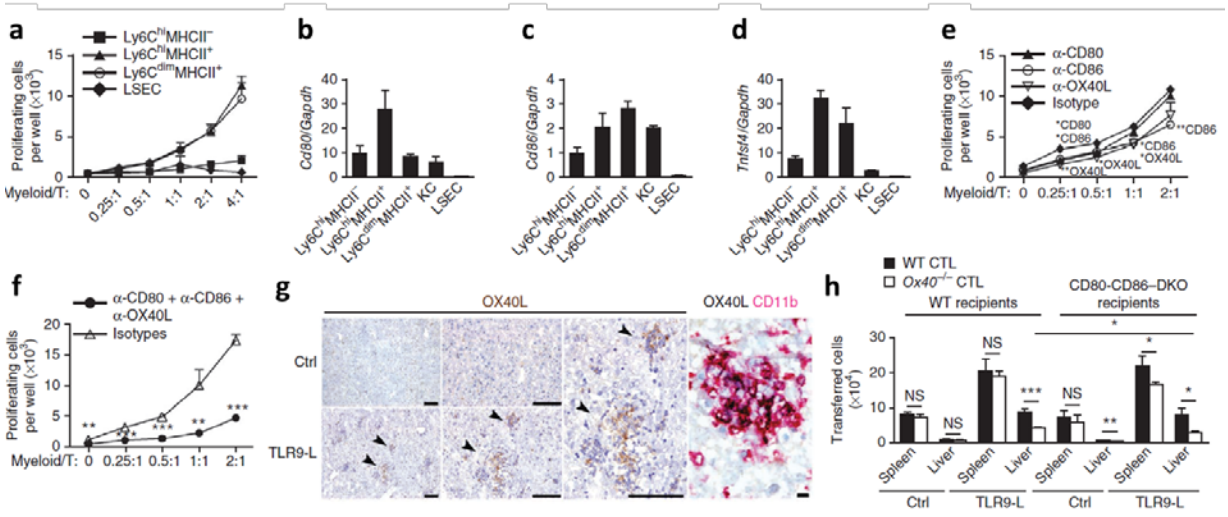

Figure 5: Hepatic myeloid cells support the expansion of the CTL population by providing costimulatory signals. (a) Proliferation of CTLs activated *in vitro* with anti-CD3, anti-CD28 and IL-12 (day 3) and cultured at various ratios (horizontal axis) with flow cytometry–sorted hepatic CD11b^{+} myeloid cell populations or liver sinusoidal endothelial cells isolated at day 3 after treatment with TLR9 ligand, assessed by incorporation of the thymidine analog EdU after 40 h of coculture. (b–d) Expression of *Cd80* mRNA (b), *Cd86* mRNA (c) and *Tnfsf4* mRNA (encoding OX40L; d) in hepatic cell populations isolated at day 3 after treatment with TLR9 ligand and sorted by flow cytometry; results are presented relative to those of the housekeeping gene *Gapdh*. (e,f) Proliferation of CTLs cultured at various ratios (horizontal axis) with flow cytometry–sorted CD11b^{+}F4/80^{+}Ly6C^{dim}MHCII^{+} cells and treated with function-blocking antibody to CD80, CD86 or OX40L, alone (e) or in combination (f), or with isotype-matched control antibody. (g) Immunohistochemical analysis of OX40L and CD11b in liver tissue on day 3 after treatment with TLR9 ligand or non–TLR9-binding control oligonucleotide. Arrowheads indicate iMATEs. Scale bars, 100 µm (left images) or 10 µm (far right). (h) Total transferred CTLs in wild-type or *Cd80*$^{-/-}$*Cd86*$^{-/-}$ (CD80-CD86–DKO) recipients (n = 3 per group) of CFSE-labeled wild-type or *Ox40*$^{-/-}$ CTLs (key), assessed on day 3 after treatment with TLR9 ligand or non–TLR9-binding control oligonucleotide. *P < 0.05, **P < 0.01 and ***P < 0.001 (unpaired Student's t-test). Data are representative of two independent experiments (triplicate assays in a–f; error bars (a–f,h), s.d.).

We transferred CFSE-labeled CD90.1$^+$ wild-type CTLs or CD90.1$^-$ CTLs deficient in OX40 (*Tnfrsf4*$^{-/-}$; called '*Ox40*$^{-/-}$' here) at ratio of 1:1 into recipient mice (data not shown) and monitored their fate in liver and spleen. We found no difference between wild-type and *Ox40*$^{-/-}$ CTLs in the spleens of wild-type mice in terms of CFSE profile or absolute number (**Fig. 5h** and data not shown), which suggested that the transferred *Ox40*$^{-/-}$ CTLs did not have an intrinsic defect in survival or proliferation *in vivo*. Mice treated with TLR9 ligand had over 50% fewer *Ox40*$^{-/-}$ CTLs than wild-type CTLs in the liver (Fig. 5h), although the CFSE-dilution profile of *Ox40*$^{-/-}$ CTLs was identical to that of the wild-type CTLs transferred together with them (data not shown). We found fewer *Ox40*$^{-/-}$ CTLs after transfer into *Cd80*$^{-/-}$*Cd86*$^{-/-}$ mice than after transfer into wild-type mice (**Fig. 5h**), but *Ox40*$^{-/-}$ CTLs again had CFSE-dilution profiles identical to those of wild-type CTLs (data not shown). Thus, OX40-dependent signaling may enhance the survival rather than the proliferation of CTLs. These results identified a crucial role for OX40 in the expansion of the CTL population in the liver and elucidated the molecular mechanism that drove the antigen-independent expansion of the CTL population caused by inflammatory DCs in iMATEs.

3.1.4.6. The iMATEs facilitate CTL-mediated viral clearance

The efficient expansion of the CTL population in the liver raised the question of whether iMATEs improved CTL immunity to viral infection in the liver. We activated ovalbumin (OVA)-specific (OT-I) CD90.1$^+$ CTLs with anti-CD3, anti-CD28 and IL-12 *in vitro* and transferred the cells, along with TLR9 ligand, into wild-type mice that we then infected with a recombinant adenovirus expressing luciferase, GFP and OVA as a fusion protein (AdLGO)[25]. The decrease in bioluminescence *in vivo* allows more sensitive quantification of antiviral CTL activity against infected hepatocytes than does measurement of serum ALT[25]. Neither transfer of OT-I CTLs nor treatment with TLR9 ligand alone resulted in lower *in vivo* bioluminescence in AdLGO-infected mice (**Fig. 6a**). Transfer of OT-I CTLs together with TLR9 ligand, however, controlled the hepatic expression of viral luciferase more rapidly than did either treatment alone (**Fig. 6a**).

Those results led us to investigate whether iMATEs enhanced antigen-specific CTL responses. We infected mice with recombinant adenovirus expressing luciferase and GFP alone (AdLG) or with AdLGO and then transferred activated OT-I CTLs into the infected mice. We found more hepatic OT-I CTLs in AdLG-infected mice after treatment with TLR9 ligand (**Fig. 6b**). However, in AdLGO-infected mice given injection of TLR9 ligand, we found sevenfold more OT-I CTLs; also, without TLR9 ligand, AdLGO-infected mice had more OT-I CTLs than did their AdLG-infected counterparts (Fig. 6b). Notably, after infection with AdLG in absence of TLR9 ligand, we observed iMATEs that did not contain OT-I CTLs, whereas iMATEs in AdLGO-infected mice contained some OT-I CTLs (**Fig. 6c**). These data suggested that viral infection of the liver caused iMATE formation and that iMATEs also

amplified antigen-specific CTL responses locally in the liver. After injection of TLR9 ligand, iMATE generation was improved, and we observed more OT-I CTLs in AdLGO-infected mice than in AdLG-infected or mock-treated mice (**Fig. 6c**); this supported the assumption of more rapid control of viral infection. Notably, we found single OT-I CTLs in the vicinity of iMATEs (**Fig. 6c**), which indicated that the OT-I CTLs executed effector functions against virus-infected hepatocytes after leaving the iMATEs.

To confirm the physiological relevance of iMATEs during viral infection, we investigated iMATE formation during infection with the replication-competent virus lymphocytic choriomeningitis virus (LCMV). During acute infection with LCMV, we observed the formation of iMATEs by $CD11b^{+}MHCII^{+}$ cells, with a peak at day 9 after infection (Fig. 6d), which coincided with the peak expansion of the CTL population. $CD8^{+}$ T cells were abundant in iMATEs during acute infection with LCMV (data not shown), which suggested that iMATEs contributed to the CTL defense against LCMV infection. Prevention of iMATE formation in CCR2-CFP-DTR mice led to less generation of H-2Db-restricted CTLs specific for LCMV glycoprotein (amino acids 33–41 (gp33); **Fig. 6e**) and failure to control LCMV replication (data not shown). This may indicate a role for iMATEs in LCMV-specific CTL immunity, although we cannot exclude the possibility that systemic depletion of $CCR2^{+}$ cells additionally influences immunity to LCMV. Those results prompted us to investigate whether iMATEs were absent from mice with chronic LCMV infection. Indeed, we observed no iMATEs in the livers of mice with chronic LCMV infection (**Fig. 6f**), but iMATEs were induced by treatment with TLR9 ligand (**Fig. 6f**), which suggested that iMATEs may be used to overcome T cell exhaustion during chronic viral infection. To test that hypothesis, we adoptively transferred in vivo–primed LCMV-specific splenic CTLs (isolated from mice with acute LCMV infection), together with TLR9 ligand or control ligand, on days 0, 7 and 10, into mice with chronic LCMV infection. Transfer of LCMV-specific CTLs or TLR9 ligand alone did not result in a greater abundance of gp33-specific CTLs; however, transfer of LCMV-specific CTLs together with TLR9 ligand did result in a greater abundance of gp33-specific CTLs in the liver at day 14 after the first transfer (**Fig. 6g**). More notably, LCMV titers in serum and liver dropped to background titers after transfer of LCMV-specific CTLs and TLR9 ligand **(Fig. 6h, i**). These results indicated that iMATEs served a role in the control of acute viral infection by facilitating TLR9 ligand–induced expansion of the CTL population and suggested that reconstitution of iMATEs that were absent during chronic infection improved CTL-mediated control of viral infection.

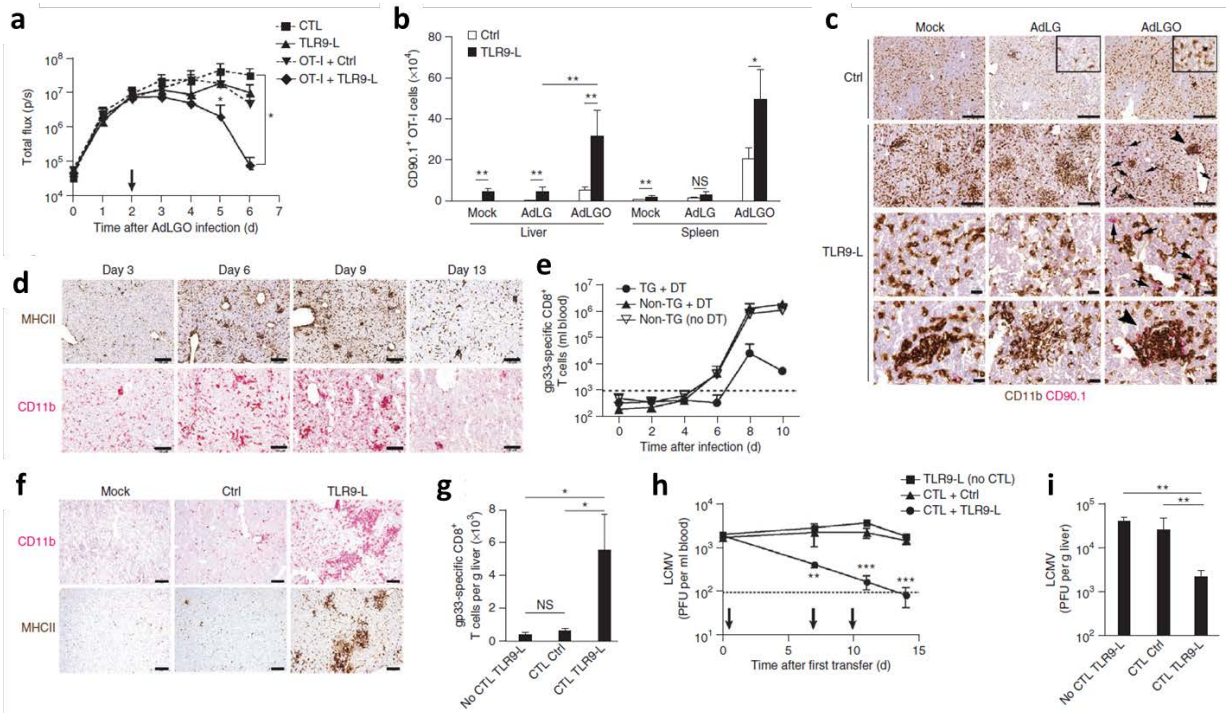

Figure 6: Improved clearance of viral infection from the liver by injection of TLR9 ligand. (a) Hepatic *in vivo* bioluminescence in mice infected with AdLGO (1×10^6 infectious units) and, 2 d later, treated (downward arrow) with TLR9 ligand or non–TLR9-binding control oligonucleotide, alone or with 1×10^4 *in vitro*–activated CD90.1$^+$ OT-I CTLs (OT-I +), assessed as reported before25. (b) Quantification of transferred CTLs in mice infected with AdLG or AdLGO (1×10^6 infectious units) and, 2 d later, given transfer of *in vitro*–activated CD90.1$^+$ OT-I CTLs (1×10^5) plus TLR9 ligand or non–TLR9-binding control oligonucleotide, assessed on day 3 after cell transfer. (c) Immunohistochemical analysis of CD11b and CD90.1 in liver tissue from the mice in b. Arrowheads indicate the same iMATE in consecutive sections; arrows indicate single CD90.1$^+$ OT-I cells in liver parenchymal tissue. Inset (top row), 5× enlargement of main image, showing iMATEs during viral infection. (d) Immunohistochemical analysis of MHC class II and CD11b in the liver after acute infection with LCMV (2×10^4 plaque-forming units). (e) Quantification of gp33-specific CTLs in blood from CCR2-CFP-DTR mice (TG) and their nontransgenic littermates (Non-TG) after infection with LCMV (2×10^4 plaque-forming units) and treatment with diphtheria toxin (+ DT); Non-TG (no DT), nontransgenic littermates not treated with diphtheria toxin. (f) Immunohistochemical analysis of MHC class II and CD11b in the liver during chronic infection with LCMV at day 3 after mock treatment or treatment with TLR9 ligand or non–TLR9-binding control oligonucleotide. (g) Quantification of hepatic gp33-specific CTLs in mice with chronic LCMV infection that received adoptive transfer of 1×10^7 *in vivo*–activated CTLs (isolated on day 7 after acute infection of donor mice with LCMV) three times (days 0, 7 and 10), together with TLR9 ligand or non–TLR9-binding control oligonucleotide, assessed at day 14 after first CTL transfer. Far left, mice given TLR9 ligand alone without CTLs. (h,i) Kinetics of LCMV titers in blood (h) and LCMV titers in the liver at day 14 after first adoptive transfer (i) in the mice in g. Downward arrows (h), transfer of gp33-specific CTLS on days 0, 7 and 10. Scale bars, 100 µm (c, top two rows, and d,f) or 10 µm (c, bottom two rows). *P < 0.05, **P < 0.01 and ***P < 0.001 (unpaired Student's *t*-test). Data are representative of two independent experiments with three to five mice per group (error bars (a,b,e,g–i), s.d.).

3.1.4.7. Successful immunotherapy of chronic liver viral infection

To explore whether the hepatic expansion of the CTL population improved defense against chronic infection with a pathogen relevant to humans, we used a model of chronic infection of immunocompetent mice by transfer of the HBV genome through the use of an adenovirus vector (AdHBV)[26]. In this model, therapeutic vaccination with DNA leads to a slightly greater abundance of circulating HBV-specific CTLs but does not control chronic infection with AdHBV26.

We treated mice with chronic AdHBV infection by vaccination with plasmid encoding HBV core antigen (HBc) or OVA, followed by injection of TLR9 ligand 12 d later. That led to a transient increase in serum ALT, indicative of liver damage, that was greatest in mice vaccinated with plasmid encoding HBc that also received TLR9 ligand (**Fig. 7a**). We did not detect iMATEs in mice with chronic AdHBV infection regardless of whether they were vaccinated with plasmid encoding HBc or OVA (**Fig. 7b**).

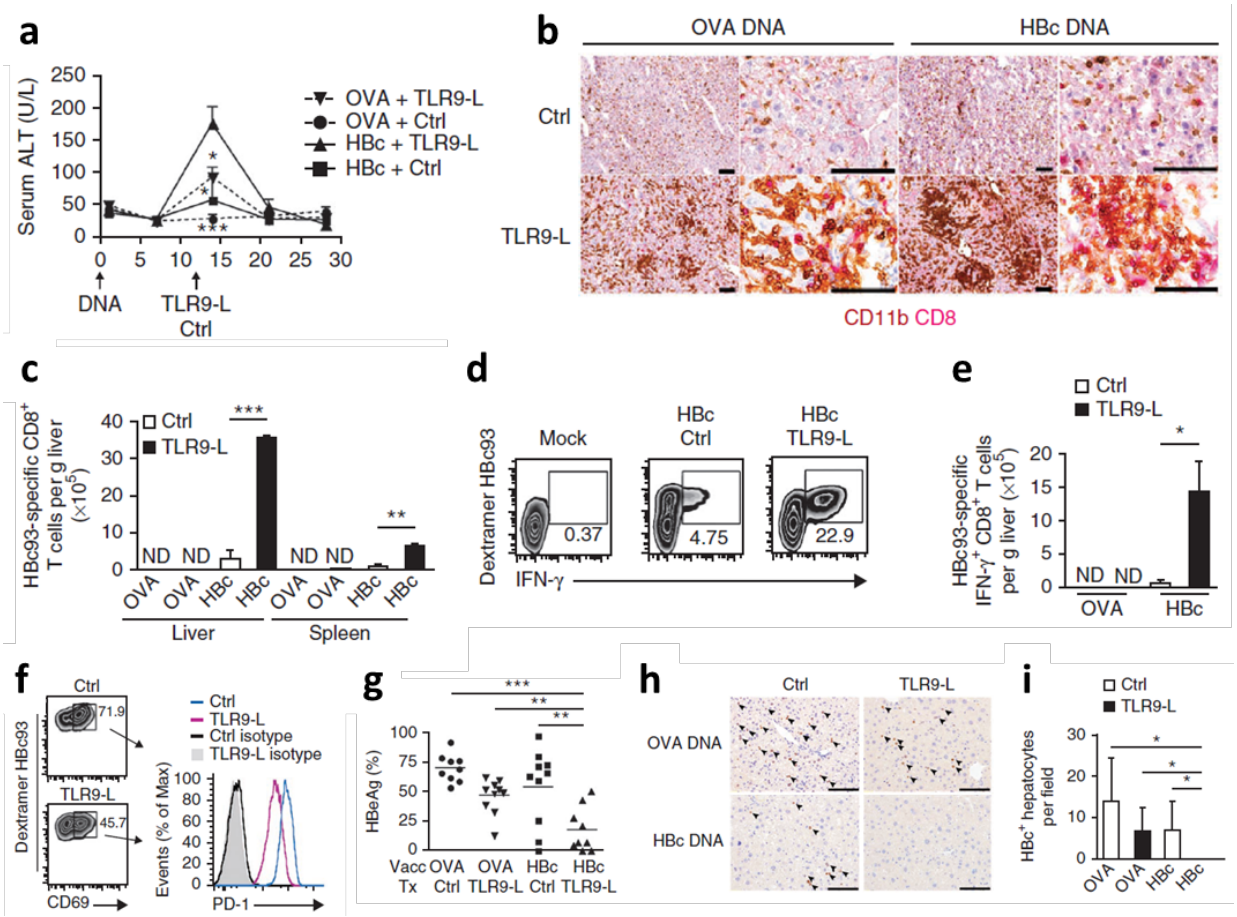

Figure 7: Elimination of chronic AdHBV infection. (a) Kinetics of serum ALT in mice (*n* = 5 per group) with chronic AdHBV infection, vaccinated with plasmid encoding HBc or OVA at day 0 (DNA) and challenged with TLR9 ligand or non–TLR9-binding control oligonucleotide at day 12. (b) Immunohistochemical analysis of CD11b and CD8 in the liver on day 15 after vaccination and challenge as in a. (c) Total HBc93-specific CTLs, detected by Dextramer staining, in spleen and liver of mice (*n* = 3 per group) on day 15 after vaccination and challenge as in a. (d) Dextramer staining (for HBc93) and intracellular cytokine staining of IFN-γ in CTLs from livers of AdHBV-infected mice given mock treatment (left) or vaccinated with plasmid encoding HBc and challenged with TLR9 ligand or non–TLR9-binding control oligonucleotide at day 12 after vaccination; cells isolated 15 d after vaccination were restimulated *ex vivo* with HBc93. Numbers below outlined areas indicate percent IFN-γ-producing HBc93-specific CTLs among total $CD8^+$ T cells. (e) Total IFN-γ-producing HBc93-specific CTLs obtained from mice (*n* = 3 per group) on day 15 after vaccination and challenge as in a and restimulated *ex vivo* with HBc93. (f) Flow cytometry of CTLs from mice vaccinated and challenged as in d, assessed immediately after isolation at day 15 after vaccination; numbers adjacent to outlined areas (left) indicate percent CD69+ HBc93-specific CTLs. Right, PD-1 expression on the CD69+ HBc93-specific CTLs at left. (g) Serum concentration of HBV e antigen (HBeAg) at day 28 after vaccination (Vacc) and challenge (Tx) of mice as in a, presented relative to those at day 1. (h,i) Immunohistochemical detection (h) and quantification (i) of HBc^+ hepatocytes at day 42 after vaccination and challenge as in a. Arrowheads (h) indicate HBc+ hepatocytes. Scale bars, 100 μm. **P* < 0.05, ***P* < 0.01 and ****P* < 0.001 (unpaired Student's *t*-test). Data are representative of three (a,c,d–g) or two (b,h,i) experiments (error bars (a,c,e,i), s.d.).

However, injection of TLR9 ligand induced iMATE formation (**Fig. 7b**), which raised the question of whether this may have facilitated expansion of the HBV-specific CTL population and subsequent clearance of chronic AdHBV infection.

Injection of TLR9 ligand at day 12 after vaccination with plasmid encoding HBc resulted in expansion of the H-2Kb-restricted CTL population specific for HBc amino acids 93–100 (HBc93) in the livers of mice with chronic AdHBV infection (**Fig. 7c**). Those HBc93-specific CTLs were functional and expressed IFN-γ after antigen-specific restimulation, whereas in the absence of TLR9 ligand, we detected few IFN-γ-expressing HBc93-specific CTLs (**Fig. 7d**,**e**). Furthermore, we observed lower expression of the costimulatory molecule PD-1 on $CD69^+$ HBc93-specific CTLs in mice treated with TLR9 ligand than on their counterparts in mice treated with control ligand (**Fig. 7f**), which suggested that DNA vaccination in combination with iMATE induction overcame immunoregulatory mechanisms. Vaccination with plasmid encoding HBc plus injection of TLR9 ligand resulted in lower serum concentrations of HBV antigens after 28 d and eventual elimination of HBV-infected hepatocytes at day 42 (**Fig. 7g–i**). These findings indicated that hepatic expansion of the HBc-specific population of CTLs eradicated HBV-infected hepatocytes during chronic infection and led to viral clearance.

3.1.5. Discussion

Here we found that activation of CTLs by simultaneous stimulation via the T cell antigen receptor, CD28 and IL-12 *in vitro*, together with the systemic application of TLR9 ligand, led to a 50-fold population expansion of CTLs locally in the liver. Myeloid-cell aggregates (iMATEs) that formed in the liver after TLR9 signaling facilitated CTL proliferation in the liver. This massive expansion of the CTL population in the liver contributed to antiviral immunity and overcame chronic viral infection in mice.

The iMATEs are distinct from the lymphoid structures that arise during chronic inflammation. Tertiary lymphoid tissues that form in the peripheral organs after chronic inflammatory signaling are functionally and structurally similar to secondary lymphatic tissue; that is, they have germinal centers and T cell zones and antigen sampling for DC-mediated population expansion of CTLs[12]. Granulomas generated during chronic inflammation or infection with intracellular bacteria are characterized by dense accumulation of macrophages surrounded by a ring of epithelial cells[27]. Tertiary lymphatic tissues and granulomas are considered long-lived yet dynamic structures that are constantly shaped by environmental factors[12, 27]. In contrast, iMATEs arose rapidly after a single injection of TLR9 ligand, were composed of monocyte-derived $CD11b^+$ cells that were not demarcated from surrounding liver tissue, and dissolved within 6–8 d. Moreover, the mechanisms that drove iMATE formation were distinct from those that operate during lymphatic tissue development. Whereas LTβR signaling is crucial

for the formation of secondary lymphatic tissue, IL-17 generates tertiary lymphatic tissue in a lymphotoxin-independent way in the lungs or the central nervous system[13, 14, 21, 28]. We found that iMATE formation did not depend on LTβR signaling but instead required signaling via TNF receptors. Monocyte-derived inflammatory DCs that formed iMATEs independently of crosstalk with lymphocytes produced TNF, which suggested that TNF acted in a local feed-forward loop to drive the efficient generation of iMATEs.

The induction of iMATEs via TLR9 signaling overcame local hepatic regulatory cues by creating a separate anatomical cocoon-like structure in the liver, where CTLs were probably sheltered from local inhibitory signals. Intravital imaging showed that T cells remained stationary or migrated within the boundaries of iMATEs. As there was no fibrous capsule or ring of fibrocytes around iMATEs, locally expressed chemotactic signals presumably kept the CTLs within the iMATEs, but the factors that determine the retention of CTLs in iMATEs or their exit from iMATEs remain to be defined. Three-dimensional reconstruction showed that CTLs were embedded within iMATEs in a matrix of monocyte-derived inflammatory DCs that probably functioned as 'nursing cells' to foster expansion of the CTL population by providing costimulatory signals through the OX40L-OX40 axis. The expansion of the CTL population in iMATEs occurred in the absence of MHC class I–restricted antigen recognition, although we cannot exclude the possibility of a role for MHC class I–induced tonic T cell antigen receptor signaling in these circumstances that is important for keeping T cells in a state in which they can respond to subsequent antigen-specific stimulation[29]. However, in the presence of their cognate antigen in infected hepatocytes, the population expansion of CTLs in iMATEs was enhanced, which indicated that inflammatory DCs may have cross-presented antigens on MHC class I to CTLs.

The generation of iMATEs during acute viral infection suggested that the iMATEs did not represent an artifact present after challenge with TLR9 ligand. The iMATEs formed during acute viral infection served as expansion hubs for antigen-specific CTLs that later contributed to the clearance of viral infection. Notably, we detected no iMATEs in the liver during chronic viral infection, which indicated that the generation of iMATEs was correlated with efficient CTL-mediated control of viral infection and opened the possibility for the use of induction of iMATEs for therapeutic vaccination.

The expansion of the CTL population in iMATEs induced by a single application of TLR9 ligand did not trigger autoimmunity. Only continuous application of TLR9 ligand over weeks, together with large numbers of autoreactive CTLs and hepatocellular expression of the auto-antigen, caused autoimmunity[30]. Moreover, chronic TLR signaling and inflammation enhances autoimmunity by enhanced MHC class I–restricted antigen presentation[31], and prolonged TLR3 signaling overcomes the tolerogenic hepatic microenvironment[32]. Thus, expansion of the CTL population in iMATEs may

improve the efficiency of therapeutic vaccines against chronic infection without causing autoimmunity.

The induction of iMATEs during chronic viral infection through application of TLR9 ligand resulted in substantial population expansion of virus-specific CTLs that were initially generated by genetic vaccination. Such expansion of the CTL population controlled chronic viral infection in hepatocytes. The combination of conventional vaccination plus TLR9 ligand–induced expansion of the CTL population in the liver augmented the efficacy of therapeutic vaccination. The hepatic expansion of the CTL population in iMATEs occurred independently of secondary lymphatic tissues and was therefore mechanistically distinct from the T cell population expansion induced by prime-boost vaccination schemes. Whereas conventional vaccination strategies aim to increase the immunogenicity of antigen-presenting cells and prolong antigen presentation to naive or central memory T cells in lymphatic tissues, iMATEs caused expansion of the population of IL-12-activated CTLs but not naive CTLs and, only to a lesser degree, memory T cells through costimulatory signals and cross-presentation in the liver.

Together our results have demonstrated the existence of a second phase of expansion of the CTL population in the liver in a distinct anatomical compartment formed by monocyte-derived inflammatory DCs. The population expansion of CTLs in iMATEs complemented the priming and proliferation of T cells in secondary lymphatic tissue that resulted in the massive population expansion of antigen-specific CTLs in the periphery. This so-far-unrecognized phase of a sudden increase in the expansion of the CTL population may be used to improve therapeutic vaccination against chronic viral infection of the liver.

3.1.6. References

1. Crispe, I.N. Hepatic T cells and liver tolerance. *Nat. Rev. Immunol*. **3**, 51–62 (2003).
2. Thomson, A.W. & Knolle, P.A. Antigen-presenting cell function in the tolerogenic liver environment. *Nat. Rev. Immunol*. **10**, 753–766 (2010).
3. Crispe, I.N. The liver as a lymphoid organ. Annu. Rev. Immunol. 27, 147–163 (2009).
4. Protzer, U., Maini, M.K. & Knolle, P.A. Living in the liver: hepatic infections. *Nat. Rev. Immunol*. **12**, 201–213 (2012).
5. Isogawa, M., Furuichi, Y. & Chisari, F.V. Oscillating CD8+ T cell effector functions after antigen recognition in the liver. *Immunity* **23**, 53–63 (2005).
6. Das, A. et al. Functional skewing of the global CD8 T cell population in chronic hepatitis B virus infection*. J. Exp. Med*. **205**, 2111–2124 (2008).

7. Lopes, A.R. et al. Bim-mediated deletion of antigen-specific CD8 T cells in patients unable to control HBV infection. *J. Clin. Invest*. **118**, 1835–1845 (2008).
8. Chakravarty, S. et al. CD8+ T lymphocytes protective against malaria liver stages are primed in skin-draining lymph nodes. *Nat. Med*. **13**, 1035–1041 (2007).
9. Cockburn, I.A. et al. Prolonged antigen presentation is required for optimal CD8+ T cell responses against malaria liver stage parasites. *PLoS Pathog*. **6**, e1000877 (2010).
10. Wong, P. & Pamer, E.G. Feedback regulation of pathogen-specific T cell priming. *Immunity* **18**, 499–511 (2003).
11. Kang, S.S. et al. Migration of cytotoxic lymphocytes in cell cycle permits local MHC I-dependent control of division at sites of viral infection. *J. Exp. Med*. **208**, 747–759 (2011).
12. Neyt, K., Perros, F., GeurtsvanKessel, C.H., Hammad, H. & Lambrecht, B.N. Tertiary lymphoid organs in infection and autoimmunity. *Trends Immunol*. **33**, 297–305 (2012).
13. Moyron-Quiroz, J.E. et al. Role of inducible bronchus associated lymphoid tissue (iBALT) in respiratory immunity. *Nat. Med*. **10**, 927–934 (2004).
14. Rangel-Moreno, J. et al. The development of inducible bronchus-associated lymphoid tissue depends on IL-17. *Nat. Immunol*. **12**, 639–646 (2011).
15. Egen, J.G. et al. Macrophage and T cell dynamics during the development and disintegration of mycobacterial granulomas. *Immunity* **28**, 271–284 (2008).
16. Egen, J.G. et al. Intravital imaging reveals limited antigen presentation and T cell effector function in mycobacterial granulomas. *Immunity* **34**, 807–819 (2011).
17. Curtsinger, J.M., Johnson, C.M. & Mescher, M.F. CD8 T cell clonal expansion and development of effector function require prolonged exposure to antigen, costimulation, and signal 3 cytokine. *J. Immunol*. **171**, 5165–5171 (2003).
18. Lee, S.W., Park, Y., Yoo, J.K., Choi, S.Y. & Sung, Y.C. Inhibition of TCR-induced CD8 T cell death by IL-12: regulation of Fas ligand and cellular FLIP expression and caspase activation by IL-12. *J. Immunol*. **170**, 2456–2460 (2003).
19. Macgregor, J.N. et al. Ex vivo culture with interleukin (IL)-12 improves CD8+ T-cell adoptive immunotherapy for murine leukemia independent of IL-18 or IFN-□ but requires perforin. *Cancer Res*. **66**, 4913–4921 (2006).
20. Gommerman, J.L. & Browning, J.L. Lymphotoxin/light, lymphoid microenvironments and autoimmune disease. *Nat. Rev. Immunol*. **3**, 642–655 (2003).
21. Drayton, D.L., Liao, S., Mounzer, R.H. & Ruddle, N.H. Lymphoid organ development: from ontogeny to neogenesis. *Nat. Immunol*. **7**, 344–353 (2006).
22. Serbina, N.V., Salazar-Mather, T.P., Biron, C.A., Kuziel, W.A. & Pamer, E.G.

TNF/iNOS-producing dendritic cells mediate innate immune defense against bacterial infection. *Immunity* **19**, 59–70 (2003).

23. Mescher, M.F. et al. Signals required for programming effector and memory development by CD8+ T cells. Immunol. Rev. 211, 81–92 (2006).
24. Croft, M. Control of immunity by the TNFR-related molecule OX40 (CD134). *Annu. Rev. Immunol*. **28**, 57–78 (2010).
25. Stabenow, D. et al. Bioluminescence imaging allows measuring CD8 T cell function in the liver. *Hepatology* **51**, 1430–1437 (2010).
26. Huang, L.R. et al. Transfer of HBV genomes using low doses of adenovirus vectors leads to persistent infection in immune competent mice. *Gastroenterology* **142**, 1447–1450 (2012).
27. Ramakrishnan, L. Revisiting the role of the granuloma in tuberculosis. *Nat. Rev. Immunol*. **12**, 352–366 (2012).
28. Peters, A. et al. Th17 cells induce ectopic lymphoid follicles in central nervous system tissue inflammation. *Immunity* **35**, 986–996 (2011).
29. Hochweller, K. et al. Dendritic cells control T cell tonic signaling required for responsiveness to foreign antigen. *Proc. Natl. Acad. Sci. USA* **107**, 5931–5936 (2010).
30. Sacher, T. et al. CpG-ODN-induced inflammation is sufficient to cause T-cell-mediated autoaggression against hepatocytes. *Eur. J. Immunol*. **32**, 3628–3637 (2002).
31. Lang, K.S. et al. Toll-like receptor engagement converts T-cell autoreactivity into overt autoimmune disease. *Nat. Med*. **11**, 138–145 (2005).
32. Lang, K.S. et al. Immunoprivileged status of the liver is controlled by Toll-like receptor 3 signaling. *J. Clin. Invest*. **116**, 2456–2463 (2006).

3.1.7. Personal contributions

In the present study we could show that Toll-like receptor signaling lead to the formation of intrahepatic myeloid cell aggregtes for T cell expansion (iMATEs) consisting of monocyte-derived $CD11b^+$ without causing any immunopathology. CTL proliferation was restricted to these 'cocoon-like' structures, protecting CTLs from immune-regulatory cues from the liver. iMATE formation was dependent on tumor-necrosis factor alpha (TNFα) and facilitated OX40 receptor dependent expansion of the CTL population. The iMATEs arose shortly after TLR9 stimulation or during acute viral infection but were lacking in chronic inflammation, yet could still be induced via TLR9 signaling facilitating control of the viral infection.

My main experimental tasks in this study were the in-detailed histological and immunohistochemical analysis of mouse livers before, during and after iMATE formation. In addition I actively contributed to the conceptual development of several hypotheses in this study.

Analyses and figures I contributed to:

Figure 1h: Immunohistochemical analysis of BrdU or CD90.1 positivity in mice on 4 consecutive days after adoptive T-cell transfer with and without TLR9 stimulation.

Figure 2b: Hematoxylin-and-eosin staining and immunohistochemical analysis of CD11b, MHC class II or CCR2 in liver tissue at day 3 after TLR9 ligand or the control oligonucleotide treatment.

Figure 2c: Immunohistochemical analysis of collagen IV, platelet-derived growth-factor receptor-β (PDGFR-β), smooth muscle actin (SMA) and gp38 in liver tissue at day 3 after TLR9 challenge.

Figure 2 d and e: Immunohistochemical analysis of CD11b (**d**) or MHC class II (**e**) in liver tissues from wild-type (WT) and CCR2-CFP-DTR mice treated with diphtheria toxin (+ DT), assessed at day 4 after TLR9 challenge

Figure 3b: Immunohistochemical analysis of MHC class II or GFP in consecutive liver sections obtained on days 1–8 after transfer of GFP^+ CTLs and treatment with TLR9 ligand.

Figure 3c: Costaining for GFP/Ki67 and MHC class II in consecutive liver sections at day 3 after treatment with TLR9 ligand or control oligonucleotide

Figure 3f: Immunohistochemical analysis of MHC class II in liver tissue at day 3 after injection of TLR9 ligand or control oligonucleotide, with or without CTLs, into wild-type and $Rag2^{-/-}$ mice.

Figure 4g and h: Immunohistochemical analysis of TNF and MHC class II (**g**) or iNOS and MHC class II (**h**) in consecutive liver sections on day 3 after treatment with TLR9 ligand or control

Figure 4i: Immunohistochemical analysis of CD11b and F4/80 in liver tissues from wild-type or TNFR1-TNFR2–deficient (TNFR-DKO) mice on day 3 after treatment with TLR9 ligand or control

Figure 5g: Immunohistochemical analysis of OX40L and CD11b in liver tissue on day 3 after TLR9 ligand or control treatment

Figure 6c: Immunohistochemical analysis of CD11b and CD90.1 in liver tissue from mice infected with AdLG or AdLGO and, 2 d later, given transfer of in vitro–activated CD90.1+ OT-I CTLs plus TLR9 ligand or non–TLR9-binding control oligonucleotide, assessed on day 3 after cell transfer.

Figure 6d: Immunohistochemical analysis of MHC class II and CD11b after acute infection with LCMV

Figure 6f: Immunohistochemical analysis of MHC class II and CD11b in the liver during chronic infection with LCMV at day 3 after mock treatment or treatment with TLR9 ligand or non–TLR9-binding control oligonucleotide

Figure 7b: Immunohistochemical analysis of CD11b and CD8 in the liver on day 15 after vaccination and challenge in mice with chronic AdHBV infection, vaccinated with plasmid encoding HBc or OVA at day 0 (DNA) and challenged with TLR9 ligand or control oligonucleotide at day 12

Figure S2a: Immunohistochemistry for MHCII and CD11b in the liver at d3 after application of different TLR agonists

Figure S2c: Quantification of the numbers of iMATEs at 1-8 days after TLR9L treatment

Figure S2e and f: Immunohistochemical analysis of cleaved caspase-3 (e) NKp46, CD19 or Ly6C + Ly6G (f) and in livers of mice at d3 after TLR9 challenge

Figure S3a: Immunohistochemistry for CD11b and CD90.1 in the liver of splenectomized FTY720-treated mice

Figure S4a: Immunohistochemistry for GFP and Ki-67 at d3 after TLR9L challenge and transfer of GFP^+CTLs.

Figure S5f: Immunohistochemistry for CD11b in the liver of wild-type or CD11c.DOG mice at d3 after TLR9L and daily diphtheria toxin treatment

Figure S7a: Immunohistochemistry for $CD11b^+$ and $CD8^+$ or Ki-67 and $CD8^+$ cells in the liver at d9 after acute LCMV infection

3.2. Specific and Nonhepatotoxic Degradation of Nuclear Hepatitis B Virus cccDNA

'Introduction', 'Material and Methods', 'Results' and 'Discussion' have been described in the following publication: Lucifora, Xia et al. *Science,* **343,** 1221-1228 (2014)

3.2.1. Authors

Julie Lucifora,* Yuchen Xia,* **Florian Reisinger**, Ke Zhang, Daniela Stadler, Xiaoming Cheng, Martin F. Sprinzl, Herwig Koppensteiner, Zuzanna Makowska, Tassilo Volz, Caroline Remouchamps, Wen-Min Chou, Wolfgang E. Thasler, Norbert Hüser, David Durantel, T. Jake Liang, Carsten Münk, Markus H. Heim, Jeffrey L. Browning, Emmanuel Dejardin, Maura Dandri, Michael Schindler, Mathias Heikenwalder,‡ Ulrike Protzer‡

*) ‡) equal contribution

3.2.2. Abstract

Current antivirals can control but not eliminate hepatitis-B-virus (HBV), because HBV establishes a stable nuclear cccDNA. Interferon-α treatment can clear HBV but is limited by systemic side effects. Here we describe how interferon-α can induce specific degradation of the nuclear viral DNA without hepatotoxicity and propose lymphotoxin-β-receptor activation as a therapeutic alternative. Interferon-α and lymphotoxin-β-receptor activation up-regulated APOBEC3A and 3B cytidine-deaminases, respectively, in HBV-infected cells, primary hepatocytes and human liver-needle biopsies. HBV-core protein mediated the interaction with nuclear cccDNA resulting in cytidine-deamination, apurinic/apyrimidinic site formation and finally cccDNA degradation that prevented HBV-reactivation. Genomic DNA was not affected. Thus, inducing nuclear deaminases - e.g., by lymphotoxin-β-receptor activation - allows development of new therapeutics that combined with existing antivirals may cure hepatitis B.

3.2.3. Introduction

Hepatitis B virus (HBV) infection remains a major public health threat with more than 350 million humans chronically infected worldwide at risk of developing end-stage liver disease and hepatocellular carcinoma. Each year, more than 600,000 humans die from consequences of chronic HBV infection. A prophylactic vaccine has been available for hepatitis B for almost thirty years, but the overall number of chronic infections re-mains high.

HBV is a small, enveloped DNA virus replicating via an RNA intermediate. The encapsidated viral genome consists of a 3.2 kb partially double-stranded relaxed circular DNA (rcDNA) molecule. The virus has optimized its life-cycle for long-term persistence in the liver (*1*). Upon translocation to the nucleus, the rcDNA genome is converted into a co-valently closed circular DNA (cccDNA), which serves as the template for viral transcription and secures HBV persistence. Nucleos(t)ide analogs are efficient antivirals but only control and do not cure HBV infection owing to the persistence of HBV cccDNA. Therefore, long-term treatment is required, which is expensive and may lead to concomitant resistance (*2*). Interferon (IFN)-α is licensed for hepatitis B therapy and treatment with this cytokine can result in virus clearance in a proportion of patients; however, its efficacy is limited and high doses are not tolerated (*3*). Thus, efficient and non-toxic elimination of cccDNA in hepatocytes is a major goal of HBV research.

Using animal models, it has been shown that HBV replication, and in particular the cccDNA content of the liver, can be affected by noncytopathic mechanisms involving cytokines such as interferons and tumor necrosis factor (TNF), which influence RNA and capsid stability (*4*–*7*). Here, we describe an antiviral mechanism that interferes with cccDNA stability and is distinct from influences of antiviral cytokines on cccDNA activity (*8*).

3.2.4. Results

3.2.4.1. High-Dose IFN-α Leads to cccDNA Degradation in HBV-Infected Hepa-tocytes

IFN-α is known to exert transcriptional, post-transcriptional and epigenetic antiviral effects on HBV (*8*–*12*). To study the effect of IFN-α on HBV cccDNA, we used HBV-infected, differentiated HepaRG (dHepaRG) cells and primary human hepatocytes (PHH). These are human cell types susceptible to HBV infection (*13*, *14*) and responsive to IFN-α treatment in vitro (data not shown). IFN-α treatment did not lead to detectable hepatotoxicity, even at very high doses (data not shown). Treating dHepaRG cells with 500 or 1000 IU/ml IFN-α controlled HBV-DNA synthesis as efficiently as 0.5 µM (5-fold EC50) of the nucleoside analog lamivudine (LAM). IFN-α, however, unlike LAM also significantly reduced expression of HBV-RNA and hepatitis B surface (HBsAg) and e (HBeAg) antigens (**Fig. 1a** and data not shown).

In patients, interruption of LAM treatment results in a rebound of HBV replication (*2*). Using IFN-α, we observed only a partial or no rebound in HBV-infected dHepaRG cells after treatment cessation (**Fig. 1a**). Because dHepaRG don't allow virus spread, reduction of HBeAg and lacking rebound indicated an effect of IFN-α on the established HBV cccDNA transcription template besides the

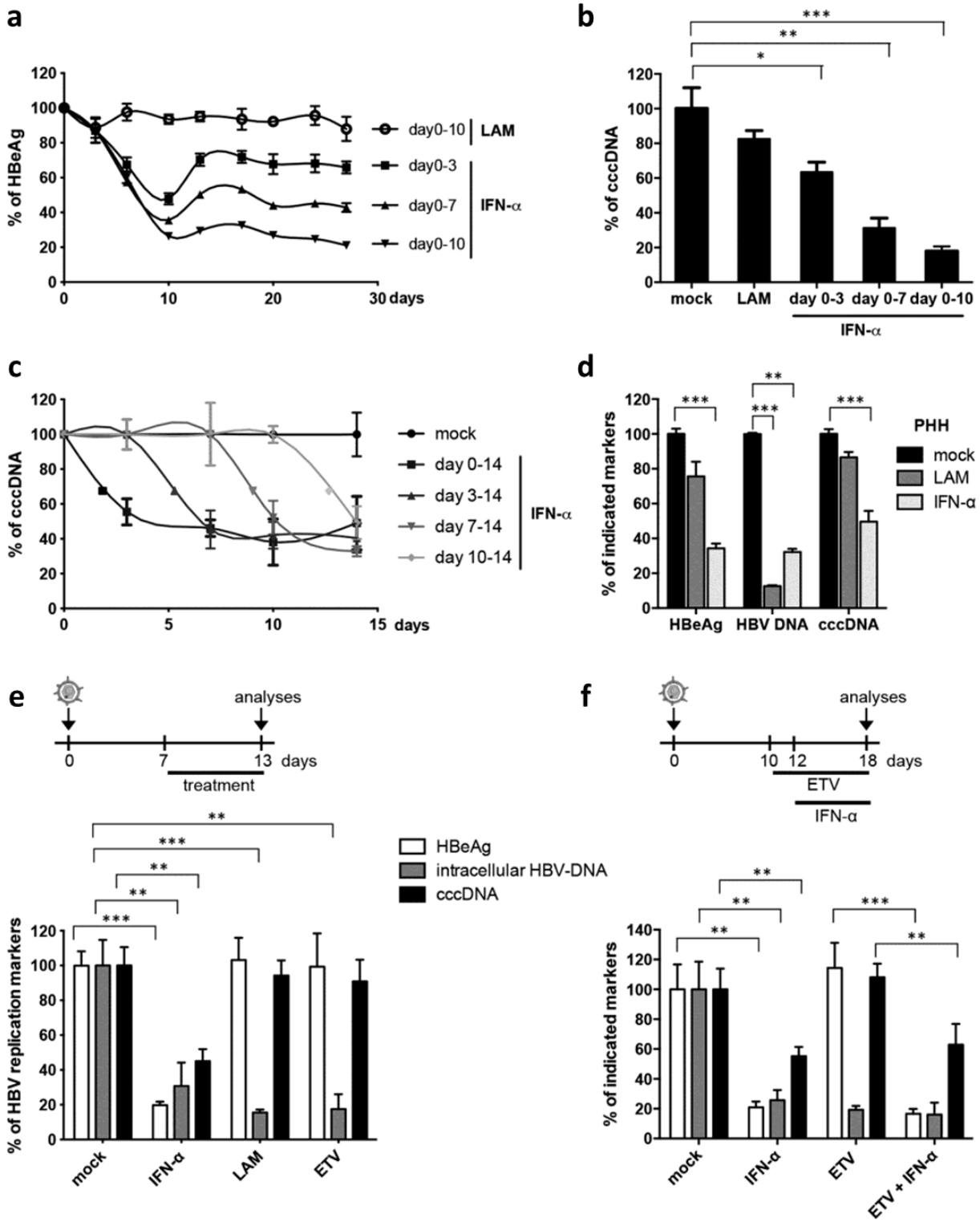

Figure 1: Degradation of cccDNA in IFN-α treated HepaRG cells and primary human hepatocytes. (a, b, c, e, and f) HBV-infected dHepaRG were treated with IFN-α at day 10 post-infection (dpi). Different regimens of treatment were applied as indicated. (d) HBV-infected primary human hepatocyte (PHH) were treated with IFN-α at dpi 3 for 13 days. Levels of HBeAg, total intracellular DNA and cccDNA are given relative to mock treated cells. LAM: lamivudine; ETV: entecavir. Mean values +/− standard deviation of replicates from independent experiments are given; data were analyzed by *t* test. * $p < 0.05$, ** $p < 0.01$ and *** $p < 0.001$.

known antiviral effects on viral replication (*14*). By cccDNA-specific qPCR, we determined an 80% reduction of cccDNA after 10 days of treatment (**Fig. 1b**). Reduction of cccDNA was confirmed by Southern blot analysis (data not shown) and was dose dependent (data not shown). cccDNA reduction could be induced at any time point (**Fig. 1c**) and persisted over time (**Fig. 1, a** and **c**). The effect was corroborated in HBV-infected primary human hepatocytes (PHH) (**Fig. 1d**). In contrast to IFN-α, LAM and even more potent nucleoside analog entecavir (ETV) at very high doses (0.5 µM, 1000-fold IC-50) only inhibited reverse transcription and thus HBV replication, but not viral persistence (**Fig. 1e**). Pretreatment with ETV did not enhance the effect of IFN-α (**Fig. 1f**) indicating that IFN-α induces the decay of established HBV cccDNA. Since the doses of IFN-α used to achieve this effect were high, we screened for other cytokines showing similar anti-viral effects at moderate doses.

3.2.4.2. LTβR Activation Controls HBV and Leads to cccDNA Degradation in HBV-Infected Cells

IFN-γ and TNF-α are known to control HBV in a noncytopathic fashion (*4*, *7*), but cannot be used as therapeutics because they cause severe side effects. We tested the effect of lymphotoxin (LT) β receptor (LTβR) activation as an alternative therapeutic option. TNF superfamily members LTα, LTβ and CD258 are the physiological ligands for LTβR and activate several inflammatory, anti-inflammatory, pro- and anti-survival pathways (*15*). Like hepatocytes (*16*), dHepaRG (*14*) and HepG2-H1.3 cells permit HBV replication (*17*) and express the LTβR (**Fig. S2a** and **b**). To activate LTβR, we used a super-agonistic tetravalent bispecific antibody (BS1) and a bivalent anti-LTβR monoclonal antibody (CBE11) (*18*, *19*). As expected, LTβR agonists activated canonical (*20*) and non-canonical nuclear factor kappa-light-chain-enhancer of activated B cells (NF-κB) pathways to trigger p100 cleavage (Fig. S2C), RelA phosphorylation (**Fig. S2d**), nuclear RelB and RelA translocation (**Fig. S2e** and **f**), and up-regulation of known target genes (**Fig. S2g**) without causing any detectable hepatocytotoxicity (**Fig. S2h**).

To test the effect of LTβR-activation on HBV infection, dHepaRG cells were treated with BS1 for 12 days starting 24 hours prior to HBV infection. LTβR-activation decreased levels of all HBV-markers, including cccDNA by approximately 90% without toxicity (**Fig. 2a**). The anti-viral effect was highly potent with an EC5O of approximately 0.01 µg/mL (data not shown). Inhibition of apoptosis did not alter antiviral activity (data not shown). Neither IFN-β nor classic IFN-stimulated genes were up-regulated upon BS1-treatment (**Fig. S2g**) and antiviral activity was independent of IFN-induction (data not shown). In vivo, activation of the murine LTβR by systemic application of an agonistic antibody (ACH6) induced RelA and RelB nuclear translocation in hepatocytes of HBV-transgenic mice (**Fig. S6a**), reduced HBV viremia (**Fig. S6b**), HBV RNA (**Fig. S6c**) and HBV core (HBc) protein expression in the

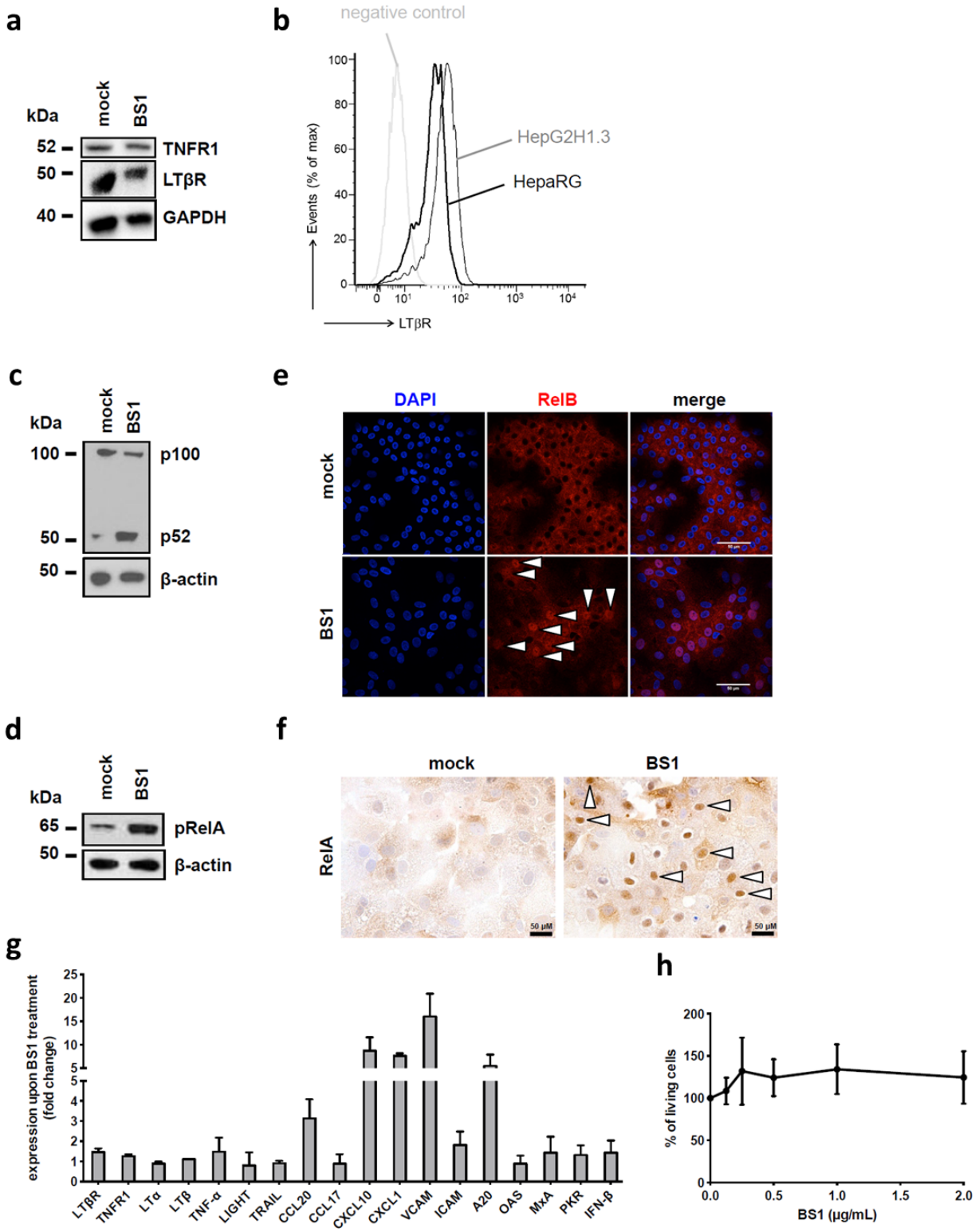

Figure S2: HBV-infected dHepaRG cells were treated with BS1. After 10 days, we analyzed (a) expression of LTβR and TNFR1 by Western blot and (b) by FACS analyses as well as (c) p100/p52 processing and (d) phosphorylation of RelA (pRelA) by Western blot. (d) Nuclear translocation of RelB and of (f) RelA by immunohistochemistry (white arrow heads indicate nuclear translocation in hepatocytes). (g) Expression analysis of indicated genes upon BS1 treatment by qRT-PCR. (h) Assessment of cell viability under different concentration of BS1 by XTT tests.

liver (**Fig. S6, d** and **e**). Neither signs of hepatocyte apoptosis (**Fig. S6f**) nor elevation of aminotransferases (ALT) (Fig. S6G, right panel) were observed indicating good in vivo tolerability of LTβR-activation. Since HBV-transgenic mice do not establish HBV cccDNA, this indicated additional antiviral effects of LTβR-activation on HBV RNA transcription or stability. Accordingly, discontinuation of LTβR-activation induced an immediate, strong rebound of HBV replication (**Fig. S6g**).

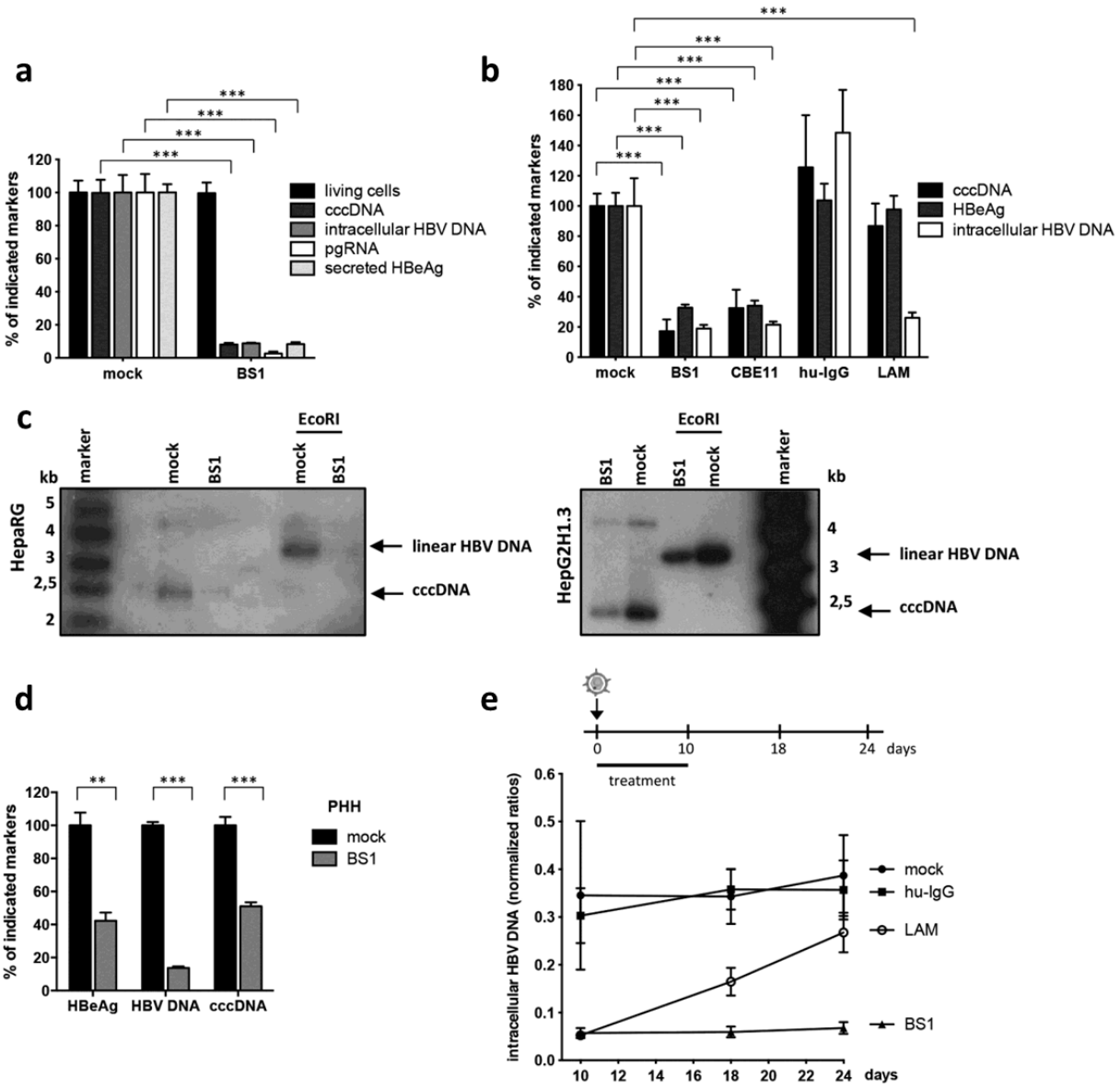

Figure 2: LTβR-activation inhibits HBV infection and leads to cccDNA degradation in HepaRG cells and PHH. (a and b) HBV-infected dHepaRG were treated with BS1, CBE11, hu-IgG control or lamivudine (LAM). (a) Treatment started 24h before infection for 12 days or (b) at 18 dpi for 10 days. Levels of the indicated HBV markers as well as cell viability are given relative to untreated controls (mock). (c) cccDNA levels were analyzed after 14 days of BS1 treatment by Southern blot in HBV-infected dHepaRG and HBV-replicating HepG2H1.3 cells. Supercoiled cccDNA bands were identified by their expected size and linearization upon *EcoRI* digestion (3,2 kb). (d) PHH were infected with HBV and treated with BS1 at 7 dpi for 10 days. Levels of the indicated HBV markers were compared to untreated PHH of the same donor (donor 3) (mock). (e) HBV-infected dHepaRG were treated with BS1, hu-IgG control or LAM. Intracellular HBV-DNA was analyzed 8 and 14 days after treatment cessation. Mean values +/− standard deviation of replicates from independent experiments are given; data were analyzed by *t*-test. * $p < 0.05$, *** $p < 0.001$.

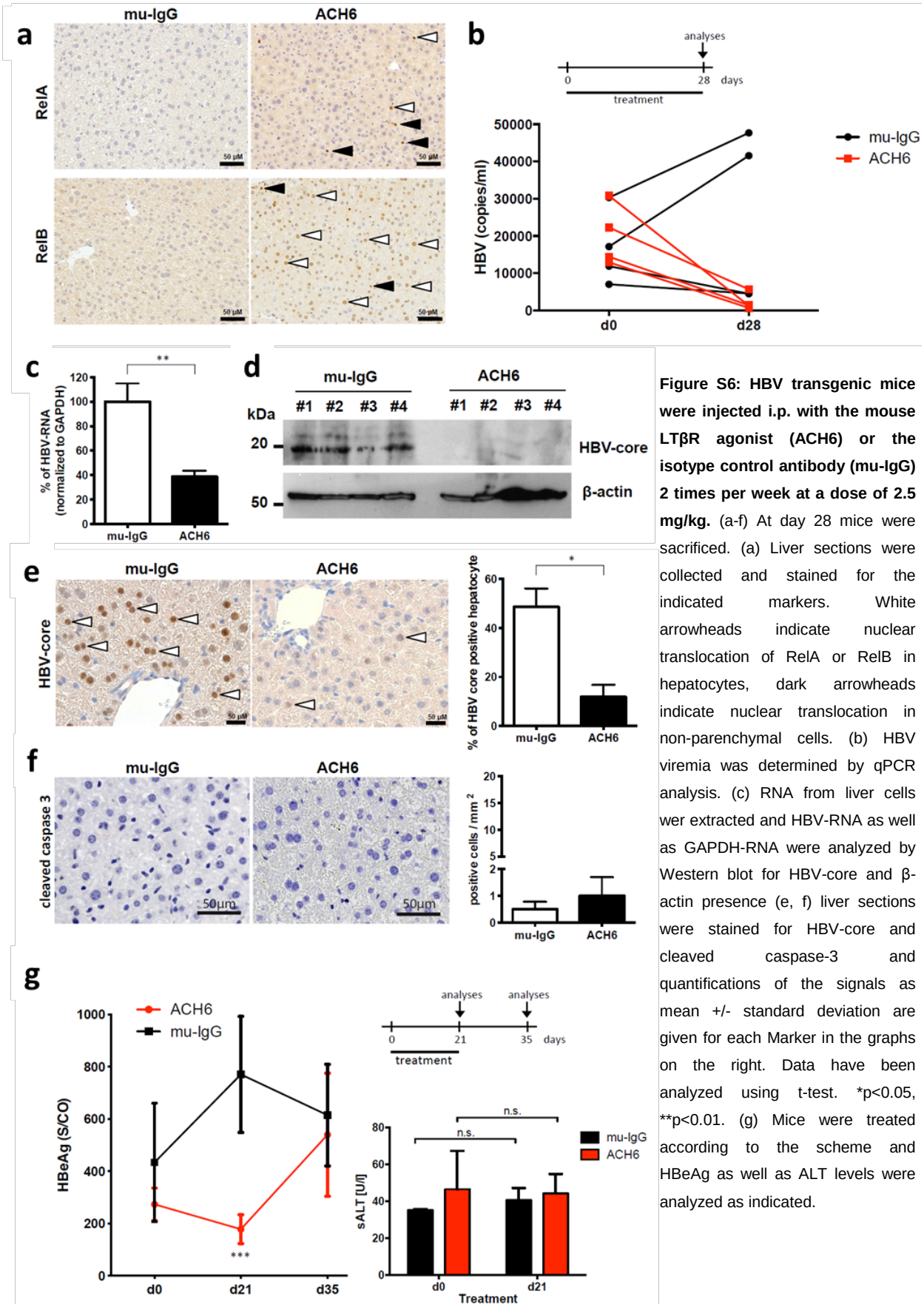

Figure S6: HBV transgenic mice were injected i.p. with the mouse LTβR agonist (ACH6) or the isotype control antibody (mu-lgG) 2 times per week at a dose of 2.5 mg/kg. (a-f) At day 28 mice were sacrificed. (a) Liver sections were collected and stained for the indicated markers. White arrowheads indicate nuclear translocation of RelA or RelB in hepatocytes, dark arrowheads indicate nuclear translocation in non-parenchymal cells. (b) HBV viremia was determined by qPCR analysis. (c) RNA from liver cells wer extracted and HBV-RNA as well as GAPDH-RNA were analyzed by Western blot for HBV-core and β-actin presence (e, f) liver sections were stained for HBV-core and cleaved caspase-3 and quantifications of the signals as mean +/- standard deviation are given for each Marker in the graphs on the right. Data have been analyzed using t-test. *p<0.05, **p<0.01. (g) Mice were treated according to the scheme and HBeAg as well as ALT levels were analyzed as indicated.

To investigate whether LTβR-activation would affect established HBV cccDNA in the context of a persistent infection and prevent HBV reactivation, dHepaRG cells were treated with LTβR agonists BS1 or CBE11 when a stable, nuclear cccDNA pool had established. All HBV markers, including HBV cccDNA, were reduced upon LTβR-activation in HBV-infected dHepaRG cells (**Fig. 2, b** and **c**, and data not shown) as well as in stably transfected HepG2H1.3 cells containing high levels of cccDNA (**Fig. 2c**). In HBV-infected primary human hepatocytes (PHH), LTβR agonisation reduced HBV cccDNA, HBeAg secretion and even more pronounced HBV-DNA replication (**Fig. 2d**). cccDNA degradation was more effective (up to 95%) when treatment was prolonged (data not shown). Treatment interruption for 10 days was almost as efficient as continuous treatment (data not shown) indicating that LTβR agonists induce a persistent antiviral effect. In contrast to LAM treatment, no rebound of HBV-replication was observed when BS1 treatment stopped (**Fig. 2e**). Hence, LTβR activation not only suppressed HBV replication but also caused nuclear cccDNA degradation, needed to achieve virus elimination.

3.2.4.3. LTβR Activation and IFN-α Treatment Induce Deamination and Apurinic/Apyrimidinic (AP) Site Formation in cccDNA

To investigate if cccDNA degradation upon LTβR-activation or IFN-α treatment was a result of DNA damage, we examined cccDNA deamination by differential DNA denaturation PCR (3D-PCR) (*21*). Low denaturing temperatures were sufficient for cccDNA amplification from HBV-infected dHepaRG cells and for PHH treated with IFN-α or BS1, compared with untreated, LAM- or ETV-treated cells (**Fig. 3a** and data not shown). Using a cocktail of recombinant proteins containing all enzymes necessary for DNA repair (preCR mix), we could reverse the denaturation of cccDNA (**Fig. 3a**, lower panels). The fact, that denaturation temperatures of mock, LAM and ETV treated cells also shifted, indicated that this modification of HBV cccDNA existed even without exposure to exogenous drugs. Deamination of cccDNA (**Fig. 3a**, right panel) and a drop in cccDNA levels after treatment with CBE11 (table S1) was confirmed in vivo in human liver chimeric uPA-SCID mice infected with HBV. Sequencing analyses showed G/A transitions occurred under treatment (**Fig. 3b** and data not shown) indicating deamination of cytidines to uridine in the HBV cccDNA minus strand. At lower denaturation temperatures G/A transitions became more obvious (**Fig. 3c** and data not shown). These data showed that both LTβR-activation and IFN-α treatment led to cccDNA deamination in vitro and in vivo, and help to explain the G/A hypermutation observed in patient samples (*21*).

Importantly, neither deamination nor mutations of genomic DNA were observed by 3D-PCR (data not shown) or by deep sequencing of selected housekeeping or IFN- and LTβR-target genes (data not shown). This indicated that DNA modifications were specifically targeted to viral cccDNA.

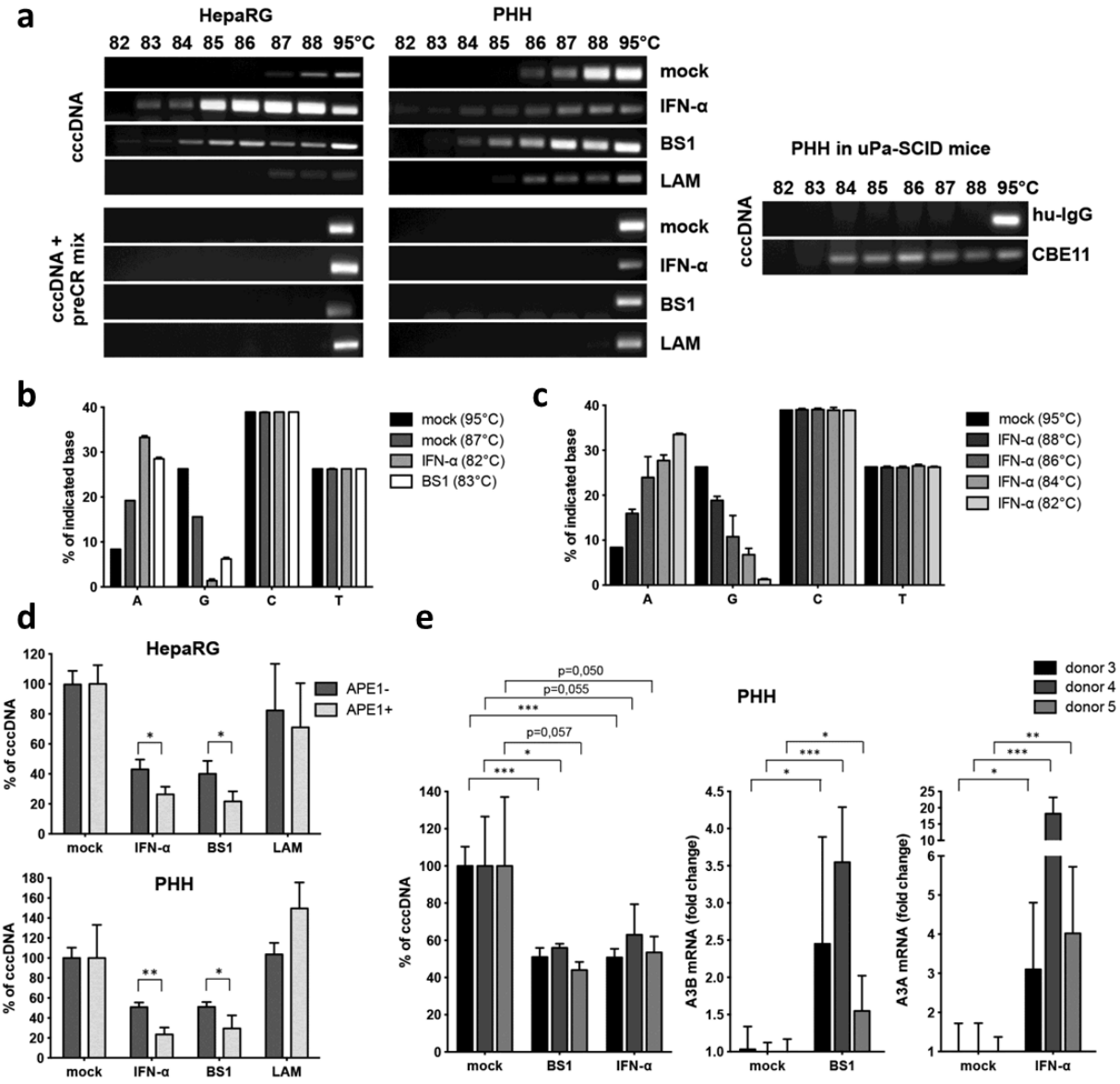

Figure 3: Deamination and AP-site formation in cccDNA upon IFN-α treatment and LTβR-activation. (a) dHepaRG (left) and PHH (middle panel) were infected with HBV and treated with IFN-α, BS1 or LAM. Human chimeric uPA/SCID mice were treated with CBE11 or hu-IgG control (right panel). 3D-PCR analyses were performed on cccDNA left either untreated (upper panels) or treated with a PreCR mix (lower panels). (b and c) 3D-PCR products from HBV-infected dHepaRG cells treated as indicated (IFN-α, BS1 or mock) were cloned and sequenced and mutations were analyzed. (d) Total DNA extracts from HBV-infected cells treated as indicated were digested with APE1, and cccDNA content was compared to mock-treated cells. In (B), (C), and (D), mean values +/− standard deviation of biological triplicates from two independent experiments are given; data were analyzed by *t* test. * $p < 0.05$, ** $p < 0.01$. (e) PHH were infected with HBV and treated with BS1 or IFN-α at 7 dpi for 10 days. Levels of the indicated cccDNA as well as A3A and A3B mRNA expression were compared to untreated PHH (mock) of the same donor.

After cytidine deamination, DNA-glycosylases recognize the damaged DNA and cleave N-glycosidic bonds to release the base and create an accessible AP site that can then be cleaved by endonucleases (*22*). These AP sites can either be repaired, can lead to mutations upon DNA replication or can induce DNA degradation (*23*). We quantified AP sites created by LTβR-activation or IFN-α treatment. However, no increase of AP sites in total DNA extracts from dHepaRG cells or PHH

treated with IFN-α or LTβR-agonists (data not shown) was found, reassuring that our treatments did not lead to detectable damage in genomic DNA. Because AP sites in the small (3.2 kb) cccDNA are very likely to be missed by this analysis, we digested total DNA extracts with an AP-endonuclease (APE1) and then amplified cccDNA by qPCR. APE digestion further decreased cccDNA extracted from dHepaRG cells and PHH treated with IFN-α or LTβR-agonists but not with LAM (**Fig. 3d**). Taken together, our data indicate that both, LTβR-activation or IFN-α treatment induced deamination and AP-site formation in HBV cccDNA leading to its degradation, but did not affect genomic DNA.

3.2.4.4. LTβR Activation and IFN-α Treatment Up-Regulate Expression of Nuclear APOBEC3 Deaminases

IFN-α is known to induce several cytidine deaminases (*23*, *24*). We performed genome-wide expression profiling of HBV-infected dHepaRG cells after LTβR-activation (**Fig. S9a**) and classified regulated genes according to their activity and properties (**Fig. S9b**). Hereby, APOBEC3B (A3B) was identified to be the most up-regulated gene with nucleic acid binding properties (**Fig. S9c**).

Analysis of all APOBEC3 family members showed that LTβR-activation leads to strong up-regulation of A3B and to minor extent A3G in HBV-infected dHepaRG and PHH, and after systemic application in human liver chimeric uPA-SCID mice (data not shown). A3B expression was induced by LTβR-activation in a dose-dependent manner and expression levels steadily increased during continuous treatment (data not shown) correlating with a concomitant increase in treatment efficacy over time (data not shown). Treatment of PHH isolated from different donors with LTβR-agonist BS1 resulted in cccDNA degradation at different levels (**Fig. 3e** and data not shown), which could neither be explained by the level of A3B upregulation (**Fig. 3e**) nor by detection of a previously described (*25*) genomic deletion of the A3B allele, which seems to correlate with HBV persistence in infected patients (data not shown).

In contrast to LTβR-activation, IFN-α treatment induced mainly A3A, but also A3F and A3G expression in HBV-infected dHepaRG cells and PHH (Fig. S12A), and A3D expression in isolated PHH. By systemic IFN treatment of chimpanzees (*26*), A3A was strongly upregulated in liver needle biopsies (data not shown). Activation of A3A, A3F and A3G after IFN-α treatment was dose- and time-dependent, and decreased after an initial peak despite continuous treatment indicating that cells become refractory to IFN-α (data not shown). In patients treated with subcutaneous pegylated IFN-α, needle biopsies obtained at different time points confirmed a rapid, strong upregulation of A3A and to a lower extend of A3G in the liver peaking at 16 hours post treatment (data not shown). Expression levels declined after this time point and remained low until day 6 post treatment confirming a fast but only transient induction of A3A by IFN-α treatment. Interestingly, the level of A3B or A3A induction in BS-

1 and IFN-α treated PHH, respectively, did not directly correlate with the level of cccDNA degradation (**Fig. 3e**). The fact that IFN-α only induces a transient A3A induction and cells rapidly become refractory to IFN-α may account for the limited effect of IFN-α treatment in HBV-infected patients.

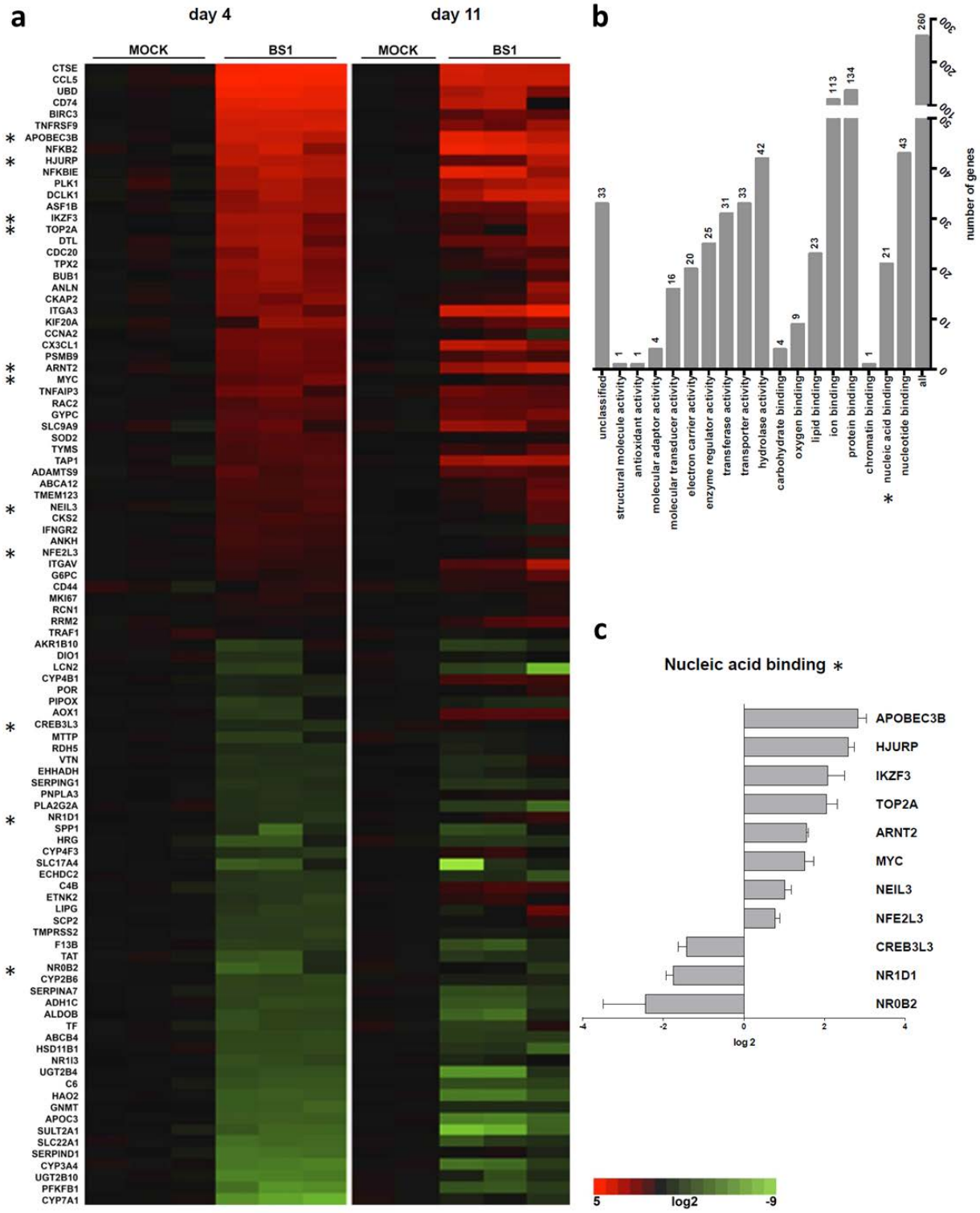

Figure S9: dHepaRG cells were infected with HBV and treated with LTβR-agonist BS1. (a) Affymetrix gene expression array was confirmed by qRT-PCR analysis of the 50 most strongly up- and down-regulatied genes. Results are shown as level of regulation according to the scale bars. (b, c) Regulated genes were classified according to their activity and binding properties. Stars indicate proteins for which nucleic acid binding properties have been described.

3.2.4.5. APOBEC3A or APOBEC3B Activity Is Essential to Induce cccDNA Degradation

Among the APOBEC3 family members up-regulated in our experiments, only A3A and A3B located to the nucleus (data not shown) where they can gain access to cccDNA. To verify that they are indeed responsible for the induction of cccDNA degradation, we overexpressed the HIV-Vif protein (known to promote the degradation of all APOBEC3 proteins except A3B (*27*, *28*)) in dHepaRG cells in a tetracycline-regulated fashion. Expression of HIV-Vif reduced A3A, A3F and A3G expression (data not shown), reverted IFN-α-induced cccDNA deamination and prevented cccDNA degradation induced by IFN-α treatment (**Fig. 4a**). However, expression of HIV-Vif did not alter A3B levels (Fig. S15B) and had no impact on cccDNA degradation by LTβR-activation (data not shown). To specifically address the role of A3A or A3B in cccDNA degradation we further knocked down A3A and A3B in dHepaRG cells under IFN-α or LTβR-agonist treatment, respectively, and observed reduced cccDNA deamination (**Fig. 4b and c, left panels**). A3A as well as A3B knock-down completely reverted cccDNA degradation, but could not rescue the additional effect of IFN-α or LTβR-activation on HBV replication (**Fig. 4b and c, right panels**).

To confirm the impact of A3A and A3B on cccDNA deamination, we overexpressed A3A and A3B, respectively, in HBV-replicating HepG2-H1.3 (**Fig. 4d and e**). Cytidine-deamination of nuclear cccDNA by A3A and A3B is in accordance with other studies showing that both localize to the nucleus (*29*) and may be involved in the elimination of foreign DNA (*23*).

3.2.4.6. APOBEC3A Interacts with the HBV Core Protein and Binds to cccDNA

APOBECs have evolved to restrict retroviral replication (*30*) as well as DNA transfer into cells. They are able to clear foreign nuclear DNA (*23*, *31*), but it remains unclear how HBV cccDNA DNA was recognized and whether it was specifically targeted in our experiments. To assess specificity, we generated cell lines replicating a mammalian replicon plasmid pEpi containing a linear HBV 1.3-fold overlength sequence. From the linear HBV-genome, HBV replication was initiated and in addition to the pEpi-H1.3 replicon HBV cccDNA was established in the nucleus. Treatment with either IFN-α or LTβR-agonist BS1 inhibited HBV replication and resulted in deamination and degradation of HBV cccDNA, but not of the HBV-sequence containing replicon (data not shown). This indicated that deamination and subsequent degradation induced by both treatments is HBV cccDNA specific.

HBV core protein associates with A3G (*32*) and HBV cccDNA (*33*) and thus was a candidate to mediate the targeting of A3 deaminases to HBV cccDNA. Confocal microscopy indicated a co-localization of A3A and A3B with HBV core in different cell lines and PHH (**Fig. 5** and data not shown). Chromatin immunoprecipitation (ChIP) experiments using stably (data not shown) or transiently transfected HepG2H1.3 cells or HBV-infected and IFN-α treated dHepaRG cells, showed that HBV

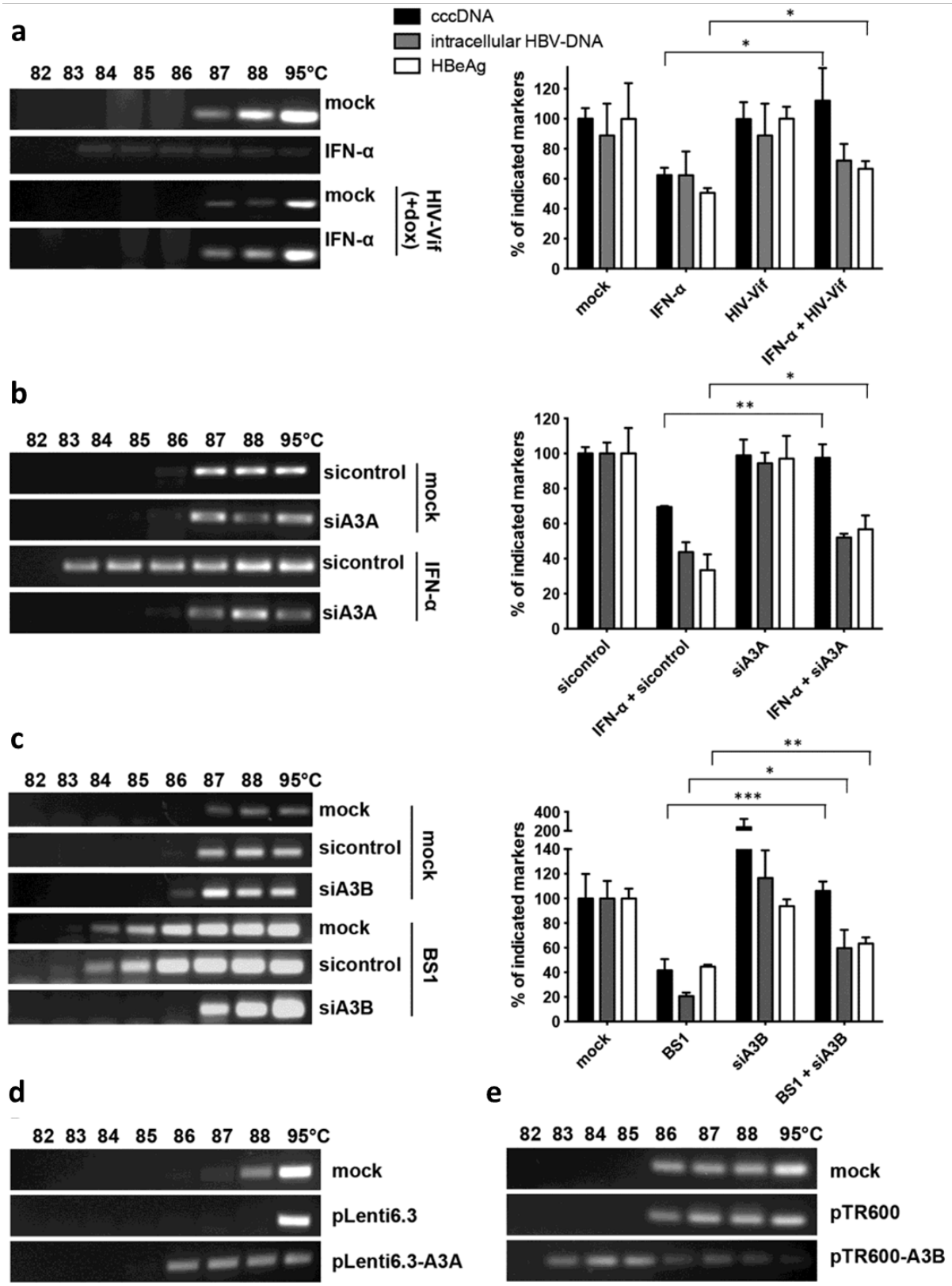

Figure 4: Analysis of cccDNA deamination and degradation. (a to c) cccDNA denaturation was analyzed by 3D-PCR (left panels); levels of HBeAg, total intracellular DNA and cccDNA are given relative to mock treated cells (right panels). (a) dHepaRG-tA-Vif cells treated with IFN-α for 10 days with and without doxycycline (dox)-induced HIV-Vif expression. HBV-infected dHepaRG cells treated with (B) IFN-α or (c) BS1 transfected with siRNA against A3A or A3B, respectively, or sequence nonspecific siRNA (sicontrol). Mean values +/− standard deviation of independent replicates and experiments are given; data were analyzed by *t* test. * $p < 0.05$, ** $p < 0.01$ and *** $p < 0.001$. (d) cccDNA denaturation analysis by 3D-PCR in HepG2-H1.3 cells overexpressing A3A or (e) A3B from lentiviral vector plasmid pLenti6.3 or pTR600, respectively, for 5 days.

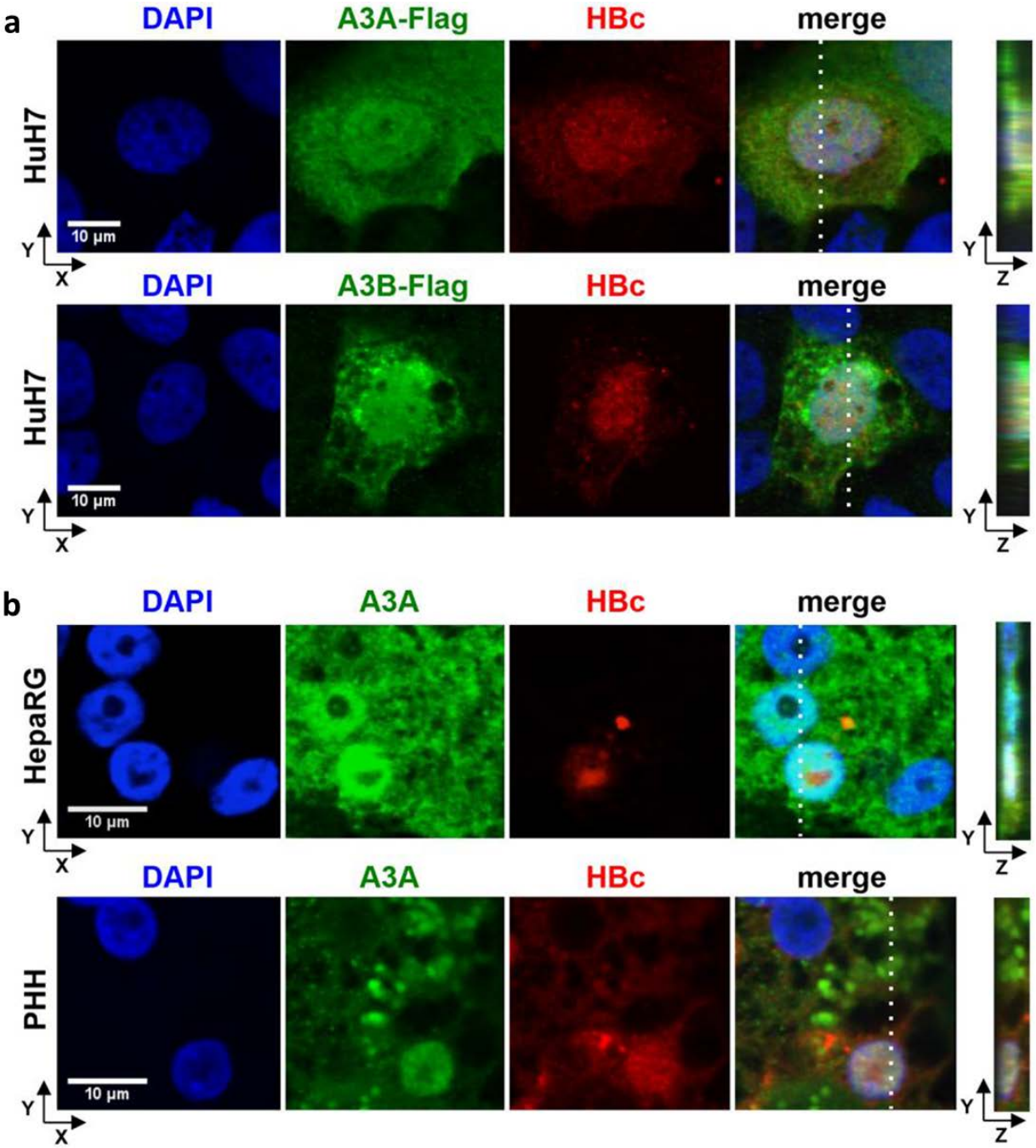

Figure 5: Co-localization of A3A and A3B with HBV core protein (HBc). (A) HuH7 cells were co-transfected with an HBV1.1-fold genome and A3A-Flag or A3B-Flag expressing plasmids and stained using DAPI, anti-HBc and anti-FLAG antibodies. (B) HBV-infected dHepaRG and PHH were treated with IFN-α at day 7 post infection for 3 days. A3A and HBc were analyzed by immunofluorescence staining. Right panels indicate z stacks taken at the dotted lines.

core protein and A3A both bind to the cccDNA minichromosome (**Fig. 6a**). Supporting the possibility that a guardian protein prevents A3A direct binding to DNA (*34*), we could not detect A3A binding to genomic DNA (data not shown) even in the presence of HBV core, which has been reported to also bind to cellular DNA (*35*).

HBV core protein co-immunoprecipitated A3A in HepG2H1.3 cells and transfected HuH7 cells indicating physical interaction with A3A (data not shown). Direct interaction of HBV core expressed after HBV infection and A3A induced by IFN-α was confirmed by proximity ligation assay (PLA) (**Fig. 6b** and data not shown) and fluorescence resonance energy transfer (FRET) analysis (**Fig. 6c**). By deletion analysis, we determined that the central region of HBc (aa 77 to 149) is involved in the interaction with A3A (**Fig. 6c** and data not shown).

These data suggest that A3A is targeted to cccDNA by interaction with HBV core. No such targeting to genomic DNA has been described so far. Since APOBEC3 deaminases are thought to act on single stranded DNA (*36*), one possibility is that A3A and A3B act on cccDNA when it is transiently rendered single-stranded by RNA polymerase II before transcription initiation.

We suggest, therefore, the following mechanism of APOBEC-dependent degradation of HBV cccDNA (**Fig. 6d**). High dose IFN-α treatment or LTβR-activation up-regulate the expression of A3A and A3B, respectively, which subsequently co-localize or directly interact with HBV core in infected hepatocytes, translocate to the nucleus, where they are brought into close contact with cccDNA by HBV core. Now, APOBECs can deaminate cccDNA that is transiently rendered single-stranded during transcription. Uracils in HBV cccDNA are recognized and excised by cellular DNA glycosylases leading to formation of AP sites, which are then recognized by cellular AP endonculeases (*23*) leading to cccDNA digestion. Why cccDNA is degraded instead of being repaired by the cellular DNA repair machinery remains elusive so far. Using a mixture of various enzymes, we were able to repair deaminated cccDNA *in tubo* (**Fig. 3a**) suggesting induction of an additional factor promoting DNA degradation or an impaired function of the repair machinery rather than a lack of recognition by the repair machinery. Thus, we can only speculate that either the number of AP sites introduced after treatment is too high and exceeds the capacity of the cellular repair machinery or that IFN-α treatment or LTβR-activation or even HBV itself (*37*) modulate the repair machinery. This may shift the equilibrium from cccDNA repair (*38*) to degradation.

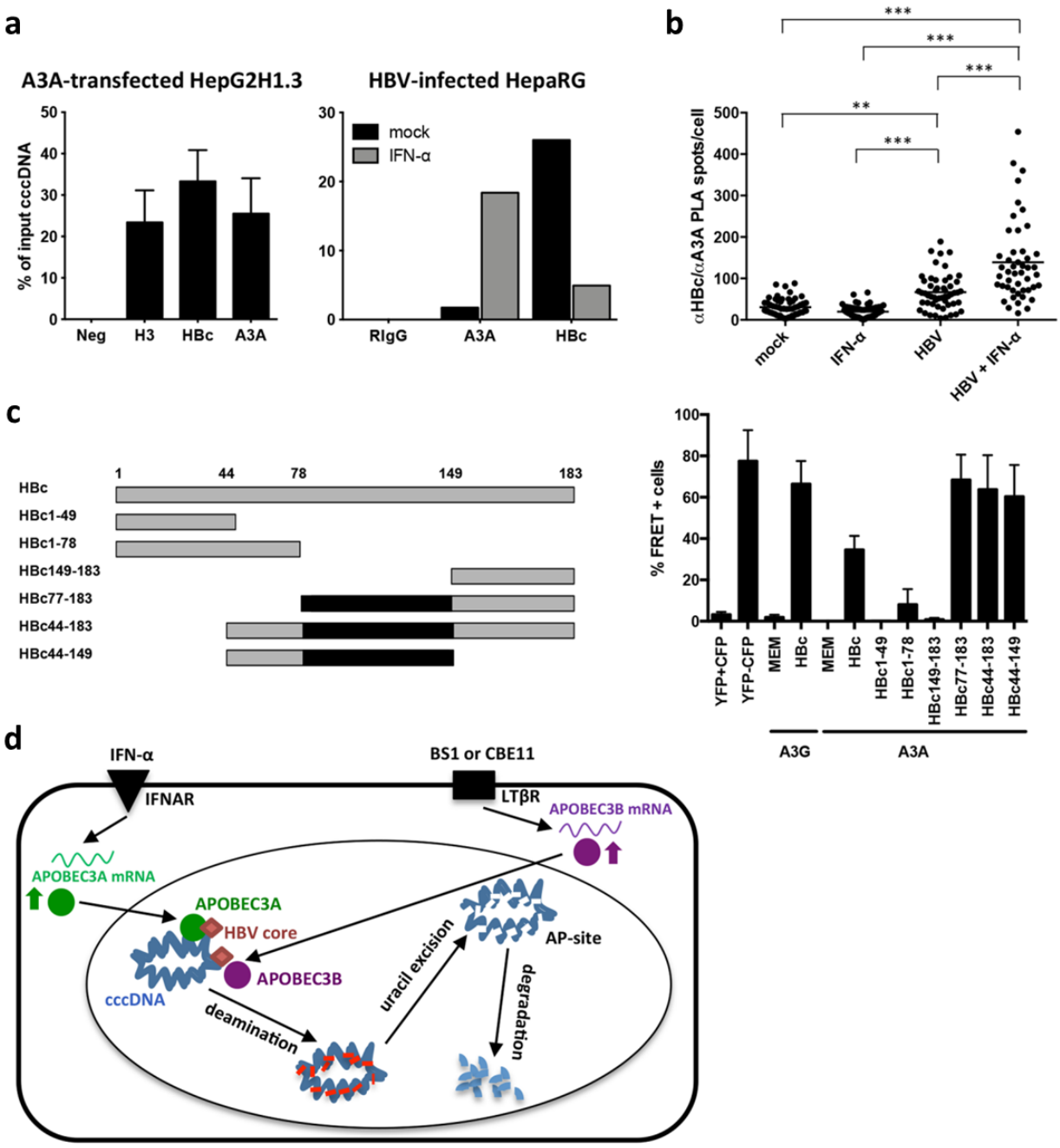

Figure 6: Interaction of A3A, HBV core protein (HBc) and cccDNA. (a) Chromatin immunoprecipitation (ChIP) was performed using lysates of HepG2H1.3 cells transfected with A3A-expressing plasmid, or HBV-infected dHepaRG cells treated with IFN-α for 3 days. IPs using antibodies against histone H3, A3A, HBc and control rabbit IgG (RIgG) were analyzed by qPCR for cccDNA. (b) Interaction between HBc and A3A was assessed by proximity ligation assay (PLA) in HBV-infected, IFN-α treated dHepaRG. PLA-spots were quantified in single cells by software-based spot-counting. Data were analyzed by one-way ANOVA. ** $p < 0.01$ and *** $p < 0.001$. (c) Serial HBV core-deletion mutants (left panel) were fused to CFP and interaction with A3A-YFP was assessed by FACS-FRET in HuH7.5 hepatoma cells (right panel). Cells cotransfected with CFP and YFP served as controls to exclude false positive FRET and subtract background signals. A CFP-YFP fusion construct was used as positive control. Mean values ± standard deviation of FRET-positive cells from 3-4 independent experiments are given. Black boxes indicate shared regions of HBc mutants giving a FRET signal. (d) Model of cccDNA degradation induced by IFN-α treatment or LTβR-activation.

3.2.5. Discussion

Ideally, a cure for HBV infection needs to eliminate cccDNA. Therefore, cytokines or cytokine-receptor agonists that can trigger HBV cccDNA deamination and its degradation are interesting antiviral candidates. Antivirals that induce A3A/B activity should be combined with nucleos(t)ide analogs to avoid the replenishment of nuclear cccDNA after degradation. LTβR-agonists were active at low doses and we did not observe any toxicity in vitro or in vivo nor did we detect any modification of genomic DNA. Constitutive overexpression of LTα/β for more than one year has been associated with inflammatory liver disease and hepatocellular carcinoma (16). As antivirals, however, LTβR-agonists would only be used for a limited period of time minimizing the risk of side effects. Moreover, LTβR-activation was already explored as a cancer treatment (18).

A recent study has shown a significantly higher frequency of an A3B deletion allele in persistent HBV carriers and hepatocellular carcinoma patients compared with healthy controls (25). This finding was further supported by the moderate deamination of cccDNA even in absence of treatment, and by the observation that knockdown of A3B in the absence of any treatment increased cccDNA levels. Although deregulated expression of A3A and A3B has been shown to correlate with genomic DNA mutations (39, 40), we did not detect any alterations of genomic DNA using analyses of AP sites, 3D-PCR analysis and deep sequencing of a set of human genes.

Our data indicate that cccDNA degradation is possible and can be induced without side-effects on the infected host cell. An important task will be testing of combinations of nucleos(t)ide analogs with novel anti-viral strategies (e.g., LTβR agonists or adoptive T-cell therapy (41)) to activate A3A or A3B to cure hepatitis B.

3.2.6. Materials and Methods

3.2.6.1. HBV inocula, cell cultures, HBV infection and treatments

HBV inolula were prepared as described (*42*) Shortly, HBV was concentrated from the supernatant of HepG2.2.15 cells using centrifugal filter devices (Centricon Plus-70, Biomax 100.000, Millipore Corp., Bedford, MA) and titered by HBV-DNA dot blot analysis after sedimentation into a CsCl density gradient to determine enveloped DNA-containing viral particles (vp). Only inocula reaching a titer between $3x10^9$ and $3x10^{10}$ vp/mL were used. Immediately after collection, the virus stock was aliquoted and stored at -80°C until used for infection. Primary Human Hepatocytes (PHH) were isolated from surgical liver resections, cultured and infected with HBV as described (43, 44). Tissue samples and annotated data were obtained and experimental procedures were performed within the

framework of the nonprofit foundation Human Tissue & Cell Research (HTCR), including the informed patient's consent (45). HepG2-H1.3, HepaRG and HepaRG-tA cell culture, differentiation and HBV infection (at a multiplicity of infection of 600 vp/cells) were also performed as described (13,46). HepaRG-tAVifAU1 cell line was obtained after transduction of HepaRG-tA cells with a lentivirus expressing the HIV-Vif gene under tetracyclin regulated promoter (Plvx-Tight-Puro lentiviral vector, Clontech, Saint-Germain-en-Laye, France) and selection using 0.25 µg/ml puromycin.

A3A or A3B overexpression in HepG2H1.3 cells was obtained by transfection of pLenti6.3, pLenti6.3-A3A, pTR600 or pTR600-A3B, respectively, using "Lipofectamine 2000 Reagent" (Invitrogen). No selection took place before experiment start. HepG2-H1.3-A3A cell line was obtained after lentiviral transduction of A3A into HepG2-H1.3 cells (47) and selection using 5ug/ml blasticidin. HepaRG cells were transfected with episomal replicon construct pEpi-H1.3 using "Lipofectamine® 2000 Reagent" (Invitrogen). pEpi-H1.3 was derived by cloning a 1.3-fold HBV genome into the extrachromosomal mammalian replicon plasmid pEpi-eGFP (kindly provided by H.J. Lipps, Witten-Herdecke, Germany). Two days after transfection, selection with 600 µg/ml geneticin was started and kept until cells expressed GFP and reached confluency and expressed GFP. HepaRG+pEpi-H1.3 cells were differentiated for 6 weeks to allow replication of HBV and establishment of HBV cccDNA by nuclear reimport of HBV rcDNA containing capsids. Lamivudine and entecavir were used at 0.5 µM (5-fold and 1000-fold IC 50, respectively), IFN-α (Roferon-A, Roche) at 1000 U/mL and BS1, CBE11 and hu-IgG at 0.5 µg/mL unless otherwise indicated.

3.2.6.2. Analysis of HBV replication intermediates

HBeAg was determined using commercial immunoassays (Siemens Molecular Diagnostics, Marburg, for cell culture supernatants; Abbott Laboratories, Wiesbaden, Germany for mouse sera). Total DNA was purified from infected cells using a "Tissue kit" (Macherey Nagel, Düren, Germany). Total RNA was extracted from infected cells (NucleoSpin® RNA II kit, Macherey Nagel) and transcribed into cDNA using SuperScript III reverse transcriptase (Invitrogen). HBVDNA, cccDNA and pgRNA were detected using specific PCR primers as described (48,17). pEpi-H1.3 was quantified using Kan-L/-R primers (see primer list). Real-time PCRs (qPCR) were performed using the LightCycler™ system (Roche Diagnostics) and analyzed using the second derivative maximum method that includes both normalization to the reference gene (*PrnP* for cccDNA and pEpi-H1.3 and GAPDH for pgRNA) and to primer efficiency (47,49).

cccDNA specific primers spanning the gap and the nick in the rc form of the HBV genome and were designed not to detect rcDNA or a linear 1.1 or 1.3-fold HBV genome. Using optimized PCR conditions on the Light Cycler instrument (95°C for 10**'**, 45 cycles at 95°C for 15**''**, 60°C for 5**''**, 72°C for 45**''**, and

detection at 88°C for 2'' after each cycle), we determined the specificity to amplify cccDNA over rcDNA to be 103 to 1. For Southern Blot analyses, cccDNA was extracted from HBV-infected cells using the KCl protein precipitation method, separated through 0.8 % agarose gel, blotted onto nylon membrane and hybridized with 32P HBV-DNA probe (50, 51). Quantification of cccDNA by qPCR was confirmed by quantification from Southern blotting as exemplarily shown in Figure S3B.

3.2.6.3. 3D-PCR

PCR products from cccDNA-specific qPCR were diluted 1/20 to 1/50 and used as templates for nested PCR using HBxin fw and HBxin rev primers (see primer list) and decreasing denaturation temperatures as indicated. PCR products were purified by gel extraction (GeneJET Gel Extraction Kit, Fermentas, Fisher Scientific - Germany, Schwerte, Germany) and cloned by TA cloning (TA Cloning® Kit, Invitrogen). DNA from individual clones was purified (GeneJET Plasmid Miniprep Kit, Fermentas, Fisher Scientific - Germany GmbH) and sequenced using primers hybridizing to the 5' and 3' plasmid backbone.

3.2.6.4. AP site quantification and repair

AP site quantification was performed with OxiSelect™ Oxidative DNA Damage Quantitation Kit (AP sites) (STA-324, Cell Biolabs, San Diego, CA, USA) according to the manufacturer's instruction using 0.5 µg of purified DNA (100 µg/mL). 1µg of total DNA were digested with 10 units of apurinic apyrimidinic endonuclease redox effector factor-1 (APE1; M0282L, New England Biolabs, Inc., Ipswich, MA, USA) or 1 µl PreCR Repair Mix (M0309L, New England Biolabs, Inc.).

3.2.6.5. qRT-PCR

For qRT-PCR RNA was extracted using commercial kits (RNeasy-kit from Qiagen, Hilden, Germany or NucleoSpin® RNA II kit, Macherey Nagel) and transcribed into cDNA with the Quantitect Reverse Transcription kit (Qiagen) or with SuperScript III reverse transcriptase (Invitrogen) according to the manufacturer's instructions. Expression levels were quantified by qRT-PCR performed on a 7900 HT qRT-PCR system (Applied Biosystems, Life Technologies Darmstadt, Germany) using the CT method or on a LightCycler™ system (Roche Diagnostics) and analyzed using the second derivative maximum method that includes both normalization to the reference genes and primer efficiency. Relative mRNA levels of all target genes were normalized to at least two house-keeping genes (HPRT; RHOT2; TBP; GAPDH) levels.

3.2.6.6. siRNA and antibodies

siRNAs were obtained from Thermo Fisher Scientific Dharmacon® (Lafayette, CO, USA) : control siRNA (D-001910-10-05 Acell non-targeting pool 5nmol), siRNA against A3B (E-017322-00-0005, Accell SMARTpool, Human A3B (9582), 5 nmol) or siRNA against A3A (#E-017432-00, Accell SMARTpool). For Western blot analyses, immunostaining and immunoprecipitation, the following primary antibodies were used: polyclonal anti-NFkB2 p100/p52 (#4882, Cell Signaling Technology, Inc, Danvers, MA, USA), anti-phospho-RelA (#RB-1638-P0, Cell Signaling Technology), monoclonal anti-GAPDH (clone 14C10) (Cell Signaling Technology), anti-β actin (clone 13E5) (Cell Signaling Technology), polyclonal anti-LTβR (#sc-8375,Santa Cruz Biotechnology, Inc, Heidelberg, Germany), anti-phospho-NIK (#4994, Santa Cruz Biotechnology), anti-TNFRI (#ab19139, Abcam, Cambridge, MA, USA), rabbit anti-HBVcore antiserum H800 (kindly provided by Heinz Schaller, Heidelberg, Germany), rabbit polyclonal anti-HBVcore (B0586, Dako, Hamburg, Germany), mouse monoclonal anti-HBVcore (F8.27.2, kindly provided by Dr. Marie-Anne Petit), anti-RelB (#sc-226, Santa Cruz Biotechnology), polyclonal anti–A3A (#AP31973PU-N, Acris Antibodies GmbH, Herford, Germany), polyclonal anti–A3F (#H00200316-A01; Abnova, Aachen, Germany), polyclonal anti–A3G (#AP23049PU-N, Acris Antibodies GmbH), polyclonal anti–AU1 (#A190-125A-2, Bethyl Laboratories, Inc., Montgomery, TX, USA), polyclonal anti-A3B (#sc-130955, Santa Cruz Biotechnology Inc), anti-Flag (F7425, Sigma), anti-TBP polyclonal antibody (H00006908-A01, Bethyl, USA), polyclonal anti–histone H3 (#ab1791, Abcam).

3.2.6.7. Deep sequencing

Target genes were amplified from total DNA by PCR using primers designed to span around 2000bp of genomic sequence containing at least one exon and one intron. PCR reaction was performed with the Advantage®-HF2 PCR-kit (Clontech). Subsequently, amplicons were separated by a 0.8% agarose gel and purified using the S.N.A.P.TM UV-free gel purification kit (Life Technologies). Purified amplicons were submitted for deep sequencing to a commercial provider (GATC Biotech, Konstanz, Germany) and analyzed using Hiseq2000 sequencing system (Illumina, San Diego, CA, USA). Sequencing data were analyzed with CLC Genomics Workbench 6.01 (CLC bio, Aarhus, Denmark).

3.2.6.8. Immunofluorescence microscopy

Cells grown on 4-well-glass slide (Lab-Tek II, Fisher Scientific - Germany, Schwerte, Germany) were fixed with 4% paraformaldehyde (PFA) in PBS pH 7.4 for 10 min at room temperature and permeabilized with 0.5% saponin. Slides were blocked in PBS containing 0.5% saponin and 10% serum from the species that the secondary antibody was raised in at room temperature for two hours. After blocking, primary antibodies diluted in PBS with 0.1% saponin and 10% blocking serum

were added overnight at 4°C. After extensive washing, slides were incubated with the secondary antibody in PBS with 0.1% saponin and 2% blocking serum for 2 hours at room temperature in the dark. Slides were mounted with Dapi Fluoromount-G (SouthernBiotech, Birmingham, Alabama, USA) and images were captured with a Olympus FV10i confocal Microscope (Olympus, Germany).

3.2.6.9. Expression profile analyses

Total RNA was amplified and labeled using WT Expression Kit (Ambion, Life Technologies) and Terminal labeling Kit (Affymetrix, Santa Clara, CA, USA) according to the manufacturer's recommendations. The amplified and fragmented, biotinylated complementary RNA was hybridized to Affymetrix Human Gene 1.0 ST Arrays (33297 probe sets) using standard procedures. The experimental setup contained a total of 8 arrays, made up of 2 groups, with each group consisting of 4 biological replicates. Arrays were assessed for quality and robust multiarray average (RMA)-normalized. Quality assessment consisted of RNA degradation plots, Affymetrix quality control metrics, sample cross-correlation, and probe-level visualizations. Normalization included (separately for each RNA-type data set) background correction, quantile normalization, and probe-level summation by RMA. Data were analyzed for differential gene expression using an empirical Bayes moderated t-test (52), implemented in the Bioconductor package Linear Models for Microarray Data LIMMA. Results were sorted by the adjusted pvalue and exported in tab-delimited format. Samples with an up- or downregulation ≥ 2 were reanalyzed by qRT-PCR. Microarray data have been submitted to the GEO database (http://www.ncbi.nlm.nih.gov/geo/) and have the accession number GSE46667.

3.2.6.10. Immunoprecipitation assays

Co-Immunoprecipitations were performed using Pierce Co-Immunoprecipitation Kit (Fisher Scientific, Schwerte, Germany) according to the manufacturer's instructions. Chromatin immunoprecipitation was performed using Pierce Agarose ChIP Kit (#26156, Fisher Scientific) or ChIP kit #ab500 (Abcam, Cambridge, UK). Non-sheared DNA for cccDNA or MNase digested DNA for genomic DNA was analyzed by specific qPCR (GAPDH, P53, SRC, cMyc promoter regions).

3.2.6.11. FACS-based FRET

For FACS-FRET analysis we used a FACS CantoII Cytometer (BD Bioscience) with 405 nm, 488 nm and 633 nm lasers. Gating strategy and experimental procedures were done as described previously (*14*). eYFP was excited with 488 nm and detected with a 529/24 filter (Semrock, New York, USA) and eCFP was excited with 405 nm and detected via the 450/40 filter (Semrock). Huh7.5 hepatoma cells transfected with 1.6 µg DNA per 250.000 cells using Lipofectamine (Life technology) were used for

FRET analysis. After 24 h, cells were washed, trypsinized and analyzed by flow cytometry using excitation at 405 nm followed by signal detection with the 529/24 filter. Mock transfected cells, eCFP and eYFP only as well as eCFP/eYFP co-transfected cells served as controls to exclude false positive FRET and subtract background signals. An eCFP-eYFP fusion construct was used as positive control. FRET constructs used within this study were all fused to eCFP/eYFP via their C-terminus using the *NheI-AgeI* restriction sites as previously described (53). PCR derived inserts were sequenced to confirm their identity.

3.2.6.12. Proximity ligation assay (PLA)

For PLA, cells were fixed with 1 % PFA, washed and permeabilized for 20 min with 1 % Saponin in PBS and blocked for 45 min with PLA blocking solution. Polyclonal rabbit anti- HBVcore and goat anti-A3A antibodies were incubated at a concentration of 1:100 in 1 % BSA for 2 h at RT. Secondary antibody probe incubation, ligation and amplification reactions were done according to the manufacturer's instructions (Duolink, Sigma Aldrich). Spinning disc microscopy with a Nikon Ti Eclipse microscope equipped with a Perkin Elmer UltraViewVox System (Yokogawa CSU-X1) was done for sample imaging. Images were analyzed with the Volocity 6.2 software package (Perkin Elmer) and the implemented automated spot counting was used to assess the number of spots per cropped cell. Statistical analysis was done with GraphPad Prism 5.0 and a one-way analysis of variances (ANOVA).

3.2.6.13. Modeling of HBc/A3A interaction

A three-dimensional structure of HBV core protein was generated by automatic modeling mode of SWISS-MODEL server (swissmodel.expasy.org) (54). The crystal structure of the human hepatitis B virus capsid (PDB code 1QGT, chains D) (55) was adapted as a template to perform the homology-modeling. In silico docking of A3A (PDB code 2M65) (56) and modeled HBVcore was carried out by using Hex protein docking server (http://hexserver.loria.fr/) (57). The result was displayed and analyzed by Rasmol 2.7.5 (58).

3.2.6.14. HBV-transgenic mice and tissue analysis

6 months old, male hepatitis B virus transgenic mice (C57BL/6, strain HBV1.3.32) (59) received murine lymphotoxin-receptor agonizing (ACH6) or isotype control antibodies intra-peritoneally (2 mg/kg, body weight) three times a week. Animals were maintained under specified pathogenfree conditions. Experiments were performed in accordance to the German legislation governing animal studies and the Principles of Laboratory Animal Care guidelines, NIH (55.1-1-54-2531.3-27-08). Mice were sacrificed at indicated time points and serum as well as liver tissues were obtained. Murine livers were fixed in phosphate buffered saline containing 4% PFA for 24 hours. Fixed liver specimens

were embedded in paraffin and 2 µm sections were mounted on glass slides. Immuno-histochemical stainings were performed with cleaved caspase 3 (Cell Signaling), HBVcore (Diagnostic Biosystems, Pleasanton, CA, USA), RelA (NeoMarkers / Lab vision corporation, Fremont, CA, USA) and RelB (Santa Cruz Biotechnology Inc.) specific antibodies employing an automated BOND-MAX™ platform (Leica Biosystems, Wetzlar, Germany). Positively stained cells were counted in five independent high-power fields and extrapolated to numbers per square millimeter tissue area. Fresh murine liver tissue were homogenized mechanically and lysed in buffer (Tris-HCL [10mM], NaCl [100mM], EDTA [5mM], Triton-X100 [5%]) containing protease inhibitor (Roche Diagnostics). Lysates (30 µg/ lane) were subjected to 15% SDS-PAGE (Bio-Rad, München, Germany) and blotted on nitrocellulose membranes (Bio-Rad) for Western blot analyses. Northern blot analyses were performed with total RNA isolated from cryopreserved liver tissue using TIRZOL® (Invitrogen).

3.2.6.15. Human chimeric uPA/SCID mice

Human liver-chimeric UPA/SCID mice were generated by transplanting one million thawed primary human hepatocytes and housed under specific pathogen-free conditions in accordance with protocols approved by the Ethical Committee of the city and state of Hamburg (permission number G12/015) (60). Levels of human chimerism were determined by measuring human serum albumin (HSA) in mouse serum (Human Albumin ELISA kit, Immunology Consultants Lab, Portland, USA) (61). HBV-infected mice received human lymphotoxin-receptor agonizing (CBE11) or isotype control antibodies intra-peritoneally (2mg/kg, body weight) once per week after macrophage depletion using clodronate liposomes (http://clodronateliposomes.org). Liver specimens collected at sacrifice were snap-frozen in 2-methylbutane for molecular analyses.

3.2.6.16. Chimpanzees

Remaining liver biopsies from a study performed on chimpanzees in 2004 were used (26). The study protocol was approved at the Southwest Foundation for Biomedical Research, San Antonio, TX (IACUC 869 PT, approved in 2004). Briefly, animals were treated with 10 million IU of recombinant human interferon-alpha2a and serial liver biopsies were performed at various time points to monitor induction of hepatic genes. Total RNA was extracted from chimpanzee liver biopsies with Trizol reagent (Life Science) and quantified using the NanoDrop spectrophotometer (NanoDrop Technologies). For each reverse transcription reaction, 360 ng of total RNA was converted into cDNA with Transcriptor First Strand cDNA Synthesis kit (Roche, Indianapolis, IN, USA) in 20 ul reaction volume. Taqman assay was used to assess the relative level of the selected transcripts by normalizing to 18s RNA with the delta/delta Ct calculation method. Primers and probes were designed and synthesized by Integration DNA Technologies (Coraville, IA). All qPCR reactions were performed in a

10 µl volume and run on ABI VIIA 7 (Applied Biosystems, Foster City, CA, USA). Each reaction contained 5 µl 2X TaqMan universal PCR master mix (Applied Biosystems,), 0.5 uM of each primer, 0.25 uM of the probe, and cDNA (equivalent to ~16 ng total RNA). The amplification profile was initiated by 10 minute incubation at 95 °C, followed by two-step amplification of 15 seconds at 95 °C and 60 seconds at 60 °C for 40 cycles. For each treatment, results were expressed relative to the expression of the pre-treated chimpanzee liver biopsies as fold-induction.

3.2.6.17. Analyses of HCV-infected patients treated with PEG-IFN-α

To investigate the effect of IFN-α treatment on APOBEC RNA expression in the human liver we used previously published microarray data of paired liver biopsies from HCV-infected patients undergoing antiviral therapy (62) (Michael T. Dill, Zuzanna Makowska, Gaia Trincucci, Andreas J. Gruber, Julia E. Vogt, Magdalena Filipowicz, Diego Calabrese, Ilona Krol, Daryl T. Lau, Luigi Terracciano, Erik van Nimwegen, Volker Roth, and Markus H. Heim. Pegylated interferon-α regulates hepatic gene expression by transient activation of the Jak-STAT pathway. Journal of Clinical Investigation, in press). This study included 18 HCV patients who all had a liver biopsy performed during the diagnostic workup and a second liver biopsy collected 4h, 16h, 48h, 96h, or 144h after the first injection of 1.5 ug/kg body weight pegIFNalpha-2b (PegIntronTM, MSD). The patients were subsequently treated with standard combination therapy of pegIFNalpha-2b and ribavirin.

3.2.7. References

1. U. Protzer, M. K. Maini, P. A. Knolle, Living in the liver: hepatic infections. *Nat. Rev. Immunol.* **12**, 201–213 (2012). doi:10.1038/nri3169 Medline
2. F. Zoulim, Hepatitis B virus resistance to antiviral drugs: where are we going? *Liver Int.* **31**, (Suppl 1), 111–116 (2011). doi:10.1111/j.1478-3231.2010.02399.x Medline
3. K. Wursthorn, M. Lutgehetmann, M. Dandri, T. Volz, P. Buggisch, B. Zollner, T. Longerich, P. Schirmacher, F. Metzler, M. Zankel, C. Fischer, G. Currie, C. Brosgart, J. Petersen, Peginterferon alpha-2b plus adefovir induce strong cccDNA decline and HBsAg reduction in patients with chronic hepatitis B. *Hepatology* **44**, 675–684 (2006). doi:10.1002/hep.21282 Medline
4. L. G. Guidotti, K. Ando, M. V. Hobbs, T. Ishikawa, L. Runkel, R. D. Schreiber, F. V. Chisari, Cytotoxic T lymphocytes inhibit hepatitis B virus gene expression by a noncytolytic mechanism in transgenic mice. *Proc. Natl. Acad. Sci. U.S.A.* **91**, 3764–3768 (1994). doi:10.1073/pnas.91.9.3764 Medline

5. L. G. Guidotti, R. Rochford, J. Chung, M. Shapiro, R. Purcell, F. V. Chisari, Viral clearance without destruction of infected cells during acute HBV infection. *Science* **284**, 825–829 (1999). doi:10.1126/science.284.5415.825 Medline
6. S. F. Wieland, H. C. Spangenberg, R. Thimme, R. H. Purcell, F. V. Chisari, Expansion and contraction of the hepatitis B virus transcriptional template in infected chimpanzees. *Proc. Natl. Acad. Sci. U.S.A.* **101**, 2129–2134 (2004). doi:10.1073/pnas.0308478100 Medline
7. H. McClary, R. Koch, F. V. Chisari, L. G. Guidotti, Relative sensitivity of hepatitis B virus and other hepatotropic viruses to the antiviral effects of cytokines. *J. Virol.* **74**, 2255–2264 (2000). doi:10.1128/JVI.74.5.2255-2264.2000 Medline
8. L. Belloni, L. Allweiss, F. Guerrieri, N. Pediconi, T. Volz, T. Pollicino, J. Petersen, G. Raimondo, M. Dandri, M. Levrero, IFN-α inhibits HBV transcription and replication in cell culture and in humanized mice by targeting the epigenetic regulation of the nuclear cccDNA minichromosome. *J. Clin. Invest.* **122**, 529–537 (2012). doi:10.1172/JCI58847 Medline
9. A. Rang, S. Günther, H. Will, Effect of interferon alpha on hepatitis B virus replication and gene expression in transiently transfected human hepatoma cells. *J. Hepatol.* **31**, 791–799 (1999). doi:10.1016/S0168-8278(99)80279-7 Medline
10. V. Pasquetto, S. F. Wieland, S. L. Uprichard, M. Tripodi, F. V. Chisari, Cytokine-sensitive replication of hepatitis B virus in immortalized mouse hepatocyte cultures. *J. Virol.* **76**, 5646–5653 (2002). doi:10.1128/JVI.76.11.5646-5653.2002 Medline
11. S. F. Wieland, L. G. Guidotti, F. V. Chisari, Intrahepatic induction of alpha/beta interferon eliminates viral RNA-containing capsids in hepatitis B virus transgenic mice. *J. Virol.* **74**, 4165–4173 (2000). doi:10.1128/JVI.74.9.4165-4173.2000 Medline
12. S. L. Uprichard, S. F. Wieland, A. Althage, F. V. Chisari, Transcriptional and posttranscriptional control of hepatitis B virus gene expression. *Proc. Natl. Acad. Sci. U.S.A.* 100, 1310–1315 (2003). doi:10.1073/pnas.252773599 Medline
13. P. Gripon, C. Diot, N. Thézé, I. Fourel, O. Loreal, C. Brechot, C. Guguen-Guillouzo, Hepatitis B virus infection of adult human hepatocytes cultured in the presence of dimethyl sulfoxide. *J. Virol.* **62**, 4136–4143 (1988). Medline
14. 14. P. Gripon, S. Rumin, S. Urban, J. Le Seyec, D. Glaise, I. Cannie, C. Guyomard, J. Lucas, C. Trepo, C. Guguen-Guillouzo, Infection of a human hepatoma cell line by hepatitis B virus. *Proc. Natl. Acad. Sci. U.S.A.* **99**, 15655–15660 (2002). doi:10.1073/pnas.232137699 Medline
15. 15. M. J. Wolf, G. M. Seleznik, N. Zeller, M. Heikenwalder, The unexpected role of lymphotoxin beta receptor signaling in carcinogenesis: from lymphoid tissue formation to liver and prostate cancer development. *Oncogene* **29**, 5006–5018 (2010). doi:10.1038/onc.2010.260 Medline

16. 16. J. Haybaeck, N. Zeller, M. J. Wolf, A. Weber, U. Wagner, M. O. Kurrer, J. Bremer, G. Iezzi, R. Graf, P. A. Clavien, R. Thimme, H. Blum, S. A. Nedospasov, K. Zatloukal, M. Ramzan, S. Ciesek, T. Pietschmann, P. N. Marche, M. Karin, M. Kopf, J. L. Browning, A. Aguzzi, M. Heikenwalder, A lymphotoxin-driven pathway to hepatocellular carcinoma. *Cancer Cell* **16**, 295–308 (2009). doi:10.1016/j.ccr.2009.08.021 Medline
17. 17. S. Jost, P. Turelli, B. Mangeat, U. Protzer, D. Trono, Induction of antiviral cytidine deaminases does not explain the inhibition of hepatitis B virus replication by interferons. *J. Virol.* **81**, 10588–10596 (2007). doi:10.1128/JVI.02489-06 Medline
18. 18. M. Lukashev, D. LePage, C. Wilson, V. Bailly, E. Garber, A. Lukashin, A. Ngam-ek, W. Zeng, N. Allaire, S. Perrin, X. Xu, K. Szeliga, K. Wortham, R. Kelly, C. Bottiglio, J. Ding, L. Griffith, G. Heaney, E. Silverio, W. Yang, M. Jarpe, S. Fawell, M. Reff, A. Carmillo, K. Miatkowski, J. Amatucci, T. Crowell, H. Prentice, W. Meier, S. M. Violette, F. Mackay, D. Yang, R. Hoffman, J. L. Browning, Targeting the lymphotoxin-beta receptor with agonist antibodies as a potential cancer therapy. *Cancer Res.* **66**, 9617–9624 (2006). doi:10.1158/0008-5472.CAN-06-0217 Medline
19. 19. X. Hu, M. A. Zimmerman, K. Bardhan, D. Yang, J. L. Waller, G. B. Liles, J. R. Lee, R. Pollock, D. Lev, C. F. Ware, E. Garber, V. Bailly, J. L. Browning, K. Liu, Lymphotoxin β receptor mediates caspase-dependent tumor cell apoptosis in vitro and tumor suppression in vivo despite induction of NF-κB activation. *Carcinogenesis* **34**, 1105–1114 (2013). doi:10.1093/carcin/bgt014 Medline
20. 20. E. Dejardin, N. M. Droin, M. Delhase, E. Haas, Y. Cao, C. Makris, Z. W. Li, M. Karin, C. F. Ware, D. R. Green, The lymphotoxin-beta receptor induces different patterns of gene expression via two NF-kappaB pathways. *Immunity* **17**, 525–535 (2002). doi:10.1016/S1074-7613(02)00423-5 Medline
21. 21. R. Suspène, D. Guétard, M. Henry, P. Sommer, S. Wain-Hobson, J. P. Vartanian, Extensive editing of both hepatitis B virus DNA strands by APOBEC3 cytidine deaminases in vitro and in vivo. *Proc. Natl. Acad. Sci. U.S.A.* **102**, 8321–8326 (2005). doi:10.1073/pnas.0408223102 Medline
22. 22. J. I. Friedman, J. T. Stivers, Detection of damaged DNA bases by DNA glycosylase enzymes. *Biochemistry* **49**, 4957–4967 (2010). doi:10.1021/bi100593a Medline
23. 23. M. D. Stenglein, M. B. Burns, M. Li, J. Lengyel, R. S. Harris, APOBEC3 proteins mediate the clearance of foreign DNA from human cells. *Nat. Struct. Mol. Biol.* **17**, 222–229 (2010). doi:10.1038/nsmb.1744 Medline
24. 24. M. Bonvin, F. Achermann, I. Greeve, D. Stroka, A. Keogh, D. Inderbitzin, D. Candinas, P. Sommer, S. Wain-Hobson, J. P. Vartanian, J. Greeve, Interferon-inducible expression of

APOBEC3 editing enzymes in human hepatocytes and inhibition of hepatitis B virus replication. *Hepatology* **43**, 1364–1374 (2006). doi:10.1002/hep.21187 Medline

25. 25. T. Zhang, J. Cai, J. Chang, D. Yu, C. Wu, T. Yan, K. Zhai, X. Bi, H. Zhao, J. Xu, W. Tan, C. Qu, D. Lin, Evidence of associations of APOBEC3B gene deletion with susceptibility to persistent HBV infection and hepatocellular carcinoma. *Hum. Mol. Genet.* **22**, 1262–1269 (2013). doi:10.1093/hmg/dds513 Medline
26. 26. Y. Huang, J. J. Feld, R. K. Sapp, S. Nanda, J. H. Lin, L. M. Blatt, M. W. Fried, K. Murthy, T. J. Liang, Defective hepatic response to interferon and activation of suppressor of cytokine signaling 3 in chronic hepatitis C. *Gastroenterology* **132**, 733–744 (2007). doi:10.1053/j.gastro.2006.11.045 Medline
27. 27. B. P. Doehle, A. Schäfer, B. R. Cullen, Human APOBEC3B is a potent inhibitor of HIV-1 infectivity and is resistant to HIV-1 Vif. *Virology* **339**, 281–288 (2005). doi:10.1016/j.virol.2005.06.005 Medline
28. G. Berger, J. Turpin, S. Cordeil, K. Tartour, X. N. Nguyen, R. Mahieux, A. Cimarelli, Functional analysis of the relationship between Vpx and the restriction factor SAMHD1. *J. Biol. Chem.* **287**, 41210–41217 (2012). doi:10.1074/jbc.M112.403816 Medline
29. H. Muckenfuss, M. Hamdorf, U. Held, M. Perkovic, J. Löwer, K. Cichutek, E. Flory, G. G. Schumann, C. Münk, APOBEC3 proteins inhibit human LINE-1 retrotransposition. *J. Biol. Chem.* **281**, 22161–22172 (2006). doi:10.1074/jbc.M601716200 Medline
30. C. Münk, A. Willemsen, I. G. Bravo, An ancient history of gene duplications, fusions and losses in the evolution of APOBEC3 mutators in mammals. *BMC Evol. Biol.* **12**, 71 (2012). doi:10.1186/1471-2148-12-71 Medline
31. M. A. Carpenter, M. Li, A. Rathore, L. Lackey, E. K. Law, A. M. Land, B. Leonard, S. M. Shandilya, M. F. Bohn, C. A. Schiffer, W. L. Brown, R. S. Harris, Methylcytosine and normal cytosine deamination by the foreign DNA restriction enzyme APOBEC3A. *J. Biol. Chem.* **287**, 34801–34808 (2012). doi:10.1074/jbc.M112.385161 Medline
32. P. Turelli, B. Mangeat, S. Jost, S. Vianin, D. Trono, Inhibition of hepatitis B virus replication by APOBEC3G. *Science* **303**, 1829 (2004). doi:10.1126/science.1092066 Medline
33. C. T. Bock, S. Schwinn, S. Locarnini, J. Fyfe, M. P. Manns, C. Trautwein, H. Zentgraf, Structural organization of the hepatitis B virus minichromosome. *J. Mol. Biol.* **307**, 183–196 (2001). doi:10.1006/jmbi.2000.4481 Medline
34. M. M. Aynaud, R. Suspène, P. O. Vidalain, B. Mussil, D. Guétard, F. Tangy, S. Wain-Hobson, J. P. Vartanian, Human Tribbles 3 protects nuclear DNA from cytidine deamination by APOBEC3A. *J. Biol. Chem.* **287**, 39182–39192 (2012). doi:10.1074/jbc.M112.372722 Medline

35. Y. Guo, W. Kang, X. Lei, Y. Li, A. Xiang, Y. Liu, J. Zhao, J. Zhang, Z. Yan, Hepatitis B viral core protein disrupts human host gene expression by binding to promoter regions. *BMC Genomics* **13**, 563 (2012). doi:10.1186/1471-2164-13-563 Medline
36. H. C. Smith, R. P. Bennett, A. Kizilyer, W. M. McDougall, K. M. Prohaska, Functions and regulation of the APOBEC family of proteins. *Semin. Cell Dev. Biol.* **23**, 258–268 (2012). doi:10.1016/j.semcdb.2011.10.004 Medline
37. T. H. Lee, S. J. Elledge, J. S. Butel, Hepatitis B virus X protein interacts with a probable cellular DNA repair protein. *J. Virol.* **69**, 1107–1114 (1995). Medline
38. K. Kitamura, Z. Wang, S. Chowdhury, M. Simadu, M. Koura, M. Muramatsu, Uracil DNA glycosylase counteracts APOBEC3G-induced hypermutation of hepatitis B viral genomes: excision repair of covalently closed circular DNA. *PLoS Pathog.* **9**, e1003361 (2013). doi:10.1371/journal.ppat.1003361 Medline
39. S. Landry, I. Narvaiza, D. C. Linfesty, M. D. Weitzman, APOBEC3A can activate the DNA damage response and cause cell-cycle arrest. *EMBO Rep.* **12**, 444–450 (2011). doi:10.1038/embor.2011.46 Medline
40. M. B. Burns, L. Lackey, M. A. Carpenter, A. Rathore, A. M. Land, B. Leonard, E. W. Refsland, D. Kotandeniya, N. Tretyakova, J. B. Nikas, D. Yee, N. A. Temiz, D. E. Donohue, R. M. McDougle, W. L. Brown, E. K. Law, R. S. Harris, APOBEC3B is an enzymatic source of mutation in breast cancer. *Nature* **494**, 366–370 (2013). doi:10.1038/nature11881 Medline
41. K. Krebs, N. Böttinger, L. R. Huang, M. Chmielewski, S. Arzberger, G. Gasteiger, C. Jäger, E. Schmitt, F. Bohne, M. Aichler, W. Uckert, H. Abken, M. Heikenwalder, P. Knolle, U. Protzer, T cells expressing a chimeric antigen receptor that binds hepatitis B virus envelope proteins control virus replication in mice. *Gastroenterology* **145**, 456–465 (2013). doi:10.1053/j.gastro.2013.04.047 Medline
42. J. Lucifora, S. Arzberger, D. Durantel, L. Belloni, M. Strubin, M. Levrero, F. Zoulim, O. Hantz, U. Protzer, Hepatitis B virus X protein is essential to initiate and maintain virus replication after infection. *J. Hepatol.* **55**, 996–1003 (2011). doi:10.1016/j.jhep.2011.02.015 Medline
43. H. Schulze-Bergkamen, A. Untergasser, A. Dax, H. Vogel, P. Büchler, E. Klar, T. Lehnert, H. Friess, M. W. Büchler, M. Kirschfink, W. Stremmel, P. H. Krammer, M. Müller, U. Protzer, Primary human hepatocytes—a valuable tool for investigation of apoptosis and hepatitis B virus infection. *J. Hepatol.* **38**, 736–744 (2003). doi:10.1016/S0168-8278(03)00120-X Medline
44. S. M. Lee, C. Schelcher, M. Demmel, M. Hauner, W. E. Thasler, Isolation of human hepatocytes by a two-step collagenase perfusion procedure. *J. Vis. Exp.* (79): (2013). Medline
45. W. E. Thasler, T. S. Weiss, K. Schillhorn, P. T. Stoll, B. Irrgang, K. W. Jauch, Charitable State-Controlled Foundation Human Tissue and Cell Research: Ethic and Legal Aspects in the Supply

of Surgically Removed Human Tissue For Research in the Academic and Commercial Sector in Germany. *Cell Tissue Bank.* **4**, 49–56 (2003). doi:10.1023/A:1026392429112 Medline

46. O. Hantz, R. Parent, D. Durantel, P. Gripon, C. Guguen-Guillouzo, F. Zoulim, Persistence of the hepatitis B virus covalently closed circular DNA in HepaRG human hepatocyte-like cells. *J. Gen. Virol.* **90**, 127–135 (2009). doi:10.1099/vir.0.004861-0 Medline
47. M. Quasdorff, M. Hösel, M. Odenthal, U. Zedler, F. Bohne, P. Gripon, H. P. Dienes, U. Drebber, D. Stippel, T. Goeser, U. Protzer, A concerted action of HNF4alpha and HNF1alpha links hepatitis B virus replication to hepatocyte differentiation. *Cell. Microbiol.* **10**, 1478–1490 (2008). doi:10.1111/j.1462-5822.2008.01141.x Medline
48. U. Protzer, S. Seyfried, M. Quasdorff, G. Sass, M. Svorcova, D. Webb, F. Bohne, M. Hösel, P. Schirmacher, G. Tiegs, Antiviral activity and hepatoprotection by heme oxygenase-1 in hepatitis B virus infection. *Gastroenterology* **133**, 1156–1165 (2007). doi:10.1053/j.gastro.2007.07.021 Medline
49. A. Untergasser, U. Zedler, A. Langenkamp, M. Hösel, M. Quasdorff, K. Esser, H. P. Dienes, B. Tappertzhofen, W. Kolanus, U. Protzer, Dendritic cells take up viral antigens but do not support the early steps of hepatitis B virus infection. *Hepatology* **43**, 539–547 (2006). doi:10.1002/hep.21048 Medline
50. J. Summers, P. M. Smith, A. L. Horwich, Hepadnavirus envelope proteins regulate covalently closed circular DNA amplification. *J. Virol.* **64**, 2819–2824 (1990). Medline
51. W. Gao, J. Hu, Formation of hepatitis B virus covalently closed circular DNA: removal of genome-linked protein. *J. Virol.* **81**, 6164–6174 (2007). doi:10.1128/JVI.02721-06 Medline
52. G. K. Smyth, Linear models and empirical bayes methods for assessing differential expression in microarray experiments. *Stat. Appl. Genet. Mol. Biol.* **3**, Article3 (2004).
53. C. Banning, J. Votteler, D. Hoffmann, H. Koppensteiner, M. Warmer, R. Reimer, F. Kirchhoff, U. Schubert, J. Hauber, M. Schindler, A flow cytometry-based FRET assay to identify and analyse protein-protein interactions in living cells. *PLoS ONE* **5**, e9344 (2010). doi:10.1371/journal.pone.0009344 Medline
54. K. Arnold, L. Bordoli, J. Kopp, T. Schwede, The SWISS-MODEL workspace: a web-based environment for protein structure homology modelling. *Bioinformatics* **22**, 195–201 (2006). doi:10.1093/bioinformatics/bti770 Medline
55. S. A. Wynne, R. A. Crowther, A. G. Leslie, The crystal structure of the human hepatitis B virus capsid. *Mol. Cell* **3**, 771–780 (1999). doi:10.1016/S1097-2765(01)80009-5 Medline
56. I. J. Byeon *et al.*, NMR structure of human restriction factor APOBEC3A reveals substrate binding and enzyme specificity. *Nat. Commun.* **4**, 1890 (2013).

57. A. W. Ghoorah, M. D. Devignes, M. Smaïl-Tabbone, D. W. Ritchie, Protein docking using case-based reasoning. *Proteins* **81**, 2150–2158 (2013). doi:10.1002/prot.24433 Medline
58. R. A. Sayle, E. J. Milner-White, RASMOL: biomolecular graphics for all. *Trends Biochem. Sci.* **20**, 374–376 (1995). doi:10.1016/S0968-0004(00)89080-5 Medline
59. L. G. Guidotti, B. Matzke, H. Schaller, F. V. Chisari, High-level hepatitis B virus replication in transgenic mice. *J. Virol.* **69**, 6158–6169 (1995). Medline
60. M. Dandri, M. R. Burda, E. Török, J. M. Pollok, A. Iwanska, G. Sommer, X. Rogiers, C. E. Rogler, S. Gupta, H. Will, H. Greten, J. Petersen, Repopulation of mouse liver with human hepatocytes and in vivo infection with hepatitis B virus. *Hepatology* **33**, 981–988 (2001). doi:10.1053/jhep.2001.23314 Medline
61. M. Lütgehetmann, T. Bornscheuer, T. Volz, L. Allweiss, J. H. Bockmann, J. M. Pollok, A. W. Lohse, J. Petersen, M. Dandri, Hepatitis B virus limits response of human hepatocytes to interferon-α in chimeric mice. *Gastroenterology* **140**, 2074–2083, e1–e2 (2011). doi:10.1053/j.gastro.2011.02.057 Medline
62. M. Sarasin-Filipowicz, E. J. Oakeley, F. H. Duong, V. Christen, L. Terracciano, W. Filipowicz, M. H. Heim, Interferon signaling and treatment outcome in chronic hepatitis C. *Proc. Natl. Acad. Sci. U.S.A.* **105**, 7034–7039 (2008). doi:10.1073/pnas.0707882105 Medline

3.2.8. Personal contributions

In the present study we investigated how interferon-α and LTβR signaling can induce degradation of nuclear HBV DNA by upregulating expression of APOBEC3A and 3B deaminases, respectively. These deaminases targeted viral cccDNA and marked it for subsequent degradation without affecting genomic DNA. HBV was cleared from infected hepatocytes and hepatoma cell lines and thus our treatment prevented viral rebound even after treatment cessation. My tasks mainly included investigation of the molecular pathways regulating APOBEC3B expression downstream of LTβR. Furthermore I actively contributed to the conceptual development of several hypotheses in this study.

Analyses and figures contributed:

FigureS2a: Western blot analysis of TNFR1 and LTbR protein expression in HepaRG cells

Figure S2b: FACS analysis of LTbR cell surface expression on HepaRG and HepG2H1.3 cells

Figure S2c and d: Western blot for p100/p52 processing (**c**) and RelA-phosphorylation (**d**) in HepaRG cells upon LTbR stimulation.

Figure S2f: Immunohistochemistry for nuclear RelA translocation in mock and LTbR stimulated HepaRG cells

Figure S2g: qRT-PCR analysis of the mRNA expression profile of HepaRG cells upon LTbR-activation

Figure S4b: Caspase-activity at d1 – d8 in BS1-treated HepaRG cells

Figure S6a: Immunohistochemistry for RelA and RelB nuclear translocation of livers from HBV1.3 transgenic mice 28d post LTbR stimulation.

Figure S6e: Immunohistochemical staining and quantification HBV-core positive hepatocytes in HBV1.3 tg mice treated for 28d with ACH6 compared to mock

Figure S6g: I injected mice (n = 6 per group) twice a week with ACH6 or CTRL- antibody for 3 weeks and evaluated ALT levels during treatment and HBeAg levels until 14 days after treatment stop

Figure S9: Differentiated HepaRG were infected with HBV and treated with LTbR agonist. I corroborated the 50 most strongly up- and down-regulated genes from an Affymetrix array by qPCR at d4 and d11 post treatment (**a**) and regulated genes wer classified according to their activity and nuclear acid binding properties (**b,c**)

Figure S10a: mRNA expression level of APOBEC family members in HepaRG cells, HepaRG-IRF3DN cells, PHH and PHH from uPA/SCID mice.

Figure S11: Dose and time dependency of APOBEC3B and G mRNA.

Figure S14b. Western blot analysis of cytosolic and nuclear fractions from differentiated HepaRG cells for A3B and A3G – HDAC2 and GAPDH serving as nuclear and cytosolic control, respectively

3.3. A positive feedback loop between RIP3 and JNK controls non-alcoholic steatohepatitis

'Introduction', 'Material and Methods', 'Results' and 'Discussion' have been described in the following publication: Gautheron, Vucur, Reisinger et al. *EMBO Molecular Medicine*, **6**,1062-1074 (2014)

3.3.1. Authors

Jérémie Gautheron,* Mihael Vucur,* **Florian Reisinger**,* David Vargas Cardenas, Christoph Roderburg, Christiane Koppe, Karina Kreggenwinkel, Anne Theres Schneider, Matthias Bartneck, Ulf Peter Neumann, Ali Canbay, Helen Louise Reeves, Mark Luedde, Frank Tacke, Christian Trautwein, Mathias Heikenwalder & Tom Luedde

* equal contribution

3.3.2. Abstract

Non-alcoholic fatty liver disease (NAFLD) represents the most common liver disease in Western countries and often progresses to non-alcoholic steatohepatitis (NASH) leading ultimately to liver fibrosis and liver cancer. The occurrence of hepatocyte cell death—so far characterized as hepatocyte apoptosis—represents a fundamental step from benign steatosis toward progressive steatohepatitis. In contrast, the function of RIP3-dependent necroptosis in NASH and NASH-induced fibrosis is currently unknown. We show that RIP3 is upregulated in human NASH and in a dietary mouse model of steatohepatitis. RIP3 mediates liver injury, inflammation, induction of hepatic progenitor cells/activated cholangiocytes, and liver fibrosis through a pathway suppressed by Caspase-8. This function of RIP3 is mediated by a positive feedback loop involving activation of Jun-(N)-terminal Kinase (JNK). Furthermore, RIP3-dependent JNK activation promotes the release of pro-inflammatory mediators like MCP-1, thereby attracting macrophages to the injured liver and further augmenting RIP3-dependent signaling, cell death, and liver fibrosis. Thus, RIP3-dependent necroptosis controls NASH-induced liver fibrosis. This pathway might represent a novel and specific target for pharmacological strategies in patients with NASH.

3.3.3. Introduction

Non-alcoholic fatty liver disease (NAFLD) is the most common chronic liver disease in the Western world (Vernon et al, 2011). The term non-alcoholic steatohepatitis (NASH) defines a more aggressive disease entity within the spectrum of NAFLD that is often associated with obesity, type 2 diabetes, and the metabolic syndrome (Schattenberg & Schuppan, 2011). In NASH, advanced fibrosis and

cirrhosis are primary determinants of an increased overall and liverrelated mortality (Schuppan & Afdhal, 2008; Bhala et al, 2011; Poelstra & Schuppan, 2011), underlining that pharmacological inhibition of liver fibrogenesis or induction of fibrosis regression is a fundamental goal in this disease (Schattenberg & Schuppan, 2011). Despite several molecular targets that were addressed in NASH patients in recent clinical trials (Schuppan & Kim, 2013), no effective pharmacological strategy against NASH-induced liver fibrosis has yet entered clinical practice, highlighting the need to identify novel-signaling pathways regulating the transition from NASH to hepatic fibrosis.

One fundamental difference between benign steatosis and progressive steatohepatitis is the occurrence of massive hepatocyte cell death, at present classified as hepatocyte apoptosis (Wree et al, 2013). Apoptosis can be triggered by ligation of death receptors like tumor necrosis factor (TNF) receptor by their cognate ligands and represents a highly synchronized procedure depending on activation of aspartate-specific proteases known as caspases (Chakraborty et al, 2012). Of these, Caspase-8 represents a key upstream caspase that engages to the death-inducing signaling complex (DISC) via the adaptor molecule FADD (Chakraborty et al, 2012). NASH is histologically characterized by hepatocyte apoptosis and varying degrees of fibrosis in the setting of hepatocyte lipid accumulation (Schattenberg & Schuppan, 2011). In line with this observation, previous functional studies in animal models and clinical studies have focused on the potential role of apoptosis in NASH development (Witek et al, 2009; Anstee et al, 2010; Ratziu et al, 2012; Hatting et al, 2013). However, necrosis and necro-inflammation are also histological characteristics of human NASH (Malhi & Gores, 2008; Schattenberg & Schuppan, 2011), suggesting that alternative cell-death forms might play a role in the pathogenesis of this disease.

It was recently discovered that necroptosis—programmed necrosis depending on the kinases RIP1 and RIP3—represents an alternative programmed cell-death pathway downstream of the TNF receptor (Cho et al, 2009; He et al, 2009; Zhang et al, 2009). RIP3 mediates necroptosis through activation of mixed lineage kinase domain-like protein (MLKL) (Sun et al, 2012). Necroptosis plays a role in the regulation of chronic inflammation in the pancreas, gut, and skin (He et al, 2009; Bonnet et al, 2011; Welz et al, 2011). Moreover, necroptosis is activated in patients with alcoholic liver injury (Roychowdhury et al, 2013), but the role of RIP3 in NASH is currently unknown.

To examine the functional role of RIP3 in NASH development, we applied the methionine- and choline-deficient (MCD) dietinduced model of steatohepatitis that mimics important features of human NASH, including the development of steatohepatitis, CYP2E1 overexpression, and increased lipid peroxidation as well as the promotion of NASH toward hepatic fibrosis (Schattenberg et al, 2006). In addition, most previous data on the relation between cell death and NASH were gained in this respective model (Csak et al, 2011; Hatting et al, 2013). We show that RIP3 controls NASH

development in a Caspase-8-dependent manner by a pathway involving activation of Jun-(N)-terminal kinase and thus might represent a promising target for future therapeutic strategies in patients with chronic metabolic liver disease.

3.3.4. Results

3.3.4.1. RIP3 mediates liver injury in MCD-diet-induced NASH

In order to examine the differential functions of RIP3-dependent necroptosis versus Caspase-8-dependent apoptosis in NASH, we generated mice with conditional deletion of Caspase-8 in liver parenchymal cells (LPC)—hepatocytes and cholangiocytes—(Casp-$8^{LPC\text{-}KO}$), constitutive ablation of Rip3 in all cells ($RIP3^{-/-}$), and mice with combined conditional and constitutive deletions of Caspase-8 and RIP3, respectively (Casp-$8^{LPC\text{-}KO}$/$RIP3^{-/-}$) (data not shown).

These groups of mice were treated for either 2 or 8 weeks with MCD-diet or normal chow as control and were first analyzed for the degree of liver injury. As described previously (Vucur et al, 2013), Casp-$8^{LPC\text{-}KO}$ mice showed a moderate increase in serum levels of aspartate aminotransferase (AST) and glutamate dehydrogenase (GLDH) but not alanine aminotransferase (ALT) in mice fed with normal chow (**Fig. 1a**). After 2 and 8 weeks of MCD-diet, serum levels of AST, ALT, and GLDH were increased in all groups compared to the respective control animals on normal chow (**Fig. 1a**). Strikingly, enzyme levels were more increased in Casp- $8^{LPC\text{-}KO}$ animals at both time points compared to all other experimental groups (**Fig. 1a**). In contrast, after 8 weeks of MCD-diet, all liver enzymes were reduced in $RIP3^{-/-}$ mice and Casp-$8^{LPC\text{-}KO}$/$RIP3^{-/-}$ animals compared to WT mice (**Fig. 1a**). Together, these findings indicate that RIP3 mediates liver injury upon MCD-diet feeding in mice.

Based on this observation, we further examined intrahepatic expression levels of RIP3 in this model. It was previously shown that necroptotic cell death in the liver or pancreas is associated with an increase in RIP3 protein levels (He et al, 2009; Vucur et al, 2013). In line, 2 weeks of MCD-diet feeding led to a strong induction of RIP3 protein levels in Western blot analysis (**Fig. 1b**). Of note, this induction of RIP3 expression was even augmented in Casp-$8^{LPC\text{-}KO}$ animals with abrogated Caspase-8-expression (**Fig. 1b**), while—as expected—no RIP3 expression was detected in Casp-$8^{LPC\text{-}KO}$/$RIP3^{-/-}$ and $RIP3^{-/-}$ livers (**Fig. 1b**).

Immunohistological analyses of livers of mice after 8 weeks of MCD-diet feeding confirmed high expression levels of RIP3 in WT mice and even stronger expression in Casp-$8^{LPC\text{-}KO}$ livers (**Fig. 1c** and **d**). In contrast, immunohistological staining for cleaved Caspase-3 revealed similarly low levels of

cleaved Casp-3+ hepatocytes in all groups (data not shown). The fact that cleavage of Caspase-3 was also detected in mouse livers with conditional deletion of Caspase-8 indicated that apoptosis in this model can be activated by Caspase-8-independent signaling cascades, e.g. via the mitochondrial pathway (Estaquier et al, 2012). In line with this finding, it was previously shown that in NASH, fatty acid accumulation enhances β-oxidation and mitochondrial electron overflow, thus triggering cell death (Seifert et al, 2010).

Finally, compensatory proliferation of parenchymal liver cells measured by staining for Ki67 correlated with overexpression of RIP3 and was most prominent in Casp-8^{LPC-KO} mice, while Casp-8^{LPC-KO}/RIP3$^{-/-}$ and RIP3$^{-/-}$ mice showed significantly less proliferating cells than MCD-diet-fed WT mice (**Fig. 1c** and **d**). Together, these observations demonstrate that activation of RIP3 represents a fundamental step in the MCD-diet NASH model mediating liver injury. Moreover, a crucial function of Caspase-8 in this model is to counterbalance RIP3-dependent liver injury.

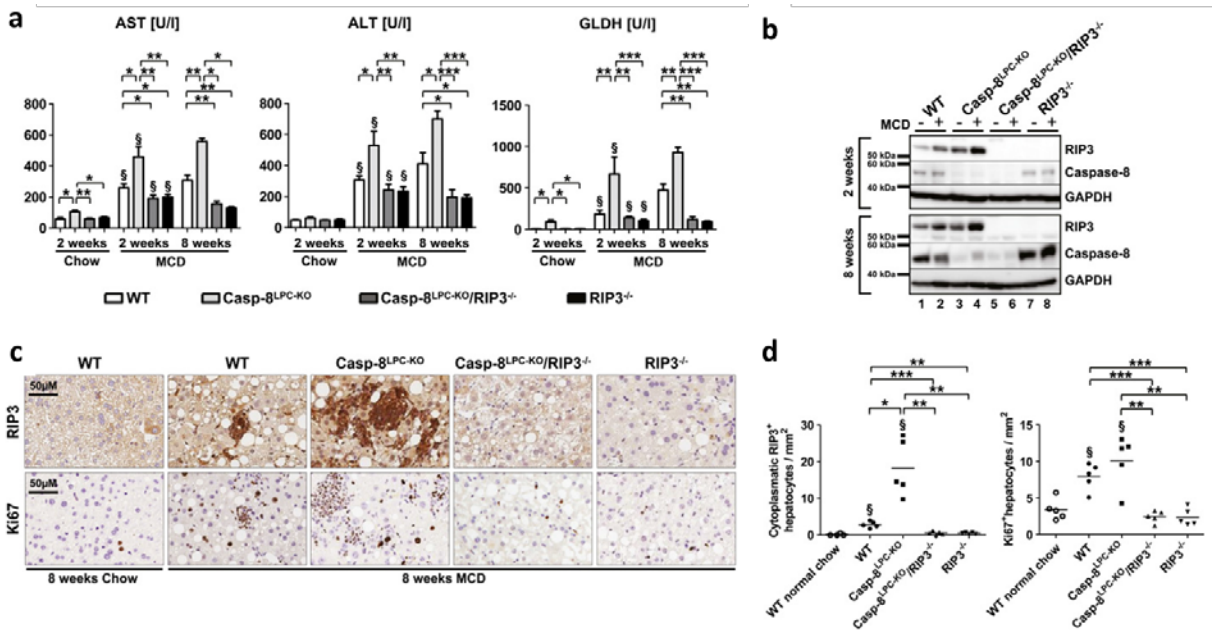

Figure 1: RIP3 is induced in murine livers following MCD-diet feeding and promotes hepatic injury in Caspase-8-deficient livers. (a) Analysis of serum levels of AST, ALT, and GLDH after 2 and 8 weeks of MCD-diet or 2 weeks of normal chow. Results are shown as mean SEM, n = 6 (2 weeks normal chow) n = 12 (2 weeks MCD), and n = 5 (8 weeks MCD). §indicates that serum levels are significantly increased from basal level. (b) Western blots analysis on liver extracts from MCD-diet-fed (2- and 8-weeks) animals and control mice with antibodies against RIP3, Caspase-8, and GAPDH as a loading control. (c) Immunohistochemical (RIP3, Ki67) analysis on representative liver sections from the indicated mice fed for 8 weeks with MCD-diet. (d) Statistical analysis of RIP3^{+} and Ki67^{+} hepatocytes. Results are shown as mean, n = 5. §indicates that RIP3^{+} and Ki67^{+} cells are significantly increased from basal WT group.

3.3.4.2. RIP3 controls the transition from NASH to liver fibrosis in a Caspase-8 dependent manner

Based on the differential functions of RIP3 and Caspase-8 in controlling liver injury in response to MCD-diet feeding, we next tested their influence on the pathogenesis of steatosis and NASH-induced liver fibrosis. Hematoxylin and eosin (H&E) staining revealed minimal steatosis in all groups of mice after 8 weeks of normal chow feeding (**Fig. 2a**). Of note, mice with combined deletions of Caspase-8 and Rip3 (Casp-8^{LPC-KO}/RIP3$^{-/-}$ mice) on normal chow already displayed increased triglyceride (TG) levels compared to the other experimental groups (**Fig. 2b**). Eight weeks of MCD-diet feeding triggered hepatic fat accumulation above control levels in all groups (**Fig. 2a and b**). In line with the control groups, MCD-diet feeding led to significantly higher intrahepatic TG contents in Casp-8^{LPC-KO}/RIP3$^{-/-}$ mice compared to all other experimental groups, suggesting that inactivation of both programmed cell-death pathways augments hepatic fat accumulation in the MCD-diet model.

The presence of apoptosis in NAFLD patients has been taken as a predictor to develop progressive fibrosis (Witek et al, 2009; Anstee et al, 2010; Ratziu et al, 2012). In contrast, while necrosis is also found as histological characteristic in human NASH (Malhi & Gores, 2008; Schattenberg & Schuppan, 2011), the functional relation to fibrosis is presently poorly defined. We therefore investigated the

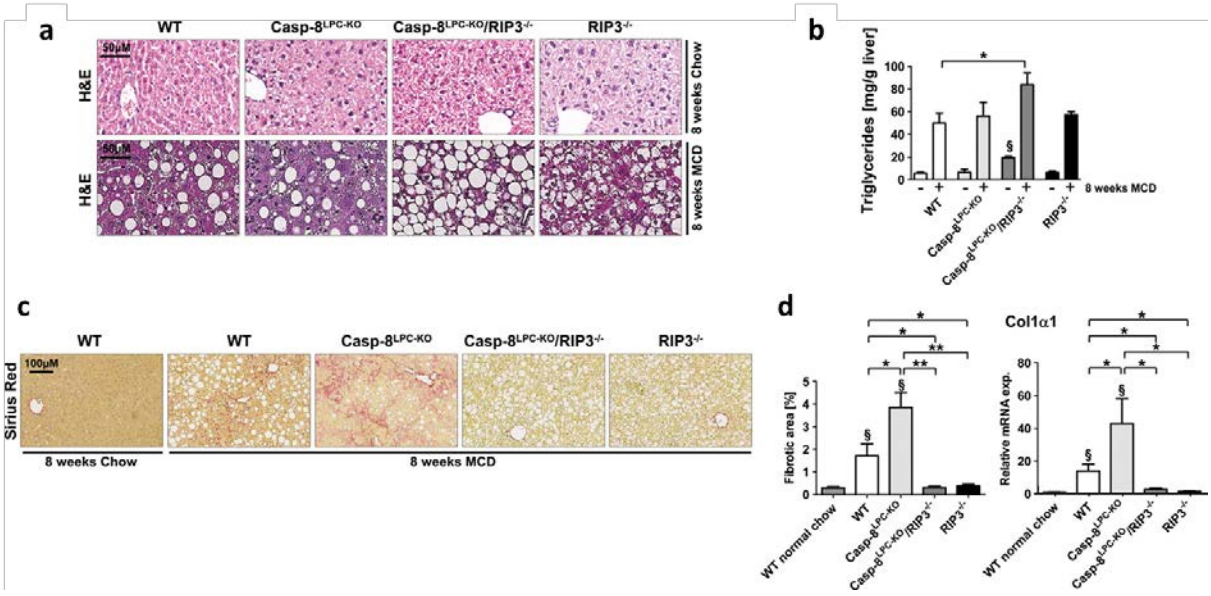

Figure 2: RIP3-dependent necroptosis promotes NASH-induced liver fibrosis and inflammation. (a)Representative H&E staining of liver slides from 16-week-old WT, Casp-8^{LPC-KO}, Casp-8^{LPC-KO}/RIP3$^{-/-}$, and RIP3$^{-/-}$ mice fed for 8 weeks with normal chow (upper panel) or MCD-diet (lower panel). (b) Intrahepatic triglycerides levels in WT, Casp-8^{LPC-KO}, Casp-8^{LPC-KO}/RIP3$^{-/-}$, and RIP3$^{-/-}$ fed for 8 weeks with MCD-diet or control chow, results are shown as mean SEM, n = 5 per group. §indicates that triglycerides are significantly increased from Casp-8^{LPC-KO}/RIP3$^{-/-}$ to the others groups of mice fed with normal chow. (c) Representative Sirius Red stainings of liver slides from 8-week-old female WT, Casp-8^{LPC-KO}, Casp-8^{LPC-KO}/RIP3$^{-/-}$, and RIP3$^{-/-}$ mice fed for 8 weeks with MCD-diet. (d) Left: statistical quantification of light polarized Sirius Red pictures, results are shown as mean, n = 5 per group. Right: Col1a1 mRNA levels in these livers were determined by qRT-PCR. Values were calculated relative to WT mice fed with normal show, and b-catenin was used as an internal standard, n = 5 per group. §indicates that values are significantly increased from basal level. Error bars represent SEM.

correlation between the occurrence of liver fibrosis and the activation of necroptosis in the MCD-diet model.

Sirius red staining and qRT-PCR analysis for Collagen-1a1 expression after 2 weeks (data not shown) and 8 weeks of MCD-diet feeding (**Fig. 2c** and **d**) revealed no significant liver fibrosis at the early time points and moderate fibrosis at the later time point in WT animals. In contrast, correlating with induction of RIP3 expression levels, Casp-$8^{LPC\text{-}KO}$ animals displayed strongly increased intrahepatic fibrosis at both time points, whereas hepatic fibrogenesis was strongly reduced in $RIP3^{-/-}$ single-mutant mice and Casp-$8^{LPC\text{-}KO}$/$RIP3^{-/-}$ double-mutant animals compared to WT and Casp-$8^{LPC\text{-}KO}$ mice (**Fig. 2c** and **d;** and data not shown). These data indicate that RIP3-dependent necroptosis promotes NASH-induced liver fibrosis. Moreover, activation of Caspase-8 inhibits RIP3-dependent liver fibrosis in NASH.

We have further addressed the question whether the previously shown pro-fibrogenic effect of RIP3 is specific for liver fibrosis in response to hepatic steatosis or represents a general principle in hepatic fibrogenesis. To test this, we used an alternative, very well established model of experimental liver fibrosis relying on repetitive injections of the substance CCl4 into mice and applied this model for 2 and 6 weeks to WT, Casp-$8^{LPC\text{-}KO}$, Casp-$8^{LPC\text{-}KO}$/$RIP3^{-/-}$, and $RIP3^{-/-}$ mice. This treatment led to the development of areas of parenchymal cell necrosis in Casp-$8^{LPC\text{-}KO}$ mice (data not shown). However, it did not result in a significantly increased degree of fibrosis between the groups of mice in quantitative analysis of Sirius Red staining (data not shown), supporting the hypothesis that RIP3 might represent a specific target in fatty liver-related liver fibrosis.

3.3.4.3. RIP3-activation in NASH promotes inflammation and hepatic recruitment of monocytes/macrophages

Inflammation represents a fundamental factor linking liver injury with hepatic fibrosis (Tacke et al, 2008; Schuppan & Kim, 2013). We therefore examined the association between liver fibrosis and inflammation in response to necroptosis upon MCD-diet feeding. As assessed by immunohistochemistry, 8 weeks of MCD-diet feeding increased the number of infiltrating CD45+ immune cells in all experimental groups of mice compared to WT mice fed with normal chow. Of note, inflammation was even higher in Casp-$8^{LPC\text{-}KO}$ mice and correlated with the strong expression of RIP3 as the number of CD45+ immune cells was reduced to WT levels in Casp-$8^{LPC\text{-}KO}$/ $RIP3^{-/-}$ mice and $RIP3^{-/-}$ animals (**Fig. 3a** and **b**).

We next investigated the impact of infiltrating monocytes, which play a pro-fibrogenic role in different experimental models of liver fibrosis as well as human liver disease (Zimmermann & Tacke, 2011). As demonstrated by immunohistochemistry, 8 weeks of MCD-diet feeding significantly

increased the number of inflammatory foci containing monocytes in WT mice and even more in Casp-8^{LPC-KO} livers (**Fig. 3a** and **b**). In contrast, the emergence of these foci was completely abrogated by the deletion of Rip3 as seen in Casp-8^{LPC-KO}/$RIP3^{-/-}$ and $RIP3^{-/-}$ animals (**Fig. 3a** and **b**). The activation role of RIP3 in the initiation of inflammation was confirmed by FACS analyses in livers of mice fed for 2 weeks with MCD-diet, revealing significantly lower numbers of F4/80+ cells in Casp-8^{LPC-KO}/$RIP3^{-/-}$ mice and $RIP3^{-/-}$ animals than seen in Casp-8^{LPC-KO} mice (Supplementary Fig. S5). Taken together, these results indicate that RIP3- dependent inflammation and recruitment of monocytes represents an important mechanism for promoting hepatic fibrosis in mice fed with MCD-diet.

We further tested which inflammatory mediators might be involved in linking necroptosis of parenchymal liver cells with monocyte recruitment and increased hepatic fibrosis. Interestingly, while many inflammatory cytokines and chemokines such as Interleukin (IL)-1a, IL-1b, IL-6, CCL1 and CCL8, and CCL17 did not show a clearly distinct regulation between WT and Casp-8^{LPC-KO} mice fed for 2 weeks with MCD-diet on mRNA level (Supplementary Fig. S6), qRT-PCR analysis and FACS-based microbeads fluorescence assay on liver extracts from the different experimental groups revealed a strong increase in intrahepatic levels of MCP-1 (CCL2) in Casp-8^{LPC-KO} mice compared to WT mice at that time point (**Fig. 3c**). In contrast, MCP-1-levels were markedly reduced in Casp-8^{LPC-KO}/$RIP3^{-/-}$, and $RIP3^{-/-}$ mice (**Fig. 3c**), which was confirmed after 8 weeks of MCD-diet feeding (**Fig. 3d**).

Given previous reports on the essential functional role of the MCP-1/CCR2 axis in monocyte recruitment and liver fibrosis (Seki et al, 2009; Baeck et al, 2012), these data indicate that MCP-1 represents one important factor linking RIP3-dependent necroptosis in NASH with liver fibrosis. Further analyses revealed increased TNF levels in WT and Casp-8^{LPC-KO} mice after 8 weeks of MCD feeding, as well as a strong correlation between RIP3 expression levels and levels of TGF-b2 (Supplementary Fig. S7), which is in line with a recent report showing a prominent role of TGF-b in the regulation of NASH-associated hepatocyte cell death (Yang et al, 2014).

The alfp-cre line used to generate Casp-8^{LPC-KO} animals mediates genetic excision exclusively in liver parenchymal cells (LPC) (Kellendonk et al, 2000), arguing for a specific function of RIP3 in this respective cell compartment in driving liver injury and subsequent fibrogenesis in Casp-8^{LPC-KO} mice upon MCD-diet feeding. However, in order to exclude that constitutive deletion of Rip3 in Casp-8^{LPC-KO}/$RIP3^{-/-}$ mice resulted in general signaling defects of immune cells as a reason for the rescue of these double-mutant animals from hepatic fibrosis, we isolated and cultured monocytes from murine bone marrow of WT, Casp-8^{LPC-KO}, Casp-8^{LPC-KO}/$RIP3^{-/-}$, and $RIP3^{-/-}$ mice. Stimulation with lipopolysaccharide (LPS) resulted in very similar patterns of chemokine and cytokine expression (data not shown), suggesting that the functional activity of macrophages is not abrogated in $RIP3^{-/-}$ and Casp-8^{LPC-KO}/$RIP3^{-/-}$ mice.

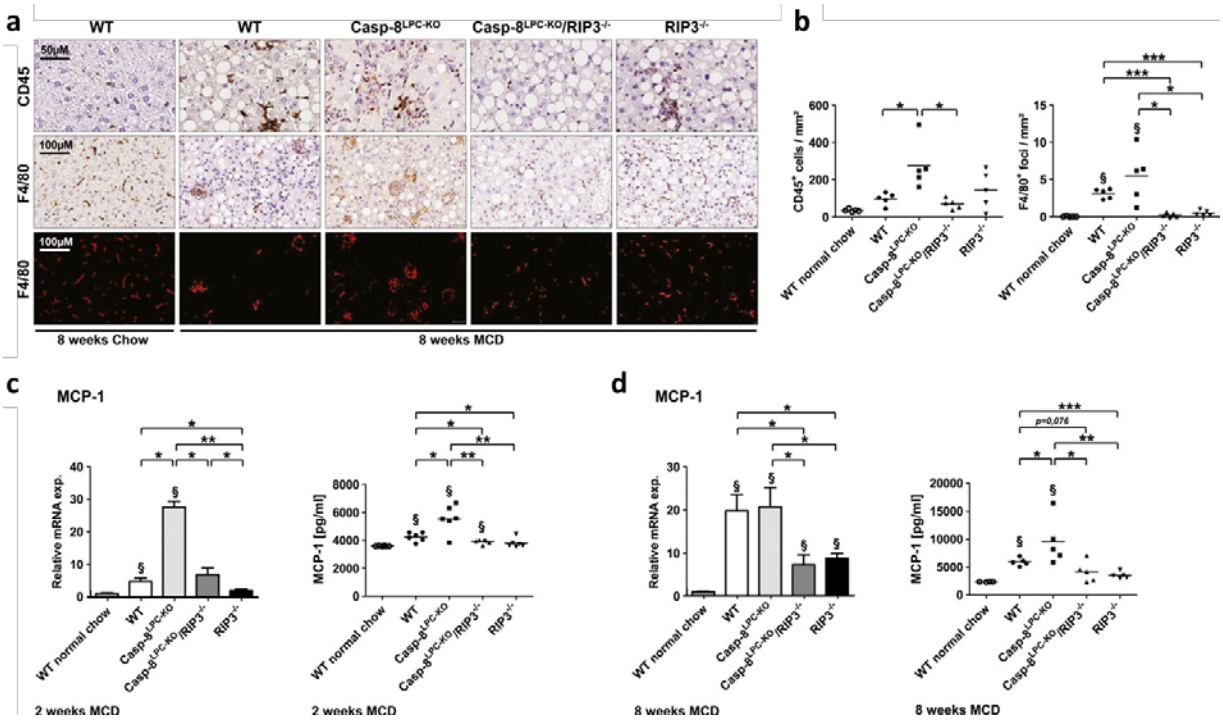

Figure 3: RIP3-dependent necroptosis promotes NASH-induced liver fibrosis through MCP-1 release. (a) Immunohistochemical analysis of CD45 (upper panel) and F4/80 (middle panel) on representative liver sections from the indicated mice fed for 8-weeks with MCDdiet or normal chow. The lower panel shows deconvoluted pictures from the F4/80 stains. (b) Statistical analysis of $CD45^+$ and $F4/80^+$ cells. Results are shown as mean, n = 5. §indicates that $F4/80^+$ foci are significantly increased from basal WT group. (c) Left: MCP-1 mRNA levels were assessed by RT-PCR after 2 weeks of MCD-diet feeding. Values were calculated relative to WT mice fed with normal chow, and bcatenin was used as an internal standard, n = 6 per group. Right: FACS-based microbeads fluorescence assay for MCP-1 expression in liver protein homogenates. Results are shown as mean, n = 6 per group. § shows that values are significantly increased from basal level. Error bars indicate SEM. (d) Left: MCP-1 mRNA levels were assessed by RT-PCR after 8 weeks of MCD-diet feeding. Values were calculated relative to WT mice fed with normal chow, and bcatenin was used as an internal standard, n = 5 per group. §indicates that values are significantly increased from basal level. Error bars represent SEM. Right: FACSbased microbeads fluorescence assay for MCP-1 expression in liver protein homogenates. Results are shown as mean, n = 5 per group. §shows that values are significantly increased from basal level. Error bars indicate SEM.

3.3.4.4. RIP3-expression in murine and human NASH livers

Most liver diseases and also NASH—once advanced—develop into a portal fibrosis with proliferation of biliary progenitors and activated cholangiocytes, which typically form small clusters and nonfunctional biliary structures (Richardson et al, 2007; Schuppan & Kim, 2013). We therefore tested the relation between RIP3-dependent necroptosis and a biliary ductular reaction in the MCD-diet model. Strikingly, immunostaining for Cytokeratin (CK)-19 revealed a strong expansion of clusters of biliary cells / progenitor cells in livers of $Casp\text{-}8^{LPC\text{-}KO}$ mice, which was not seen in combined or single RIP3-mutants (**Fig. 4a** and **b**). Of note, immunostaining for RIP3 and specific analysis in areas of ductular reactions revealed that many cholangiocytes expressed even higher levels of RIP3 than the surrounding hepatocytes (**Fig. 4c**).

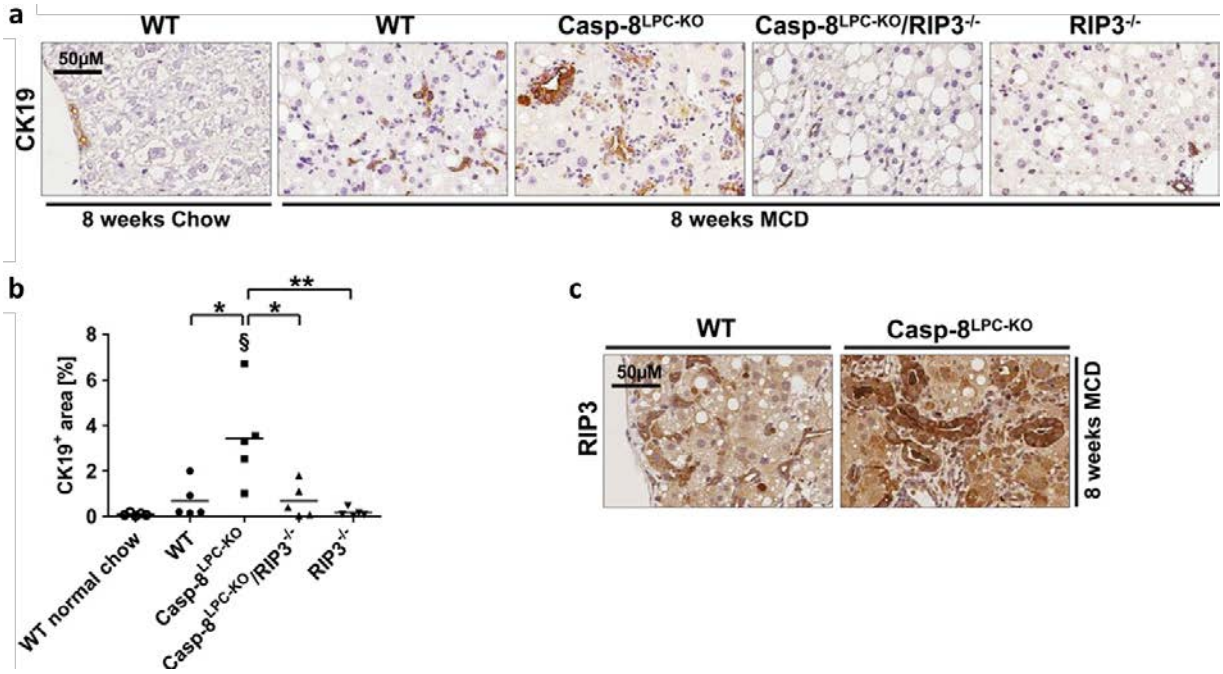

Figure 4: RIP3-dependent necroptosis mediates expansion of progenitor cells that expressed high levels of RIP3. (a) Immunohistochemical (CK19) analysis on representative liver sections from the indicated mice fed for 8-weeks with MCD-diet. (b) Statistical analysis of $CK19^+$ cells. Results are shown as mean, n = 5. §shows that $CK19^+$ cells are significantly increased from basal WT group. (c) Immunohistochemical (RIP3) analysis on representative liver sections from WT and Casp-8LPC-KO mice fed for 8 weeks with MCD-diet.

It was previously demonstrated in liver samples from human NASH patients that RIP3 is strongly upregulated on RNA level to more than 40-fold compared to healthy controls (Csak et al, 2011). In order to provide further evidence for a function of RIP3 in human NASH, we examined RIP3 expression in livers of NASH patients (as demonstrated histologically by increased NAS score, see **Fig. 5a**) by Western blot and immunohistochemistry. On protein levels, RIP3 was strongly upregulated in NASH patients compared to controls (**Fig. 5b**). Immunostaining of NASH patient livers revealed strong RIP3 expression in hepatocytes, often neighboring areas of fat deposition (**Fig. 5c**). Of note, RIP3 often showed a granule-like staining pattern (**Fig. 5c**), similar to previous imaging results in MEF cells with activated RIP3 signaling depicting clustering of RIP1/RIP3 (Li et al, 2012).

Finally, RIP3 was often overexpressed in cells morphologically reflecting cholangiocytes / bile duct cells (**Fig. 5c**), similar to our previous findings in mouse livers. These findings support the hypothesis that also in human NASH, liver cells are sensitized to necroptotic cell death. Moreover, in murine as well as human NASH, biliary cells express high levels of RIP3, pointing toward celltype-specific functions of this pathway in the liver.

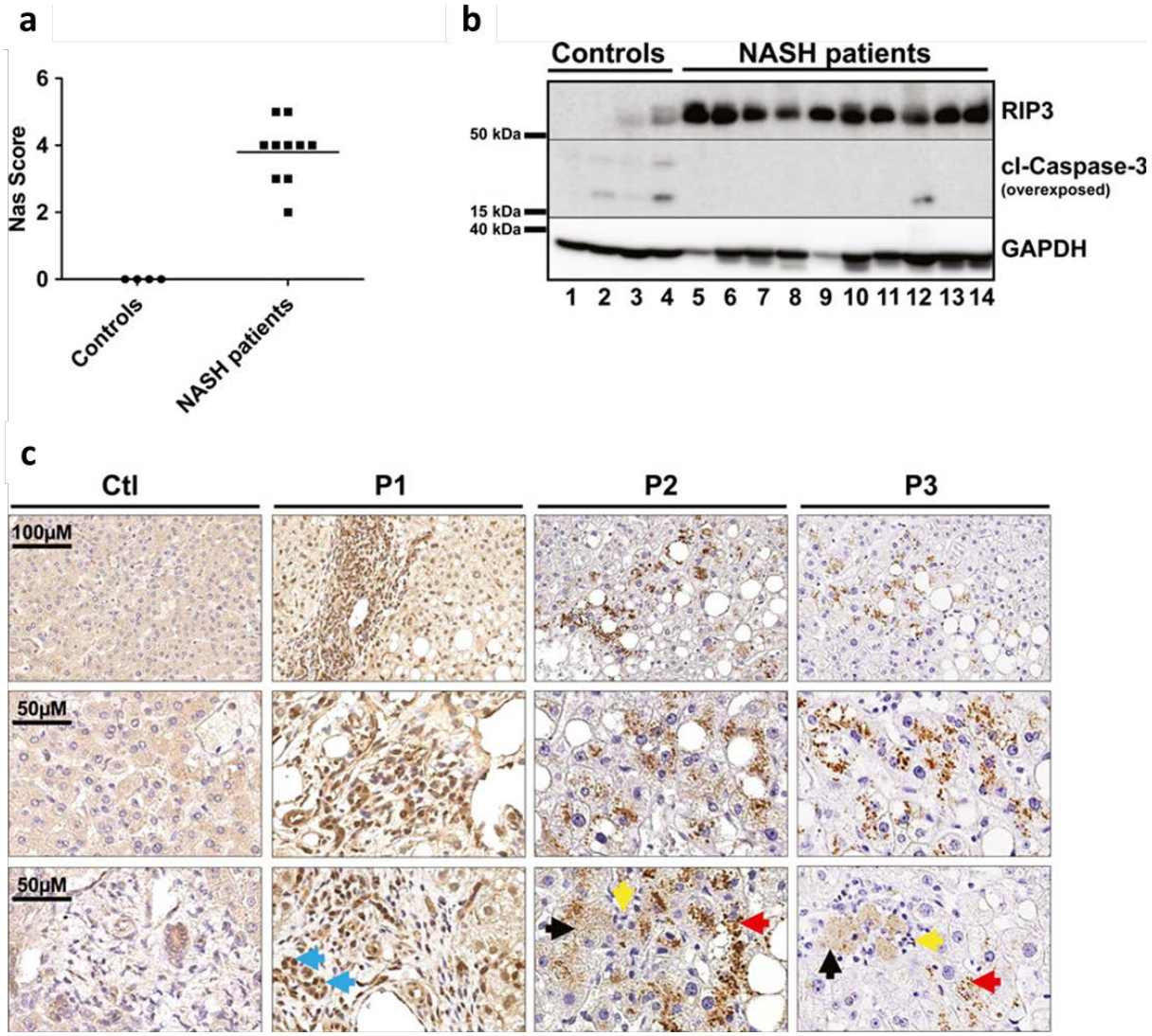

Figure 5: RIP3 is overexpressed in livers of human NASH patients. (a) Western blot analysis of RIP3 in control livers (n = 4) and human NASH patients (n = 10), using antibodies against RIP3, cleaved Caspase-3, and GAPDH as a loading control. (b) NAS scores of control livers and human NASH samples, corresponding to the Western blot analysis for RIP3. (c) Immunostaining analyses of RIP3 in control livers and human NASH patients (P1, P2, P3) (blue arrows indicate progenitor/biliary cells, black arrows indicate necrotic hepatocytes, red arrows show clusters of RIP3 in hepatocytes, and yellow arrows indicate inflammatory cells grouped around dying hepatocytes). Pictures are representative for 27 samples examined.

3.3.4.5. A positive feedback loop involving activation of Jun-(N)-terminal Kinase (JNK) mediates RIP3-dependent inflammation and hepatic fibrosis upon MCD feeding

We finally aimed at further evaluating which potential downstream pathway mediated RIP3-dependent liver injury, inflammation, and fibrosis upon MCD feeding. To test this, we first examined the activation status of stress-related signaling cascades in the different knockout models after 2 weeks of MCD-diet feeding. As shown by Western blot analysis using phospho-specific antibodies, increased activation of RIP3 and fibrosis upon MCD-diet feeding correlated with increased phosphorylation and activation of the kinase Jun-(N)-terminal Kinase (JNK) in WT and even more in

Casp-8^{LPC-KO} livers (**Fig. 6a**), which was abolished in Casp-8^{LPC-KO}/RIP3$^{-/-}$ and RIP3$^{-/-}$mice (**Fig. 6a**). In contrast, activation of AKT and p38 didnot show a clear association with the activation status of RIP3(**Fig. 6a**).

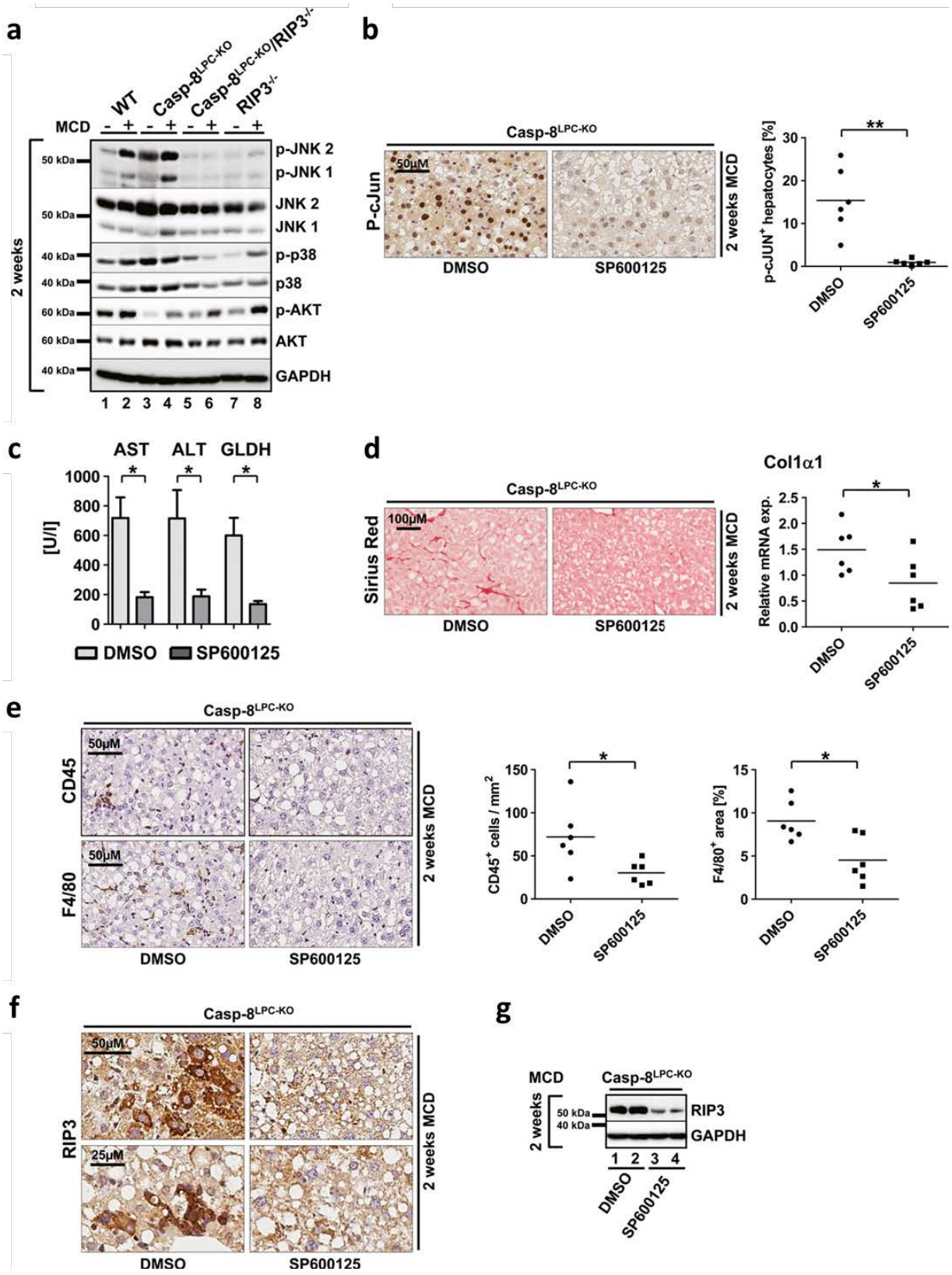

Figure 6: RIP3 mediates MCD-diet-induced NASH and liver fibrosis through activation of Jun-(N)-terminal kinase (JNK). (a) Western blot analysis of whole liver protein extracts from WT, Casp-8^{LPC-KO}, Casp-8^{LPC-KO}/RIP3$^{-/-}$, and RIP3$^{-/-}$ mice fed with MCD-diet for 14 days, using antibodies against the phosphorylated and active forms of JNK, AKT, p38 and GAPDH, JNK, AKT, and p38 as loading controls. (b) Immunohistochemical (left) and statistical analysis (right) of nuclear p-c-Jun^{+} hepatocytes on representative liver sections from Casp-8LPC-KO mice treated with SP600125 or vehicle (DMSO) for 2 weeks under MCD-diet, n = 6 per group. (c) Analysis of serum levels of AST, ALT, and GLDH of vehicle-treated and SP600125-treated mice after 2 weeks of MCD-diet feeding. Results are shown as mean SEM, n = 6 per group. (d) Left: representative Sirius Red stainings of mice treated with vehicle substance (DMSO) or SP600125 for 2 weeks. Right: Col1α1 mRNA levels quantification by qRTPCR, n = 6 per group. Error bars represent SEM. (e) Immunohistochemical (left) and statistical analysis (right) of CD45^{+} and F4/80^{+} cells on representative liver sections from Casp-8^{LPC-KO} mice treated with SP600125 or vehicle (DMSO) for 2 weeks with MCD-diet, n = 6 per group. (f) Immunostaining analysis of RIP3 in Casp-8^{LPC-KO} mice treated with SP600125 or vehicle (DMSO) for 2 weeks with MCD-diet. (g) Western blot analysis of RIP3 in Casp-8^{LPC-KO} mice treated with SP600125 or vehicle (DMSO) for 2 weeks with MCD-diet.

Given previous reports on the crucial function of JNK in the mediation of NASH fibrosis (Schattenberg et al, 2006), we further examined the functional role of JNK in RIP3-dependent NASH fibrosis and treated groups of Casp-8^{LPC-KO} mice with repetitive injections of the well-established JNK-inhibitor SP600125 or vehicle substance as control in parallel to MCD-diet feeding. This treatment resulted in effective inhibition of phosphorylation of the JNK-target c-Jun (**Fig. 6b**). JNK inhibition significantly ameliorated liver injury as shown by decreased levels of serum aminotransferases and GLDH in SP600125-treated mice (**Fig. 6c**). In line, JNK inhibition ameliorated liver fibrosis as shown by Sirius Red staining and qRT-PCR analysis for expression of Collagen-Iα1 (**Fig. 6d**). Moreover, decreased fibrosis in these livers went along with reduced intrahepatic numbers of CD45^{+} and F4/80^{+} cells (Fig. 6E), correlating with reduced levels of MCP-1 (data not shown). Interestingly, immunostaining and Western blot analysis revealed that inhibition of JNK during MCD-diet feeding significantly reduced expression levels of RIP3 in parenchymal liver cells (**Fig. 6f** and **g**).

To further confirm a mutual interaction between RIP3 and JNK signaling, we used L929 cells and confirmed that these cells undergo necroptosis upon stimulation with the pan-Caspase-inhibitor zVAD (Supplementary Fig. S10). Of note, additional treatment with the necroptosis inhibitor Nec-1 (Degterev et al, 2013) and also with SP600125 abolished zVAD-induced cell death. Moreover, JNK inhibition was associated with reduced RIP3 expression levels (data not shown). These data suggest that activation of JNK in LPC and probably non-parenchymal cells (NPC) further augments hepatic RIP3 signaling in terms of a positive feedback loop.

3.3.5. Discussion

For years, the term apoptosis, describing a form of cell death depending on the activation of caspases, was used synonymously for programmed cell death (Najimi et al, 2009). Apoptotic death of hepatocytes is a common feature of non-alcoholic steatohepatitis, and it was shown that both extrinsic and intrinsic apoptotic pathways are involved in NASH-induced hepatocyte death (Feldstein et al, 2003; Feldstein & Gores, 2005). Apoptosis has been considered as a driving force of NASH-induced liver fibrosis (Chakraborty et al, 2012), as it promotes activation of hepatic stellate cells to hepatic myofibroblasts, promoting deposition of extracellular matrix and scar formation in the liver (Chakraborty et al, 2012). Biomarkers of apoptosis like Cytokeratin-18 are strongly increased in NASH patients and distinguish between simple steatosis and NASH (Wieckowska et al, 2006; Younossi et al, 2008). Finally, the paradigmatic concept of apoptosis in NASH fibrosis has led to translational approaches into clinical studies, testing the use of apoptosis inhibitors in NASH patients (Ratziu et al, 2012).

Recently, however, it became evident that next to apoptosis, “necroptosis” represents an alternative programmed cell-death pathway (Han et al, 2011). Here, we demonstrate for the first time that RIP3-dependent necroptosis represents an important regulatory pathway driving the transition from NAFLD to NASH and subsequent liver fibrosis. Therefore, this pathway might represent a promising novel target for therapeutic strategies in NASH. Moreover, in contrast to previous assumptions (Hatting et al, 2013), our findings indicate that the main function of Caspase-8 in the MCDNASH model is to counterbalance the deleterious hyperactivation of RIP3-dependent necroptosis, underlining the mutual inhibitory functions of RIP3 and Caspase-8 that were previously demonstrated, for example in embryonic development (Kaiser et al, 2011) and skin homeostasis (Weinlich et al, 2013).

The relevance of apoptosis for NASH progression is supported by several studies. As such, it was clearly demonstrated that usage of the pan-Caspase-inhibitor VX-166 significantly reduced liver injury and liver fibrosis in MCD-diet-fed db/db mice (Witek et al, 2009). However, pan-caspase inhibitors inhibit numerous caspases including the downstream executioner caspases. In addition, chemical pan-caspase inhibitors act also on Caspase-1, which mediates proteolytic cleavage of Interleukin molecules including IL-1b (Chang & Yang, 2000; Das et al, 2009). Given recent data that specific inhibition of Caspase-1 inhibits NASH fibrosis (Dixon et al, 2013), it is possible that targeting of this respective pathway might also contribute to the beneficial effects of pan-caspase inhibitors in NASH fibrosis.

Moreover, our finding that also in Caspase-8-deficient livers apoptosis of hepatocytes is detected on a low level upon MCD-diet feeding suggests that Caspase-8-independent apoptosis are primarily activated in the MCD-diet model, which is supported by the fact that Casp-8^{LPC-KO}/RIP3$^{-/-}$ mice still showed significant liver injury in this respective model. Taken together, our present study together with previous findings indicate that both programmed cell-death pathways—(Caspase-8-independent) apoptosis and necroptosis—are involved in the pathogenesis of NASH and NASH-induced liver fibrosis. Of note, the degree of steatosis in our different genetically modified mouse models did not strictly correlate with the extent of liver injury upon MCD-diet feeding. Instead, blockage of both cell-death pathways (necroptosis and Caspase-8-dependent apoptosis) in Casp-8^{LPC-KO}/RIP3$^{-/-}$ mice resulted in an increase in intrahepatic fat accumulation in this model compared with WT or single-mutant animals, suggesting that absence of these two programmed cell-death pathways might increase the tolerance of hepatocytes to store lipids without undergoing cell death. Alternatively, given that multiple molecular interactions between programmed cell-death pathways and autophagy have been suggested (Pattingre et al, 2005; Yousefi et al, 2006), simultaneous inhibition of Caspase-8-dependent apoptosis and necroptosis might alter the activity of cellular pathways controlling lipolysis in hepatocytes (Liu & Czaja, 2013).

Our present findings diverge from a previous publication showing reduced liver damage in the MCD-diet model upon Caspase-8-deletion in hepatocytes (Hatting et al, 2013). It is important to note that in our study, we used the alfp-cre line (Kellendonk et al, 2000) that mediates highly efficient deletion of floxed genes at an early developmental time point in all parenchymal liver cells including cholangiocytes and progenitor cells, while in contrast, in the previous study, the albumin-cre (alb-cre) line was used (Postic et al, 1999). Of note, comparison of RIP3-expression levels between alfpcre/Caspase-8^{Fl} and alb-cre/Caspase-8^{Fl} confirmed high RIP3 expression upon alfp-cre-mediated Caspase-8 deletion (Supplementary Fig. S11), which is in line with previous reports on Caspase-8 deletion in other organs like skin (Weinlich et al, 2013). In contrast, we did not detect RIP3 upregulation upon albumin-cre-mediated deletion, further supporting the association between RIP3 expression levels and necroptotic liver injury.

In our experiments, we identified the stress-activated kinase JNK as a prominent mediator of RIP3-dependent liver injury and fibrogenesis in the MCD-diet model. Moreover, we show that mutual interactions exist between JNK- and RIP3-activation, as chemical inhibition of JNK not only ameliorated liver injury and fibrosis downstream of RIP3, but also led to reduced expression levels of RIP3 in liver parenchymal cells (LPC). Importantly, it is presently not clear whether the striking effect of chemical JNK inhibition in our model was mediated through JNK inhibition in hepatocytes or rather in non-parenchymal liver cells (NPLC). Previous data using conditional JNK-knockout mice in the

Concanavalin-A model of hepatitis suggested that JNK activation in NPLC but not in LPC represents a major control mechanism in the regulation of hepatitis (Das et al, 2009). Hence, it is possible that JNK activation in LPC promotes RIP3-dependent liver injury through generation of inflammatory cytokines, which in turn augments RIP3 expression and activation in LPC. However, our experiments in L929 cells suggest that a cell-autonomous or intercellular feedback loop exists in hepatocytes between RIP3- and JNK-signaling. Further experiments with conditional JNK-knockout mice are needed to functionally clarify the cell-specific relation between RIP3 and JNK in vivo.

Another prominent finding in our study was the strong, RIP3-dependent induction of biliary cells in the MCD-diet model. Activated cholangiocytes are related, if not identical to biliary progenitor cells (Schuppan & Kim, 2013). These cells can proliferate in response to hepatocyte growth arrest or cell death and were shown to secrete factors that attract and activate hepatic stellate cells for ECM deposition (Richardson et al, 2007; Schuppan & Kim, 2013). Moreover, biliary cells were previously suggested to be more resistant to oxidative stress and cell death than hepatocytes (Richardson et al, 2007). Thus, their expansion in Casp-$8^{LPC\text{-}KO}$ mice might reflect a biliary regenerative response in a context of necroptotic hepatocytes, but might also represent a functional amplification loop in the mediation of RIP3-dependent liver fibrosis upon NASH.

Interestingly, our findings indicated that biliary cells seemed to express high levels of RIP3 compared to hepatocytes, a finding currently lacking a functional explanation. It is possible that, given their putative resistance to cell death (Schuppan & Kim, 2013), biliary or precursor cells might tolerate higher levels of RIP3 in the absence of functional Caspase-8 before undergoing cell death. Future experiments with bile duct-specific cre-lines could also reveal a previously unrecognized role of RIP3 or Caspase-8 in biliary homeostasis, regeneration, or the intercellular communication between biliary cells and hepatocytes.

We have recently shown that Caspase-8-dependent apoptosis but not RIP3-dependent necroptosis promoted liver fibrosis and hepatocarcinogenesis in a model of liver injury caused by conditional deletion of the kinase TGF-b-activated Kinase-1 (Tak1) in parenchymal liver cells (Vucur et al, 2013). In this light, our present findings showing a protective function of Caspase-8 and an injury-promoting role of RIP3 are opposing their roles in the TAK1 model, indicating that activation modes and outcomes of distinct programmed cell death-forms depend on the initiating stimulus and pathogenic context. Given that chemical apoptosis inhibitors have already been tested in clinical studies in patients with NASH (Ratziu et al, 2012), pharmacological targeting of the necroptosis pathway might potentially have additive beneficial effects in a combinatory approach together with apoptosis inhibitors that do not specifically target Caspase-8 in these patients. In addition, previous studies showed that serum parameters reflecting activation of apoptosis might serve as biomarkers in NASH

(Chakraborty et al, 2012). Therefore, enhanced activation of necroptosis could serve as an indicator for more progressive liver disease, which should be evaluated in future prospective studies.

3.3.6. Materials and Methods

3.3.6.1. Study approval

All animal experiments were approved by the Federal Ministry for Nature, Environment and Consumers' Protection of the state of North Rhine-Westphalia and were performed in accordance to the respective national, federal, and institutional regulations.

3.3.6.2. Generation of conditional knockout mice

Mice carrying loxP-site-flanked (floxed) alleles of the Caspase-8-gene (Caspase-8 fl) (Salmena et al, 2003) were crossed to alfp-cre transgenic mice (Kellendonk et al, 2000) to generate a liver parenchymal cell (LPC)-specific knockout (Caspase-$8^{LPC\text{-}KO}$). Mice with constitutive deletion of RIP3 ($RIP3^{-/-}$) were described before (Newton et al, 2004). Mice with double knockout of conditional deletion of Caspase-8 and constitutive ablation of Rip3 (Caspase-$8^{LPC\text{-}KO}$/$RIP3^{-/-}$) were generated by intercrossing the respective lines. Alb-Cre Caspase-8Floxed transgenic mice were described previously (Hatting et al, 2013). In all experiments, littermates carrying the respective loxP-flanked alleles but lacking expression of Cre recombinase were used as wild-type (WT) controls. Mice were bred on a C57BL/6 genetic background. Only sex-matched animals were compared.

3.3.6.3. Animal experiments

Mice were fed with a methionine choline-deficient (MCD) diet (MP Biomedicals) for 2 weeks (short term) or 8 weeks (long term). Livers from these mice were collected, fixed in 4% PFA, and embedded in paraffin for histological evaluation. Intraperitoneal injection of the JNK-Inhibitor SP600125 (15 µl/1 mg) (Absource Diagnostics) or vehicle (DMSO) was performed twice a day over 2 weeks of MCD feeding.

3.3.6.4. Human liver tissue

Human liver biopsy specimens and clinicopathological data were obtained from Newcastle upon Tyne University / Hepatopancreatobiliary and Gastroenterology Research Tissue Bank and Essen University. The project was authorized by the local ethics committees and conducted in accordance with the ethical standards laid down in the Declaration of Helsinki (Newcastle and North Tyneside 1 Research Ethics Committee, Newcastle upon Tyne, Reference number 10/10906/41 and Research

Ethics Committee, Essen University, Reference number 09-4252). Histological scoring system for non-alcoholic fatty liver disease (NAFLD) was performed according to the NAS score system (Kleiner et al, 2005).

3.3.6.5. Serum analysis

Serum ALT, AST, and GLDH activities were measured by standard procedures in the Institute of Clinical Chemistry of the RWTH University Hospital Aachen.

3.3.6.6. Triglyceride assay

The intrahepatic triglyceride tenor was measured by TG liquicolor mono (Human Diagnostics) according to the manufacturer's instructions from homogenized frozen liver sample.

3.3.6.7. Western blot analysis

Liver tissue was homogenized in NP-40 lysis buffer using a tissue grind pestle (Kimble/Chase) to obtain protein lysates. These were separated by SDS–polyacrylamide gel electrophoresis (PAGE), transferred to PVDF membrane, and analyzed by immunoblotting. Membranes were probed with the following antibodies: anti p-AKT, anti p-ERK, anti p-JNK, anti p-p38 (Cell Signaling), anti-Caspase-8 (Enzo), anti-RIP3 (IMGENEX) and anti-GAPDH (ABD Serotec). As secondary antibodies, anti-rabbit-HRP and anti-mouse-HRP (Amersham) were used.

3.3.6.8. Flow cytometry

Multicolor staining was conducted using combinations of the following mAbs: F4/80 (Serotec), CD11b (eBioscience), CD45, and Ly6G (BD). Flow cytometric analysis was performed on a FACS-Canto II (BD). Absolute cell numbers were determined by adding 2 × 104 Calibrite APC beads (BD) to each sample before measurement as internal reference standard. Data were analyzed using FlowJo software (Tree Star). For measurement of MCP-1 in total liver protein extracts, we used the mouse FlowCytomix kit (eBioscience) according to the manufacturer's instructions using a FACSCanto II System (BD).

3.3.6.9. Histological examination

Paraffin sections (2 μm) were stained with H/E or various primary and secondary antibodies. Paraformaldehyde (4%)-fixed and paraffin-embedded liver tissue were incubated in Bond Primary antibody diluent (Leica), and staining was performed on a BOND-MAX immunohistochemistry robot (Leica Biosystems) using BOND polymer refine detection solution for DAB. The following antibodies were used: Antibodies against F4/80 (BMA Biomedicals AG, 1:120), anti-CD45 (BD, 1:200) anti-CK19 (TROMAIIIc, Hybridoma bank, 1:500), anti-Ki67 (NeoMarkers; 1:200), anti-cleaved Caspase-3 (Cell

Signaling; 1:300), anti-phospho c-Jun (Abcam, 1:100), and anti-RIP3 (Enzo, 1:500). Image acquisition was performed on an Olympus BX53 microscope with a Leica SCN400 slide scanner. The number of hepatocytes positively stained for the different nuclear markers (e.g. Ki67, pc-Jun) was determined using SlidePath TissueIA image analysis software (Leica) on whole tissue sections (paraffin embedded) and normalized to tissue area or hepatocyte number, respectively. Hepatocytes positively stained for cleaved Caspase-3 and RIP3 as well as macrophages positive for F4/80, immune cells positively stained for CD45 or MHCII, and fibrotic fibers stained with Sirius Red were quantified numerically (positive cells per total tissue area) or densitometrically (area stained per total tissue area) using SlidePath TissueIA image analysis software (Leica) on whole tissue sections and normalized to total tissue area.

3.3.6.10. Cell culture

L929 cells were cultured in Dulbecco's modified Eagle's medium supplemented with 10% fetal calf serum, penicillin (100 IU/ml), streptomycin (0.1 mg/ml), and L-glutamine (0.03%). Bone marrow cells were isolated from femur and tibia of 8-week-old C57BL6/J and $RIP3^{-/-}$ mice. To obtain fibroblast conditioned medium (FCM) which is known to contain the macrophage colony-stimulating factor (MCSF, CSF1), L929 fibroblasts were cultured in RPMI medium containing 10% fetal calf serum (FCS) for 3 days, and the supernatant was collected, filtered, and stored until usage at -80°C. For the generation of bone marrow derived macrophages (BMM), bone marrow cells were cultured in RPMI medium containing 10% FCS and 20% FCM for 1 week on bacterial grade plastic plates (Greiner). At day 7, cells were either left untreated or stimulated for additional 24 h with lipopolysaccharides (LPS, 1 lg/ml) (Sigma-Aldrich).

3.3.6.11. Analysis of cell survival

L929 cells were cultured overnight in 12-well plates and used at 50% of confluence. After pre-treatment with zVAD (20 µM) (Millipore) for 1 h, the cells were incubated with Necrostatin-1 (10 µM) (Santa Cruz), SP600125 (20 µM) (Absource), or DMSO as control. Nineteen hours later, the cells were incubated with 1 ng/ml of MTT reagent (Life Technologies) for 2 h. Once MTT crystals were developed and controlled under light microscopy, they were dissolved in DMSO and quantified by measuring absorbance at 540 nm.

3.3.6.12. Quantitative real-time PCR

Total RNA was purified from liver tissue using TRIzol reagent (Invitrogen) and an RNeasy Mini kit (Qiagen). The quantity and quality of the RNA were determined spectroscopically using a nanodrop (Thermo Scientific). Total RNA (1 µg) was used to synthesize cDNA using the Transcriptor cDNA First-

Strand Synthesis Kit (Roche) according to the manufacturer's protocol and was resuspended in 50 µl of H2O. cDNA samples (2 µl) were used for real-time PCR in a total volume of 25 µl using SYBR Green Reagent (Invitrogen) and specific primers on a qPCR machine (Applied Biosystems 7300 Sequence Detection System). All real-time PCRs were performed in duplicates. Data were generated and analyzed using SDS 2.3 and RQ manager 1.2 software. Primer sequences are available upon request. All values were normalized to the level of beta-actin mRNA.

3.3.6.13. Statistical analysis

Data were analyzed using PRISM software (GraphPad, Inc., La Jolla, CA) and are expressed as SEM. Statistical significance between experimental groups was assessed using unpaired two-sample t-test, Mann–Whitney test, and unpaired two-sample t-test with Welch's correction (*P < 0.05; **P < 0.01; ***P < 0.001). The exact P-values of each experiment and specific tests used are provided in Supplementary Table S1.

3.3.7. References

Anstee QM, Concas D, Kudo H, Levene A, Pollard J, Charlton P, Thomas HC, Thursz MR, Goldin RD. Impact of pan-caspase inhibition in animal models of established steatosis and non-alcoholic steatohepatitis. *J Hepatol*. 2010;**53**:542–550.

Baeck C, Wehr A, Karlmark KR, Heymann F, Vucur M, Gassler N, Huss S, Klussmann S, Eulberg D, Luedde T, et al. Pharmacological inhibition of the chemokine CCL2 (MCP-1) diminishes liver macrophage infiltration and steatohepatitis in chronic hepatic injury. *Gut*. 2012;**61**:416–426.

Bhala N, Angulo P, van der Poorten D, Lee E, Hui JM, Saracco G, Adams LA, Charatcharoenwitthaya P, Topping JH, Bugianesi E, et al. The natural history of nonalcoholic fatty liver disease with advanced fibrosis or cirrhosis: an international collaborative study. *Hepatology*. 2011;**54**:1208–1216.

Bonnet MC, Preukschat D, Welz PS, van Loo G, Ermolaeva MA, Bloch W, Haase I, Pasparakis M. The adaptor protein FADD protects epidermal keratinocytes from necroptosis in vivo and prevents skin inflammation. *Immunity*. 2011;**35**:572–582.

Chakraborty JB, Oakley F, Walsh MJ. Mechanisms and biomarkers of apoptosis in liver disease and fibrosis. *Int J Hepatol*. 2012;2012:648915.

Chang HY, Yang X. Proteases for cell suicide: functions and regulation of caspases. *Microbiol Mol Biol Rev.* 2000;**64**:821–846.

Cho YS, Challa S, Moquin D, Genga R, Ray TD, Guildford M, Chan FK. Phosphorylation-driven assembly of the RIP1-RIP3 complex regulates programmed necrosis and virus-induced inflammation. *Cell*. 2009;**137**:1112–1123.

Csak T, Dolganiuc A, Kodys K, Nath B, Petrasek J, Bala S, Lippai D, Szabo G. Mitochondrial antiviral signaling protein defect links impaired antiviral response and liver injury in steatohepatitis in mice. *Hepatology*. 2011;**53**:1917–1931.

Das M, Sabio G, Jiang F, Rincon M, Flavell RA, Davis RJ. Induction of hepatitis by JNK-mediated expression of TNF-alpha. *Cell*. 2009;**136**:249–260.

Degterev A, Maki JL, Yuan J. Activity and specificity of necrostatin-1, small-molecule inhibitor of RIP1 kinase. *Cell Death Differ*. 2013;**20**:366.

Dixon LJ, Flask CA, Papouchado BG, Feldstein AE, Nagy LE. Caspase-1 as a central regulator of high fat diet-induced non-alcoholic steatohepatitis*. PLoS ONE*. 2013;**8**:e56100.

Estaquier J, Vallette F, Vayssiere JL, Mignotte B. The mitochondrial pathways of apoptosis. *Adv Exp Med Biol*. 2012;**942**:157–183.

Feldstein AE, Canbay A, Angulo P, Taniai M, Burgart LJ, Lindor KD, Gores GJ. Hepatocyte apoptosis and fas expression are prominent features of human nonalcoholic steatohepatitis. *Gastroenterology*. 2003;**125**:437–443.

Feldstein AE, Gores GJ. Apoptosis in alcoholic and nonalcoholic steatohepatitis. Front Biosci. 2005;10:3093–3099.

Han J, Zhong CQ, Zhang DW. Programmed necrosis: backup to and competitor with apoptosis in the immune system. *Nat Immunol*. 2011;**12**:1143–1149.

Hatting M, Zhao G, Schumacher F, Sellge G, Al Masaoudi M, Gabetaler N, Boekschoten M, Muller M, Liedtke C, Cubero FJ, et al. Hepatocyte caspase-8 is an essential modulator of steatohepatitis in rodents. *Hepatology*. 2013;**57**:2189–2201.

He S, Wang L, Miao L, Wang T, Du F, Zhao L, Wang X. Receptor interacting protein kinase-3 determines cellular necrotic response to TNF-alpha. *Cell*. 2009;**137**:1100–1111.

Kaiser WJ, Upton JW, Long AB, Livingston-Rosanoff D, Daley-Bauer LP, Hakem R, Caspary T, Mocarski ES. RIP3 mediates the embryonic lethality of caspase-8-deficient mice. *Nature*. 2011;**471**:368–372.

Kellendonk C, Opherk C, Anlag K, Schutz G, Tronche F. Hepatocyte-specific expression of Cre recombinase. *Genesis*. 2000;**26**:151–153.

Kleiner DE, Brunt EM, Van Natta M, Behling C, Contos MJ, Cummings OW, Ferrell LD, Liu YC, Torbenson MS, Unalp-Arida A, et al. Design and validation of a histological scoring system for nonalcoholic fatty liver disease. *Hepatology*. 2005;**41**:1313–1321.

Li J, McQuade T, Siemer AB, Napetschnig J, Moriwaki K, Hsiao YS, Damko E, Moquin D, Walz T, McDermott A, et al. The RIP1/RIP3 necrosome forms a functional amyloid signaling complex required for programmed necrosis. *Cell*. 2012;**150**:339–350.

Liu K, Czaja MJ. Regulation of lipid stores and metabolism by lipophagy. *Cell Death Differ*. 2013;**20**:3–11.

Malhi H, Gores GJ. Molecular mechanisms of lipotoxicity in nonalcoholic fatty liver disease. *Semin Liver Dis*. 2008;**28**:360–369.

Najimi M, Smets F, Sokal E. Hepatocyte apoptosis. Methods Mol Biol. 2009;481:59–74.

Newton K, Sun X, Dixit VM. Kinase RIP3 is dispensable for normal NF-kappa Bs, signaling by the B-cell and T-cell receptors, tumor necrosis factor receptor 1, and Toll-like receptors 2 and 4. *Mol Cell Biol*. 2004;**24**:1464–1469.

Pattingre S, Tassa A, Qu X, Garuti R, Liang XH, Mizushima N, Packer M, Schneider MD, Levine B. Bcl-2 antiapoptotic proteins inhibit Beclin 1-dependent autophagy. *Cell*. 2005;**122**:927–939.

Poelstra K, Schuppan D. Targeted therapy of liver fibrosis/cirrhosis and its complications*. J Hepatol.* 2011;**55**:726–728.

Postic C, Shiota M, Niswender KD, Jetton TL, Chen Y, Moates JM, Shelton KD, Lindner J, Cherrington AD, Magnuson MA. Dual roles for glucokinase in glucose homeostasis as determined by liver and pancreatic beta cell-specific gene knock-outs using Cre recombinase. *J Biol Chem*. 1999;**274**:305–315.

Ratziu V, Sheikh MY, Sanyal AJ, Lim JK, Conjeevaram H, Chalasani N, Abdelmalek M, Bakken A, Renou C, Palmer M, et al. A phase 2, randomized, double-blind, placebo-controlled study of GS-9450 in subjects with nonalcoholic steatohepatitis. *Hepatology*. 2012;**55**:419–428.

Richardson MM, Jonsson JR, Powell EE, Brunt EM, Neuschwander-Tetri BA, Bhathal PS, Dixon JB, Weltman MD, Tilg H, Moschen AR, et al. Progressive fibrosis in nonalcoholic steatohepatitis: association with altered regeneration and a ductular reaction. *Gastroenterology.* 2007;**133**:80–90.

Roychowdhury S, McMullen MR, Pisano SG, Liu X, Nagy LE. Absence of receptor interacting protein kinase 3 prevents ethanol-induced liver injury. *Hepatology*. 2013;**57**:1773–1783.

Salmena L, Lemmers B, Hakem A, Matysiak-Zablocki E, Murakami K, Au PY, Berry DM, Tamblyn L, Shehabeldin A, Migon E, et al. Essential role for caspase 8 in T-cell homeostasis and T-cell-mediated immunity. *Genes Dev*. 2003;**17**:883–895.

Schattenberg JM, Singh R, Wang Y, Lefkowitch JH, Rigoli RM, Scherer PE, Czaja MJ. JNK1 but not JNK2 promotes the development of steatohepatitis in mice. *Hepatology*. 2006;**43**:163–172.

Schattenberg JM, Schuppan D. Nonalcoholic steatohepatitis: the therapeutic challenge of a global epidemic. *Curr Opin Lipidol*. 2011;**22**:479–488.

Schuppan D, Afdhal NH. Liver cirrhosis. *Lancet*. 2008;**371**:838–851.

Schuppan D, Kim YO. Evolving therapies for liver fibrosis. *J Clin Invest*. 2013;**123**:1887–1901.

Seifert EL, Estey C, Xuan JY, Harper ME. Electron transport chain-dependent and -independent mechanisms of mitochondrial H2O2 emission during long-chain fatty acid oxidation. *J Biol Chem*. 2010;**285**:5748–5758.

Seki E, de Minicis S, Inokuchi S, Taura K, Miyai K, van Rooijen N, Schwabe RF, Brenner DA. CCR2 promotes hepatic fibrosis in mice. *Hepatology*. 2009;**50**:185–197.

Sun L, Wang H, Wang Z, He S, Chen S, Liao D, Wang L, Yan J, Liu W, Lei X, et al. Mixed lineage kinase domain-like protein mediates necrosis signaling downstream of RIP3 kinase. *Cell*. 2012;**148**:213–227.

Tacke F, Luedde T, Trautwein C. Inflammatory pathways in liver homeostasis and liver injury. *Clin Rev Allergy Immunol*. 2008;**36**:4–12.

Vernon G, Baranova A, Younossi ZM. Systematic review: the epidemiology and natural history of non-alcoholic fatty liver disease and non-alcoholic steatohepatitis in adults. *Aliment Pharmacol Ther*. 2011;**34**:274–285.

Vucur M, Reisinger F, Gautheron J, Janssen J, Roderburg C, Cardenas DV, Kreggenwinkel K, Koppe C, Hammerich L, Hakem R, et al. RIP3 inhibits inflammatory hepatocarcinogenesis but promotes cholestasis by controlling caspase-8- and JNK-dependent compensatory cell proliferation. *Cell Rep*. 2013;**4**:776–790.

Weinlich R, Oberst A, Dillon CP, Janke LJ, Milasta S, Lukens JR, Rodriguez DA, Gurung P, Savage C, Kanneganti TD, et al. Protective roles for caspase-8 and cFLIP in adult homeostasis. *Cell Rep.* 2013;**5**:340–348.

Welz PS, Wullaert A, Vlantis K, Kondylis V, Fernandez-Majada V, Ermolaeva M, Kirsch P, Sterner-Kock A, van Loo G, Pasparakis M. FADD prevents RIP3-mediated epithelial cell necrosis and chronic intestinal inflammation. *Nature*. 2011;**477**:330–334.

Wieckowska A, Zein NN, Yerian LM, Lopez AR, McCullough AJ, Feldstein AE. In vivo assessment of liver cell apoptosis as a novel biomarker of disease severity in nonalcoholic fatty liver disease. *Hepatology*. 2006;**44**:27–33.

Witek RP, Stone WC, Karaca FG, Syn WK, Pereira TA, Agboola KM, Omenetti A, Jung Y, Teaberry V, Choi SS, et al. Pan-caspase inhibitor VX-166 reduces fibrosis in an animal model of nonalcoholic steatohepatitis. *Hepatology*. 2009;**50**:1421–1430.

Wree A, Broderick L, Canbay A, Hoffman HM, Feldstein AE. From NAFLD to NASH to cirrhosis-new insights into disease mechanisms. *Nat Rev Gastroenterol Hepatol*. 2013;**10**:627–636.

Yang L, Roh YS, Song J, Zhang B, Liu C, Loomba R, Seki E. Transforming growth factor beta signaling in hepatocytes participates in steatohepatitis through regulation of cell death and lipid metabolism in mice. *Hepatology*. 2014;**59**:483–495.

Younossi ZM, Jarrar M, Nugent C, Randhawa M, Afendy M, Stepanova M, Rafiq N, Goodman Z, Chandhoke V, Baranova A. A novel diagnostic biomarker panel for obesity-related nonalcoholic steatohepatitis (NASH) *Obes Surg*. 2008;**18**:1430–1437.

Yousefi S, Perozzo R, Schmid I, Ziemiecki A, Schaffner T, Scapozza L, Brunner T, Simon HU. Calpain-mediated cleavage of Atg5 switches autophagy to apoptosis. *Nat Cell Biol.* 2006;**8**:1124–1132.

Zhang DW, Shao J, Lin J, Zhang N, Lu BJ, Lin SC, Dong MQ, Han J. RIP3, an energy metabolism regulator that switches TNF-induced cell death from apoptosis to necrosis. *Science*. 2009;**325**:332–336.

Zimmermann HW, Tacke F. Modification of chemokine pathways and immune cell infiltration as a novel therapeutic approach in liver inflammation and fibrosis. *Inflamm Allergy Drug Targets*. 2011;**10**:509–536.

3.3.8. Personal contributions

Hepatocyte cell death – until lately mainly characterized as hepatocyte apoptosis – is an essential step in the progression from NAFLD to NASH. In this study we could show that RIP3, the main initiating molecule of necroptosis, was upregulated in human NASH patients and in the MCD-diet NASH mosue model. RIP3 mediated liver damage, inflammation and hepatic progenitor cell activation, while as Caspase-8 showed a protective function and counterbalanced RIP3-induced liver damage. My main task in this study was the evaluation of inflammation, liver damage, fibrosis and the underlying signaling molecules on histological and immunohistochemical level. In addition I actively contributed to the conceptual development of several hypotheses in this study.

Analyses and figures contributed:

Figure 1c and d: Immunohistochemical (RIP3, Ki67) analysis on representative liver sections from the indicated mice fed for 8 weeks with MCD-diet (**c**) and statistical analysis of RIP^+ and $Ki67^+$ hepatocytes.(**d**) Results are shown as mean, n = 5.

Figure 2A and B Representative H&E staining (**a**) and Sirius Red staining (**b**) of liver slides from 16-week-old WT, Casp-$8^{LPC\text{-}KO}$, Casp-$8^{LPC\text{-}KO}$/$RIP3^{-/-}$, and $RIP3^{-/-}$ mice fed for 8 weeks with normal chow or MCD-diet

Figure 2d: Quantification of fibrotic area upon MCD-diet

Figure 3a and b: Immunohistochemicyl staining (**a**) and quantification of $CD45^+$ cells and $F4/80^+$ foci (**b**)

Figure 4: Immunohistocemical staining for CK19 (**a**) and quantification of CK19-positive area (**b**). Immunohistocemical staining for RIP3 in WT and Caspase-$8^{LPC\text{-}KO}$ mice upon MCD-diet feeding

Figure 5c: Immunohistocemical staining for RIP3 in control livers compared to NASH patients

Figure6b: Immunohistochemical and statistical analysis of phosphor-cJUN-positive hepatocytes in Caspase-$8^{LPC\text{-}KO+}$ mice upon JNK-inhibition and MCD-diet

Figure 6e: Immunohistochemical and statistical analysis of CD45 and F4/80 in Caspase-$8^{LPC\text{-}KO}$ mice upon JNK-inhibition and MCD-diet

Figure 6f: Immunohistocemical staining for RIP3 in Caspase-$8^{LPC\text{-}KO}$ mice upon JNK-inhibition and MCD-diet

3.4. RIP3 Inhibits Inflammatory Hepatocarcinogenesis but Promotes Cholestasis by Controlling Caspase-8- and JNK-Dependent Compensatory Cell Proliferation

'Introduction', 'Material and Methods', 'Results' and 'Discussion' have been described in the following publication:Vucur, Reisinger, Gautheron et al*. Cell Reports* (2013) 4(4), 776-90

3.4.1. Authors

Mihael Vucur,* **Florian Reisinger**,* Jérémie Gautheron,* Joern Janssen, Christoph Roderburg, David Vargas Cardenas, Karina Kreggenwinkel, Christiane Koppe, Linda Hammerich, Razq Hakem, Kristian Unger, Achim Weber, Nikolaus Gassler, Mark Luedde, Norbert Frey, Ulf Peter Neumann, Frank Tacke, Christian Trautwein, Mathias Heikenwalder, and Tom Luedde

* equal contribution

3.4.2. Summary

For years, the term ''apoptosis'' was used synonymously with programmed cell death. However, it was recently discovered that receptor interacting protein 3 (RIP3)-dependent ''necroptosis'' represents an alternative programmed cell death pathway activated in many inflamed tissues. Here, we show in a genetic model of chronic hepatic inflammation that activation of RIP3 limits immune responses and compensatory proliferation of liver parenchymal cells (LPC) by inhibiting Caspase-8-dependent activation of Jun-(N)-terminal kinase in LPC and nonparenchymal liver cells. In this way, RIP3 inhibits intrahepatic tumor growth and impedes the Caspase-8-dependent establishment of specific chromosomal aberrations that mediate resistance to tumor-necrosis-factor-induced apoptosis and underlie hepatocarcinogenesis. Moreover, RIP3 promotes the development of jaundice and cholestasis, because its activation suppresses compensatory proliferation of cholangiocytes and hepatic stem cells. These findings demonstrate a function of RIP3 in regulating carcinogenesis and cholestasis. Controlling RIP3 or Caspase-8 might represent a chemopreventive or therapeutic strategy against hepatocellular carcinoma and biliary disease.

3.4.3. Introduction

Hepatocellular carcinoma (HCC), the most common primary liver tumor, arises almost exclusively in a setting of chronic hepatic inflammation (Sherman, 2010). However, the knowledge on the clear association between inflammation and cancer has not yet translated into a chemopreventive pharmacological strategy against HCC development, underlining the need for a better understanding

of molecular processes controlling the transition from inflammation to cancer. Cell death represents a dominant trigger for inflammation, thus contributing to multiple hallmark capabilities of cancer (Hanahan and Weinberg, 2011). In chronic liver disease, hepatocyte cell death is a prominent feature driving progression to hepatic fibrosis and finally HCC (Zhang and Friedman, 2012).

For years, the term apoptosis was used synonymously for programmed cell death, whereas necrosis was considered a passive, not specifically regulated, and ATP-independent process (Chakraborty et al., 2012). Apoptosis is triggered by ligation of death receptors, like tumor necrosis factor (TNF) receptor, by their cognate ligands and represents a highly synchronized procedure depending on activation of aspartate-specific proteases, known as caspases (Chakraborty et al., 2012). In viral hepatitis, immune cell-triggered apoptosis of virally infected hepatocytes represents a key step in viral clearance (Fung et al., 2009). Moreover, apoptotic death of hepatocytes is a common feature of alcoholic and nonalcoholic steatohepatitis and is associated with fibrosis (Feldstein and Gores, 2005).

It was recently discovered that, next to apoptosis, necroptosis— programmed necrosis depending on the kinases receptor interacting protein 1 (RIP1) and RIP3—represents an alternative programmed cell-death pathway downstream of the TNF-receptor (Cho et al., 2009; He et al., 2009; Zhang et al., 2009). It can be induced by viral infection and can serve as an alternative when caspase-dependent apoptosis is inhibited or absent (Han et al., 2011). Necroptosis plays a role in the regulation of chronic inflammation in the pancreas, gut, and skin (Bonnet et al., 2011; He et al., 2009; Welz et al., 2011). In human patients, necroptosis is activated in alcoholic liver injury (Roychowdhury et al., 2013) as one of the leading causes of liver cirrhosis and HCC in the western world (Sherman, 2010). However, the functional role of RIP3 in controlling the consequences of chronic inflammation in the liver and other organs is presently not known. In this study, we examined the role of RIP3 in a model of inflammatory hepatocarcinogenesis based on conditional deletion of the mitogenactivated protein 3 (MAP3)-kinase transforming growth factor b (TGF-b)-activated-kinase-1 (TAK1) in liver parenchymal cells (LPC) ($TAK1^{LPC\text{-}KO}$) (Bettermann et al., 2010).

3.4.4. Results

3.4.4.1. RIP3 Is Activated in TAK1-Deficient Livers and Promotes Jaundice and Cholestasis by Inhibiting a Sufficient Ductular Reaction

Mice with conditional deletion of Tak1 in LPC ($TAK1^{LPC\text{-}KO}$ mice) display severe hepatic inflammation at a young age characterized by spontaneous LPC apoptosis and LPC necrosis, proceeding over time to liver fibrosis and liver cancer but also to severe lethal cholestasis (Bettermann et al., 2010). In order

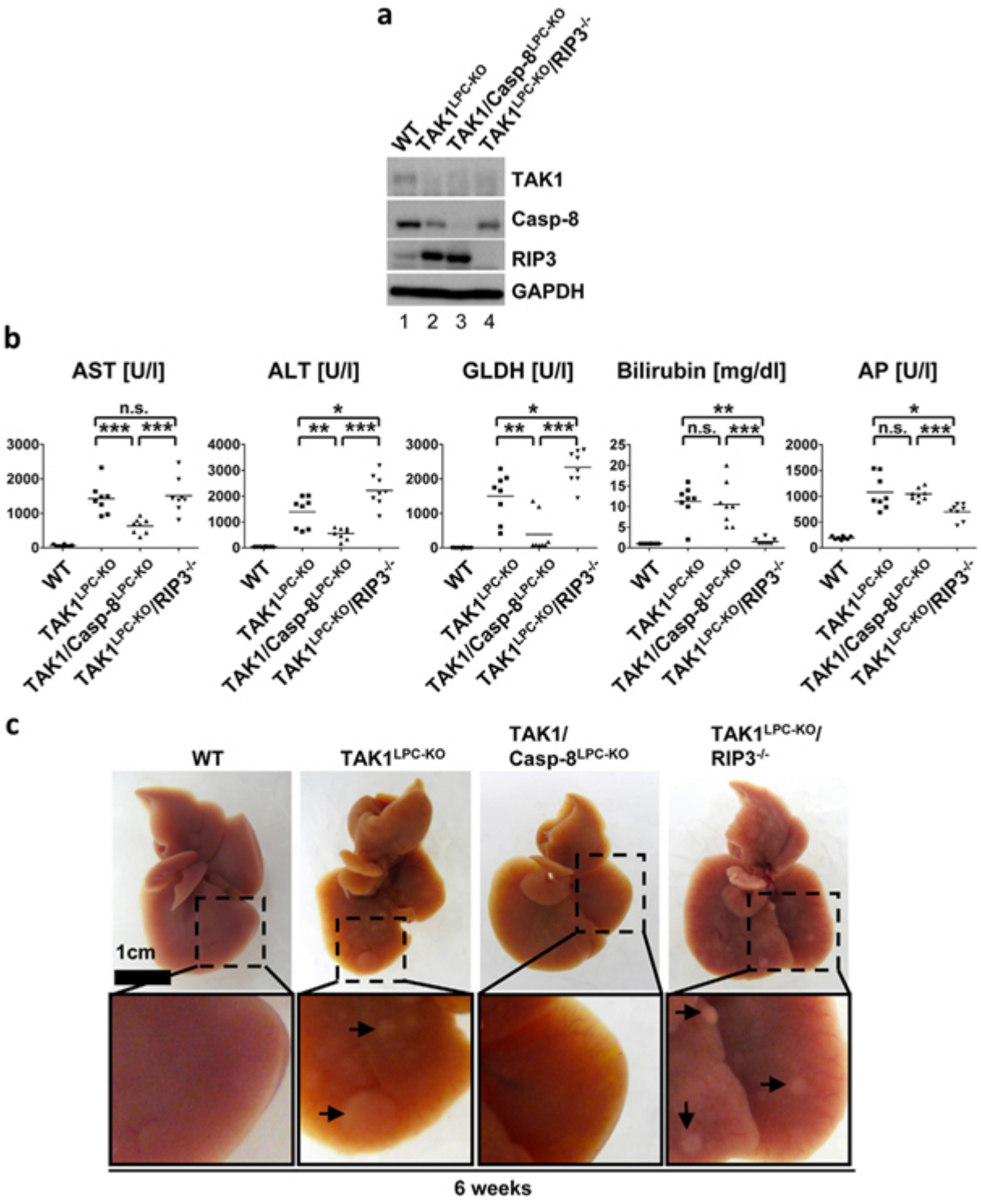

Figure 1: Apoptosis and Necroptosis Differentially Regulate Dysplasia, Cholestasis, and Liver Injury in Mice with LPC-specific Tak1 Deletion. (a) Western blot analysis of whole liver protein extracts from 6-week-old male TAK1^{LPC-KO}, TAK1/Casp-8^{LPC-KO}, TAK1^{LPC-KO}/RIP3$^{-/-}$, and control littermate mice (WT) using antibodies against TAK1, RIP3, Caspase-8, and glyceraldehyde 3-phosphate dehydrogenase (GAPDH) as loading control. (b) Serum level analysis of AST, ALT, glutamate dehydrogenase (GLDH), total bilirubin, and AP in 6-week-old male mice. Results are shown as mean. Double asterisks denote $p < 0.01$ and triple asterisks denote $p < 0.001$ ($n = 8$ each genotype). (c) Representative macroscopic pictures of 6-week-old male WT, TAK1^{LPC-KO}, TAK1/Casp-8^{LPC-KO}, and TAK1^{LPC-KO}/RIP3$^{-/-}$ livers. Small nodular structures are observed in livers of TAK1^{LPC-KO} and TAK1^{LPC-KO}/RIP3$^{-/-}$ mice but not on TAK1/Casp-8^{LPC-KO} livers. Arrows indicate nodules. Additionally, TAK1^{LPC-KO} and TAK1/Casp-8^{LPC-KO} but not TAK1^{LPC-KO}/RIP3$^{-/-}$ livers display a cholestatic, yellow color. The scale bars represent 1 cm.

to investigate the function of RIP3 in hepatocarcinogenesis, we generated mice with ablation of TAK1in LPC together with a full knockout of Rip3 ($TAK1^{LPC\text{-}KO}/RIP3^{-/-}$) or combined ablations of TAK1 and Caspase-8 in LPC ($TAK1/Casp\text{-}8^{LPC\text{-}KO}$) and first compared their phenotypes with wild-type (WT) and TAK1 single mutant mice ($TAK1^{LPC\text{-}KO}$) at the age of 6 weeks (**Fig. 1a**).

We detected strongly increased protein levels of RIP3 in liver extracts from $TAK1^{LPC\text{-}KO}$ and $TAK1/Casp\text{-}8^{LPC\text{-}KO}$ mice (**Fig. 1a**), suggesting that LPC in these mice might be sensitized to necrosis (He et al., 2009). Measurements of serum enzymes from 6-week-old male mice confirmed that $TAK1^{LPC\text{-}KO}$ mice showed a strong rise in serum aminotransferases (alanine aminotransferase [ALT] and aspartate aminotransferase [AST]) and serum glutamate dehydrogenase (GLDH) levels compared to WT mice as marker for hepatitis and LPC damage (**Fig. 1b**).

Macroscopic analysis revealed that this coincided with yellow color of livers and elevated serum bilirubin and alkaline phosphatase (AP) levels (Figures 1B and 1C), reflecting severe jaundice and cholestasis as shown previously by electron-microscopical analysis of bile canaliculi in $TAK1^{LPC\text{-}KO}$ animals (Bettermann et al., 2010). Moreover, $TAK1^{LPC\text{-}KO}$ livers displayed macroscopically visible nodules on the surface of livers (Figure 1C). Deletion of Caspase-8 in $TAK1^{LPC\text{-}KO}$ mice led to significant reduction in ALT, AST, and GLDH serum levels, and disappearance of macroscopic nodules on the surface of liver lobes compared to $TAK1^{LPC\text{-}KO}$ mice. However, no rescue in hyperbilirubinemia and AP elevation was found (Figures 1B and 1C). In contrast, deletion of Rip3 in $TAK1^{LPC\text{-}KO}$ mice led to a normalization of bilirubin and reduced AP levels but worsened hepatitis, indicated by significantly elevated ALT and GLDH levels in $TAK1^{LPC\text{-}KO}/ RIP3^{-/-}$ mice compared to $TAK1^{LPC\text{-}KO}$ animals (**Fig. 1b**).

Moreover, while at 6 weeks of age, $TAK1^{LPC\text{-}KO}/RIP3^{-/-}$ livers lacked a yellow color as a sign of jaundice; they displayed multiple small nodules on their surface (**Fig. 1c**). Histological analysis of liver sections from 6-week-old male mice revealed that jaundice in $TAK1^{LPC\text{-}KO}$ mice correlated with the presence of areas of hepatocyte necrosis, which were detected even to a higher extent in $TAK1/Casp\text{-}8^{LPC\text{-}KO}$ animals, whereas necrosis was absent in $TAK1^{LPC\text{-}KO}/RIP3^{-/-}$ mice at this age (**Fig. 2a** and **2b**). In parallel to the absence of necrosis, $TAK1^{LPC\text{-}KO}/RIP3^{-/-}$ mice showed a strong ductular reaction with expansion of A6+ (oval) cells (**Fig. 2a–2d**), likely reflecting a necessary process to maintain biliary homeostasis in a setting of chronic inflammation (Desmet, 2011; Glaser et al., 2009). Strikingly, this ductular reaction was absent in $TAK1^{LPC\text{-}KO}$ and $TAK1/ Casp\text{-}8^{LPC\text{-}KO}$ mice (**Fig. 2a, 2c**, and **2d**). These data demonstrate that, in chronic hepatitis, Caspase-8-dependent apoptosis primarily causes elevation of free circulating aminotransferases and GLDH in the serum. In contrast, RIP3-dependent necroptosis promotes jaundice and cholestasis in $TAK1^{LPC\text{-}KO}$ livers, because it is not linked with a ductular reaction.

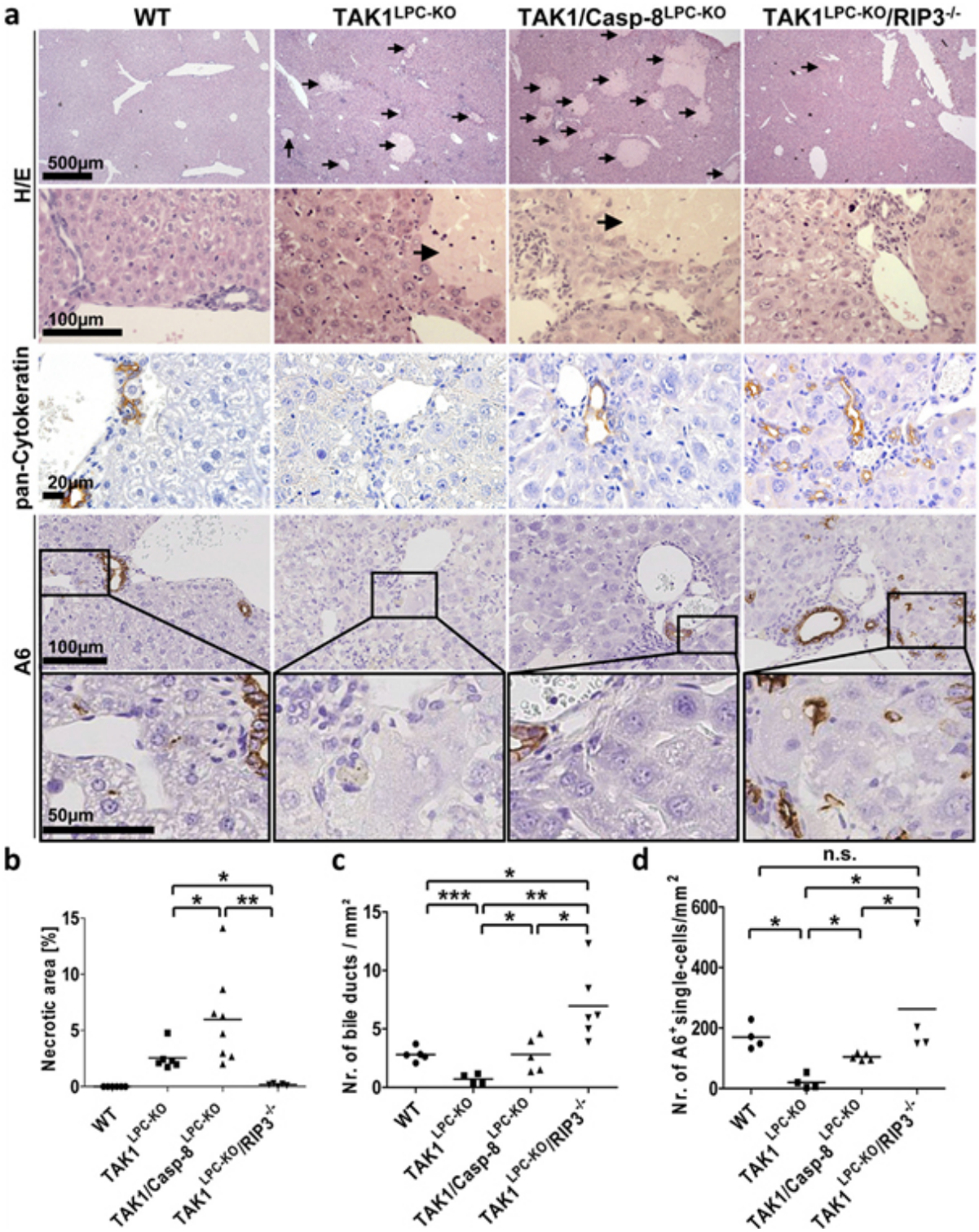

Figure 2: RIP3-Dependent Necroptosis Mediates Cholestasis and Biliary Ductopenia by Suppressing Caspase-8-Dependent Ductular Reaction in Livers of Mice with LPC-Specific Tak1 Deletion. (a) Histological (H&E) and immunohistochemical (pancytokeratin, A6) analysis on representative liver sections from 6-week-old male mice. Arrows indicate necrotic areas. Scale bars represent (from top to bottom) 500 mm, 100 mm, 20 mm, 100 mm, and 50 mm. (b) Evaluation of necrotic areas from H&E staining. WT (n = 6), TAK1^{LPC-KO} (n = 6), TAK1/Casp-8^{LPC-KO} (n = 6), and TAK1^{LPC-KO}/RIP3$^{-/-}$ (n = 5) livers. Results are shown as mean. The asterisk denotes $p < 0.05$ and double asterisks denote $p < 0.01$.(C) Statistical quantification of number of bile ducts per mm2 in WT (n = 5), TAK1^{LPC-KO} (n = 4), TAK1/Casp-8^{LPC-KO} (n = 5), and TAK1^{LPC-KO}/RIP3$^{-/-}$ (n = 6) livers. TAK1^{LPC-KO} livers show decreasing of bile ducts, whereas, in TAK1^{LPC-KO}/RIP3$^{-/-}$, livers increase the number of bile ducts compared with the other genotypes. Results are shown as mean. The asterisk denotes $p < 0.05$, double asterisks denote $p < 0.01$, and triple asterisks denote $p < 0.001$. (d) Statistical analysis of A6+ single-oval cells/mm2 in the respective 6-week-old mice. Results are shown as mean (n = 4, except for TAK1/Casp-8^{LPC-KO} mice, where n = 5); *$p < 0.05$; n.s., not significant.

3.4.4.2. Activation of RIP3 Limits Compensatory Proliferation of Hepatocytes and Biliary Epithelial Cells in the Chronically Inflamed Liver

We further analyzed the influence of RIP3 and Caspase-8 on cell death in TAK1$^{LPC\text{-}KO}$ animals. In line with previous findings (Bettermann et al., 2010), TAK1$^{LPC\text{-}KO}$ mice displayed significant spontaneous LPC apoptosis as shown by immunohistochemistry and western blot analyses for cleaved Caspase-3 (**Fig. 3a–3c**). Additional deletion of Caspase-8 resulted in complete inhibition of Caspase-3 cleavage, whereas additional deletion of Rip3 in TAK1$^{LPC\text{-}KO}$ mice resulted in a significant increase in Caspase-3 cleavage when compared to TAK1$^{LPC\text{-}KO}$ mice (**Fig. 3a–3c**). Therefore, Caspase-8-dependent apoptosis and RIP3-dependent necroptosis counterbalance and compete with each other in the regulation of LPC death in TAK1$^{LPC\text{-}KO}$ livers (compare Figures 2A and 2B and Figures 3A–3C).

We next examined the functions of Caspase-8 and RIP3 in LPC proliferation in Tak1-deficient livers. Ki67 staining and western blot analyses of the cell cycle proteins proliferating cell nuclear antigen (PCNA) and cyclin D1 confirmed a high proportion of proliferating LPC in TAK1$^{LPC\text{-}KO}$ mice (Figures 3A–3C). Additional deletion of Caspase-8 dramatically reduced the number of proliferating LPC and the degree of PCNA/cyclin D1 expression, whereas proliferation remained high or was even higher by tendency in mice with combined deletions of Tak1 and Rip3 (**Fig. 3a–3c**). This indicates that Caspase-8-dependent LPC apoptosis induces strong compensatory proliferation of other adjacent LPC, which is not the case in terms of LPC necroptosis. Interestingly, not only hepatocytes but also biliary cells in TAK1$^{LPC\text{-}KO}$/RIP3$^{-/-}$ mice displayed increased apoptosis and proliferation, as indicated by costainings for pancytokeratin and Ki67 or cleaved Caspase-3 (**Fig. 3d–3f**). Thus, differential degrees of compensatory cell proliferation upon apoptosis versus necroptosis are a likely cause for the presence or absence of a sufficient ductular reaction and cholestasis in TAK1$^{LPC\text{-}KO}$/RIP3$^{-/-}$ and TAK1/Casp-8$^{LPC\text{-}KO}$ mice, respectively.

To evaluate the effect of Caspase-8 deletion in LPC, we further performed serological and histological analyses on Casp-8$^{LPC\text{-}KO}$ mice. This analysis revealed mild liver injury, indicated by elevated serum ALT, AST, and GLDH, but no changes in the biliary system or infiltration with myelomonocytic cells (data not shown). In addition, we tested whether the molecules Caspase-8 or RIP3 might have limiting effects on LPC proliferation and performed partial hepatectomy (PH) experiments in Casp-8$^{LPC\text{-}KO}$ mice or mice with constitutive deletion of Rip3 (RIP3$^{-/-}$). Whereas WT and RIP3$^{-/-}$ animals showed similar expression levels of cell cycle markers cyclin D1 and PCNA in western blot and Ki67-expression in immunohistochemical analysis, Casp-8$^{LPC\text{-}KO}$ animals even displayed a slight acceleration in cell-cycle progression (data not shown). This indicates that the differences in the proliferative response between TAK1$^{LPC\text{-}KO}$/RIP3$^{-/-}$ and TAK1/Casp-8$^{LPC\text{-}KO}$ animals were not caused by direct effects

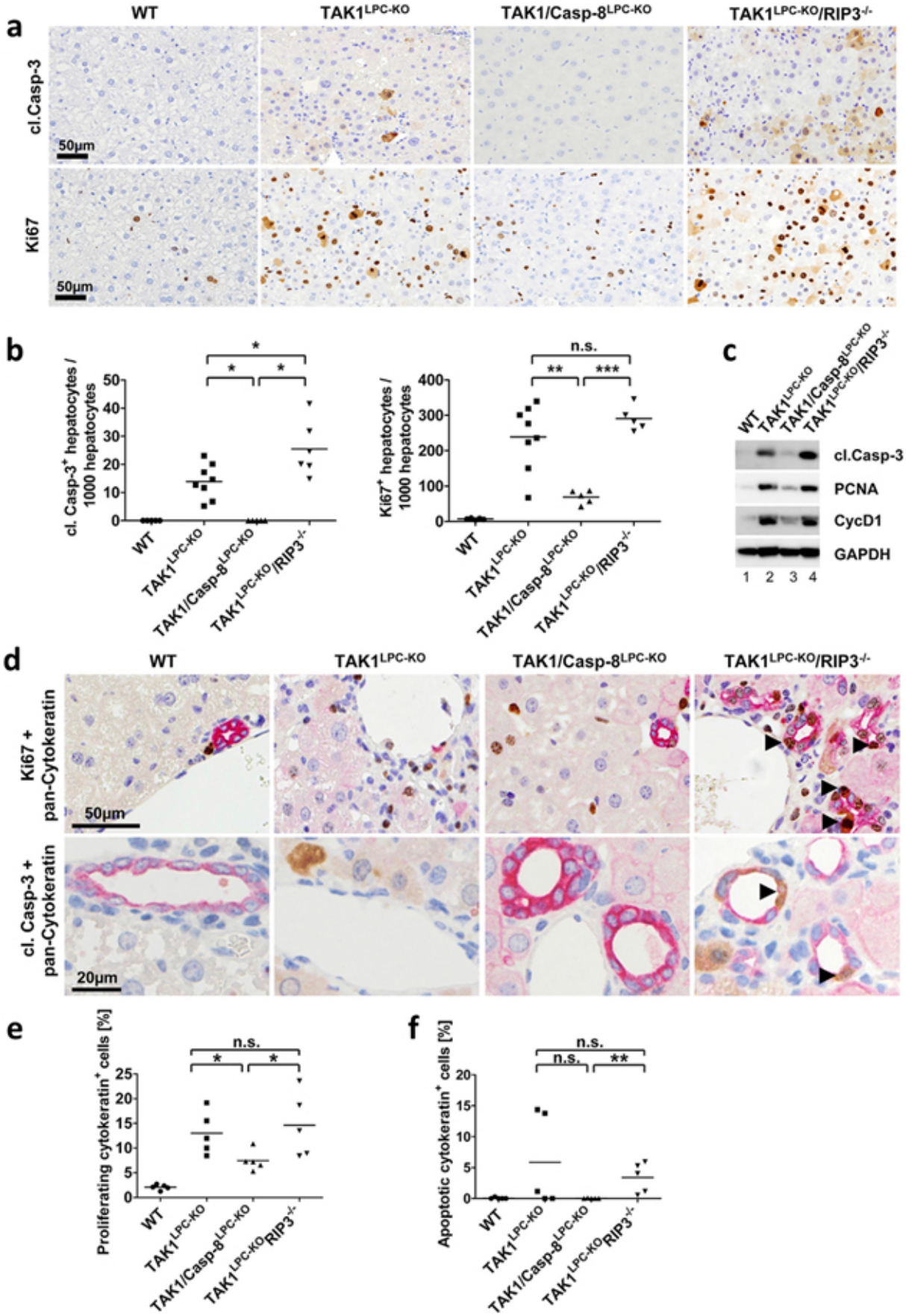
a
WT
TAK1LPC-KO
TAK1/Casp-8LPC-KO
TAK1LPC-KO/RIP3-/-
cl.Casp-3
Ki67
50µm
50µm
b
cl. Casp-3+ hepatocytes / 1000 hepatocytes
Ki67+ hepatocytes / 1000 hepatocytes
n.s.
WT
TAK1LPC-KO
TAK1/Casp-8LPC-KO
TAK1LPC-KO/RIP3-/-
c
cl.Casp-3
PCNA
CycD1
GAPDH
1 2 3 4
d
Ki67 + pan-Cytokeratin
cl. Casp-3 + pan-Cytokeratin
50µm
20µm
e
Proliferating cytokeratin+ cells [%]
f
Apoptotic cytokeratin+ cells [%]

Figure 3: Apoptosis but Not Necroptosis Induces Strong Compensatory Proliferation of Hepatocytes and Biliary Epithelial Cells upon Chronic Liver Injury. (a) Immunohistochemical analysis on representative liver paraffin sections from 6-week-old male mice of the indicated genotypes. Upper panel: cleaved (cl.) Caspase-3 staining. Lower panel: Ki67 staining. The scale bars represent 50 mm. (b) Statistical analysis of $Ki67^{+}$ and cl. $Casp\text{-}3^{+}$ hepatocytes. Results are shown as mean (cl. Casp-3 staining: WT [n = 5]; $TAK1^{LPC\text{-}KO}$ [n = 8]; TAK1/$Casp\text{-}8^{LPC\text{-}KO}$ [n = 5]; $TAK1^{LPC\text{-}KO}/RIP3^{-/-}$ [n = 6] and Ki67 staining:WT[n = 5]; $TAK1^{LPC\text{-}KO}$ [n = 8]; TAK1/$Casp\text{-}8^{LPC\text{-}KO}$ [n = 5]; $TAK1^{LPC\text{-}KO}/RIP3^{-/-}$ [n = 5]). *p < 0.05, **p < 0.01, ***p < 0.001. (c) Western blot analysis of whole liver protein extracts from 6-week-old male $TAK1^{LPC\text{-}KO}$, TAK1/$Casp\text{-}8^{LPC\text{-}KO}$, $TAK1^{LPC\text{-}KO}/RIP3^{-/-}$, and control littermate mice (WT) using antibodies against PCNA, CycD1, cl. Casp-3, and GAPDH as loading control. (d) Double stainings of pancytokeratin with Ki67 (upper panel; pancytokeratin is stained pink, Ki67 is stained brown) or cl. Casp-3 (lower panel; pancytokeratin is stained pink, cl. Casp-3 is stained brown). Arrowheads indicate double-stained cells. (e) Statistical analysis of double-stained pancytokeratin^{+} and $Ki67^{+}$ biliary epithelial cells in the respective 6-week-old mice. Results are shown as mean (n = 5); *p < 0.05; n.s., not significant. (f) Statistical analysis of double-stained pancytokeratin^{+} and cl. $Casp\text{-}3^{+}$ biliary epithelial cells in the respective 6-week-old mice. Results are shown as mean (n = 5). **p < 0.01.

of Caspase-8 or RIP3 on the cell-cycle machinery, however, suggest that apoptosis but not necroptosis of LPC represents a strong trigger for compensatory LPC proliferation.

The kinase TAK1 integrates signals from several upstream ligands and regulates various inflammatory and stress-related signaling pathways (Delaney and Mlodzik, 2006). We therefore tested whether, besides apoptosis and necroptosis, other signaling pathways might be involved in hepatitis and cholestasis development in Tak1-deficient livers and generated mice with combined deletions of Tak1 and Caspase-8 in LPC together with full knockout of Rip3 (TAK1/$Casp\text{-}8^{LPC\text{-}KO}/RIP3^{-/-}$ mice; **Figure S2A**). On macroscopic, serological, and histological level, combined deletions of Caspase-8 and Rip3 completely rescued hepatitis, liver injury, cholestasis, and biliary ductopenia seen in TAK1 single mutants (**Figures S2b–S2d**). This highlights that apoptosis and necroptosis represent the major pathways mediating the severe phenotype in Tak1-deficient livers. Further, this argues against significant influences of potential dysregulation of biliary transporters or structural cell proteins in biliary epithelial cells in response to Tak1 deletion.

3.4.4.3. Activation of RIP3 Inhibits Hepatic Tumor Growth

Based on the differential functional relations between apoptotic versus necroptotic cell death and compensatory LPC proliferation, we next evaluated if RIP3 and Caspase-8 might also differentially regulate hepatocarcinogenesis. Hence, we examined the spontaneous phenotype of 25- to 38-week-old animals, because TAK1 single mutants develop HCC at that age (Bettermann et al., 2010). Macroscopic analyses of livers confirmed the presence of hepatic tumors in $TAK1^{LPC\text{-}KO}$ mice (**Fig. 4a**). Surprisingly, TAK1/$Casp\text{-}8^{LPC\text{-}KO}$ animals did not show any signs of macroscopically detectable hepatic tumors at this age. In contrast, $TAK1^{LPC\text{-}KO}/RIP3^{-/-}$ mice exhibited a massive hepatic tumor burden already visible on macroscopic level (**Fig. 4a**). The high hepatic tumor burden in these mice

corresponded with a significant increase in the liver-to-body weight ratio in TAK1^{LPC-KO}/RIP3$^{-/-}$ animals compared to TAK1 single mutants or TAK1/Casp-8 combined mutants (**Fig. 4b**). On the histological level, we confirmed increased development of hepatic tumors with histological criteria of HCC in TAK1^{LPC-KO}/RIP3$^{-/-}$ mice by hematoxylin and eosin staining (H&E) staining and immunohistochemical analysis for collagen-IV expression.

Conversely, no histologically malignant hepatic tumor or preneoplastic lesions could be detected in TAK1/Casp-8^{LPC-KO} animals (**Fig. 4c** and **4d**). Thus, Caspase-8-dependent apoptosis promotes HCC development in TAK1^{LPC-KO} mice. In contrast, the higher tumor burden in TAK1^{LPC-KO}/RIP3$^{-/-}$ mice compared to TAK1^{LPC-KO} mice and the absence of hepatic tumors in TAK1/Casp-8^{LPC-KO} livers exhibiting pure necroptosis suggest that activation of RIP3 has an inhibitory effect on tumor growth.

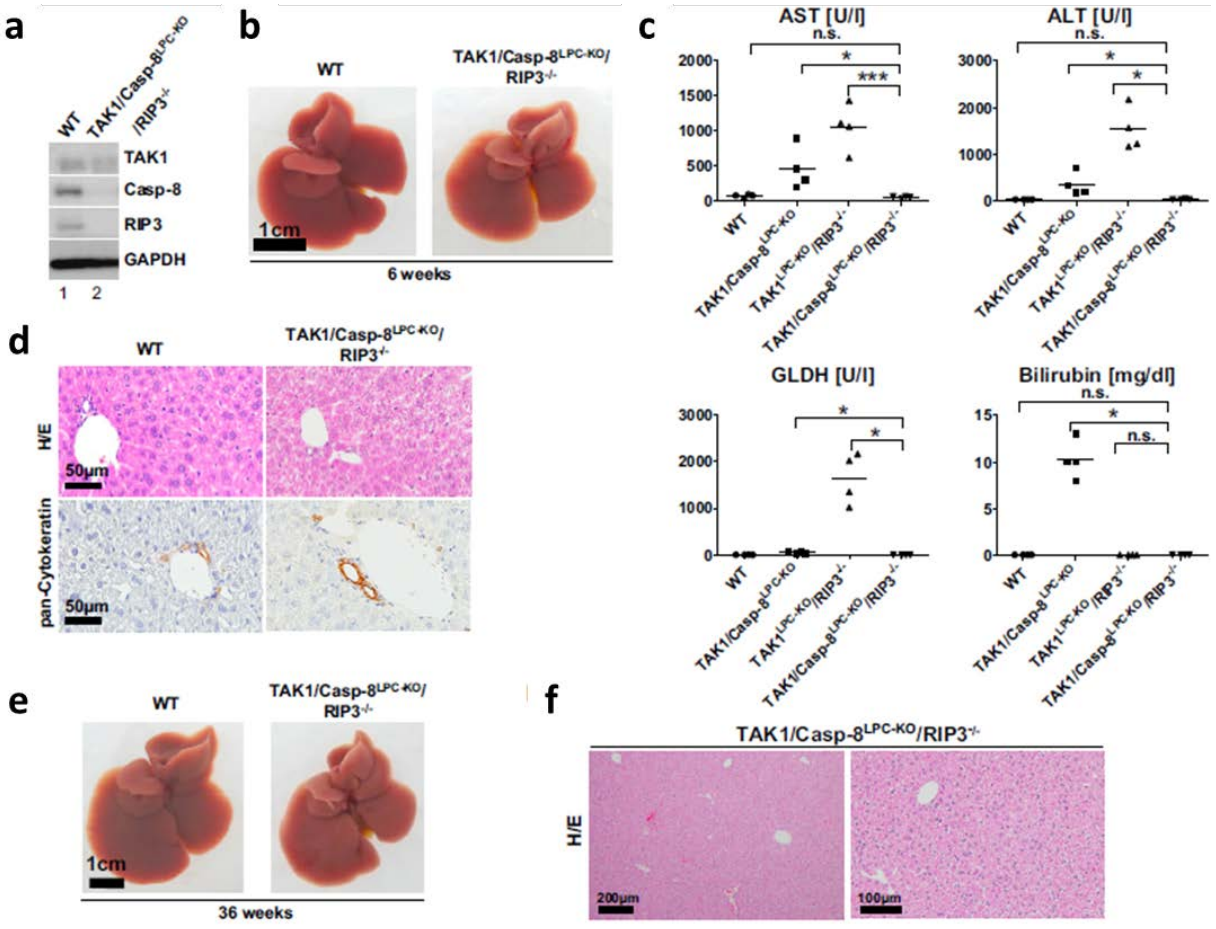

Figure S2: Complete Rescue of Hepatitis, Liver Injury, Cholestasis, and Hepatocarcinogenesis in TAK1/Caspase-8^{LPC-KO}/RIP3$^{-/-}$ Mice. (a) Western blot analysis of whole liver-protein extracts from 6-week-old male TAK1/Casp-8^{LPC-KO}/RIP3$^{-/-}$ and control littermate mice (WT) using antibodies against TAK1, Caspase-8, RIP3 and GAPDH as loading control. (b) Representative macroscopic pictures of 6-week-old male WT (left) and TAK1/Caspase-8^{LPC-KO}/RIP3$^{-/-}$ (right) livers. Scale bars: 1 cm. (c) Serumlevel analysis of aspartate aminotransferase (AST), alanine aminotransferase (ALT), glutamate dehydrogenase (GLDH) and total bilirubin in 6-week-old male mice. Results are shown as mean. (n = 4 each genotype). *p < 0.05, ***p < 0.001. (d) Histological and immunohistochemical analysis on representative liver paraffin sections from 6-week-old male mice. Scale bars: 50 mm. (e) Representative macroscopic pictures of 36-week-old male WT (left) and TAK1/Caspase-8^{LPC-KO}/RIP3$^{-/-}$ (right) livers. Scale bars: 1 cm. (f) Histological analysis on representative liver paraffin sections from 36-week-old male mice. Scale bars: 200 mm (left) and 100 mm (right).

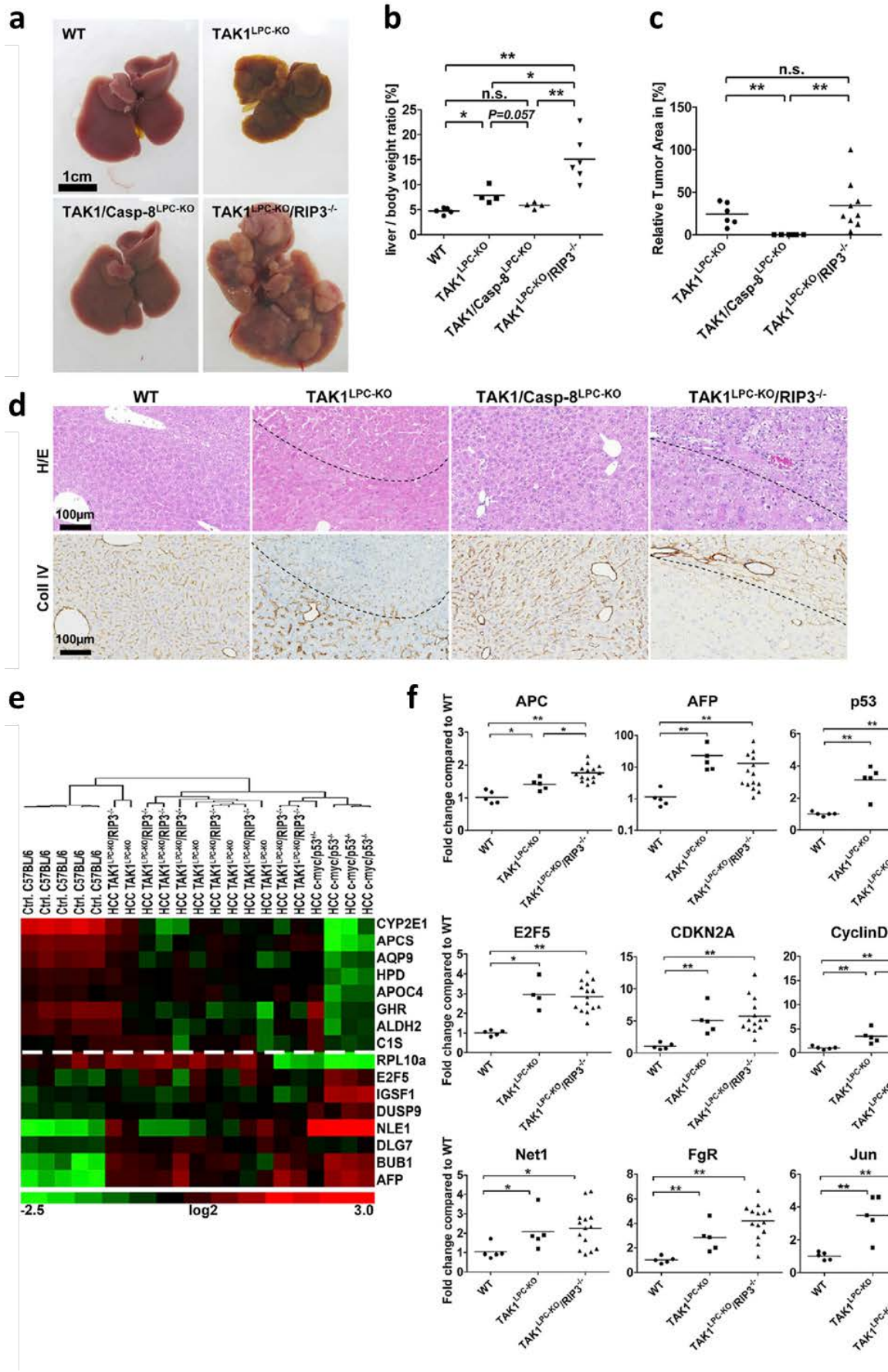
a
WT
TAK1LPC-KO
1cm
TAK1/Casp-8LPC-KO
TAK1LPC-KO/RIP3-/-
b
liver / body weight ratio [%]
n.s.
P=0.057
WT
TAK1LPC-KO
TAK1/Casp-8LPC-KO
TAK1LPC-KO/RIP3-/-
c
Relative Tumor Area in [%]
n.s.
d
H/E
Coll IV
100µm
e
CYP2E1
APCS
AQP9
HPD
APOC4
GHR
ALDH2
C1S
RPL10a
E2F5
IGSF1
DUSP9
NLE1
DLG7
BUB1
AFP
-2.5
log2
3.0
f
APC
AFP
p53
E2F5
CDKN2A
CyclinD1
Net1
FgR
Jun
Fold change compared to WT

Figure 4: Apoptosis Promotes Hepatocarcinogenesis, whereas Necroptosis Inhibits Cancer Growth in Livers of TAK1^{LPC-KO} Mice. (a) Representative macroscopic pictures of 33- to 35-week-old male WT (from left to the right), TAK1^{LPC-KO}, TAK1/Casp-8^{LPC-KO}, and TAK1^{LPC-KO}/RIP3$^{-/-}$ livers. Scale bars represent 1 cm. (b) Body-weight ratio of 25- to 38-week-old male WT (n = 6), TAK1^{LPC-KO} (n = 4), TAK1/Casp-8^{LPC-KO} (n = 4), and TAK1^{LPC-KO}/RIP3$^{-/-}$ (n = 6) mice. *p < 0.05, **p < 0.01. (c) Evaluation of tumor areas from H&E staining. TAK1^{LPC-KO} (n = 6), TAK1/Casp-8^{LPC-KO} (n = 6), and TAK1^{LPC-KO}/RIP3$^{-/-}$(n = 9) livers. Results are shown as mean. **p < 0.01. (d) Representative slides from livers of a 28-week-old WT, TAK1^{LPC-KO}, TAK1/Casp-8^{LPC-KO}, and TAK1^{LPC-KO}/RIP3$^{-/-}$ mouse stained with H&E and collagen IV. Tumor borders are indicated by a dashed line. (e) Sixteen gene profile analysis (heat map) of HCC derived from TAK1^{LPC-KO} and TAK1^{LPC-KO}/RIP3$^{-/-}$ livers (25- to 38-week-old mice). HCC were compared to aggressive liver tumors from WHV/N-myc2 p53$^{+/delta}$ mice and control WT mice. Below the dashed line, genes indicating a proliferative phenotype are listed, whereas genes above the dashed white line represent a less proliferative, more differentiated phenotype. HCC derived from TAK1^{LPC-KO} and TAK1^{LPC-KO}/RIP3$^{-/-}$ livers show a similar proliferating phenotype. (f) Relative (rel.) messenger RNA (mRNA) expression of the indicated oncogenes/tumor suppressor genes (APC, AFP, tumor protein p53 [p53], E2F5, CDKN2A, cyclin D1, Net1, Gardner-Rasheed feline sarcoma viral oncogene homolog [FgR], Jun oncogene [Jun]) of HCC derived from 25- to 38-week-old TAK1^{LPC-KO} (n = 5) and TAK1^{LPC-KO}/RIP3$^{-/-}$ (n = 14) mice as well as normal tissue from littermate control (WT) (n = 5). * p < 0.05, **p < 0.01.

Importantly, the fact that the massive tumor development in TAK1^{LPC-KO}/RIP3$^{-/-}$ mice could be completely abolished by cell-specific ablation of Caspase-8 in LPC (TAK1/Casp-8^{LPC-KO}/RIP3$^{-/-}$ mice) (**Figures S2e** and **S2f**) argues against a significant effect of Rip3 deletion in nonparenchymal hepatic cells in the regulation of hepatocarcinogenesis in TAK1^{LPC-KO}/RIP3$^{-/-}$ mice, which have an LPC-specific knockout of Tak1 but full knockout of Rip3.

The finding that TAK1/Casp-8^{LPC-KO} mice did not develop any HCC, whereas TAK1^{LPC-KO}/RIP3$^{-/-}$ mice showed larger HCC than TAK1^{LPC-KO} single mutant animals, suggested that activation of RIP3 controls hepatocarcinogenesis in terms of the hepatic tumor burden. To test if RIP3 also influences hepatic tumor biology, HCC samples from TAK1^{LPC-KO} and TAK1^{LPC-KO}/RIP3$^{-/-}$ mice were profiled by qRT-PCR with a 16 gene signature that identifies and stratifies liver tumors according to their degree of differentiation and proliferation rate (Cairo et al., 2008). For control, normal liver samples as well as samples of aggressive liver tumors from woodchuck hepatitis virus (WHV)/N-myc2 p53$^{+/delta}$ mice (Renard et al., 2000) were added to the analysis. Unsupervised analysis of the samples profiled showed coclustering of nearly all TAK1^{LPC-KO} and TAK1^{LPC-KO}/RIP3$^{-/-}$ tumors (**Fig. 4e**).

We also examined expression of alpha fetoprotein (AFP) and selected oncogenes and tumor suppressor genes (antigen-presenting cell [APC], p53, E2F transcription factor 5 [E2F5], cyclin-dependent kinase inhibitor 2A [CDKN2A], cyclin D1, neuroepithelial cell transforming 1 [Net1], FgR, and Jun) in HCC from both mouse lines. Despite elevated cyclin D1 and APC levels in TAK1^{LPC-KO}/RIP3$^{-/-}$ tumors, most other genes examined showed similar transcriptional levels in HCC from TAK1^{LPC-KO} and TAK1^{LPC-KO}/RIP3$^{-/-}$livers (**Fig. 4f**). Together, these findings indicate similar tumor biology of HCC in both mouse lines, suggesting that activation of RIP3 in TAK1^{LPC-KO} mice inhibits hepatocarcinogenesis by a dominant effect on tumor initiation and proliferation of tumor cells.

3.4.4.4. RIP3 Controls the Transition from Inflammation to Cancer by Inhibiting Caspase-8-Induced Chromosomal Aberrations Associated with Immortalization of Hepatocytes

To further analyze the functional roles of necroptosis and apoptosis on hepatocarcinogenesis, we performed array-comparative genomic hybridization (aCGH) analyses on histologically characterized and microdissected HCCs from TAK1$^{LPC\text{-}KO}$ and TAK1$^{LPC\text{-}KO}$/RIP3$^{-/-}$ mice and areas of disturbed microarchitecture (histologically not HCC or dysplastic nodules) in TAK1/Casp-8$^{LPC\text{-}KO}$ animals (**Fig. 5a**). As previously shown for TAK1$^{LPC\text{-}KO}$ mice (Bettermann et al., 2010) and corroborated on three HCCs in this study, TAK1$^{LPC\text{-}KO}$ displays large chromosomal amplifications mainly on chromosomes 4, 8, and 13.

Interestingly, amplifications on these chromosomes were also found in most tumors of TAK1$^{LPC\text{-}KO}$/RIP3$^{-/-}$ mice. However, the majority of TAK1$^{LPC\text{-}KO}$/RIP3$^{-/-}$ tumors displayed multiple additional chromosomal aberrations, of which many were not found in tumors of most TAK1$^{LPC\text{-}KO}$ animals (chromosomes 1, 5–6, 9, and 11–12; **Fig. 5a**; Bettermann et al., 2010). In contrast, TAK1/Casp-8$^{LPC\text{-}KO}$ animals hardly displayed any significant chromosomal aberrations in their livers (**Fig. 5a**). These data suggest that, in chronic hepatitis, apoptosis but not necroptosis specifically promotes the development of liver cancer by favoring an environment that drives genetic aberrations. Moreover, necroptosis not only inhibits tumor growth but also counterbalances the establishment of genetic alterations in HCC.

The striking pattern of chromosomal aberrations detected in TAK1$^{LPC\text{-}KO}$ and TAK1$^{LPC\text{-}KO}$/RIP3$^{-/-}$ tumors but not livers of TAK1/Casp-8$^{LPC\text{-}KO}$ mice prompted us to further investigate if these genetic changes might withhold a functional role in the transition from inflammation to cancer (e.g., by driving LPC specifically resistant to apoptotic cell death). To test this, we isolated primary hepatocytes from 8-week-old WT, TAK1/Casp-8$^{LPC\text{-}KO}$, and TAK1$^{LPC\text{-}KO}$/RIP3$^{-/-}$ mice, lacking immunohistochemical and molecular evidence for malignant tumors (data not shown).

Twenty-four hours after isolation, cells were washed carefully to remove dead cells and then stimulated with recombinant murine TNF, a treatment that induces cell-death of Tak1-deficient but not WT hepatocytes, due to their inability to activate nuclear factor (NF)-κB (Bettermann et al., 2010). Twenty-four hours after TNF stimulation, TAK1/Casp-8$^{LPC\text{-}KO}$ but not WT hepatocytes lost attachment to the plate and showed morphological signs of cell death (**Fig. 5b**), indicating that TNF treatment led to necroptosis of hepatocytes in vitro. Whereas also many hepatocytes isolated from TAK1$^{LPC\text{-}KO}$/RIP3$^{-/-}$ livers showed morphological signs of cell death, some cells with large nuclei survived TNF treatment and were collected for preparation of genomic DNA followed by aCGH analysis for their genetic status.

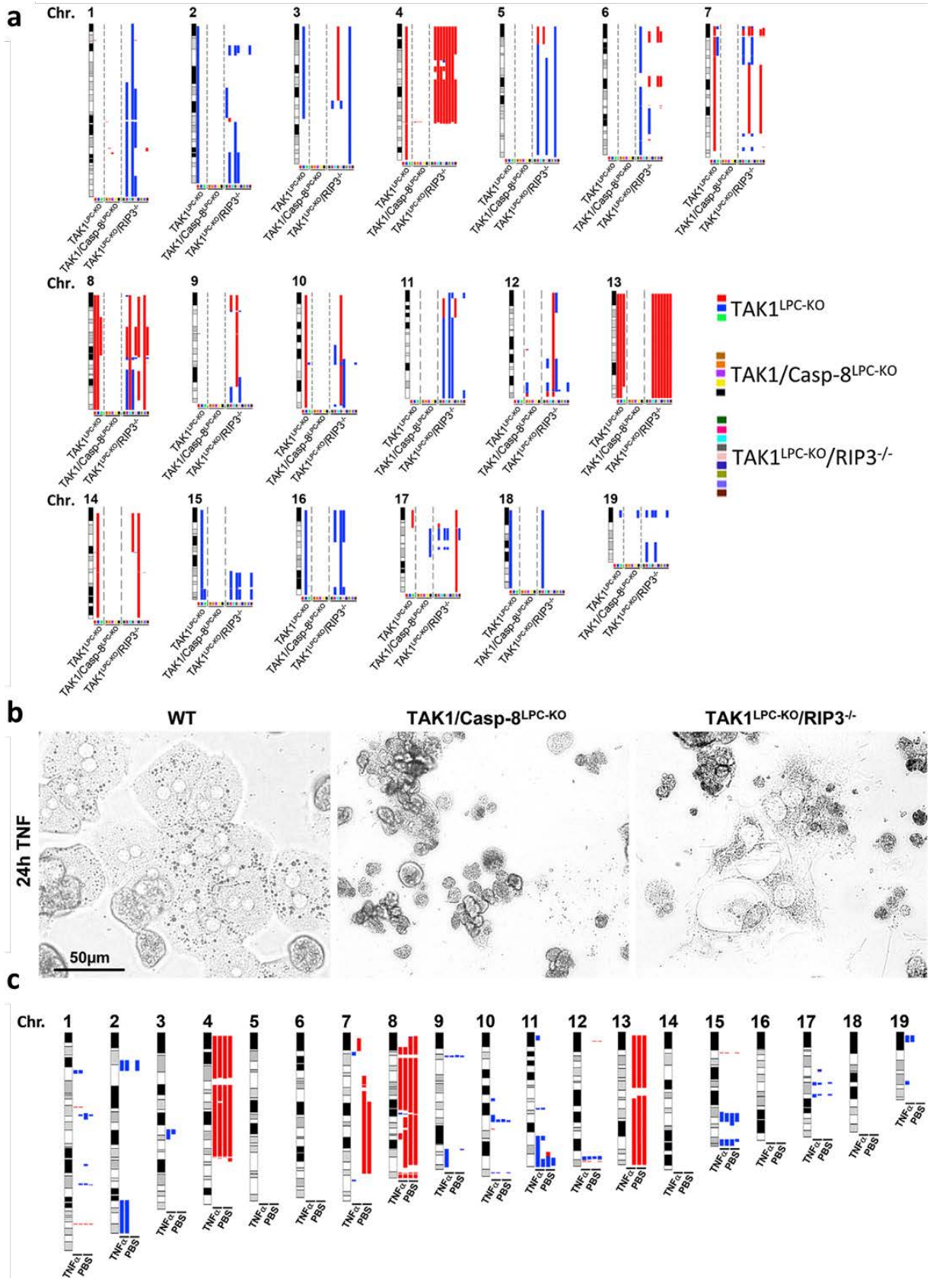
a
Chr. 1
2
3
4
5
6
7
Chr. 8
9
10
11
12
13
Chr. 14
15
16
17
18
19
TAK1LPC-KO
TAK1/Casp-8LPC-KO
TAK1LPC-KO/RIP3-/-
b
WT
TAK1/Casp-8LPC-KO
TAK1LPC-KO/RIP3-/-
24h TNF
50μm
c
Chr. 1 2 3 4 5 6 7 8 9 10 11 12 13 14 15 16 17 18 19
TNFα
PBS

Figure 5: RIP3 Controls the Transition from Inflammation to Cancer by Inhibiting Chromosomal Aberrations Associated with Resistance of Hepatocytes toward Caspase-8-Dependent Apoptosis (a) Summary of CGH analysis from three different hepatic tumors of three TAK1^{LPC-KO} mice, nine different tumors of nine TAK1^{LPC-KO}/RIP3$^{-/-}$ mice, and five samples of areas with disturbed histological architecture (no obvious tumors) from five TAK1/Casp-8^{LPC-KO} mice. The q-arm of each chromosome is shown and chromosome numbers are indicated. Dark horizontal bars within the symbolized chromosomes represent G bands. Chromosomal deletions are indicated in blue and amplifications in red. Individual mice are labeled by horizontal collared bars. (b) Microscopic pictures of TNF-α-treated primary hepatocytes from WT, TAK1/Casp-8^{LPC-KO}, and TAK1^{LPC-KO}/RIP3$^{-/-}$ mice. (c) Summary of CGH analysis from untreated and survived TNF-α-treated primary hepatocytes from TAK1^{LPC-KO}/RIP3$^{-/-}$ mice. Chromosomal amplifications and deletions are indicated in red and blue, respectively. IFN, interferon

Strikingly, cells displayed the same pattern of chromosomal aberrations on chromosomes 4, 8, and 13 as seen previously in HCC from these animals as well as additional chromosomal aberrations (**Fig. 5c**). These data provide evidence that the specific, Caspase-8-dependent pattern of chromosomal aberrations on chromosomes 4, 8, and 13 in TAK1^{LPC-KO}/RIP3$^{-/-}$ mice arises already at an early step of hepatocarcinogenesis and is associated with immortalization of hepatocytes in a setting of Caspase-8-dependent apoptosis. In line with this hypothesis, we identified focal areas free of Caspase-3 activation already in 6-week-old TAK1^{LPC-KO}/RIP3$^{-/-}$ mice (data not shown), probably reflecting in vivo a corresponding early step of clonal immortalization.

3.4.4.5. Caspase-8-Dependent Apoptosis but Not RIP3-Dependent Necroptosis Is Associated with a Strong Inflammatory Response and Liver Fibrosis

We aimed at further characterizing mediators of compensatory LPC proliferation activated in response to Caspase-8 but not RIP3-dependent necroptosis. Liver regeneration was previously shown to involve the production of inflammatory cytokines secreted by hepatic macrophages/Kupffer cells (Michalopoulos and DeFrances, 2005), suggesting that differential inflammatory responses to LPC apoptosis versus necroptosis might be associated with the differences in LPC proliferation between both respective mouse lines. Fluorescence-activated cell sorting (FACS) analysis revealed stronger infiltration of myeloid cells and CD4$^+$ and CD8$^+$ T cells but similar levels of B cells in both TAK1^{LPC-KO} and TAK1^{LPC-KO}/ RIP3$^{-/-}$ mice compared with WT and TAK1/Casp-8^{LPC-KO} animals (**Fig 6a**; data not shown). Immunohistochemical analysis confirmed a clear trend toward higher numbers of F4/80$^+$ cells in TAK1^{LPC-KO}/RIP3$^{-/-}$ mice compared with TAK1/Casp-8^{LPC-KO} animals (**Fig. 6b**).

To further examine expression levels of cytokines typically secreted by activated macrophages, we performed a FACS-based microbeads fluorescence assay on liver homogenates, which revealed significantly higher protein levels of interleukin (IL)-1a, IL-6, and IL-10 in TAK1^{LPC-KO} and TAK1^{LPC-KO}/RIP3$^{-/-}$ compared to TAK1/Casp-8^{LPC-KO} animals (**Fig. 6c**), of which IL-1a and IL-6 represent key cytokines driving compensatory proliferation and HCC development in response to hepatocyte death (Maeda et al., 2005; Sakurai et al., 2008). Thus, in contrast to previous concepts of oncotic necrosis

versus necrosis (Jaeschke and Lemasters, 2003), we show here that LPC apoptosis rather than necroptosis drives inflammation in response to chronic injury.

We further tested for the presence of liver fibrosis by Sirius red stainings on liver slides from 6-week-old WT, TAK1/Casp-8^{LPC-KO}, and TAK1^{LPC-KO}/RIP3$^{-/-}$ mice. This analysis showed only a slight increase in fibrosis in TAK1/Casp-8^{LPC-KO} livers at that age, which in turn was significantly lower than seen in TAK1^{LPC-KO}/RIP3$^{-/-}$ animals (data not shown). Additional RT-PCR analysis on whole liver RNA extracts revealed only a trend toward higher levels of TGF-β1 and TGF-β3 in TAK1^{LPC-KO}/RIP3$^{-/-}$ mice compared with TAK1/Casp-8^{LPC-KO} livers (data not shown). Whereas levels of active TGF-β ligands might not be fully reflected on RNA levels, due to potential differences in cleavage processes (Dubois et al., 2001), these data suggest that apoptosis but not necroptosis induces hepatic fibrogenesis and activation of stellate cells by various profibrogenic and proinflammatory stimuli.

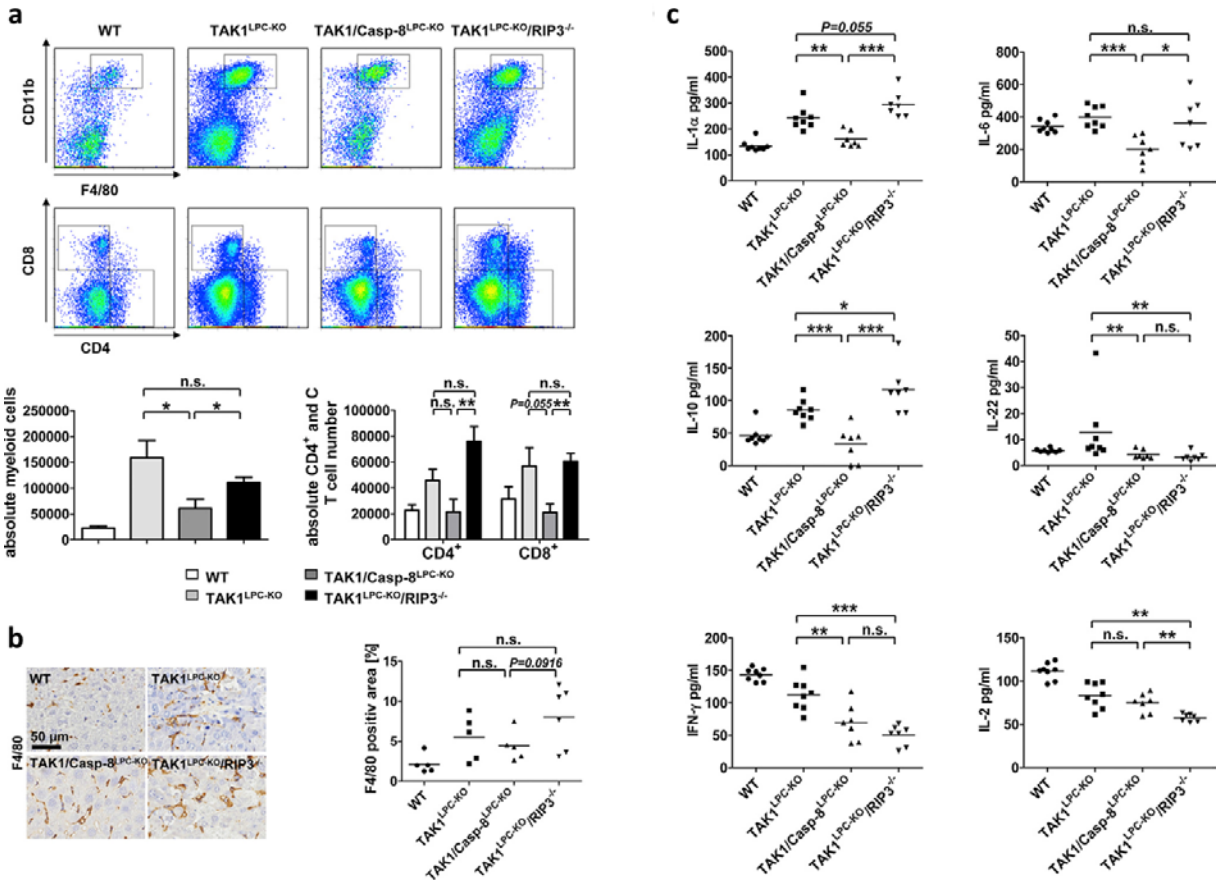

Figure 6: Differential Inductions of Inflammatory Responses by Apoptosis and Necroptosis in Tak1-Deficient Livers. (a) FACS-based analysis of infiltrating myeloid cells and T cells into liver tissue of TAK1^{LPC-KO}, TAK1/Casp-8^{LPC-KO}, and TAK1^{LPC-KO}/RIP3$^{-/-}$ mice. Results are shown as mean; error bars indicate SEM n = 5; *p < 0.05, **p < 0.01. (b) Immunohistochemistry of liver paraffin sections and densitometric analysis for F4/80 in TAK1^{LPC-KO}, TAK1/Casp-8^{LPC-KO}, TAK1^{LPC-KO}/RIP3$^{-/-}$, and WT livers. Results are shown as mean; n = 5 for WT and TAK1/Casp-8^{LPC-KO}; n = 6 for TAK1^{LPC-KO}/RIP3$^{-/-}$. The scale bar represents 50 mm. (c) FACS-based microbeads fluorescence assay for cytokine expression in liver protein homogenates. Results are shown as mean. n = 8 for WT and TAK1^{LPC-KO} and n = 7 for TAK1/Casp-8^{LPC-KO} and TAK1^{LPC-KO}/RIP3$^{-/-}$; *p < 0.05, **p < 0.01, ***p < 0.001.

3.4.4.6. Caspase-8-Dependent Apoptosis Drives Compensatory LPC Proliferation by Activation of JNK in Parenchymal and Nonparenchymal Liver Cells

We further examined which intracellular signaling pathways might connect the two different modes of cell death with activation or inhibition of compensatory proliferation and cancer development. In Drosophila, activation of Jun-(N)-terminal kinase (JNK) by the initiator caspase Dronc is driving apoptosis-induced compensatory proliferation (Huh et al., 2004; Kondo et al., 2006). Moreover, it was suggested that JNK activation is part of a nonapoptotic, procarcinogenic pathway downstream of CD95/Fas/APO-1 (Chen et al., 2010).

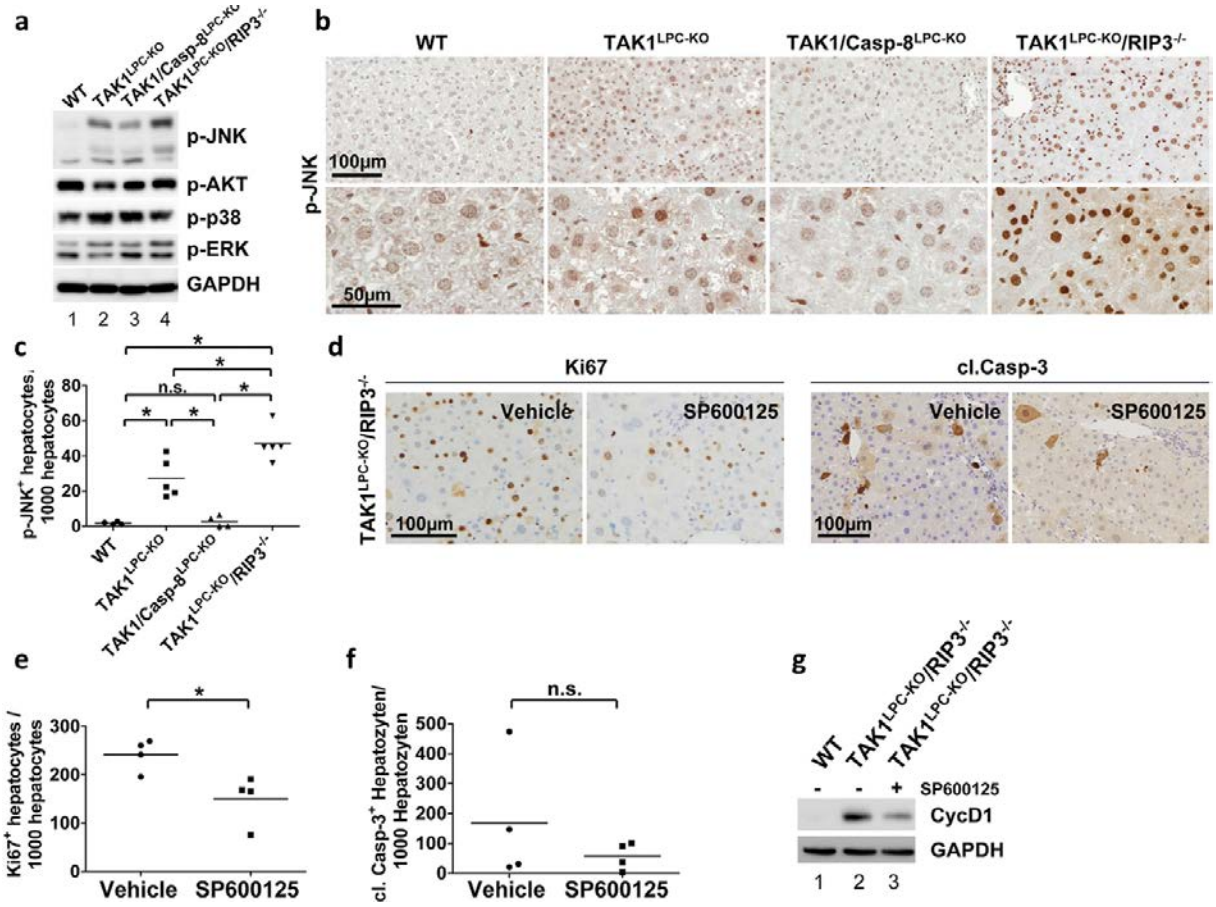

Figure 7: RIP3 Limits Compensatory Cell Proliferation through Inhibition of Caspase-8-Dependent JNK Activation (a) Western blot analysis of whole liver-protein extracts from 6-week-old male TAK1^{LPC-KO}, TAK1/Casp-8^{LPC-KO}, TAK1^{LPC-KO}/RIP3$^{-/-}$, and control littermate mice (WT) using antibodies against the phosphorylated and active form of JNK, AKT, p38, ERK, and GAPDH as loading control. (b) Immunohistochemistry of representative liver paraffin sections for phospho-JNK in 6-week-old mice. The scale bars represent 100 mm and 50 mm. (c) Statistical analysis of p-JNK^{+} hepatocytes. Results are shown as mean. WT (n = 4), TAK1^{LPC-KO} (n = 5), TAK1/Casp-8^{LPC-KO} (n = 4), and TAK1^{LPC-KO}/RIP3$^{-/-}$ (n = 5) mice; *p < 0.05. (d) Representative immunohistochemical analysis for Ki67 and cl. Casp-3 in 6-week-old mice treated with the JNK inhibitor SP600125 or vehicle as control. (e) Statistical analysis of Ki67^{+} hepatocytes in animals treated with SP600125 compared to vehicle control-treated animals. Results are shown as mean. (n = 4); *p < 0.05. (f) Statistical analysis of cl. Casp-3^{+} hepatocytes in TAK1^{LPC-KO}/RIP3$^{-/-}$ treated with SP600125 compared to vehicle control-treated mice. Results are shown as mean. (n = 4). (g) Western blot analysis of whole liver protein extracts from 6-week-old male TAK1^{LPC-KO}/RIP3$^{-/-}$ and WT mice treated with SP600125 or vehicle using antibodies against CycD1 and GAPDH as loading control.

Western blot analysis on liver extracts from 6-week-old mice revealed strong spontaneous phosphorylation and activation of JNK but not p38a, AKT, or ERK in livers of TAK1^{LPC-KO}/RIP3$^{-/-}$ compared with TAK1/Casp-8^{LPC-KO} and WT animals (**Fig. 7a**). Immunohistochemical staining for the phosphorylated JNK forms confirmed significantly more phosphorylated JNK (p-JNK)+ hepatocytes in TAK1^{LPC-KO}/RIP3$^{-/-}$ compared to TAK1/Casp-8^{LPC-KO} and WT animals (**Fig. 7b**). Importantly, TAK1^{LPC-KO}/RIP3$^{-/-}$ livers even displayed significantly more p-JNK^{+} hepatocytes than TAK1^{LPC-KO} single knockouts (**Fig. 7c**). In addition, TAK1^{LPC-KO}/RIP3$^{-/-}$ livers showed a significantly higher fraction of p-JNK^{+} liver nonparenchymal cells (NPC) than all other genotypes, although to a much lower extent than observed in terms of hepatocytes (data not shown).

Finally, to functionally evaluate the role of JNK in mediating apoptosis and compensatory proliferation in TAK1^{LPC-KO}/RIP3$^{-/-}$ mice, we injected TAK1^{LPC-KO}/RIP3$^{-/-}$ mice with the well-established JNK-inhibitor SP600125, which significantly decreased the amount of Ki67^{+} cells and lowered cyclin D1 expression when compared to vehicle-treated animals (**Fig. 7d, 7e**, and **7g**). Additional analysis of cleaved Casp-3^{+} cells lacked a significant difference between the two groups (**Fig. 7d** and **7f**).

These data suggest that JNK activation represents an important step in mediating compensatory proliferation downstream of Caspase-8, whereas, in contrast, RIP3 inhibits the activation of JNK in livers of TAK1^{LPC-KO} mice.

3.4.5. Experimental Procedures

3.4.5.1. Generation of Conditional Knockout Mice and Animal Experiments

Mice carrying loxP-site-flanked (floxed) alleles of the Tak1 gene Map3k7 (Tak1fl) (Sato et al., 2005) or Caspase-8 (Caspase-8fl) (Salmena et al., 2003) were crossed to Alfp-Cre transgenic mice (Kellendonk et al., 2000) to generate a LPC-specific knockout of the respective genes (TAK1^{LPC-KO}, Caspase-8^{LPC-KO}). Mice with constitutive deletion of RIP3 (RIP3$^{-/-}$) were described before (Newton et al., 2004). Mice with combined conditional knockouts of Map3k7 and constitutive ablation of Rip3 (TAK1^{LPC-KO}/RIP3$^{-/-}$) as well as combined conditional ablations of Map3k7 and Caspase-8 (TAK1/Casp8^{LPC-KO}) as well as mice with constitutive ablations of Rip3 and conditional ablations of Map3k7 and Caspase-8 in LPC (TAK1/Casp-8^{LPC-KO}/ RIP3$^{-/-}$) were generated by intercrossing the respective lines. In all experiments, littermates carrying the respective loxP-flanked alleles but lacking expression of Cre recombinase were used as WT controls. Mice were bred on a mixed C57/BL6 -SV129Ola genetic background. Only sex-matched animals were compared. All animal experiments were approved by the Federal Ministry

for Nature, Environment and Consumers' Protection of the state of North Rhine-Westphalia and were performed in accordance to the respective national, federal, and institutional regulations.

Surgery (partial hepatectomy) was performed on male mice of 6–8 weeks of age. Mice were anesthetized by isoflurane inhalation and treated with buprenorphine for analgesia. The abdominal cavity was opened by a midline laparotomy. The right median lobe, left median lobe, and left lateral lobe were identified and individually ligated. Mice were sacrificed at the indicated time points. Intraperitoneal injection of 15 ml SP600125 (1 mg/ABSOURCE) or vehicle (DMSO) was performed twice a day over 4 days on male mice of 5 weeks of age. Mice were sacrificed 3 hr after the last injection.

3.4.5.2. Statistics

Data were analyzed using PRISM software (GraphPad Software) and are expressed as mean. Statistical significance between experimental groups was assessed using an unpaired two-sample t test or Mann-Whitney test.

3.4.5.3. Serum Analysis

Serum ALT, AST, GLDH, AP activities and total serum bilirubin levels were measured by standard procedures in the Institute of Clinical Chemistry of the RWTH University Hospital Aachen.

3.4.5.4. Western Blot Analysis

Liver tissue was homogenized in NP-40 lysis buffer using a tissue grind pestle (Kontes) to gain protein lysates. These were separated by SDS-polyacrylamide gel electrophoresis (PAGE), transferred to PVDF membrane and analyzed by immunoblotting as previously described (Luedde et al., 2003). Membranes were probed with the following antibodies: anti-Cyclin D1 (Santa Cruz), anti-cleaved-Caspase-3, anti p-AKT, anti p-ERK, anti p-JNK, anti p-p38, (Cell Signaling), anti-Caspase-8 (Enzo), anti-PCNA (ZYMED), anti-TAK1, anti-RIP3 (IMGENEX) and anti-GAPDH (ABD Serotec). As secondary antibodies, anti-rabbit-HRP, anti-mouse-HRP (Amersham) and anti-rat-HRP (Santa Cruz) were used.

3.4.5.5. Quantitative Real-Time PCR

Total RNA was purified from liver tissue using Trizol reagent (Invitrogen) and an RNeasy Mini Kit (QIAGEN). The quantity and quality of the RNA was determined spectroscopically using a nanodrop (Thermo Scientific). Total RNA (1 mg) was used to synthesize cDNA using the Transcriptor cDNA First-Strand Synthesis Kit (Roche) according to the manufacturer's protocol, and was resuspended in 50 ml of H2O. cDNA samples (2 ml) were used for real-time PCR in a total volume of 25 ml using SYBR Green Reagent (Invitrogen) and specific primers on a qPCR machine (Applied Biosystems 7300

Sequence Detection System). All real-time PCR reactions were performed in duplicates. Data were generated and analyzed using SDS 2.3 and RQ manager 1.2 software. Primer sequences are available upon request. All values were normalized to the level of beta-actin mRNA.

3.4.5.6. Stainings

Paraffin sections (2mm) were stained with H/E or various primary and secondary antibodies. Paraformaldehyde (4%) fixed and paraffin embedded liver tissue was incubated in Bond Primary antibody diluent (Leica) and staining was performed on a BONDMAX immunohistochemistry robot (Leica Biosystems) using BOND polymer refine detection solution for DAB or BOND polymer refine red detection for AP, respectively. The following antibodies were used: Antibodies against F4/80 (BMA Biomedicals AG, 1:120), anti-pan-cytokeratin (Dako A/S; 1:300), anti-Collagen IV (Cedarlane; 1:50), anti-A6 (1:50) (antibody kindly provided by Dr. Valentina Factor), anti-Ki67 (NeoMarkers; 1:200), anti-cleaved Caspase-3 (Cell Signaling; 1:300) and anti-Phospho-JNK (Cell Signaling; 1:50). Image acquisition was either performed on an Olympus BX53 microscope equipped with an Olympus DP72 digital camera or with a Leica SCN400 slide scanner. Collagen deposition was quantified by Sirius Red staining using polarization microscopy as previously described (Bettermann et al., 2010).

3.4.5.7. Analysis and Quantification of Immunohistochemical Staining

The number of cells positively stained for the different nuclear markers (e.g., Ki67, p-JNK) in various cell types (e.g., hepatocytes or non-parenchymal cells) was determined using SlidePath TissueIA image analysis software (Leica) on whole tissue sections (paraffin embedded) and normalized to tissue area or total cell number, respectively. Alternatively, 4 different areas were randomly selected and analyzed in a blinded fashion and normalized to tissue area or total cell number on an Olympus Microscope BX53, a DP72 camera using the ‘‘cell sense’’ software (Olympus).

Numbers of bile ducts or bile duct cells, positively stained for cytokeratin or A6 were counted manually or automatically (using a SlidePath TissueIA image analysis software (Leica)) on whole liver sections (paraffin embedded) and normalized to tissue area. Hepatocytes positively stained for cleaved Caspase-3 as well as macrophages positive for F4/80 were quantified numerically (positive cells per total cells) or densitometrically (area stained per total area) using SlidePath TissueIA image analysis software (Leica) on whole tissue sections and normalized to the total number of hepatocytes or total tissue area, respectively. For double stainings the number of bile duct cells, positively double-stained for pan-cytokeratin and Ki67 or cleaved Caspase-3 respectively, were counted manually on whole liver sections and normalized to the total number of cytokeratin-positive cells. Pictures for representation were either taken by an Olympus Microscope BX53 and a DP72 camera using the Cell

sense dimensions 1.7 software (Olympus) or by scanning in whole tissue sections using a Leica SCN400 slide scanner.

3.4.5.8. Quantification of Necrotic Areas

Necrotic areas were quantified on H/E stained paraffin sections. The lateral right lobe of mice was examined using a Nikon ECLIPSE 80i microscope and 10x magnification. The area of the lobe and the necrotic areas were measured using NIS 3.0 software and the percentage of necrotic tissue was calculated.

3.4.5.9. aCGH Analysis

In order to characterize copy number alterations, oligo array CGH using the Agilent (Boeblingen, Germany) platform was performed. Genomic DNA was extracted from formalin-fixed paraffin-embedded (FFPE) tissue sections, after enrichment for tumor cells by micro-dissection, using the DNAeasy FFPE kit (QIAGEN, Hildesheim, Germany). DNA extracted from 4 normal liver tissues was pooled and used as reference DNA. 250ng of test and reference DNA were differentially labeled with Cy3-dUTP (test) and Cy5-dUTP (reference) by random primed labeling using the CGH labeling kit for oligo arrays (Enzo, Loerrach, Germany). Hybridization, washing and scanning was performed according to the manufacturer's protocol and the data were extracted from the Feature Extraction Software (Agilent, Boeblingen, Germany) as tab-delimited text files. The arrays used were custom-designed 8x60k arrays (AMADID 41078) with approx. 60000 probes covering the whole mouse genome. The probe set includes the Agilent 44k (AMADID 15028) in order to enable merging of the 60k data with 44k data. The raw data were imported into the R statistical platform (R Development Core Team. R: A language and environment for statistical computing. R Foundation for Statistical Computing, Vienna, Austria. ISBN 3-900051-07-0, URL: http://www.R-project.org/) and the background subtracted median intensity signals were used to build the log2 ratios. After median normalization values were quality filtered using flags as defined by the Agilent Feature extraction software.

The log2 ratios were subsequently segmented called and copy number regions were defined using functions from the CGHcall (van de Wiel et al., 2007) and CGHregions (van de Wiel and van Wieringen, 2007) packages. For the CGHcall function 75% estimated proportion of tumor cells based on microscopic assessment of Haematoxylin stained FFPE sections, was used. In order to include profiles of liver tumors that developed in TAK1^{LPC-KO} mice from a former study (Bettermann et al., 2010), raw data from two samples (GSM473549 and GSM473553) were downloaded from Gene Expression Omnibus (GEO, http://www.ncbi.nlm.nih.gov/geo/), analyzed as described above and the

resulting data were merged with the 60k array data. The copy number profiles were karyogram- style plotted using an in-house written R function.

Cultured primary hepatocytes from TAK1/Casp-8^{LPC-KO}, TAK1^{LPC-KO}/RIP3$^{-/-}$ and WT mice were treated with murine recombinant TNF-a (20ng/ml) or PBS (control) for 24h and harvest afterwards for DNA extraction. CGH analysis was performed with surviving primary hepatocytes from TAK1^{LPC-KO}/RIP3$^{-/-}$ mice by the same procedure as described above.

3.4.5.10. Transcriptional Profiling of Liver Tumors

cDNA synthesis and qRT-PCR on mouse liver samples was performed as described elsewhere (Haybaeck et al., 2009). The following genes were included into transcriptional profiles: a) genes indicative for high proliferation: Afp (alpha fetoprotein); Bub1 (BUB1 budding unhibited by benzimidazoles 1 homolog (Yeast), Dlg7 [discs, large chromosome 7 (Drosophila)], Dusp9 (dual specificity phosphatase 9), E2f5 (E2F transcription factor 5, p130-binding), Igsf1 (immunoglobulin superfamily, member 1), Rpl10a (ribosomal protein L10a). b) genes indicative for differentiation: Aldh2 [aldehyde dehydrogenase 2 family (mitochondrial)], Apcs (amyloid P component, serum), Apoc4 (apolipoprotein C-IV), Aqp9 (aquaporin 9), Cyp2e1 (cytochrome P450, family 2, subfamily E, polypeptide 1), C1s (complement component 1 subcomponent), Ghr (growth hormone factor), Hpd (4-hydroxyphenylpyruvate dioxygenase), Nle [notchless homolog 1 (Drosophila)]. Unification of sample replicates and Heatmap visualization was done by using dCHIP v1.6 software.

3.4.5.11. Flow Cytometry

Six-color staining was conducted using combinations of the following mAbs: F4/80 (Serotec), CD11b (eBioscience), CD45, Ly6G, CD19, CD8, CD4 (all BD). Flow cytometric analysis was performed on a FACS-Canto II (BD). Absolute cell numbers were determined by adding 2x104 Calibrite APC beads (BD) to each sample before measurement as internal reference standard. Data were analyzed using FlowJo (Tree Star).

3.4.5.12. Measurement of Cytokines

For measurement of cytokines in total liver Protein-extracts, we used the mouse FlowCytomix kit (eBioscience) according to the manufacturer's instructions using a FACS-Canto II System (BD).

3.4.6. References

Andreu, P., Johansson, M., Affara, N.I., Pucci, F., Tan, T., Junankar, S., Korets, L., Lam, J., Tawfik, D., DeNardo, D.G., et al. (2010). FcRgamma activation regulates inflammation-associated squamous carcinogenesis. *Cancer Cell* **17**, 121–134.

Bantel, H., and Schulze-Osthoff, K. (2012). Mechanisms of cell death in acute liver failure. *Front. Physiol*. **3**, 79.

Bettermann, K., Vucur, M., Haybaeck, J., Koppe, C., Janssen, J., Heymann, F., Weber, A., Weiskirchen, R., Liedtke, C., Gassler, N., et al. (2010). TAK1 suppresses a NEMO-dependent but NF-kappaB-independent pathway to liver cancer. *Cancer Cell* **17**, 481–496.

Bonnet, M.C., Preukschat, D., Welz, P.S., van Loo, G., Ermolaeva, M.A., Bloch, W., Haase, I., and Pasparakis, M. (2011). The adaptor protein FADD protects epidermal keratinocytes from necroptosis in vivo and prevents skin inflammation. *Immunity* **35**, 572–582.

Cairo, S., Armengol, C., De Reynie` s, A., Wei, Y., Thomas, E., Renard, C.A., Goga, A., Balakrishnan, A., Semeraro, M., Gresh, L., et al. (2008). Hepatic stem-like phenotype and interplay of Wnt/beta-catenin and Myc signaling in aggressive childhood liver cancer. *Cancer Cell* **14**, 471–484.

Chakraborty, J.B., Oakley, F., and Walsh, M.J. (2012). Mechanisms and biomarkers of apoptosis in liver disease and fibrosis. *Int. J. Hepatol*. 2012, 648915.

Chan, J.K., Roth, J., Oppenheim, J.J., Tracey, K.J., Vogl, T., Feldmann, M., Horwood, N., and Nanchahal, J. (2012). Alarmins: awaiting a clinical response. *J. Clin. Invest*. **122**, 2711–2719.

Chang, L., Kamata, H., Solinas, G., Luo, J.L., Maeda, S., Venuprasad, K., Liu, Y.C., and Karin, M. (2006). The E3 ubiquitin ligase itch couples JNK activation to TNFalpha-induced cell death by inducing c-FLIP(L) turnover. *Cell* **124**, 601–613.

Chen, L., Park, S.M., Tumanov, A.V., Hau, A., Sawada, K., Feig, C., Turner, J.R., Fu, Y.X., Romero, I.L., Lengyel, E., and Peter, M.E. (2010). CD95 promotes tumour growth. *Nature* **465**, 492–496.

Cho, Y.S., Challa, S., Moquin, D., Genga, R., Ray, T.D., Guildford, M., and Chan, F.K. (2009). Phosphorylation-driven assembly of the RIP1-RIP3 complex regulates programmed necrosis and virus-induced inflammation. *Cell* **137**, 1112–1123.

Das, M., Garlick, D.S., Greiner, D.L., and Davis, R.J. (2011). The role of JNK in the development of hepatocellular carcinoma. *Genes Dev*. **25**, 634–645.

Delaney, J.R., and Mlodzik, M. (2006). TGF-beta activated kinase-1: new insights into the diverse roles of TAK1 in development and immunity. *Cell Cycle* **5**, 2852–2855.

Desmet, V.J. (2011). Ductal plates in hepatic ductular reactions. Hypothesis and implications. I. Types of ductular reaction reconsidered. *Virchows Arch*. **458**, 251–259.

Dubois, C.M., Blanchette, F., Laprise, M.H., Leduc, R., Grondin, F., and Seidah, N.G. (2001). Evidence that furin is an authentic transforming growth factor-beta1-converting enzyme. *Am. J. Pathol*. **158**, 305–316.

Feldstein, A.E., and Gores, G.J. (2005). Apoptosis in alcoholic and nonalcoholic steatohepatitis. *Front. Biosci.* **10**, 3093–3099.

Fung, J., Lai, C.L., and Yuen, M.F. (2009). Hepatitis B and C virus-related carcinogenesis. *Clin. Microbiol. Infect*. **15**, 964–970.

Glaser, S.S., Gaudio, E., Miller, T., Alvaro, D., and Alpini, G. (2009). Cholangiocyte proliferation and liver fibrosis. *Expert Rev. Mol. Med*. **11**, e7.

Greten, F.R., Eckmann, L., Greten, T.F., Park, J.M., Li, Z.W., Egan, L.J., Kagnoff, M.F., and Karin, M. (2004). IKKbeta links inflammation and tumorigenesis in a mouse model of colitis-associated cancer. *Cell* **118**, 285–296.

Guerra, C., Schuhmacher, A.J., Can˜ amero, M., Grippo, P.J., Verdaguer, L., Pe´ rez-Gallego, L., Dubus, P., Sandgren, E.P., and Barbacid, M. (2007). Chronic pancreatitis is essential for induction of pancreatic ductal adenocarcinoma by K-Ras oncogenes in adult mice. *Cancer Cell* **11**, 291–302.

Han, J., Zhong, C.Q., and Zhang, D.W. (2011). Programmed necrosis: backup to and competitor with apoptosis in the immune system. *Nat. Immunol*. **12**, 1143–1149.

Hanahan, D., and Weinberg, R.A. (2011). Hallmarks of cancer: the next generation. *Cell* **144**, 646–674.

He, S., Wang, L., Miao, L., Wang, T., Du, F., Zhao, L., and Wang, X. (2009). Receptor interacting protein kinase-3 determines cellular necrotic response to TNF-alpha. *Cell* **137**, 1100–1111.

Huh, J.R., Guo, M., and Hay, B.A. (2004). Compensatory proliferation induced by cell death in the Drosophila wing disc requires activity of the apical cell death caspase Dronc in a nonapoptotic role. *Curr. Biol*. **14**, 1262–1266.

Inokuchi, S., Aoyama, T., Miura, K., Osterreicher, C.H., Kodama, Y., Miyai, K., Akira, S., Brenner, D.A., and Seki, E. (2010). Disruption of TAK1 in hepatocytes causes hepatic injury, inflammation, fibrosis, and carcinogenesis. *Proc. Natl. Acad. Sci. USA* **107**, 844–849.

Jaeschke, H., and Lemasters, J.J. (2003). Apoptosis versus oncotic necrosis in hepatic ischemia/reperfusion injury. *Gastroenterology* **125**, 1246–1257.

Karin, M., and Gallagher, E. (2009). TNFR signaling: ubiquitin-conjugated TRAFfic signals control stop-and-go for MAPK signaling complexes. *Immunol. Rev*. **228**, 225–240.

Kellendonk, C., Opherk, C., Anlag, K., Schu¨ tz, G., and Tronche, F. (2000). Hepatocyte-specific expression of Cre recombinase. *Genesis* **26**, 151–153.

Kondo, S., Senoo-Matsuda, N., Hiromi, Y., and Miura, M. (2006). DRONC coordinates cell death and compensatory proliferation. *Mol. Cell. Biol*. **26**, 7258–7268.

Llovet, J.M., Burroughs, A., and Bruix, J. (2003). Hepatocellular carcinoma. *Lancet* **362**, 1907–1917.

Luedde, T., and Schwabe, R.F. (2011). NF-kB in the liver—linking injury, fibrosis and hepatocellular carcinoma. Nat. Rev. Gastroenterol. *Hepatol*. **8**, 108–118.

Luedde, T., Beraza, N., Kotsikoris, V., van Loo, G., Nenci, A., De Vos, R., Roskams, T., Trautwein, C., and Pasparakis, M. (2007). Deletion of NEMO/IKKgamma in liver parenchymal cells causes steatohepatitis and hepatocellular carcinoma. *Cancer Cell* **11**, 119–132.

Maeda, S., Kamata, H., Luo, J.L., Leffert, H., and Karin, M. (2005). IKKbeta couples hepatocyte death to cytokine-driven compensatory proliferation that promotes chemical hepatocarcinogenesis. *Cell* **121**, 977–990.

Michalopoulos, G.K., and DeFrances, M. (2005). Liver regeneration. *Adv. Biochem. Eng. Biotechnol*. **93**, 101–134.

Newton, K., Sun, X., and Dixit, V.M. (2004). Kinase RIP3 is dispensable for normal NF-kappa Bs, signaling by the B-cell and T-cell receptors, tumor necrosis factor receptor 1, and Toll-like receptors 2 and 4. *Mol. Cell. Biol*. **24**, 1464–1469.

Pockros, P.J., Schiff, E.R., Shiffman, M.L., McHutchison, J.G., Gish, R.G., Afdhal, N.H., Makhviladze, M., Huyghe, M., Hecht, D., Oltersdorf, T., and Shapiro, D.A. (2007). Oral IDN-6556, an antiapoptotic caspase inhibitor, may lower aminotransferase activity in patients with chronic hepatitis C. *Hepatology* **46**, 324–329.

Ratziu, V., Sheikh, M.Y., Sanyal, A.J., Lim, J.K., Conjeevaram, H., Chalasani, N., Abdelmalek, M., Bakken, A., Renou, C., Palmer, M., et al. (2012). A phase 2, randomized, double-blind, placebo-controlled study of GS-9450 in subjects with nonalcoholic steatohepatitis. *Hepatology* **55**, 419–428.

Renard, C.A., Fourel, G., Bralet, M.P., Degott, C., De La Coste, A., Perret, C.,Tiollais, P., and Buendia, M.A. (2000). Hepatocellular carcinoma in WHV/Nmyc2 transgenic mice: oncogenic mutations of beta-catenin and synergistic effect of p53 null alleles. *Oncogene* **19**, 2678–2686.

Roychowdhury, S., McMullen, M.R., Pisano, S.G., Liu, X., and Nagy, L.E. (2013). Absence of receptor interacting protein kinase 3 prevents ethanolinduced liver injury. *Hepatology* **57**, 1773–1783.

Ryoo, H.D., and Bergmann, A. (2012). The role of apoptosis-induced proliferation for regeneration and cancer. *Cold Spring Harb. Perspect. Biol*. **4**, a008797.

Sakurai, T., Maeda, S., Chang, L., and Karin, M. (2006). Loss of hepatic NFkappa B activity enhances chemical hepatocarcinogenesis through sustained c-Jun N-terminal kinase 1 activation. *Proc. Natl. Acad. Sci. USA* **103**, 10544– 10551.

Sakurai, T., He, G., Matsuzawa, A., Yu, G.Y., Maeda, S., Hardiman, G., and Karin, M. (2008). Hepatocyte necrosis induced by oxidative stress and IL-1 alpha release mediate carcinogen-induced compensatory proliferation and liver tumorigenesis. *Cancer Cell* **14**, 156–165.

Salmena, L., Lemmers, B., Hakem, A., Matysiak-Zablocki, E., Murakami, K., Au, P.Y., Berry, D.M., Tamblyn, L., Shehabeldin, A., Migon, E., et al. (2003). Essential role for caspase 8 in T-cell homeostasis and T-cell-mediated immunity. *Genes Dev*. **17**, 883–895.

Sato, S., Sanjo, H., Takeda, K., Ninomiya-Tsuji, J., Yamamoto, M., Kawai, T., Matsumoto, K., Takeuchi, O., and Akira, S. (2005). Essential function for the kinase TAK1 in innate and adaptive immune responses. *Nat. Immunol*. **6**, 1087–1095.

Sherman, M. (2010). Hepatocellular carcinoma: epidemiology, surveillance, and diagnosis. *Semin. Liver Dis*. **30**, 3–16.

Takahashi, H., Ogata, H., Nishigaki, R., Broide, D.H., and Karin, M. (2010). Tobacco smoke promotes lung tumorigenesis by triggering IKKbeta- and JNK1-dependent inflammation. *Cancer Cell* **17**, 89–97.

Vanlangenakker, N., Vanden Berghe, T., Bogaert, P., Laukens, B., Zobel, K., Deshayes, K., Vucic, D., Fulda, S., Vandenabeele, P., and Bertrand, M.J. (2011). cIAP1 and TAK1 protect cells from TNF-induced necrosis by preventing RIP1/RIP3-dependent reactive oxygen species production. *Cell Death Differ*. **18**, 656–665.

Vucur, M., Roderburg, C., Bettermann, K., Tacke, F., Heikenwalder, M., Trautwein, C., and Luedde, T. (2010). Mouse models of hepatocarcinogenesis: what can we learn for the prevention of human hepatocellular carcinoma? *Oncotarget* **1**, 373–378.

Welz, P.S., Wullaert, A., Vlantis, K., Kondylis, V., Ferna´ ndez-Majada, V., Ermolaeva, M., Kirsch, P., Sterner-Kock, A., van Loo, G., and Pasparakis, M. (2011). FADD prevents RIP3-mediated epithelial cell necrosis and chronic intestinal inflammation. *Nature* **477**, 330–334.

Wunderlich, F.T., Luedde, T., Singer, S., Schmidt-Supprian, M., Baumgartl, J., Schirmacher, P., Pasparakis, M., and Brüning, J.C. (2008). Hepatic NF-kappa B essential modulator deficiency prevents obesity-induced insulin resistance but synergizes with high-fat feeding in tumorigenesis. *Proc. Natl. Acad. Sci. USA* **105**, 1297–1302.

Yang, L., Inokuchi, S., Roh, Y.S., Song, J., Loomba, R., Park, E.J., and Seki, E. (2013). Transforming growth factor-b signaling in hepatocytes promotes hepatic fibrosis and carcinogenesis in mice with hepatocyte-specific deletion of TAK1. *Gastroenterology* **144**, 1042–1054.e4.

Zhang, D.Y., and Friedman, S.L. (2012). Fibrosis-dependent mechanisms of hepatocarcinogenesis. *Hepatology* **56**, 769–775.

3.4.7. Personal contributions

Hepatocyte cell death and compensatory proliferation play a crucial role in the development of HCC in the setting of a chronic inflammation. Most studies so far mainly focused on the role of Caspase-8-dependent apoptis in hepatocarcinogenesis but we could show in the present study that RIP-3 dependent necroptosis limits immune responses and counteracts compensatory proliferation therefore preventing HCC formation. However, as chronic inflammation leads also to a loss of bilary cells, RIP3 mediates jaundice and cholestasis by suppressing compensatory proliferation of biliary cells.

My tasks in this study were conceptional development of the project and the immunohistochemical analysis of inflammation-driven HCC development, biochemical and histological analyses of tumor promoting factors as well as tumor-promoting chromosomal abberrations.

Analyses and figures contributed:

Figure 2a: Histological (H/E) and immunohistochemical (pan-cytokeratin, A6) analysis of 6-weeks old knock-out and wt mice

Figure 2b – d: Quantification of necrotic area (**b**), number of bile-ducts (**c**) and A6-positive oval cells (**d**) in the different mice indicated.

Figure 3a and b: Immunohistochemical (**a**) and statistical (**b**) analyses of apoptotic and proliferating hepatocytes

Figure 3d – f: Double stainings for Ki67/pan-Cytokeratin and cleaved Caspase-3/pan-Cytokeratin (**d**) and quantification of proliferating (**e**) and apoptotic (**f**) biliary cells.

Figure 4**c**: Quantification of tumor area

Figure 4**d**: Histologic (H/E) and immunohistochemical (Collagen IV) analysis of mice at time of tumor development

Figure 4e and f: 16-gene profile analysis (**e**) and oncogene anlysis (**f**) of WT, $TAK1^{LPC\text{-}KO}$ and $TAK1^{LPC\text{-}KO}/RIP3^{-/-}$ mice.

Figure 5a and c: Array CGH analysis for chromosomal aberration in livers of different knock-out compared to WT mice (**a**) primary hepatocytes isolated from $TAK1^{LPC\text{-}KO}/RIP3^{-/-}$ mice resistant to TNFα-induced cell death (**c**).

Figure 6b: Immunohistochemistry of liver paraffin sections and densitometric analysis for F4/80 positivity in WT and knock-out mice

Figure 7b and c: Immunohistochemical (**b**) and statistical (**c**) analyses of phospho-JNK-positive hepatocytes.

Figure 7d: Immunohistochemical analysis of proliferating and apoptic hepatocytes upon JNK inhibtion

Figure 7e and f: Statistical evaluation of proliferating (**e**) and apoptotic (**f**) hepatocytes upon JNK-inhibtion

Figure S1c: Pan-Cytokeratin and F4/80 staining from 6-week-old male mice

Figure S1e and f: Immunohistochemical (**e**) and statistical (**f**) analysis of $Ki67^{+}$ hepatocytes 48h after partial hepatectomy

Figure S2d and f: Histologic (H/E) and immunohistochemical (pan-Cytokeratin) analysis of young (**d**) and old (**f**) TAK1/$Casp\text{-}8^{LPC\text{-}KO}/RIP3^{-/-}$ triple-knock-out mice

Figure S3: Immunohistochemistry of Liver Paraffin Sections for cleaved Caspase-3 in 6-week-old $TAK1^{LPC\text{-}KO}/RIP3^{-/-}$ mice

Figure S5: Immunohistochemical (**a**) and statistical (**b**) analysis of phosphor-JNK-positive non-parenchymal cells in 6-week-old mice

4. Discussion

The liver is an organ with vital functions in the metabolism of proteins, lipids and carbodydrates, the clearance of pathogens by regulating immune responses and detoxification of foreign substances like drugs and alcohol.[1] To prevent local organ damage by immune responses directed against metabolites processed in the liver, the liver microenvironment induces an immune tolerant state. But this tight regulation of immune responses can also be exploited by pathogens that are specifically targeting and infecting hepatocytes, like for example hepatitis B (HBV) and hepatitis C (HCV) virus. Although the immune system can in many cases clear the viral infection, more than 500 million people worldwide are suffering from chronic infections with either HBV or HCV putting people at risk of developing immune cell mediated liver damage, fibrosis, cirrhosis and hepatocellular carcinoma (HCC). [2] Despite the availability of a preventive vaccine, more than 50% of all HCC cases develop on the background of chronic HBV infection.[93] Hence, HBV remains a major health problem and new therapeutic options for curing chronically HBV infected patients are urgently needed.

4.1. Clearing of chronic viral liver infections

In the present thesis my colleagues and I were able to provide two possibilities to clear chronically HBV infected hepatocytes either by overcoming liver immune tolerance or by activating a hepatocyte intrinsic defense mechanism leading to degradation of the episomal viral DNA in a non-cytopathic manner.

In the first study published under the title 'Intrahepatic myeloid-cell aggregates enable local proliferation of CD8+ T cells and successful immunotherapy against chronic viral liver infection'[140] we found that concomitant *in vitro* stimulation of the T cell receptor, CD28 and IL-12 together with Toll-like receptor 9 (TLR9) treatment, resulted in a 50-fold increased expansion of cytotoxic T lymphocytes (CTLs) in the liver. TLR9 signaling as well as viral infection were capable to mediate the formation of previously unrecognized intrahepatic myeloid-cell aggregates of T-cell expansion (iMATEs). These iMATEs enabled extremely efficient local CTL proliferation and antiviral immunity finally leading to the clearance chronic viral infection in mice. This indicated that iMATEs not only constitute a morphological hub in which T-cells can expand but also release functionally active antiviral T-cells. Of note, iMATEs were distinct from long-lived tertiary lymphoid structures[141] or granulomas[142], arose shortly after TLR9 ligand injection and dissolved within 6-8 days. In line, inhibition of the LTβR-signalling pathway by application of the fusion molecule LTβR-Ig did not diminish iMATE formation or function.

iMATEs seem to represent a cocoon-like structure formed by monocyte-derived $CD11b^+$ dendritic cells (DC) shielding CTLs from immune-regulatory signals present in the liver. Furthermore, iMATEs were not only formed after TLR9L injection but also during acute viral infection (e.g. LCMV) but were lacking in chronic viral liver infection, indicating a correlation of these structures with efficient viral control by CTLs. When we induced iMATEs by TLR9 stimulation in the course of a chronic viral infection, we could see a significant expansion in virus-specific CTLs which were then able to control viral infection in the liver. Furthermore, by combining conventional therapeutic vaccination and TLR9 ligand injection we could increase the efficacy of the therapeutic vaccination. Hence, we believe that the induction of iMATEs by TLR9 stimulation may be used to improve therapeutic vaccination against chronic viral liver infections.

In the second study 'Specific and Nonhepatotoxic Degradation of Nuclear Hepatitis B Virus cccDNA'[143] we used a different approach for clearing chronic HBV infection from hepatocytes. One of the major problems during chronic HBV infection is, that upon infection HBV establishes a stably expressed episomal DNA, the so called covalently closed circular (ccc) DNA in the nuclei of hepatocytes.[27] Treatment with nucleo(t)side analogous can control viral replication, but life-long treatment is necessary, as the cccDNA will stay in the nucleus leading to viral rebound after treatment cessation. However, in previous studies it was shown that pro-inflammatory cytokines like interferons or tumor necrosis factor alpha (TNFα) affect among other steps of the HBV life cycle also cccDNA stability. However, clear mechanistic underpinnings were partly lacking.[34-37] Here we could describe for the first time how inflammatory cytokine signaling via interferon alpha (IFNα) or lymphotoxin beta receptor (LTβR) influences cccDNA stability by activating a host cell specific defense mechanism.

High doses of IFNα or LTβR-activation with agonistic antibodies lead to an up-regulation of APOBEC3A (A3A) or APOBEC3B (A3B) deaminases in HBV-infected HepaRG cells and primary human hepatocytes (PHH). Our findings suggest that these enzymes then co-localize with HBV core protein which mediates nuclear translocation and binding to cccDNA were the APOBEC molecules can deaminate cccDNA without affecting genomic DNA. Deaminated bases in the cccDNA are then recognized by DNA glycosylases marking cccDNA for further degradation. Why cccDNA is degraded instead of being repaired by the cellular repair machinery remains so far elusive and needs further investigation.

However, our study shows that cytokines or cytokine receptor agonists which can induce HBV cccDNA deamination and subsequent degradation are interesting candidates for treatment of chronically HBV infected patients. In combination with nucleo(t)side analogues which can inhibit nuclear replenishment of cccDNA, induction of A3A and A3B could potentially clear chronic HBV infection. Especially LTβR-agonists were, in contrast to INFα, effective at very low doses and

furthermore did neither show any toxicity nor modifications of genomic DNA. Of note, constitutive activation of the LTβR signaling pathway for more than one year was reported to lead to necro-inflammation and HCC in mice.[85] Furthermore, A3A and A3B have been shown to be able to induce mutations in genomic DNA and can therefore lead to cancer development.[144-146] However, we did not observe any modifications on genomic DNA level and the agonistic antibodies used in our experiments have already been tested in pre-clinical and clinical settings as anti-cancer therapy.[147] Moreover, as antivirals these antibodies would only be used for a very short period of time as we saw very effective viral clearance (>95%) already after 10 days post treatment using differentiated cell lines or primary human hepatocytes. Supportive for our findings of APOBEC-mediated HBV inhibition is a recent study which reported a significantly higher frequency of an A3B deletion allele in chronic HBV infected and HCC patients compared to healthy controls.[148]

Summarizing one can say that effective HBV clearance either by immunotherapy, inducing a sufficient number of CTLs that can efficiently kill infected hepatocytes, or by activation of cell intrinsic defense mechanisms like the APOBECs is possible. It might also be that these new treatment options we propose can even be interlinked as CTLs are known to express high levels of lymphotoxin[121] and therefore might in addition to their cytotoxic effects even induce APOBEC3B expression in target cells.

4.2. The role or necroptotic signaling in development of NASH

Despite HBV being the major cause for developing liver fibrosis, cirrhosis, and HCC in south-east Asia and sub-Saharan Africa[93], in industrialized countries non-alcoholic liver disease (NAFLD) has become the most commonly diagnosed chronic liver disease and the main causative underlying liver disease for development of HCC.[57, 93] Consequently, HCC is today the fastest increasing type of cancer in the U.S.[47]

An important step in the progression from benign steatosis (fatty liver) to destructive non-alcoholic steatohepatitis (NASH) is the induction of hepatocyte death by immune cells.[52] So far, studies have mainly focused on the role of caspase-mediated apoptotic pathways in the progression from NAFLD to NASH.[149, 150] However, NASH shows also histological features of necrosis and necro-inflammation[52, 151] suggesting a role of other cell death pathways in the pathology of the disease. Necroptosis, a recently discovered form of cell death downstream of TNF receptor depending on the kinases RIP1 and RIP3, has already been shown to play important roles in the induction of chronic inflammatory reaction in pancreas, gut and skin.[152-154] Furthermore, it was already shown that necroptotic cell death is present in patients with alcoholic liver disease [155] but the study 'A positive feedback loop

between RIP3 and JNK controls non-alcoholic steatohepatitis' presented within in this thesis is the first one to address to role of necroptosis in development of NASH. In the methionine-choline-deficient (MCD) dietary mouse model of NASH we demonstrate that RIP3-dependent necroptosis represents an important programmed cell death pathway in the transition from NAFLD to NASH.

Our results indicate that, in contrast to previous findings[156], Caspase-8 is counterbalancing the harmful hyperactivation of RIP3 dependent necroptosis. Therefore, our discoveries are in line with previous studies were it was demonstrated that RIP3 and Capase-8 mutually inhibit each other for example in embryonic development[157] and skin homeostasis.[158] However, the importance of apoptosis in the induction of NASH has already been demonstrated in several previously and pan-Caspase inhibitors proofed to be beneficial by reducing liver injury and fibrosis in mice fed with MCD-diet[159] and human NASH patients.[160] But one has to state, that these inhibitors not only inhibit Caspase-8 but also downstream effector caspases like for example Caspase-1 which has recently been shown to be a driver of NASH-induced fibrosis.[161] In line with that, we observed also apoptotic hepatocytes in *Caspase-8*-deficient livers and significant liver damage Caspase-$8^{LPC\text{-}KO}$/$RIP3^{-/-}$ mice upon MCD-diet feeding pointing to a role of Caspase-8 independent apoptosis in this mouse model.

Hence, our results suggest that both – Caspase-8 independent apoptosis as well as RIP3-dependent necroptosis are important mediators in the progression from NAFLD to NASH and NASH-induced fibrosis. Therefore, we think that pharmacological inhibition of the necroptotic pathway together with caspase-inhibitors might have additive beneficial effects in the treatment of patients suffering from NASH.

4.3. The role of necroptotic signaling in the development of HCC

In more than 80% – 90% of cases development of hepatocellular carcinoma (HCC), independent of the underlying liver disease, is preceded by a relatively uniform sequence of steps comprising of inflammation, hepatocyte death, compensatory proliferation, fibrogenesis and cirrhosis. Despite knowing this connection between inflammation, cell death and hepatocarcinogenesis for years, the exact molecular pathways regulating this transition from inflammation to liver cancer remain still elusive.[80] As we could show in the study described above, Caspase-8-independent apoptosis as well RIP3-dependent necroptosis play crucial roles in the development of NASH and NASH-induced liver damage, we were also interested whether these pathways also interact in the development of HCC.

To address this question we used the $TAK1^{LPC\text{-}KO}$ mouse model in which the TGFβ-activated kinase (TAK1) has been specifically knocked-out in liver parenchymal cells (LPC). This model mimics most of

the important steps found in human liver cancer formation, like inflammation, hepatocyte death, compensatory proliferation and finally HCC development. Lack of TAK1 has been shown to block NF-κB signaling and therefore rendering LPC more sensitive to spontaneous apoptosis.[127] Additionally, in another study TAK1 was associated with the inhibition of RIP1/RIP3 complexes and therefore preventing necroptosis.[162] Therefore, TAK1 seems to be one of the main regulators of cell death in the liver. By backcrossing $TAK^{LPC\text{-}KO}$ mice to $RIP3^{-/-}$ mice or Caspase-$8^{LPC\text{-}KO}$ mice we generated mice in which programmed cell death of LPC could either only occur via apoptosis or necroptosis, respectively.

In general, apoptosis is described as a form of cell death, without the release of intracellular contents and therefore no induction of inflammation, whereas necrosis is regarded as a cellular burst causing damage of surrounding by releasing cellular content and initiation of an inflammatory response.[163] However, in our mouse model we could show that apoptosis, induced a strong inflammatory response, enhanced compensatory proliferation and increased tumor development compared to TAK1-only knock-out mice. In contrast, when LPC were only able to undergo necroptotic cell death, there was only minor inflammation, reduced compensatory proliferation and consequently no tumor formation. Interestingly, $TAK1^{LPC\text{-}KO}/RIP3^{-/-}$ mice which showed strong and aggressive liver tumor development could be almost completely rescued in terms of hepatocyte death, compensatory proliferation and carcinogenesis when being back-crossed to Caspase-$8^{LPC\text{-}KO}$ mice. Hence, our results suggest that Caspase-8-dependent apoptosis is a main driver in HCC development while as RIP3-dependent necroptosis has a protective function in the $TAK1^{LPC\text{-}KO}$ model.

These results are in contrast to the study described above where we saw a protective role of Caspase- 8 and a liver damage-promoting function of RIP3 in the course of NASH-induced fibrosis. This clearly indicates that, despite the similar sequence of events in inflammation induced liver damage and hepatocarcinogenesis, the underlying molecular pathways might be totally different in the various etiologies causing chronic liver disease. Therefore, the use of apoptosis or necroptosis inhibitors needs to be carefully evaluated, depending on the initial stimulus and the pathogenic context of the underlying liver disease.

References

1. Renz-Polster, H., Krautzig, S. & Braun, J. Basislehrbuch Innere Medizin (2006).
2. Protzer, U., Maini, M.K. & Knolle, P.A. Living in the liver: hepatic infections. *Nat Rev Immunol* 12, 201-13 (2012).
3. Thomson, A.W. & Knolle, P.A. Antigen-presenting cell function in the tolerogenic liver environment. *Nat Rev Immunol* 10, 753-66 (2010).
4. Pei, R.J., Chen, X.W. & Lu, M.J. Control of hepatitis B virus replication by interferons and Toll-like receptor signaling pathways. *World J Gastroenterol* 20, 11618-11629 (2014).
5. Saito, T., Owen, D.M., Jiang, F., Marcotrigiano, J. & Gale, M., Jr. Innate immunity induced by composition-dependent RIG-I recognition of hepatitis C virus RNA. *Nature* 454, 523-7 (2008).
6. Wang, B. et al. Toll-like receptor activated human and murine hepatic stellate cells are potent regulators of hepatitis C virus replication. *J Hepatol* 51, 1037-45 (2009).
7. Wu, J. et al. Hepatitis B virus suppresses toll-like receptor-mediated innate immune responses in murine parenchymal and nonparenchymal liver cells. *Hepatology* 49, 1132-40 (2009).
8. Biswas, S.K. & Lopez-Collazo, E. Endotoxin tolerance: new mechanisms, molecules and clinical significance. *Trends Immunol* 30, 475-87 (2009).
9. Limmer, A. et al. Efficient presentation of exogenous antigen by liver endothelial cells to CD8+ T cells results in antigen-specific T-cell tolerance. *Nat Med* 6, 1348-54 (2000).
10. Isogawa, M., Furuichi, Y. & Chisari, F.V. Oscillating CD8(+) T cell effector functions after antigen recognition in the liver. *Immunity* 23, 53-63 (2005).
11. Cooper, A., Tal, G., Lider, O. & Shaul, Y. Cytokine induction by the hepatitis B virus capsid in macrophages is facilitated by membrane heparan sulfate and involves TLR2. *J Immunol* 175, 3165-76 (2005).
12. Dolganiuc, A. et al. Hepatitis C core and nonstructural 3 proteins trigger toll-like receptor 2-mediated pathways and inflammatory activation. *Gastroenterology* 127, 1513-24 (2004).
13. Dunn, C. et al. Temporal analysis of early immune responses in patients with acute hepatitis B virus infection. *Gastroenterology* 137, 1289-300 (2009).
14. Gehring, S. et al. Kupffer cells abrogate cholestatic liver injury in mice. *Gastroenterology* 130, 810-22 (2006).
15. Hosel, M. et al. Not interferon, but interleukin-6 controls early gene expression in hepatitis B virus infection. *Hepatology* 50, 1773-82 (2009).
16. Klein, C. et al. The IL-6-gp130-STAT3 pathway in hepatocytes triggers liver protection in T cell-mediated liver injury. *J Clin Invest* 115, 860-9 (2005).
17. von Hahn, T. et al. Hepatitis C virus continuously escapes from neutralizing antibody and T-cell responses during chronic infection in vivo. *Gastroenterology* 132, 667-78 (2007).

18. Chakravarty, S. et al. CD8+ T lymphocytes protective against malaria liver stages are primed in skin-draining lymph nodes. *Nat Med* 13, 1035-41 (2007).
19. Cockburn, I.A. et al. Prolonged antigen presentation is required for optimal CD8+ T cell responses against malaria liver stage parasites. *PLoS Pathog* 6, e1000877 (2010).
20. Holz, L.E. et al. Intrahepatic murine CD8 T-cell activation associates with a distinct phenotype leading to Bim-dependent death. *Gastroenterology* 135, 989-97 (2008).
21. Lopes, A.R. et al. Bim-mediated deletion of antigen-specific CD8 T cells in patients unable to control HBV infection. *J Clin Invest* 118, 1835-45 (2008).
22. Radziewicz, H. et al. Impaired hepatitis C virus (HCV)-specific effector CD8+ T cells undergo massive apoptosis in the peripheral blood during acute HCV infection and in the liver during the chronic phase of infection. *J Virol* 82, 9808-22 (2008).
23. Schurich, A. et al. Role of the coinhibitory receptor cytotoxic T lymphocyte antigen-4 on apoptosis-Prone CD8 T cells in persistent hepatitis B virus infection. *Hepatology* 53, 1494-503 (2011).
24. Larrubia, J.R. et al. Bim-mediated apoptosis and PD-1/PD-L1 pathway impair reactivity of PD1(+)/CD127(-) HCV-specific CD8(+) cells targeting the virus in chronic hepatitis C virus infection. *Cell Immunol* 269, 104-14 (2011).
25. Dienstag, J.L. Hepatitis B virus infection. *N Engl J Med* 359, 1486-500 (2008).
26. Fattovich, G., Bortolotti, F. & Donato, F. Natural history of chronic hepatitis B: special emphasis on disease progression and prognostic factors. *J Hepatol* 48, 335-52 (2008).
27. Grimm, D., Thimme, R. & Blum, H.E. HBV life cycle and novel drug targets. *Hepatol Int* 5, 644-53 (2011).
28. Tarocchi, M., Polvani, S., Marroncini, G. & Galli, A. Molecular mechanism of hepatitis B virus-induced hepatocarcinogenesis. *World J Gastroenterol* 20, 11630-11640 (2014).
29. Summers, J. & Mason, W.S. Replication of the genome of a hepatitis B--like virus by reverse transcription of an RNA intermediate. *Cell* 29, 403-15 (1982).
30. Yan, H. et al. Sodium taurocholate cotransporting polypeptide is a functional receptor for human hepatitis B and D virus. *Elife* 1, e00049 (2012).
31. Beck, J. & Nassal, M. Hepatitis B virus replication. *World J Gastroenterol* 13, 48-64 (2007).
32. Levrero, M. et al. Control of cccDNA function in hepatitis B virus infection. *J Hepatol* 51, 581-92 (2009).
33. Zoulim, F. & Locarnini, S. Hepatitis B virus resistance to nucleos(t)ide analogues. *Gastroenterology* 137, 1593-608 e1-2 (2009).
34. Guidotti, L.G. et al. Cytotoxic T lymphocytes inhibit hepatitis B virus gene expression by a noncytolytic mechanism in transgenic mice. *Proc Natl Acad Sci U S A* 91, 3764-8 (1994).

35. Guidotti, L.G. et al. Viral clearance without destruction of infected cells during acute HBV infection. *Science* 284, 825-9 (1999).
36. McClary, H., Koch, R., Chisari, F.V. & Guidotti, L.G. Relative sensitivity of hepatitis B virus and other hepatotropic viruses to the antiviral effects of cytokines. *J Virol* 74, 2255-64 (2000).
37. Wieland, S.F., Spangenberg, H.C., Thimme, R., Purcell, R.H. & Chisari, F.V. Expansion and contraction of the hepatitis B virus transcriptional template in infected chimpanzees. *Proc Natl Acad Sci U S A* 101, 2129-34 (2004).
38. Kock, J. & Blum, H.E. Hypermutation of hepatitis B virus genomes by APOBEC3G, APOBEC3C and APOBEC3H. *J Gen Virol* 89, 1184-91 (2008).
39. Rosler, C. et al. APOBEC-mediated interference with hepadnavirus production. *Hepatology* 42, 301-9 (2005).
40. Vartanian, J.P. et al. Massive APOBEC3 editing of hepatitis B viral DNA in cirrhosis. *PLoS Pathog* 6, e1000928 (2010).
41. Weber, A., Boege, Y., Reisinger, F. & Heikenwalder, M. Chronic liver inflammation and hepatocellular carcinoma: persistence matters. *Swiss Med Wkly* 141, w13197 (2011).
42. Bostan, N. & Mahmood, T. An overview about hepatitis C: a devastating virus. *Crit Rev Microbiol* 36, 91-133 (2010).
43. Kaplan, M.M. & Gershwin, M.E. Primary biliary cirrhosis. *N Engl J Med* 353, 1261-73 (2005).
44. Krawitt, E.L. Autoimmune hepatitis. *N Engl J Med* 354, 54-66 (2006).
45. Lucey, M.R., Mathurin, P. & Morgan, T.R. Alcoholic hepatitis. *N Engl J Med* 360, 2758-69 (2009).
46. Tujios, S. & Fontana, R.J. Mechanisms of drug-induced liver injury: from bedside to bench. *Nat Rev Gastroenterol Hepatol* 8, 202-11 (2011).
47. Wolf, M.J. & al, e. Metabolic activation of intrahepatic CD8+ and NKT-cells causes nonalcoholic steatohepatitis and hepatocellular carcinoma via cross-talk with hepatocytes. *Cancer cell* in press (2014).
48. Riehle, K.J., Dan, Y.Y., Campbell, J.S. & Fausto, N. New concepts in liver regeneration. *J Gastroenterol Hepatol* 26 Suppl 1, 203-12 (2011).
49. Cavazza, A. et al. Incidence, risk factors, and survival of hepatocellular carcinoma in primary biliary cirrhosis: comparative analysis from two centers. *Hepatology* 50, 1162-8 (2009).
50. Yeoman, A.D. et al. Evaluation of risk factors in the development of hepatocellular carcinoma in autoimmune hepatitis: Implications for follow-up and screening. *Hepatology* 48, 863-70 (2008).
51. Ringelhan, M., Protzer, U., O'Connor, T. & Heikenwalder, M. The direct and indirect role of HBV in liver cancer: Prospective markers for HCC-screening and potential therapeutic targets. *J Pathol* (2014).

52. Schattenberg, J.M. & Schuppan, D. Nonalcoholic steatohepatitis: the therapeutic challenge of a global epidemic. *Curr Opin Lipidol* 22, 479-88 (2011).
53. Weiss, J., Rau, M. & Geier, A. Non-alcoholic fatty liver disease: epidemiology, clinical course, investigation, and treatment. *Dtsch Arztebl Int* 111, 447-52 (2014).
54. Nakagawa, H. et al. ER Stress Cooperates with Hypernutrition to Trigger TNF-Dependent Spontaneous HCC Development. *Cancer Cell* 26, 331-43 (2014).
55. Blachier, M., Leleu, H., Peck-Radosavljevic, M., Valla, D.C. & Roudot-Thoraval, F. The burden of liver disease in Europe: a review of available epidemiological data. *J Hepatol* 58, 593-608 (2013).
56. Younossi, Z.M. et al. Changes in the prevalence of the most common causes of chronic liver diseases in the United States from 1988 to 2008. *Clin Gastroenterol Hepatol* 9, 524-530 e1; quiz e60 (2011).
57. Vernon, G., Baranova, A. & Younossi, Z.M. Systematic review: the epidemiology and natural history of non-alcoholic fatty liver disease and non-alcoholic steatohepatitis in adults. *Aliment Pharmacol Ther* 34, 274-85 (2011).
58. Chalasani, N. et al. The diagnosis and management of non-alcoholic fatty liver disease: practice Guideline by the American Association for the Study of Liver Diseases, American College of Gastroenterology, and the American Gastroenterological Association. *Hepatology* 55, 2005-23 (2012).
59. Leite, N.C., Salles, G.F., Araujo, A.L., Villela-Nogueira, C.A. & Cardoso, C.R. Prevalence and associated factors of non-alcoholic fatty liver disease in patients with type-2 diabetes mellitus. *Liver Int* 29, 113-9 (2009).
60. Clark, J.M., Brancati, F.L. & Diehl, A.M. The prevalence and etiology of elevated aminotransferase levels in the United States. *Am J Gastroenterol* 98, 960-7 (2003).
61. Caballero, F. et al. Enhanced free cholesterol, SREBP-2 and StAR expression in human NASH. *J Hepatol* 50, 789-96 (2009).
62. Dyson, J.K., Anstee, Q.M. & McPherson, S. Non-alcoholic fatty liver disease: a practical approach to diagnosis and staging. *Frontline Gastroenterol* 5, 211-218 (2014).
63. Caldwell, S.H. & Crespo, D.M. The spectrum expanded: cryptogenic cirrhosis and the natural history of non-alcoholic fatty liver disease. *J Hepatol* 40, 578-84 (2004).
64. Virchow, R. An Address on the Value of Pathological Experiments. *Br Med J* 2, 198-203 (1881).
65. Balkwill, F. & Mantovani, A. Inflammation and cancer: back to Virchow? *Lancet* 357, 539-45 (2001).
66. Demaria, S. et al. Cancer and inflammation: promise for biologic therapy. *J Immunother* 33, 335-51 (2010).

67. Colotta, F., Allavena, P., Sica, A., Garlanda, C. & Mantovani, A. Cancer-related inflammation, the seventh hallmark of cancer: links to genetic instability. *Carcinogenesis* 30, 1073-81 (2009).
68. Hanahan, D. & Weinberg, R.A. The hallmarks of cancer. *Cell* 100, 57-70 (2000).
69. Hanahan, D. & Weinberg, R.A. Hallmarks of cancer: the next generation. *Cell* 144, 646-74 (2011).
70. Cover, T.L. & Blaser, M.J. Helicobacter pylori in health and disease. *Gastroenterology* 136, 1863-73 (2009).
71. Mostafa, M.H., Sheweita, S.A. & O'Connor, P.J. Relationship between schistosomiasis and bladder cancer. *Clin Microbiol Rev* 12, 97-111 (1999).
72. Nishiyama, R. et al. Hepatocellular carcinoma associated with autoimmune hepatitis. *J Hepatobiliary Pancreat Surg* 11, 215-9 (2004).
73. Pohl, C., Hombach, A. & Kruis, W. Chronic inflammatory bowel disease and cancer. *Hepatogastroenterology* 47, 57-70 (2000).
74. Park, E.J. et al. Dietary and genetic obesity promote liver inflammation and tumorigenesis by enhancing IL-6 and TNF expression. *Cell* 140, 197-208 (2010).
75. Grivennikov, S.I., Greten, F.R. & Karin, M. Immunity, inflammation, and cancer. *Cell* 140, 883-99 (2010).
76. Wolf, M.J., Seleznik, G.M., Zeller, N. & Heikenwalder, M. The unexpected role of lymphotoxin beta receptor signaling in carcinogenesis: from lymphoid tissue formation to liver and prostate cancer development. *Oncogene* 29, 5006-18 (2010).
77. Thorgeirsson, S.S. & Grisham, J.W. Molecular pathogenesis of human hepatocellular carcinoma. *Nat Genet* 31, 339-46 (2002).
78. Ferlay, J., Parkin, D.M. & Steliarova-Foucher, E. Estimates of cancer incidence and mortality in Europe in 2008. *Eur J Cancer* 46, 765-81 (2010).
79. Yu, J.B., Blitzblau, R.C., Patel, S.C., Decker, R.H. & Wilson, L.D. Surveillance, Epidemiology, and End Results (SEER) database analysis of microcystic adnexal carcinoma (sclerosing sweat duct carcinoma) of the skin. *Am J Clin Oncol* 33, 125-7 (2010).
80. El-Serag, H.B. Hepatocellular carcinoma. *N Engl J Med* 365, 1118-27 (2011).
81. Guidotti, L.G. & Chisari, F.V. Immunobiology and pathogenesis of viral hepatitis. *Annu Rev Pathol* 1, 23-61 (2006).
82. Protzer, U. & Schaller, H. Immune escape by hepatitis B viruses. *Virus Genes* 21, 27-37 (2000).
83. Fattovich, G., Stroffolini, T., Zagni, I. & Donato, F. Hepatocellular carcinoma in cirrhosis: incidence and risk factors. *Gastroenterology* 127, S35-50 (2004).
84. Nakamoto, Y., Guidotti, L.G., Kuhlen, C.V., Fowler, P. & Chisari, F.V. Immune pathogenesis of hepatocellular carcinoma. *J Exp Med* 188, 341-50 (1998).

85. Haybaeck, J. et al. A lymphotoxin-driven pathway to hepatocellular carcinoma. *Cancer Cell* 16, 295-308 (2009).
86. Sung, W.K. et al. Genome-wide survey of recurrent HBV integration in hepatocellular carcinoma. *Nat Genet* 44, 765-9 (2012).
87. Bonilla Guerrero, R. & Roberts, L.R. The role of hepatitis B virus integrations in the pathogenesis of human hepatocellular carcinoma. *J Hepatol* 42, 760-77 (2005).
88. Heikenwalder, M. & Protzer, U. LINE(1)s of evidence in HBV-driven liver cancer. *Cell Host Microbe* 15, 249-50 (2014).
89. Bouchard, M.J. & Navas-Martin, S. Hepatitis B and C virus hepatocarcinogenesis: lessons learned and future challenges. *Cancer Lett* 305, 123-43 (2011).
90. Ou, D.P., Tao, Y.M., Tang, F.Q. & Yang, L.Y. The hepatitis B virus X protein promotes hepatocellular carcinoma metastasis by upregulation of matrix metalloproteinases. *Int J Cancer* 120, 1208-14 (2007).
91. Paterlini, P., Poussin, K., Kew, M., Franco, D. & Brechot, C. Selective accumulation of the X transcript of hepatitis B virus in patients negative for hepatitis B surface antigen with hepatocellular carcinoma. *Hepatology* 21, 313-21 (1995).
92. Pollicino, T. & Saitta, C. Occult hepatitis B virus and hepatocellular carcinoma. *World J Gastroenterol* 20, 5951-61 (2014).
93. Forner, A., Llovet, J.M. & Bruix, J. Hepatocellular carcinoma. *Lancet* 379, 1245-55 (2012).
94. Donato, F. et al. Alcohol and hepatocellular carcinoma: the effect of lifetime intake and hepatitis virus infections in men and women. *Am J Epidemiol* 155, 323-31 (2002).
95. Calle, E.E., Rodriguez, C., Walker-Thurmond, K. & Thun, M.J. Overweight, obesity, and mortality from cancer in a prospectively studied cohort of U.S. adults. *N Engl J Med* 348, 1625-38 (2003).
96. Moller, H., Mellemgaard, A., Lindvig, K. & Olsen, J.H. Obesity and cancer risk: a Danish record-linkage study. *Eur J Cancer* 30A, 344-50 (1994).
97. Wolk, A. et al. A prospective study of obesity and cancer risk (Sweden). *Cancer Causes Control* 12, 13-21 (2001).
98. Villanueva, A., Hernandez-Gea, V. & Llovet, J.M. Medical therapies for hepatocellular carcinoma: a critical view of the evidence. *Nat Rev Gastroenterol Hepatol* 10, 34-42 (2013).
99. Mazzaferro, V. et al. Risk of HBV reinfection after liver transplantation in HBsAg-positive cirrhosis. Primary hepatocellular carcinoma is not a predictor for HBV recurrence. The European Cooperative Study Group on Liver Cancer and Transplantation. *Liver* 16, 117-22 (1996).

100. Cheng, A.L. et al. Efficacy and safety of sorafenib in patients in the Asia-Pacific region with advanced hepatocellular carcinoma: a phase III randomised, double-blind, placebo-controlled trial. *Lancet Oncol* 10, 25-34 (2009).
101. Llovet, J.M. et al. Sorafenib in advanced hepatocellular carcinoma. *N Engl J Med* 359, 378-90 (2008).
102. Llovet, J.M. & Hernandez-Gea, V. Hepatocellular carcinoma: reasons for phase III failure and novel perspectives on trial design. *Clin Cancer Res* 20, 2072-9 (2014).
103. Bhoj, V.G. & Chen, Z.J. Ubiquitylation in innate and adaptive immunity. *Nature* 458, 430-7 (2009).
104. Gilmore, T.D., Kalaitzidis, D., Liang, M.C. & Starczynowski, D.T. The c-Rel transcription factor and B-cell proliferation: a deal with the devil. *Oncogene* 23, 2275-86 (2004).
105. Hoffmann, A. & Baltimore, D. Circuitry of nuclear factor kappaB signaling. *Immunol Rev* 210, 171-86 (2006).
106. Vallabhapurapu, S. & Karin, M. Regulation and function of NF-kappaB transcription factors in the immune system. *Annu Rev Immunol* 27, 693-733 (2009).
107. Xiao, C. & Ghosh, S. NF-kappaB, an evolutionarily conserved mediator of immune and inflammatory responses. *Adv Exp Med Biol* 560, 41-5 (2005).
108. Kida, Y. et al. Interleukin-1 stimulates cytokines, prostaglandin E2 and matrix metalloproteinase-1 production via activation of MAPK/AP-1 and NF-kappaB in human gingival fibroblasts. *Cytokine* 29, 159-68 (2005).
109. Osborn, L., Kunkel, S. & Nabel, G.J. Tumor necrosis factor alpha and interleukin 1 stimulate the human immunodeficiency virus enhancer by activation of the nuclear factor kappa B. *Proc Natl Acad Sci U S A* 86, 2336-40 (1989).
110. Qin, H., Wilson, C.A., Lee, S.J., Zhao, X. & Benveniste, E.N. LPS induces CD40 gene expression through the activation of NF-kappaB and STAT-1alpha in macrophages and microglia. *Blood* 106, 3114-22 (2005).
111. Aggarwal, B.B. Signalling pathways of the TNF superfamily: a double-edged sword. *Nat Rev Immunol* 3, 745-56 (2003).
112. Pomerantz, J.L. & Baltimore, D. Two pathways to NF-kappaB. *Mol Cell* 10, 693-5 (2002).
113. Remouchamps, C., Boutaffala, L., Ganeff, C. & Dejardin, E. Biology and signal transduction pathways of the Lymphotoxin-alphabeta/LTbetaR system. *Cytokine Growth Factor Rev* 22, 301-10 (2011).
114. Coope, H.J. et al. CD40 regulates the processing of NF-kappaB2 p100 to p52. *EMBO J* 21, 5375-85 (2002).

115. Weih, F. & Caamano, J. Regulation of secondary lymphoid organ development by the nuclear factor-kappaB signal transduction pathway. *Immunol Rev* 195, 91-105 (2003).
116. Zhu, M. & Fu, Y.X. The role of core TNF/LIGHT family members in lymph node homeostasis and remodeling. *Immunol Rev* 244, 75-84 (2011).
117. Vandenabeele, P., Galluzzi, L., Vanden Berghe, T. & Kroemer, G. Molecular mechanisms of necroptosis: an ordered cellular explosion. *Nat Rev Mol Cell Biol* 11, 700-14 (2010).
118. Naugler, W.E. & Karin, M. NF-kappaB and cancer-identifying targets and mechanisms. *Curr Opin Genet Dev* 18, 19-26 (2008).
119. Srinivasula, S.M. & Ashwell, J.D. IAPs: what's in a name? *Mol Cell* 30, 123-35 (2008).
120. Luedde, T., Kaplowitz, N. & Schwabe, R.F. Cell Death and Cell Death Responses in Liver Disease: Mechanisms and Clinical Relevance. *Gastroenterology* 147, 765-783 e4 (2014).
121. Bauer, J. et al. Lymphotoxin, NF-kB, and cancer: the dark side of cytokines. *Dig Dis* 30, 453-68 (2012).
122. Luedde, T. & Schwabe, R.F. NF-kappaB in the liver--linking injury, fibrosis and hepatocellular carcinoma. *Nat Rev Gastroenterol Hepatol* 8, 108-18 (2011).
123. Liu, P. et al. Activation of NF-kappa B, AP-1 and STAT transcription factors is a frequent and early event in human hepatocellular carcinomas. *J Hepatol* 37, 63-71 (2002).
124. Kim, H.R., Lee, S.H. & Jung, G. The hepatitis B viral X protein activates NF-kappaB signaling pathway through the up-regulation of TBK1. *FEBS Lett* 584, 525-30 (2010).
125. Tai, D.I. et al. Activation of nuclear factor kappaB in hepatitis C virus infection: implications for pathogenesis and hepatocarcinogenesis. *Hepatology* 31, 656-64 (2000).
126. Shi, H. et al. TLR4 links innate immunity and fatty acid-induced insulin resistance. *J Clin Invest* 116, 3015-25 (2006).
127. Bettermann, K. et al. TAK1 suppresses a NEMO-dependent but NF-kappaB-independent pathway to liver cancer. *Cancer Cell* 17, 481-96 (2010).
128. Inokuchi, S. et al. Disruption of TAK1 in hepatocytes causes hepatic injury, inflammation, fibrosis, and carcinogenesis. *Proc Natl Acad Sci U S A* 107, 844-9 (2010).
129. Luedde, T. et al. Deletion of NEMO/IKKgamma in liver parenchymal cells causes steatohepatitis and hepatocellular carcinoma. *Cancer Cell* 11, 119-32 (2007).
130. van de Wiel, M.A. et al. CGHcall: calling aberrations for array CGH tumor profiles. *Bioinformatics* 23, 892-4 (2007).
131. van de Wiel, M.A. & Wieringen, W.N. CGHregions: dimension reduction for array CGH data with minimal information loss. *Cancer Inform* 3, 55-63 (2007).
132. Lucifora, J. et al. Hepatitis B virus X protein is essential to initiate and maintain virus replication after infection. *J Hepatol* 55, 996-1003 (2011).

133. Lee, S.M., Schelcher, C., Demmel, M., Hauner, M. & Thasler, W.E. Isolation of human hepatocytes by a two-step collagenase perfusion procedure. *J Vis Exp* (2013).
134. Schulze-Bergkamen, H. et al. Primary human hepatocytes--a valuable tool for investigation of apoptosis and hepatitis B virus infection. *J Hepatol* 38, 736-44 (2003).
135. Thasler, W.E. et al. Charitable State-Controlled Foundation Human Tissue and Cell Research: Ethic and Legal Aspects in the Supply of Surgically Removed Human Tissue For Research in the Academic and Commercial Sector in Germany. *Cell Tissue Bank* 4, 49-56 (2003).
136. Gripon, P. et al. Hepatitis B virus infection of adult human hepatocytes cultured in the presence of dimethyl sulfoxide. *J Virol* 62, 4136-43 (1988).
137. Hantz, O. et al. Persistence of the hepatitis B virus covalently closed circular DNA in HepaRG human hepatocyte-like cells. *J Gen Virol* 90, 127-35 (2009).
138. Quasdorff, M. et al. A concerted action of HNF4alpha and HNF1alpha links hepatitis B virus replication to hepatocyte differentiation. *Cell Microbiol* 10, 1478-90 (2008).
139. Dandri, M. et al. Repopulation of mouse liver with human hepatocytes and in vivo infection with hepatitis B virus. *Hepatology* 33, 981-8 (2001).
140. Huang, L.R. et al. Intrahepatic myeloid-cell aggregates enable local proliferation of CD8(+) T cells and successful immunotherapy against chronic viral liver infection. *Nat Immunol* 14, 574-83 (2013).
141. Neyt, K., Perros, F., GeurtsvanKessel, C.H., Hammad, H. & Lambrecht, B.N. Tertiary lymphoid organs in infection and autoimmunity. *Trends Immunol* 33, 297-305 (2012).
142. Ramakrishnan, L. Revisiting the role of the granuloma in tuberculosis. *Nat Rev Immunol* 12, 352-66 (2012).
143. Lucifora, J. et al. Specific and nonhepatotoxic degradation of nuclear hepatitis B virus cccDNA. *Science* 343, 1221-8 (2014).
144. Burns, M.B. et al. APOBEC3B is an enzymatic source of mutation in breast cancer. *Nature* 494, 366-70 (2013).
145. Burns, M.B., Temiz, N.A. & Harris, R.S. Evidence for APOBEC3B mutagenesis in multiple human cancers. *Nat Genet* 45, 977-83 (2013).
146. Landry, S., Narvaiza, I., Linfesty, D.C. & Weitzman, M.D. APOBEC3A can activate the DNA damage response and cause cell-cycle arrest. *EMBO Rep* 12, 444-50 (2011).
147. Lukashev, M. et al. Targeting the lymphotoxin-beta receptor with agonist antibodies as a potential cancer therapy. *Cancer Res* 66, 9617-24 (2006).
148. Zhang, T. et al. Evidence of associations of APOBEC3B gene deletion with susceptibility to persistent HBV infection and hepatocellular carcinoma. *Hum Mol Genet* 22, 1262-9 (2013).

149. Feldstein, A.E. et al. Hepatocyte apoptosis and fas expression are prominent features of human nonalcoholic steatohepatitis. *Gastroenterology* 125, 437-43 (2003).
150. Feldstein, A.E. & Gores, G.J. Apoptosis in alcoholic and nonalcoholic steatohepatitis. *Front Biosci* 10, 3093-9 (2005).
151. Malhi, H. & Gores, G.J. Molecular mechanisms of lipotoxicity in nonalcoholic fatty liver disease. *Semin Liver Dis* 28, 360-9 (2008).
152. Bonnet, M.C. et al. The adaptor protein FADD protects epidermal keratinocytes from necroptosis in vivo and prevents skin inflammation. *Immunity* 35, 572-82 (2011).
153. He, S. et al. Receptor interacting protein kinase-3 determines cellular necrotic response to TNF-alpha. *Cell* 137, 1100-11 (2009).
154. Welz, P.S. et al. FADD prevents RIP3-mediated epithelial cell necrosis and chronic intestinal inflammation. *Nature* 477, 330-4 (2011).
155. Roychowdhury, S., McMullen, M.R., Pisano, S.G., Liu, X. & Nagy, L.E. Absence of receptor interacting protein kinase 3 prevents ethanol-induced liver injury. *Hepatology* 57, 1773-83 (2013).
156. Hatting, M. et al. Hepatocyte caspase-8 is an essential modulator of steatohepatitis in rodents. *Hepatology* 57, 2189-201 (2013).
157. Kaiser, W.J. et al. RIP3 mediates the embryonic lethality of caspase-8-deficient mice. *Nature* 471, 368-72 (2011).
158. Weinlich, R. et al. Protective roles for caspase-8 and cFLIP in adult homeostasis. *Cell Rep* 5, 340-8 (2013).
159. Witek, R.P. et al. Pan-caspase inhibitor VX-166 reduces fibrosis in an animal model of nonalcoholic steatohepatitis. *Hepatology* 50, 1421-30 (2009).
160. Ratziu, V. et al. A phase 2, randomized, double-blind, placebo-controlled study of GS-9450 in subjects with nonalcoholic steatohepatitis. *Hepatology* 55, 419-28 (2012).
161. Dixon, L.J., Flask, C.A., Papouchado, B.G., Feldstein, A.E. & Nagy, L.E. Caspase-1 as a central regulator of high fat diet-induced non-alcoholic steatohepatitis. *PLoS One* 8, e56100 (2013).
162. Vanlangenakker, N. et al. cIAP1 and TAK1 protect cells from TNF-induced necrosis by preventing RIP1/RIP3-dependent reactive oxygen species production. *Cell Death Differ* 18, 656-65 (2011).
163. Jaeschke, H. & Lemasters, J.J. Apoptosis versus oncotic necrosis in hepatic ischemia/reperfusion injury. *Gastroenterology* 125, 1246-57 (2003).

Apendix I - Reprint permissions

Reprint permission *Nature Immunology*

Thank you for contacting Nature Publishing Group. As an author, you have the right to use this manuscript and figures, as per the licence-to-publish you signed:

Ownership of copyright in the article remains with the Authors, and provided that, when reproducing the Contribution or extracts from it, the Authors acknowledge first and reference publication in the Journal, the Authors retain the following non-exclusive rights:

a) **To reproduce the Contribution in whole or in part in any printed volume (book or thesis) of which they are the author(s).**

b) They and any academic institution where they work at the time may reproduce the Contribution for the purpose of course teaching.

c) To post a copy of the Contribution as accepted for publication after peer review (in Word or Tex format) on the Authors' own web site or institutional repository, or the Authors' funding body's designated archive, six months after publication of the printed or online edition of the Journal, provided that they also give a hyperlink from the Contribution to the Journals web site.

d) To reuse figures or tables created by them and contained in the Contribution in other works created by them.

Reprint permission *Science*

AAAS Author License to Publish Policy

OUR PHILOSOPHY

The American Association for the Advancement of Science (AAAS), the non-profit publisher of the *Science* family of journals, recognizes the importance of openness in research as well as the increasingly global nature of the scientific enterprise. The broad public communication of peer-reviewed research, and information-sharing within the scientific community, are essential to advancing science in the service of society.

This is why AAAS makes all of its peer-reviewed research content freely available with registration via the *Science* Web site twelve months after publication. AAAS also makes any

articles of urgent public-health importance freely and immediately available to the public, and it participates in various efforts to provide no-cost research content to the world's poorest countries.

As part of our mission, AAAS seeks to enhance communication among scientists, engineers, and the public, worldwide. Toward that end, AAAS does not require a copyright transfer from authors. Instead, authors are asked to grant AAAS an exclusive license to publish their work.

FURTHER DISSEMINATION

Authors are encouraged to further disseminate the accepted version of their manuscript, for release on the following schedule:

• Immediately following publication of the work by AAAS: o To the author's personal website

o To the author's institution's archival database

• Six months following publication of the work by AAAS: o To the funder's designated repository, if any

Additionally, authors and their institutions are encouraged—without further permission from AAAS—to use the final, published version of their work for educational purposes such as presentations, class handouts, dissertations, or photocopies for colleagues, so long as that use is not commercial in nature.

Further details about the AAAS author license to publish agreement appear below.

OUR LICENSE TO PUBLISH

1. **It's a license to publish, not a copyright transfer agreement.**

AAAS does not require copyright transfer from the authors of editorial content, including research reports, brevia, reviews, policy forums, perspectives, essays, and technical comments. AAAS requires instead a License to Publish, as described here. Ownership of the copyright will remain with the author. AAAS will be the title holder for purposes of registration

2. **Authors grant to AAAS an exclusive license to publish.**

In consideration of publication by AAAS in one of its *Science* journals, the author grants to AAAS an exclusive license to publish and to reproduce, adapt, and distribute the work as well as related supplemental content as broadly as possible, in various languages and forms, worldwide.

3. **Authors can immediately use final works for non-profit purposes—no permission needed.**

The author retains the non-exclusive right to use the final, published version of the work, immediately after it is made public by AAAS and without further permission, for educational and other non-commercial purposes. Such purposes include, for example, print collections of the author's own writings; completion of the author's thesis or dissertation; oral presentations by the author; educational courses taught by the author or offered by the author's institution; and distribution of photocopies by the author to colleagues for non-commercial purposes (not for further re-distribution). Figures from the final, published version of the work also can be used, with attribution, in future works by the author, including journal articles, book chapters, presentation slides, and posters, for example.

4. **Authors also can hyperlink to the final work through the AAAS "referrer linking service."**

Authors have the right to take advantage of the AAAS referrer linking service in order to provide free access to their final, published work via their personal or institutional Web site. AAAS will provide authors with one free referrer link per article. Information on the service will be e-mailed to the corresponding author the week following publication by AAAS.

5. **Authors can immediately post the accepted work to their personal or institutional archive.**

Authors also retain the right and are encouraged to post the accepted version of their manuscript to their personal Web site or institutional repository, immediately following publication by AAAS. (The accepted version is the paper that was accepted for publication by AAAS, including changes resulting from peer review, but prior to AAAS copyediting.) In such cases, authors must include a hyperlink to the final version published on the *Science* Web site, along with an explanatory note that includes the full citation, as follows: "This is the author's version of the work. It is posted here by permission of the AAAS for personal use, not for redistribution. The definitive version was published in *[Science* Journal Title] on [Volume number and date], DOI: [insert DOI number]."

6. **Authors and their institutions can use the accepted work for non-profit research purposes.**

Information-sharing is a key to scientific progress. Authors and their institutions therefore can use the accepted version of manuscripts for non-commercial research purposes, including sharing results with colleagues, or for replication or adaptation of the work so long as such use is not for any commercial advantage or exploitation. No further permission is needed from AAAS. Authors and their institutions cannot license the work, except to AAAS.

7. **Authors can release the accepted work to designated repositories, as required by funders.**

Authors of research articles, reports, brevia, reviews, or technical comments can release the accepted version of their work to PubMedCentral or another designated repository no sooner than six months after publication by AAAS. The accepted work can be *submitted* to the funder's repository immediately upon publication by AAAS, but authors must ensure that it is not scheduled for posting or public release for at least six months.

8. **Authors pledge that the work is original, true, and not previously published.**

The author(s) warrant that the work is original, that all facts are true and accurate, that it has not been published elsewhere, and does not infringe on any copyright, proprietary, or personal right of any third party. If the work contains materials owned or controlled by a third party, the author must certify that s/he has obtained permission for its use by attaching documentation to the License to Publish form and by clearly attributing the source within the text of the manuscript.

9. **University or institutional restrictions require a waiver.**

If university or other institutional restrictions might limit the authors' ability to grant to AAAS any of the rights described in AAAS's license, they must obtain an approved waiver from their institution.

10. Publication by AAAS will require a signed copy of AAAS's License to Publish form.

This License to Publish must be signed and returned to AAAS before a manuscript can be accepted for publication. Each author must sign the form. If the contribution is owned by the author's employer, an authorized representative must sign the form.

11. Authors must sign AAAS's form even if the Work was created under U.S. Government Contract.

The AAAS recognizes the U.S. Government's non-exclusive rights to use the work for non-commercial, governmental purposes where such rights are established in the grant or contract.

12. Authors employed by the U.S. Government should sign in the appropriate section of AAAS's form.

The area designated for U.S. Government employees confirms that the Work was written as part of your official duties as an employee of the U.S. Government, and therefore the Work is in the public domain.

Reprint permission *EMBO Molecular Medicine* AND *Cell Reports*

License

"Distribute" means to make available to the public the original and copies of the Work or Adaptation, as appropriate, through sale or other transfer of ownership.

"Licensor" means the individual, individuals, entity or entities that offer(s) the Work under the terms of this License.

"Original Author" means, in the case of a literary or artistic work, the individual, individuals, entity or entities who created the Work or if no individual or entity can be identified, the publisher; and in addition (i) in the case of a performance the actors, singers, musicians, dancers, and other persons who act, sing, deliver, declaim, play in, interpret or otherwise perform literary or artistic works or expressions of folklore; (ii) in the case of a phonogram the producer being the person or legal entity who first fixes the sounds of a performance or other sounds; and, (iii) in the case of broadcasts, the organization that transmits the broadcast.

"Work" means the literary and/or artistic work offered under the terms of this License including without limitation any production in the literary, scientific and artistic domain, whatever may be the mode or form of its expression including digital form, such as a book, pamphlet and other writing; a lecture, address, sermon or other work of the same nature; a dramatic or dramatico-musical work; a choreographic work or entertainment in dumb show; a musical composition with or without words; a cinematographic work to which are assimilated works expressed by a process analogous to cinematography; a work of drawing, painting, architecture, sculpture, engraving or lithography; a photographic work to which are assimilated works expressed by a process analogous to photography; a work of applied art; an illustration, map, plan, sketch or three-dimensional work relative to geography, topography, architecture or science; a performance; a broadcast; a phonogram; a compilation of data to the extent it is protected as a copyrightable work; or a work performed by a variety or circus performer to the extent it is not otherwise considered a literary or artistic work.

"You" means an individual or entity exercising rights under this License who has not previously violated the terms of this License with respect to the Work, or who has received express permission from the Licensor to exercise rights under this License despite a previous violation.

"Publicly Perform" means to perform public recitations of the Work and to communicate to the public those public recitations, by any means or process, including by wire or wireless means or public digital performances; to make available to the public Works in such a way that members of the public may access these Works from a place and at a place individually chosen by them; to perform the Work to the public by any means or process and the communication to the public of the performances of the Work, including by public digital performance; to broadcast and rebroadcast the Work by any means including signs, sounds or images.

"Reproduce" means to make copies of the Work by any means including without limitation by sound or visual recordings and the right of fixation and reproducing fixations of the Work, including storage of a protected performance or phonogram in digital form or other electronic medium.

2. Fair Dealing Rights. Nothing in this License is intended to reduce, limit, or restrict any uses free from copyright or rights arising from limitations or exceptions that are provided for in connection with the copyright protection under copyright law or other applicable laws.

3. License Grant. Subject to the terms and conditions of this License, Licensor hereby grants You a worldwide, royalty-free, non-exclusive, perpetual (for the duration of the applicable copyright) license to exercise the rights in the Work as stated below:

a. to Reproduce the Work, to incorporate the Work into one or more Collections, and to Reproduce the Work as incorporated in the Collections;
b. to create and Reproduce Adaptations provided that any such Adaptation, including any translation in any medium, takes reasonable steps to clearly label, demarcate or otherwise identify that changes were made to the original Work. For example, a translation could be marked "The original work was translated from English to Spanish," or a modification could indicate "The original work has been modified.";
c. to Distribute and Publicly Perform the Work including as incorporated in Collections; and,
d. to Distribute and Publicly Perform Adaptations.
e. For the avoidance of doubt:

i. **Non-waivable Compulsory License Schemes**. In those jurisdictions in which the right to collect royalties through any statutory or compulsory licensing scheme cannot be

waived, the Licensor reserves the exclusive right to collect such royalties for any exercise by You of the rights granted under this License;

ii. **Waivable Compulsory License Schemes**. In those jurisdictions in which the right to collect royalties through any statutory or compulsory licensing scheme can be waived, the Licensor waives the exclusive right to collect such royalties for any exercise by You of the rights granted under this License; and,

iii. **Voluntary License Schemes**. The Licensor waives the right to collect royalties, whether individually or, in the event that the Licensor is a member of a collecting society that administers voluntary licensing schemes, via that society, from any exercise by You of the rights granted under this License.

The above rights may be exercised in all media and formats whether now known or hereafter devised. The above rights include the right to make such modifications as are technically necessary to exercise the rights in other media and formats. Subject to Section 8(f), all rights not expressly granted by Licensor are hereby reserved.

4. Restrictions. The license granted in Section 3 above is expressly made subject to and limited by the following restrictions:

a. You may Distribute or Publicly Perform the Work only under the terms of this License. You must include a copy of, or the Uniform Resource Identifier (URI) for, this License with every copy of the Work You Distribute or Publicly Perform. You may not offer or impose any terms on the Work that restrict the terms of this License or the ability of the recipient of the Work to exercise the rights granted to that recipient under the terms of the License. You may not sublicense the Work. You must keep intact all notices that refer to this License and to the disclaimer of warranties with every copy of the Work You Distribute or Publicly Perform. When You Distribute or Publicly Perform the Work, You may not impose any effective technological measures on the Work that restrict the ability of a recipient of the Work from You to exercise the rights granted to that recipient under the terms of the License. This Section 4(a) applies to the Work as incorporated in a Collection, but this does not require the Collection apart from the Work itself to be made subject to the terms of this License. If You create a Collection, upon notice from any Licensor You must, to the extent practicable, remove from the Collection any credit as required by Section 4(b), as

requested. If You create an Adaptation, upon notice from any Licensor You must, to the extent practicable, remove from the Adaptation any credit as required by Section 4(b), as requested.

b. If You Distribute, or Publicly Perform the Work or any Adaptations or Collections, You must, unless a request has been made pursuant to Section 4(a), keep intact all copyright notices for the Work and provide, reasonable to the medium or means You are utilizing: (i) the name of the Original Author (or pseudonym, if applicable) if supplied, and/or if the Original Author and/or Licensor designate another party or parties (e.g., a sponsor institute, publishing entity, journal) for attribution ("Attribution Parties") in Licensor's copyright notice, terms of service or by other reasonable means, the name of such party or parties; (ii) the title of the Work if supplied; (iii) to the extent reasonably practicable, the URI, if any, that Licensor specifies to be associated with the Work, unless such URI does not refer to the copyright notice or licensing information for the Work; and (iv) , consistent with Section 3(b), in the case of an Adaptation, a credit identifying the use of the Work in the Adaptation (e.g., "French translation of the Work by Original Author," or "Screenplay based on original Work by Original Author"). The credit required by this Section 4 (b) may be implemented in any reasonable manner; provided, however, that in the case of a Adaptation or Collection, at a minimum such credit will appear, if a credit for all contributing authors of the Adaptation or Collection appears, then as part of these credits and in a manner at least as prominent as the credits for the other contributing authors. For the avoidance of doubt, You may only use the credit required by this Section for the purpose of attribution in the manner set out above and, by exercising Your rights under this License, You may not implicitly or explicitly assert or imply any connection with, sponsorship or endorsement by the Original Author, Licensor and/or Attribution Parties, as appropriate, of You or Your use of the Work, without the separate, express prior written permission of the Original Author, Licensor and/or Attribution Parties.

c. Except as otherwise agreed in writing by the Licensor or as may be otherwise permitted by applicable law, if You Reproduce, Distribute or Publicly Perform the Work either by itself or as part of any Adaptations or Collections, You must not distort, mutilate, modify or take other derogatory action in relation to the Work

which would be prejudicial to the Original Author's honor or reputation. Licensor agrees that in those jurisdictions (e.g. Japan), in which any exercise of the right granted in Section 3(b) of this License (the right to make Adaptations) would be deemed to be a distortion, mutilation, modification or other derogatory action prejudicial to the Original Author's honor and reputation, the Licensor will waive or not assert, as appropriate, this Section, to the fullest extent permitted by the applicable national law, to enable You to reasonably exercise Your right under Section 3(b) of this License (right to make Adaptations) but not otherwise.

5. Representations, Warranties and Disclaimer

UNLESS OTHERWISE MUTUALLY AGREED TO BY THE PARTIES IN WRITING, LICENSOR OFFERS THE WORK AS-IS AND MAKES NO REPRESENTATIONS OR WARRANTIES OF ANY KIND CONCERNING THE WORK, EXPRESS, IMPLIED, STATUTORY OR OTHERWISE, INCLUDING, WITHOUT LIMITATION, WARRANTIES OF TITLE, MERCHANTIBILITY, FITNESS FOR A PARTICULAR PURPOSE, NONINFRINGEMENT, OR THE ABSENCE OF LATENT OR OTHER DEFECTS, ACCURACY, OR THE PRESENCE OF ABSENCE OF ERRORS, WHETHER OR NOT DISCOVERABLE. SOME JURISDICTIONS DO NOT ALLOW THE EXCLUSION OF IMPLIED WARRANTIES, SO SUCH EXCLUSION MAY NOT APPLY TO YOU.

6. Limitation on Liability. EXCEPT TO THE EXTENT REQUIRED BY APPLICABLE LAW, IN NO EVENT WILL LICENSOR BE LIABLE TO YOU ON ANY LEGAL THEORY FOR ANY SPECIAL, INCIDENTAL, CONSEQUENTIAL, PUNITIVE OR EXEMPLARY DAMAGES ARISING OUT OF THIS LICENSE OR THE USE OF THE WORK, EVEN IF LICENSOR HAS BEEN ADVISED OF THE POSSIBILITY OF SUCH DAMAGES.

7. Termination

a. This License and the rights granted hereunder will terminate automatically upon any breach by You of the terms of this License. Individuals or entities who have received Adaptations or Collections from You under this License, however, will not have their licenses terminated provided such individuals or entities remain in full compliance with those licenses. Sections 1, 2, 5, 6, 7, and 8 will survive any termination of this License.
b. Subject to the above terms and conditions, the license granted here is perpetual (for the duration of the applicable copyright in the Work). Notwithstanding the above,

Licensor reserves the right to release the Work under different license terms or to stop distributing the Work at any time; provided, however that any such election will not serve to withdraw this License (or any other license that has been, or is required to be, granted under the terms of this License), and this License will continue in full force and effect unless terminated as stated above.

8. Miscellaneous

a. Each time You Distribute or Publicly Perform the Work or a Collection, the Licensor offers to the recipient a license to the Work on the same terms and conditions as the license granted to You under this License.
b. Each time You Distribute or Publicly Perform an Adaptation, Licensor offers to the recipient a license to the original Work on the same terms and conditions as the license granted to You under this License.
c. If any provision of this License is invalid or unenforceable under applicable law, it shall not affect the validity or enforceability of the remainder of the terms of this License, and without further action by the parties to this agreement, such provision shall be reformed to the minimum extent necessary to make such provision valid and enforceable.
d. No term or provision of this License shall be deemed waived and no breach consented to unless such waiver or consent shall be in writing and signed by the party to be charged with such waiver or consent.
e. This License constitutes the entire agreement between the parties with respect to the Work licensed here. There are no understandings, agreements or representations with respect to the Work not specified here. Licensor shall not be bound by any additional provisions that may appear in any communication from You. This License may not be modified without the mutual written agreement of the Licensor and You.
f. The rights granted under, and the subject matter referenced, in this License were drafted utilizing the terminology of the Berne Convention for the Protection of Literary and Artistic Works (as amended on September 28, 1979), the Rome Convention of 1961, the WIPO Copyright Treaty of 1996, the WIPO Performances and Phonograms Treaty of 1996 and the Universal Copyright Convention (as revised on July 24, 1971). These rights and subject matter take effect in the relevant jurisdiction

in which the License terms are sought to be enforced according to the corresponding provisions of the implementation of those treaty provisions in the applicable national law. If the standard suite of rights granted under applicable copyright law includes additional rights not granted under this License, such additional rights are deemed to be included in the License; this License is not intended to restrict the license of any rights under applicable law.

Appendix II – Curriculum Vitae

Personal details	
First names / Surname	Florian Johannes REISINGER
Address	56 Drautendorf, 4174 Niederwaldkirchen, Austria
Nationality	Austrian
Date of birth	28.09.1983
Gender	Male
Educational qualifications	
Dates	October 2010 – today
Occupation or position held	PhD Student
Main activities and responsibilities	• Working on HBV infection, chronic liver inflammation and liver cancer • Developing new treatment options for HBV infection • Histological analyses of liver pathology during viral infection and carcinogenesis
Dates	May 2007 – August 2009
Title of qualification awarded	Master der Naturwissenschaften (Master of Science)
Name and type of organisation providing education and training	University of Salzburg and University of Linz (Austria)
Main activities and responsibilities	• Production of murine monoclonal antibodies by Hybridoma technique • Purification and structural analysis of proteins with HPLC and Circular Dichroism Spectroscopy • Analysis of blood sera of allergic persons by radioallergosorbent tests (RAST)
Dates	October 2003 – April 2007
Title of qualification awarded	Bachelor der Naturwissenschaften (Bachelor of Science)
Name and type of organisation providing education and training	University of Salzburg and University of Linz (Austria)
Dates	September 1994 – May 2002
Occupation or position held	Highschool-Student
Research publications	Listed in Apendix III

Apendix III - List of publications

Peer-reviewed, scientific articles

Gautheron J*, Vucur M*, **Reisinger F***, Cardenas DV, Roderburg C, Koppe C, Kreggenwinkel K, Schneider AT, Bartneck M, Neumann UP, Canbay A, Reeves HL, Luedde M, Tacke F, Trautwein C, Heikenwalder M, Luedde T.

* equal contribution

A positive feedback loop between RIP3 and JNK controls non-alcoholic steatohepatitis.

***EMBO Molecular Medicine* 2014 Jun 24;6(8):1062-74**.

Xia Y, Lucifora J, **Reisinger F**, Heikenwalder M, Protzer U.

Virology. Response to Comment on "Specific and nonhepatotoxic degradation of nuclear hepatitis B virus cccDNA".

***Science*. 2014 Jun 13;344(6189):1237**

Luedde M, Lutz M, Carter N, Sosna J, Jacoby C, Vucur M, Gautheron J, Roderburg C, Borg N, **Reisinger F**, Hippe HJ, Linkermann A, Wolf MJ, Rose-John S, Lüllmann-Rauch R, Adam D, Flögel U, Heikenwalder M, Luedde T, Frey N.

RIP3, a kinase promoting necroptotic cell death, mediates adverse remodelling after myocardial infarction.

***Cardiovascular Research*. 2014 Jul 15;103(2):206-16**

Lucifora J*, Xia Y*, **Reisinger F**, Zhang K, Stadler D, Cheng X, Sprinzl MF, Koppensteiner H, Makowska Z, Volz T, Remouchamps C, Chou WM, Thasler WE, Hüser N, Durantel D, Liang TJ, Münk C, Heim MH, Browning JL, Dejardin E, Dandri M, Schindler M, Heikenwalder M[#], Protzer U[#].

* [#] equal contribution

Specific and nonhepatotoxic degradation of nuclear hepatitis B virus cccDNA.

***Science*. 2014 Mar 14;343(6176):1221-8**

Vucur M*, **Reisinger F***, Gautheron J*, Janssen J, Roderburg C, Cardenas DV, Kreggenwinkel K, Koppe C, Hammerich L, Hakem R, Unger K, Weber A, Gassler N, Luedde M, Frey N, Neumann UP, Tacke F, Trautwein C, Heikenwalder M, Luedde T.

* equal contribution

RIP3 inhibits inflammatory hepatocarcinogenesis but promotes cholestasis by controlling caspase-8- and JNK-dependent compensatory cell proliferation.

***Cell Reports*. 2013 Aug 29;4(4):776-90.**

Huang LR, Wohlleber D, **Reisinger F**, Jenne CN, Cheng RL, Abdullah Z, Schildberg FA, Odenthal M, Dienes HP, van Rooijen N, Schmitt E, Garbi N, Croft M, Kurts C, Kubes P, Protzer U, Heikenwalder M, Knolle PA.

Intrahepatic myeloid-cell aggregates enable local proliferation of CD8(+) T cells and successful immunotherapy against chronic viral liver infection.

***Nature Immunology*. 2013 Jun;14(6):574-83**

Sprinzl MF, **Reisinger F**, Puschnik A, Ringelhan M, Ackermann K, Hartmann D, Schiemann M, Weinmann A, Galle PR, Schuchmann M, Friess H, Otto G, Heikenwalder M, Protzer U.

Sorafenib perpetuates cellular anticancer effector functions by modulating the crosstalk between macrophages and natural killer cells.

***Hepatology.* 2013 Jun;57(6):2358-68**

Reviews

Lucifora J, Xia Y, **Reisinger F**, Stadler D, Heikenwälder M, Protzer U.

[Specific degradation of nuclear hepatitis B virus covalently closed circular DNA].

***Médecine/Sciences (Paris).* 2014 Aug-Sep;30(8-9):724-6**

Bauer J, Namineni S, **Reisinger F**, Zöller J, Yuan D, Heikenwälder M.

Lymphotoxin, NF-κB, and cancer: the dark side of cytokines.

***Digestive Disease*. 2012;30(5):453-68**

Weber A, Boege Y, **Reisinger** F, Heikenwälder M.

Chronic liver inflammation and hepatocellular carcinoma: persistence matters.

***Swiss Medical Weekly*. 2011 May 10;141:w13197**

Acknowledgements

I would like to thank all the people who supported me during these four years of my PhD. First of all I am deeply thankful to my parents and my brother Michael who always beliefed in me, my decisions and my work. Furthermore, with their financial support they enabled me to undertake my graduate and post-graduate studies and reaching my goal of a doctoral degree.

Next, I would like to thank my girlfriend Sylvia who was always there for me during good times, celebrating my successes as well as in not so easy times, when experiments failed or things were not running so smoothly. She was also incredible patient and supported me in my work, despite the long working hours preventing me from spending as much time with her as she would have deserved and I would have wanted to.

Then of course I would like to thank my fantastic colleagues and lab members who are probably the best team in the world making the last four years an unforgetable time. I would like to thank Daniel, Ruth and Olga for their always helpful hands, their technical support and know-how, Jeanette for taking care of my mice and Reiner for interesting discussions, Sukumar, Paul Tracy and Arlind for always giving a helping hand or an open ear for scientific consultations. A special thanks goes to Jessi, Judith, Marc, Anna, Detian, Nicole, Barbara, and also Andi who almost spent the whole four years together with me in the laboratory and have become much more then colleagues supporting me inside and outside of the lab with scientific and non-scientific discussions and also one or the other beer or coffee during breaks and evenings.

Besides I would like to thank all my collaboration partners, escpecially Julie, Mihael, Jérémie and Tom without whom my PhD would not have been that successful.

Last but not least I would like to thank Mathias for giving me the opportunity to undertake my PhD in his laboratory. I am very thankful for his basicially unlimited scientific and financial support, for even providing me with food during long working hours at night and for pushing me to my limits and sometimes beyond making my time as doctoral student a great success!

nature immunology

Intrahepatic myeloid-cell aggregates enable local proliferation of CD8+ T cells and successful immunotherapy against chronic viral liver infection

Li-Rung Huang[1], Dirk Wohlleber[1], Florian Reisinger[2], Craig N Jenne[3], Ru-Lin Cheng[1], Zeinab Abdullah[1], Frank A Schildberg[1], Margarete Odenthal[4], Hans-Peter Dienes[4], Nico van Rooijen[5], Edgar Schmitt[6], Natalio Garbi[1], Michael Croft[7], Christian Kurts[1], Paul Kubes[3], Ulrike Protzer[2], Mathias Heikenwalder[2] & Percy A Knolle[1,8,9]

Chronic infection is difficult to overcome because of exhaustion or depletion of cytotoxic effector CD8+ T cells (cytotoxic T lymphoytes (CTLs)). Here we report that signaling via Toll-like receptors (TLRs) induced intrahepatic aggregates of myeloid cells that enabled the population expansion of CTLs (iMATEs: 'intrahepatic myeloid-cell aggregates for T cell population expansion') without causing immunopa thology. In the liver, CTL proliferation was restricted to iMATEs that were composed of inflammatory monocyte–derived CD11b+ cells. Signaling via tumor-necrosis factor (TNF) caused iMATE formation that facilitated costimulation dependent on the receptor OX40 for expansion of the CTL population. The iMATEs arose during acute viral infection but were absent during chronic viral infection, yet they were still induced by TLR signaling. Such hepatic expansion of the CTL population controlled chronic viral infection of the liver after vaccination with DNA. Thus, iMATEs are dynamic structures that overcome regulatory cues that limit the population expansion of CTLs during chronic infection and can be used in new therapeutic vaccination strategies.

The liver has unique immunological functions that are determined by its particular microenvironment and its organ-resident antigen-presenting cells[1,2]. Because of this distinct regulation of T cell responses, the liver is considered a lymphoid organ[3]. Although the immune system can clear liver infections, hepatotropic pathogens such as hepatitis B virus (HBV), hepatitis C virus or malaria parasites can persist and establish chronic infections, which affect hundreds of millions of people worldwide[4]. Mechanisms that limit the function and population expansion of cytotoxic CD8+ T cells (cytotoxic T lymphocytes (CTLs)) in the liver include expression of the inhibitory molecules PD-L1 and galectin-9 or of arginase, which metabolizes amino acids required for the proliferation of CTLs, or the release of immunoregulatory cytokines such as interleukin 10 (IL-10) and transforming growth factor-β[4]. Such regulatory cues limit CTL function, which may protect the infected liver from overwhelming immunopathology by inducing oscillatory CTL effector function[5] but may also functionally compromise pathogen-specific CTLs[6,7]. However, large numbers of parasite-specific CTLs can eradicate infected hepatocytes[8,9], which indicates that large numbers of CTLs are needed to find and eliminate infected hepatocytes in the extensive maze of liver sinusoids. At present, no convincing immunotherapy exists for the treatment of chronic viral infection of the liver.

The generation of sufficient numbers of CTLs for defense against pathogens is regulated by the extent of antigen presentation in secondary lymphatic tissue by appropriately matured dendritic cells (DCs)[9,10]. CTLs may also proliferate in infected tissues after major histocompatibility complex (MHC) class I–restricted activation through the T cell antigen receptor[11], but local regulatory cues in the liver limit or even prevent such local proliferation. Tertiary lymphatic tissue generated during chronic inflammation is reported to increase CTL numbers in chronically inflamed tissue and augment immunity during infection of the lungs with influenza virus[12–14]. The relevance of tertiary lymphatic tissue for chronic infection of the liver is unclear. However, in hepatic granulomas formed after infection with mycobacteria, macrophage–T cell interactions, which lead to local antigen presentation in granulomas, trigger CTL effector function[15,16].

Here we report that induction of intrahepatic myeloid cell aggregates after signaling via Toll-like receptor 9 (TLR9) enabled massive expansion of the CTL population locally in the liver. Those myeloid-cell aggregates rapidly formed within 2 d after TLR9 signaling and provided a nonperfused cocoon-like anatomic structure for local proliferation of CTLs dependent on the T cell–costimulatory receptor OX40.

[1]Institutes of Molecular Medicine and Experimental Immunology, University of Bonn, Bonn, Germany. [2]Institute of Virology Technische Universität München/Helmholtz Zentrum München, München, Germany. [3]Calvin, Phoebe, and Joan Snyder Institute for Infection, Immunity and Inflammation, University of Calgary, Calgary, Canada. [4]Institute of Pathology, University of Köln, Köln, Germany. [5]Molecular Cell Biology and Immunology, VU Medical Center, Amsterdam, The Netherlands. [6]Institute of Immunology, University of Mainz, Mainz, Germany. [7]Division of Immune Regulation, La Jolla Institute for Allergy and Immunology, La Jolla, California, USA. [8]Institute of Virology, Technische Universität München, München, Germany. [9]Institute of Molecular Immunology, Technische Universität München, München, Germany. Correspondence should be addressed to P.A.K. (percy.knolle@ukb.uni-bonn.de) or M.H. (heikenwalder@helmholtz-muenchen.de).

Received 20 December 2012; accepted 20 February 2013; published online 14 April 2013; doi:10.1038/ni.2573

Such population expansion of CTLs in the liver controlled acute and chronic viral infection of the liver and eradicated chronic viral infection.

RESULTS

TLR9 signaling leads to population expansion of CTLs in the liver

In the liver, many layers of inhibitory mechanisms prevent the local population expansion and execution of effector functions of CTLs[4]. By adoptive transfer of CTLs, we studied which beneficial factors influence the CTLs or the microenvironment to achieve hepatic proliferation of CTLs. Through the use of antibody-coated microbeads as artificial antigen-presenting particles, we discovered that activation of CTLs by combined stimulation *in vitro* with antibody to the invariant signaling protein of the T cell receptor CD3 (anti-CD3) and antibody to the coreceptor CD28 (anti-CD28) together with IL-12 resulted in better *in vivo* survival of CTLs in the spleen and liver than did stimulation with antibody alone (**Supplementary Fig. 1a**). Costimulation with IL-12 improves CTL survival and promotes the differentiation of CTLs into effector and memory T cells[17–19]. Other stimulatory signals such as type I interferon (IFN-α/β), IFN-γ or retinoic acid together with transforming growth factor-β did not augment CTL numbers in the liver (data not shown).

We next investigated whether hepatic inflammation resulted in more proliferation of CTLs. We activated CD90.1$^+$ CTLs *in vitro* with anti-CD3, anti-CD28 and IL-12 and transferred the cells into CD90.2$^+$ host mice, then challenged the recipient mice by intravenous injection of TLR ligands. We found no greater abundance of CTLs in the liver or lungs but found fewer CTLs in the spleen at 4 h after injection of TLR9 ligand (**Fig. 1a**). At day 4 after challenge with TLR9 ligand, we found no greater abundance of splenic CTLs but over 20-fold more hepatic CTLs in mice treated with TLR9 ligand than in mice injected with a non–TLR9-binding control oligonucleotide (**Fig. 1b**). Challenge with a TLR4 ligand also elicited hepatic proliferation of CTLs, but TLR3 ligand or TLR7 ligand had little or no effect (**Supplementary Fig. 1b**). Dose-titration studies showed that a single application of TLR9 ligand sufficed for hepatic population expansion of CTLs (**Supplementary Fig. 1c**) but did not cause substantial liver damage (**Supplementary Fig. 1d**). The TLR9 ligand acted on recipient cells but not on transferred CTLs, as shown by the lack of proliferation of CTLs in *Tlr9*$^{-/-}$ mice (**Fig. 1c**); this also demonstrated the specificity of the TLR9 ligand used. These results suggested that TLR9 signaling caused changes in the liver that supported the hepatic proliferation of CTLs.

TLR9-induced proliferation of CTLs, as determined by expression of the proliferation marker Ki67, was most prominent in the liver and lungs (**Fig. 1d**), a result we confirmed by dilution of the cytosolic dye CFSE in CTLs (**Supplementary Fig. 1e**). Also, endogenous CTLs underwent proliferation in the liver after injection of TLR9 ligand (**Supplementary Fig. 1f**), which raised the question of whether naive or memory CD8$^+$ T cells had proliferated. We sorted splenic naive CD44^{lo}KLRG1$^-$CD8$^+$ T cells or memory CD44^{hi}KLRG1$^-$CD127$^+$CD8$^+$ T cells by flow cytometry from CD45.1$^+$ mice and then adoptively transferred those cells into CD45.2$^+$ recipient mice. Intrahepatic transferred naive CD8$^+$ T cells did not incorporate the thymidine analog BrdU, and we detected only low absolute numbers of T cells (**Supplementary Fig. 1g–i**). Transferred memory T cells present in the liver, however, incorporated BrdU after challenge with TLR9 ligand, which led to sevenfold more cells, but we

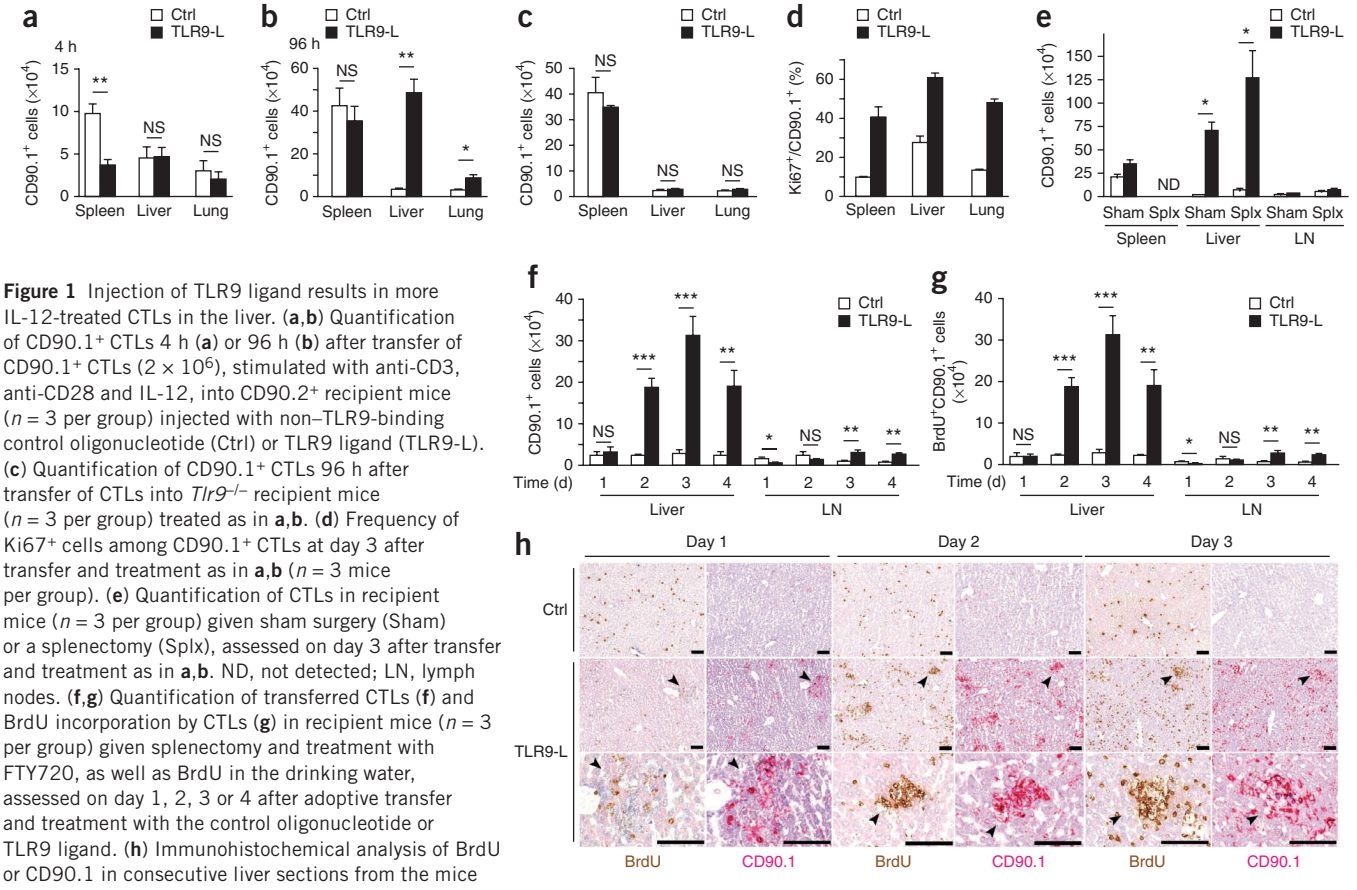

Figure 1 Injection of TLR9 ligand results in more IL-12-treated CTLs in the liver. (**a**,**b**) Quantification of CD90.1$^+$ CTLs 4 h (**a**) or 96 h (**b**) after transfer of CD90.1$^+$ CTLs (2 × 10^6), stimulated with anti-CD3, anti-CD28 and IL-12, into CD90.2$^+$ recipient mice (n = 3 per group) injected with non–TLR9-binding control oligonucleotide (Ctrl) or TLR9 ligand (TLR9-L). (**c**) Quantification of CD90.1$^+$ CTLs 96 h after transfer of CTLs into *Tlr9*$^{-/-}$ recipient mice (n = 3 per group) treated as in **a**,**b**. (**d**) Frequency of Ki67$^+$ cells among CD90.1$^+$ CTLs at day 3 after transfer and treatment as in **a**,**b** (n = 3 mice per group). (**e**) Quantification of CTLs in recipient mice (n = 3 per group) given sham surgery (Sham) or a splenectomy (Splx), assessed on day 3 after transfer and treatment as in **a**,**b**. ND, not detected; LN, lymph nodes. (**f**,**g**) Quantification of transferred CTLs (**f**) and BrdU incorporation by CTLs (**g**) in recipient mice (n = 3 per group) given splenectomy and treatment with FTY720, as well as BrdU in the drinking water, assessed on day 1, 2, 3 or 4 after adoptive transfer and treatment with the control oligonucleotide or TLR9 ligand. (**h**) Immunohistochemical analysis of BrdU or CD90.1 in consecutive liver sections from the mice in **f**,**g**. Arrowheads indicate the same position in consecutive sections. Scale bars, 100 μm. NS, not significant; $^*P < 0.05$, $^{**}P < 0.01$ and $^{***}P < 0.001$ (unpaired Student's t-test). Data are representative of two independent experiments (error bars (**a**–**g**), s.d.).

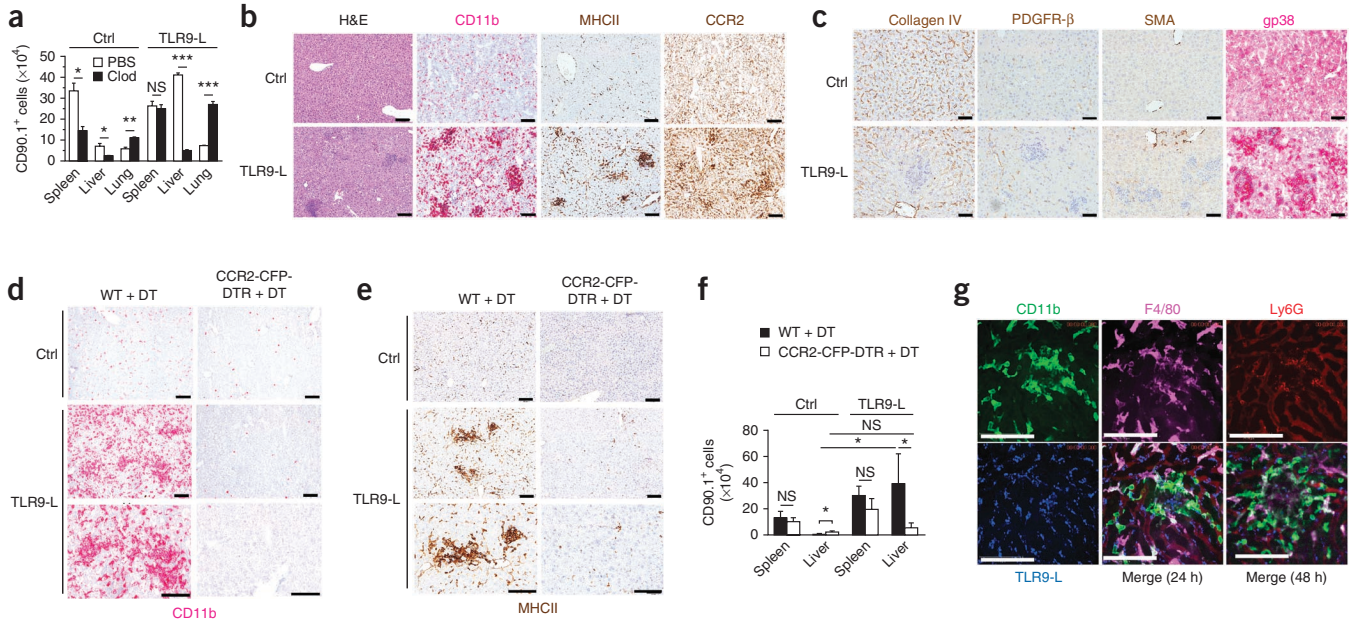

Figure 2 Characterization of iMATEs in the liver after injection of TLR9 ligand. (**a**) Quantification of CD90.1$^+$ CTLs after adoptive transfer into mice ($n = 4$ per group) treated with PBS or clodronate liposomes (Clod; for depletion of phagocytes), assessed at day 3 after challenge with TLR9 ligand or non–TLR9-binding control oligonucleotide. (**b**) Hematoxylin-and-eosin staining (far left) and immunohistochemical analysis of CD11b, MHC class II or CCR2 in liver tissue at day 3 after challenge with TLR9 ligand or the control oligonucleotide. (**c**) Immunohistochemical analysis of collagen IV, platelet-derived growth-factor receptor-β (PDGFR-β), smooth muscle actin (SMA) and gp38 in liver tissue at day 3 after challenge as in **b**. (**d**,**e**) Immunohistochemical analysis of CD11b (**d**) or MHC class II (**e**) in liver tissues from wild-type (WT) and CCR2-CFP-DTR mice treated with diphtheria toxin (+ DT), assessed at day 4 after challenge as in **b**. (**f**) Quantification of CD90.1$^+$ CTLs after transfer into wild-type or CCR2-CFP-DTR mice ($n = 3$ per group) treated with diphtheria toxin, assessed at day 4 after challenge as in **b**. (**g**) Images of intravital spinning-disc confocal microscopy of liver tissues obtained from mice 24 h or 48 h after injection of indodicarbocyanine-labeled TLR9 ligand and fluorochrome-labeled antibodies. Scale bars, 100 μm. $^*P < 0.05$, $^{**}P < 0.01$ and $^{***}P < 0.001$ (unpaired Student's *t*-test). Data are representative of two independent experiments (error bars (**a**,**f**), s.d.).

detected lower absolute numbers of cells than after transfer of *in vitro*–activated CTLs (**Supplementary Fig. 1g–i**).

The greater abundance of hepatic CTLs resulted from local proliferation but not from recirculation after activation in the spleen, as CTLs also proliferated in the liver after splenectomy (**Fig. 1e**). We obtained further evidence of hepatic expansion of the CTL population independently of lymphatic tissue by removing spleens from mice and treating the mice with the sphingosine 1-phosphate antagonist FTY720, which prevents egress of lymphocytes from the lymph nodes. As expected, treatment with FTY720 resulted in fewer endogenous CTLs in the liver and spleen (**Supplementary Fig. 1j**). We transferred CD90.1$^+$ CTLs into mice treated as described above (splenectomy plus FTY720) and found that the transferred cells increased in number in the livers and incorporated BrdU after challenge with TLR9 ligand (**Fig. 1f**,**g**), consistent with hepatic proliferation of CTLs rather than relocation from lymphatic tissue. Furthermore, BrdU$^+$CD90.1$^+$ CTLs accumulated in the liver in mice treated with TLR9 ligand (**Fig. 1h**). Notably, BrdU$^+$CD90.1$^+$ CTLs accumulated in certain areas in the liver, which raised the question of whether the proliferation of CTLs was related to their local clustering in the liver after challenge with TLR9 ligand.

Clustering of CD11b$^+$ cells promotes hepatic proliferation of CTLs

The lack of TLR9-induced hepatic proliferation of CTLs in *Tlr9*$^{-/-}$ mice indicated that recipient cells but not CTLs were the target of the TLR9 ligand. Depletion of phagocytic cells in mice completely abrogated the hepatic proliferation of CTLs but led to more CTLs in the lungs (**Fig. 2a**). This finding indicated that the CTL proliferation in the lung was independent of phagocytes and may have occurred in a compensatory way in the absence of phagocyte-dependent proliferation of CTLs in the liver.

Immunohistochemistry showed the presence of CD11b$^+$, MHC class II–positive (MHCII$^+$) and CCR2$^+$ cells after challenge with TLR9 ligand; these cells formed intrahepatic aggregates throughout the hepatic parenchyma (**Fig. 2b**). We observed aggregates formed by CD11b$^+$ cells only in mice treated with TLR9 ligand or TLR4 ligand, associated with hepatic proliferation of CTLs, but did not find such aggregates in mice treated with TLR3 ligand or TLR7 ligand (**Supplementary Fig. 2a**). Those aggregates were not separated from the surrounding liver tissue by collagen IV or by cells that expressed platelet-derived growth-factor receptor-β or smooth muscle actin, but we did detect expression of gp38, a marker of stromal cells, on CD11b$^+$MHCII$^+$ cells in the aggregates (**Fig. 2c** and data not shown). These results demonstrated a fundamental difference between hepatic aggregates of CD11b$^+$MHCII$^+$ cells generated by TLR9 ligand and the tertiary lymphoid structures formed during chronic inflammation[20,21]. Pursuant to that, we found no role for signaling via the lymphotoxin-β receptor (LTβR) in the TLR9 ligand–mediated proliferation of CTLs (**Supplementary Fig. 2b**).

We depleted CCR2-CFP-DTR mice (which have transgenic expression of a cyan fluorescent protein (CFP) reporter fused to the diphtheria toxin receptor (DTR) under the control of the promoter of the gene encoding the chemokine receptor CCR2) of CCR2$^+$ cells by injecting them with diphtheria toxin and found that aggregates of CD11b$^+$MHCII$^+$ cells did not form, which coincided with the loss of population expansion of CTLs (**Fig. 2d–f**). That observation led us to call this structure 'iMATE' ('intrahepatic myeloid-cell aggregate for T cell population expansion'). We found that iMATEs developed in a dynamic way after treatment with TLR9 ligand and gradually disappeared by day 8 (**Supplementary Fig. 2c**,**d**). There was little liver damage

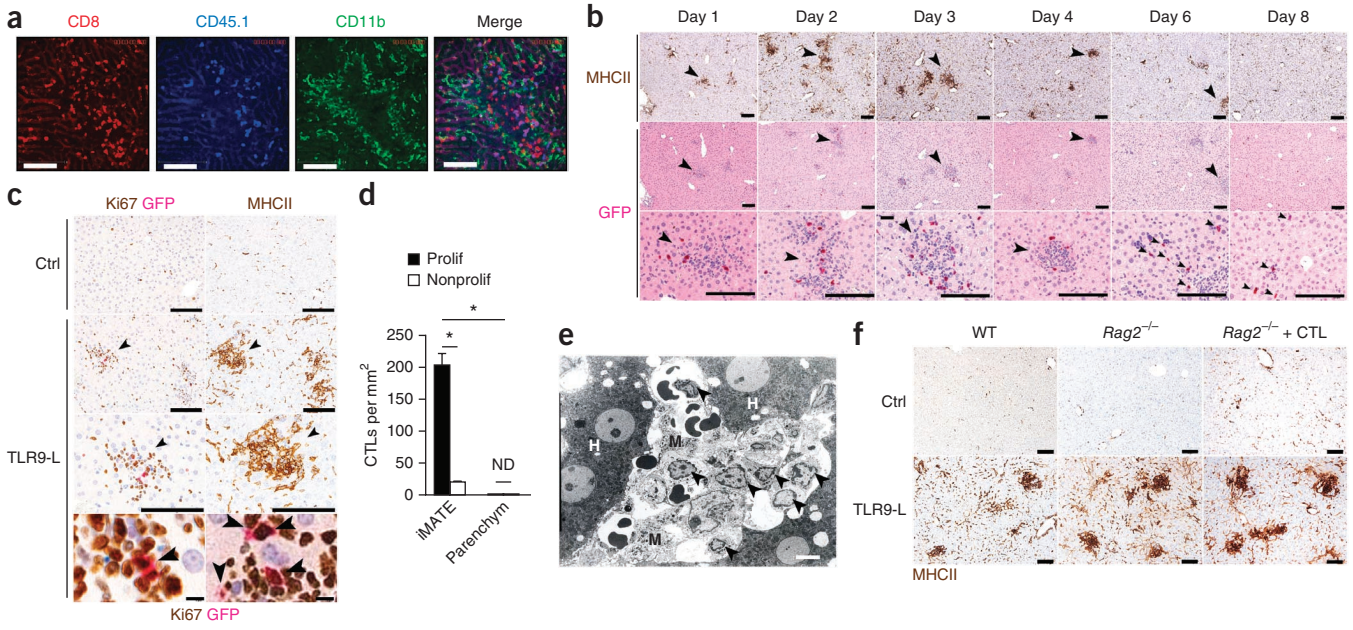

Figure 3 CTL proliferation in iMATEs. (**a**) Images of intravital spinning-disc confocal microscopy of an iMATE at day 3 after transfer of CD45.1$^+$ CTLs and treatment with TLR9 ligand; samples were costained for CD11b$^+$ cells (green), CD45.1$^+$ CTLs (blue) and total CD8$^+$ T cells (red). (**b**) Immunohistochemical analysis of MHC class II or GFP in consecutive liver sections obtained on days 1–8 (time, above images) after transfer of GFP$^+$ CTLs (3×10^6) and treatment with TLR9 ligand. Large arrowheads indicate the same iMATE in consecutive sections; small arrowheads indicate single CTLs outside iMATEs. (**c**) Costaining for GFP, Ki67 and MHC class II in consecutive liver sections at day 3 after treatment with TLR9 ligand or non–TLR9-binding control oligonucleotide. Arrowheads indicate the same position in consecutive sections (middle two rows) or dividing GFP$^+$ CTLs (bottom row). (**d**) Quantification of proliferating (Prolif; Ki67$^+$) and nonproliferating (Nonprolif; Ki67$^-$) transferred GFP$^+$ CTLs at day 3 after injection of TLR9 ligand, presented as cells per mm^2 liver tissue. $^*P < 0.01$ (unpaired Student's *t*-test). (**e**) Ultrastructural analysis of iMATEs by electron microscopy at day 3 after treatment with TLR9 ligand, showing CTLs (arrowheads) interacting with myeloid cells (M) in the vicinity of hepatocytes (H). (**f**) Immunohistochemical analysis of MHC class II in liver tissue at day 3 after injection of TLR9 ligand or control oligonucleotide, with (right) or without (left and middle) CTLs, into wild-type mice and mice deficient in recombination-activating gene 2 (*Rag2*$^{-/-}$). Scale bars, 100 μm (**a**,**b**,**f** and **c**, top three rows), 10 μm (**c**, bottom row) or 7 μm (**e**). Data are representative of two independent experiments with three mice per group (error bars (**d**), s.d.).

associated with the formation of iMATEs, as evaluated by cleavage of caspase-3 (**Supplementary Fig. 2e**) and slightly higher serum concentrations of alanine aminotransferase (ALT; **Supplementary Fig. 1d**). We found few infiltrating natural killer (NK) cells or B cells in iMATEs (**Supplementary Fig. 2f**). Instead, cells in iMATEs stained with antibody to the marker Gr-1 (**Supplementary Fig. 2f**), which identifies inflammatory monocytes (Ly6C) and neutrophils (Ly6G).

Anti-Ly6G-mediated depletion of neutrophils did not affect the hepatic proliferation of CTLs (**Supplementary Fig. 2g**), which excluded the possibility of a prominent role for neutrophils in this. We depleted mice of CD11b$^+$ neutrophils and treated them with TLR9 ligand, then used intravital time-lapse spinning-disc microscopy to characterize the role of CD11b$^+$ monocytes in iMATE formation. Circulating CD11b$^+$F4/80$^-$ monocytes did not adhere to sinusoids immediately after treatment with TLR9 ligand (**Supplementary Videos 1** and **2**), but 4 h later, some CD11b$^+$F4/80$^-$ monocytes adhered without affecting sinusoidal perfusion (**Supplementary Videos 3** and **4**). At 24 h and 48 h after treatment with TLR9 ligand, CD11b$^+$ monocytes with low to undetectable expression of F4/80 clustered in sinusoids (**Fig. 2g** and **Supplementary Videos 5–8**). These results suggested that iMATEs arose from inflammatory monocytes, but not Kupffer cells, that adhered to sinusoidal cells and thereby formed a nonperfused anatomical structure distinct from lymphatic tissue in which T cell proliferation occurred.

Hepatic CTL proliferation is restricted to iMATEs

After activation *in vitro* with anti-CD3, anti-CD28 and IL-12, CD45.1$^+$ CTLs or CTLs with transgenic expression of green fluorescent protein (GFP) localized together with CD11b$^+$MHCII$^+$ cells in iMATEs (**Fig. 3a** and **Supplementary Video 9**); this colocalization was constant (**Fig. 3b**) and independent of the proliferation of CTLs in the spleen or lymph nodes (**Supplementary Fig. 3a**). BrdU incorporation was greater in CTLs isolated from the liver than in those isolated from lymph nodes, and it continuously increased from day 1 to day 3 (**Supplementary Fig. 3b**). This suggested local proliferation of CTLs in iMATEs. Proliferating Ki67$^+$ CTLs were located in iMATEs but not elsewhere in parenchymal liver tissue, as shown by immunohistochemistry of serial liver sections (**Fig. 3c**). Quantification showed over 200-fold more Ki67$^+$ CTLs in iMATEs than in the remaining liver tissue (**Fig. 3d**).

We observed three distinct iMATE structures: a condensed form with either few proliferating CTLs or many proliferating CTLs; a dispersed form with many proliferating CTLs; and a diffuse form with few Ki67$^+$ CTLs (**Supplementary Fig. 4a**). Three-dimensional reconstruction of serial sections recapitulated the distinct forms of iMATEs (**Supplementary Fig. 4b** and **Supplementary Videos 10–12**), which allowed us to quantify the mean volume of iMATEs (73,851 μm^3 ± 50,184 μm^3) and number of CTLs per iMATE (94.4 ± 15). Ultrastructural analysis showed that monocyte-derived cells closely interacted with CTLs in iMATEs that were not demarcated from surrounding hepatocytes (**Fig. 3e**). The formation of iMATEs did not require crosstalk between myeloid cells and lymphocytes, as injection of TLR9 ligand into mice deficient in recombination-activating gene 2, which lack B cells and T cells, was sufficient to induce iMATEs,

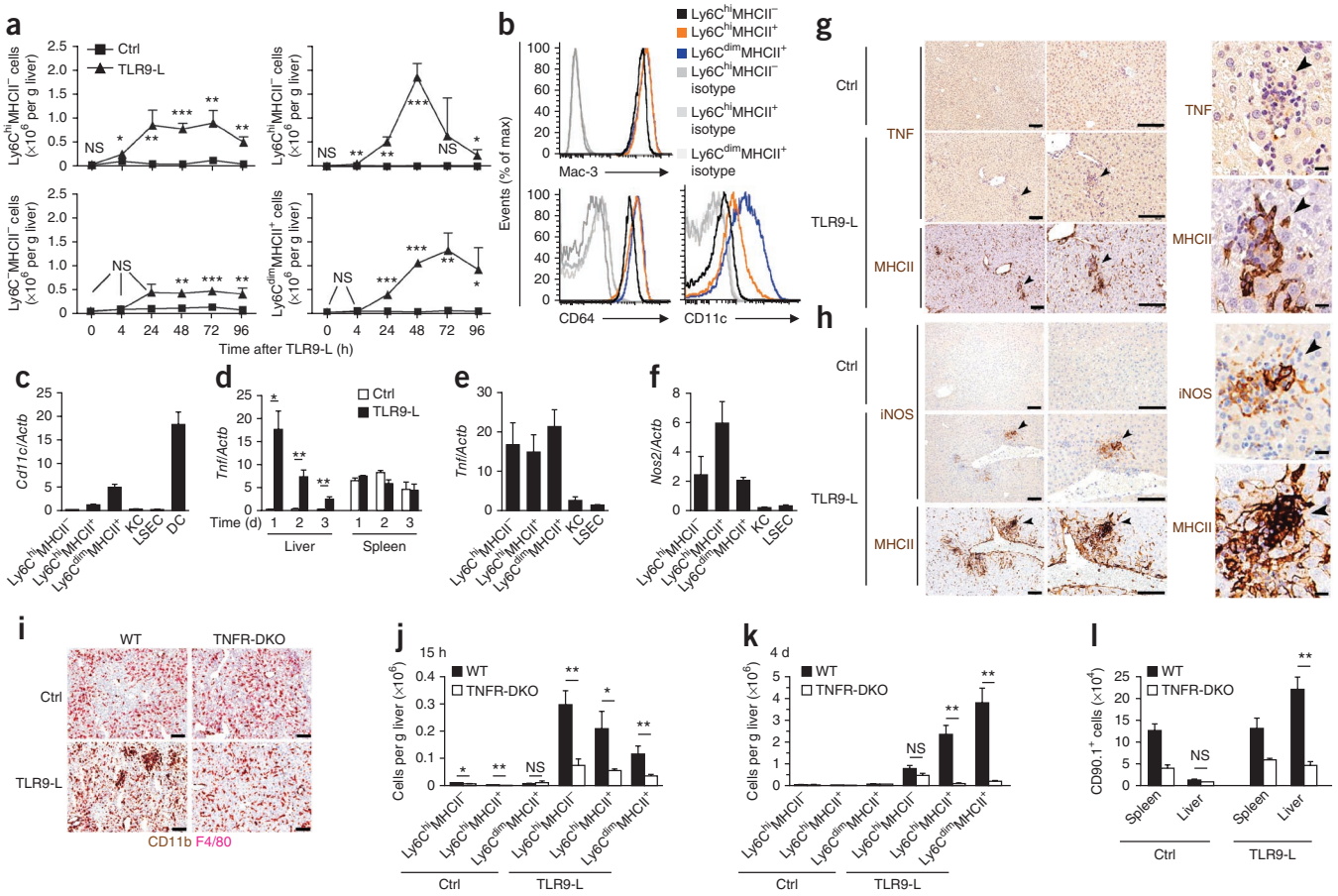

Figure 4 Phenotype of myeloid cells in iMATEs. (**a**) Kinetics of changes in the abundance of subpopulations of NKp46$^-$Ly6G$^-$F4/80$^+$CD11b$^+$ cells in livers from mice ($n = 3$ per group per time point) treated with TLR9 ligand or non–TLR9-binding control oligonucleotide. (**b**) Expression of CD64, CD11c and intracellular Mac-3 by subpopulations of NKp46$^-$Ly6G$^-$F4/80$^+$CD11b$^+$ cells, assessed by flow cytometry. Isotype, immunoglobulin isotype–matched control antibody. (**c**) Quantitative real-time PCR analysis of *Cd11c* in hepatic cell populations (left five bars) or splenic DCs (far right) obtained on day 3 after injection of TLR9 ligand and sorted by flow cytometry; results are presented relative to those of *Actb* (encoding β-actin). KC, Kupffer cell; LSEC, liver sinusoidal endothelial cell. (**d**) Time course of *Tnf* expression in livers and spleens from mice ($n = 3$ per group) treated with TLR9 ligand or control (as in **a**); presented as in **c**. (**e**,**f**) Quantitative real-time PCR analysis of *Tnf* (**e**) and *Nos2* (encoding iNOS; **f**) in cells as in **c** (presented as in **c**). (**g**,**h**) Immunohistochemical analysis of TNF and MHC class II (**g**) or iNOS and MHC class II (**h**) in consecutive liver sections on day 3 after treatment with TLR9 ligand or control (as in **a**). Arrowheads indicate the same position in consecutive sections. (**i**) Immunohistochemical analysis of CD11b and F4/80 in liver tissues from wild-type or TNFR1-TNFR2–deficient (TNFR-DKO) mice on day 3 after treatment with TLR9 ligand or control (as in **a**). (**j**,**k**) Total Ly6C^{hi}MHCII$^-$, Ly6C^{hi}MHCII$^+$ and Ly6C^{dim}MHCII$^+$ cells among NKp46$^-$Ly6G$^-$F4/80$^+$CD11b$^+$ cells in the liver at 15 h (**j**) or day 4 (**k**) after treatment of wild-type or TNFR1-TNFR2–deficient mice ($n = 3$ per group) with TLR9 ligand or control (as in **a**). (**l**) Quantification of CD90.1$^+$ CTLs from wild-type mice at day 3 after transfer into wild-type or TNFR1-TNFR2–deficient mice treated with TLR9 ligand or control (as in **a**). Scale bars, 100 μm (**g**,**h**, left two columns, and **i**) or 10 μm (**g**,**h**, right column). $^*P < 0.05$, $^{**}P < 0.01$ and $^{***}P < 0.001$ (unpaired Student's *t*-test). Data are representative of two independent experiments (error bars (**a**,**c**–**f**,**j**–**l**), s.d.).

and this was not further improved by the transfer of additional CTLs (**Fig. 3f**). Thus, iMATE formation was triggered by inflammatory signals and did not require the presence of lymphocytes.

Phenotype of myeloid cells in iMATEs

The results reported above raised the issue of how CD11b$^+$ cells (neutrophils, NK cells, Kupffer cells, monocytes and macrophages or DCs) facilitate the hepatic proliferation of CTLs. As neither neutrophils nor NK cells were present in iMATEs, we analyzed hepatic NKp46$^-$Ly6G$^-$CD11b$^+$ cells. Profiling by flow cytometry (gating strategy, **Supplementary Fig. 5a**) showed more F4/80^{hi} Kupffer cells or F4/80$^-$CD11b$^+$ cells in mice treated with TLR9 ligand than in mice treated with the control (non-TLR9) ligand, whereas the number of CD11b$^+$ non-Kupffer cells that were F4/80$^+$ paralleled the hepatic proliferation of CTLs (**Fig. 1f** and **Supplementary Fig. 5b**,**c**); this prompted us to investigate the role of inflammatory monocytes and DCs in the hepatic proliferation of CTLs[22]. Those NKp46$^-$Ly6G$^-$CD11b$^+$F4/80$^+$ cells were distinct from F4/80^{hi} Kupffer cells, as assessed by Ly6C expression (**Supplementary Fig. 5d**). We categorized them into two main populations on the basis of their Ly6C expression in combination with expression of MHC class II or the common DC marker CD11c (**Supplementary Fig. 5e**); this defined Ly6C^{hi} inflammatory monocytes that were MHCII$^-$ with low CD11c expression, and MHCII$^+$ cells with lower Ly6C expression and intermediate CD11c expression. After treatment with TLR9 ligand, there was a rapid increase in Ly6C^{hi}MHCII$^-$ inflammatory monocytes, a transient increase in Ly6C^{hi}MHCII$^+$CD11b$^+$ cells and a persistent increase in Ly6C^{dim}MHCII$^+$CD11b$^+$ cells in the liver (**Fig. 4a**). All those CD11b$^+$ cells expressed the macrophage-specific markers Mac-3 and CD64 (**Fig. 4b**), consistent with their monocytic origin.

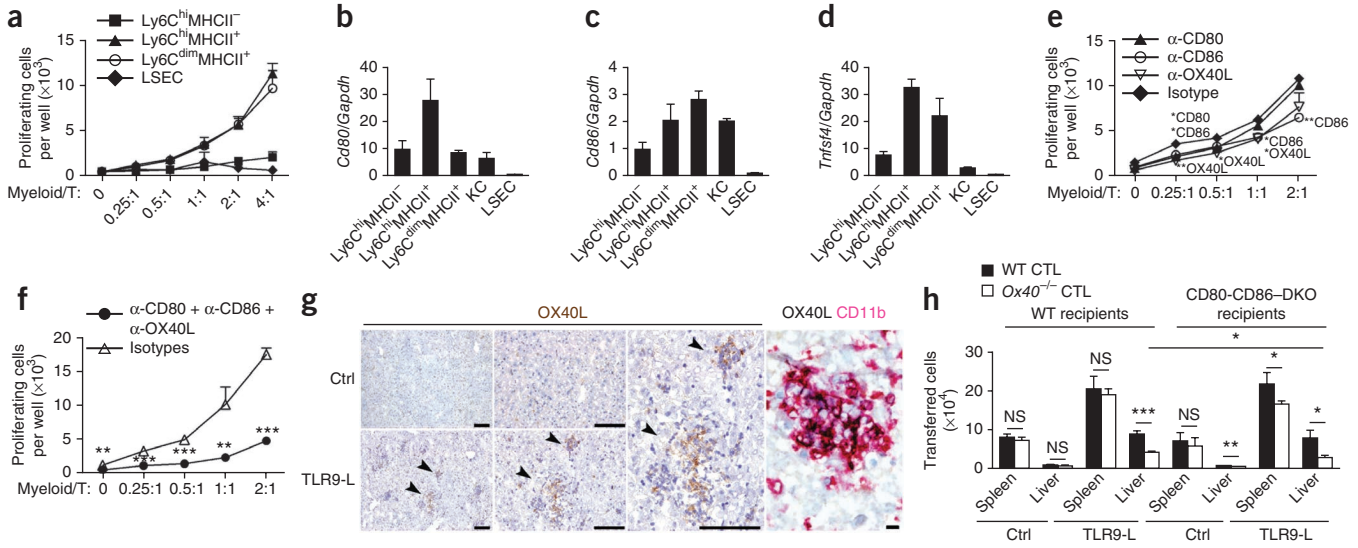

Figure 5 Hepatic myeloid cells support the expansion of the CTL population by providing costimulatory signals. (**a**) Proliferation of CTLs activated *in vitro* with anti-CD3, anti-CD28 and IL-12 (day 3) and cultured at various ratios (horizontal axis) with flow cytometry–sorted hepatic CD11b$^+$ myeloid cell populations or liver sinusoidal endothelial cells isolated at day 3 after treatment with TLR9 ligand, assessed by incorporation of the thymidine analog EdU after 40 h of coculture. (**b**–**d**) Expression of *Cd80* mRNA (**b**), *Cd86* mRNA (**c**) and *Tnfsf4* mRNA (encoding OX40L; **d**) in hepatic cell populations isolated at day 3 after treatment with TLR9 ligand and sorted by flow cytometry; results are presented relative to those of the housekeeping gene *Gapdh*. (**e**,**f**) Proliferation of CTLs cultured at various ratios (horizontal axis) with flow cytometry–sorted CD11b$^+$F4/80$^+$Ly6C^{dim}MHCII$^+$ cells and treated with function-blocking antibody to CD80, CD86 or OX40L, alone (**e**) or in combination (**f**), or with isotype-matched control antibody. (**g**) Immunohistochemical analysis of OX40L and CD11b in liver tissue on day 3 after treatment with TLR9 ligand or non–TLR9-binding control oligonucleotide. Arrowheads indicate iMATEs. Scale bars, 100 µm (left images) or 10 µm (far right). (**h**) Total transferred CTLs in wild-type or *Cd80*$^{-/-}$ *Cd86*$^{-/-}$ (CD80-CD86–DKO) recipients ($n = 3$ per group) of CFSE-labeled wild-type or *Ox40*$^{-/-}$ CTLs (key), assessed on day 3 after treatment with TLR9 ligand or non–TLR9-binding control oligonucleotide. $^*P < 0.05$, $^{**}P < 0.01$ and $^{***}P < 0.001$ (unpaired Student's *t*-test). Data are representative of two independent experiments (triplicate assays in **a**–**f**; error bars (**a**–**f**,**h**), s.d.).

Ly6C^{dim}MHCII$^+$ cells also had CD11c expression, albeit less than that of conventional DCs (**Fig. 4b**,**c**). Notably, when we depleted CD11c.DOG mice (which have transgenic expression of DTR under control of the promoter of the gene encoding CD11c) of DCs by injection of diphtheria toxin, we found that this did not eliminate those CD11b$^+$CD11c^{int} cells in the liver and did not affect the hepatic proliferation of CTLs or iMATE formation (**Supplementary Fig. 5f**–**h**). Thus, monocytes and monocyte-derived inflammatory DCs, but not conventional DCs, were responsible for the hepatic proliferation of CTLs.

After injection of TLR9 ligand into wild-type mice, there was substantial expression of tumor-necrosis factor (TNF) in the liver but not in the spleen (**Fig. 4d**). Analysis of gene expression showed that the CD11b$^+$ cells expressed TNF and inducible nitric oxide synthetase (iNOS; **Fig. 4e**,**f**). We found TNF- and iNOS-expressing cells in iMATEs (**Fig. 4g**,**h**), which indicated a critical role for signaling via the TNF receptor. Indeed, no iMATEs formed in mice doubly deficient in the TNF receptors TNFR1 and TNFR2 (TNFR1-TNFR2–deficient) after treatment with TLR9 ligand (**Fig. 4i**); similarly, the recruitment of inflammatory monocytes and proliferation of CD11b$^+$MHCII$^+$ cells were impaired in these mice (**Fig. 4j**,**k**). Predictably, there was less hepatic CTL proliferation in TNFR1-TNFR2–deficient mice than in wild-type mice after challenge with TLR9 (**Fig. 4l**). Signaling via the TNF receptor in T cells was not involved, as TNFR1-TNFR2–deficient CTLs proliferated in TNF receptor–sufficient mice after treatment with TLR9 ligand (data not shown). These data demonstrated a critical role for inflammatory monocytes or inflammatory DCs in the formation of iMATEs and local hepatic proliferation of CTLs after challenge with TLR9 ligand.

Functional characterization of myeloid cells in iMATEs

To investigate the relevance of CD11b$^+$MHCII$^+$ cells to CTL proliferation, we analyzed Ly6C^{hi}MHCII$^-$ inflammatory monocytes and MHCII$^+$CD11b$^+$ cells sorted from the liver of wild-type mice after treatment with TLR9 ligand. Only MHCII$^+$ inflammatory DCs induced CTL proliferation independently of antigen presentation; inflammatory monocytes or liver sinusoidal endothelial cells did not (**Fig. 5a**). Costimulatory signals are important for the proliferation and survival of T cells[23,24]. Only CD11b$^+$MHCII$^+$ cells had higher expression of mRNA encoding the costimulatory molecules CD80, CD86 and OX40L than did MHCII$^-$ cells, Kupffer cells or liver sinusoidal endothelial cells (**Fig. 5b**–**d**). Individual blockade of CD86 or OX40L had some effect on but did not abrogate CTL proliferation (**Fig. 5e**), whereas simultaneous blockade of CD80, CD86 and OX40L led to almost complete inhibition of CTL proliferation (**Fig. 5f**).

CTLs activated i*n vitro* with anti-CD3, anti-CD28 and IL-12 expressed CD28, and approximately 50% of these CTLs expressed OX40 (**Supplementary Fig. 6a**), which suggested that costimulation might be relevant for the hepatic expansion of the CTL population *in vivo*. In the liver, OX40L expression was restricted to CD11b$^+$ cells in iMATEs but not in parenchymal liver tissue (**Fig. 5g**). We transferred CFSE-labeled CD90.1$^+$ wild-type CTLs or CD90.1$^-$ CTLs deficient in OX40 (*Tnfrsf4*$^{-/-}$; called '*Ox40*$^{-/-}$' here) at ratio of 1:1 into recipient mice (**Supplementary Fig. 6b**) and monitored their fate in liver and spleen. We found no difference between wild-type and *Ox40*$^{-/-}$ CTLs in the spleens of wild-type mice in terms of CFSE profile or absolute number (**Supplementary Fig. 6c** and **Fig. 5h**), which suggested that the transferred *Ox40*$^{-/-}$ CTLs did not have an intrinsic defect in survival or proliferation *in vivo*. Mice treated with TLR9

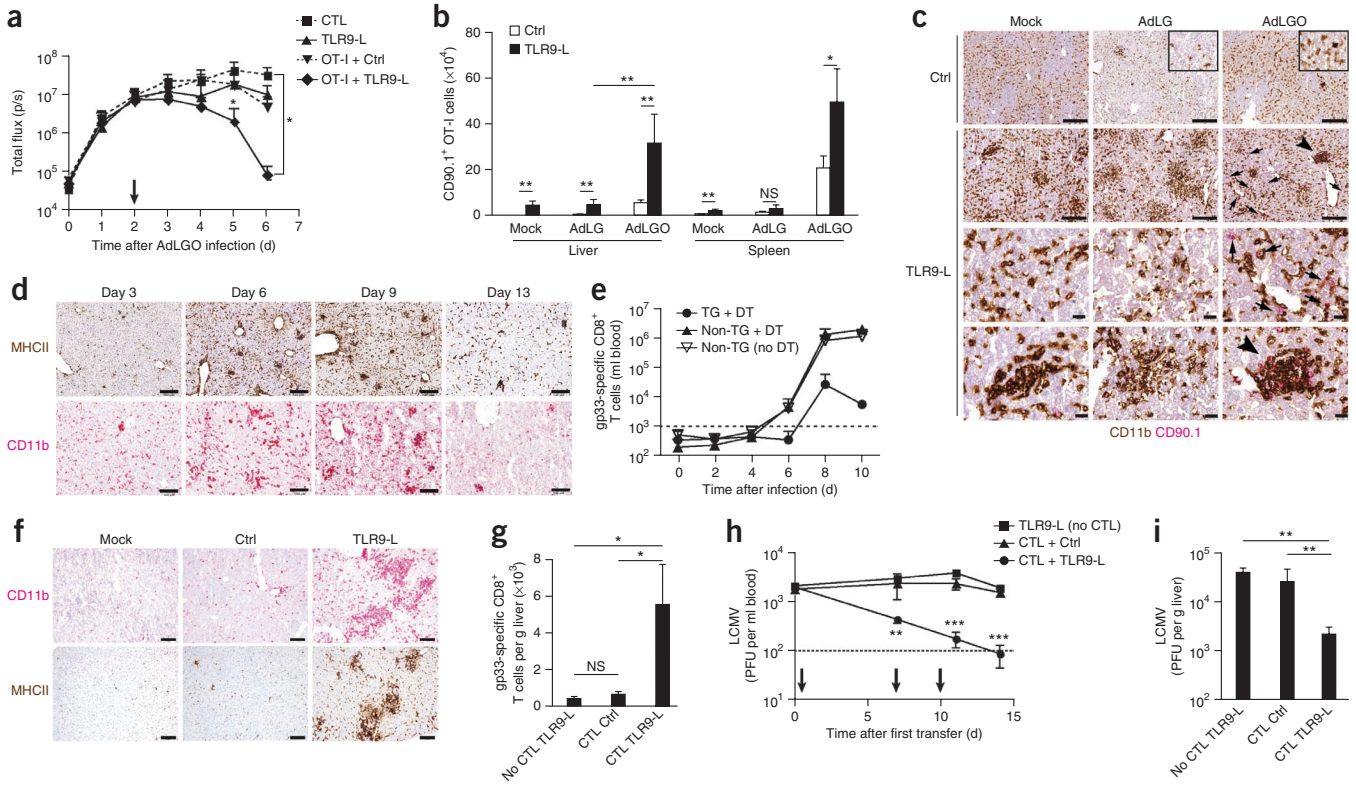

Figure 6 Improved clearance of viral infection from the liver by injection of TLR9 ligand. (**a**) Hepatic *in vivo* bioluminescence in mice infected with AdLGO (1×10^6 infectious units) and, 2 d later, treated (downward arrow) with TLR9 ligand or non–TLR9-binding control oligonucleotide, alone or with 1×10^4 *in vitro*–activated CD90.1$^+$ OT-I CTLs (OT-I +), assessed as reported before[25]. (**b**) Quantification of transferred CTLs in mice infected with AdLG or AdLGO (1×10^6 infectious units) and, 2 d later, given transfer of *in vitro*–activated CD90.1$^+$ OT-I CTLs (1×10^5) plus TLR9 ligand or non–TLR9-binding control oligonucleotide, assessed on day 3 after cell transfer. (**c**) Immunohistochemical analysis of CD11b and CD90.1 in liver tissue from the mice in **b**. Arrowheads indicate the same iMATE in consecutive sections; arrows indicate single CD90.1$^+$ OT-I cells in liver parenchymal tissue. Inset (top row), 5× enlargement of main image, showing iMATEs during viral infection. (**d**) Immunohistochemical analysis of MHC class II and CD11b in the liver after acute infection with LCMV (2×10^4 plaque-forming units). (**e**) Quantification of gp33-specific CTLs in blood from CCR2-CFP-DTR mice (TG) and their nontransgenic littermates (Non-TG) after infection with LCMV (2×10^4 plaque-forming units) and treatment with diphtheria toxin (+ DT); Non-TG (no DT), nontransgenic littermates not treated with diphtheria toxin. (**f**) Immunohistochemical analysis of MHC class II and CD11b in the liver during chronic infection with LCMV at day 3 after mock treatment or treatment with TLR9 ligand or non–TLR9-binding control oligonucleotide. (**g**) Quantification of hepatic gp33-specific CTLs in mice with chronic LCMV infection that received adoptive transfer of 1×10^7 *in vivo*–activated CTLs (isolated on day 7 after acute infection of donor mice with LCMV) three times (days 0, 7 and 10), together with TLR9 ligand or non–TLR9-binding control oligonucleotide, assessed at day 14 after first CTL transfer. Far left, mice given TLR9 ligand alone without CTLs. (**h**,**i**) Kinetics of LCMV titers in blood (**h**) and LCMV titers in the liver at day 14 after first adoptive transfer (**i**) in the mice in **g**. Downward arrows (**h**), transfer of gp33-specific CTLS on days 0, 7 and 10. Scale bars, 100 μm (**c**, top two rows, and **d**,**f**) or 10 μm (**c**, bottom two rows). $^*P < 0.05$, $^{**}P < 0.01$ and $^{***}P < 0.001$ (unpaired Student's *t*-test). Data are representative of two independent experiments with three to five mice per group (error bars (**a**,**b**,**e**,**g**–**i**), s.d.).

ligand had over 50% fewer *Ox40*$^{-/-}$ CTLs than wild-type CTLs in the liver (**Fig. 5h**), although the CFSE-dilution profile of *Ox40*$^{-/-}$ CTLs was identical to that of the wild-type CTLs transferred together with them (**Supplementary Fig. 6c**). We found fewer *Ox40*$^{-/-}$ CTLs after transfer into *Cd80*$^{-/-}$*Cd86*$^{-/-}$ mice than after transfer into wild-type mice (**Fig. 5h**), but *Ox40*$^{-/-}$ CTLs again had CFSE-dilution profiles identical to those of wild-type CTLs (**Supplementary Fig. 6d**). Thus, OX40-dependent signaling may enhance the survival rather than the proliferation of CTLs. These results identified a crucial role for OX40 in the expansion of the CTL population in the liver and elucidated the molecular mechanism that drove the antigen-independent expansion of the CTL population caused by inflammatory DCs in iMATEs.

The iMATEs facilitate CTL-mediated viral clearance

The efficient expansion of the CTL population in the liver raised the question of whether iMATEs improved CTL immunity to viral infection in the liver. We activated ovalbumin (OVA)-specific (OT-I) CD90.1$^+$ CTLs with anti-CD3, anti-CD28 and IL-12 *in vitro* and transferred the cells, along with TLR9 ligand, into wild-type mice that we then infected with a recombinant adenovirus expressing luciferase, GFP and OVA as a fusion protein (AdLGO)[25]. The decrease in bioluminescence *in vivo* allows more sensitive quantification of antiviral CTL activity against infected hepatocytes than does measurement of serum ALT[25]. Neither transfer of OT-I CTLs nor treatment with TLR9 ligand alone resulted in lower *in vivo* bioluminescence in AdLGO-infected mice (**Fig. 6a**). Transfer of OT-I CTLs together with TLR9 ligand, however, controlled the hepatic expression of viral luciferase more rapidly than did either treatment alone (**Fig. 6a**).

Those results led us to investigate whether iMATEs enhanced antigen-specific CTL responses. We infected mice with recombinant adenovirus expressing luciferase and GFP alone (AdLG) or with AdLGO and then transferred activated OT-I CTLs into the infected mice. We found more hepatic OT-I CTLs in AdLG-infected mice after

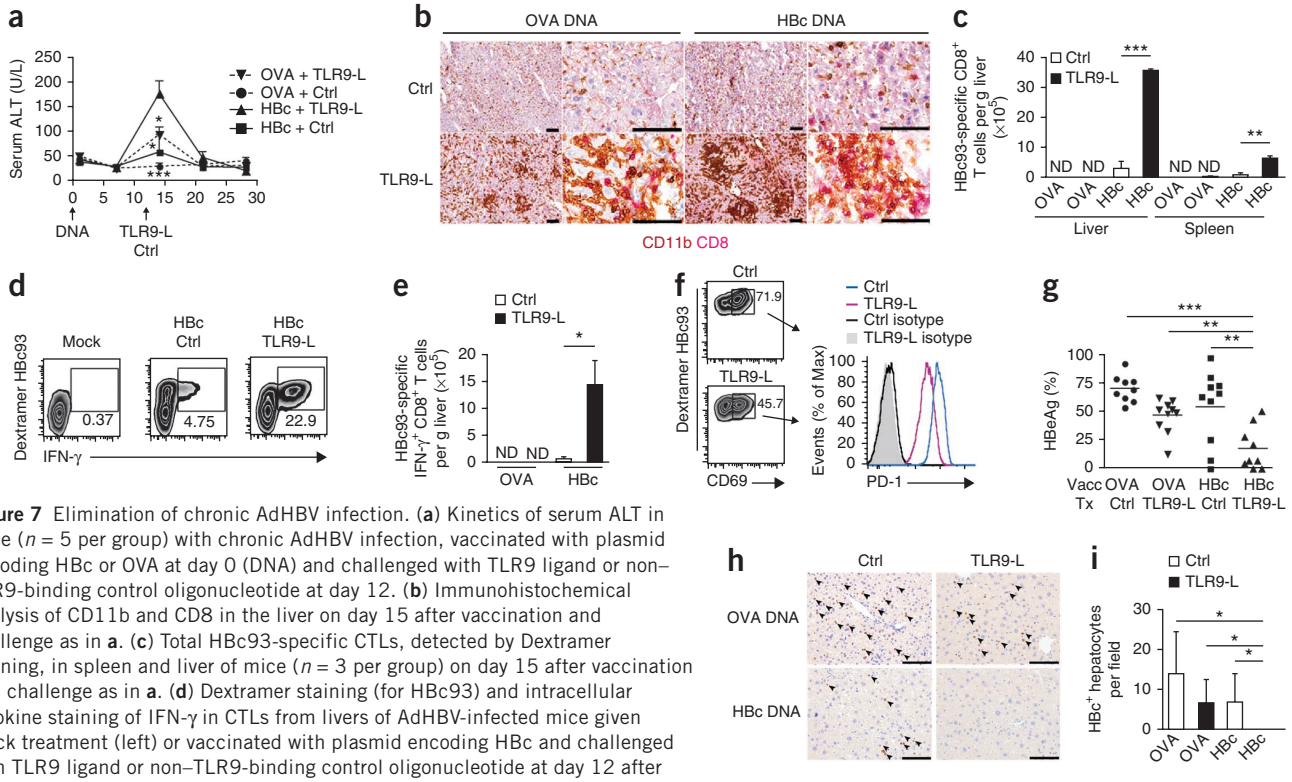

Figure 7 Elimination of chronic AdHBV infection. (**a**) Kinetics of serum ALT in mice ($n = 5$ per group) with chronic AdHBV infection, vaccinated with plasmid encoding HBc or OVA at day 0 (DNA) and challenged with TLR9 ligand or non–TLR9-binding control oligonucleotide at day 12. (**b**) Immunohistochemical analysis of CD11b and CD8 in the liver on day 15 after vaccination and challenge as in **a**. (**c**) Total HBc93-specific CTLs, detected by Dextramer staining, in spleen and liver of mice ($n = 3$ per group) on day 15 after vaccination and challenge as in **a**. (**d**) Dextramer staining (for HBc93) and intracellular cytokine staining of IFN-γ in CTLs from livers of AdHBV-infected mice given mock treatment (left) or vaccinated with plasmid encoding HBc and challenged with TLR9 ligand or non–TLR9-binding control oligonucleotide at day 12 after vaccination; cells isolated 15 d after vaccination were restimulated *ex vivo* with HBc93. Numbers below outlined areas indicate percent IFN-γ-producing HBc93-specific CTLs among total CD8$^+$ T cells. (**e**) Total IFN-γ-producing HBc93-specific CTLs obtained from mice ($n = 3$ per group) on day 15 after vaccination and challenge as in **a** and restimulated *ex vivo* with HBc93. (**f**) Flow cytometry of CTLs from mice vaccinated and challenged as in **d**, assessed immediately after isolation at day 15 after vaccination; numbers adjacent to outlined areas (left) indicate percent CD69$^+$ HBc93-specific CTLs. Right, PD-1 expression on the CD69$^+$ HBc93-specific CTLs at left. (**g**) Serum concentration of HBV e antigen (HBeAg) at day 28 after vaccination (Vacc) and challenge (Tx) of mice as in **a**, presented relative to those at day 1. (**h**,**i**) Immunohistochemical detection (**h**) and quantification (**i**) of HBc$^+$ hepatocytes at day 42 after vaccination and challenge as in **a**. Arrowheads (**h**) indicate HBc$^+$ hepatocytes. Scale bars, 100 μm. $^*P < 0.05$, $^{**}P < 0.01$ and $^{***}P < 0.001$ (unpaired Student's *t*-test). Data are representative of three (**a**,**c**,**d**–**g**) or two (**b**,**h**,**i**) experiments (error bars (**a**,**c**,**e**,**i**), s.d.).

treatment with TLR9 ligand (**Fig. 6b**). However, in AdLGO-infected mice given injection of TLR9 ligand, we found sevenfold more OT-I CTLs; also, without TLR9 ligand, AdLGO-infected mice had more OT-I CTLs than did their AdLG-infected counterparts (**Fig. 6b**). Notably, after infection with AdLG in absence of TLR9 ligand, we observed iMATEs that did not contain OT-I CTLs, whereas iMATEs in AdLGO-infected mice contained some OT-I CTLs (**Fig. 6c**). These data suggested that viral infection of the liver caused iMATE formation and that iMATEs also amplified antigen-specific CTL responses locally in the liver. After injection of TLR9 ligand, iMATE generation was improved, and we observed more OT-I CTLs in AdLGO-infected mice than in AdLG-infected or mock-treated mice (**Fig. 6c**); this supported the assumption of more rapid control of viral infection. Notably, we found single OT-I CTLs in the vicinity of iMATEs (**Fig. 6c**), which indicated that the OT-I CTLs executed effector functions against virus-infected hepatocytes after leaving the iMATEs.

To confirm the physiological relevance of iMATEs during viral infection, we investigated iMATE formation during infection with the replication-competent virus lymphocytic choriomeningitis virus (LCMV). During acute infection with LCMV, we observed the formation of iMATEs by CD11b$^+$MHCII$^+$ cells, with a peak at day 9 after infection (**Fig. 6d**), which coincided with the peak expansion of the CTL population. CD8$^+$ T cells were abundant in iMATEs during acute infection with LCMV (**Supplementary Fig. 7a**), which suggested that iMATEs contributed to the CTL defense against LCMV infection. Prevention of iMATE formation in CCR2-CFP-DTR mice led to less generation of H-2D^b-restricted CTLs specific for LCMV glycoprotein (amino acids 33–41 (gp33); **Fig. 6e**) and failure to control LCMV replication (**Supplementary Fig. 7b**). This may indicate a role for iMATEs in LCMV-specific CTL immunity, although we cannot exclude the possibility that systemic depletion of CCR2$^+$ cells additionally influences immunity to LCMV. Those results prompted us to investigate whether iMATEs were absent from mice with chronic LCMV infection. Indeed, we observed no iMATEs in the livers of mice with chronic LCMV infection (**Fig. 6f**), but iMATEs were induced by treatment with TLR9 ligand (**Fig. 6f**), which suggested that iMATEs may be used to overcome T cell exhaustion during chronic viral infection. To test that hypothesis, we adoptively transferred *in vivo*–primed LCMV-specific splenic CTLs (isolated from mice with acute LCMV infection), together with TLR9 ligand or control ligand, on days 0, 7 and 10, into mice with chronic LCMV infection. Transfer of LCMV-specific CTLs or TLR9 ligand alone did not result in a greater abundance of gp33-specific CTLs; however, transfer of LCMV-specific CTLs together with TLR9 ligand did result in a greater abundance of gp33-specific CTLs in the liver at day 14 after the first transfer (**Fig. 6g**). More notably, LCMV titers in serum and liver dropped to background titers after transfer of LCMV-specific CTLs and TLR9 ligand (**Fig. 6h**,**i**). These results indicated that iMATEs served a role in the control of acute viral infection by facilitating TLR9 ligand–induced expansion of the CTL population and suggested that

reconstitution of iMATEs that were absent during chronic infection improved CTL-mediated control of viral infection.

Successful immunotherapy of chronic liver viral infection

To explore whether the hepatic expansion of the CTL population improved defense against chronic infection with a pathogen relevant to humans, we used a model of chronic infection of immunocompetent mice by transfer of the HBV genome through the use of an adenovirus vector (AdHBV)[26]. In this model, therapeutic vaccination with DNA leads to a slightly greater abundance of circulating HBV-specific CTLs but does not control chronic infection with AdHBV[26]. We treated mice with chronic AdHBV infection by vaccination with plasmid encoding HBV core antigen (HBc) or OVA, followed by injection of TLR9 ligand 12 d later. That led to a transient increase in serum ALT, indicative of liver damage, that was greatest in mice vaccinated with plasmid encoding HBc that also received TLR9 ligand (**Fig. 7a**). We did not detect iMATEs in mice with chronic AdHBV infection regardless of whether they were vaccinated with plasmid encoding HBc or OVA (**Fig. 7b**). However, injection of TLR9 ligand induced iMATE formation (**Fig. 7b**), which raised the question of whether this may have facilitated expansion of the HBV-specific CTL population and subsequent clearance of chronic AdHBV infection.

Injection of TLR9 ligand at day 12 after vaccination with plasmid encoding HBc resulted in expansion of the H-2K^b-restricted CTL population specific for HBc amino acids 93–100 (HBc93) in the livers of mice with chronic AdHBV infection (**Fig. 7c**). Those HBc93-specific CTLs were functional and expressed IFN-γ after antigen-specific restimulation, whereas in the absence of TLR9 ligand, we detected few IFN-γ-expressing HBc93-specific CTLs (**Fig. 7d,e**). Furthermore, we observed lower expression of the costimulatory molecule PD-1 on CD69$^+$ HBc93-specific CTLs in mice treated with TLR9 ligand than on their counterparts in mice treated with control ligand (**Fig. 7f**), which suggested that DNA vaccination in combination with iMATE induction overcame immunoregulatory mechanisms. Vaccination with plasmid encoding HBc plus injection of TLR9 ligand resulted in lower serum concentrations of HBV antigens after 28 d and eventual elimination of HBV-infected hepatocytes at day 42 (**Fig. 7g–i**). These findings indicated that hepatic expansion of the HBc-specific population of CTLs eradicated HBV-infected hepatocytes during chronic infection and led to viral clearance.

DISCUSSION

Here we found that activation of CTLs by simultaneous stimulation via the T cell antigen receptor, CD28 and IL-12 *in vitro*, together with the systemic application of TLR9 ligand, led to a 50-fold population expansion of CTLs locally in the liver. Myeloid-cell aggregates (iMATEs) that formed in the liver after TLR9 signaling facilitated CTL proliferation in the liver. This massive expansion of the CTL population in the liver contributed to antiviral immunity and overcame chronic viral infection in mice.

The iMATEs are distinct from the lymphoid structures that arise during chronic inflammation. Tertiary lymphoid tissues that form in the peripheral organs after chronic inflammatory signaling are functionally and structurally similar to secondary lymphatic tissue; that is, they have germinal centers and T cell zones and antigen sampling for DC-mediated population expansion of CTLs[12]. Granulomas generated during chronic inflammation or infection with intracellular bacteria are characterized by dense accumulation of macrophages surrounded by a ring of epithelial cells[27]. Tertiary lymphatic tissues and granulomas are considered long-lived yet dynamic structures that are constantly shaped by environmental factors[12,27]. In contrast, iMATEs arose rapidly after a single injection of TLR9 ligand, were composed of monocyte-derived CD11b$^+$ cells that were not demarcated from surrounding liver tissue, and dissolved within 6–8 d. Moreover, the mechanisms that drove iMATE formation were distinct from those that operate during lymphatic tissue development. Whereas LTβR signaling is crucial for the formation of secondary lymphatic tissue, IL-17 generates tertiary lymphatic tissue in a lymphotoxin-independent way in the lungs or the central nervous system[13,14,21,28]. We found that iMATE formation did not depend on LTβR signaling but instead required signaling via TNF receptors. Monocyte-derived inflammatory DCs that formed iMATEs independently of crosstalk with lymphocytes produced TNF, which suggested that TNF acted in a local feed-forward loop to drive the efficient generation of iMATEs.

The induction of iMATEs via TLR9 signaling overcame local hepatic regulatory cues by creating a separate anatomical cocoon-like structure in the liver, where CTLs were probably sheltered from local inhibitory signals. Intravital imaging showed that T cells remained stationary or migrated within the boundaries of iMATEs. As there was no fibrous capsule or ring of fibrocytes around iMATEs, locally expressed chemotactic signals presumably kept the CTLs within the iMATEs, but the factors that determine the retention of CTLs in iMATEs or their exit from iMATEs remain to be defined. Three-dimensional reconstruction showed that CTLs were embedded within iMATEs in a matrix of monocyte-derived inflammatory DCs that probably functioned as 'nursing cells' to foster expansion of the CTL population by providing costimulatory signals through the OX40L-OX40 axis. The expansion of the CTL population in iMATEs occurred in the absence of MHC class I–restricted antigen recognition, although we cannot exclude the possibility of a role for MHC class I–induced tonic T cell antigen receptor signaling in these circumstances that is important for keeping T cells in a state in which they can respond to subsequent antigen-specific stimulation[29]. However, in the presence of their cognate antigen in infected hepatocytes, the population expansion of CTLs in iMATEs was enhanced, which indicated that inflammatory DCs may have cross-presented antigens on MHC class I to CTLs.

The generation of iMATEs during acute viral infection suggested that the iMATEs did not represent an artifact present after challenge with TLR9 ligand. The iMATEs formed during acute viral infection served as expansion hubs for antigen-specific CTLs that later contributed to the clearance of viral infection. Notably, we detected no iMATEs in the liver during chronic viral infection, which indicated that the generation of iMATEs was correlated with efficient CTL-mediated control of viral infection and opened the possibility for the use of induction of iMATEs for therapeutic vaccination.

The expansion of the CTL population in iMATEs induced by a single application of TLR9 ligand did not trigger autoimmunity. Only continuous application of TLR9 ligand over weeks, together with large numbers of autoreactive CTLs and hepatocellular expression of the auto-antigen, caused autoimmunity[30]. Moreover, chronic TLR signaling and inflammation enhances autoimmunity by enhanced MHC class I–restricted antigen presentation[31], and prolonged TLR3 signaling overcomes the tolerogenic hepatic microenvironment[32]. Thus, expansion of the CTL population in iMATEs may improve the efficiency of therapeutic vaccines against chronic infection without causing autoimmunity.

The induction of iMATEs during chronic viral infection through application of TLR9 ligand resulted in substantial population expansion of virus-specific CTLs that were initially generated by genetic vaccination. Such expansion of the CTL population controlled chronic viral infection in hepatocytes. The combination of conventional

vaccination plus TLR9 ligand–induced expansion of the CTL population in the liver augmented the efficacy of therapeutic vaccination. The hepatic expansion of the CTL population in iMATEs occurred independently of secondary lymphatic tissues and was therefore mechanistically distinct from the T cell population expansion induced by prime-boost vaccination schemes. Whereas conventional vaccination strategies aim to increase the immunogenicity of antigen-presenting cells and prolong antigen presentation to naive or central memory T cells in lymphatic tissues, iMATEs caused expansion of the population of IL-12-activated CTLs but not naive CTLs and, only to a lesser degree, memory T cells through costimulatory signals and cross-presentation in the liver.

Together our results have demonstrated the existence of a second phase of expansion of the CTL population in the liver in a distinct anatomical compartment formed by monocyte-derived inflammatory DCs. The population expansion of CTLs in iMATEs complemented the priming and proliferation of T cells in secondary lymphatic tissue that resulted in the massive population expansion of antigen-specific CTLs in the periphery. This so-far-unrecognized phase of a sudden increase in the expansion of the CTL population may be used to improve therapeutic vaccination against chronic viral infection of the liver.

METHODS

Methods and any associated references are available in the online version of the paper.

Note: Supplementary information is available in the online version of the paper.

ACKNOWLEDGMENTS

We thank D. Kull, R. Hillermann, O. Seelbach, N. Simonavicius, M. Wolf and the flow cytometry core facility of the Institutes of Molecular Medicine and Experimental Immunology, University of Bonn for technical support. Supported by the Helmholtz Association (M.H.), the Hofschneider Foundation (M.H.), the European Research Council (LiverCancerMech; M.H.), the Helmholtz Alliance Preclinical Comprehensive Cancer Center (M.H.), Sonderforschungsbereich (36 to M.H., and 704, TR57 and 670 to P.K.), the Helmholtz Alliance on Immunotherapy of Cancer (P.K.), the Bundesministerium für Bildung und Forschung projects Virtual Liver and PeTra (P.K.) and the Excellence Cluster ImmunoSensation (P.K.).

AUTHOR CONTRIBUTIONS

L.-R.H., D.W., F.R., R.-L.C., Z.A. and F.A.S. did the experiments; C.N.J. and P.K. designed and did intravital microscopy experiments; M.O. and H.-P.D. did electron microscopy studies; N.v.R., E.S., N.G. and M.C. contributed reagents and contributed to experimental design; C.K., U.P., M.H. and P.A.K. designed experiments; and L.-R.H., M.H. and P.A.K. wrote the manuscript.

COMPETING FINANCIAL INTERESTS

The authors declare no competing financial interests.

1. Crispe, I.N. Hepatic T cells and liver tolerance. *Nat. Rev. Immunol.* **3**, 51–62 (2003).
2. Thomson, A.W. & Knolle, P.A. Antigen-presenting cell function in the tolerogenic liver environment. *Nat. Rev. Immunol.* **10**, 753–766 (2010).
3. Crispe, I.N. The liver as a lymphoid organ. *Annu. Rev. Immunol.* **27**, 147–163 (2009).
4. Protzer, U., Maini, M.K. & Knolle, P.A. Living in the liver: hepatic infections. *Nat. Rev. Immunol.* **12**, 201–213 (2012).
5. Isogawa, M., Furuichi, Y. & Chisari, F.V. Oscillating CD8+ T cell effector functions after antigen recognition in the liver. *Immunity* **23**, 53–63 (2005).
6. Das, A. *et al.* Functional skewing of the global CD8 T cell population in chronic hepatitis B virus infection. *J. Exp. Med.* **205**, 2111–2124 (2008).
7. Lopes, A.R. *et al.* Bim-mediated deletion of antigen-specific CD8 T cells in patients unable to control HBV infection. *J. Clin. Invest.* **118**, 1835–1845 (2008).
8. Chakravarty, S. *et al.* CD8+ T lymphocytes protective against malaria liver stages are primed in skin-draining lymph nodes. *Nat. Med.* **13**, 1035–1041 (2007).
9. Cockburn, I.A. *et al.* Prolonged antigen presentation is required for optimal CD8+ T cell responses against malaria liver stage parasites. *PLoS Pathog.* **6**, e1000877 (2010).
10. Wong, P. & Pamer, E.G. Feedback regulation of pathogen-specific T cell priming. *Immunity* **18**, 499–511 (2003).
11. Kang, S.S. *et al.* Migration of cytotoxic lymphocytes in cell cycle permits local MHC I-dependent control of division at sites of viral infection. *J. Exp. Med.* **208**, 747–759 (2011).
12. Neyt, K., Perros, F., GeurtsvanKessel, C.H., Hammad, H. & Lambrecht, B.N. Tertiary lymphoid organs in infection and autoimmunity. *Trends Immunol.* **33**, 297–305 (2012).
13. Moyron-Quiroz, J.E. *et al.* Role of inducible bronchus associated lymphoid tissue (iBALT) in respiratory immunity. *Nat. Med.* **10**, 927–934 (2004).
14. Rangel-Moreno, J. *et al.* The development of inducible bronchus-associated lymphoid tissue depends on IL-17. *Nat. Immunol.* **12**, 639–646 (2011).
15. Egen, J.G. *et al.* Macrophage and T cell dynamics during the development and disintegration of mycobacterial granulomas. *Immunity* **28**, 271–284 (2008).
16. Egen, J.G. *et al.* Intravital imaging reveals limited antigen presentation and T cell effector function in mycobacterial granulomas. *Immunity* **34**, 807–819 (2011).
17. Curtsinger, J.M., Johnson, C.M. & Mescher, M.F. CD8 T cell clonal expansion and development of effector function require prolonged exposure to antigen, costimulation, and signal 3 cytokine. *J. Immunol.* **171**, 5165–5171 (2003).
18. Lee, S.W., Park, Y., Yoo, J.K., Choi, S.Y. & Sung, Y.C. Inhibition of TCR-induced CD8 T cell death by IL-12: regulation of Fas ligand and cellular FLIP expression and caspase activation by IL-12. *J. Immunol.* **170**, 2456–2460 (2003).
19. Macgregor, J.N. *et al. Ex vivo* culture with interleukin (IL)-12 improves CD8+ T-cell adoptive immunotherapy for murine leukemia independent of IL-18 or IFN-γ but requires perforin. *Cancer Res.* **66**, 4913–4921 (2006).
20. Gommerman, J.L. & Browning, J.L. Lymphotoxin/light, lymphoid microenvironments and autoimmune disease. *Nat. Rev. Immunol.* **3**, 642–655 (2003).
21. Drayton, D.L., Liao, S., Mounzer, R.H. & Ruddle, N.H. Lymphoid organ development: from ontogeny to neogenesis. *Nat. Immunol.* **7**, 344–353 (2006).
22. Serbina, N.V., Salazar-Mather, T.P., Biron, C.A., Kuziel, W.A. & Pamer, E.G. TNF/iNOS-producing dendritic cells mediate innate immune defense against bacterial infection. *Immunity* **19**, 59–70 (2003).
23. Mescher, M.F. *et al.* Signals required for programming effector and memory development by CD8+ T cells. *Immunol. Rev.* **211**, 81–92 (2006).
24. Croft, M. Control of immunity by the TNFR-related molecule OX40 (CD134). *Annu. Rev. Immunol.* **28**, 57–78 (2010).
25. Stabenow, D. *et al.* Bioluminescence imaging allows measuring CD8 T cell function in the liver. *Hepatology* **51**, 1430–1437 (2010).
26. Huang, L.R. *et al.* Transfer of HBV genomes using low doses of adenovirus vectors leads to persistent infection in immune competent mice. *Gastroenterology* **142**, 1447–1450 (2012).
27. Ramakrishnan, L. Revisiting the role of the granuloma in tuberculosis. *Nat. Rev. Immunol.* **12**, 352–366 (2012).
28. Peters, A. *et al.* Th17 cells induce ectopic lymphoid follicles in central nervous system tissue inflammation. *Immunity* **35**, 986–996 (2011).
29. Hochweller, K. *et al.* Dendritic cells control T cell tonic signaling required for responsiveness to foreign antigen. *Proc. Natl. Acad. Sci. USA* **107**, 5931–5936 (2010).
30. Sacher, T. *et al.* CpG-ODN-induced inflammation is sufficient to cause T-cell-mediated autoaggression against hepatocytes. *Eur. J. Immunol.* **32**, 3628–3637 (2002).
31. Lang, K.S. *et al.* Toll-like receptor engagement converts T-cell autoreactivity into overt autoimmune disease. *Nat. Med.* **11**, 138–145 (2005).
32. Lang, K.S. *et al.* Immunoprivileged status of the liver is controlled by Toll-like receptor 3 signaling. *J. Clin. Invest.* **116**, 2456–2463 (2006).

ONLINE METHODS

Mice. C57BL/6j and C57BL/6N mice, actin-EGFP mice, CD11c.DOG mice, CCR2-CFP-DTR mice[33], *Tnfrsf4*$^{-/-}$ (OX40-deficient) mice, *Tlr9*$^{-/-}$ mice, *Tnfrsf1a*$^{-/-}$*Tnfrsf1b*$^{-/-}$ (TNFR1-TNFR2–deficient) mice, mice deficient in recombination-activating gene 2, and *Cd80*$^{-/-}$*Cd86*$^{-/-}$ mice were maintained under specific pathogen–free conditions in the animal facility of the University of Bonn and the La Jolla Institute for Allergy and Immunology. All animal experiments were done in accordance with German legislation governing animal studies and the *Principles of Laboratory Animal Care* guidelines (US National Institutes of Health publication 85-23, 1996 revision).

Reagents. Antibodies used for flow cytometry were as follows (all from eBioscience unless indicated otherwise): peridinin chlorophyll protein–cyanine 5.5 or phycoerythrin-conjugated anti-CD8α (53-6.7), allophycocyanin-conjugated anti-CD45.1 (A20), allophycocyanin-conjugated anti-CD90.1 (HIS51), fluorescein isothiocyanate–conjugated anti-KLRG1 (2F1), phycoerythrin-conjugated anti-CD44 (IM7), allophycocyanin-conjugated anti-CD127 (A7R34), fluorescein isothiocyanate–, peridinin chlorophyll protein–cyanine 5.5– or phycoerythrin-conjugated anti-CD11b (M1/70), phycoerythrin-conjugated anti-NKp46 (29A1.4), Alexa Fluor 647–, Alexa Fluor 488– or Alexa Fluor 405–conjugated anti-mouse CD146 (ME-9F1), allophycocyanin–eFluor 780–conjugated anti–MHC class II (I-A and I-E; M5/114.15.2), phycoerythrin-conjugated anti-I-A^{b} (AF6-120.1), allophycocyanin-conjugated anti-Ly6C (HK1.4), allophycocyanin–eFluor 780– or phycoerythrin-indodicarbocyanine–conjugated anti-F4/80 (BM8), allophycocyanin- or Alexa Fluor 488–conjugated anti-CD11c (N418), phycoerythrin-conjugated anti-CD107b (Mac-3; M3/84), phycoerythrin-conjugated anti-CD19 (eBio1D3), phycoerythrin-conjugated anti-PD-1 (J43), fluorescein isothiocyanate–conjugated anti-CD69 (H1.2F3), phycoerythrin-conjugated anti-OX40 (OX-86), phycoerythrin-conjugated anti-CD28 (37.51), fluorescein isothiocyanate–conjugated anti-Ly6C (1G7.G10; Miltenyi Biotec), phycoerythrin-conjugated anti-Ly6G (1A8; BioLegend) and allophycocyanin-conjugated anti-CD64 (X54-5/7.1; BioLegend).

TLR9 ligand (CpG oligodeoxynuleotide 1668: 5′-S-TCCATGACGTTC CTGATGCT-3′) and control non-TLR9 ligand (non-CpG oligodeoxynuleotide 1720: 5′-S-TCCATGAGCTTCCTGATGCT-3′) were from TIB MOLBIOL; indodicarbocyanine-labeled TLR9 ligand was from Sigma-Aldrich; and TLR3 ligand (poly(I:C) VacciGrade), TLR4 ligand (MPLA VacciGrade) and TLR7 ligand (Imiquimod VacciGrade) were from InvivoGen.

For cell type–specific depletion, mice were treated 1 d before and 1 d after treatment with TLR9 ligand as follows: for depletion of phagocytic cells, clodronate liposomes; for depletion of Ly6G^{+} neutrophils, anti-Ly6G (100 μg; 1A8; Bio X cell); for depletion of NK cells, anti-NK1.1 (300 μg; PK136; prepared in-house); and intraperitoneal injection of diphtheria toxin (10 ng or 30 ng per gram body weight; Sigma-Aldrich;) into CCR2-CFP-DTR or CD11c.DOG mice). Mice were treated with FTY720 at a dose of 1 mg per kg body weight daily from 1 d before to day 3 after treatment with TLR9 ligand. BrdU (bromodeoxyuridine; 0.8 mg/ml) was provided in the drinking water and incorporation was detected with a BrdU Flow Kit (BD Biosciences).

Generation of activated CD8^{+} T cells (CTLs). Splenic CD8^{+} T cells isolated by immunomagnetic separation (Miltenyi Biotec) were stimulated for 3 d with T-activator Dynabeads labeled with anti-CD3 plus anti-CD28 (Invitrogen) and 5 ng/ml IL-12 (p70 subunit). For *in vivo* tracking of CTLs, cells without congenic markers were labeled with 2 μM CFSE (carboxyfluorescein diacetate succinimidyl esterl; Invitrogen). If not stated otherwise, 2×10^6 activated CTLs were transferred.

Isolation of nonparenchymal liver cells. Livers were perfused via the portal vein with a solution of 0.05% collagenase, then mechanically disrupted. The products of that disruption were digested for 20 min at 37 °C in Gey's balanced-salt solution with 0.04% collagenase, then filtered through a 250-μm cell strainer. Cells were resuspended in 10 ml PBS and separated by centrifugation at 1,350*g* for 30 min at 4 °C in 25% and 50% Percoll gradient. After centrifugation, nonparenchymal cells were collected from the interface and were analyzed or sorted by flow cytometry.

Flow cytometry. Antibody staining was done in presence of Fc receptor blockade (monoclonal antibody 2.4G2 to mouse CD16-CD32 (10 μg/ml); prepared in-house) in flow cytometry buffer. A FACSCanto II or Fortessa (BD Biosciences) and FlowJo sofware (TreeStar) were used for acquisition and data analysis. Hoechst 33258 (10 μg/ml; Sigma-Aldrich) or LIVE/DEAD Fixable Dead Cell Stain Kit (Invitrogen) was used for exclusion of dead cells. For sorting by flow cytometry, nonparenchymal cells were isolated as described above from mice depleted of NK cells and neutrophils, followed by the addition of Hoechst 33258 for exclusion of dead cells, then staining and filtering through a 100-μm mesh, then cells were sorted with a FACSDiva (BD Biosciences). For flow sorting of CD44^{lo}KLRG1^{-}CD8α^{+} (naive) or CD44^{hi}CD127^{+}KLRG1^{-}CD8α^{+} (memory) T cells, total CD8^{+} T cells from spleen (single-cell suspensions) were treated with ammonium chloride–potassium bicarbonate buffer, followed by enrichment with a CD8α^{+} isolation kit II (Miltenyi Biotec).

***In vitro* T cell–proliferation assay.** Activated CD90.1^{+} CTLs (3×10^4) were incubated with 'titrated' numbers of various hepatic nonparenchymal cells obtained from mice at day 3 after challenge with TLR9 ligand. Anti-CD80 (16-10A1), anti-CD86 (GL1), anti-OX40L (RM134L) and isotype-matched control immunoglobulins (eBio299Arm, eBR2a and eB149/10H5; all from eBioscience) were added at a concentration of 10 μg/ml for functional blockade. After 40 h of coculture, 4 μM EdU (5-ethynyl-2′-deoxyuridine) was added for 6 h, then CTLs were collected and incorporation of EdU was measured with a with Click-iT EdU kit (Invitrogen). The absolute number of proliferating EdU^{+} CTLs per well was determined by flow cytometry with CountBright absolute counting beads.

Viral infection. AdLGO (recombinant adenovirus expressing a fusion protein of click-beetle luciferase (Promega), GFP and an H-2K^{b}-restricted OVA epitope of amino acids 257–264 (SIINFEKL)) or AdLG (recombinant adenovirus expressing only luciferase and GFP) was used to infect C57BL/6j mice, at a dose of 1×10^6 infectious units. At day 2 after infection, 1×10^4 or 1×10^5 CD90.1^{+} OT-I CTLs activated with T-activator Dynabeads labeled with anti-CD3 plus anti-CD28 (Invitrogen) and 5 ng/ml IL-12 were transferred into mice together with 20 μg of TLR9 ligand or non–TLR9-binding control oligonucleotide. *In vivo* bioluminescence to was determined as reported[25,34].

Chronic infection with LCMV was induced by infection of newborn mice with 1×10^6 plaque-forming units of LCMV (WE strain). At 8 weeks after infection, mice were used for experiments. LCMV-specific CTLs were obtained from spleens at day 7 after acute infection with LCMV (2×10^4 plaque-forming units).

C57BL/6j mice were infected intravenously with 1×10^8 infectious units of AdHBV, which led to chronic infection with AdHBV, as reported[26]. DNA immunization was done as described[26]. After immunization, serum ALT activity were measured with a Reflovet Plus (Roche). Analysis of CTL number and function *ex vivo* was done as described[26].

H-2K^{b}-restricted HBc93-specific CTLs and H-2D^{b}-restricted gp33-specific CTLs were detected by Dextramer staining (Immudex).

Immunohistochemistry, electron microcopy and spinning-disc confocal intravital microscopy. The preparation of liver sections for immunohistochemistry has been described[35,36]. CD11b, MHC class II, CCR2, GFP, Ki67, CD90.1, NKp46, CD19, Ly6C-Ly6G, OX40L and BrdU were detected with M1/70 (BMA Biomedicals), M5/114.15.2 (Novus Biologicals), MC-21 (ref. 37), polyclonal anti-GFP (20R-GR011; Fitzgerald Industries), SP6 (Lab Vision), polyclonal anti-NKp46 (BAF2225; R&D Systems), 1D3 (BD Pharmingen), AL-21 (BD Pharmingen), 1A8 (BD Pharmingen), OX89 (MyBioSource) and B44 (BD), respectively. Preparation of liver tissues for electron microcopy was done as described[34]. Intravital imaging of the migration of cell of the immune system in the liver was done as described[38].

Quantitative real-time PCR. Total RNA from tissue or from flow cytometry–sorted cells was purified by TRIzol reagent (Life technologies) and reverse-transcribed into cDNA with a SuperScript VILO cDNA synthesis kit (Invitrogen). A LightCycler 480 (Roche) and TagMan PCR reagents, including proprietary primers (Invitrogen), were used for quantitative real-time PCR analysis of

doi:10.1038/ni.2573

Gapdh, *Cd80*, *Cd86* and *Ox40l*. Faster SYBR Green (Roche) was used for quantification of the following genes: *Tnf* forward, 5′-CATCTTCTCAAAATTCGAGTGACAA-3′, and *Tnf* reverse, 5′-TGGGAGTAGACAAGGTACAACCC-3′; *Cd11c* forward, 5′-CTGGATAGCCTTTCTTCTGCTG-3′, and *Cd11c* reverse, 5′-GCACACTGTGTCCGAACTCA-3′; *Nos2* forward, 5′-CTGTGTGCCTGGAGGT-TCTG–3′, and *Nos2* reverse, 5′-CCAATCTCTGCCTATCCGTCTC-3′; *Actb* forward, 5′-AGAGGGAAATCGTGCGTGAC-3′, and *Actb* reverse, 5′-CAATAGTGACCTGGCCGT-3′. The abundance of *Gapdh* or *Actb* mRNA was used for reference.

Statistical analysis. GraphPad Prism 5 and Student's *t*-test were used for statistical analysis.

33. Hohl, T.M. *et al.* Inflammatory monocytes facilitate adaptive CD4 T cell responses during respiratory fungal infection. *Cell Host Microbe* **6**, 470–481 (2009).
34. Wohlleber, D. *et al.* TNF-induced target cell killing by CTL activated through cross-presentation. *Cell Reports* **2**, 478–487 (2012).
35. Haybaeck, J. *et al.* A lymphotoxin-driven pathway to hepatocellular carcinoma. *Cancer Cell* **16**, 295–308 (2009).
36. Wolf, M.J. *et al.* Endothelial CCR2 signaling induced by colon carcinoma cells enables extravasation via the JAK2-Stat5 and p38MAPK pathway. *Cancer Cell* **22**, 91–105 (2012).
37. Mildner, A. *et al.* CCR2^{+}Ly-6C^{hi} monocytes are crucial for the effector phase of autoimmunity in the central nervous system. *Brain* **132**, 2487–2500 (2009).
38. Jenne, C.N., Wong, C.H., Petri, B. & Kubes, P. The use of spinning-disk confocal microscopy for the intravital analysis of platelet dynamics in response to systemic and local inflammation. *PLoS ONE* **6**, e25109 (2011).

Sciencexpress Research Articles

Specific and Nonhepatotoxic Degradation of Nuclear Hepatitis B Virus cccDNA

Julie Lucifora,[1,2]* Yuchen Xia,[1]* Florian Reisinger,[1] Ke Zhang,[1] Daniela Stadler,[1] Xiaoming Cheng,[1] Martin F. Sprinzl,[1,3] Herwig Koppensteiner,[1] Zuzanna Makowska,[4] Tassilo Volz,[5] Caroline Remouchamps,[6] Wen-Min Chou,[1] Wolfgang E. Thasler,[7] Norbert Hüser,[8] David Durantel,[9] T. Jake Liang,[10] Carsten Münk,[11] Markus H. Heim,[4] Jeffrey L. Browning,[12] Emmanuel Dejardin,[6] Maura Dandri,[2,5] Michael Schindler,[1] Mathias Heikenwalder,[1]†‡ Ulrike Protzer[1,2]†‡

[1]Institute of Virology, Technische Universität München–Helmholtz Zentrum München, 81675 Munich, Germany. [2]German Center for Infection Research (DZIF), Munich and Hamburg sites, Germany. [3]1st Medical Department, University Hospital Mainz, 55131 Mainz, Germany. [4]Department of Biomedicine, University Hospital Basel, 4031 Basel, Switzerland. [5]Department of Internal Medicine, University Medical Center Hamburg-Eppendorf, 20246 Hamburg, Germany. [6]GIGA-Research Laboratory of Molecular Immunology and Signal Transduction, University of Liège, 4000 Liège, Belgium. [7]Department of General, Visceral, Transplantation, Vascular and Thoracic Surgery, Grosshadern Hospital, Ludwig Maximilians University, 81377 Munich, Germany. [8]Department of Surgery, University Hospital Rechts der Isar, Technische Universität München, 85748 Munich, Germany. [9]INSERM U1052, CNRS UMR 5286, Cancer Research Center of Lyon, University of Lyon, LabEx DEVweCAN, 69007 Lyon, France. [10]Liver Diseases Branch, National Institute of Diabetes and Digestive and Kidney Diseases, Bethesda, MD 20892, USA. [11]Clinic for Gastroenterology, Hepatology and Infectiology, Medical Faculty, Heinrich-Heine University, 40225 Düsseldorf, Germany. [12]Department of Immunobiology, Biogen Idec, Cambridge, MA 02142, USA.

*These authors contributed equally to this work.

†Corresponding author. E-mail: protzer@tum.de (U.P.); heikenwaelder@helmholtz-muenchen.de (M.H.)

‡These authors contributed equally to this work.

Current antivirals can control but not eliminate hepatitis-B-virus (HBV), because HBV establishes a stable nuclear cccDNA. Interferon-α treatment can clear HBV but is limited by systemic side effects. Here we describe how interferon-α can induce specific degradation of the nuclear viral DNA without hepatotoxicity and propose lymphotoxin-β-receptor activation as a therapeutic alternative. Interferon-α and lymphotoxin-β-receptor activation up-regulated APOBEC3A and 3B cytidine-deaminases, respectively, in HBV-infected cells, primary hepatocytes and human liver-needle biopsies. HBV-core protein mediated the interaction with nuclear cccDNA resulting in cytidine-deamination, apurinic/apyrimidinic site formation and finally cccDNA degradation that prevented HBV-reactivation. Genomic DNA was not affected. Thus, inducing nuclear deaminases - e.g., by lymphotoxin-β-receptor activation - allows development of new therapeutics that combined with existing antivirals may cure hepatitis B.

Hepatitis B virus (HBV) infection remains a major public health threat with more than 350 million humans chronically infected worldwide at risk of developing end-stage liver disease and hepatocellular carcinoma. Each year, more than 600,000 humans die from consequences of chronic HBV infection. A prophylactic vaccine has been available for hepatitis B for almost thirty years, but the overall number of chronic infections remains high.

HBV is a small, enveloped DNA virus replicating via an RNA intermediate. The encapsidated viral genome consists of a 3.2 kb partially double-stranded relaxed circular DNA (rcDNA) molecule. The virus has optimized its life-cycle for long-term persistence in the liver (*1*). Upon translocation to the nucleus, the rcDNA genome is converted into a covalently closed circular DNA (cccDNA), which serves as the template for viral transcription and secures HBV persistence. Nucleos(t)ide analogs are efficient antivirals but only control and do not cure HBV infection owing to the persistence of HBV cccDNA. Therefore, long-term treatment is required, which is expensive and may lead to concomitant resistance (*2*). Interferon (IFN)-α is licensed for hepatitis B therapy and treatment with this cytokine can result in virus clearance in a proportion of patients; however, its efficacy is limited and high doses are not tolerated (*3*). Thus, efficient and non-toxic elimination of cccDNA in hepatocytes is a major goal of HBV research.

Using animal models, it has been shown that HBV replication, and in particular the cccDNA content of the liver, can be affected by noncytopathic mechanisms involving cytokines such as interferons and tumor necrosis factor (TNF), which influence RNA and capsid stability (*4–7*). Here, we describe an antiviral mechanism that interferes with cccDNA stability and is distinct from influences of antiviral cytokines on cccDNA activity (*8*).

High-Dose IFN-α Leads to cccDNA Degradation in HBV-Infected Hepatocytes

IFN-α is known to exert transcriptional, post-transcriptional and epigenetic antiviral effects on HBV (*8–12*). To study the effect of IFN-α on HBV cccDNA, we used HBV-infected, differentiated HepaRG (dHepaRG) cells and primary human hepatocytes (PHH). These are human cell types susceptible to HBV infection (*13, 14*) and responsive to IFN-α treatment in vitro (fig. S1A). IFN-α treatment did not lead to detectable hepatotoxicity, even at very high doses (fig. S1B). Treating dHepaRG cells with 500 or 1000 IU/ml IFN-α controlled HBV-DNA synthesis as efficiently as 0.5 μM (5-fold EC50) of the nucleoside analog lamivudine (LAM). IFN-α, however, unlike LAM also significantly reduced expression of HBV-RNA and hepatitis B surface (HBsAg) and e (HBeAg) antigens (Fig. 1A and fig. S1C).

In patients, interruption of LAM treatment results in a rebound of HBV replication (*2*). Using IFN-α, we observed only a partial or no rebound in HBV-infected dHepaRG cells after treatment cessation (Fig. 1A). Because dHepaRG don't allow virus spread, reduction of HBeAg and lacking rebound indicated an effect of IFN-α on the established HBV cccDNA transcription template besides the known antiviral effects on viral replication (*14*). By cccDNA-specific qPCR, we determined an 80% reduction of cccDNA after 10 days of treatment (Fig. 1B). Reduction of cccDNA was confirmed by Southern blot analysis (fig. S1D) and was dose dependent (fig. S1E). cccDNA reduction could be induced at any time point (Fig. 1C) and persisted over time (Fig. 1, A and C). The

effect was corroborated in HBV-infected primary human hepatocytes (PHH) (Fig. 1D). In contrast to IFN-α, LAM and even more potent nucleoside analog entecavir (ETV) at very high doses (0.5 μM, 1000-fold IC-50) only inhibited reverse transcription and thus HBV replication, but not viral persistence (Fig. 1E). Pretreatment with ETV did not enhance the effect of IFN-α (Fig. 1F) indicating that IFN-α induces the decay of established HBV cccDNA. Since the doses of IFN-α used to achieve this effect were high, we screened for other cytokines showing similar antiviral effects at moderate doses.

LTβR Activation Controls HBV and Leads to cccDNA Degradation in HBV-Infected Cells

IFN-γ and TNF-α are known to control HBV in a noncytopathic fashion (*4*, *7*), but cannot be used as therapeutics because they cause severe side effects. We tested the effect of lymphotoxin (LT) β receptor (LTβR) activation as an alternative therapeutic option. TNF superfamily members LTα, LTβ and CD258 are the physiological ligands for LTβR and activate several inflammatory, anti-inflammatory, pro- and anti-survival pathways (*15*). Like hepatocytes (*16*), dHepaRG (*14*) and HepG2-H1.3 cells permit HBV replication (*17*) and express the LTβR (fig. S2, A and B). To activate LTβR, we used a super-agonistic tetravalent bispecific antibody (BS1) and a bivalent anti-LTβR monoclonal antibody (CBE11) (*18*, *19*). As expected, LTβR agonists activated canonical (*20*) and non-canonical nuclear factor kappa-light-chain-enhancer of activated B cells (NF-κB) pathways to trigger p100 cleavage (fig. S2C), RelA phosphorylation (fig. S2D), nuclear RelB and RelA translocation (fig. S2, E and F), and up-regulation of known target genes (fig. S2G) without causing any detectable hepatocytotoxicity (fig. S2H).

To test the effect of LTβR-activation on HBV infection, dHepaRG cells were treated with BS1 for 12 days starting 24 hours prior to HBV infection. LTβR-activation decreased levels of all HBV-markers, including cccDNA by approximately 90% without toxicity (Fig. 2A). The antiviral effect was highly potent with an EC_{50} of approximately 0.01 μg/mL (fig. S3A). Inhibition of apoptosis did not alter antiviral activity (fig. S4). Neither IFN-β nor classic IFN-stimulated genes were up-regulated upon BS1-treatment (fig. S2G) and antiviral activity was independent of IFN-induction (fig. S5).

In vivo, activation of the murine LTβR by systemic application of an agonistic antibody (ACH6) induced RelA and RelB nuclear translocation in hepatocytes of HBV-transgenic mice (fig. S6A), reduced HBV viremia (fig. S6B), HBV RNA (fig. S6C) and HBV core (HBc) protein expression in the liver (fig. S6, D and E). Neither signs of hepatocyte apoptosis (fig. S6F) nor elevation of aminotransferases (ALT) (fig. S6G, right panel) were observed indicating good in vivo tolerability of LTβR-activation. Since HBV-transgenic mice do not establish HBV cccDNA, this indicated additional antiviral effects of LTβR-activation on HBV RNA transcription or stability. Accordingly, discontinuation of LTβR-activation induced an immediate, strong rebound of HBV replication (fig. S6G).

To investigate whether LTβR-activation would affect established HBV cccDNA in the context of a persistent infection and prevent HBV reactivation, dHepaRG cells were treated with LTβR agonists BS1 or CBE11 when a stable, nuclear cccDNA pool had established. All HBV markers, including HBV cccDNA, were reduced upon LTβR-activation in HBV-infected dHepaRG cells (Fig. 2, B and C, and fig. S3) as well as in stably transfected HepG2H1.3 cells containing high levels of cccDNA (Fig. 2C). In HBV-infected primary human hepatocytes (PHH), LTβR agonisation reduced HBV cccDNA, HBeAg secretion and even more pronounced HBV-DNA replication (Fig. 2D). cccDNA degradation was more effective (up to 95%) when treatment was prolonged (fig. S3, C and D). Treatment interruption for 10 days was almost as efficient as continuous treatment (fig. S3C) indicating that LTβR agonists induce a persistent antiviral effect. In contrast to LAM treatment, no rebound of HBV-replication was observed when BS1 treatment stopped (Fig. 2E). Hence, LTβR activation not only suppressed HBV replication but also caused nuclear cccDNA degradation, needed to achieve virus elimination.

LTβR Activation and IFN-α Treatment Induce Deamination and Apurinic/Apyrimidinic (AP) Site Formation in cccDNA

To investigate if cccDNA degradation upon LTβR-activation or IFN-α treatment was a result of DNA damage, we examined cccDNA deamination by differential DNA denaturation PCR (3D-PCR) (*21*). Low denaturing temperatures were sufficient for cccDNA amplification from HBV-infected dHepaRG cells and for PHH treated with IFN-α or BS1, compared with untreated, LAM- or ETV-treated cells (Fig. 3A and fig. S7, C and D). Using a cocktail of recombinant proteins containing all enzymes necessary for DNA repair (preCR mix), we could reverse the denaturation of cccDNA (Fig. 3A, lower panels). The fact, that denaturation temperatures of mock, LAM and ETV treated cells also shifted, indicated that this modification of HBV cccDNA existed even without exposure to exogenous drugs. Deamination of cccDNA (Fig. 3A, right panel) and a drop in cccDNA levels after treatment with CBE11 (table S1) was confirmed in vivo in human liver chimeric uPA-SCID mice infected with HBV. Sequencing analyses showed G/A transitions occurred under treatment (Fig. 3B and fig. S7, A and B) indicating deamination of cytidines to uridine in the HBV cccDNA minus strand. At lower denaturation temperatures G/A transitions became more obvious (Fig. 3C and fig. S7A). These data showed that both LTβR-activation and IFN-α treatment led to cccDNA deamination in vitro and in vivo, and help to explain the G/A hypermutation observed in patient samples (*21*).

Importantly, neither deamination nor mutations of genomic DNA were observed by 3D-PCR (fig. S8A) or by deep sequencing of selected housekeeping or IFN- and LTβR-target genes (fig. S8B). This indicated that DNA modifications were specifically targeted to viral cccDNA.

After cytidine deamination, DNA-glycosylases recognize the damaged DNA and cleave N-glycosidic bonds to release the base and create an accessible AP site that can then be cleaved by endonucleases (*22*). These AP sites can either be repaired, can lead to mutations upon DNA replication or can induce DNA degradation (*23*). We quantified AP sites created by LTβR-activation or IFN-α treatment. However, no increase of AP sites in total DNA extracts from dHepaRG cells or PHH treated with IFN-α or LTβR-agonists (fig. S8C) was found, reassuring that our treatments did not lead to detectable damage in genomic DNA. Because AP sites in the small (3.2 kb) cccDNA are very likely to be missed by this analysis, we digested total DNA extracts with an AP-endonuclease (APE1) and then amplified cccDNA by qPCR. APE digestion further decreased cccDNA extracted from dHepaRG cells and PHH treated with IFN-α or LTβR-agonists but not with LAM (Fig. 3D). Taken together, our data indicate that both, LTβR-activation or IFN-α treatment induced deamination and AP-site formation in HBV cccDNA leading to its degradation, but did not affect genomic DNA.

LTβR Activation and IFN-α Treatment Up-Regulate Expression of Nuclear APOBEC3 Deaminases

IFN-α is known to induce several cytidine deaminases (*23*, *24*). We performed genome-wide expression profiling of HBV-infected dHepaRG cells after LTβR-activation (fig. S9A) and classified regulated genes according to their activity and properties (fig. S9B). Hereby, APOBEC3B (A3B) was identified to be the most up-regulated gene with nucleic acid binding properties (fig. S9C).

Analysis of all APOBEC3 family members showed that LTβR-activation leads to strong up-regulation of A3B and to minor extent A3G in HBV-infected dHepaRG and PHH, and after systemic application in human liver chimeric uPA-SCID mice (fig. S10A). A3B expression was

induces by LTβR-activation in a dose-dependent manner and expression levels steadily increased during continuous treatment (fig. S11) correlating with a concomitant increase in treatment efficacy over time (fig. S3C). Treatment of PHH isolated from different donors with LTβR-agonist BS1 resulted in cccDNA degradation at different levels (Fig. 3E and fig. S10B), which could neither be explained by the level of A3B upregulation (Fig. 3E) nor by detection of a previously described (*25*) genomic deletion of the A3B allele, which seems to correlate with HBV persistence in infected patients (fig. S10, B and C).

In contrast to LTβR-activation, IFN-α treatment induced mainly A3A, but also A3F and A3G expression in HBV-infected dHepaRG cells and PHH (fig. S12A), and A3D expression in isolated PHH. By systemic IFN treatment of chimpanzees (*26*), A3A was strongly upregulated in liver needle biopsies (fig. S12B). Activation of A3A, A3F and A3G after IFN-α treatment was dose- and time-dependent, and decreased after an initial peak despite continuous treatment indicating that cells become refractory to IFN-α (fig. S13). In patients treated with subcutaneous pegylated IFN-α, needle biopsies obtained at different time points confirmed a rapid, strong upregulation of A3A and to a lower extend of A3G in the liver peaking at 16 hours post treatment (fig. S12C). Expression levels declined after this time point and remained low until day 6 post treatment confirming a fast but only transient induction of A3A by IFN-α treatment. Interestingly, the level of A3B or A3A induction in BS-1 and IFN-α treated PHH, respectively, did not directly correlate with the level of cccDNA degradation (Fig. 3E). The fact that IFN-α only induces a transient A3A induction and cells rapidly become refractory to IFN-α may account for the limited effect of IFN-α treatment in HBV-infected patients (*3*).

APOBEC3A or APOBEC3B Activity Is Essential to Induce cccDNA Degradation

Among the APOBEC3 family members up-regulated in our experiments, only A3A and A3B located to the nucleus (fig. S14) where they can gain access to cccDNA. To verify that they are indeed responsible for the induction of cccDNA degradation, we overexpressed the HIV-Vif protein (known to promote the degradation of all APOBEC3 proteins except A3B (*27*, *28*)) in dHepaRG cells in a tetracycline-regulated fashion. Expression of HIV-Vif reduced A3A, A3F and A3G expression (fig. S15A), reverted IFN-α-induced cccDNA deamination and prevented cccDNA degradation induced by IFN-α treatment (Fig. 4A). However, expression of HIV-Vif did not alter A3B levels (fig. S15B) and had no impact on cccDNA degradation by LTβR-activation (fig. S15C). To specifically address the role of A3A or A3B in cccDNA degradation we further knocked down A3A and A3B in dHepaRG cells under IFN-α or LTβR-agonist treatment, respectively, and observed reduced cccDNA deamination (Fig. 4, B and C, left panels). A3A as well as A3B knock-down completely reverted cccDNA degradation, but could not rescue the additional effect of IFN-α or LTβR-activation on HBV replication (Fig. 4, B and C, right panels).

To confirm the impact of A3A and A3B on cccDNA deamination, we overexpressed A3A and A3B, respectively, in HBV-replicating HepG2-H1.3 (Fig. 4, D and E). Cytidine-deamination of nuclear cccDNA by A3A and A3B is in accordance with other studies showing that both localize to the nucleus (*29*) and may be involved in the elimination of foreign DNA (*23*).

APOBEC3A Interacts with the HBV Core Protein and Binds to cccDNA

APOBECs have evolved to restrict retroviral replication (*30*) as well as DNA transfer into cells. They are able to clear foreign nuclear DNA (*23*, *31*), but it remains unclear how HBV cccDNA DNA was recognized and whether it was specifically targeted in our experiments. To assess specificity, we generated cell lines replicating a mammalian replicon plasmid pEpi containing a linear HBV 1.3-fold overlength sequence. From the linear HBV-genome, HBV replication was initiated and in addition to the pEpi-H1.3 replicon HBV cccDNA was established in the nucleus. Treatment with either IFN-α or LTβR-agonist BS1 inhibited HBV replication and resulted in deamination and degradation of HBV cccDNA, but not of the HBV-sequence containing replicon (fig. S16). This indicated that deamination and subsequent degradation induced by both treatments is HBV cccDNA specific.

HBV core protein associates with A3G (*32*) and HBV cccDNA (*33*) and thus was a candidate to mediate the targeting of A3 deaminases to HBV cccDNA. Confocal microscopy indicated a co-localization of A3A and A3B with HBV core in different cell lines and PHH (Fig. 5 and fig. S17). Chromatin immunoprecipitation (ChIP) experiments using stably (fig. S18A) or transiently transfected HepG2H1.3 cells or HBV-infected and IFN-α treated dHepaRG cells, showed that HBV core protein and A3A both bind to the cccDNA minichromosome (Fig. 6A). Supporting the possibility that a guardian protein prevents A3A direct binding to DNA (*34*), we could not detect A3A binding to genomic DNA (fig. S18B) even in the presence of HBV core, which has been reported to also bind to cellular DNA (*35*).

HBV core protein co-immunoprecipitated A3A in HepG2H1.3 cells and transfected HuH7 cells indicating physical interaction with A3A (fig. S19). Direct interaction of HBV core expressed after HBV infection and A3A induced by IFN-α was confirmed by proximity ligation assay (PLA) (Fig. 6B and fig. S20) and fluorescence resonance energy transfer (FRET) analysis (Fig. 6C). By deletion analysis, we determined that the central region of HBc (aa 77 to 149) is involved in the interaction with A3A (Fig. 6C and fig. S21).

These data suggest that A3A is targeted to cccDNA by interaction with HBV core. No such targeting to genomic DNA has been described so far. Since APOBEC3 deaminases are thought to act on single stranded DNA (*36*), one possibility is that A3A and A3B act on cccDNA when it is transiently rendered single-stranded by RNA polymerase II before transcription initiation.

We suggest, therefore, the following mechanism of APOBEC-dependent degradation of HBV cccDNA (Fig. 6D). High dose IFN-α treatment or LTβR-activation up-regulate the expression of A3A and A3B, respectively, which subsequently co-localize or directly interact with HBV core in infected hepatocytes, translocate to the nucleus, where they are brought into close contact with cccDNA by HBV core. Now, APOBECs can deaminate cccDNA that is transiently rendered single-stranded during transcription. Uracils in HBV cccDNA are recognized and excised by cellular DNA glycosylases leading to formation of AP sites, which are then recognized by cellular AP endonucleases (*23*) leading to cccDNA digestion. Why cccDNA is degraded instead of being repaired by the cellular DNA repair machinery remains elusive so far. Using a mixture of various enzymes, we were able to repair deaminated cccDNA *in tubo* (Fig. 3A) suggesting induction of an additional factor promoting DNA degradation or an impaired function of the repair machinery rather than a lack of recognition by the repair machinery. Thus, we can only speculate that either the number of AP sites introduced after treatment is too high and exceeds the capacity of the cellular repair machinery or that IFN-α treatment or LTβR-activation or even HBV itself (*37*) modulate the repair machinery. This may shift the equilibrium from cccDNA repair (*38*) to degradation.

Ideally, a cure for HBV infection needs to eliminate cccDNA. Therefore, cytokines or cytokine-receptor agonists that can trigger HBV cccDNA deamination and its degradation are interesting antiviral candidates. Antivirals that induce A3A/B activity should be combined with nucleos(t)ide analogs to avoid the replenishment of nuclear cccDNA after degradation. LTβR-agonists were active at low doses and we did not observe any toxicity in vitro or in vivo nor did we detect any modification of genomic DNA. Constitutive overexpression of LTα/β for more

than one year has been associated with inflammatory liver disease and hepatocellular carcinoma (*16*). As antivirals, however, LTβR-agonists would only be used for a limited period of time minimizing the risk of side effects. Moreover, LTβR-activation was already explored as a cancer treatment (*18*).

A recent study has shown a significantly higher frequency of an A3B deletion allele in persistent HBV carriers and hepatocellular carcinoma patients compared with healthy controls (*25*). This finding was further supported by the moderate deamination of cccDNA even in absence of treatment, and by the observation that knockdown of A3B in the absence of any treatment increased cccDNA levels. Although deregulated expression of A3A and A3B has been shown to correlate with genomic DNA mutations (*39*, *40*), we did not detect any alterations of genomic DNA using analyses of AP sites, 3D-PCR analysis and deep sequencing of a set of human genes.

Our data indicate that cccDNA degradation is possible and can be induced without side-effects on the infected host cell. An important task will be testing of combinations of nucleos(t)ide analogs with novel antiviral strategies (e.g., LTβR agonists or adoptive T-cell therapy (*41*)) to activate A3A or A3B to cure hepatitis B.

References and Notes

1. U. Protzer, M. K. Maini, P. A. Knolle, Living in the liver: hepatic infections. *Nat. Rev. Immunol.* **12**, 201–213 (2012). doi:10.1038/nri3169 Medline
2. F. Zoulim, Hepatitis B virus resistance to antiviral drugs: where are we going? *Liver Int.* **31**, (Suppl 1), 111–116 (2011). doi:10.1111/j.1478-3231.2010.02399.x Medline
3. K. Wursthorn, M. Lutgehetmann, M. Dandri, T. Volz, P. Buggisch, B. Zollner, T. Longerich, P. Schirmacher, F. Metzler, M. Zankel, C. Fischer, G. Currie, C. Brosgart, J. Petersen, Peginterferon alpha-2b plus adefovir induce strong cccDNA decline and HBsAg reduction in patients with chronic hepatitis B. *Hepatology* **44**, 675–684 (2006). doi:10.1002/hep.21282 Medline
4. L. G. Guidotti, K. Ando, M. V. Hobbs, T. Ishikawa, L. Runkel, R. D. Schreiber, F. V. Chisari, Cytotoxic T lymphocytes inhibit hepatitis B virus gene expression by a noncytolytic mechanism in transgenic mice. *Proc. Natl. Acad. Sci. U.S.A.* **91**, 3764–3768 (1994). doi:10.1073/pnas.91.9.3764 Medline
5. L. G. Guidotti, R. Rochford, J. Chung, M. Shapiro, R. Purcell, F. V. Chisari, Viral clearance without destruction of infected cells during acute HBV infection. *Science* **284**, 825–829 (1999). doi:10.1126/science.284.5415.825 Medline
6. S. F. Wieland, H. C. Spangenberg, R. Thimme, R. H. Purcell, F. V. Chisari, Expansion and contraction of the hepatitis B virus transcriptional template in infected chimpanzees. *Proc. Natl. Acad. Sci. U.S.A.* **101**, 2129–2134 (2004). doi:10.1073/pnas.0308478100 Medline
7. H. McClary, R. Koch, F. V. Chisari, L. G. Guidotti, Relative sensitivity of hepatitis B virus and other hepatotropic viruses to the antiviral effects of cytokines. *J. Virol.* **74**, 2255–2264 (2000). doi:10.1128/JVI.74.5.2255-2264.2000 Medline
8. L. Belloni, L. Allweiss, F. Guerrieri, N. Pediconi, T. Volz, T. Pollicino, J. Petersen, G. Raimondo, M. Dandri, M. Levrero, IFN-α inhibits HBV transcription and replication in cell culture and in humanized mice by targeting the epigenetic regulation of the nuclear cccDNA minichromosome. *J. Clin. Invest.* **122**, 529–537 (2012). doi:10.1172/JCI58847 Medline
9. A. Rang, S. Günther, H. Will, Effect of interferon alpha on hepatitis B virus replication and gene expression in transiently transfected human hepatoma cells. *J. Hepatol.* **31**, 791–799 (1999). doi:10.1016/S0168-8278(99)80279-7 Medline
10. V. Pasquetto, S. F. Wieland, S. L. Uprichard, M. Tripodi, F. V. Chisari, Cytokine-sensitive replication of hepatitis B virus in immortalized mouse hepatocyte cultures. *J. Virol.* **76**, 5646–5653 (2002). doi:10.1128/JVI.76.11.5646-5653.2002 Medline
11. S. F. Wieland, L. G. Guidotti, F. V. Chisari, Intrahepatic induction of alpha/beta interferon eliminates viral RNA-containing capsids in hepatitis B virus transgenic mice. *J. Virol.* **74**, 4165–4173 (2000). doi:10.1128/JVI.74.9.4165-4173.2000 Medline
12. S. L. Uprichard, S. F. Wieland, A. Althage, F. V. Chisari, Transcriptional and posttranscriptional control of hepatitis B virus gene expression. *Proc. Natl. Acad. Sci. U.S.A.* **100**, 1310–1315 (2003). doi:10.1073/pnas.252773599 Medline
13. P. Gripon, C. Diot, N. Thézé, I. Fourel, O. Loreal, C. Brechot, C. Guguen-Guillouzo, Hepatitis B virus infection of adult human hepatocytes cultured in the presence of dimethyl sulfoxide. *J. Virol.* **62**, 4136–4143 (1988). Medline
14. P. Gripon, S. Rumin, S. Urban, J. Le Seyec, D. Glaise, I. Cannie, C. Guyomard, J. Lucas, C. Trepo, C. Guguen-Guillouzo, Infection of a human hepatoma cell line by hepatitis B virus. *Proc. Natl. Acad. Sci. U.S.A.* **99**, 15655–15660 (2002). doi:10.1073/pnas.232137699 Medline
15. M. J. Wolf, G. M. Seleznik, N. Zeller, M. Heikenwalder, The unexpected role of lymphotoxin beta receptor signaling in carcinogenesis: from lymphoid tissue formation to liver and prostate cancer development. *Oncogene* **29**, 5006–5018 (2010). doi:10.1038/onc.2010.260 Medline
16. J. Haybaeck, N. Zeller, M. J. Wolf, A. Weber, U. Wagner, M. O. Kurrer, J. Bremer, G. Iezzi, R. Graf, P. A. Clavien, R. Thimme, H. Blum, S. A. Nedospasov, K. Zatloukal, M. Ramzan, S. Ciesek, T. Pietschmann, P. N. Marche, M. Karin, M. Kopf, J. L. Browning, A. Aguzzi, M. Heikenwalder, A lymphotoxin-driven pathway to hepatocellular carcinoma. *Cancer Cell* **16**, 295–308 (2009). doi:10.1016/j.ccr.2009.08.021 Medline
17. S. Jost, P. Turelli, B. Mangeat, U. Protzer, D. Trono, Induction of antiviral cytidine deaminases does not explain the inhibition of hepatitis B virus replication by interferons. *J. Virol.* **81**, 10588–10596 (2007). doi:10.1128/JVI.02489-06 Medline
18. M. Lukashev, D. LePage, C. Wilson, V. Bailly, E. Garber, A. Lukashin, A. Ngam-ek, W. Zeng, N. Allaire, S. Perrin, X. Xu, K. Szeliga, K. Wortham, R. Kelly, C. Bottiglio, J. Ding, L. Griffith, G. Heaney, E. Silverio, W. Yang, M. Jarpe, S. Fawell, M. Reff, A. Carmillo, K. Miatkowski, J. Amatucci, T. Crowell, H. Prentice, W. Meier, S. M. Violette, F. Mackay, D. Yang, R. Hoffman, J. L. Browning, Targeting the lymphotoxin-beta receptor with agonist antibodies as a potential cancer therapy. *Cancer Res.* **66**, 9617–9624 (2006). doi:10.1158/0008-5472.CAN-06-0217 Medline
19. X. Hu, M. A. Zimmerman, K. Bardhan, D. Yang, J. L. Waller, G. B. Liles, J. R. Lee, R. Pollock, D. Lev, C. F. Ware, E. Garber, V. Bailly, J. L. Browning, K. Liu, Lymphotoxin β receptor mediates caspase-dependent tumor cell apoptosis in vitro and tumor suppression in vivo despite induction of NF-κB activation. *Carcinogenesis* **34**, 1105–1114 (2013). doi:10.1093/carcin/bgt014 Medline
20. E. Dejardin, N. M. Droin, M. Delhase, E. Haas, Y. Cao, C. Makris, Z. W. Li, M. Karin, C. F. Ware, D. R. Green, The lymphotoxin-beta receptor induces different patterns of gene expression via two NF-kappaB pathways. *Immunity* **17**, 525–535 (2002). doi:10.1016/S1074-7613(02)00423-5 Medline
21. R. Suspène, D. Guétard, M. Henry, P. Sommer, S. Wain-Hobson, J. P. Vartanian, Extensive editing of both hepatitis B virus DNA strands by APOBEC3 cytidine deaminases in vitro and in vivo. *Proc. Natl. Acad. Sci. U.S.A.* **102**, 8321–8326 (2005). doi:10.1073/pnas.0408223102 Medline
22. J. I. Friedman, J. T. Stivers, Detection of damaged DNA bases by DNA glycosylase enzymes. *Biochemistry* **49**, 4957–4967 (2010). doi:10.1021/bi100593a Medline
23. M. D. Stenglein, M. B. Burns, M. Li, J. Lengyel, R. S. Harris, APOBEC3 proteins mediate the clearance of foreign DNA from human cells. *Nat. Struct. Mol. Biol.* **17**, 222–229 (2010). doi:10.1038/nsmb.1744 Medline
24. M. Bonvin, F. Achermann, I. Greeve, D. Stroka, A. Keogh, D. Inderbitzin, D. Candinas, P. Sommer, S. Wain-Hobson, J. P. Vartanian, J. Greeve, Interferon-inducible expression of APOBEC3 editing enzymes in human hepatocytes and inhibition of hepatitis B virus replication. *Hepatology* **43**, 1364–1374 (2006). doi:10.1002/hep.21187 Medline
25. T. Zhang, J. Cai, J. Chang, D. Yu, C. Wu, T. Yan, K. Zhai, X. Bi, H. Zhao, J. Xu, W. Tan, C. Qu, D. Lin, Evidence of associations of APOBEC3B gene deletion with susceptibility to persistent HBV infection and hepatocellular carcinoma. *Hum. Mol. Genet.* **22**, 1262–1269 (2013). doi:10.1093/hmg/dds513 Medline
26. Y. Huang, J. J. Feld, R. K. Sapp, S. Nanda, J. H. Lin, L. M. Blatt, M. W. Fried, K. Murthy, T. J. Liang, Defective hepatic response to interferon and activation of suppressor of cytokine signaling 3 in chronic hepatitis C. *Gastroenterology* **132**, 733–744 (2007). doi:10.1053/j.gastro.2006.11.045 Medline
27. B. P. Doehle, A. Schäfer, B. R. Cullen, Human APOBEC3B is a potent inhibitor of HIV-1 infectivity and is resistant to HIV-1 Vif. *Virology* **339**, 281–288 (2005). doi:10.1016/j.virol.2005.06.005 Medline

28. G. Berger, J. Turpin, S. Cordeil, K. Tartour, X. N. Nguyen, R. Mahieux, A. Cimarelli, Functional analysis of the relationship between Vpx and the restriction factor SAMHD1. *J. Biol. Chem.* **287**, 41210–41217 (2012). doi:10.1074/jbc.M112.403816 Medline
29. H. Muckenfuss, M. Hamdorf, U. Held, M. Perkovic, J. Löwer, K. Cichutek, E. Flory, G. G. Schumann, C. Münk, APOBEC3 proteins inhibit human LINE-1 retrotransposition. *J. Biol. Chem.* **281**, 22161–22172 (2006). doi:10.1074/jbc.M601716200 Medline
30. C. Münk, A. Willemsen, I. G. Bravo, An ancient history of gene duplications, fusions and losses in the evolution of APOBEC3 mutators in mammals. *BMC Evol. Biol.* **12**, 71 (2012). doi:10.1186/1471-2148-12-71 Medline
31. M. A. Carpenter, M. Li, A. Rathore, L. Lackey, E. K. Law, A. M. Land, B. Leonard, S. M. Shandilya, M. F. Bohn, C. A. Schiffer, W. L. Brown, R. S. Harris, Methylcytosine and normal cytosine deamination by the foreign DNA restriction enzyme APOBEC3A. *J. Biol. Chem.* **287**, 34801–34808 (2012). doi:10.1074/jbc.M112.385161 Medline
32. P. Turelli, B. Mangeat, S. Jost, S. Vianin, D. Trono, Inhibition of hepatitis B virus replication by APOBEC3G. *Science* **303**, 1829 (2004). doi:10.1126/science.1092066 Medline
33. C. T. Bock, S. Schwinn, S. Locarnini, J. Fyfe, M. P. Manns, C. Trautwein, H. Zentgraf, Structural organization of the hepatitis B virus minichromosome. *J. Mol. Biol.* **307**, 183–196 (2001). doi:10.1006/jmbi.2000.4481 Medline
34. M. M. Aynaud, R. Suspène, P. O. Vidalain, B. Mussil, D. Guétard, F. Tangy, S. Wain-Hobson, J. P. Vartanian, Human Tribbles 3 protects nuclear DNA from cytidine deamination by APOBEC3A. *J. Biol. Chem.* **287**, 39182–39192 (2012). doi:10.1074/jbc.M112.372722 Medline
35. Y. Guo, W. Kang, X. Lei, Y. Li, A. Xiang, Y. Liu, J. Zhao, J. Zhang, Z. Yan, Hepatitis B viral core protein disrupts human host gene expression by binding to promoter regions. *BMC Genomics* **13**, 563 (2012). doi:10.1186/1471-2164-13-563 Medline
36. H. C. Smith, R. P. Bennett, A. Kizilyer, W. M. McDougall, K. M. Prohaska, Functions and regulation of the APOBEC family of proteins. *Semin. Cell Dev. Biol.* **23**, 258–268 (2012). doi:10.1016/j.semcdb.2011.10.004 Medline
37. T. H. Lee, S. J. Elledge, J. S. Butel, Hepatitis B virus X protein interacts with a probable cellular DNA repair protein. *J. Virol.* **69**, 1107–1114 (1995). Medline
38. K. Kitamura, Z. Wang, S. Chowdhury, M. Simadu, M. Koura, M. Muramatsu, Uracil DNA glycosylase counteracts APOBEC3G-induced hypermutation of hepatitis B viral genomes: excision repair of covalently closed circular DNA. *PLoS Pathog.* **9**, e1003361 (2013). doi:10.1371/journal.ppat.1003361 Medline
39. S. Landry, I. Narvaiza, D. C. Linfesty, M. D. Weitzman, APOBEC3A can activate the DNA damage response and cause cell-cycle arrest. *EMBO Rep.* **12**, 444–450 (2011). doi:10.1038/embor.2011.46 Medline
40. M. B. Burns, L. Lackey, M. A. Carpenter, A. Rathore, A. M. Land, B. Leonard, E. W. Refsland, D. Kotandeniya, N. Tretyakova, J. B. Nikas, D. Yee, N. A. Temiz, D. E. Donohue, R. M. McDougle, W. L. Brown, E. K. Law, R. S. Harris, APOBEC3B is an enzymatic source of mutation in breast cancer. *Nature* **494**, 366–370 (2013). doi:10.1038/nature11881 Medline
41. K. Krebs, N. Böttinger, L. R. Huang, M. Chmielewski, S. Arzberger, G. Gasteiger, C. Jäger, E. Schmitt, F. Bohne, M. Aichler, W. Uckert, H. Abken, M. Heikenwalder, P. Knolle, U. Protzer, T cells expressing a chimeric antigen receptor that binds hepatitis B virus envelope proteins control virus replication in mice. *Gastroenterology* **145**, 456–465 (2013). doi:10.1053/j.gastro.2013.04.047 Medline
42. J. Lucifora, S. Arzberger, D. Durantel, L. Belloni, M. Strubin, M. Levrero, F. Zoulim, O. Hantz, U. Protzer, Hepatitis B virus X protein is essential to initiate and maintain virus replication after infection. *J. Hepatol.* **55**, 996–1003 (2011). doi:10.1016/j.jhep.2011.02.015 Medline
43. H. Schulze-Bergkamen, A. Untergasser, A. Dax, H. Vogel, P. Büchler, E. Klar, T. Lehnert, H. Friess, M. W. Büchler, M. Kirschfink, W. Stremmel, P. H. Krammer, M. Müller, U. Protzer, Primary human hepatocytes—a valuable tool for investigation of apoptosis and hepatitis B virus infection. *J. Hepatol.* **38**, 736–744 (2003). doi:10.1016/S0168-8278(03)00120-X Medline
44. S. M. Lee, C. Schelcher, M. Demmel, M. Hauner, W. E. Thasler, Isolation of human hepatocytes by a two-step collagenase perfusion procedure. *J. Vis. Exp.* (79): (2013). Medline
45. W. E. Thasler, T. S. Weiss, K. Schillhorn, P. T. Stoll, B. Irrgang, K. W. Jauch, Charitable State-Controlled Foundation Human Tissue and Cell Research: Ethic and Legal Aspects in the Supply of Surgically Removed Human Tissue For Research in the Academic and Commercial Sector in Germany. *Cell Tissue Bank.* **4**, 49–56 (2003). doi:10.1023/A:1026392429112 Medline
46. O. Hantz, R. Parent, D. Durantel, P. Gripon, C. Guguen-Guillouzo, F. Zoulim, Persistence of the hepatitis B virus covalently closed circular DNA in HepaRG human hepatocyte-like cells. *J. Gen. Virol.* **90**, 127–135 (2009). doi:10.1099/vir.0.004861-0 Medline
47. M. Quasdorff, M. Hösel, M. Odenthal, U. Zedler, F. Bohne, P. Gripon, H. P. Dienes, U. Drebber, D. Stippel, T. Goeser, U. Protzer, A concerted action of HNF4alpha and HNF1alpha links hepatitis B virus replication to hepatocyte differentiation. *Cell. Microbiol.* **10**, 1478–1490 (2008). doi:10.1111/j.1462-5822.2008.01141.x Medline
48. U. Protzer, S. Seyfried, M. Quasdorff, G. Sass, M. Svorcova, D. Webb, F. Bohne, M. Hösel, P. Schirmacher, G. Tiegs, Antiviral activity and hepatoprotection by heme oxygenase-1 in hepatitis B virus infection. *Gastroenterology* **133**, 1156–1165 (2007). doi:10.1053/j.gastro.2007.07.021 Medline
49. A. Untergasser, U. Zedler, A. Langenkamp, M. Hösel, M. Quasdorff, K. Esser, H. P. Dienes, B. Tappertzhofen, W. Kolanus, U. Protzer, Dendritic cells take up viral antigens but do not support the early steps of hepatitis B virus infection. *Hepatology* **43**, 539–547 (2006). doi:10.1002/hep.21048 Medline
50. J. Summers, P. M. Smith, A. L. Horwich, Hepadnavirus envelope proteins regulate covalently closed circular DNA amplification. *J. Virol.* **64**, 2819–2824 (1990). Medline
51. W. Gao, J. Hu, Formation of hepatitis B virus covalently closed circular DNA: removal of genome-linked protein. *J. Virol.* **81**, 6164–6174 (2007). doi:10.1128/JVI.02721-06 Medline
52. G. K. Smyth, Linear models and empirical bayes methods for assessing differential expression in microarray experiments. *Stat. Appl. Genet. Mol. Biol.* **3**, Article3 (2004).
53. C. Banning, J. Votteler, D. Hoffmann, H. Koppensteiner, M. Warmer, R. Reimer, F. Kirchhoff, U. Schubert, J. Hauber, M. Schindler, A flow cytometry-based FRET assay to identify and analyse protein-protein interactions in living cells. *PLoS ONE* **5**, e9344 (2010). doi:10.1371/journal.pone.0009344 Medline
54. K. Arnold, L. Bordoli, J. Kopp, T. Schwede, The SWISS-MODEL workspace: a web-based environment for protein structure homology modelling. *Bioinformatics* **22**, 195–201 (2006). doi:10.1093/bioinformatics/bti770 Medline
55. S. A. Wynne, R. A. Crowther, A. G. Leslie, The crystal structure of the human hepatitis B virus capsid. *Mol. Cell* **3**, 771–780 (1999). doi:10.1016/S1097-2765(01)80009-5 Medline
56. I. J. Byeon *et al.*, NMR structure of human restriction factor APOBEC3A reveals substrate binding and enzyme specificity. *Nat. Commun.* **4**, 1890 (2013).
57. A. W. Ghoorah, M. D. Devignes, M. Smaïl-Tabbone, D. W. Ritchie, Protein docking using case-based reasoning. *Proteins* **81**, 2150–2158 (2013). doi:10.1002/prot.24433 Medline
58. R. A. Sayle, E. J. Milner-White, RASMOL: biomolecular graphics for all. *Trends Biochem. Sci.* **20**, 374–376 (1995). doi:10.1016/S0968-0004(00)89080-5 Medline
59. L. G. Guidotti, B. Matzke, H. Schaller, F. V. Chisari, High-level hepatitis B virus replication in transgenic mice. *J. Virol.* **69**, 6158–6169 (1995). Medline
60. M. Dandri, M. R. Burda, E. Török, J. M. Pollok, A. Iwanska, G. Sommer, X. Rogiers, C. E. Rogler, S. Gupta, H. Will, H. Greten, J. Petersen, Repopulation of mouse liver with human hepatocytes and in vivo infection with hepatitis B virus. *Hepatology* **33**, 981–988 (2001). doi:10.1053/jhep.2001.23314 Medline
61. M. Lütgehetmann, T. Bornscheuer, T. Volz, L. Allweiss, J. H. Bockmann, J. M. Pollok, A. W. Lohse, J. Petersen, M. Dandri, Hepatitis B virus limits response of human hepatocytes to interferon-α in chimeric mice. *Gastroenterology* **140**, 2074–2083, e1–e2 (2011). doi:10.1053/j.gastro.2011.02.057 Medline
62. M. Sarasin-Filipowicz, E. J. Oakeley, F. H. Duong, V. Christen, L. Terracciano, W. Filipowicz, M. H. Heim, Interferon signaling and treatment outcome in chronic hepatitis C. *Proc. Natl. Acad. Sci. U.S.A.* **105**, 7034–7039 (2008). doi:10.1073/pnas.0707882105 Medline

Acknowledgments: We would like to thank Romina Bester, Theresa Asen, Kerstin Ackermann, Kathrin Kappes, Martin Feuerherd, Robert Baier, Ruth Hillermann, Ute Finkel, Aikatherini Krikoni and Fang Zhang for their

technical support, Prof. Luigi Terracciano for analysis of acute hepatitis patients, Prof. Frank Chisari for providing HBV transgenic mice (HBV 1.3.32), Prof. Thorsten Buch and Olivia Prazeres da Costa for help with array analysis and data discussions, Lena Allweiss and Anne Groth for help by generating and treating humanized uPA/SCID mice, as well as Siemens Healthcare Diagnostics for providing reagents. The study was supported by grants from FCC (Fédération belge Contre le Cancer) to ED, an ERC Starting grant (LiverCancerMechanism) to MH, the German Research Foundation (SFB 841 to MD, SFB TR 36 to MH, SFB TR 22), the Peter-Hans Hofschneider foundation and the Helmholtz Alliances HAIT (to UP) and PCCC (to MH). We acknowledge the support of the nonprofit foundation HTCR, which holds human tissue on trust, making it broadly available for research on an ethical and legal basis. Patent application EP12006XXX filed at the European patent office: 'Lymphotoxin signaling activation and its downstream mediators eliminate HBV ccc DNA'. Microarray data have been submitted to the GEO database (http://www.ncbi.nlm.nih.gov/geo/) and have the accession number GSE46667. Human liver-chimeric UPA/SCID mice were handled in accordance with protocols approved by the Ethical Committee of the city and state of Hamburg (permission number G12/015). Experiments with HBV-transgenic mice were performed in accordance to the German legislation governing animal studies and the Principles of Laboratory Animal Care guidelines, NIH (55.1-1-54-2531.3-27-08). The study protocol for the experiment with Chimpanzee was approved at the Southwest Foundation for Biomedical Research, San Antonio, TX (IACUC 869 PT, approved in 2004).

Supplementary Materials
www.sciencemag.org/cgi/content/full/science.1243462/DC1
Materials and Methods
Figs. S1 to S21
Table S1
References (*42*–*62*)

18 July 2013; accepted 5 February 2014

Published online 20 February 2014
10.1126/science.1243462

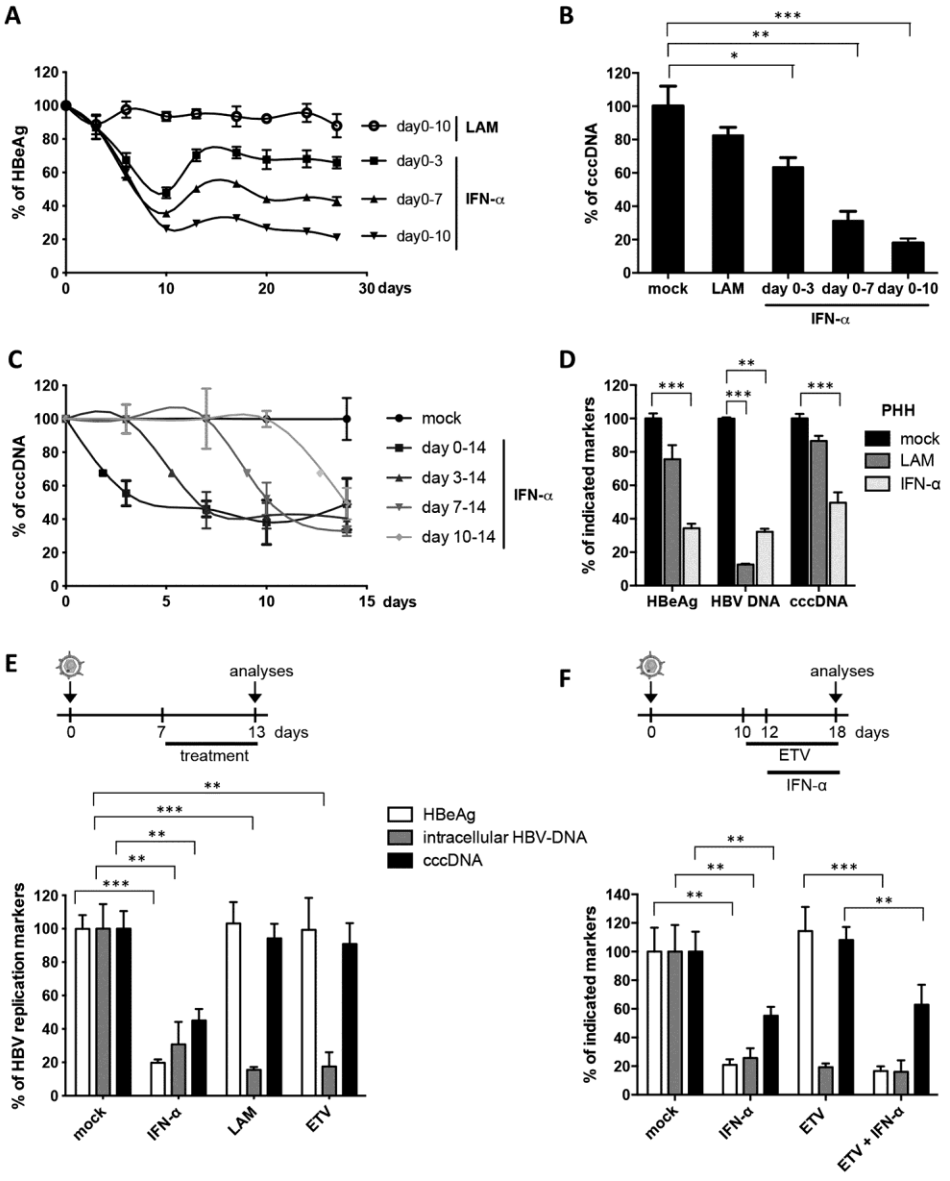

Fig. 1. Degradation of cccDNA in IFN-α treated HepaRG cells and primary human hepatocytes. (**A**, **B**, **C**, **E**, and **F**) HBV-infected dHepaRG were treated with IFN-α at day 10 post-infection (dpi). Different regimens of treatment were applied as indicated. (**D**) HBV-infected primary human hepatocyte (PHH) were treated with IFN-α at dpi 3 for 13 days. Levels of HBeAg, total intracellular DNA and cccDNA are given relative to mock treated cells. LAM: lamivudine; ETV: entecavir. Mean values +/− standard deviation of replicates from independent experiments are given; data were analyzed by *t* test. * $p < 0.05$, ** $p < 0.01$ and *** $p < 0.001$.

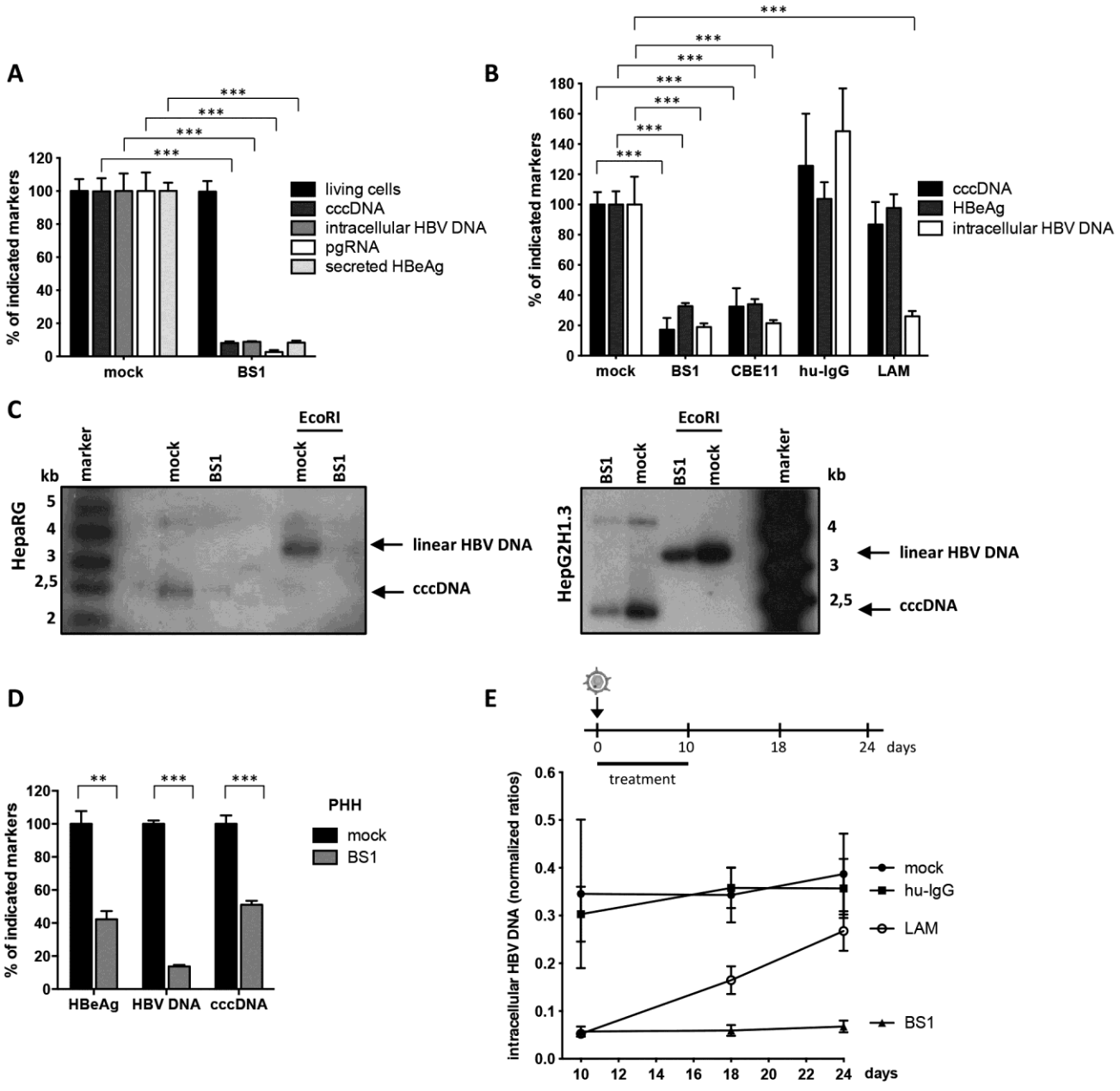

Fig. 2. LTβR-activation inhibits HBV infection and leads to cccDNA degradation in HepaRG cells and PHH. (**A** and **B**) HBV-infected dHepaRG were treated with BS1, CBE11, hu-IgG control or lamivudine (LAM). (A) Treatment started 24h before infection for 12 days or (B) at 18 dpi for 10 days. Levels of the indicated HBV markers as well as cell viability are given relative to untreated controls (mock). (**C**) cccDNA levels were analyzed after 14 days of BS1 treatment by Southern blot in HBV-infected dHepaRG and HBV-replicating HepG2H1.3 cells. Supercoiled cccDNA bands were identified by their expected size and linearization upon *EcoRI* digestion (3,2 kb). (**D**) PHH were infected with HBV and treated with BS1 at 7 dpi for 10 days. Levels of the indicated HBV markers were compared to untreated PHH of the same donor (donor 3) (mock). (**E**) HBV-infected dHepaRG were treated with BS1, hu-IgG control or LAM. Intracellular HBV-DNA was analyzed 8 and 14 days after treatment cessation. Mean values +/− standard deviation of replicates from independent experiments are given; data were analyzed by *t* test. * $p < 0.05$, *** $p < 0.001$.

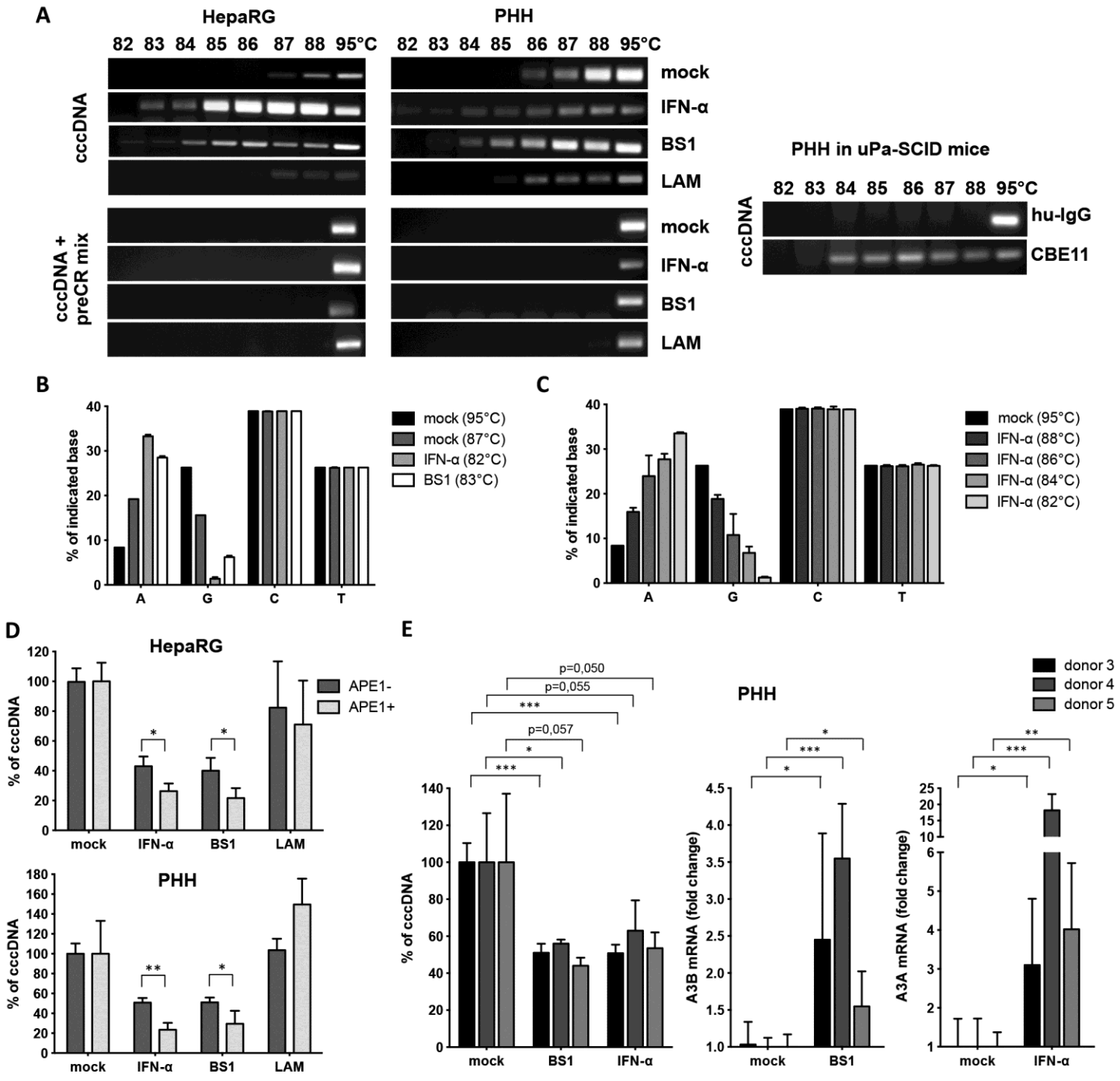

Fig. 3. Deamination and AP-site formation in cccDNA upon IFN-α treatment and LTβR-activation. (**A**) dHepaRG (left) and PHH (middle panel) were infected with HBV and treated with IFN-α, BS1 or LAM. Human chimeric uPA/SCID mice were treated with CBE11 or hu-IgG control (right panel). 3D-PCR analyses were performed on cccDNA left either untreated (upper panels) or treated with a PreCR mix (lower panels). (**B** and **C**) 3D-PCR products from HBV-infected dHepaRG cells treated as indicated (IFN-α, BS1 or mock) were cloned and sequenced and mutations were analyzed. (**D**) Total DNA extracts from HBV-infected cells treated as indicated were digested with APE1, and cccDNA content was compared to mock-treated cells. In (B), (C), and (D), mean values +/− standard deviation of biological triplicates from two independent experiments are given; data were analyzed by *t* test. * $p < 0.05$, ** $p < 0.01$. (**E**) PHH were infected with HBV and treated with BS1 or IFN-α at 7 dpi for 10 days. Levels of the indicated cccDNA as well as A3A and A3B mRNA expression were compared to untreated PHH (mock) of the same donor.

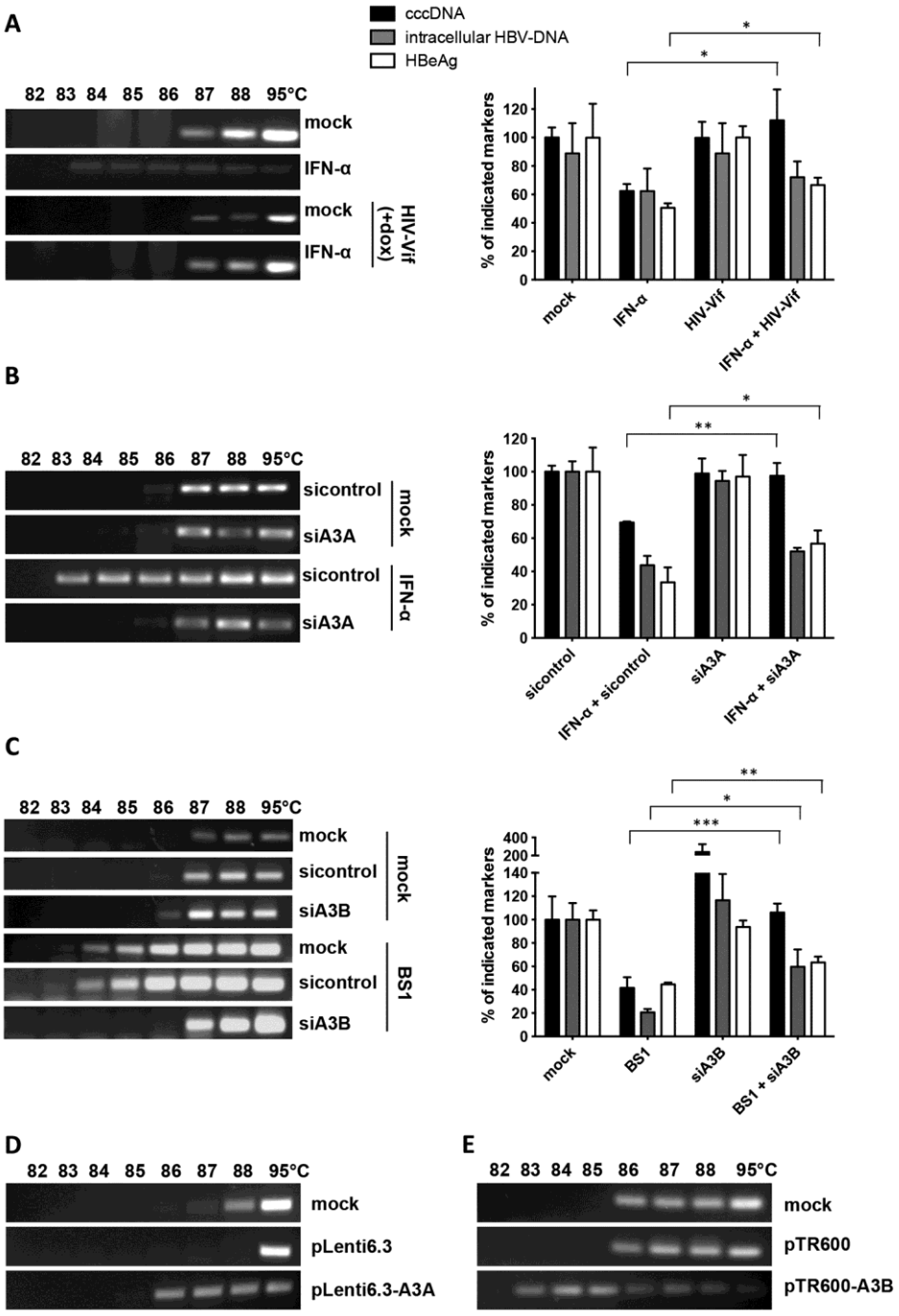

Fig. 4. Analysis of cccDNA deamination and degradation. (**A** to **C**) cccDNA denaturation was analyzed by 3D-PCR (left panels); levels of HBeAg, total intracellular DNA and cccDNA are given relative to mock treated cells (right panels). (A) dHepaRG-tA-Vif cells treated with IFN-α for 10 days with and without doxycycline (dox)-induced HIV-Vif expression. HBV-infected dHepaRG cells treated with (B) IFN-α or (C) BS1 transfected with siRNA against A3A or A3B, respectively, or sequence nonspecific siRNA (sicontrol). Mean values +/− standard deviation of independent replicates and experiments are given; data were analyzed by *t* test. * $p < 0.05$, ** $p < 0.01$ and *** $p < 0.001$. (**D**) cccDNA denaturation analysis by 3D-PCR in HepG2-H1.3 cells overexpressing A3A or (**E**) A3B from lentiviral vector plasmid pLenti6.3 or pTR600, respectively, for 5 days.

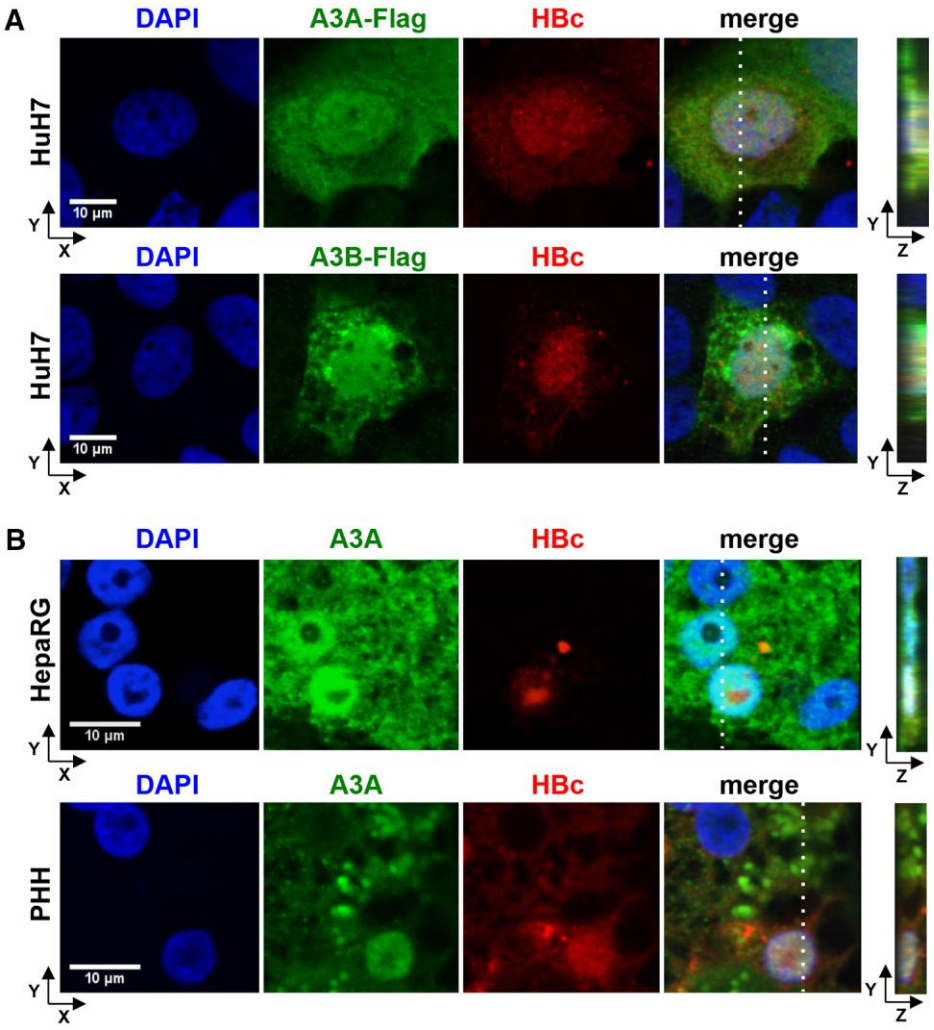

Fig. 5. Co-localization of A3A and A3B with HBV core protein (**HBc**). (**A**) HuH7 cells were co-transfected with an HBV1.1-fold genome and A3A-Flag or A3B-Flag expressing plasmids and stained using DAPI, anti-HBc and anti-FLAG antibodies. (**B**) HBV-infected dHepaRG and PHH were treated with IFN-α at day 7 post infection for 3 days. A3A and HBc were analyzed by immunofluorescence staining. Right panels indicate z stacks taken at the dotted lines.

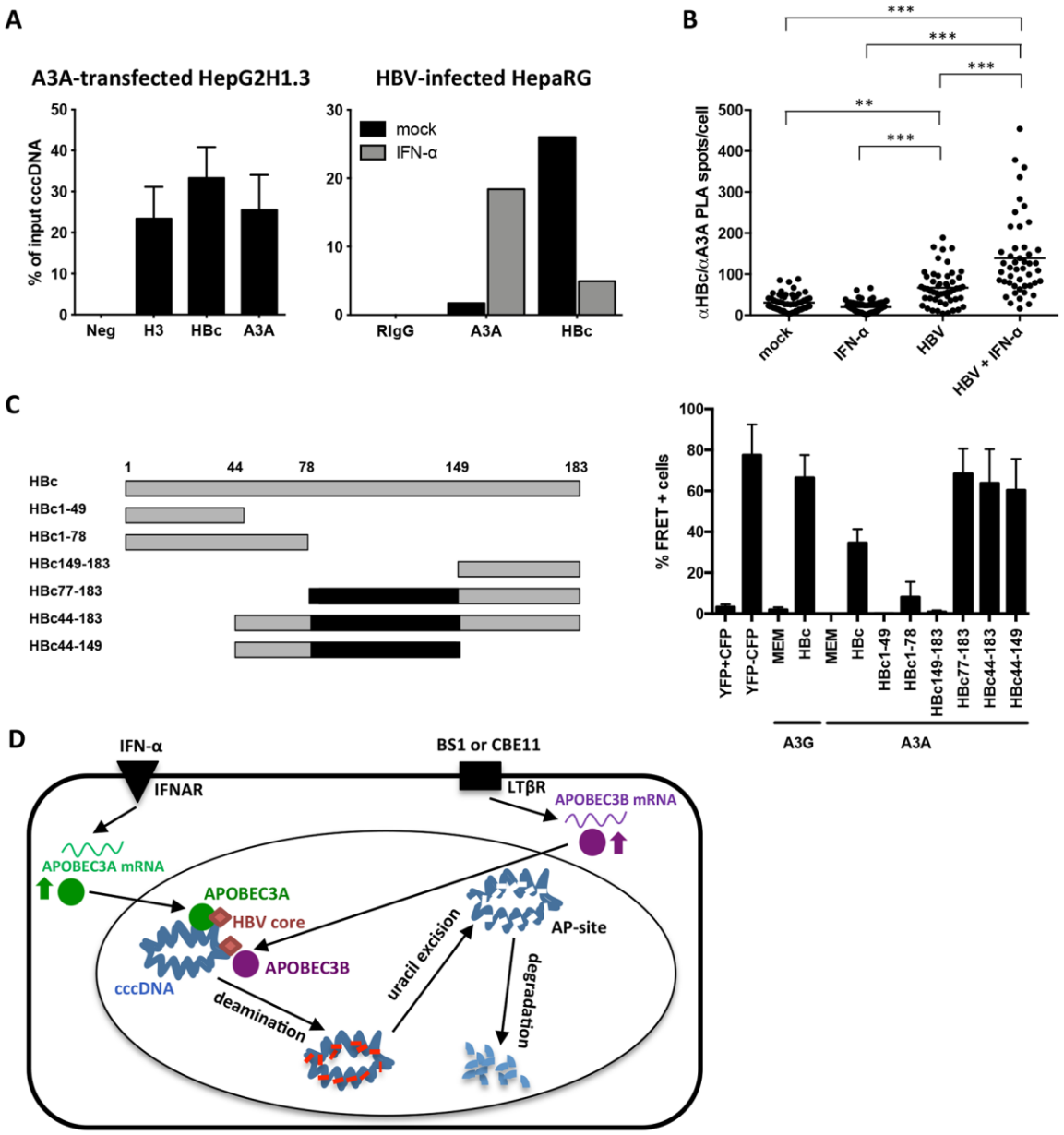

Fig. 6. Interaction of A3A, HBV core protein (HBc) and cccDNA. (**A**) Chromatin immunoprecipitation (ChIP) was performed using lysates of HepG2H1.3 cells transfected with A3A-expressing plasmid, or HBV-infected dHepaRG cells treated with IFN-α for 3 days. IPs using antibodies against histone H3, A3A, HBc and control rabbit IgG (RIgG) were analyzed by qPCR for cccDNA. (**B**) Interaction between HBc and A3A was assessed by proximity ligation assay (PLA) in HBV-infected, IFN-α treated dHepaRG. PLA-spots were quantified in single cells by software-based spot-counting. Data were analyzed by one-way ANOVA. ** $p < 0.01$ and *** $p < 0.001$. (**C**) Serial HBV core-deletion mutants (left panel) were fused to CFP and interaction with A3A-YFP was assessed by FACS-FRET in HuH7.5 hepatoma cells (right panel). Cells cotransfected with CFP and YFP served as controls to exclude false positive FRET and subtract background signals. A CFP-YFP fusion construct was used as positive control. Mean values ± standard deviation of FRET-positive cells from 3-4 independent experiments are given. Black boxes indicate shared regions of HBc mutants giving a FRET signal. (**D**) Model of cccDNA degradation induced by IFN-α treatment or LTβR-activation.

Research Article

SOURCE DATA | TRANSPARENT PROCESS | OPEN ACCESS

EMBO Molecular Medicine

A positive feedback loop between RIP3 and JNK controls non-alcoholic steatohepatitis

Jérémie Gautheron[1,2,†], Mihael Vucur[1,†], Florian Reisinger[3,†], David Vargas Cardenas[1], Christoph Roderburg[1], Christiane Koppe[1], Karina Kreggenwinkel[1], Anne Theres Schneider[1], Matthias Bartneck[1], Ulf Peter Neumann[4], Ali Canbay[5], Helen Louise Reeves[6], Mark Luedde[7], Frank Tacke[1], Christian Trautwein[1], Mathias Heikenwalder[3] & Tom Luedde[1,*]

Abstract

Non-alcoholic fatty liver disease (NAFLD) represents the most common liver disease in Western countries and often progresses to non-alcoholic steatohepatitis (NASH) leading ultimately to liver fibrosis and liver cancer. The occurrence of hepatocyte cell death —so far characterized as hepatocyte apoptosis—represents a fundamental step from benign steatosis toward progressive steatohepatitis. In contrast, the function of RIP3-dependent necroptosis in NASH and NASH-induced fibrosis is currently unknown. We show that RIP3 is upregulated in human NASH and in a dietary mouse model of steatohepatitis. RIP3 mediates liver injury, inflammation, induction of hepatic progenitor cells/activated cholangiocytes, and liver fibrosis through a pathway suppressed by Caspase-8. This function of RIP3 is mediated by a positive feedback loop involving activation of Jun-(N)-terminal Kinase (JNK). Furthermore, RIP3-dependent JNK activation promotes the release of pro-inflammatory mediators like MCP-1, thereby attracting macrophages to the injured liver and further augmenting RIP3-dependent signaling, cell death, and liver fibrosis. Thus, RIP3-dependent necroptosis controls NASH-induced liver fibrosis. This pathway might represent a novel and specific target for pharmacological strategies in patients with NASH.

Keywords biliary ductular reaction; Caspase-8; liver fibrosis; MCP-1; necroptosis

Subject Categories Digestive System; Metabolism

DOI 10.15252/emmm.201403856 | Received 15 January 2014 | Revised 22 May 2014 | Accepted 22 May 2014 | Published online 24 June 2014

EMBO Mol Med (2014) 6: 1062–1074

Introduction

Non-alcoholic fatty liver disease (NAFLD) is the most common chronic liver disease in the Western world (Vernon *et al*, 2011). The term non-alcoholic steatohepatitis (NASH) defines a more aggressive disease entity within the spectrum of NAFLD that is often associated with obesity, type 2 diabetes, and the metabolic syndrome (Schattenberg & Schuppan, 2011). In NASH, advanced fibrosis and cirrhosis are primary determinants of an increased overall and liver-related mortality (Schuppan & Afdhal, 2008; Bhala *et al*, 2011; Poelstra & Schuppan, 2011), underlining that pharmacological inhibition of liver fibrogenesis or induction of fibrosis regression is a fundamental goal in this disease (Schattenberg & Schuppan, 2011). Despite several molecular targets that were addressed in NASH patients in recent clinical trials (Schuppan & Kim, 2013), no effective pharmacological strategy against NASH-induced liver fibrosis has yet entered clinical practice, highlighting the need to identify novel-signaling pathways regulating the transition from NASH to hepatic fibrosis.

One fundamental difference between benign steatosis and progressive steatohepatitis is the occurrence of massive hepatocyte cell death, at present classified as hepatocyte apoptosis (Wree *et al*, 2013). Apoptosis can be triggered by ligation of death receptors like tumor necrosis factor (TNF) receptor by their cognate ligands and represents a highly synchronized procedure depending on activation of aspartate-specific proteases known as caspases (Chakraborty *et al*, 2012). Of these, Caspase-8 represents a key upstream caspase that engages to the death-inducing signaling complex (DISC) via the adaptor molecule FADD (Chakraborty *et al*, 2012). NASH is histologically characterized by hepatocyte apoptosis and varying degrees of fibrosis in the setting of hepatocyte lipid accumulation (Schattenberg & Schuppan, 2011). In line with this observation, previous

1 Department of Gastroenterology, Digestive Diseases and Intensive Care Medicine (Department of Medicine III), University Hospital RWTH Aachen, Aachen, Germany
2 Interdisciplinary Centre for Clinical Research Aachen, University Hospital RWTH Aachen, Aachen, Germany
3 Institute of Virology, Technische Universität München and Helmholtz Zentrum München für Gesundheit und Umwelt (HMGU), Munich, Germany
4 Department of Visceral and Transplantation Surgery, University Hospital RWTH Aachen, Aachen, Germany
5 Department of Gastroenterology and Hepatology, University Hospital, University Duisburg-Essen, Essen, Germany
6 The Liver Group, Department of Medicine, Freeman Hospital, Newcastle-upon-Tyne Hospitals NHS Foundation Trust, Newcastle-upon-Tyne, UK
7 Department of Cardiology and Angiology, University Hospital Kiel, Kiel, Germany
*Corresponding author. Tel: +49 241 80 35609; E-mail: tluedde@ukaachen.de
†These authors contributed equally to this work

functional studies in animal models and clinical studies have focused on the potential role of apoptosis in NASH development (Witek *et al*, 2009; Anstee *et al*, 2010; Ratziu *et al*, 2012; Hatting *et al*, 2013). However, necrosis and necro-inflammation are also histological characteristics of human NASH (Malhi & Gores, 2008; Schattenberg & Schuppan, 2011), suggesting that alternative cell-death forms might play a role in the pathogenesis of this disease. It was recently discovered that necroptosis—programmed necrosis depending on the kinases RIP1 and RIP3—represents an alternative programmed cell-death pathway downstream of the TNF receptor (Cho *et al*, 2009; He *et al*, 2009; Zhang *et al*, 2009). RIP3 mediates necroptosis through activation of mixed lineage kinase domain-like protein (MLKL) (Sun *et al*, 2012). Necroptosis plays a role in the regulation of chronic inflammation in the pancreas, gut, and skin (He *et al*, 2009; Bonnet *et al*, 2011; Welz *et al*, 2011). Moreover, necroptosis is activated in patients with alcoholic liver injury (Roychowdhury *et al*, 2013), but the role of RIP3 in NASH is currently unknown.

To examine the functional role of RIP3 in NASH development, we applied the methionine- and choline-deficient (MCD) diet-induced model of steatohepatitis that mimics important features of human NASH, including the development of steatohepatitis, CYP2E1 overexpression, and increased lipid peroxidation as well as the promotion of NASH toward hepatic fibrosis (Schattenberg *et al*, 2006). In addition, most previous data on the relation between cell death and NASH were gained in this respective model (Csak *et al*, 2011; Hatting *et al*, 2013). We show that RIP3 controls NASH development in a Caspase-8-dependent manner by a pathway involving activation of Jun-(N)-terminal kinase and thus might represent a promising target for future therapeutic strategies in patients with chronic metabolic liver disease.

Results

RIP3 mediates liver injury in MCD-diet-induced NASH

In order to examine the differential functions of RIP3-dependent necroptosis versus Caspase-8-dependent apoptosis in NASH, we generated mice with conditional deletion of *Caspase-8* in liver parenchymal cells (LPC)—hepatocytes and cholangiocytes—(Casp-$8^{LPC\text{-}KO}$), constitutive ablation of *Rip3* in all cells ($RIP3^{-/-}$), and mice with combined conditional and constitutive deletions of Caspase-8 and RIP3, respectively (Casp-$8^{LPC\text{-}KO}$/$RIP3^{-/-}$) (Supplementary Fig S1). These groups of mice were treated for either 2 or 8 weeks with MCD-diet or normal chow as control and were first analyzed for the degree of liver injury. As described previously (Vucur *et al*, 2013), Casp-$8^{LPC\text{-}KO}$ mice showed a moderate increase in serum levels of aspartate aminotransferase (AST) and glutamate dehydrogenase (GLDH) but not alanine aminotransferase (ALT) in mice fed with normal chow (Fig 1A). After 2 and 8 weeks of MCD-diet, serum levels of AST, ALT, and GLDH were increased in all groups compared to the respective control animals on normal chow (Fig 1A). Strikingly, enzyme levels were more increased in Casp-$8^{LPC\text{-}KO}$ animals at both time points compared to all other experimental groups (Fig 1A). In contrast, after 8 weeks of MCD-diet, all liver enzymes were reduced in $RIP3^{-/-}$ mice and Casp-$8^{LPC\text{-}KO}$/$RIP3^{-/-}$ animals compared to WT mice (Fig 1A). Together, these findings indicate that RIP3 mediates liver injury upon MCD-diet feeding in mice.

Based on this observation, we further examined intrahepatic expression levels of RIP3 in this model. It was previously shown that necroptotic cell death in the liver or pancreas is associated with an increase in RIP3 protein levels (He *et al*, 2009; Vucur *et al*, 2013). In line, 2 weeks of MCD-diet feeding led to a strong induction of RIP3 protein levels in Western blot analysis (Fig 1B). Of note, this induction of RIP3 expression was even augmented in Casp-$8^{LPC\text{-}KO}$ animals with abrogated Caspase-8-expression (Fig 1B), while—as expected—no RIP3 expression was detected in Casp-$8^{LPC\text{-}KO}$/$RIP3^{-/-}$ and $RIP3^{-/-}$ livers (Fig 1B). Immunohistological analyses of livers of mice after 8 weeks of MCD-diet feeding confirmed high expression levels of RIP3 in WT mice and even stronger expression in Casp-$8^{LPC\text{-}KO}$ livers (Fig 1C and D). In contrast, immunohistological staining for cleaved Caspase-3 revealed similarly low levels of cleaved Casp-3^{+} hepatocytes in all groups (Supplementary Fig S2). The fact that cleavage of Caspase-3 was also detected in mouse livers with conditional deletion of Caspase-8 indicated that apoptosis in this model can be activated by Caspase-8-independent signaling cascades, e.g. via the mitochondrial pathway (Estaquier *et al*, 2012). In line with this finding, it was previously shown that in NASH, fatty acid accumulation enhances β-oxidation and mitochondrial electron overflow, thus triggering cell death (Seifert *et al*, 2010). Finally, compensatory proliferation of parenchymal liver cells measured by staining for Ki67 correlated with overexpression of RIP3 and was most prominent in Casp-$8^{LPC\text{-}KO}$ mice, while Casp-$8^{LPC\text{-}KO}$/$RIP3^{-/-}$ and $RIP3^{-/-}$ mice showed significantly less proliferating cells than MCD-diet-fed WT mice (Fig 1C and D). Together, these observations demonstrate that activation of RIP3 represents a fundamental step in the MCD-diet NASH model mediating liver injury. Moreover, a crucial function of Caspase-8 in this model is to counterbalance RIP3-dependent liver injury.

RIP3 controls the transition from NASH to liver fibrosis in a Caspase-8 dependent manner

Based on the differential functions of RIP3 and Caspase-8 in controlling liver injury in response to MCD-diet feeding, we next tested their influence on the pathogenesis of steatosis and NASH-induced liver fibrosis. Hematoxylin and eosin (H&E) staining revealed minimal steatosis in all groups of mice after 8 weeks of normal chow feeding (Fig 2A). Of note, mice with combined deletions of *Caspase-8* and *Rip3* (Casp-$8^{LPC\text{-}KO}$/$RIP3^{-/-}$ mice) on normal chow already displayed increased triglyceride (TG) levels compared to the other experimental groups (Fig 2B). Eight weeks of MCD-diet feeding triggered hepatic fat accumulation above control levels in all groups (Fig 2A and B). In line with the control groups, MCD-diet feeding led to significantly higher intrahepatic TG contents in Casp-$8^{LPC\text{-}KO}$/$RIP3^{-/-}$ mice compared to all other experimental groups, suggesting that inactivation of both programmed cell-death pathways augments hepatic fat accumulation in the MCD-diet model.

The presence of apoptosis in NAFLD patients has been taken as a predictor to develop progressive fibrosis (Witek *et al*, 2009; Anstee *et al*, 2010; Ratziu *et al*, 2012). In contrast, while necrosis is also found as histological characteristic in human NASH (Malhi & Gores, 2008; Schattenberg & Schuppan, 2011), the functional relation to fibrosis is presently poorly defined. We therefore investigated

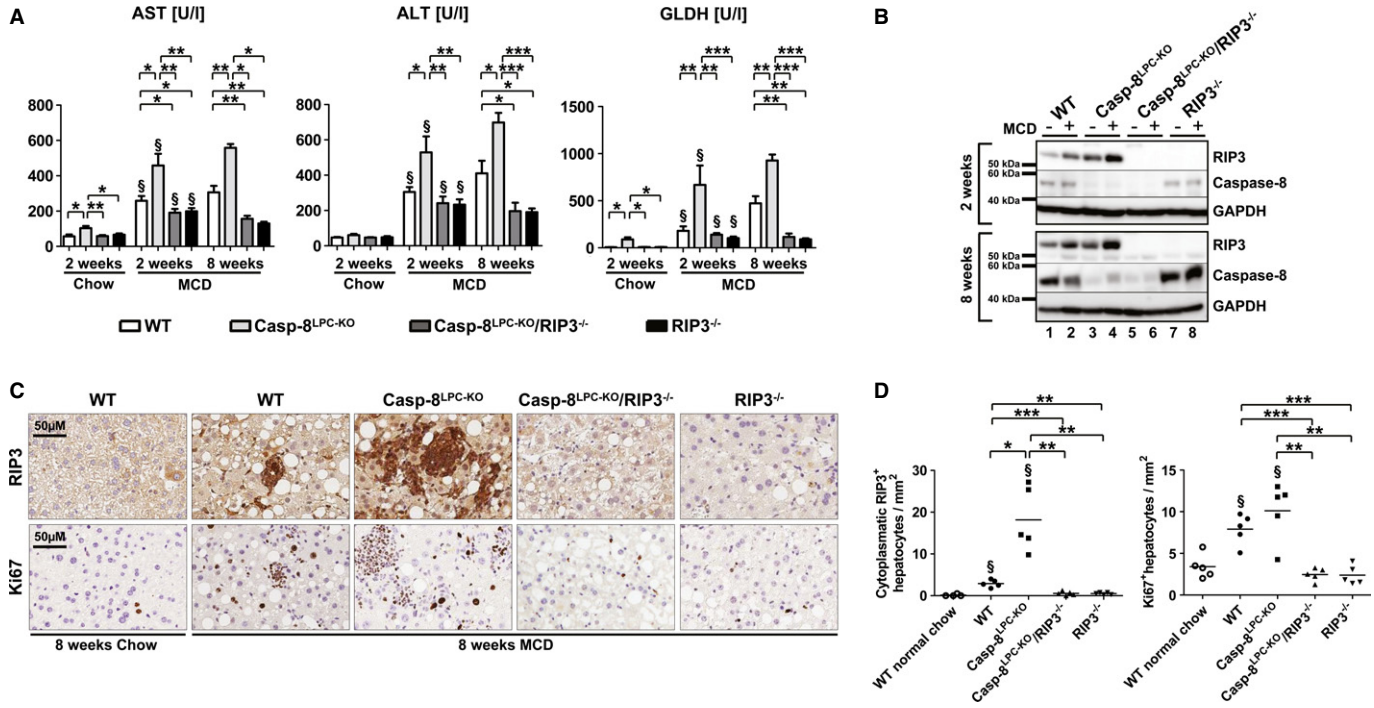

Figure 1. RIP3 is induced in murine livers following MCD-diet feeding and promotes hepatic injury in Caspase-8-deficient livers.

A Analysis of serum levels of AST, ALT, and GLDH after 2 and 8 weeks of MCD-diet or 2 weeks of normal chow. Results are shown as mean ± SEM, n = 6 (2 weeks normal chow) n = 12 (2 weeks MCD), and n = 5 (8 weeks MCD). §indicates that serum levels are significantly increased from basal level.

B Western blots analysis on liver extracts from MCD-diet-fed (2- and 8-weeks) animals and control mice with antibodies against RIP3, Caspase-8, and GAPDH as a loading control.

C Immunohistochemical (RIP3, Ki67) analysis on representative liver sections from the indicated mice fed for 8 weeks with MCD-diet.

D Statistical analysis of RIP3$^+$ and Ki67$^+$ hepatocytes. Results are shown as mean, n = 5. §indicates that RIP3$^+$ and Ki67$^+$ cells are significantly increased from basal WT group.

Data information: The exact P-values of each experiment and specific tests used are provided in the Supplementary Table S1.
Source data is available online for this figure.

the correlation between the occurrence of liver fibrosis and the activation of necroptosis in the MCD-diet model. Sirius red staining and qRT-PCR analysis for Collagen-1α1 expression after 2 weeks (Supplementary Fig S3) and 8 weeks of MCD-diet feeding (Fig 2C and D) revealed no significant liver fibrosis at the early time points and moderate fibrosis at the later time point in WT animals. In contrast, correlating with induction of RIP3 expression levels, Casp-8$^{LPC\text{-}KO}$ animals displayed strongly increased intrahepatic fibrosis at both time points, whereas hepatic fibrogenesis was strongly reduced in RIP3$^{-/-}$ single-mutant mice and Casp-8$^{LPC\text{-}KO}$/RIP3$^{-/-}$ double-mutant animals compared to WT and Casp-8$^{LPC\text{-}KO}$ mice (Fig 2C and D; Supplementary Fig S3). These data indicate that RIP3-dependent necroptosis promotes NASH-induced liver fibrosis. Moreover, activation of Caspase-8 inhibits RIP3-dependent liver fibrosis in NASH.

We have further addressed the question whether the previously shown pro-fibrogenic effect of RIP3 is specific for liver fibrosis in response to hepatic steatosis or represents a general principle in hepatic fibrogenesis. To test this, we used an alternative, very well-established model of experimental liver fibrosis relying on repetitive injections of the substance CCl_4 into mice and applied this model for 2 and 6 weeks to WT, Casp-8$^{LPC\text{-}KO}$, Casp-8$^{LPC\text{-}KO}$/RIP3$^{-/-}$, and RIP3$^{-/-}$ mice. This treatment led to the development of areas of parenchymal cell necrosis in Casp-8$^{LPC\text{-}KO}$ mice (Supplementary Fig S4). However, it did not result in a significantly increased degree of fibrosis between the groups of mice in quantitative analysis of Sirius Red staining (Supplementary Fig S4), supporting the hypothesis that RIP3 might represent a specific target in fatty liver-related liver fibrosis.

RIP3-activation in NASH promotes inflammation and hepatic recruitment of monocytes/macrophages

Inflammation represents a fundamental factor linking liver injury with hepatic fibrosis (Tacke *et al*, 2008; Schuppan & Kim, 2013). We therefore examined the association between liver fibrosis and inflammation in response to necroptosis upon MCD-diet feeding. As assessed by immunohistochemistry, 8 weeks of MCD-diet feeding increased the number of infiltrating CD45$^+$ immune cells in all experimental groups of mice compared to WT mice fed with normal chow. Of note, inflammation was even higher in Casp-8$^{LPC\text{-}KO}$ mice and correlated with the strong expression of RIP3 as the number of CD45$^+$ immune cells was reduced to WT levels in Casp-8$^{LPC\text{-}KO}$/RIP3$^{-/-}$ mice and RIP3$^{-/-}$ animals (Fig 3A and B). We next investigated the impact of infiltrating monocytes, which play a pro-fibrogenic role in different experimental models of liver fibrosis as well as human liver disease (Zimmermann & Tacke, 2011). As

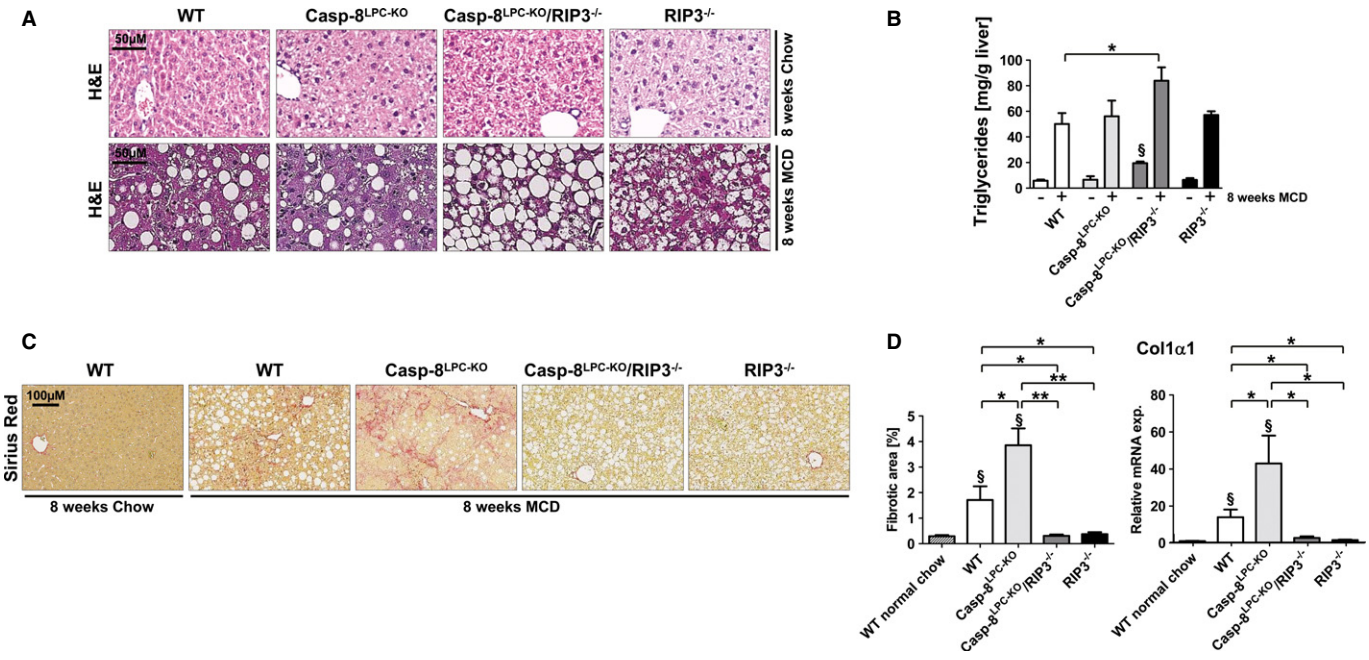

Figure 2. RIP3-dependent necroptosis promotes NASH-induced liver fibrosis and inflammation.

A Representative H&E staining of liver slides from 16-week-old WT, Casp-8^{LPC-KO}, Casp-8^{LPC-KO}/RIP3$^{-/-}$, and RIP3$^{-/-}$ mice fed for 8 weeks with normal chow (upper panel) or MCD-diet (lower panel).

B Intrahepatic triglycerides levels in WT, Casp-8^{LPC-KO}, Casp-8^{LPC-KO}/RIP3$^{-/-}$, and RIP3$^{-/-}$ fed for 8 weeks with MCD-diet or control chow, results are shown as mean ± SEM, n = 5 per group. §indicates that triglycerides are significantly increased from Casp-8^{LPC-KO}/RIP3$^{-/-}$ to the others groups of mice fed with normal chow.

C Representative Sirius Red stainings of liver slides from 8-week-old female WT, Casp-8^{LPC-KO}, Casp-8^{LPC-KO}/RIP3$^{-/-}$, and RIP3$^{-/-}$ mice fed for 8 weeks with MCD-diet.

D Left: statistical quantification of light polarized Sirius Red pictures, results are shown as mean, n = 5 per group. Right: *Col1α1* mRNA levels in these livers were determined by qRT-PCR. Values were calculated relative to WT mice fed with normal show, and β-catenin was used as an internal standard, n = 5 per group. §indicates that values are significantly increased from basal level. Error bars represent SEM.

Data information: The exact *P*-values of each experiment and specific tests used are provided in the Supplementary Table S1.

demonstrated by immunohistochemistry, 8 weeks of MCD-diet feeding significantly increased the number of inflammatory foci containing monocytes in WT mice and even more in Casp-8^{LPC-KO} livers (Fig 3A and B). In contrast, the emergence of these foci was completely abrogated by the deletion of *Rip3* as seen in Casp-8^{LPC-KO}/RIP3$^{-/-}$ and RIP3$^{-/-}$ animals (Fig 3A and B). The activation role of RIP3 in the initiation of inflammation was confirmed by FACS analyses in livers of mice fed for 2 weeks with MCD-diet, revealing significantly lower numbers of F4/80^{+} cells in Casp-8^{LPC-KO}/RIP3$^{-/-}$ mice and RIP3$^{-/-}$ animals than seen in Casp-8^{LPC-KO} mice (Supplementary Fig S5). Taken together, these results indicate that RIP3-dependent inflammation and recruitment of monocytes represents an important mechanism for promoting hepatic fibrosis in mice fed with MCD-diet.

We further tested which inflammatory mediators might be involved in linking necroptosis of parenchymal liver cells with monocyte recruitment and increased hepatic fibrosis. Interestingly, while many inflammatory cytokines and chemokines such as Interleukin (IL)-1α, IL-1β, IL-6, CCL1 and CCL8, and CCL17 did not show a clearly distinct regulation between WT and Casp-8^{LPC-KO} mice fed for 2 weeks with MCD-diet on mRNA level (Supplementary Fig S6), qRT-PCR analysis and FACS-based microbeads fluorescence assay on liver extracts from the different experimental groups revealed a strong increase in intrahepatic levels of MCP-1 (CCL2) in Casp-8^{LPC-KO} mice compared to WT mice at that time point (Fig 3C). In contrast, MCP-1-levels were markedly reduced in Casp-8^{LPC-KO}/RIP3$^{-/-}$, and RIP3$^{-/-}$ mice (Fig 3C), which was confirmed after 8 weeks of MCD-diet feeding (Fig 3D). Given previous reports on the essential functional role of the MCP-1/CCR2 axis in monocyte recruitment and liver fibrosis (Seki *et al*, 2009; Baeck *et al*, 2012), these data indicate that MCP-1 represents one important factor linking RIP3-dependent necroptosis in NASH with liver fibrosis. Further analyses revealed increased TNF levels in WT and Casp-8^{LPC-KO} mice after 8 weeks of MCD feeding, as well as a strong correlation between RIP3 expression levels and levels of TGF-β2 (Supplementary Fig S7), which is in line with a recent report showing a prominent role of TGF-β in the regulation of NASH-associated hepatocyte cell death (Yang *et al*, 2014).

The *alfp*-cre line used to generate Casp-8^{LPC-KO} animals mediates genetic excision exclusively in liver parenchymal cells (LPC) (Kellendonk *et al*, 2000), arguing for a specific function of RIP3 in this respective cell compartment in driving liver injury and subsequent fibrogenesis in Casp-8^{LPC-KO} mice upon MCD-diet feeding. However, in order to exclude that constitutive deletion of *Rip3* in Casp-8^{LPC-KO}/RIP3$^{-/-}$ mice resulted in general signaling defects of immune cells as a reason for the rescue of these double-mutant animals from hepatic fibrosis, we isolated and cultured monocytes from murine bone marrow of WT, Casp-8^{LPC-KO}, Casp-8^{LPC-KO}/RIP3$^{-/-}$, and RIP3$^{-/-}$ mice. Stimulation with lipopolysaccharide (LPS) resulted in very similar patterns of chemokine and cytokine expression

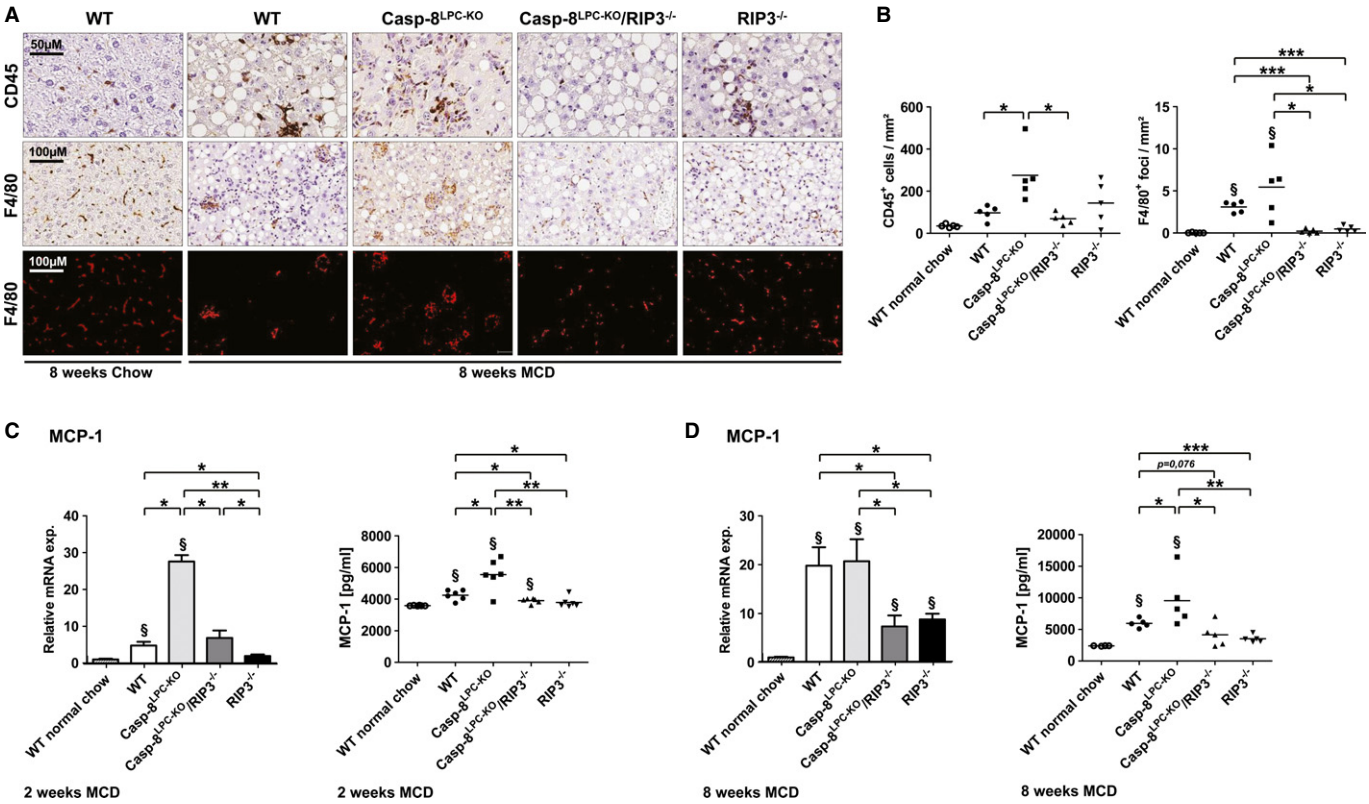

Figure 3. RIP3-dependent necroptosis promotes NASH-induced liver fibrosis through MCP-1 release.

A Immunohistochemical analysis of CD45 (upper panel) and F4/80 (middle panel) on representative liver sections from the indicated mice fed for 8-weeks with MCD-diet or normal chow. The lower panel shows deconvoluted pictures from the F4/80 stains.

B Statistical analysis of $CD45^+$ and $F4/80^+$ cells. Results are shown as mean, $n = 5$. §indicates that $F4/80^+$ foci are significantly increased from basal WT group.

C Left: *MCP-1* mRNA levels were assessed by RT-PCR after 2 weeks of MCD-diet feeding. Values were calculated relative to WT mice fed with normal chow, and β-catenin was used as an internal standard, $n = 6$ per group. Right: FACS-based microbeads fluorescence assay for MCP-1 expression in liver protein homogenates. Results are shown as mean, $n = 6$ per group. § shows that values are significantly increased from basal level. Error bars indicate SEM.

D Left: *MCP-1* mRNA levels were assessed by RT-PCR after 8 weeks of MCD-diet feeding. Values were calculated relative to WT mice fed with normal chow, and β-catenin was used as an internal standard, $n = 5$ per group. §indicates that values are significantly increased from basal level. Error bars represent SEM. Right: FACS-based microbeads fluorescence assay for MCP-1 expression in liver protein homogenates. Results are shown as mean, $n = 5$ per group. §shows that values are significantly increased from basal level. Error bars indicate SEM.

Data information: The exact *P*-values of each experiment and specific tests used are provided in the Supplementary Table S1.

(Supplementary Fig S8), suggesting that the functional activity of macrophages is not abrogated in $RIP3^{-/-}$ and Casp-$8^{LPC\text{-}KO}$/$RIP3^{-/-}$ mice.

RIP3-expression in murine and human NASH livers

Most liver diseases and also NASH—once advanced—develop into a portal fibrosis with proliferation of biliary progenitors and activated cholangiocytes, which typically form small clusters and non-functional biliary structures (Richardson *et al*, 2007; Schuppan & Kim, 2013). We therefore tested the relation between RIP3-dependent necroptosis and a biliary ductular reaction in the MCD-diet model. Strikingly, immunostaining for Cytokeratin (CK)-19 revealed a strong expansion of clusters of biliary cells / progenitor cells in livers of Casp-$8^{LPC\text{-}KO}$ mice, which was not seen in combined or single RIP3-mutants (Fig 4A and B). Of note, immunostaining for RIP3 and specific analysis in areas of ductular reactions revealed that many cholangiocytes expressed even higher levels of RIP3 than the surrounding hepatocytes (Fig 4C).

It was previously demonstrated in liver samples from human NASH patients that RIP3 is strongly upregulated on RNA level to more than 40-fold compared to healthy controls (Csak *et al*, 2011). In order to provide further evidence for a function of RIP3 in human NASH, we examined RIP3 expression in livers of NASH patients (as demonstrated histologically by increased NAS score, see Fig 5A) by Western blot and immunohistochemistry. On protein levels, RIP3 was strongly upregulated in NASH patients compared to controls (Fig. 5B). Immunostaining of NASH patient livers revealed strong RIP3 expression in hepatocytes, often neighboring areas of fat deposition (Fig 5C). Of note, RIP3 often showed a granule-like staining pattern (Fig 5C), similar to previous imaging results in MEF cells with activated RIP3 signaling depicting clustering of RIP1/RIP3 (Li *et al*, 2012). Finally, RIP3 was often overexpressed in cells morphologically reflecting cholangiocytes / bile duct cells (Fig 5C), similar to our previous findings in mouse livers. These findings support the hypothesis that also in human NASH, liver cells are sensitized to necroptotic cell death. Moreover, in murine as well as human

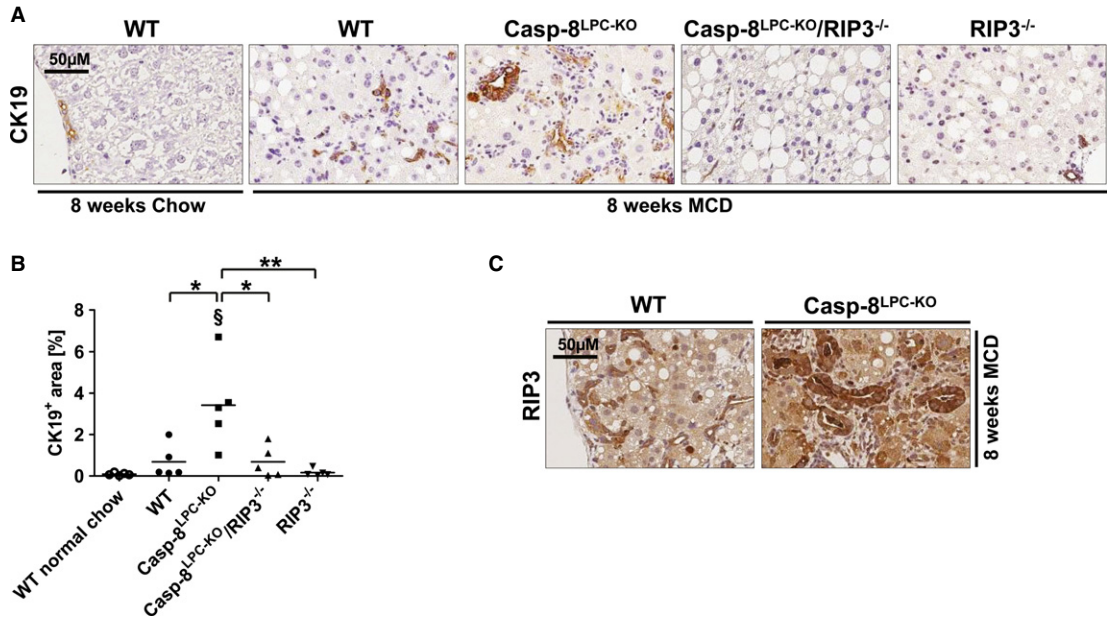

Figure 4. RIP3-dependent necroptosis mediates expansion of progenitor cells that expressed high levels of RIP3.

A Immunohistochemical (CK19) analysis on representative liver sections from the indicated mice fed for 8-weeks with MCD-diet.

B Statistical analysis of $CK19^+$ cells. Results are shown as mean, $n = 5$. §shows that $CK19^+$ cells are significantly increased from basal WT group.

C Immunohistochemical (RIP3) analysis on representative liver sections from WT and Casp-$8^{LPC\text{-}KO}$ mice fed for 8 weeks with MCD-diet.

Data information: The exact *P*-values of each experiment and specific tests used are provided in the Supplementary Table S1.

NASH, biliary cells express high levels of RIP3, pointing toward cell-type specific functions of this pathway in the liver.

A positive feedback loop involving activation of Jun-(N)-terminal Kinase (JNK) mediates RIP3-dependent inflammation and hepatic fibrosis upon MCD feeding

We finally aimed at further evaluating which potential downstream pathway mediated RIP3-dependent liver injury, inflammation, and fibrosis upon MCD feeding. To test this, we first examined the activation status of stress-related signaling cascades in the different knockout models after 2 weeks of MCD-diet feeding. As shown by Western blot analysis using phospho-specific antibodies, increased activation of RIP3 and fibrosis upon MCD-diet feeding correlated with increased phosphorylation and activation of the kinase Jun-(N)-terminal Kinase (JNK) in WT and even more in Casp-$8^{LPC\text{-}KO}$ livers (Fig 6A), which was abolished in Casp-$8^{LPC\text{-}KO}$/$RIP3^{-/-}$ and $RIP3^{-/-}$ mice (Fig 6A). In contrast, activation of AKT and p38α did not show a clear association with the activation status of RIP3 (Fig 6A).

Given previous reports on the crucial function of JNK in the mediation of NASH fibrosis (Schattenberg *et al*, 2006), we further examined the functional role of JNK in RIP3-dependent NASH fibrosis and treated groups of Casp-$8^{LPC\text{-}KO}$ mice with repetitive injections of the well-established JNK-inhibitor SP600125 or vehicle substance as control in parallel to MCD-diet feeding. This treatment resulted in effective inhibition of phosphorylation of the JNK-target c-Jun (Fig 6B). JNK inhibition significantly ameliorated liver injury as shown by decreased levels of serum aminotransferases and GLDH in SP600125-treated mice (Fig 6C). In line, JNK inhibition ameliorated liver fibrosis as shown by Sirius Red staining and qRT-PCR analysis for expression of Collagen-Iα1 (Fig 6D). Moreover, decreased fibrosis in these livers went along with reduced intrahepatic numbers of $CD45^+$ and $F4/80^+$ cells (Fig 6E), correlating with reduced levels of MCP-1 (Supplementary Fig S9). Interestingly, immunostaining and Western blot analysis revealed that inhibition of JNK during MCD-diet feeding significantly reduced expression levels of RIP3 in parenchymal liver cells (Fig 6F and G). To further confirm a mutual interaction between RIP3 and JNK signaling, we used L929 cells and confirmed that these cells undergo necroptosis upon stimulation with the pan-Caspase-inhibitor zVAD (Supplementary Fig S10). Of note, additional treatment with the necroptosis inhibitor Nec-1 (Degterev *et al*, 2013) and also with SP600125 abolished zVAD-induced cell death. Moreover, JNK inhibition was associated with reduced RIP3 expression levels (Supplementary Fig S10). These data suggest that activation of JNK in LPC and probably non-parenchymal cells (NPC) further augments hepatic RIP3 signaling in terms of a positive feedback loop.

Discussion

For years, the term apoptosis, describing a form of cell death depending on the activation of caspases, was used synonymously for programmed cell death (Najimi *et al*, 2009). Apoptotic death of hepatocytes is a common feature of non-alcoholic steatohepatitis, and it was shown that both extrinsic and intrinsic apoptotic pathways are involved in NASH-induced hepatocyte death (Feldstein *et al*, 2003; Feldstein & Gores, 2005). Apoptosis has been considered as a driving force of NASH-induced liver fibrosis

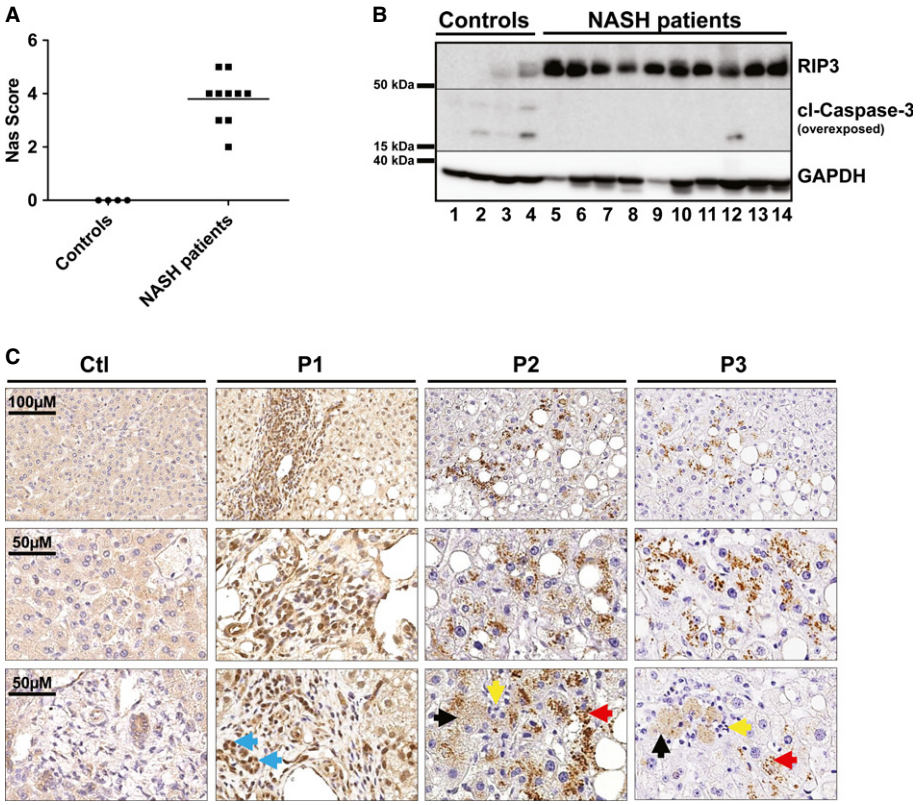

Figure 5. RIP3 is overexpressed in livers of human NASH patients.

A Western blot analysis of RIP3 in control livers (n = 4) and human NASH patients (n = 10), using antibodies against RIP3, cleaved Caspase-3, and GAPDH as a loading control.

B NAS scores of control livers and human NASH samples, corresponding to the Western blot analysis for RIP3.

C Immunostaining analyses of RIP3 in control livers and human NASH patients (P1, P2, P3) (blue arrows indicate progenitor/biliary cells, black arrows indicate necrotic hepatocytes, red arrows show clusters of RIP3 in hepatocytes, and yellow arrows indicate inflammatory cells grouped around dying hepatocytes). Pictures are representative for 27 samples examined.

Source data are available online for this figure.

(Chakraborty *et al*, 2012), as it promotes activation of hepatic stellate cells to hepatic myofibroblasts, promoting deposition of extracellular matrix and scar formation in the liver (Chakraborty *et al*, 2012). Biomarkers of apoptosis like Cytokeratin-18 are strongly increased in NASH patients and distinguish between simple steatosis and NASH (Wieckowska *et al*, 2006; Younossi *et al*, 2008). Finally, the paradigmatic concept of apoptosis in NASH fibrosis has led to translational approaches into clinical studies, testing the use of apoptosis inhibitors in NASH patients (Ratziu *et al*, 2012). Recently, however, it became evident that next to apoptosis, "necroptosis" represents an alternative programmed cell-death pathway (Han *et al*, 2011). Here, we demonstrate for the first time that RIP3-dependent necroptosis represents an important regulatory pathway driving the transition from NAFLD to NASH and subsequent liver fibrosis. Therefore, this pathway might represent a promising novel target for therapeutic strategies in NASH. Moreover, in contrast to previous assumptions (Hatting *et al*, 2013), our findings indicate that the main function of Caspase-8 in the MCD-NASH model is to counterbalance the deleterious hyperactivation of RIP3-dependent necroptosis, underlining the mutual inhibitory functions of RIP3 and Caspase-8 that were previously demonstrated, for example in embryonic development (Kaiser *et al*, 2011) and skin homeostasis (Weinlich *et al*, 2013).

The relevance of apoptosis for NASH progression is supported by several studies. As such, it was clearly demonstrated that usage of the pan-Caspase-inhibitor VX-166 significantly reduced liver injury and liver fibrosis in MCD-diet-fed db/db mice (Witek *et al*, 2009). However, pan-caspase inhibitors inhibit numerous caspases including the downstream executioner caspases. In addition, chemical pan-caspase inhibitors act also on Caspase-1, which mediates proteolytic cleavage of Interleukin molecules including IL-1β (Chang & Yang, 2000; Das *et al*, 2009). Given recent data that specific inhibition of Caspase-1 inhibits NASH fibrosis (Dixon *et al*, 2013), it is possible that targeting of this respective pathway might also contribute to the beneficial effects of pan-caspase inhibitors in NASH fibrosis. Moreover, our finding that also in *Caspase-8*-deficient livers apoptosis of hepatocytes is detected on a low level upon MCD-diet feeding suggests that Caspase-8-independent apoptosis are primarily activated in the MCD-diet model, which is supported by the fact that Casp-8$^{LPC\text{-}KO}$/RIP3$^{-/-}$ mice still showed significant liver injury in this respective model. Taken together, our present study together with previous findings indicate that both programmed cell-death

pathways—(Caspase-8-independent) apoptosis and necroptosis—are involved in the pathogenesis of NASH and NASH-induced liver fibrosis. Of note, the degree of steatosis in our different genetically modified mouse models did not strictly correlate with the extent of liver injury upon MCD-diet feeding. Instead, blockage of both cell-death pathways (necroptosis and Caspase-8-dependent apoptosis) in Casp-$8^{LPC\text{-}KO}$/$RIP3^{-/-}$ mice resulted in an increase in intrahepatic fat accumulation in this model compared with WT or single-mutant animals, suggesting that absence of these two programmed cell-death pathways might increase the tolerance of hepatocytes to store lipids without undergoing cell death. Alternatively, given that multiple molecular interactions between programmed cell-death pathways and autophagy have been suggested (Pattingre *et al*, 2005; Yousefi *et al*, 2006), simultaneous inhibition of Caspase-8-dependent apoptosis and necroptosis might alter the activity of cellular pathways controlling lipolysis in hepatocytes (Liu & Czaja, 2013).

Our present findings diverge from a previous publication showing reduced liver damage in the MCD-diet model upon Caspase-8-deletion in hepatocytes (Hatting *et al*, 2013). It is important to note that in our study, we used the alfp-cre line (Kellendonk *et al*, 2000) that mediates highly efficient deletion of floxed genes at an early developmental time point in all parenchymal liver cells including cholangiocytes and progenitor cells, while in contrast, in the previous study, the albumin-cre (alb-cre) line was used (Postic *et al*, 1999). Of note, comparison of RIP3-expression levels between alfp-cre/Caspase-8Fl and alb-cre/Caspase-8Fl confirmed high RIP3 expression upon alfp-cre-mediated Caspase-8 deletion (Supplementary Fig S11), which is in line with previous reports on Caspase-8 deletion in other organs like skin (Weinlich *et al*, 2013). In contrast, we did not detect RIP3 upregulation upon albumin-cre-mediated deletion, further supporting the association between RIP3 expression levels and necroptotic liver injury.

In our experiments, we identified the stress-activated kinase JNK as a prominent mediator of RIP3-dependent liver injury and fibrogenesis in the MCD-diet model. Moreover, we show that mutual interactions exist between JNK- and RIP3-activation, as chemical inhibition of JNK not only ameliorated liver injury and fibrosis downstream of RIP3, but also led to reduced expression levels of RIP3 in liver parenchymal cells (LPC). Importantly, it is presently not clear whether the striking effect of chemical JNK inhibition in our model was mediated through JNK inhibition in hepatocytes or rather in non-parenchymal liver cells (NPLC). Previous data using conditional JNK-knockout mice in the Concanavalin-A model of hepatitis suggested that JNK activation in NPLC but not in LPC represents a major control mechanism in the regulation of hepatitis (Das *et al*, 2009). Hence, it is possible that JNK activation in LPC promotes RIP3-dependent liver injury through generation of inflammatory cytokines, which in turn augments RIP3 expression and activation in LPC. However, our experiments in L929 cells suggest that a cell-autonomous or intercellular feedback loop exists in hepatocytes between RIP3- and JNK-signaling. Further experiments with conditional JNK-knockout mice are needed to functionally clarify the cell-specific relation between RIP3 and JNK *in vivo*.

Another prominent finding in our study was the strong, RIP3-dependent induction of biliary cells in the MCD-diet model. Activated cholangiocytes are related, if not identical to biliary progenitor cells (Schuppan & Kim, 2013). These cells can proliferate in response to hepatocyte growth arrest or cell death and were shown to secrete factors that attract and activate hepatic stellate cells for ECM deposition (Richardson *et al*, 2007; Schuppan & Kim, 2013). Moreover, biliary cells were previously suggested to be more resistant to oxidative stress and cell death than hepatocytes (Richardson *et al*, 2007). Thus, their expansion in Casp-$8^{LPC\text{-}KO}$ mice might reflect a biliary regenerative response in a context of necroptotic hepatocytes, but might also represent a functional amplification loop in the mediation of RIP3-dependent liver fibrosis upon NASH. Interestingly, our findings indicated that biliary cells seemed to express high levels of RIP3 compared to hepatocytes, a finding currently lacking a functional explanation. It is possible that, given their putative resistance to cell death (Schuppan & Kim, 2013), biliary or precursor cells might tolerate higher levels of RIP3 in the absence of functional Caspase-8 before undergoing cell death. Future experiments with bile duct-specific cre-lines could also reveal a previously unrecognized role of RIP3 or Caspase-8 in biliary homeostasis, regeneration, or the intercellular communication between biliary cells and hepatocytes.

We have recently shown that Caspase-8-dependent apoptosis but not RIP3-dependent necroptosis promoted liver fibrosis and hepatocarcinogenesis in a model of liver injury caused by conditional deletion of the kinase TGF-β-activated Kinase-1 (*Tak1*) in parenchymal liver cells (Vucur *et al*, 2013). In this light, our present findings showing a protective function of Caspase-8 and an injury-promoting role of RIP3 are opposing their roles in the TAK1 model, indicating that activation modes and outcomes of distinct programmed cell death-forms depend on the initiating stimulus and pathogenic context. Given that chemical apoptosis inhibitors have already been tested in clinical studies in patients with NASH (Ratziu *et al*, 2012), pharmacological targeting of the necroptosis pathway might potentially have additive beneficial effects in a combinatory approach together with apoptosis inhibitors that do not specifically target Caspase-8 in these patients. In addition, previous studies showed that serum parameters reflecting activation of apoptosis might serve as biomarkers in NASH (Chakraborty *et al*, 2012). Therefore, enhanced activation of necroptosis could serve as an indicator for more progressive liver disease, which should be evaluated in future prospective studies.

Materials and Methods

Study approval

All animal experiments were approved by the Federal Ministry for Nature, Environment and Consumers' Protection of the state of North Rhine-Westphalia and were performed in accordance to the respective national, federal, and institutional regulations.

Generation of conditional knockout mice

Mice carrying loxP-site-flanked (floxed) alleles of the *Caspase-8*-gene (Caspase-8 fl) (Salmena *et al*, 2003) were crossed to *alfp*-cre transgenic mice (Kellendonk *et al*, 2000) to generate a liver parenchymal cell (LPC)-specific knockout (Caspase-$8^{LPC\text{-}KO}$). Mice with constitutive deletion of *RIP3* ($RIP3^{-/-}$) were described before (Newton *et al*, 2004). Mice with double knockout of conditional deletion of *Caspase-8* and constitutive ablation of *Rip3* (Caspase-$8^{LPC\text{-}KO}$/$RIP3^{-/-}$)

were generated by intercrossing the respective lines. *Alb*-Cre Caspase-8^{Floxed} transgenic mice were described previously (Hatting *et al*, 2013). In all experiments, littermates carrying the respective loxP-flanked alleles but lacking expression of Cre recombinase were used as wild-type (WT) controls. Mice were bred on a C57BL/6 genetic background. Only sex-matched animals were compared.

Animal experiments

Mice were fed with a methionine choline-deficient (MCD) diet (MP Biomedicals) for 2 weeks (short term) or 8 weeks (long term). Livers from these mice were collected, fixed in 4% PFA, and embedded in paraffin for histological evaluation. Intraperitoneal injection of the JNK-Inhibitor SP600125 (15 μl/1 mg) (Absource Diagnostics) or vehicle (DMSO) was performed twice a day over 2 weeks of MCD feeding.

Human liver tissue

Human liver biopsy specimens and clinicopathological data were obtained from Newcastle upon Tyne University / Hepatopancreatobiliary and Gastroenterology Research Tissue Bank and Essen University. The project was authorized by the local ethics committees and conducted in accordance with the ethical standards laid down in the Declaration of Helsinki (Newcastle and North Tyneside 1 Research Ethics Committee, Newcastle upon Tyne, Reference number 10/10906/41 and Research Ethics Committee, Essen University, Reference number 09-4252). Histological scoring system for non-alcoholic fatty liver disease (NAFLD) was performed according to the NAS score system (Kleiner *et al*, 2005).

Serum analysis

Serum ALT, AST, and GLDH activities were measured by standard procedures in the Institute of Clinical Chemistry of the RWTH University Hospital Aachen.

Triglyceride assay

The intrahepatic triglyceride tenor was measured by TG liquicolor mono (Human Diagnostics) according to the manufacturer's instructions from homogenized frozen liver sample.

Western blot analysis

Liver tissue was homogenized in NP-40 lysis buffer using a tissue grind pestle (Kimble/Chase) to obtain protein lysates. These were separated by SDS–polyacrylamide gel electrophoresis (PAGE), transferred to PVDF membrane, and analyzed by immunoblotting. Membranes were probed with the following antibodies: anti p-AKT, anti p-ERK, anti p-JNK, anti p-p38 (Cell Signaling), anti-Caspase-8 (Enzo), anti-RIP3 (IMGENEX) and anti-GAPDH (ABD Serotec). As secondary antibodies, anti-rabbit-HRP and anti-mouse-HRP (Amersham) were used.

Flow cytometry

Multicolor staining was conducted using combinations of the following mAbs: F4/80 (Serotec), CD11b (eBioscience), CD45, and Ly6G (BD). Flow cytometric analysis was performed on a FACS-Canto II (BD). Absolute cell numbers were determined by adding 2 × 104 Calibrite APC beads (BD) to each sample before measurement as internal reference standard. Data were analyzed using FlowJo software (Tree Star). For measurement of MCP-1 in total liver protein extracts, we used the mouse FlowCytomix kit (eBioscience) according to the manufacturer's instructions using a FACSCanto II System (BD).

Histological examination

Paraffin sections (2 μm) were stained with H/E or various primary and secondary antibodies. Paraformaldehyde (4%)-fixed and paraffin-embedded liver tissue were incubated in Bond Primary antibody diluent (Leica), and staining was performed on a BOND-MAX immunohistochemistry robot (Leica Biosystems) using BOND polymer refine detection solution for DAB. The following antibodies were used: Antibodies against F4/80 (BMA Biomedicals AG, 1:120), anti-CD45 (BD, 1:200) anti-CK19 (TROMAIIIc, Hybridoma bank, 1:500), anti-Ki67 (NeoMarkers; 1:200), anti-cleaved Caspase-3 (Cell Signaling; 1:300), anti-phospho c-Jun (Abcam, 1:100), and anti-RIP3 (Enzo, 1:500). Image acquisition was performed on an Olympus BX53 microscope with a Leica SCN400 slide scanner. The number of hepatocytes positively stained for the different nuclear markers (e.g. Ki67, pc-Jun) was determined using SlidePath TissueIA image analysis software (Leica) on whole tissue sections (paraffin embed-

Figure 6. RIP3 mediates MCD-diet-induced NASH and liver fibrosis through activation of Jun-(N)-terminal kinase (JNK).

A Western blot analysis of whole liver protein extracts from WT, Casp-8^{LPC-KO}, Casp-8^{LPC-KO}/RIP3$^{-/-}$, and RIP3$^{-/-}$ mice fed with MCD-diet for 14 days, using antibodies against the phosphorylated and active forms of JNK, AKT, p38 and GAPDH, JNK, AKT, and p38 as loading controls.

B Immunohistochemical (left) and statistical analysis (right) of nuclear p-c-Jun^{+} hepatocytes on representative liver sections from Casp-8^{LPC-KO} mice treated with SP600125 or vehicle (DMSO) for 2 weeks under MCD-diet, n = 6 per group.

C Analysis of serum levels of AST, ALT, and GLDH of vehicle-treated and SP600125-treated mice after 2 weeks of MCD-diet feeding. Results are shown as mean ± SEM, n = 6 per group.

D Left: representative Sirius Red stainings of mice treated with vehicle substance (DMSO) or SP600125 for 2 weeks. Right: *Col1α1* mRNA levels quantification by qRT-PCR, n = 6 per group. Error bars represent SEM.

E Immunohistochemical (left) and statistical analysis (right) of CD45^{+} and F4/80^{+} cells on representative liver sections from Casp-8^{LPC-KO} mice treated with SP600125 or vehicle (DMSO) for 2 weeks with MCD-diet, n = 6 per group.

F Immunostaining analysis of RIP3 in Casp-8^{LPC-KO} mice treated with SP600125 or vehicle (DMSO) for 2 weeks with MCD-diet.

G Western blot analysis of RIP3 in Casp-8^{LPC-KO} mice treated with SP600125 or vehicle (DMSO) for 2 weeks with MCD-diet.

Data information: The exact *P*-values of each experiment and specific tests used are provided in the Supplementary Table S1.
Source data are available online for this figure.

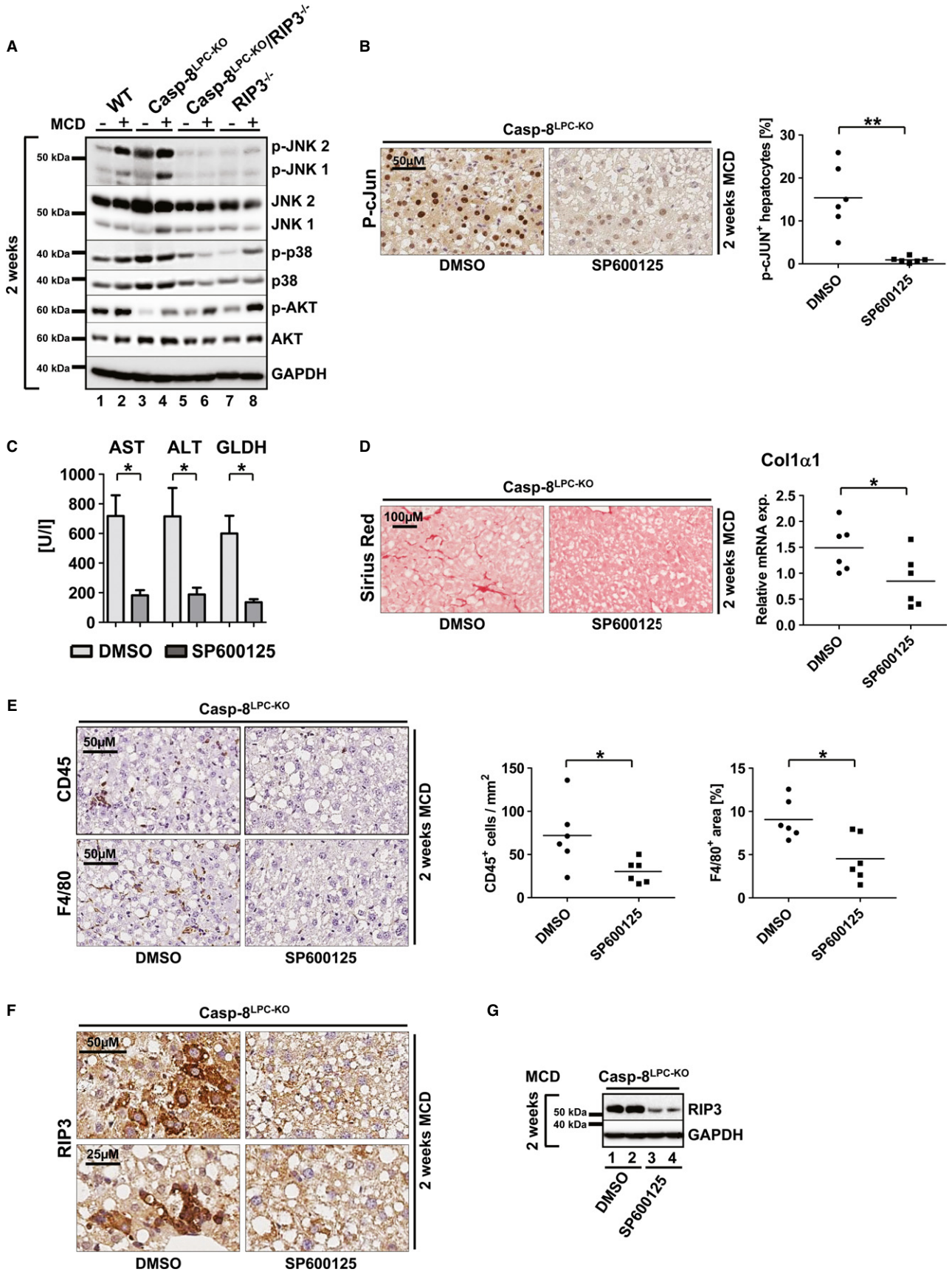

Figure 6.

ded) and normalized to tissue area or hepatocyte number, respectively. Hepatocytes positively stained for cleaved Caspase-3 and RIP3 as well as macrophages positive for F4/80, immune cells positively stained for CD45 or MHCII, and fibrotic fibers stained with Sirius Red were quantified numerically (positive cells per total tissue area) or densitometrically (area stained per total tissue area) using SlidePath TissueIA image analysis software (Leica) on whole tissue sections and normalized to total tissue area.

Cell culture

L929 cells were cultured in Dulbecco's modified Eagle's medium supplemented with 10% fetal calf serum, penicillin (100 IU/ml), streptomycin (0.1 mg/ml), and L-glutamine (0.03%). Bone marrow cells were isolated from femur and tibia of 8-week-old C57BL6/J and RIP3$^{-/-}$ mice. To obtain fibroblast-conditioned medium (FCM) which is known to contain the macrophage colony-stimulating factor (MCSF, CSF1), L929 fibroblasts were cultured in RPMI medium containing 10% fetal calf serum (FCS) for 3 days, and the supernatant was collected, filtered, and stored until usage at −80°C. For the generation of bone marrow derived macrophages (BMM), bone marrow cells were cultured in RPMI medium containing 10% FCS and 20% FCM for 1 week on bacterial grade plastic plates (Greiner). At day 7, cells were either left untreated or stimulated for additional 24 h with lipopolysaccharides (LPS, 1 μg/ml) (Sigma-Aldrich).

Analysis of cell survival

L929 cells were cultured overnight in 12-well plates and used at 50% of confluence. After pre-treatment with zVAD (20 μM) (Millipore) for 1 h, the cells were incubated with Necrostatin-1 (10 μM) (Santa Cruz), SP600125 (20 μM) (Absource), or DMSO as control. Nineteen hours later, the cells were incubated with 1 ng/ml of MTT reagent (Life Technologies) for 2 h. Once MTT crystals were developed and controlled under light microscopy, they were dissolved in DMSO and quantified by measuring absorbance at 540 nm.

Quantitative real-time PCR

Total RNA was purified from liver tissue using TRIzol reagent (Invitrogen) and an RNeasy Mini kit (Qiagen). The quantity and quality of the RNA were determined spectroscopically using a nanodrop (Thermo Scientific). Total RNA (1 μg) was used to synthesize cDNA using the Transcriptor cDNA First-Strand Synthesis Kit (Roche) according to the manufacturer's protocol and was resuspended in 50 μl of H_2O. cDNA samples (2 μl) were used for real-time PCR in a total volume of 25 μl using SYBR Green Reagent (Invitrogen) and specific primers on a qPCR machine (Applied Biosystems 7300 Sequence Detection System). All real-time PCRs were performed in duplicates. Data were generated and analyzed using SDS 2.3 and RQ manager 1.2 software. Primer sequences are available upon request. All values were normalized to the level of beta-actin mRNA.

Statistical analysis

Data were analyzed using PRISM software (GraphPad, Inc., La Jolla, CA) and are expressed as SEM. Statistical significance between experimental groups was assessed using unpaired two-sample *t*-test, Mann–Whitney test, and unpaired two-sample *t*-test with Welch's correction ($^*P < 0.05$; $^{**}P < 0.01$; $^{***}P < 0.001$). The exact *P*-values of each experiment and specific tests used are provided in Supplementary Table S1.

The paper explained

Problem
Apoptosis was previously considered as the main driver of NASH development in patients with fatty liver disease. In this line, Caspase-8 was suggested as a promising target for novel pharmacological strategies, but it was unknown whether other programmed cell-death pathways than apoptosis might be involved in the pathophysiology of NASH.

Results
We show that RIP3-dependent necroptosis represents a major driving force mediating NASH-induced liver fibrosis. This function of RIP3 was mediated by activation of JNK as its pharmacological inhibition reduced intrahepatic level of RIP3 and subsequently liver fibrosis and was associated with MCP-1-mediated recruitment of monocytes and an expansion of intrahepatic biliary / progenitor cells. Finally, in contrast to previous assumptions, we demonstrate that the main function of Caspase-8 in this context is to suppress the deleterious effect of RIP3-dependent necroptosis.

Impact
The novel RIP3/JNK axis in the liver might represent a novel pharmacological target and/or biomarker in the clinical context of NASH and NASH-induced liver fibrosis. In contrast, pharmacological targeting of Caspase-8 might have deleterious effects in NASH patients, as this might activate necroptosis and trigger liver fibrosis.

Supplementary information for this article is available online:
http://embomolmed.embopress.org

Acknowledgements
The authors thank Drs. V. Dixit (Genentech, San Francisco, USA) and R. Hakem (Cancer Institute, Ontario, Canada) for kindly providing RIP3$^{-/-}$ and Caspase-8$^{LPC\text{-}KO}$ mice, respectively. We thank Dr. G. Courtois (CEA, Grenoble, France) and M.P. Gautheron for their valuable comments and support. Work in the laboratory of TL was supported by the German-Research-Foundation (SFB-TRR57 / P06), the German Cancer Aid (Deutsche Krebshilfe 110043), an ERC Starting Grant (ERC-2007-Stg/208237-Luedde-Med3-Aachen), the EMBO Young Investigator Program, and the Ernst-Jung-Foundation/Hamburg. JG was supported by the Interdisciplinary-Centre-for-Clinical-Research (IZKF) and the medical faculty of the RWTH Aachen. MH was supported by the Helmholtz Foundation, the Hofschneider Foundation, the German-Research-Foundation (SFB-TR36), the Helmholtz alliance preclinical comprehensive center (PCCC), and an ERC Starting grant (LiverCancerMechanisms). ML was supported by the Deutsche Stiftung Herzforschung (12/12).

Author contributions
TL and JG conceived and designed the experiments, made the figures, and wrote the manuscript with the contribution from other authors; JG, MV, and FR performed experiments and statistical analysis with the assistance of CR, DVC, CK, and ATS; DVC and KK maintained mouse lines and performed genotyping; MB helped in the isolation of monocytes; UPN, HLR, and AC provided human NASH samples; CT provided *alb*-cre line

samples; MH, ML, UPN, and FT provided intellectual input; MH and TL supervised experiments.

Conflict of interest

The authors declare that they have no conflict of interest.

References

Anstee QM, Concas D, Kudo H, Levene A, Pollard J, Charlton P, Thomas HC, Thursz MR, Goldin RD (2010) Impact of pan-caspase inhibition in animal models of established steatosis and non-alcoholic steatohepatitis. *J Hepatol* 53: 542 – 550

Baeck C, Wehr A, Karlmark KR, Heymann F, Vucur M, Gassler N, Huss S, Klussmann S, Eulberg D, Luedde T *et al* (2012) Pharmacological inhibition of the chemokine CCL2 (MCP-1) diminishes liver macrophage infiltration and steatohepatitis in chronic hepatic injury. *Gut* 61: 416 – 426

Bhala N, Angulo P, van der Poorten D, Lee E, Hui JM, Saracco G, Adams LA, Charatcharoenwitthaya P, Topping JH, Bugianesi E *et al* (2011) The natural history of nonalcoholic fatty liver disease with advanced fibrosis or cirrhosis: an international collaborative study. *Hepatology* 54: 1208 – 1216

Bonnet MC, Preukschat D, Welz PS, van Loo G, Ermolaeva MA, Bloch W, Haase I, Pasparakis M (2011) The adaptor protein FADD protects epidermal keratinocytes from necroptosis in vivo and prevents skin inflammation. *Immunity* 35: 572 – 582

Chakraborty JB, Oakley F, Walsh MJ (2012) Mechanisms and biomarkers of apoptosis in liver disease and fibrosis. *Int J Hepatol* 2012: 648915

Chang HY, Yang X (2000) Proteases for cell suicide: functions and regulation of caspases. *Microbiol Mol Biol Rev* 64: 821 – 846

Cho YS, Challa S, Moquin D, Genga R, Ray TD, Guildford M, Chan FK (2009) Phosphorylation-driven assembly of the RIP1-RIP3 complex regulates programmed necrosis and virus-induced inflammation. *Cell* 137: 1112 – 1123

Csak T, Dolganiuc A, Kodys K, Nath B, Petrasek J, Bala S, Lippai D, Szabo G (2011) Mitochondrial antiviral signaling protein defect links impaired antiviral response and liver injury in steatohepatitis in mice. *Hepatology* 53: 1917 – 1931

Das M, Sabio G, Jiang F, Rincon M, Flavell RA, Davis RJ (2009) Induction of hepatitis by JNK-mediated expression of TNF-alpha. *Cell* 136: 249 – 260

Degterev A, Maki JL, Yuan J (2013) Activity and specificity of necrostatin-1, small-molecule inhibitor of RIP1 kinase. *Cell Death Differ* 20: 366

Dixon LJ, Flask CA, Papouchado BG, Feldstein AE, Nagy LE (2013) Caspase-1 as a central regulator of high fat diet-induced non-alcoholic steatohepatitis. *PLoS ONE* 8: e56100

Estaquier J, Vallette F, Vayssiere JL, Mignotte B (2012) The mitochondrial pathways of apoptosis. *Adv Exp Med Biol* 942: 157 – 183

Feldstein AE, Canbay A, Angulo P, Taniai M, Burgart LJ, Lindor KD, Gores GJ (2003) Hepatocyte apoptosis and fas expression are prominent features of human nonalcoholic steatohepatitis. *Gastroenterology* 125: 437 – 443

Feldstein AE, Gores GJ (2005) Apoptosis in alcoholic and nonalcoholic steatohepatitis. *Front Biosci* 10: 3093 – 3099

Han J, Zhong CQ, Zhang DW (2011) Programmed necrosis: backup to and competitor with apoptosis in the immune system. *Nat Immunol* 12: 1143 – 1149

Hatting M, Zhao G, Schumacher F, Sellge G, Al Masaoudi M, Gabetaler N, Boekschoten M, Muller M, Liedtke C, Cubero FJ *et al* (2013) Hepatocyte caspase-8 is an essential modulator of steatohepatitis in rodents. *Hepatology* 57: 2189 – 2201

He S, Wang L, Miao L, Wang T, Du F, Zhao L, Wang X (2009) Receptor interacting protein kinase-3 determines cellular necrotic response to TNF-alpha. *Cell* 137: 1100 – 1111

Kaiser WJ, Upton JW, Long AB, Livingston-Rosanoff D, Daley-Bauer LP, Hakem R, Caspary T, Mocarski ES (2011) RIP3 mediates the embryonic lethality of caspase-8-deficient mice. *Nature* 471: 368 – 372

Kellendonk C, Opherk C, Anlag K, Schutz G, Tronche F (2000) Hepatocyte-specific expression of Cre recombinase. *Genesis* 26: 151 – 153

Kleiner DE, Brunt EM, Van Natta M, Behling C, Contos MJ, Cummings OW, Ferrell LD, Liu YC, Torbenson MS, Unalp-Arida A *et al* (2005) Design and validation of a histological scoring system for nonalcoholic fatty liver disease. *Hepatology* 41: 1313 – 1321

Li J, McQuade T, Siemer AB, Napetschnig J, Moriwaki K, Hsiao YS, Damko E, Moquin D, Walz T, McDermott A *et al* (2012) The RIP1/RIP3 necrosome forms a functional amyloid signaling complex required for programmed necrosis. *Cell* 150: 339 – 350

Liu K, Czaja MJ (2013) Regulation of lipid stores and metabolism by lipophagy. *Cell Death Differ* 20: 3 – 11

Malhi H, Gores GJ (2008) Molecular mechanisms of lipotoxicity in nonalcoholic fatty liver disease. *Semin Liver Dis* 28: 360 – 369

Najimi M, Smets F, Sokal E (2009) Hepatocyte apoptosis. *Methods Mol Biol* 481: 59 – 74

Newton K, Sun X, Dixit VM (2004) Kinase RIP3 is dispensable for normal NF-kappa Bs, signaling by the B-cell and T-cell receptors, tumor necrosis factor receptor 1, and Toll-like receptors 2 and 4. *Mol Cell Biol* 24: 1464 – 1469

Pattingre S, Tassa A, Qu X, Garuti R, Liang XH, Mizushima N, Packer M, Schneider MD, Levine B (2005) Bcl-2 antiapoptotic proteins inhibit Beclin 1-dependent autophagy. *Cell* 122: 927 – 939

Poelstra K, Schuppan D (2011) Targeted therapy of liver fibrosis/cirrhosis and its complications. *J Hepatol* 55: 726 – 728

Postic C, Shiota M, Niswender KD, Jetton TL, Chen Y, Moates JM, Shelton KD, Lindner J, Cherrington AD, Magnuson MA (1999) Dual roles for glucokinase in glucose homeostasis as determined by liver and pancreatic beta cell-specific gene knock-outs using Cre recombinase. *J Biol Chem* 274: 305 – 315

Ratziu V, Sheikh MY, Sanyal AJ, Lim JK, Conjeevaram H, Chalasani N, Abdelmalek M, Bakken A, Renou C, Palmer M *et al* (2012) A phase 2, randomized, double-blind, placebo-controlled study of GS-9450 in subjects with nonalcoholic steatohepatitis. *Hepatology* 55: 419 – 428

Richardson MM, Jonsson JR, Powell EE, Brunt EM, Neuschwander-Tetri BA, Bhathal PS, Dixon JB, Weltman MD, Tilg H, Moschen AR *et al* (2007) Progressive fibrosis in nonalcoholic steatohepatitis: association with altered regeneration and a ductular reaction. *Gastroenterology* 133: 80 – 90

Roychowdhury S, McMullen MR, Pisano SG, Liu X, Nagy LE (2013) Absence of receptor interacting protein kinase 3 prevents ethanol-induced liver injury. *Hepatology* 57: 1773 – 1783

Salmena L, Lemmers B, Hakem A, Matysiak-Zablocki E, Murakami K, Au PY, Berry DM, Tamblyn L, Shehabeldin A, Migon E *et al* (2003) Essential role for caspase 8 in T-cell homeostasis and T-cell-mediated immunity. *Genes Dev* 17: 883 – 895

Schattenberg JM, Singh R, Wang Y, Lefkowitch JH, Rigoli RM, Scherer PE, Czaja MJ (2006) JNK1 but not JNK2 promotes the development of steatohepatitis in mice. *Hepatology* 43: 163 – 172

Schattenberg JM, Schuppan D (2011) Nonalcoholic steatohepatitis: the therapeutic challenge of a global epidemic. *Curr Opin Lipidol* 22: 479 – 488

Schuppan D, Afdhal NH (2008) Liver cirrhosis. *Lancet* 371: 838 – 851

Schuppan D, Kim YO (2013) Evolving therapies for liver fibrosis. *J Clin Invest* 123: 1887 – 1901

Seifert EL, Estey C, Xuan JY, Harper ME (2010) Electron transport chain-dependent and -independent mechanisms of mitochondrial H2O2 emission during long-chain fatty acid oxidation. *J Biol Chem* 285: 5748 – 5758

Seki E, de Minicis S, Inokuchi S, Taura K, Miyai K, van Rooijen N, Schwabe RF, Brenner DA (2009) CCR2 promotes hepatic fibrosis in mice. *Hepatology* 50: 185 – 197

Sun L, Wang H, Wang Z, He S, Chen S, Liao D, Wang L, Yan J, Liu W, Lei X *et al* (2012) Mixed lineage kinase domain-like protein mediates necrosis signaling downstream of RIP3 kinase. *Cell* 148: 213 – 227

Tacke F, Luedde T, Trautwein C (2008) Inflammatory pathways in liver homeostasis and liver injury. *Clin Rev Allergy Immunol* 36: 4 – 12

Vernon G, Baranova A, Younossi ZM (2011) Systematic review: the epidemiology and natural history of non-alcoholic fatty liver disease and non-alcoholic steatohepatitis in adults. *Aliment Pharmacol Ther* 34: 274 – 285

Vucur M, Reisinger F, Gautheron J, Janssen J, Roderburg C, Cardenas DV, Kreggenwinkel K, Koppe C, Hammerich L, Hakem R *et al* (2013) RIP3 inhibits inflammatory hepatocarcinogenesis but promotes cholestasis by controlling caspase-8- and JNK-dependent compensatory cell proliferation. *Cell Rep* 4: 776 – 790

Weinlich R, Oberst A, Dillon CP, Janke LJ, Milasta S, Lukens JR, Rodriguez DA, Gurung P, Savage C, Kanneganti TD *et al* (2013) Protective roles for caspase-8 and cFLIP in adult homeostasis. *Cell Rep* 5: 340 – 348

Welz PS, Wullaert A, Vlantis K, Kondylis V, Fernandez-Majada V, Ermolaeva M, Kirsch P, Sterner-Kock A, van Loo G, Pasparakis M (2011) FADD prevents RIP3-mediated epithelial cell necrosis and chronic intestinal inflammation. *Nature* 477: 330 – 334

Wieckowska A, Zein NN, Yerian LM, Lopez AR, McCullough AJ, Feldstein AE (2006) In vivo assessment of liver cell apoptosis as a novel biomarker of disease severity in nonalcoholic fatty liver disease. *Hepatology* 44: 27 – 33

Witek RP, Stone WC, Karaca FG, Syn WK, Pereira TA, Agboola KM, Omenetti A, Jung Y, Teaberry V, Choi SS *et al* (2009) Pan-caspase inhibitor VX-166 reduces fibrosis in an animal model of nonalcoholic steatohepatitis. *Hepatology* 50: 1421 – 1430

Wree A, Broderick L, Canbay A, Hoffman HM, Feldstein AE (2013) From NAFLD to NASH to cirrhosis-new insights into disease mechanisms. *Nat Rev Gastroenterol Hepatol* 10: 627 – 636

Yang L, Roh YS, Song J, Zhang B, Liu C, Loomba R, Seki E (2014) Transforming growth factor beta signaling in hepatocytes participates in steatohepatitis through regulation of cell death and lipid metabolism in mice. *Hepatology* 59: 483 – 495

Younossi ZM, Jarrar M, Nugent C, Randhawa M, Afendy M, Stepanova M, Rafiq N, Goodman Z, Chandhoke V, Baranova A (2008) A novel diagnostic biomarker panel for obesity-related nonalcoholic steatohepatitis (NASH). *Obes Surg* 18: 1430 – 1437

Yousefi S, Perozzo R, Schmid I, Ziemiecki A, Schaffner T, Scapozza L, Brunner T, Simon HU (2006) Calpain-mediated cleavage of Atg5 switches autophagy to apoptosis. *Nat Cell Biol* 8: 1124 – 1132

Zhang DW, Shao J, Lin J, Zhang N, Lu BJ, Lin SC, Dong MQ, Han J (2009) RIP3, an energy metabolism regulator that switches TNF-induced cell death from apoptosis to necrosis. *Science* 325: 332 – 336

Zimmermann HW, Tacke F (2011) Modification of chemokine pathways and immune cell infiltration as a novel therapeutic approach in liver inflammation and fibrosis. *Inflamm Allergy Drug Targets* 10: 509 – 536

Cell Reports
Article

RIP3 Inhibits Inflammatory Hepatocarcinogenesis but Promotes Cholestasis by Controlling Caspase-8- and JNK-Dependent Compensatory Cell Proliferation

Mihael Vucur,[1,11] Florian Reisinger,[5,11] Jérémie Gautheron,[1,2,11] Joern Janssen,[1] Christoph Roderburg,[1] David Vargas Cardenas,[1] Karina Kreggenwinkel,[1] Christiane Koppe,[1] Linda Hammerich,[1] Razq Hakem,[7] Kristian Unger,[6] Achim Weber,[8] Nikolaus Gassler,[3] Mark Luedde,[9] Norbert Frey,[9] Ulf Peter Neumann,[4] Frank Tacke,[1] Christian Trautwein,[1] Mathias Heikenwalder,[5,10] and Tom Luedde[1,*]

[1]Department of Medicine III
[2]Interdisciplinary Centre for Clinical Research (IZKF)
[3]Institute of Pathology
[4]Department of Visceral and Transplantation Surgery
University Hospital RWTH Aachen, D-52074 Aachen, Germany
[5]Institute of Virology, Helmholtz Zentrum München für Gesundheit und Umwelt (HMGU), D-81675 Munich, Germany
[6]Research Unit of Radiation Cytogenetics, Helmholtz-Zentrum München für Gesundheit und Umwelt (HMGU), D-85764 Neuherberg, Germany
[7]Departments of Medical Biophysics and Immunology, Ontario Cancer Institute, University of Toronto, Toronto, ON M5G 2C1, Canada
[8]Institute of Surgical Pathology, University Hospital Zurich, CH-8091 Zurich, Switzerland
[9]Department of Cardiology and Angiology, University Hospital Kiel, D-24105 Kiel, Germany
[10]Institute of Virology, Technische Universität München (TUM), D-81675 Munich, Germany
[11]These authors contributed equally to this work
*Correspondence: tluedde@ukaachen.de
http://dx.doi.org/10.1016/j.celrep.2013.07.035

SUMMARY

For years, the term "apoptosis" was used synonymously with programmed cell death. However, it was recently discovered that receptor interacting protein 3 (RIP3)-dependent "necroptosis" represents an alternative programmed cell death pathway activated in many inflamed tissues. Here, we show in a genetic model of chronic hepatic inflammation that activation of RIP3 limits immune responses and compensatory proliferation of liver parenchymal cells (LPC) by inhibiting Caspase-8-dependent activation of Jun-(N)-terminal kinase in LPC and non-parenchymal liver cells. In this way, RIP3 inhibits intrahepatic tumor growth and impedes the Caspase-8-dependent establishment of specific chromosomal aberrations that mediate resistance to tumor-necrosis-factor-induced apoptosis and underlie hepatocarcinogenesis. Moreover, RIP3 promotes the development of jaundice and cholestasis, because its activation suppresses compensatory proliferation of cholangiocytes and hepatic stem cells. These findings demonstrate a function of RIP3 in regulating carcinogenesis and cholestasis. Controlling RIP3 or Caspase-8 might represent a chemopreventive or therapeutic strategy against hepatocellular carcinoma and biliary disease.

INTRODUCTION

Hepatocellular carcinoma (HCC), the most common primary liver tumor, arises almost exclusively in a setting of chronic hepatic inflammation (Sherman, 2010). However, the knowledge on the clear association between inflammation and cancer has not yet translated into a chemopreventive pharmacological strategy against HCC development, underlining the need for a better understanding of molecular processes controlling the transition from inflammation to cancer. Cell death represents a dominant trigger for inflammation, thus contributing to multiple hallmark capabilities of cancer (Hanahan and Weinberg, 2011). In chronic liver disease, hepatocyte cell death is a prominent feature driving progression to hepatic fibrosis and finally HCC (Zhang and Friedman, 2012).

For years, the term apoptosis was used synonymously for programmed cell death, whereas necrosis was considered a passive, not specifically regulated, and ATP-independent process (Chakraborty et al., 2012). Apoptosis is triggered by ligation of death receptors, like tumor necrosis factor (TNF) receptor, by their cognate ligands and represents a highly synchronized procedure depending on activation of aspartate-specific proteases, known as caspases (Chakraborty et al., 2012). In viral hepatitis, immune cell-triggered apoptosis of virally infected hepatocytes represents a key step in viral clearance (Fung et al., 2009). Moreover, apoptotic death of hepatocytes is a common feature of alcoholic and nonalcoholic steatohepatitis and is associated with fibrosis (Feldstein and Gores, 2005).

It was recently discovered that, next to apoptosis, necroptosis—programmed necrosis depending on the kinases receptor interacting protein 1 (RIP1) and RIP3—represents an alternative programmed cell-death pathway downstream of the TNF-receptor (Cho et al., 2009; He et al., 2009; Zhang et al., 2009). It can be induced by viral infection and can serve as an alternative when caspase-dependent apoptosis is inhibited or absent (Han et al., 2011). Necroptosis plays a role in the regulation of chronic inflammation in the pancreas, gut, and skin (Bonnet et al., 2011; He et al., 2009; Welz et al., 2011). In human patients, necroptosis is activated in alcoholic liver injury (Roychowdhury et al., 2013) as one of the leading causes of liver cirrhosis and HCC in the western world (Sherman, 2010). However, the functional role of RIP3 in controlling the consequences of chronic inflammation in the liver and other organs is presently not known. In this study, we examined the role of RIP3 in a model of inflammatory hepatocarcinogenesis based on conditional deletion of the mitogen-activated protein 3 (MAP3)-kinase transforming growth factor β (TGF-β)-activated-kinase-1 (TAK1) in liver parenchymal cells (LPC) (TAK1$^{LPC\text{-}KO}$) (Bettermann et al., 2010).

RESULTS

RIP3 Is Activated in TAK1-Deficient Livers and Promotes Jaundice and Cholestasis by Inhibiting a Sufficient Ductular Reaction

Mice with conditional deletion of *Tak1* in LPC (TAK1$^{LPC\text{-}KO}$ mice) display severe hepatic inflammation at a young age characterized by spontaneous LPC apoptosis and LPC necrosis, proceeding over time to liver fibrosis and liver cancer but also to severe lethal cholestasis (Bettermann et al., 2010). In order to investigate the function of RIP3 in hepatocarcinogenesis, we generated mice with ablation of TAK1 in LPC together with a full knockout of *Rip3* (TAK1$^{LPC\text{-}KO}$/RIP3$^{-/-}$) or combined ablations of TAK1 and Caspase-8 in LPC (TAK1/Casp-8$^{LPC\text{-}KO}$) and first compared their phenotypes with wild-type (WT) and TAK1 single mutant mice (TAK1$^{LPC\text{-}KO}$) at the age of 6 weeks (Figure 1A).

We detected strongly increased protein levels of RIP3 in liver extracts from TAK1$^{LPC\text{-}KO}$ and TAK1/Casp-8$^{LPC\text{-}KO}$ mice (Figure 1A), suggesting that LPC in these mice might be sensitized to necrosis (He et al., 2009). Measurements of serum enzymes from 6-week-old male mice confirmed that TAK1$^{LPC\text{-}KO}$ mice showed a strong rise in serum aminotransferases (alanine aminotransferase [ALT] and aspartate aminotransferase [AST]) and serum glutamate dehydrogenase (GLDH) levels compared to WT mice as marker for hepatitis and LPC damage (Figure 1B). Macroscopic analysis revealed that this coincided with yellow color of livers and elevated serum bilirubin and alkaline phosphatase (AP) levels (Figures 1B and 1C), reflecting severe jaundice and cholestasis as shown previously by electron-microscopical analysis of bile canaliculi in TAK1$^{LPC\text{-}KO}$ animals (Bettermann et al., 2010). Moreover, TAK1$^{LPC\text{-}KO}$ livers displayed macroscopically visible nodules on the surface of livers (Figure 1C). Deletion of *Caspase-8* in TAK1$^{LPC\text{-}KO}$ mice led to significant reduction in ALT, AST, and GLDH serum levels, and disappearance of macroscopic nodules on the surface of liver lobes compared to TAK1$^{LPC\text{-}KO}$ mice. However, no rescue in hyperbilirubinemia and AP elevation was found (Figures 1B and 1C). In contrast, deletion of *Rip3* in TAK1$^{LPC\text{-}KO}$ mice led to a normalization of bilirubin and reduced AP levels but worsened hepatitis, indicated by significantly elevated ALT and GLDH levels in TAK1$^{LPC\text{-}KO}$/RIP3$^{-/-}$ mice compared to TAK1$^{LPC\text{-}KO}$ animals (Figure 1B). Moreover, while at 6 weeks of age, TAK1$^{LPC\text{-}KO}$/RIP3$^{-/-}$ livers lacked a yellow color as a sign of jaundice; they displayed multiple small nodules on their surface (Figure 1C).

Histological analysis of liver sections from 6-week-old male mice revealed that jaundice in TAK1$^{LPC\text{-}KO}$ mice correlated with the presence of areas of hepatocyte necrosis, which were detected even to a higher extent in TAK1/Casp-8$^{LPC\text{-}KO}$ animals, whereas necrosis was absent in TAK1$^{LPC\text{-}KO}$/RIP3$^{-/-}$ mice at this age (Figures 2A and 2B). In parallel to the absence of necrosis, TAK1$^{LPC\text{-}KO}$/RIP3$^{-/-}$ mice showed a strong ductular reaction with expansion of A6^{+} (oval) cells (Figures 2A–2D), likely reflecting a necessary process to maintain biliary homeostasis in a setting of chronic inflammation (Desmet, 2011; Glaser et al., 2009). Strikingly, this ductular reaction was absent in TAK1$^{LPC\text{-}KO}$ and TAK1/Casp-8$^{LPC\text{-}KO}$ mice (Figures 2A, 2C, and 2D). These data demonstrate that, in chronic hepatitis, Caspase-8-dependent apoptosis primarily causes elevation of free circulating aminotransferases and GLDH in the serum. In contrast, RIP3-dependent necroptosis promotes jaundice and cholestasis in TAK1$^{LPC\text{-}KO}$ livers, because it is not linked with a ductular reaction.

Activation of RIP3 Limits Compensatory Proliferation of Hepatocytes and Biliary Epithelial Cells in the Chronically Inflamed Liver

We further analyzed the influence of RIP3 and Caspase-8 on cell death in TAK1$^{LPC\text{-}KO}$ animals. In line with previous findings (Bettermann et al., 2010), TAK1$^{LPC\text{-}KO}$ mice displayed significant spontaneous LPC apoptosis as shown by immunohistochemistry and western blot analyses for cleaved Caspase-3 (Figures 3A–3C). Additional deletion of *Caspase-8* resulted in complete inhibition of Caspase-3 cleavage, whereas additional deletion of *Rip3* in TAK1$^{LPC\text{-}KO}$ mice resulted in a significant increase in Caspase-3 cleavage when compared to TAK1$^{LPC\text{-}KO}$ mice (Figures 3A–3C). Therefore, Caspase-8-dependent apoptosis and RIP3-dependent necroptosis counterbalance and compete with each other in the regulation of LPC death in TAK1$^{LPC\text{-}KO}$ livers (compare Figures 2A and 2B and Figures 3A–3C).

We next examined the functions of Caspase-8 and RIP3 in LPC proliferation in *Tak1*-deficient livers. Ki67 staining and western blot analyses of the cell cycle proteins proliferating cell nuclear antigen (PCNA) and cyclin D1 confirmed a high proportion of proliferating LPC in TAK1$^{LPC\text{-}KO}$ mice (Figures 3A–3C). Additional deletion of *Caspase-8* dramatically reduced the number of proliferating LPC and the degree of PCNA/cyclin D1 expression, whereas proliferation remained high or was even higher by tendency in mice with combined deletions of *Tak1* and *Rip3* (Figures 3A–3C). This indicates that Caspase-8-dependent LPC apoptosis induces strong compensatory proliferation of other adjacent LPC, which is not the case in terms of LPC necroptosis. Interestingly, not only hepatocytes but also biliary cells in TAK1$^{LPC\text{-}KO}$/RIP3$^{-/-}$ mice displayed increased apoptosis and proliferation, as indicated by costainings for pancytokeratin and Ki67 or cleaved Caspase-3 (Figures 3D–3F). Thus, differential degrees of compensatory cell proliferation

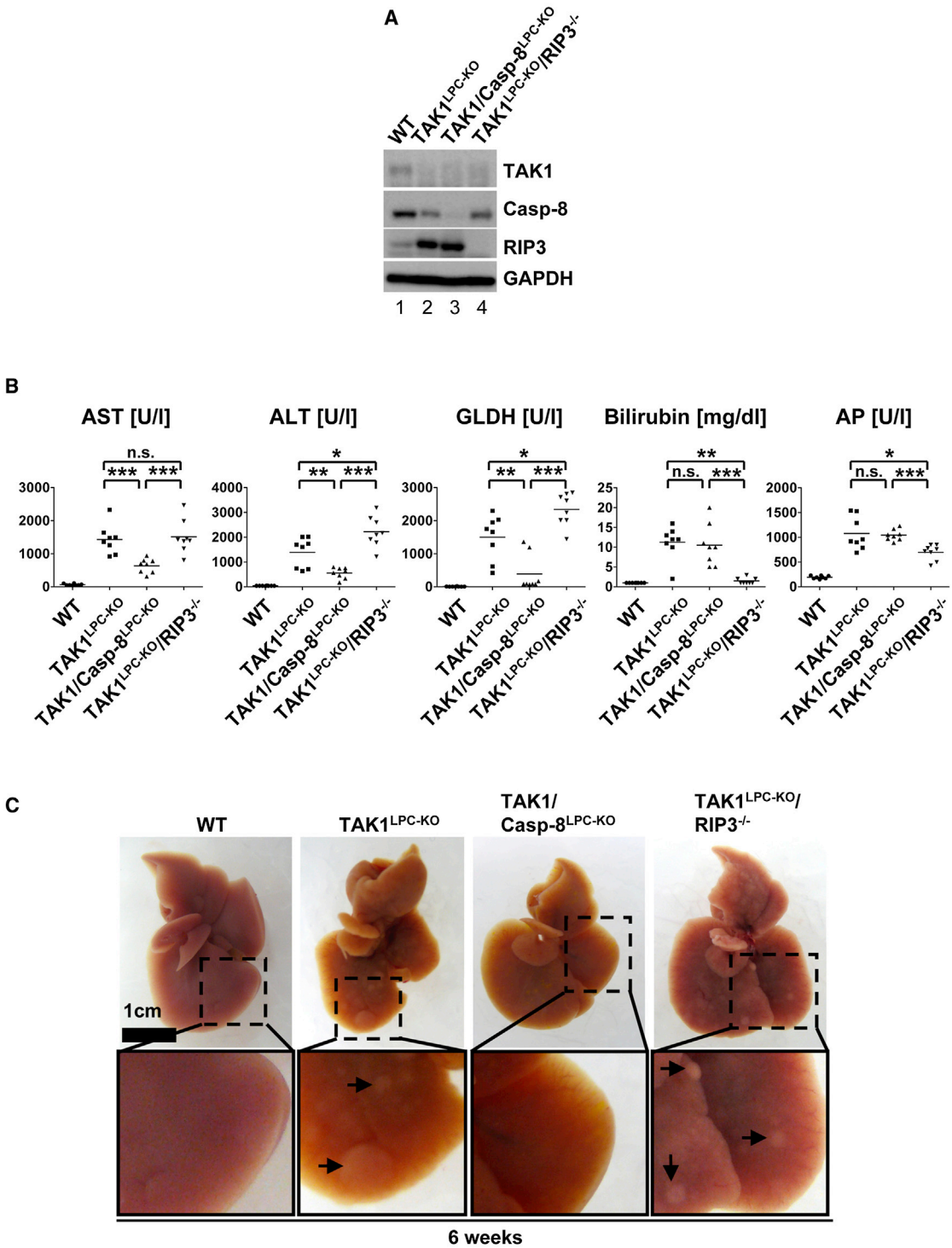

Figure 1. Apoptosis and Necroptosis Differentially Regulate Dysplasia, Cholestasis, and Liver Injury in Mice with LPC-specific *Tak1* Deletion

(A) Western blot analysis of whole liver protein extracts from 6-week-old male TAK1^{LPC-KO}, TAK1/Casp-8^{LPC-KO}, TAK1^{LPC-KO}/RIP3$^{-/-}$, and control littermate mice (WT) using antibodies against TAK1, RIP3, Caspase-8, and glyceraldehyde 3-phosphate dehydrogenase (GAPDH) as loading control.

(B) Serum level analysis of AST, ALT, glutamate dehydrogenase (GLDH), total bilirubin, and AP in 6-week-old male mice. Results are shown as mean. Double asterisks denote $p < 0.01$ and triple asterisks denote $p < 0.001$ ($n = 8$ each genotype).

(C) Representative macroscopic pictures of 6-week-old male WT, TAK1^{LPC-KO}, TAK1/Casp-8^{LPC-KO}, and TAK1^{LPC-KO}/RIP3$^{-/-}$ livers. Small nodular structures are observed in livers of TAK1^{LPC-KO} and TAK1^{LPC-KO}/RIP3$^{-/-}$ mice but not on TAK1/Casp-8^{LPC-KO} livers. Arrows indicate nodules. Additionally, TAK1^{LPC-KO} and TAK1/Casp-8^{LPC-KO} but not TAK1^{LPC-KO}/RIP3$^{-/-}$ livers display a cholestatic, yellow color. The scale bars represent 1 cm.

upon apoptosis versus necroptosis are a likely cause for the presence or absence of a sufficient ductular reaction and cholestasis in TAK1$^{LPC\text{-}KO}$/RIP3$^{-/-}$ and TAK1/Casp-8$^{LPC\text{-}KO}$ mice, respectively.

To evaluate the effect of *Caspase-8* deletion in LPC, we further performed serological and histological analyses on Casp-8$^{LPC\text{-}KO}$ mice. This analysis revealed mild liver injury, indicated by elevated serum ALT, AST, and GLDH, but no changes in the biliary system or infiltration with myelomonocytic cells (Figures S1A–S1C). In addition, we tested whether the molecules Caspase-8 or RIP3 might have limiting effects on LPC proliferation and performed partial hepatectomy (PH) experiments in Casp-8$^{LPC\text{-}KO}$ mice or mice with constitutive deletion of *Rip3* (RIP3$^{-/-}$). Whereas WT and RIP3$^{-/-}$ animals showed similar expression levels of cell cycle markers cyclin D1 and PCNA in western blot and Ki67-expression in immunohistochemical analysis, Casp-8$^{LPC\text{-}KO}$ animals even displayed a slight acceleration in cell-cycle progression (Figures S1D–S1F). This indicates that the differences in the proliferative response between TAK1$^{LPC\text{-}KO}$/RIP3$^{-/-}$ and TAK1/Casp-8$^{LPC\text{-}KO}$ animals were not caused by direct effects of Caspase-8 or RIP3 on the cell-cycle machinery, however, suggest that apoptosis but not necroptosis of LPC represents a strong trigger for compensatory LPC proliferation.

The kinase TAK1 integrates signals from several upstream ligands and regulates various inflammatory and stress-related signaling pathways (Delaney and Mlodzik, 2006). We therefore tested whether, besides apoptosis and necroptosis, other signaling pathways might be involved in hepatitis and cholestasis development in *Tak1*-deficient livers and generated mice with combined deletions of *Tak1* and *Caspase-8* in LPC together with full knockout of *Rip3* (TAK1/Casp-8$^{LPC\text{-}KO}$/RIP3$^{-/-}$ mice; Figure S2A). On macroscopic, serological, and histological level, combined deletions of *Caspase-8* and *Rip3* completely rescued hepatitis, liver injury, cholestasis, and biliary ductopenia seen in TAK1 single mutants (Figures S2B–S2D). This highlights that apoptosis and necroptosis represent the major pathways mediating the severe phenotype in *Tak1*-deficient livers. Further, this argues against significant influences of potential dysregulation of biliary transporters or structural cell proteins in biliary epithelial cells in response to *Tak1* deletion.

Activation of RIP3 Inhibits Hepatic Tumor Growth

Based on the differential functional relations between apoptotic versus necroptotic cell death and compensatory LPC proliferation, we next evaluated if RIP3 and Caspase-8 might also differentially regulate hepatocarcinogenesis. Hence, we examined the spontaneous phenotype of 25- to 38-week-old animals, because TAK1 single mutants develop HCC at that age (Bettermann et al., 2010). Macroscopic analyses of livers confirmed the presence of hepatic tumors in TAK1$^{LPC\text{-}KO}$ mice (Figure 4A). Surprisingly, TAK1/Casp-8$^{LPC\text{-}KO}$ animals did not show any signs of macroscopically detectable hepatic tumors at this age. In contrast, TAK1$^{LPC\text{-}KO}$/RIP3$^{-/-}$ mice exhibited a massive hepatic tumor burden already visible on macroscopic level (Figure 4A). The high hepatic tumor burden in these mice corresponded with a significant increase in the liver-to-body weight ratio in TAK1$^{LPC\text{-}KO}$/RIP3$^{-/-}$ animals compared to TAK1 single mutants or TAK1/Casp-8 combined mutants (Figure 4B). On the histological level, we confirmed increased development of hepatic tumors with histological criteria of HCC in TAK1$^{LPC\text{-}KO}$/RIP3$^{-/-}$ mice by hematoxylin and eosin staining (H&E) staining and immunohistochemical analysis for collagen-IV expression. Conversely, no histologically malignant hepatic tumor or preneoplastic lesions could be detected in TAK1/Casp-8$^{LPC\text{-}KO}$ animals (Figures 4C and 4D). Thus, Caspase-8-dependent apoptosis promotes HCC development in TAK1$^{LPC\text{-}KO}$ mice. In contrast, the higher tumor burden in TAK1$^{LPC\text{-}KO}$/RIP3$^{-/-}$ mice compared to TAK1$^{LPC\text{-}KO}$ mice and the absence of hepatic tumors in TAK1/Casp-8$^{LPC\text{-}KO}$ livers exhibiting pure necroptosis suggest that activation of RIP3 has an inhibitory effect on tumor growth. Importantly, the fact that the massive tumor development in TAK1$^{LPC\text{-}KO}$/RIP3$^{-/-}$ mice could be completely abolished by cell-specific ablation of *Caspase-8* in LPC (TAK1/Casp-8$^{LPC\text{-}KO}$/RIP3$^{-/-}$ mice) (Figures S2E and S2F) argues against a significant effect of *Rip3* deletion in nonparenchymal hepatic cells in the regulation of hepatocarcinogenesis in TAK1$^{LPC\text{-}KO}$/RIP3$^{-/-}$ mice, which have an LPC-specific knockout of *Tak1* but full knockout of *Rip3*.

The finding that TAK1/Casp-8$^{LPC\text{-}KO}$ mice did not develop any HCC, whereas TAK1$^{LPC\text{-}KO}$/RIP3$^{-/-}$ mice showed larger HCC than TAK1$^{LPC\text{-}KO}$ single mutant animals, suggested that activation of RIP3 controls hepatocarcinogenesis in terms of the hepatic tumor burden. To test if RIP3 also influences hepatic tumor biology, HCC samples from TAK1$^{LPC\text{-}KO}$ and TAK1$^{LPC\text{-}KO}$/RIP3$^{-/-}$ mice were profiled by qRT-PCR with a 16 gene signature that identifies and stratifies liver tumors according to their degree of differentiation and proliferation rate (Cairo et al., 2008). For control, normal liver samples as well as samples of aggressive liver tumors from woodchuck hepatitis virus (WHV)/N-myc2 p53^{+}/delta mice (Renard et al., 2000) were added to the analysis. Unsupervised analysis of the samples profiled showed coclustering of nearly all TAK1$^{LPC\text{-}KO}$ and TAK1$^{LPC\text{-}KO}$/RIP3$^{-/-}$ tumors (Figure 4E). We also examined expression of alpha fetoprotein (AFP) and selected oncogenes and tumor suppressor genes (antigen-presenting cell [APC], p53, E2F transcription factor 5 [E2F5], cyclin-dependent kinase inhibitor 2A [CDKN2A], cyclin D1, neuroepithelial cell transforming 1 [Net1], FgR, and Jun) in HCC from both mouse lines. Despite elevated cyclin D1 and APC levels in TAK1$^{LPC\text{-}KO}$/RIP3$^{-/-}$ tumors, most other genes examined showed similar transcriptional levels in HCC from TAK1$^{LPC\text{-}KO}$ and TAK1$^{LPC\text{-}KO}$/RIP3$^{-/-}$ livers (Figure 4F). Together, these findings indicate similar tumor biology of HCC in both mouse lines, suggesting that activation of RIP3 in TAK1$^{LPC\text{-}KO}$ mice inhibits hepatocarcinogenesis by a dominant effect on tumor initiation and proliferation of tumor cells.

RIP3 Controls the Transition from Inflammation to Cancer by Inhibiting Caspase-8-Induced Chromosomal Aberrations Associated with Immortalization of Hepatocytes

To further analyze the functional roles of necroptosis and apoptosis on hepatocarcinogenesis, we performed array-comparative genomic hybridization (aCGH) analyses on histologically characterized and microdissected HCCs from TAK1$^{LPC\text{-}KO}$

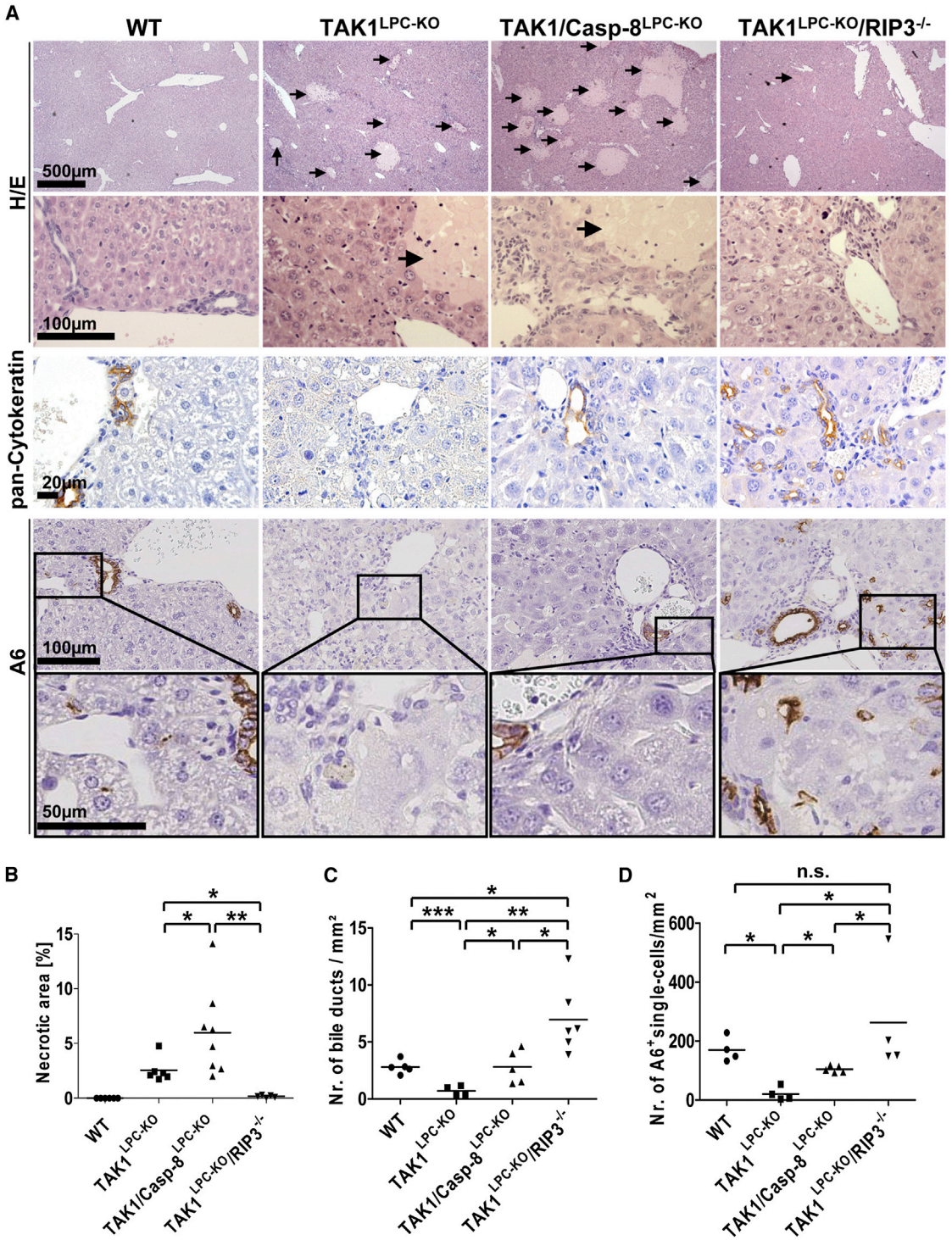

Figure 2. RIP3-Dependent Necroptosis Mediates Cholestasis and Biliary Ductopenia by Suppressing Caspase-8-Dependent Ductular Reaction in Livers of Mice with LPC-Specific *Tak1* Deletion

(A) Histological (H&E) and immunohistochemical (pancytokeratin, A6) analysis on representative liver sections from 6-week-old male mice. Arrows indicate necrotic areas. The scale bars represent (from top to bottom) 500 μm, 100 μm, 20 μm, 100 μm, and 50 μm.

(B) Evaluation of necrotic areas from H&E staining. WT (n = 6), TAK1^{LPC-KO} (n = 6), TAK1/Casp-8^{LPC-KO} (n = 6), and TAK1^{LPC-KO}/RIP3$^{-/-}$ (n = 5) livers. Results are shown as mean. The asterisk denotes $p < 0.05$ and double asterisks denote $p < 0.01$.

(legend continued on next page)

and TAK1$^{LPC\text{-}KO}$/RIP3$^{-/-}$ mice and areas of disturbed microarchitecture (histologically not HCC or dysplastic nodules) in TAK1/Casp-8$^{LPC\text{-}KO}$ animals (Figure 5A). As previously shown for TAK1$^{LPC\text{-}KO}$ mice (Bettermann et al., 2010) and corroborated on three HCCs in this study, TAK1$^{LPC\text{-}KO}$ displays large chromosomal amplifications mainly on chromosomes 4, 8, and 13. Interestingly, amplifications on these chromosomes were also found in most tumors of TAK1$^{LPC\text{-}KO}$/RIP3$^{-/-}$ mice. However, the majority of TAK1$^{LPC\text{-}KO}$/RIP3$^{-/-}$ tumors displayed multiple additional chromosomal aberrations, of which many were not found in tumors of most TAK1$^{LPC\text{-}KO}$ animals (chromosomes 1, 5–6, 9, and 11–12; Figure 5A; Bettermann et al., 2010). In contrast, TAK1/Casp-8$^{LPC\text{-}KO}$ animals hardly displayed any significant chromosomal aberrations in their livers (Figure 5A). These data suggest that, in chronic hepatitis, apoptosis but not necroptosis specifically promotes the development of liver cancer by favoring an environment that drives genetic aberrations. Moreover, necroptosis not only inhibits tumor growth but also counterbalances the establishment of genetic alterations in HCC.

The striking pattern of chromosomal aberrations detected in TAK1$^{LPC\text{-}KO}$ and TAK1$^{LPC\text{-}KO}$/RIP3$^{-/-}$ tumors but not livers of TAK1/Casp-8$^{LPC\text{-}KO}$ mice prompted us to further investigate if these genetic changes might withhold a functional role in the transition from inflammation to cancer (e.g., by driving LPC specifically resistant to apoptotic cell death). To test this, we isolated primary hepatocytes from 8-week-old WT, TAK1/Casp-8$^{LPC\text{-}KO}$, and TAK1$^{LPC\text{-}KO}$/RIP3$^{-/-}$ mice, lacking immunohistochemical and molecular evidence for malignant tumors (data not shown). Twenty-four hours after isolation, cells were washed carefully to remove dead cells and then stimulated with recombinant murine TNF, a treatment that induces cell-death of *Tak1*-deficient but not WT hepatocytes, due to their inability to activate nuclear factor (NF)-κB (Bettermann et al., 2010). Twenty-four hours after TNF stimulation, TAK1/Casp-8$^{LPC\text{-}KO}$ but not WT hepatocytes lost attachment to the plate and showed morphological signs of cell death (Figure 5B), indicating that TNF treatment led to necroptosis of hepatocytes in vitro. Whereas also many hepatocytes isolated from TAK1$^{LPC\text{-}KO}$/RIP3$^{-/-}$ livers showed morphological signs of cell death, some cells with large nuclei survived TNF treatment and were collected for preparation of genomic DNA followed by aCGH analysis for their genetic status. Strikingly, cells displayed the same pattern of chromosomal aberrations on chromosomes 4, 8, and 13 as seen previously in HCC from these animals as well as additional chromosomal aberrations (Figure 5C). These data provide evidence that the specific, Caspase-8-dependent pattern of chromosomal aberrations on chromosomes 4, 8, and 13 in TAK1$^{LPC\text{-}KO}$/RIP3$^{-/-}$ mice arises already at an early step of hepatocarcinogenesis and is associated with immortalization of hepatocytes in a setting of Caspase-8-dependent apoptosis. In line with this hypothesis, we identified focal areas free of Caspase-3 activation already in 6-week-old TAK1$^{LPC\text{-}KO}$/RIP3$^{-/-}$ mice (Figure S3), probably reflecting in vivo a corresponding early step of clonal immortalization.

Caspase-8-Dependent Apoptosis but Not RIP3-Dependent Necroptosis Is Associated with a Strong Inflammatory Response and Liver Fibrosis

We aimed at further characterizing mediators of compensatory LPC proliferation activated in response to Caspase-8 but not RIP3-dependent necroptosis. Liver regeneration was previously shown to involve the production of inflammatory cytokines secreted by hepatic macrophages/Kupffer cells (Michalopoulos and DeFrances, 2005), suggesting that differential inflammatory responses to LPC apoptosis versus necroptosis might be associated with the differences in LPC proliferation between both respective mouse lines. Fluorescence-activated cell sorting (FACS) analysis revealed stronger infiltration of myeloid cells and CD4$^+$ and CD8$^+$ T cells but similar levels of B cells in both TAK1$^{LPC\text{-}KO}$ and TAK1$^{LPC\text{-}KO}$/RIP3$^{-/-}$ mice compared with WT and TAK1/Casp-8$^{LPC\text{-}KO}$ animals (Figure 6A; data not shown). Immunohistochemical analysis confirmed a clear trend toward higher numbers of F4/80$^+$ cells in TAK1$^{LPC\text{-}KO}$/RIP3$^{-/-}$ mice compared with TAK1/Casp-8$^{LPC\text{-}KO}$ animals (Figure 6B). To further examine expression levels of cytokines typically secreted by activated macrophages, we performed a FACS-based microbeads fluorescence assay on liver homogenates, which revealed significantly higher protein levels of interleukin (IL)-1α, IL-6, and IL-10 in TAK1$^{LPC\text{-}KO}$ and TAK1$^{LPC\text{-}KO}$/RIP3$^{-/-}$ compared to TAK1/Casp-8$^{LPC\text{-}KO}$ animals (Figure 6C), of which IL-1α and IL-6 represent key cytokines driving compensatory proliferation and HCC development in response to hepatocyte death (Maeda et al., 2005; Sakurai et al., 2008). Thus, in contrast to previous concepts of oncotic necrosis versus necrosis (Jaeschke and Lemasters, 2003), we show here that LPC apoptosis rather than necroptosis drives inflammation in response to chronic injury.

We further tested for the presence of liver fibrosis by Sirius red stainings on liver slides from 6-week-old WT, TAK1/Casp-8$^{LPC\text{-}KO}$, and TAK1$^{LPC\text{-}KO}$/RIP3$^{-/-}$ mice. This analysis showed only a slight increase in fibrosis in TAK1/Casp-8$^{LPC\text{-}KO}$ livers at that age, which in turn was significantly lower than seen in TAK1$^{LPC\text{-}KO}$/RIP3$^{-/-}$ animals (Figure S4A). Additional RT-PCR analysis on whole liver RNA extracts revealed only a trend toward higher levels of TGF-β1 and TGF-β3 in TAK1$^{LPC\text{-}KO}$/RIP3$^{-/-}$ mice compared with TAK1/Casp-8$^{LPC\text{-}KO}$ livers (Figure S4B). Whereas levels of active TGF-β ligands might not be fully reflected on RNA levels, due to potential differences in cleavage processes (Dubois et al., 2001), these data suggest that apoptosis but not necroptosis induces hepatic fibrogenesis and activation of stellate cells by various profibrogenic and proinflammatory stimuli.

(C) Statistical quantification of number of bile ducts per mm^2 in WT (n = 5), TAK1$^{LPC\text{-}KO}$ (n = 4), TAK1/Casp-8$^{LPC\text{-}KO}$ (n = 5), and TAK1$^{LPC\text{-}KO}$/RIP3$^{-/-}$ (n = 6) livers. TAK1$^{LPC\text{-}KO}$ livers show decreasing of bile ducts, whereas, in TAK1$^{LPC\text{-}KO}$/RIP3$^{-/-}$, livers increase the number of bile ducts compared with the other genotypes. Results are shown as mean. The asterisk denotes $p < 0.05$, double asterisks denote $p < 0.01$, and triple asterisks denote $p < 0.001$.
(D) Statistical analysis of A6$^+$ single-oval cells per mm^2 in the respective 6-week-old mice. Results are shown as mean (n = 4, except for TAK1/Casp-8$^{LPC\text{-}KO}$ mice, where n = 5); *$p < 0.05$; n.s., not significant.

Cell PRESS
Open ACCESS

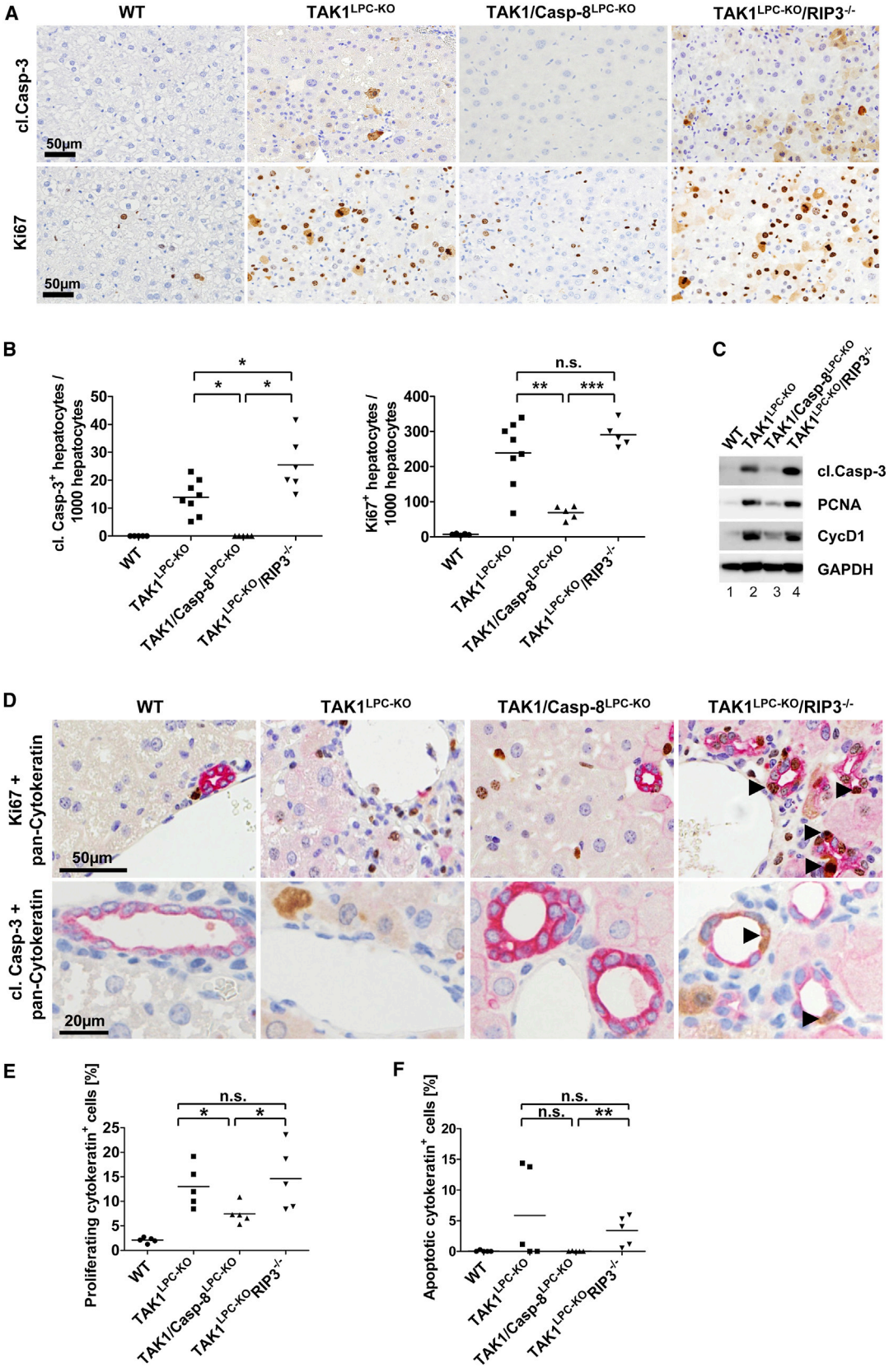

(legend on next page)

Caspase-8-Dependent Apoptosis Drives Compensatory LPC Proliferation by Activation of JNK in Parenchymal and Nonparenchymal Liver Cells

We further examined which intracellular signaling pathways might connect the two different modes of cell death with activation or inhibition of compensatory proliferation and cancer development. In *Drosophila*, activation of Jun-(N)-terminal kinase (JNK) by the initiator caspase Dronc is driving apoptosis-induced compensatory proliferation (Huh et al., 2004; Kondo et al., 2006). Moreover, it was suggested that JNK activation is part of a nonapoptotic, procarcinogenic pathway downstream of CD95/Fas/APO-1 (Chen et al., 2010). Western blot analysis on liver extracts from 6-week-old mice revealed strong spontaneous phosphorylation and activation of JNK but not p38α, AKT, or ERK in livers of TAK1$^{LPC\text{-}KO}$/RIP3$^{-/-}$ compared with TAK1/Casp-8$^{LPC\text{-}KO}$ and WT animals (Figure 7A). Immunohistochemical staining for the phosphorylated JNK forms confirmed significantly more phosphorylated JNK (p-JNK)$^{+}$ hepatocytes in TAK1$^{LPC\text{-}KO}$/RIP3$^{-/-}$ compared to TAK1/Casp-8$^{LPC\text{-}KO}$ and WT animals (Figure 7B). Importantly, TAK1$^{LPC\text{-}KO}$/RIP3$^{-/-}$ livers even displayed significantly more p-JNK^{+} hepatocytes than TAK1$^{LPC\text{-}KO}$ single knockouts (Figure 7C). In addition, TAK1$^{LPC\text{-}KO}$/RIP3$^{-/-}$ livers showed a significantly higher fraction of p-JNK^{+} liver nonparenchymal cells (NPC) than all other genotypes, although to a much lower extent than observed in terms of hepatocytes (Figure S5). Finally, to functionally evaluate the role of JNK in mediating apoptosis and compensatory proliferation in TAK1$^{LPC\text{-}KO}$/RIP3$^{-/-}$ mice, we injected TAK1$^{LPC\text{-}KO}$/RIP3$^{-/-}$ mice with the well-established JNK-inhibitor SP600125, which significantly decreased the amount of Ki67^{+} cells and lowered cyclin D1 expression when compared to vehicle-treated animals (Figures 7D, 7E, and 7G). Additional analysis of cleaved Casp-3^{+} cells lacked a significant difference between the two groups (Figures 7D and 7F). These data suggest that JNK activation represents an important step in mediating compensatory proliferation downstream of Caspase-8, whereas, in contrast, RIP3 inhibits the activation of JNK in livers of TAK1$^{LPC\text{-}KO}$ mice.

DISCUSSION

The natural course of chronic hepatic disease is characterized by a relatively uniform pattern, featuring constant hepatocyte cell death, inflammation and compensatory hepatocyte proliferation, hepatic fibrogenesis, and ultimately the development of HCC (Sherman, 2010). Although this sequence has been known for many years, it has not been well characterized which exact molecular pathways are regulating the critical transition from inflammation to cancer, which explains why, up to now, no nonpathogen-specific chemopreventive strategy has been developed against HCC in patients with chronic liver disease. We show that, in a setting of chronic inflammation induced by LPC-specific deletion of *Tak1*, RIP3-dependent necroptosis represents a pathway regulating the consequences of chronic inflammation in the liver by counteracting against Caspase-8-dependent compensatory proliferation of hepatocytes, immune cell activation, hepatic fibrogenesis, and the development of chromosomal aberrations leading to hepatocarcinogenesis.

Studies have demonstrated that necroptosis serves as an alternative when caspase-dependent apoptosis is inhibited or absent (Han et al., 2011). Of note, our findings indicated the simultaneous activation of both apoptosis and necroptosis in livers of TAK1$^{LPC\text{-}KO}$ animals, mediating either carcinogenesis or cholestasis. *Tak1* deletion in LPC results in inhibition of NF-κB activation (Bettermann et al., 2010), which in turn leads to increased sensitivity against spontaneous apoptosis, as demonstrated in mice with conditional deletion of the NF-κB-activating kinase subunit NF-κB essential modulator (NEMO) (Luedde et al., 2007; Wunderlich et al., 2008). On the other hand, it was recently shown in vitro that TAK1 can prevent necroptosis by inhibiting the action of RIP1/RIP3 complexes (Vanlangenakker et al., 2011), supporting the hypothesis that TAK1 inhibits activation of both programmed cell death pathways in LPC. Based on our findings, it is likely that, in the absence of *Rip3*, LPC are "forced" to die by apoptosis, leading to increased inflammation and a higher tumor burden in TAK1$^{LPC\text{-}KO}$/RIP3$^{-/-}$ mice. TAK1 is therefore a master regulator of liver cell death induced, for example, by the cytokines TNF-α and TGF-β (Inokuchi et al., 2010; Yang et al., 2013). Moreover, the fact that cultured primary TAK1-deficient hepatocytes show a decreased survival in serum-free conditions (Bettermann et al., 2010) indicates also an intrinsic component of cell death in these cells.

As stated before, livers with conditional deletion of *Tak1* in LPC show defective NF-κB activation and—similar to other mouse models with genetic defects in the NF-κB pathway

Figure 3. Apoptosis but Not Necroptosis Induces Strong Compensatory Proliferation of Hepatocytes and Biliary Epithelial Cells upon Chronic Liver Injury

(A) Immunohistochemical analysis on representative liver paraffin sections from 6-week-old male mice of the indicated genotypes. Upper panel: cleaved (cl.) Caspase-3 staining. Lower panel: Ki67 staining. The scale bars represent 50 μm.

(B) Statistical analysis of Ki67^{+} and cl. Casp-3^{+} hepatocytes. Results are shown as mean (cl. Casp-3 staining: WT [n = 5]; TAK1$^{LPC\text{-}KO}$ [n = 8]; TAK1/Casp-8$^{LPC\text{-}KO}$ [n = 5]; TAK1$^{LPC\text{-}KO}$/RIP3$^{-/-}$ [n = 6] and Ki67 staining: WT [n = 5]; TAK1$^{LPC\text{-}KO}$ [n = 8]; TAK1/Casp-8$^{LPC\text{-}KO}$ [n = 5]; TAK1$^{LPC\text{-}KO}$/RIP3$^{-/-}$ [n = 5]). The asterisk denotes $p < 0.05$, double asterisks denote $p < 0.01$, and triple asterisks denote $p < 0.001$.

(C) Western blot analysis of whole liver protein extracts from 6-week-old male TAK1$^{LPC\text{-}KO}$, TAK1/Casp-8$^{LPC\text{-}KO}$, TAK1$^{LPC\text{-}KO}$/RIP3$^{-/-}$, and control littermate mice (WT) using antibodies against PCNA, CycD1, cl. Casp-3, and GAPDH as loading control.

(D) Double stainings of pancytokeratin with Ki67 (upper panel; pancytokeratin is stained pink, Ki67 is stained brown) or cl. Casp-3 (lower panel; pancytokeratin is stained pink, cl. Casp-3 is stained brown). Arrowheads indicate double-stained cells.

(E) Statistical analysis of double-stained pancytokeratin^{+} and Ki67^{+} biliary epithelial cells in the respective 6-week-old mice. Results are shown as mean (n = 5); *$p < 0.05$; n.s., not significant.

(F) Statistical analysis of double-stained pancytokeratin^{+} and cl. Casp-3^{+} biliary epithelial cells in the respective 6-week-old mice. Results are shown as mean (n = 5). Double asterisks denote $p < 0.01$.

See also Figures S1 and S2.

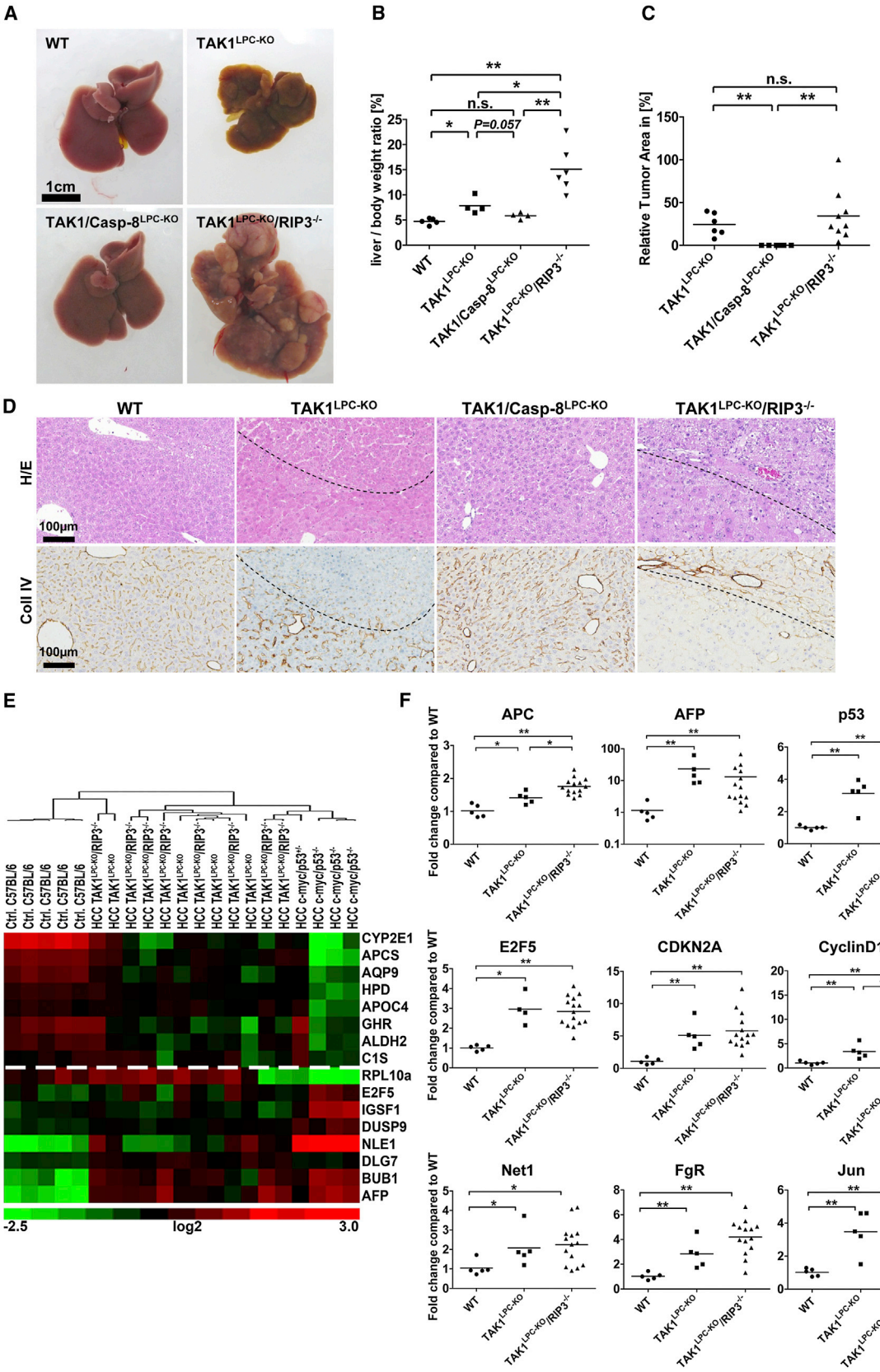

(legend on next page)

(Luedde and Schwabe, 2011)—are therefore extremely sensitive to LPS/TNF-induced liver failure and LPC apoptosis (Bettermann et al., 2010). However, we show that, already in livers of young TAK1^{LPC-KO}/RIP3$^{-/-}$ mice, a fraction of hepatocytes gained resistance toward TNF-dependent apoptosis, despite the absence of *Tak1*, and showed a pattern of chromosomal aberrations that was later found in HCC from these mice. These findings indicate that the specific chromosomal aberration pattern on chromosomes 4, 8, and 13 is not particularly acquired in late stages of tumor promotion but represents a fundamental genetic event involved in the earliest steps of tumor initiation in chronic inflammation in TAK1^{LPC-KO} mice. The exact nature of these genetic abnormalities is currently not clear, but they might lead to resistance toward apoptosis through the amplification of antiapoptotic genes or defective transcription of genes driving apoptosis in *Tak1*-deficient cells. Thus, further cytogenetic or transcriptomic analysis of TAK1^{LPC-KO}-HCCs might reveal novel candidate molecules or micro-RNAs involved in the regulation of apoptosis in *Tak1*-deficient cells. In addition, these findings might shed new light on the enigmatic processes of how chronic inflammation leads to genetic alterations in human patients with chronic liver disease.

In original definitions of apoptosis detected, for example, during organ development, intracellular contents are not released, and a consequent inflammatory response fails to develop, whereas the typical oncotic necrosis induced, for example, by ischemia is associated with release of cellular contents, initiating an inflammatory response (Jaeschke and Lemasters, 2003). By our genetic approach, we demonstrated that LPC apoptosis occurring in a pathological condition represents a much stronger trigger for inflammation and subsequent liver fibrosis than necroptosis. Given the concordant regulations between inflammation and fibrosis in TAK1^{LPC-KO}/RIP3$^{-/-}$ versus TAK1/Casp-8^{LPC-KO} livers, further comparative analyses in serum and cell culture supernatants between these two mouse models might allow the identification of novel paracrine factors linking apoptotic cell death of LPC with immune activation and hepatic fibrosis. Moreover, our data show that apoptosis and necroptosis have a fundamentally opposing function in regulating compensatory cell proliferation of surrounding cells in vivo. Whereas Caspase-8-dependent apoptosis in TAK1^{LPC-KO}/RIP3$^{-/-}$ mice led to a strong biliary reaction and expansion of bile ducts and oval cells in young animals, the "hyporegenerative" nature of necroptosis resulted in a disturbed biliary homeostasis and cholestasis. Interestingly, the intrahepatic number of bile ducts was significantly lower in TAK1^{LPC-KO} livers with combined presence of apoptosis and necroptosis than in TAK1/Casp-8^{LPC-KO} mice showing only necroptosis. This indicates that the complex biliary architecture might be even more sensitive to the onset of necroptosis in a setting with constant massive hepatocyte regeneration when apoptosis is simultaneously present. Whereas the mechanisms and functional implications of biliary ductular reactions are presently not well understood, the TAK1 model might shed new light on these processes and on paracrine mediators, linking cell death with differentiation and proliferation of bile duct cells.

Our data suggest that the MAP kinase JNK plays a critical role in the mediation of compensatory LPC proliferation in response to apoptosis. The function of JNK in liver cancer development was previously studied mainly in the model of diethylnitrosamine-dependent hepatocarcinogenesis, resulting in conflicting results with regards to a tumor promoting versus a tumor suppressive function in hepatocytes (Das et al., 2011; Sakurai et al., 2006). However, the proregenerative and presumably procarcinogenic function of JNK suggested by our data might depend on the presence of chronic inflammation preceding malignant transformation of hepatocytes, a situation present in most patients developing liver cancer (Llovet et al., 2003; Vucur et al., 2010). Moreover, our findings suggest that JNK not only acts upstream of Caspase-8 to control apoptosis, as previously shown (Chang et al., 2006), but is also regulated in response to Caspase-8, because ablation of Caspase-8 significantly dampened JNK activation in *Tak1*-deficient livers. Whether Caspase-8 controls JNK activation by cell-intrinsic signals (e.g., alternative MAP-3 kinases and their interaction with TNF receptor-associated factor or RIP modules [Karin and Gallagher, 2009]), or by cell-extrinsic mechanisms is presently unclear. Again, it is possible that, during carcinogenesis, certain genetic aberrations resulting in a condition similar to "undead cells" might promote JNK-dependent proliferation in response to apoptosis, a concept previously suggested in

Figure 4. Apoptosis Promotes Hepatocarcinogenesis, whereas Necroptosis Inhibits Cancer Growth in Livers of TAK1^{LPC-KO} Mice

(A) Representative macroscopic pictures of 33- to 35-week-old male WT (from left to the right), TAK1^{LPC-KO}, TAK1/Casp-8^{LPC-KO}, and TAK1^{LPC-KO}/RIP3$^{-/-}$ livers. The scale bars represent 1 cm.

(B) Body-weight ratio of 25- to 38-week-old male WT (n = 6), TAK1^{LPC-KO} (n = 4), TAK1/Casp-8^{LPC-KO} (n = 4), and TAK1^{LPC-KO}/RIP3$^{-/-}$ (n = 6) mice. The asterisk denotes $p < 0.05$ and double asterisks denote $p < 0.01$.

(C) Evaluation of tumor areas from H&E staining. TAK1^{LPC-KO} (n = 6), TAK1/Casp-8^{LPC-KO} (n = 6), and TAK1^{LPC-KO}/RIP3$^{-/-}$ (n = 9) livers. Results are shown as mean. Double asterisks denote $p < 0.01$.

(D) Representative slides from livers of a 28-week-old WT, TAK1^{LPC-KO}, TAK1/Casp-8^{LPC-KO}, and TAK1^{LPC-KO}/RIP3$^{-/-}$ mouse stained with H&E and collagen IV. Tumor borders are indicated by a dashed line.

(E) Sixteen gene profile analysis (heat map) of HCC derived from TAK1^{LPC-KO} and TAK1^{LPC-KO}/RIP3$^{-/-}$ livers (25- to 38-week-old mice). HCC were compared to aggressive liver tumors from WHV/N-myc2 p53^{+}/delta mice and control WT mice. Below the dashed line, genes indicating a proliferative phenotype are listed, whereas genes above the dashed white line represent a less proliferative, more differentiated phenotype. HCC derived from TAK1^{LPC-KO} and TAK1^{LPC-KO}/RIP3$^{-/-}$ livers show a similar proliferating phenotype.

(F) Relative (rel.) messenger RNA (mRNA) expression of the indicated oncogenes/tumor suppressor genes (APC, AFP, tumor protein p53 [p53], E2F5, CDKN2A, cyclin D1, Net1, Gardner-Rasheed feline sarcoma viral oncogene homolog [FgR], Jun oncogene [Jun]) of HCC derived from 25- to 38-week-old TAK1^{LPC-KO} (n = 5) and TAK1^{LPC-KO}/RIP3$^{-/-}$ (n = 14) mice as well as normal tissue from littermate control (WT) (n = 5). The asterisk denotes $p < 0.05$ and double asterisks denote $p < 0.01$.

See also Figure S2.

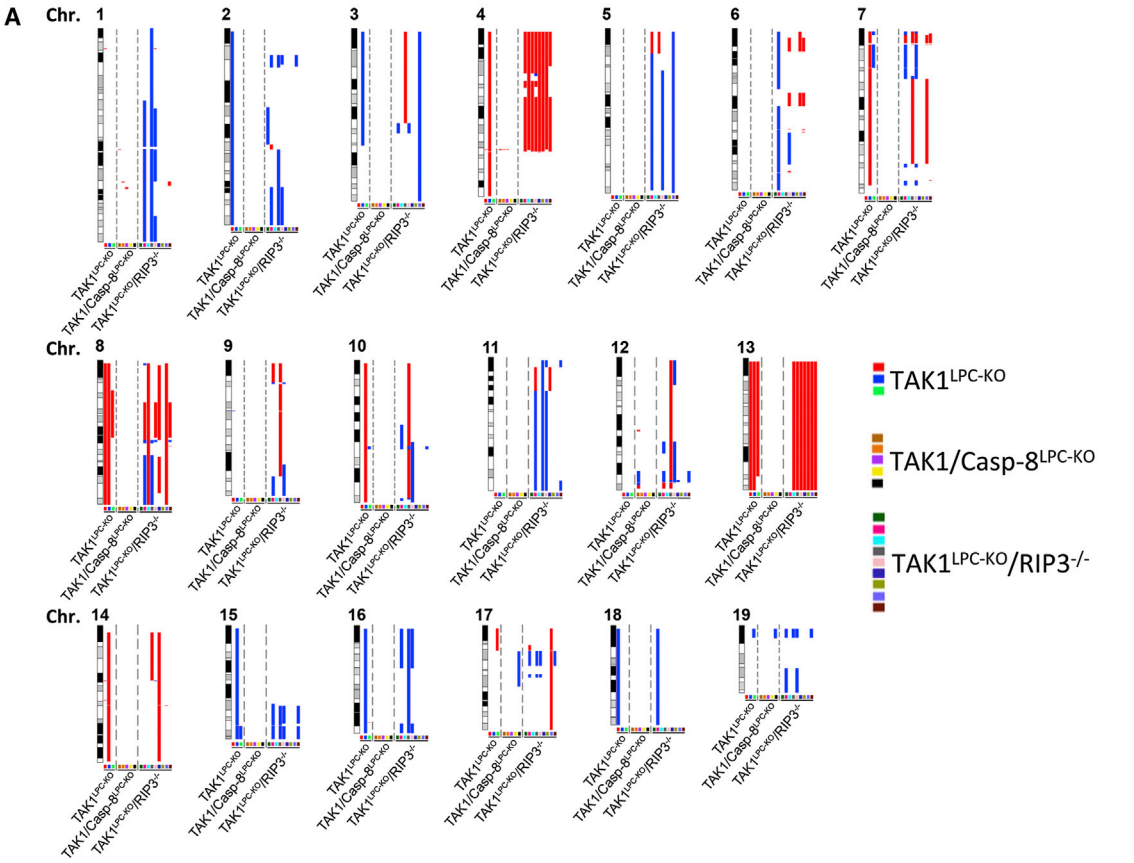

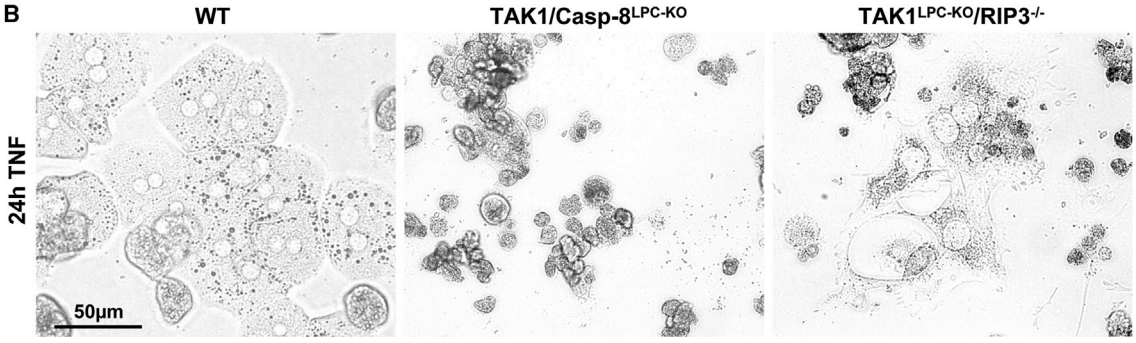

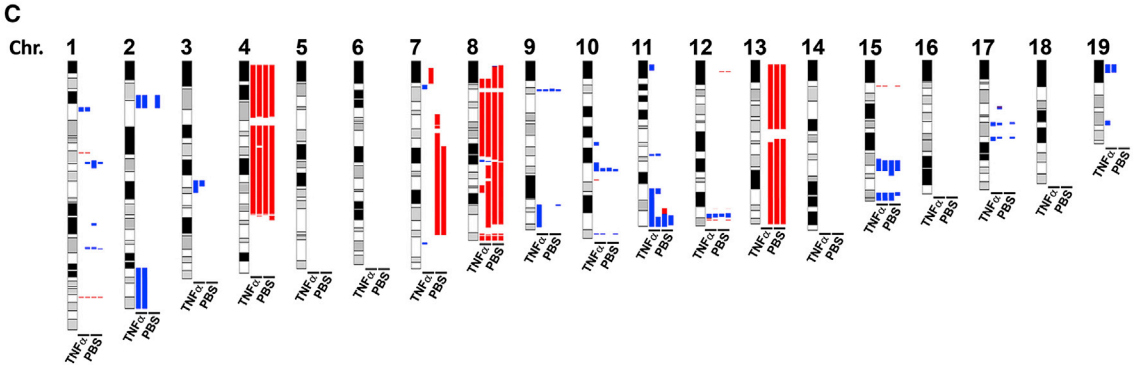

(legend on next page)

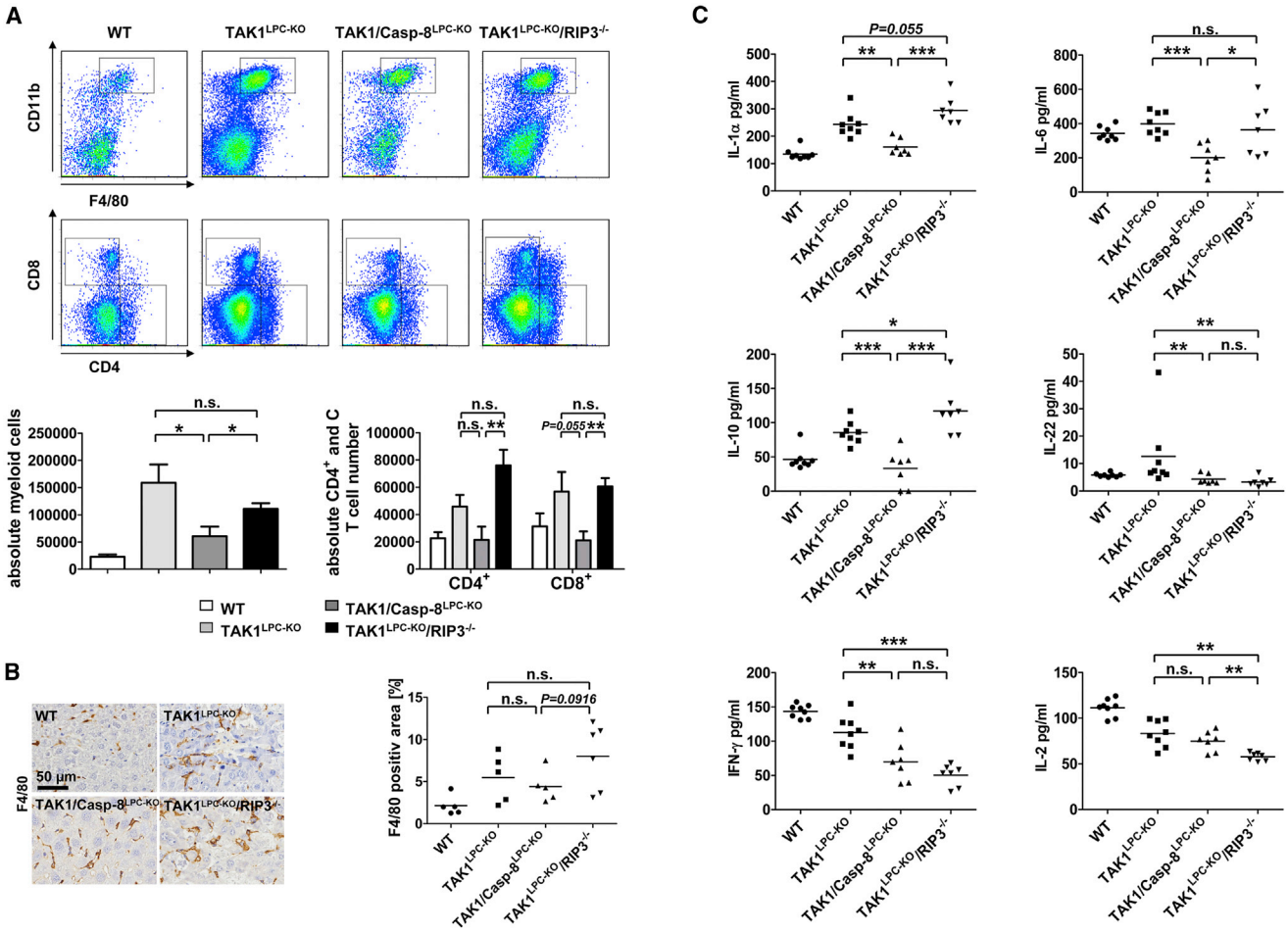

Figure 6. Differential Inductions of Inflammatory Responses by Apoptosis and Necroptosis in *Tak1*-Deficient Livers

(A) FACS-based analysis of infiltrating myeloid cells and T cells into liver tissue of TAK1^{LPC-KO}, TAK1/Casp-8^{LPC-KO}, and TAK1^{LPC-KO}/RIP3$^{-/-}$ mice. Results are shown as mean; error bars indicate SEM n = 5; *p < 0.05, **p < 0.01.

(B) Immunohistochemistry of liver paraffin sections and densitometric analysis for F4/80 in TAK1^{LPC-KO}, TAK1/Casp-8^{LPC-KO}, TAK1^{LPC-KO}/RIP3$^{-/-}$, and WT livers. Results are shown as mean; n = 5 for WT and TAK1/Casp-8^{LPC-KO}; n = 6 for TAK1^{LPC-KO}/RIP3$^{-/-}$. The scale bar represents 50 μm.

(C) FACS-based microbeads fluorescence assay for cytokine expression in liver protein homogenates. Results are shown as mean. n = 8 for WT and TAK1^{LPC-KO} and n = 7 for TAK1/Casp-8^{LPC-KO} and TAK1^{LPC-KO}/RIP3$^{-/-}$; *p < 0.05, **p < 0.01, ***p < 0.001.

See also Figure S4.

Drosophila (Ryoo and Bergmann, 2012). Interestingly, JNK activation was strongly increased in LPC (28-fold increase compared to WT) and less pronounced in NPC of TAK1^{LPC-KO}/RIP3$^{-/-}$ mice (1.18-fold increase compared to WT), favoring a parenchymal function of JNK. Moreover, it is presently unclear which specific factors released by apoptotic but not necroptotic parenchymal cells are involved in the activation process of immune cells, induction of chromosomal aberrations, and HCC development, but these processes might involve damage-associated molecular patterns/alarmins, such as high-mobility group protein 1, HMGN1, HSP60/HSP70, or β-defensins (Chan et al., 2012).

Figure 5. RIP3 Controls the Transition from Inflammation to Cancer by Inhibiting Chromosomal Aberrations Associated with Resistance of Hepatocytes toward Caspase-8-Dependent Apoptosis

(A) Summary of CGH analysis from three different hepatic tumors of three TAK1^{LPC-KO} mice, nine different tumors of nine TAK1^{LPC-KO}/RIP3$^{-/-}$ mice, and five samples of areas with disturbed histological architecture (no obvious tumors) from five TAK1/Casp-8^{LPC-KO} mice. The q-arm of each chromosome is shown and chromosome numbers are indicated. Dark horizontal bars within the symbolized chromosomes represent G bands. Chromosomal deletions are indicated in blue and amplifications in red. Individual mice are labeled by horizontal collared bars.

(B) Microscopic pictures of TNF-α-treated primary hepatocytes from WT, TAK1/Casp-8^{LPC-KO}, and TAK1^{LPC-KO}/RIP3$^{-/-}$ mice.

(C) Summary of CGH analysis from untreated and survived TNF-α-treated primary hepatocytes from TAK1^{LPC-KO}/RIP3$^{-/-}$ mice. Chromosomal amplifications and deletions are indicated in red and blue, respectively. IFN, interferon.

See also Figure S3.

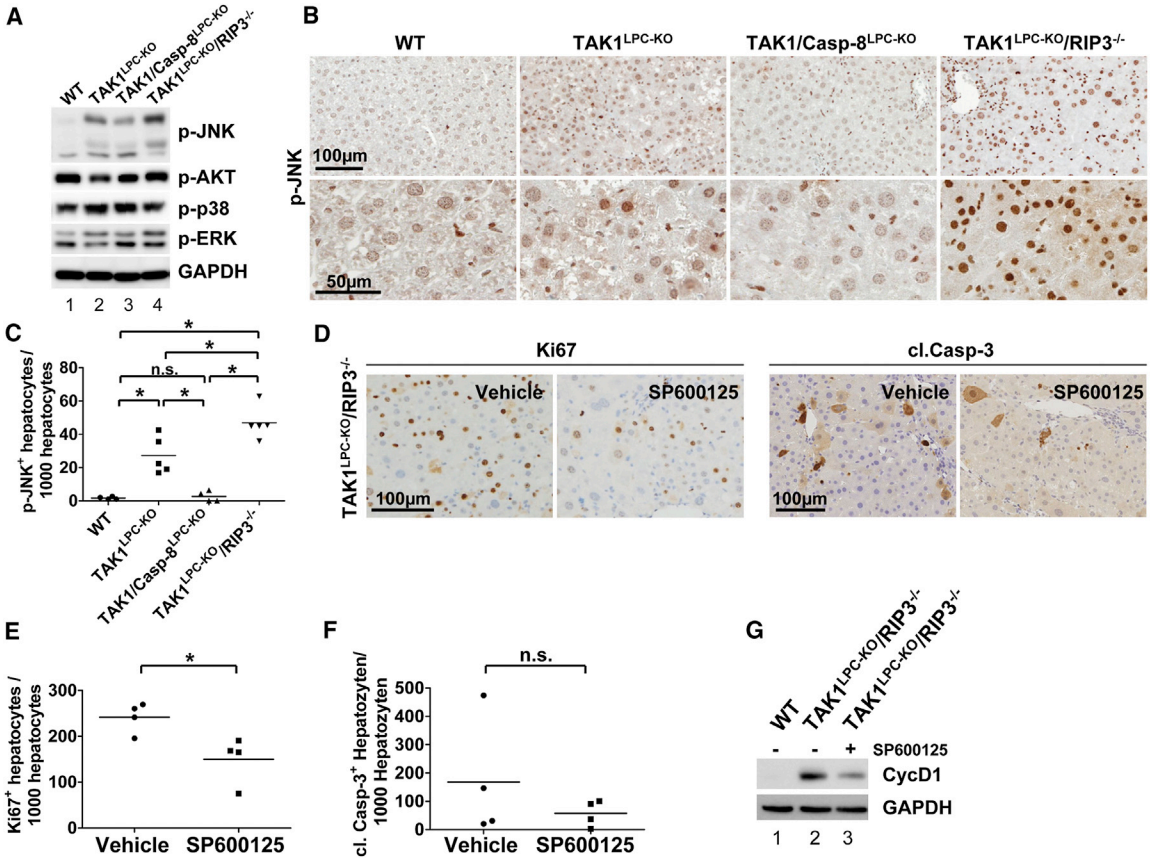

Figure 7. RIP3 Limits Compensatory Cell Proliferation through Inhibition of Caspase-8-Dependent JNK Activation

(A) Western blot analysis of whole liver-protein extracts from 6-week-old male TAK1^{LPC-KO}, TAK1/Casp-8^{LPC-KO}, TAK1^{LPC-KO}/RIP3$^{-/-}$, and control littermate mice (WT) using antibodies against the phosphorylated and active form of JNK, AKT, p38, ERK, and GAPDH as loading control.

(B) Immunohistochemistry of representative liver paraffin sections for phospho-JNK in 6-week-old mice. The scale bars represent 100 μm and 50 μm.

(C) Statistical analysis of p-JNK^{+} hepatocytes. Results are shown as mean. WT (n = 4), TAK1^{LPC-KO} (n = 5), TAK1/Casp-8^{LPC-KO} (n = 4), and TAK1^{LPC-KO}/RIP3$^{-/-}$ (n = 5) mice; *p < 0.0.

(D) Representative immunohistochemical analysis for Ki67 and cl. Casp-3 in 6-week-old mice treated with the JNK inhibitor SP600125 or vehicle as control.

(E) Statistical analysis of Ki67^{+} hepatocytes in animals treated with SP600125 compared to vehicle control-treated animals. Results are shown as mean. (n = 4); *p < 0.05.

(F) Statistical analysis of cl. Casp-3^{+} hepatocytes in TAK1^{LPC-KO}/RIP3$^{-/-}$ treated with SP600125 compared to vehicle control-treated mice. Results are shown as mean. (n = 4).

(G) Western blot analysis of whole liver protein extracts from 6-week-old male TAK1^{LPC-KO}/RIP3$^{-/-}$ and WT mice treated with SP600125 or vehicle using antibodies against CycD1 and GAPDH as loading control.

See also Figure S5.

Our findings indicate that mechanisms regulating the balance between necroptosis and apoptosis might be of great relevance for human liver disease and are in line with the clinical observation that an overbalance of necrotic over apoptotic hepatic cell death in acute liver failure is associated with a decreased regenerative capacity of the liver as a basis for a worse outcome (Bantel and Schulze-Osthoff, 2012). In addition, RIP3 mediates ethanol-induced liver injury (Roychowdhury et al., 2013). Thus, inhibition of RIP3-dependent or independent necrotic signaling pathways by novel molecular inhibitors might represent a promising approach in these settings. In addition, our findings indicate that LPC apoptosis plays a dominant role for the progression of chronic liver injury to liver cancer. Therefore, molecular inhibitors of caspases recently studied in patients with chronic hepatitis C virus infection (Pockros et al., 2007) or nonalcoholic steatohepatitis (Ratziu et al., 2012) might be especially useful in preventing the transition from chronic inflammation to hepatocarcinogenesis. Finally, inflammation is not only driving hepatocarcinogenesis but also the development of, for example, cancer of the colon (Greten et al., 2004), pancreas (Guerra et al., 2007), lung (Takahashi et al., 2010), or skin (Andreu et al., 2010). Hence, further studies in other cellular systems and organs are needed to examine if the paradigmatic functions of RIP3 versus Caspase-8 in regulating cellular compensatory proliferation and tumor growth in the liver represent a general principle in the control of epithelial cell homeostasis and cancer development.

EXPERIMENTAL PROCEDURES

Generation of Conditional Knockout Mice and Animal Experiments

Mice carrying loxP-site-flanked (floxed) alleles of the *Tak1* gene *Map3k7* (Tak1^{fl}) (Sato et al., 2005) or *Caspase-8* (Caspase-8^{fl}) (Salmena et al., 2003) were crossed to *Alfp*-Cre transgenic mice (Kellendonk et al., 2000) to generate a LPC-specific knockout of the respective genes (TAK1$^{LPC\text{-}KO}$, Caspase-8$^{LPC\text{-}KO}$). Mice with constitutive deletion of RIP3 (RIP3$^{-/-}$) were described before (Newton et al., 2004). Mice with combined conditional knockouts of *Map3k7* and constitutive ablation of *Rip3* (TAK1$^{LPC\text{-}KO}$/RIP3$^{-/-}$) as well as combined conditional ablations of *Map3k7* and *Caspase-8* (TAK1/Casp8$^{LPC\text{-}KO}$) as well as mice with constitutive ablations of *Rip3* and conditional ablations of *Map3k7* and *Caspase-8* in LPC (TAK1/Casp-8$^{LPC\text{-}KO}$/RIP3$^{-/-}$) were generated by intercrossing the respective lines. In all experiments, littermates carrying the respective loxP-flanked alleles but lacking expression of Cre recombinase were used as WT controls. Mice were bred on a mixed C57/BL6 - SV129Ola genetic background. Only sex-matched animals were compared. All animal experiments were approved by the Federal Ministry for Nature, Environment and Consumers' Protection of the state of North Rhine-Westphalia and were performed in accordance to the respective national, federal, and institutional regulations.

Surgery (partial hepatectomy) was performed on male mice of 6–8 weeks of age. Mice were anesthetized by isoflurane inhalation and treated with buprenorphine for analgesia. The abdominal cavity was opened by a midline laparotomy. The right median lobe, left median lobe, and left lateral lobe were identified and individually ligated. Mice were sacrificed at the indicated time points. Intraperitoneal injection of 15 μl SP600125 (1 mg/ABSOURCE) or vehicle (DMSO) was performed twice a day over 4 days on male mice of 5 weeks of age. Mice were sacrificed 3 hr after the last injection.

Statistics

Data were analyzed using PRISM software (GraphPad Software) and are expressed as mean. Statistical significance between experimental groups was assessed using an unpaired two-sample t test or Mann-Whitney test.

Further description of the Experimental Procedures is included within the Supplemental Information (Extended Experimental Procedures).

ACCESSION NUMBERS

The aCGH data have been deposited into the ArrayExpress database under accession number E-MTAB-1559 (http://www.ebi.ac.uk/arrayexpress/).

SUPPLEMENTAL INFORMATION

Supplemental Information includes Extended Experimental Procedures and five figures and can be found with this article online at http://dx.doi.org/10.1016/j.celrep.2013.07.035.

ACKNOWLEDGMENTS

The authors thank Dr. V. Dixit (Genentech, San Francisco, CA, USA) for kindly providing RIP3$^{-/-}$ mice, Dr. Shizuo Akira (Osaka, Japan) for kindly providing TAK1$^{fl/fl}$ mice, and Dr. Valentina M. Factor for kindly providing the A6 antibody. The authors are thankful for excellent technical support from Ruth Hillermann, Daniel Kull, and Olga Seelbach. T.L. was supported by the German Cancer Aid (Deutsche Krebshilfe 110043), an ERC Starting Grant (ERC-2007-Stg/208237-Luedde-Med3-Aachen), the German Research Foundation (SFB-TRR57/P06), the EMBO Young Investigator Program, the Interdisciplinary Centre for Clinical Research "BIOMAT" Aachen, the Ernst Jung Foundation Hamburg, and a grant from the medical faculty of the RWTH Aachen. M.H. was supported by the Helmholtz Foundation, the Hofschneider Foundation, the German Research Foundation (SFB-TR36), the Helmholtz Alliance Preclinical Comprehensive Center, and an ERC Starting Grant (LiverCancerMechanisms). M.L. was supported by the Deutsche Stiftung Herzforschung (12/12). This paper is dedicated to Dr. Uwe Walter Luedde (Bremerhaven/Germany) on the occasion of his 70th birthday.

Received: April 8, 2013
Revised: June 18, 2013
Accepted: July 26, 2013
Published: August 22, 2013

REFERENCES

Andreu, P., Johansson, M., Affara, N.I., Pucci, F., Tan, T., Junankar, S., Korets, L., Lam, J., Tawfik, D., DeNardo, D.G., et al. (2010). FcRgamma activation regulates inflammation-associated squamous carcinogenesis. Cancer Cell *17*, 121–134.

Bantel, H., and Schulze-Osthoff, K. (2012). Mechanisms of cell death in acute liver failure. Front. Physiol. *3*, 79.

Bettermann, K., Vucur, M., Haybaeck, J., Koppe, C., Janssen, J., Heymann, F., Weber, A., Weiskirchen, R., Liedtke, C., Gassler, N., et al. (2010). TAK1 suppresses a NEMO-dependent but NF-kappaB-independent pathway to liver cancer. Cancer Cell *17*, 481–496.

Bonnet, M.C., Preukschat, D., Welz, P.S., van Loo, G., Ermolaeva, M.A., Bloch, W., Haase, I., and Pasparakis, M. (2011). The adaptor protein FADD protects epidermal keratinocytes from necroptosis in vivo and prevents skin inflammation. Immunity *35*, 572–582.

Cairo, S., Armengol, C., De Reyniès, A., Wei, Y., Thomas, E., Renard, C.A., Goga, A., Balakrishnan, A., Semeraro, M., Gresh, L., et al. (2008). Hepatic stem-like phenotype and interplay of Wnt/beta-catenin and Myc signaling in aggressive childhood liver cancer. Cancer Cell *14*, 471–484.

Chakraborty, J.B., Oakley, F., and Walsh, M.J. (2012). Mechanisms and biomarkers of apoptosis in liver disease and fibrosis. Int. J. Hepatol. *2012*, 648915.

Chan, J.K., Roth, J., Oppenheim, J.J., Tracey, K.J., Vogl, T., Feldmann, M., Horwood, N., and Nanchahal, J. (2012). Alarmins: awaiting a clinical response. J. Clin. Invest. *122*, 2711–2719.

Chang, L., Kamata, H., Solinas, G., Luo, J.L., Maeda, S., Venuprasad, K., Liu, Y.C., and Karin, M. (2006). The E3 ubiquitin ligase itch couples JNK activation to TNFalpha-induced cell death by inducing c-FLIP(L) turnover. Cell *124*, 601–613.

Chen, L., Park, S.M., Tumanov, A.V., Hau, A., Sawada, K., Feig, C., Turner, J.R., Fu, Y.X., Romero, I.L., Lengyel, E., and Peter, M.E. (2010). CD95 promotes tumour growth. Nature *465*, 492–496.

Cho, Y.S., Challa, S., Moquin, D., Genga, R., Ray, T.D., Guildford, M., and Chan, F.K. (2009). Phosphorylation-driven assembly of the RIP1-RIP3 complex regulates programmed necrosis and virus-induced inflammation. Cell *137*, 1112–1123.

Das, M., Garlick, D.S., Greiner, D.L., and Davis, R.J. (2011). The role of JNK in the development of hepatocellular carcinoma. Genes Dev. *25*, 634–645.

Delaney, J.R., and Mlodzik, M. (2006). TGF-beta activated kinase-1: new insights into the diverse roles of TAK1 in development and immunity. Cell Cycle *5*, 2852–2855.

Desmet, V.J. (2011). Ductal plates in hepatic ductular reactions. Hypothesis and implications. I. Types of ductular reaction reconsidered. Virchows Arch. *458*, 251–259.

Dubois, C.M., Blanchette, F., Laprise, M.H., Leduc, R., Grondin, F., and Seidah, N.G. (2001). Evidence that furin is an authentic transforming growth factor-beta1-converting enzyme. Am. J. Pathol. *158*, 305–316.

Feldstein, A.E., and Gores, G.J. (2005). Apoptosis in alcoholic and nonalcoholic steatohepatitis. Front. Biosci. *10*, 3093–3099.

Fung, J., Lai, C.L., and Yuen, M.F. (2009). Hepatitis B and C virus-related carcinogenesis. Clin. Microbiol. Infect. *15*, 964–970.

Glaser, S.S., Gaudio, E., Miller, T., Alvaro, D., and Alpini, G. (2009). Cholangiocyte proliferation and liver fibrosis. Expert Rev. Mol. Med. *11*, e7.

Greten, F.R., Eckmann, L., Greten, T.F., Park, J.M., Li, Z.W., Egan, L.J., Kagnoff, M.F., and Karin, M. (2004). IKKbeta links inflammation and tumorigenesis in a mouse model of colitis-associated cancer. Cell *118*, 285–296.

Guerra, C., Schuhmacher, A.J., Cañamero, M., Grippo, P.J., Verdaguer, L., Pérez-Gallego, L., Dubus, P., Sandgren, E.P., and Barbacid, M. (2007). Chronic pancreatitis is essential for induction of pancreatic ductal adenocarcinoma by K-Ras oncogenes in adult mice. Cancer Cell *11*, 291–302.

Han, J., Zhong, C.Q., and Zhang, D.W. (2011). Programmed necrosis: backup to and competitor with apoptosis in the immune system. Nat. Immunol. *12*, 1143–1149.

Hanahan, D., and Weinberg, R.A. (2011). Hallmarks of cancer: the next generation. Cell *144*, 646–674.

He, S., Wang, L., Miao, L., Wang, T., Du, F., Zhao, L., and Wang, X. (2009). Receptor interacting protein kinase-3 determines cellular necrotic response to TNF-alpha. Cell *137*, 1100–1111.

Huh, J.R., Guo, M., and Hay, B.A. (2004). Compensatory proliferation induced by cell death in the Drosophila wing disc requires activity of the apical cell death caspase Dronc in a nonapoptotic role. Curr. Biol. *14*, 1262–1266.

Inokuchi, S., Aoyama, T., Miura, K., Osterreicher, C.H., Kodama, Y., Miyai, K., Akira, S., Brenner, D.A., and Seki, E. (2010). Disruption of TAK1 in hepatocytes causes hepatic injury, inflammation, fibrosis, and carcinogenesis. Proc. Natl. Acad. Sci. USA *107*, 844–849.

Jaeschke, H., and Lemasters, J.J. (2003). Apoptosis versus oncotic necrosis in hepatic ischemia/reperfusion injury. Gastroenterology *125*, 1246–1257.

Karin, M., and Gallagher, E. (2009). TNFR signaling: ubiquitin-conjugated TRAFfic signals control stop-and-go for MAPK signaling complexes. Immunol. Rev. *228*, 225–240.

Kellendonk, C., Opherk, C., Anlag, K., Schütz, G., and Tronche, F. (2000). Hepatocyte-specific expression of Cre recombinase. Genesis *26*, 151–153.

Kondo, S., Senoo-Matsuda, N., Hiromi, Y., and Miura, M. (2006). DRONC coordinates cell death and compensatory proliferation. Mol. Cell. Biol. *26*, 7258–7268.

Llovet, J.M., Burroughs, A., and Bruix, J. (2003). Hepatocellular carcinoma. Lancet *362*, 1907–1917.

Luedde, T., and Schwabe, R.F. (2011). NF-κB in the liver—linking injury, fibrosis and hepatocellular carcinoma. Nat. Rev. Gastroenterol. Hepatol. *8*, 108–118.

Luedde, T., Beraza, N., Kotsikoris, V., van Loo, G., Nenci, A., De Vos, R., Roskams, T., Trautwein, C., and Pasparakis, M. (2007). Deletion of NEMO/IKKgamma in liver parenchymal cells causes steatohepatitis and hepatocellular carcinoma. Cancer Cell *11*, 119–132.

Maeda, S., Kamata, H., Luo, J.L., Leffert, H., and Karin, M. (2005). IKKbeta couples hepatocyte death to cytokine-driven compensatory proliferation that promotes chemical hepatocarcinogenesis. Cell *121*, 977–990.

Michalopoulos, G.K., and DeFrances, M. (2005). Liver regeneration. Adv. Biochem. Eng. Biotechnol. *93*, 101–134.

Newton, K., Sun, X., and Dixit, V.M. (2004). Kinase RIP3 is dispensable for normal NF-kappa Bs, signaling by the B-cell and T-cell receptors, tumor necrosis factor receptor 1, and Toll-like receptors 2 and 4. Mol. Cell. Biol. *24*, 1464–1469.

Pockros, P.J., Schiff, E.R., Shiffman, M.L., McHutchison, J.G., Gish, R.G., Afdhal, N.H., Makhviladze, M., Huyghe, M., Hecht, D., Oltersdorf, T., and Shapiro, D.A. (2007). Oral IDN-6556, an antiapoptotic caspase inhibitor, may lower aminotransferase activity in patients with chronic hepatitis C. Hepatology *46*, 324–329.

Ratziu, V., Sheikh, M.Y., Sanyal, A.J., Lim, J.K., Conjeevaram, H., Chalasani, N., Abdelmalek, M., Bakken, A., Renou, C., Palmer, M., et al. (2012). A phase 2, randomized, double-blind, placebo-controlled study of GS-9450 in subjects with nonalcoholic steatohepatitis. Hepatology *55*, 419–428.

Renard, C.A., Fourel, G., Bralet, M.P., Degott, C., De La Coste, A., Perret, C., Tiollais, P., and Buendia, M.A. (2000). Hepatocellular carcinoma in WHV/N-myc2 transgenic mice: oncogenic mutations of beta-catenin and synergistic effect of p53 null alleles. Oncogene *19*, 2678–2686.

Roychowdhury, S., McMullen, M.R., Pisano, S.G., Liu, X., and Nagy, L.E. (2013). Absence of receptor interacting protein kinase 3 prevents ethanol-induced liver injury. Hepatology *57*, 1773–1783.

Ryoo, H.D., and Bergmann, A. (2012). The role of apoptosis-induced proliferation for regeneration and cancer. Cold Spring Harb. Perspect. Biol. *4*, a008797. http://dx.doi.org/10.1101/cshperspect.a008797.

Sakurai, T., Maeda, S., Chang, L., and Karin, M. (2006). Loss of hepatic NF-kappa B activity enhances chemical hepatocarcinogenesis through sustained c-Jun N-terminal kinase 1 activation. Proc. Natl. Acad. Sci. USA *103*, 10544–10551.

Sakurai, T., He, G., Matsuzawa, A., Yu, G.Y., Maeda, S., Hardiman, G., and Karin, M. (2008). Hepatocyte necrosis induced by oxidative stress and IL-1 alpha release mediate carcinogen-induced compensatory proliferation and liver tumorigenesis. Cancer Cell *14*, 156–165.

Salmena, L., Lemmers, B., Hakem, A., Matysiak-Zablocki, E., Murakami, K., Au, P.Y., Berry, D.M., Tamblyn, L., Shehabeldin, A., Migon, E., et al. (2003). Essential role for caspase 8 in T-cell homeostasis and T-cell-mediated immunity. Genes Dev. *17*, 883–895.

Sato, S., Sanjo, H., Takeda, K., Ninomiya-Tsuji, J., Yamamoto, M., Kawai, T., Matsumoto, K., Takeuchi, O., and Akira, S. (2005). Essential function for the kinase TAK1 in innate and adaptive immune responses. Nat. Immunol. *6*, 1087–1095.

Sherman, M. (2010). Hepatocellular carcinoma: epidemiology, surveillance, and diagnosis. Semin. Liver Dis. *30*, 3–16.

Takahashi, H., Ogata, H., Nishigaki, R., Broide, D.H., and Karin, M. (2010). Tobacco smoke promotes lung tumorigenesis by triggering IKKbeta- and JNK1-dependent inflammation. Cancer Cell *17*, 89–97.

Vanlangenakker, N., Vanden Berghe, T., Bogaert, P., Laukens, B., Zobel, K., Deshayes, K., Vucic, D., Fulda, S., Vandenabeele, P., and Bertrand, M.J. (2011). cIAP1 and TAK1 protect cells from TNF-induced necrosis by preventing RIP1/RIP3-dependent reactive oxygen species production. Cell Death Differ. *18*, 656–665.

Vucur, M., Roderburg, C., Bettermann, K., Tacke, F., Heikenwalder, M., Trautwein, C., and Luedde, T. (2010). Mouse models of hepatocarcinogenesis: what can we learn for the prevention of human hepatocellular carcinoma? Oncotarget *1*, 373–378.

Welz, P.S., Wullaert, A., Vlantis, K., Kondylis, V., Fernández-Majada, V., Ermolaeva, M., Kirsch, P., Sterner-Kock, A., van Loo, G., and Pasparakis, M. (2011). FADD prevents RIP3-mediated epithelial cell necrosis and chronic intestinal inflammation. Nature *477*, 330–334.

Wunderlich, F.T., Luedde, T., Singer, S., Schmidt-Supprian, M., Baumgartl, J., Schirmacher, P., Pasparakis, M., and Brüning, J.C. (2008). Hepatic NF-kappa B essential modulator deficiency prevents obesity-induced insulin resistance but synergizes with high-fat feeding in tumorigenesis. Proc. Natl. Acad. Sci. USA *105*, 1297–1302.

Yang, L., Inokuchi, S., Roh, Y.S., Song, J., Loomba, R., Park, E.J., and Seki, E. (2013). Transforming growth factor-β signaling in hepatocytes promotes hepatic fibrosis and carcinogenesis in mice with hepatocyte-specific deletion of TAK1. Gastroenterology *144*, 1042–1054.e4.

Zhang, D.Y., and Friedman, S.L. (2012). Fibrosis-dependent mechanisms of hepatocarcinogenesis. Hepatology *56*, 769–775.

Zhang, D.W., Shao, J., Lin, J., Zhang, N., Lu, B.J., Lin, S.C., Dong, M.Q., and Han, J. (2009). RIP3, an energy metabolism regulator that switches TNF-induced cell death from apoptosis to necrosis. Science *325*, 332–336.